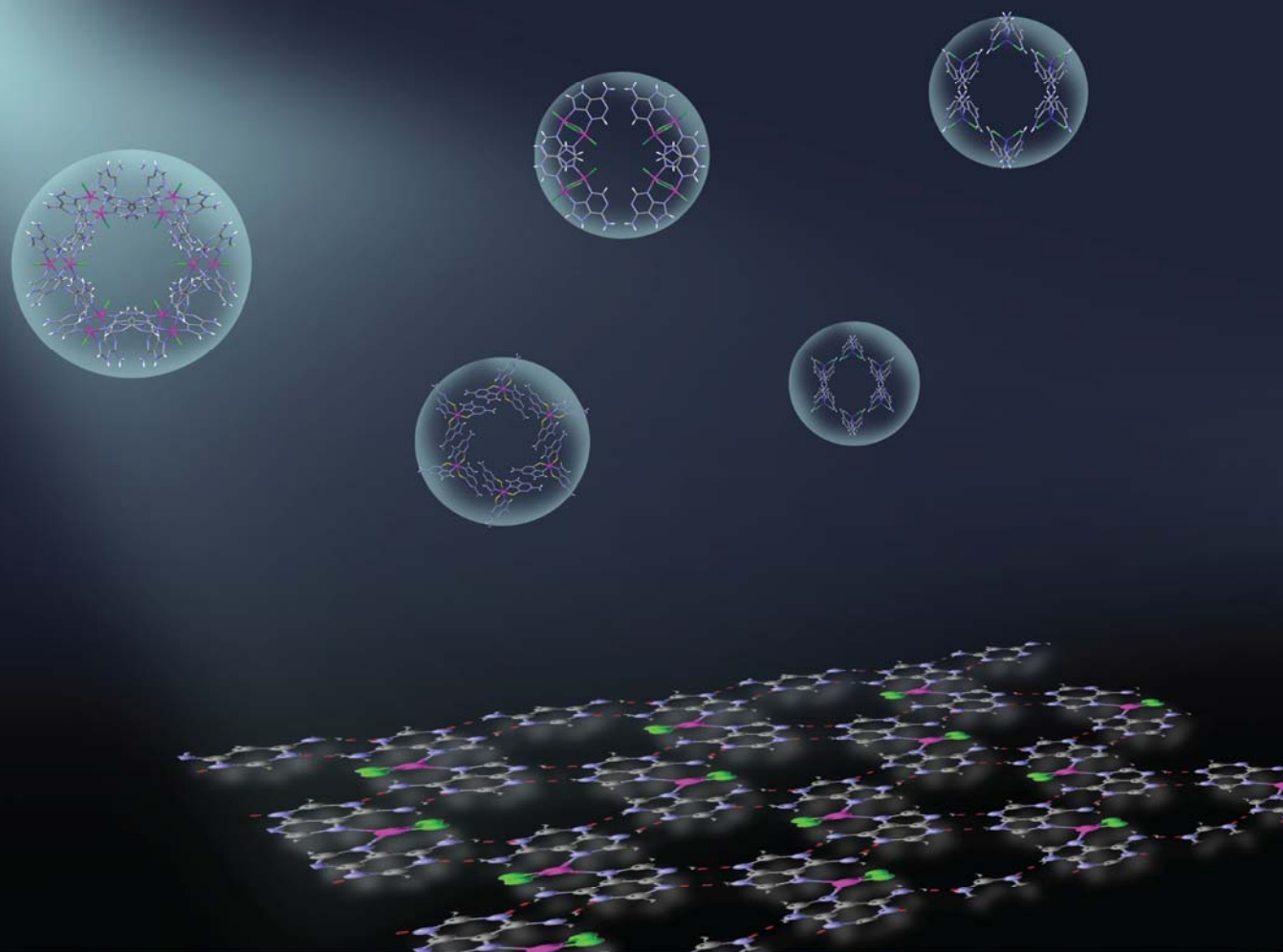


SupraMOFs: Supramolecular porous materials assembled from metal–nucleobase discrete entities



Jintha Thomas
July 2015



Universidad del País Vasco
Euskal Herriko Unibertsitatea



ZTF-FCT
Zientzia eta Teknologia Fakultatea
Facultad de Ciencia y Tecnología



ZTF-FCT
Zientzia eta Teknologia Fakultatea
Facultad de Ciencia y Tecnología



emán ta zabal zazu
Universidad del País Vasco
Euskal Herriko Unibertsitatea

UPV/EHU
FACULTAD DE CIENCIA Y TECNOLOGÍA
DEPARTAMENTO DE QUÍMICA INORGÁNICA

SupraMOFs: Supramolecular porous materials assembled from metal–nucleobase discrete entities

A thesis submitted to the University of the Basque Country
in partial fulfilment of the requirements for the degree of
Doctor of Philosophy in
Chemistry

by
JINTHA THOMAS
Leioa, July, 2015

Words of Gratitude.....

This thesis originated out of years of research and by that time I have worked with a great number of people, whose contributions helped the research and the making of the thesis in assorted ways. They all deserve special mention and it is a pleasure to convey my gratitude to all of them in my humble acknowledgement.

First, I want to express my deeply felt thanks to my directors Dr. Oscar Castillo García, Professor of the Department of Inorganic Chemistry, University of the Basque Country and Dr. Pascual Román Polo, the Director of the Department of Inorganic Chemistry, University of the Basque Country for their valuable guidance and constant support. With extreme gratitude I remember Dr. Oscar Castillo García, who with his profound knowledge have enlightened me during my stint here as a research scholar. I am indebted to him for his expertise, kindness, and valuable guidance and above all for his patience and optimism which helped a lot in instilling confidence in me. I sincerely thank him for continuously orienting me in the correct research direction and guiding me to write this thesis through his constant encouragement and advice. He was very affectionate and was ready to help me even in the midst of his busy schedule and without his guidance this thesis would have been a distant possibility. I would like to express my great gratitude to Prof. Pascual Román Polo for his encouragement, advices and constructive criticisms that contributed to the fruitful completion of my research work. He always supported me with valuable suggestions and inspirational words. I remember him with a deep sense of gratitude and affection.

I would like to extend my gratitude to Professor Antonio Luque Arrebola, who was always there with valuable suggestions. I am really thankful to him for the helps that he offered me for the successful completion of this work. With great happiness I acknowledge his contributions to this work. I cannot move forth without acknowledging the immense support and contribution from Dr Garikoitz Beobide Pacheco, who was always willing to offer help and clarifying doubts even when with his busy schedules. He was a source of knowledge and open hearted to discuss about new possibilities and with whom I learnt many scientific skills. I am extremely grateful for his efficient guidance, creative discussions, constant encouragement and support.

I gratefully remember my colleagues Sonia Pérez, Javier Cepeda, Mónica Lanchas, and Daniel Vallejo for their guidance, support and affection. I would say that

God has showered his blessings on me in the form of these friends. They had always been there to help me in all the issues either academic or personal. Their cheerful and refreshing company added colour to my research life. I remember that I had full freedom to approach them whenever I needed their help. No words would be enough to express my love and gratitude for them. I am extremely thankful to Sonia for being my help and for her contributions, especially during the last stages of this work. I would like to extend my special thanks to Mónica, who is like an elder sister for me and she always offered me support whenever I needed. I am also thankful to Javi and Dani, who always found time to clear my doubts. With great pleasure I remember the good moments shared with Sandra Arcediano, Fabio Scé, Rubén Pérez, Ahmed Reyad, Asier Bárbara, Xabi and Fran Llano. I remember the good moments I have shared with Javi Salado and Eider Goikolea and all other members of the Department of Inorganic Chemistry. With great affection I remember Eneritz Couciero and also Julen who have always been a source of happiness for me.

I would like to thank the University of the Basque country (UPV/EHU) for the financial support and the 'Servicios Generales de Investigación' (SGIker) of the University of the Basque Country for their technical and human support. I remember with gratitude the helps received from Pablo Vitoria, Leire San Felices, Aitor Larrañaga and Javier Sangüesa.

I owe immensely to all my teachers right from my schooling days to the post graduate level for having constantly kept my thirst for knowledge burning. I also thank all my friends who have come across the journey of my life and each and everyone who has been in help though I cannot name them all here.

I am indebted to Elena Aunty for her constant love and care. She was always there with her kind words and support whenever I needed. I would like to give special words of thanks to Dr. Julia Gonzáles, Dr. Josu Solaberrieta, Prof. Itziar Elexpuru and Silvia Martínez for their consideration and encouragement. I would also like to thank Alan Wrafter, Sharon Lloyd, Nora Fernández, Irene Sendra, Terry Howard and Katherine Shirrell from the American School of Bilbao, for their kind support. With great joy I cherish the friendship shared with Aritz Plaza, Zvezdana Topalovic, Sashwati Mishra, Angom Delhi, Alfred-Asha, Saji-Anitha, Azis Ikka, Barca-friends, Fr. Binu Kumar, S. Suja, E. M. Biji, P. K. Saritha, M. V. Lekha and all my friends from school days.

Let me also take this opportunity to thank my family for their incessant love and cooperation. I know that words are insufficient to express the depth of my love and gratitude to my beloved parents and my brother. Pappa, mummy and my little brother Jinu Thomas, had always been in my side for my good and bad. This thesis would not have been realized without their prayers and sacrifice. With tears in my eyes, I remember my late grandmothers who could not wait to see me accomplishing this goal, as it was their dream too. I express my extreme gratitude to my parents in law for their wholehearted support and prayers. With great pleasure and gratitude I remember all my aunts, uncles, cousins, neighbours and all other family members for the immense love, care and encouragement they showed on me throughout my life. With great affection I remember Vishal Wilson and Akash Wilson for their innocent love and care.

Even though words cannot express the depth of my love and gratitude to my husband Dr. Gipson Varghese, I am taking this opportunity to thank him for his love, patience, encouragement and sacrifice. From the moment I knew him, he had been my mentor and guide and without his wholehearted support it would not have been possible for me to complete this work. I thankfully remember all his efforts for my success and by completing this thesis I am fulfilling his dream as well, because he is the one behind my achievements.

Now with all my love I would like to thank my little darlings Aiden Georgie and Aislin Maria who were gifted to me during this journey of research. They were always beside me with their innocent smile even though they might have missed the warmth and comfort of being with their mum. In return, I dedicate this thesis to my kids.

Above all, I bow my head in humility before my Saviour and Lord for giving me the knowledge and strength to complete this work and guiding me all through my life.

To,

My parents and brother

My husband

My children

CONTENTS

1. INTRODUCTION

1.1 OVERVIEW OF CRYSTAL ENGINEERING	3
1.2 POROUS MATERIALS BASED ON COORDINATION BONDS (METAL–ORGANIC FRAMEWORKS, MOFs)	5
1.3 SUPRAMOLECULAR CRYSTAL ENGINEERING	11
1.4 NUCLEOBASES AS COORDINATION BONDING LINKERS	17
1.5 NUCLEOBASES AS HYDROGEN BONDING LINKERS	25
1.6 OBJECTIVE	33

2. SUPRAMOLECULAR ARCHITECTURES BASED ON METAL/CYTOSINE SYSTEMS

2.1 INTRODUCTION	37
2.2 SYNTHESIS AND CHARACTERISATION	41
2.2.1 <i>Synthesis</i>	41
2.2.1.1 <i>Synthesis of COCYTCL</i>	41
2.2.1.2 <i>Synthesis of COCYTBR</i>	42
2.2.1.3 <i>Synthesis of ZNCYTCL</i>	42
2.2.1.4 <i>Synthesis of CUCYTCL–B</i>	42
2.2.1.5 <i>Synthesis of CUCYTBR</i>	43
2.2.1.6 <i>Synthesis of CUCYTSO4</i>	43
2.3 RESULTS AND DISCUSSION	43
2.3.1 <i>Crystallographic analysis</i>	43
2.3.2 <i>Structural Description</i>	46
2.3.2.1 <i>Structure of COCYTCL</i>	46
2.3.2.2 <i>Structures of COCYTBR and ZNCYTCL</i>	49
2.3.2.3 <i>Structure of CUCYTCL–B</i>	52
2.3.2.4 <i>Structure of CUCYTBR</i>	54
2.3.2.5 <i>Structure of CUCYTSO4</i>	56
2.3.3 <i>Thermal analysis</i>	62
2.4 CONCLUSIONS	63

3. SUPRAMOLECULAR METAL–ORGANIC FRAMEWORKS BASED ON METAL/PURINE SYSTEMS

3.1 INTRODUCTION	69
3.2 SYNTHESIS AND CHEMICAL CHARACTERISATION	76

3.2.1	<i>Synthesis</i>	76
3.2.1.1	<i>Synthesis of compound CUADECL–A</i>	77
3.2.1.2	<i>Synthesis of compound CUADECL–B (SMOF–1)</i>	77
3.2.1.3	<i>Synthesis of compound CUADECL–C (SMOF–3)</i>	77
3.2.1.4	<i>Synthesis of compound CUADEBR–A (SMOF–2)</i>	78
3.2.1.5	<i>Synthesis of compound CUADEBR–B</i>	78
3.2.1.6	<i>Synthesis of compound CUADEOH (SMOF–9)</i>	79
3.2.1.7	<i>Synthesis of compound CUADECO₃ (SMOF–8).</i>	79
3.2.1.8	<i>Synthesis of compound CO₃ADECL</i>	79
3.2.1.9	<i>Synthesis of compound COADECL (SMOF–5)</i>	79
3.2.1.10	<i>Synthesis of compound COADEBR (SMOF–6)</i>	80
3.2.1.11	<i>Synthesis of compound CO–9–MEADECL</i>	80
3.2.1.12	<i>Synthesis of compound CU–9–MEADEACE</i>	81
3.2.1.13	<i>Synthesis of compound CO–6–CLPUR</i>	81
3.2.1.14	<i>Synthesis of compound CUGUACL</i>	81
3.2.1.15	<i>Synthesis of compound CO–6–THIOG (SMOF–4)</i>	82
3.3	RESULTS AND DISCUSSION	82
3.3.1	<i>Crystallographic analysis</i>	82
3.3.2	<i>Structural Description</i>	87
3.3.2.1	Structural Description of [Cu ₂ (μ–Hade) ₄ Cl ₂]Cl ₂ ·8H ₂ O; (CUADECL–A)	87
3.3.2.2	Structural description of [Cu ₂ (μ– Hade) ₄ (Cl) ₂]Cl ₂ ·2MeOH; (CUADECL–B/ SMOF–1) and [Cu ₂ (μ–Hade) ₄ (Br) ₂]Br ₂ ·~2MeOH; (CUADEBR– A/SMOF–2)	90
3.3.2.2.1	<i>Thermogravimetric analysis of CUADECL–B (SMOF–1) and CUADEBR–A (SMOF–2)</i>	97
3.3.2.2.2	<i>Gas adsorption experiments on CUADECL–B (SMOF–1) and CUADEBR–A (SMOF–2).</i>	99
3.3.2.3	Structural description of [Cu ₂ (μ–Hade) ₂ (μ– Cl) ₂ (Cl) ₂]·2MeOH; CUADECL–C (SMOF–3) and [Cu ₂ (μ–Hade) ₂ (μ–Br) ₂ (Br) ₂]·2PrOH; CUADEBR–B	107
3.3.2.4	Structural description of [Cu ₂ (μ–ade) ₃ (μ– OH)(H ₂ O)(CH ₃ OH)] _n ·n(solvent); CUADEOH (SMOF– 9)	116
3.3.2.5	Structural description of [Co ₃ (μ–Hade) ₂ (μ– Cl) ₄ Cl ₂ (H ₂ O) ₄]·2H ₂ O; (CO ₃ ADECL)	120

3.3.2.6	Structural description of $[\text{Cu}_4(\mu_3\text{-ade})_2(\mu_2\text{-ade})_2(\text{pentylNH}_2)_2(\text{CH}_3\text{OH})_2(\text{CO}_3)_2(\text{H}_2\text{O})_2] \cdot n(\text{solvent})$ <i>CUADECO3 (SMOF-8)</i>	124
3.3.2.7	Structural description of $[\text{Co}(\text{Hade})_2\text{Cl}_2]$ <i>COADECL (SMOF-5)</i> and $[\text{Co}(\text{Hade})_2\text{Br}_2]$ <i>COADEBR (SMOF-6)</i>	128
3.3.2.8	Structural Description of $[\text{Co}(9\text{-MeAde})_2(\text{H}_2\text{O})_4]\text{Cl}_2 \cdot 2\text{H}_2\text{O}$; <i>CO-9-MEADECL</i>	134
3.3.2.9	Structural Description of $[\text{Cu}_2(\mu\text{-CH}_3\text{COO})_4(\mu\text{-9-MeAde})]_n \cdot n\text{CH}_3\text{OH}$; <i>CU-9-MEADEACE</i>	139
3.3.2.10	Structural description of $[\text{Cu}_2(\text{Hgua})_2(\text{H}_2\text{gua})_2(\mu\text{-Cl})_2\text{Cl}_2(\text{H}_2\text{O})][\text{CuCl}_4]$; <i>CUGUACL</i>	143
3.3.2.11	Structural description of $[\text{Co}(6\text{-ClPur})_2(\text{H}_2\text{O})_4] \cdot 4\text{H}_2\text{O}$; <i>CO-6-CLPUR</i>	146
3.3.2.12	Structural description of $[\text{Co}(\text{ThioG})_3] \cdot n\text{H}_2\text{O}$; <i>CO-6-THIOG (SMOF-4)</i>	150
3.4	CONCLUSIONS	157
4.	CONCLUSIONS AND FUTURE PERSPECTIVES	
4.1	CONCLUSIONS	161
4.2	FUTURE WORK	165
5.	REFERENCES	
5.1	INTRODUCTION:	169
5.2	REFERENCES:	169
6.	APPENDICES	
A.1	CHEMICALS	197
A.2	INSTRUMENTAL TECHNIQUES	198
A.3	IR SPECTRA	202
A.4	THERMOGRAVIMETRIC ANALYSIS	207
A.5	EXPERIMENTAL AND THEORETICAL ADSORPTION MEASUREMENTS	209
A.6	ARTICLES PUBLISHED FROM THIS WORK	216

List of Tables

Table 2.1:	Synthesised new compounds.	41
Table 2.2:	Single crystal data and structural refinement details of metal–cytosine.	45
Table 2.3:	Selected coordination bonds (Å) and angles (°) in compound COCYTCL.	46
Table 2.4:	Supramolecular interactions (Å, °) of COCYTCL.	47
Table 2.5:	Selected coordination bonds (Å) and angles (°) in compounds COCYTBR and ZNCYTCL.	50
Table 2.6:	Supramolecular interactions (Å, °) of COCYTBR/ZNCYTCL.	50
Table 2.7:	Selected coordination bonds (Å) and angles (°) in compound CUCYTCL–A and CUCYTCL–B.	53
Table 2.8:	Supramolecular interactions (Å, °) of CUCYTCL.	54
Table 2.9:	Selected coordination bonds (Å) and angles (°) in compound CUCYTBR.	55
Table 2.10:	Supramolecular interactions (Å, °) of CUCYTBR.	56
Table 2.11:	Selected coordination bonds (Å) and angles (°) in compound CUCYTSO4.	59
Table 2.12:	Hydrogen bonding interactions (Å, °) of COCYTSO4.	59
Table 2.13:	Distances for coordination bonds and intermolecular interaction between two $[\text{Cu}(\text{Hcyt})_4]^{2+}$ in the optimized structure and crystal structure.	61
Table 2.14:	Thermoanalytic data for the compounds COCYTBR, CUCYTCL, CUCYTBR.	63
Table 3.1:	Compounds synthesised	76
Table 3.2:	Single crystal data and structural refinement details of compounds CUADECL–A, CUADECL–B (SMOF–1), CUADEBR–A (SMOF–2), CUADECL–C (SMOF–3) and CUADEBR–B.	84
Table 3.3:	Single crystal data and structural refinement details of compounds CUADEOH (SMOF–9), CUADECO3 (SMOF–8), CO3ADECL, COADECL (SMOF–5) and CUGUACL	84
Table 3.4:	Single crystal data and structural refinement details of compounds CO–9–MEADECL, CU–9–MEADEACE, CO–6–CLPUR, CO–6–THIOG (SMOF–4).	86
Table 3.5:	Selected bond lengths (Å) and angles (°) of the compound CUADECL–A.	88
Table 3.6:	Selected bond lengths (Å) and angles (°) for CUADECL–B and CUADEBR–A.	92

Table 3.7:	Hydrogen bonding interactions (\AA , $^\circ$) in compound CUADECL-B (SMOF-1).	94
Table 3.8:	Hydrogen bonding interactions (\AA , $^\circ$) in CUADEBR-A (SMOF-2).	94
Table 3.9:	Thermogravimetric data of CUADECL-B (SMOF-1) and CUADEBR-A (SMOF-2).	98
Table 3.10:	Calculated onset point values for CUADECL-B (SMOF-1).	102
Table 3.11:	Selected bond lengths (\AA) and angles ($^\circ$) for the coordination polyhedron of CUADECL-C (SMOF-3) and CUADEBR-B	109
Table 3.12:	Supramolecular interactions (\AA , $^\circ$) in CUADECL-C (SMOF-3).	110
Table 3.13:	Hydrogen bonding interactions (\AA , $^\circ$) in the compound CUADEBR-B.	113
Table 3.14:	The thermogravimetric data for compounds CUADECL-C (SMOF-3) and	114
Table 3.15:	Selected bond lengths (\AA) and angles ($^\circ$) of the coordination sphere of CUADEOH (SMOF-9).	119
Table 3.16:	Hydrogen bonding interactions (\AA , $^\circ$) in CUADEOH (SMOF-9).	119
Table 3.17:	Selected coordination bond lengths (\AA) and angles ($^\circ$) in CO3ADECL.	122
Table 3.18:	Hydrogen bonding interactions (\AA , $^\circ$) in CO3ADECL.	122
Table 3.19:	The coordination bond lengths (\AA) and angles ($^\circ$) for CUADECO3 (SMOF-8)	128
Table 3.20:	Hydrogen bonding interactions (\AA , $^\circ$) in CUADECO3 (SMOF-8).	128
Table 3.21:	Coordination bond lengths (\AA) and angles ($^\circ$) in COADECL-A (SMOF-5).	129
Table 3.22:	Hydrogen bonding interactions (\AA , $^\circ$) in COADECL (SMOF-5).	130
Table 3.23:	Thermogravimetric data for COADECL (SMOF-5) and COADEBR	132
Table 3.24:	Coordination bond lengths (\AA) and angles ($^\circ$) for compound CO-9-MEADECL.	136
Table 3.25:	Supramolecular interactions (\AA , $^\circ$) in CO-9-MEADECL.	137
Table 3.26:	The thermogravimetric data of CO-9-MEADECL.	139
Table 3.27:	Selected bond lengths (\AA) and angles ($^\circ$) of compound CU-9-MEADEACE	141

Table 3.28:	Hydrogen bonding interactions (Å, °) in CU-9-MEADFACE.	142
Table 3.29:	Thermogravimetric data of CU-9-MEADFACE.	143
Table 3.30:	Coordination bond lengths (Å) and angles (°) of CUGUACL.	144
Table 3.31:	Supramolecular interactions (Å, °) for compound CUGUACL.	145
Table 3.32:	Selected coordination bond lengths (Å) and angles (°) of the compound	147
Table 3.33:	Supramolecular interactions (Å, °) in CO-6-CLPUR.	149
Table 3.34:	Thermogravimetric data of CO-6-CLPUR.	150
Table 3.35:	Selected bond lengths (Å) and angles (°) of the compound CO-6-THIOG (SMOF-4).	151
Table 3.36:	Supramolecular interactions (Å, °) in CO-6-THIOG (SMOF-4).	153
Table 3.37:	Thermogravimetric data of CO-6-THIOG (SMOF-4).	156
Table 4.1:	A summary table showing the effect of the key factors determining the formation of porous SMOFs.	163
Table A.1.1:	Reactants used.	197
Table A.1.1:	Ligands used.	197
Table A.5.1:	Lennard-Jones parameters and point charges.	213
Table A.5.2:	Lennard-Jones parameters and partial charges.	214
Table A.5.3:	Resulting ESP charges upon the atoms of the structural model of the CUADECL-B (SMOF-1), CUADEBR-A (SMOF-2).and CUADECL-C (SMOF-3)	215

List of Figures

Figure 1.1:	Examples of bridging ligands used as connectors in crystal engineering.	6
Figure 1.2:	Different structural possibilities by the combination of metal centres (nodes) and ligands (connectors).	7
Figure 1.3:	Different structures obtained using blocking ligands to create nodes with new geometries.	7
Figure 1.4:	Examples of isorecticular MOFs based on Zn_4O clusters	8
Figure 1.5:	Structural breakdown of the compound $[Zn_4O(bdc)_3]_n$ (MOF-5, bdc: benzene-1,4-dicarboxylate).	9
Figure 1.6:	Examples of common SBUs.	9
Figure 1.7:	Examples of some common representative supramolecular synthons (taken from reference 5).	12
Figure 1.8:	The self-assembly from molecule to crystal through supramolecular synthons.	13
Figure 1.9:	Scheme showing the “tecton-synthon” concept using trimesic acid as example.	14
Figure 1.10:	Examples of organic synthons formed through hydrogen bonding interaction. Hydrogen bonded synthons are highlighted within the circles.	16
Figure 1.11:	(a) The building unit of $[Cu_2((S)-2-(1,8-naphthalimido)propanoate)_4(THF)_2]$; (b) Section of the overall structure of sustained through π - π interactions.	17
Figure 1.12:	Structure and numbering pattern of the nucleobases.	19
Figure 1.13:	Crystal structure of $\{[Cu_2(\mu\text{-adeninato})_4(H_2O)_2][Cu(ox)(H_2O)]_2\}_n$.	20
Figure 1.14:	SBUs and the resulting crystal structures of compounds (a) $(Me_2NH_2)_2[Zn_8(\mu_4\text{-adeninato})_4(\mu\text{-BPDC})_6(\mu_4\text{-O})]\cdot 8DMF\cdot 11H_2O$, and (b) $(Me_2NH_2)_4[Zn_8(\mu_4\text{-adeninato})_4(\mu\text{-BPDC})_6(\mu\text{-O})]\cdot 49DMF\cdot 31H_2O$.	21
Figure 1.15:	Porous crystal structure of $[M(\mu_3\text{-adeninato})(\mu_2\text{-carboxylato})]_n$ compounds (M being Co^{2+} , Ni^{2+} , Cu^{2+} or Zn^{2+}).	23
Figure 1.16:	Metal coordination environment and final crystal structures of compounds (a) $[Zn(\mu\text{-purinato-}\kappa N7:\kappa N9)_2]_n$, and (b) $[Zn(\mu\text{-adeninato-}\kappa N7:\kappa N9)(\mu\text{-isonicotinato-}\kappa N:\kappa O)]_n$.	25
Figure 1.17:	Canonical Adenine...Thymine and Guanine...Cytosine complementary base pairing pattern through Watson-Crick faces.	27
Figure 1.18:	The hydrogen bonding interactions established between the same types of nucleobases with adenine as an example.	27

Figure 1.19:	Examples of other nucleobases derivatives.	28
Figure 1.20:	Discrete entities of adenine with different nuclearities—(a) monomers, (b) dimers, (c) trimers, (d) tetramers, (e) hexamers and (f) octamers.	29
Figure 1.21:	Discrete entities of other nucleobases; (a) monomeric compound of cytosine, (b) thymine, (c) monomeric compound of xanthine, (d) dimeric compound of guanine, (e) dimeric compound of hypoxanthine, and (f) trimeric compound of uracil and cytosine and (g) 6-mercaptopurine.	30
Figure 1.22:	Examples of compounds in which base-pairing interactions lead to supramolecular polymerization, like, (a) trans-bis(Adeninato)-bis(tri-n-butylphosphine)-palladium(II) methanol solvate, (b) (Adeninato-N9)-methyl-mercury(II) monohydrate, (c) Tetra-aqua-bis(9-methyladenine)-copper(II) dichloride dehydrate, (d) Dichloro-bis(cytosine-N3)-copper(II), (e) bis(9-Methylguanine)-tetraaqua-cadmium(II) dinitrate, (f) tetrakis(Cytosine)-copper(II) diperchlorate dehydrate, and (g) trans-bis(Guanine)-aqua-(formate)-copper(ii) perchlorate formic acid solvate monohydrate.	32
Figure 1.23:	Similarity between (a) coordination bonds and (b) hydrogen bonding interactions.	33
Figure 2.1:	(a) The numbering scheme of cytosine and (b) coordination modes of neutral cytosine.	38
Figure 2.2:	Coordination modes of cytosinate anion	38
Figure 2.3:	Examples of cytosine- $\kappa N3$ coordinated transition metal complexes.	39
Figure 2.4:	(a) Cytosine nucleobase edges, (b) guanine...cytosine triple complementary hydrogen bond and (c) cytosine...cytosine double complementary hydrogen bonding patterns.	40
Figure 2.5:	Hydrogen bonding interaction between coordinated cytosine- $\kappa N3$ nucleobases.	40
Figure 2.6:	Building units of compound COCYTCL showing the labelling scheme.	46
Figure 2.7:	(a) Supramolecular ribbons of cytosinium cations and cytosine molecules. (b) π - π stacking interactions among adjacent supramolecular ribbons. (c) Crystal packing of COCYTCL viewed along [1 1 0] direction. Single dashed lines indicate H-bonds whereas double dashed ones correspond to π - π stacking interactions.	48
Figure 2.8:	Ortep drawing of (a) $[\text{CoBr}_2(\text{C}_4\text{H}_5\text{N}_3\text{O})_2]$ and (b) $[\text{ZnCl}_2(\text{C}_4\text{H}_5\text{N}_3\text{O})_2]$ entities in COCYTBR and ZNCYTCL, respectively.	49

Figure 2.9:	(a) Supramolecular dimeric entity. (b) Infinite chains joined by non-complementary supramolecular interactions. (c) Supramolecular chains formed through base pairing interactions. (d) Crystal packing of COCYTBR viewed along the crystallographic b axis.	51
Figure 2.10:	Drawing showing the structure of the $[\text{CuCl}_2(\text{C}_4\text{H}_5\text{N}_3\text{O})_2]$ discrete entity of (a) CUCYTCL-B and (b) CUCYTCL-A. (c) Overlay of both structures.	53
Figure 2.11:	(a) Supramolecular chain of cytosine...cytosine complementary hydrogen bonded $[\text{CuCl}_2(\text{C}_4\text{H}_5\text{N}_3\text{O})_2]$ discrete entities and (b) crystal packing in CUCYTCL-B.	54
Figure 2.12:	Ortep drawing of $[\text{CuBr}_2(\text{C}_4\text{H}_5\text{N}_3\text{O})_2]$ complex with labelling scheme.	55
Figure 2.13:	Ortep drawing of $[\text{Cu}(\text{C}_4\text{H}_5\text{N}_3\text{O})_4]^{2+}$ complex entity in CUCYTISO4.	57
Figure 2.14:	Intramolecular bifurcated hydrogen bonding.	57
Figure 2.15:	Hypothetical complementary base pairing interactions between the sugar edges of cytosine moieties in CUCYTISO4.	58
Figure 2.16:	(a) Hydrogen bonding interactions between the $[\text{Cu}(\text{C}_4\text{H}_5\text{N}_3\text{O})_4]^{2+}$ complex entity in CUCYTISO4. (b) Hydrogen bonding interactions of the $[\text{Cu}(\text{C}_4\text{H}_5\text{N}_3\text{O})_4]^{2+}$ units with the sulphate counterions.	59
Figure 2.17:	Structural model for the DFT-D geometry optimization showing the numbering scheme.	60
Figure 2.18:	(Left) Electrostatic potential upon an electronic isosurface of 0.01 a.u. (Right) Electrostatic potential (ESP) charges for metal center and for atoms implied in the intermolecular interactions.	61
Figure 2.19:	Thermogravimetric analysis of COCYTBR, CUCYTCL, CUCYTBR.	62
Figure 3.1:	Metal-nucleobase discrete entities suitable for the synthesis of <i>SupraMOFs</i> .	69
Figure 3.2:	Numbering pattern of the atoms in adenine molecule.	71
Figure 3.3:	Coordination modes of the adenine ligand with the number of examples for each mode found in the CSD.	72
Figure 3.4:	The pKa values of adenine.	73
Figure 3.5:	(a) Structure and numbering pattern of Guanine. (b) Different coordination modes as found in the CSD database.	74
Figure 3.6:	Complementary hydrogen bonds between adenines.	75
Figure 3.7:	Complementary hydrogen bonds between guanines.	75

- Figure 3.8: Structure of the dimeric complex cation $[\text{Cu}_2(\mu\text{-adenine})_4\text{Cl}_2]^{2+}$ present in CUADECL–A together with labeling scheme. 88
- Figure 3.9: Graphical insight into the crystal structure of CUADECL–A complex. (a) Complex layer of $[\text{Cu}_2(\mu\text{-adenine})_4\text{Cl}_2]^{2+}$ units and water molecules. (b) Projection along the crystallographic a axis. Notice that the chloride counterions and interlayer water molecules are disordered. 89
- Figure 3.10: Structural unit of CUADECL–B and CUADEBR–A with the atomic numbering scheme (where X = Cl^- or Br^-). 91
- Figure 3.11: Details of the adenine \cdots adenine and adenine \cdots chloride interactions in the crystal packing of CUADECL–B (SMOF–1). 93
- Figure 3.12: Perspective view of the 3D framework along the c -axis showing the pores in compound CUADECL–B (SMOF–1). Solvated methanol molecules are omitted for clarity. 95
- Figure 3.13: Crystal structure features of CUADEBR–A (SMOF–2): (a) Structural unit. (b) Details of the adenine base pairing interaction through the Watson–Crick face (WCF) and of the Hoogsteen Face (HF) mediated adenine \cdots bromide interaction (free bromide anions are represented as orange spheres). (c) Perspective view of the 3D framework along the c -axis showing the pores. 96
- Figure 3.14: (a) Watson–Crick base pairing generated four-connected uninodal 3D net, (b) Hoogsteen edge \cdots bromide hydrogen bond generated net and (c) supramolecular network considering both interactions in CUADEBR–A (SMOF–2). 97
- Figure 3.15: Thermoanalytic data for the compounds CUADECL–B (SMOF–1), CUADEBR–A (SMOF–2) performed upon synthetic air atmosphere (79% N_2 , 21% O_2). 98
- Figure 3.16: Thermogravimetric plots of (a) CUADECL–B (SMOF–1) and (b) CUADEBR–A (SMOF–2). 99
- Figure 3.17: Adsorption isotherms for N_2 (77 K), H_2 (77 K), CO_2 (273 K), and CH_4 (298 K) for fresh samples of compounds CUADECL–B (SMOF–1) (a) and CUADEBR–A (SMOF–2) (b). 101
- Figure 3.18: (a) CO_2 adsorption/desorption isotherms measured at 273 K showing the aging of CUADECL–B (SMOF–1). (b) CO_2 isotherms at 273 and 298 K. The onset pressure value is indicated for each case. 103
- Figure 3.19: Comparison between experimental PXRD patterns collected at different CO_2 pressures and simulated PXRD pattern for the pristine crystal structure of CUADECL–B (SMOF–1). 105

Figure 3.20:	PXRD data for CUADECL-B (SMOF-1) within 6–10°: (a) experimental patterns with increasing CO ₂ pressure. (b) Simulated PXRD patterns from GCMC low energy configurations with increasing CO ₂ uptake per unit cell.	106
Figure 3.21:	Average occupation profiles for CO ₂ at 298 K in CUADECL-B (SMOF-1).	107
Figure 3.22:	Ortep representation of the [Cu ₂ (μ-ade) ₂ (μ-X) ₂ X ₂] units in CUADECL-C (SMOF-3) and CUADEBR-B.	108
Figure 3.23:	Crystal packing features in CUADECL-C (SMOF-3): (a) Strips of [Cu ₂ (μ-adenine) ₂ (μ-Cl) ₂ (Cl) ₂] dinuclear complexes growth by Watson-Crick base pairing interactions. (b, c) Dinuclear entities interacting through Cl···Hoogsteen face and π-π interactions. (d, e) View of the crystal packing through [1 0 0] direction and overall supramolecular connectivity. Dashed lines indicate hydrogen bonds, while double plus signals represent π-π interactions.	111
Figure 3.24:	A view of the crystal packing through [1 0 0] direction in CUADEBR-B. Black dotted lines indicate hydrogen bonding interactions, while orange dashed lines indicate halido···π contacts.	112
Figure 3.25:	The thermogravimetric data for compounds CUADECL-C (SMOF-3) and CUADEBR-B	113
Figure 3.26:	Thermodiffractometric data of CUADECL-C (SMOF-3) and proposed rearrangement scheme for the structural phase transition.	115
Figure 3.27:	CO ₂ adsorption isotherm CUADECL-C (SMOF-3) at 273 K.	116
Figure 3.28:	Ortep representation of the the asymmetric unit of CUADEOH (SMOF-9) together with the numbering scheme.	117
Figure 3.29:	(a) The coordination polymeric chain and (b) supramolecular complementary base pairing interactions among the adeninate entities in compound CUADEOH (SMOF-9).	118
Figure 3.30:	(a) Porous supramolecular architecture of CUADEOH (SMOF-9) (b) the available void space shown in green colour.	120
Figure 3.31:	Ortep representation of [Co ₃ (μ-Hade) ₂ (μ-Cl) ₄ Cl ₂ (H ₂ O) ₄] trimeric unit in CO3ADECL.	121
Figure 3.32:	The head to tail hydrogen bonding interactions between the neighbouring trimeric units in CO3ADECL.	123
Figure 3.33:	Projection of the crystal structure of compound CO3ADECL along the crystallographic <i>a</i> (a), <i>b</i> (b) and <i>c</i> (c) axes.	124

Figure 3.34:	Structural unit of CUADECO3 (SMOF-8) with the atomic numbering scheme.	125
Figure 3.35:	(a) Complementary hydrogen bonding interaction through the Watson-Crick faces of the adenines. (b) Supramolecular sheets sustained through Watson-Crick faces interaction CUADECO3 (SMOF-8).	126
Figure 3.36:	(a) Projection of the crystal structure of compound CUADECO3 (SMOF-8) along the crystallographic <i>c</i> axis and (b) green coloured regions representing the solvent accessible void.	127
Figure 3.37:	X-ray powder diffractograms of and COADEBR (SMOF-6) and simulated pattern resulting from the replacement of chloride by bromide in the crystal structure of COADECL (SMOF-5).	129
Figure 3.38:	(a) Ortep representation of the monomeric entity [Co(Hade) ₂ Cl ₂] together with the labelling scheme and (b) Complementary hydrogen bonding interactions taking place between the [Co(Hade) ₂ Cl ₂] units.	130
Figure 3.39:	(a) Crystal structure of an individual supramolecular subnet of COADECL (SMOF-5) and (b) real crystal structure resulting from the interpenetration of three individual subnets depicted using different colours.	131
Figure 3.40:	TG and DTA curves of the COADECL (SMOF-5) and COADEBR (SMOF-6) under synthetic air atmosphere	132
Figure 3.41:	Coordination modes of 9-methyladenine and their appearance frequency.	135
Figure 3.42:	Ortep view of the complex cation present in compound CO-9-MEADECL.	136
Figure 3.43:	Supramolecular chain of [Co(9-MeAde) ₂ (H ₂ O) ₄] ²⁺ complex cations.	137
Figure 3.44:	The availability of hydrogen bonding faces for free adenine and <i>N</i> 7-coordinated 9-methyladenine.	138
Figure 3.45:	Thermogravimetric analysis of CO-9-MEADECL.	139
Figure 3.46:	(a) A fragment of the polymeric chain of CU-9-MEADEACE (b) and the intramolecular hydrogen bond between <i>N</i> 6-H and oxygen atoms of the carboxylate anions.	141
Figure 3.47:	Crystal packing of CU-9-MEADEACE viewed along the crystallographic <i>b</i> axis.	142
Figure 3.48:	Thermogravimetric analysis of CU-9-MEADEACE.	142
Figure 3.49:	Disordered dimeric [Cu ₂ (Hgua) ₂ (H ₂ gua) ₂ (μ-Cl) ₂ Cl ₂] ²⁺ and [Cu ₂ (Hgua) ₂ (H ₂ gua) ₂ (μ-Cl) ₂ Cl ₂ (H ₂ O)] ²⁺ cations of compound CUGUACL.	144

Figure 3.50:	Hydrogen bonding interaction in the crystal structure of CUGUACL. Only the water coordinated dimeric entities are depicted here for clarity purposes.	145
Figure 3.51:	Packing of compound CUGUACL.	146
Figure 3.52:	The monomeric entity of CO-6-CLPUR.	147
Figure 3.53:	Coordination modes of 6-chloropurine/6-chloropurinate as found in the CSD data base.	148
Figure 3.54:	(a) Packing of compound CO-6-CLPUR and (b) hydrogen bonding (blue dashed lines) and π - π stacking interactions (red double dashed lines).	148
Figure 3.55:	Thermogravimetric studies of CO-6-CLPUR.	150
Figure 3.56:	6-thiopurinate sides available for complementary hydrogen bonding interaction when chelating to a metal centre through S6 and N7.	151
Figure 3.57:	[Co(ThioG) ₃] entity (a) of compound CO-6-THIOG (SMOF-4) and (b) available supramolecular hydrogen bonding scheme.	152
Figure 3.58:	Nucleobase...nucleobase base pairing interactions.	153
Figure 3.59:	2D supramolecular sheet assembled by means of base pairing interactions among the 6-thioguanine nucleobases with a Shubnikov hexagonal hcb topology in CO-6-THIOG (SMOF-4).	154
Figure 3.60:	Projection of the crystal packing of SMOF-4 along the crystallographic <i>c</i> axis. Green coloured regions represent the solvent accessible void.	155
Figure 3.61:	Thermogravimetric studies of CO-6-THIOG (SMOF-4)	156
Figure 3.62:	Adsorption isotherms for N ₂ (77 K) and CO ₂ (273 K), of a fresh sample of CO-6-THIOG (SMOF-4).	157
Figure 4.1:	Similarity between (a) coordination bonds and (b) hydrogen bonding interactions.	161
Figure A.2.1:	FTIR spectrophotometer 8000S Shimadzu	156
Figure A.2.2:	Thermobalance TA instrument SDT 2960	156
Figure A.2.3:	Single crystal X-ray diffractometer (a) Oxford Diffraction Xcalibur and (b) Stoe IPDS 2T	156
Figure A.3.1:	IR spectra of Metal-cytosine compounds	202
Figure A.3.2:	IR spectra of Metal-adenine compounds	203
Figure A.3.3:	IR spectra of Metal- adenine compounds	204
Figure A.3.4:	IR spectra of CU-9-MEADEACE and CO-9-MEADECL compounds	205
Figure A.3.5:	IR spectra of CO-6-CLPUR	205
Figure A.3.6:	IR spectra of CUGUACL and CO-6-THIOG	206

Figure A.4.1: Thermogravimetric analysis	207
Figure A.4.1: (contd.)Thermogravimetric analysis	208
Figure A.5.1: Different types of adsorption isotherms	209
Figure A.5.2: Models for N ₂ , CO ₂ and H ₂	213
Figure A.5.3: Average occupation profiles for CO ₂ at 298 K in CUADECL-B (SMOF-1)	215

Chapter 1

Introduction

- 1.1 Overview of crystal engineering**
- 1.2 Porous materials based on coordination bonds
(metal–organic frameworks, MOFs)**
- 1.3 Supramolecular crystal engineering**
- 1.4 Nucleobases as coordination bonding linkers**
- 1.5 Nucleobases as hydrogen bonding linkers**
- 1.6 Objective**

1.1 OVERVIEW OF CRYSTAL ENGINEERING

Historically, materials with appealing properties like mechanical, electrical, magnetic, thermal, optical, etc were discovered by serendipity and not because of a planned synthetic approach to achieve those properties. The development of crystal structure elucidation techniques at early 20th century arouse the interest of the scientific community in the correlation between the structural features and the properties of the materials, which, later on, sowed the seed of the pursuit for the general synthetic strategies to design materials with tuned functionalities, i.e. crystal engineering. Systematic crystal engineering was launched with Schmidt with his notable contributions in the 1950's and 1960's on solid state photochemical reactivity.¹ Although there is an earlier report by Pepinsky² wherein the term is actually mentioned for the first time, Schmidt³ is usually credited with having introduced the term crystal engineering into the chemical literature with his works on topochemistry.

In spite of the large trail of time, crystal engineering did not reach its current importance until a handful of referential works were published in 1990's, by outstanding authors such as Dunitz,⁴ Desiraju,⁵ Anthony,⁶ etc. Dunitz in 1991, identified an organic crystal as a supramolecule par excellence.⁴ The works of Desiraju focused on the transformation from a molecule to crystal as the key issue in crystal engineering.⁵ He further defines crystal engineering as '*the understanding of intermolecular interactions in the context of crystal packing and in the utilization of such understanding in the design of new solids with desired physical and chemical properties*'.⁷ In line with this, the modern crystal engineering follows the three principles as follows, (i) the study of intermolecular interactions; (ii) the study of packing modes in the context of these interactions with the aim of designing a strategy for crystal construction and (iii) the study of crystal properties.⁸

¹ Schmidt, G. M. J. *Pure Appl. Chem.* **1971**, 27, 647.

² Pepinsky, R. *Phys. Rev.* **1955**, 100, 971.

³ Schmidt, G. M. J.; Gerdhard, M. J. et al. *Solid State Photochemistry*, D. Ginsburg(ed), Verlag Chemie, Weinheim, 1976.

⁴ Dunitz, J. D. *Pure Appl. Chem.* **1991**, 63, 177.

⁵ Desiraju, G. R. *Angew. Chem. Int. Ed. Engl.* **1995**, 34, 2311.

⁶ Anthony, A. et al. *Cryst. Eng.* **1998**, 1, 1.

⁷ Desiraju, G. R. *Crystal Engineering: The design of organic solids*, Amsterdam: Elsevier, 1989.

⁸ Desiraju, G. R. *Angew. Chem. Int. Ed.* **2007**, 46, 8342.

In crystal engineering, for the construction of solids with predetermined properties, not only the building blocks are important, but the way in which they are assembled too.⁹ So crystal engineering is concerned with the construction of crystal structures or organic and metal–organic species, using design principles that are derived from an understanding of the intermolecular interactions that prevail in molecular solids.⁷ Hence, the aims of crystal engineering are the understanding of intermolecular interactions and their application in the design of crystal structures with specific architectures and properties. Within a crystal, there exists medium range isotropic interactions, which are responsible for gross shapes and close packing effects while long range, isotropic interactions and those of electrostatic origin like hydrogen bonds account for all the fine effects and intermolecular orientations. In the case of metal organic systems, the metal–metal bonds and metal–ligand coordination bonds are to be considered.¹⁰ So the understanding of the intermolecular interactions and coordination bonds has become very important in the control of molecular and ionic organization in the solid state.

Crystal engineering has grown to a very wide scope and the concepts of crystal engineering are applicable to any kind of intermolecular assembly, like a protein ligand recognition, system for drug delivery or the design of supramolecular polymers including MOFs.¹¹ In fact, one of the most active objective of crystal engineering is the design of new host systems in order to obtain nanoporous solids and this could be achieved by preventing the close packing, creating voids and thereby promoting inclusion of guest molecules.⁶ These materials have become very important in the field of chemistry and material science due to their promising applications in catalysis,¹² energy storage,¹³ sensing,¹⁴ and separation.¹⁵

⁹ Rowsell, J. L. C. et al. *Micropor. Mesopor. Mat.* **2004**, *73*, 3.

¹⁰ Desiraju, G. R. *J. Mol. Struct.* **2003**, *656*, 5.

¹¹ Desiraju, G. R. *J. Chem. Sci.* **2010**, *122*, 667.

¹² (a) Phann, A. et al. *Inorg. Chem.* **2011**, *50*, 7388. (b) Dhakshinamoorthy, A. et al. *Dalton Trans.* **2011**, *40*, 6344. (c) Corma, A. et al. *Chem. Rev.* **2010**, *110*, 4606. (d) Farrusseng, D. et al. *Angew. Chem. Int. Ed.* **2009**, *48*, 7502. (e) Dhakshinamoorthy, A.; Garcia, H. *Chem. Soc. Rev.* **2014**, *43*, 5750. (f) Liu, J. et al. *Chem. Soc. Rev.* **2014**, *43*, 6011.

¹³ (a) Zhao, D. et al. *Acc. Chem. Res.* **2011**, *44*, 123. (b) Murray, L. J. et al. *Chem. Soc. Rev.* **2009**, *38*, 1294. (c) Czaja, A. U. et al. *Chem. Soc. Rev.* **2009**, *38*, 1284. (d) Muller, U. et al. *J. Mater. Chem.* **2006**, *38*, 626. (e) He, Y. et al. *Chem. Soc. Rev.* **2014**, *43*, 5657.

1.2 POROUS MATERIALS BASED ON COORDINATION BONDS (METAL–ORGANIC FRAMEWORKS, MOFs)

Over the past few decades a vast number of solids that contain metal ions linked by molecular species have been indistinctly termed as coordination polymers, hybrid organic–inorganic materials and metal–organic frameworks. At this point, it is relevant to point out the difference between Coordination Polymers (CPs) and Metal–Organic Frameworks (MOFs). In 2013, the IUPAC published a series of recommendations to face the controversial use of terms in this area.¹⁶ The term coordination polymers means an extended system of metal centers and ligands connected through coordination bonds, while for a solid to be named as metal–organic framework, it should be a coordination polymer with an open framework containing potential voids.¹⁷

The concept of crystal engineering based on coordination bonds, especially the case of metal–organic frameworks has aroused the interest of the scientific world for the last few decades because they are facile to prepare, aesthetically appealing and because of their inherent modularity, prototypal for a diverse range of structures that are amenable to crystal engineering design strategies.¹⁸ In the new era of crystal engineering, the design and synthesis of coordination compounds has become apparently easy. The proper selection of the metal ions and ligands allow a rational design of the compounds with required or predetermined physical and chemical properties. For this purpose, it is important to have knowledge about the coordination geometries of the central metal ion and the coordination modes of the ligands.¹⁹ The ligands may provide different modes of connectivity like, linear, angular, triangular, tetrahedral, etc (Figure 1.1).

¹⁴ (a) Chen, B. et al. *Acc. Chem. Res.* **2010**, *43*, 1115. (b) Liu, S. et al. *Inorg. Chem. Commun.* **2010**, *13*, 870. (c) Green, M. A. *Nat. Mater.* **2010**, *9*, 539. (d) Lan, A. et al. *Angew. Chem. Int. Ed.* **2009**, *48*, 2334. (e) Hu, Z. et al. *Chem. Soc. Rev.* **2014**, *43*, 5815. (f) Falcaro, P. *Chem. Soc. Rev.* **2014**, *43*, 5513.

¹⁵ (a) Basu, S. et al. *J. Sep. Purif. Technol.* **2011**, *81*, 31. (b) Qiu, S.; Zhu, G. *Coord. Chem. Rev.* **2009**, *253*, 2891. (c) Manos, M. J. et al. *Angew. Chem. Intl. Ed.* **2005**, *44*, 3552. (d) Lee, H. et al. *Nature* **2003**, *425*, 385. (e) Czaja, A. U. et al. *Chem. Soc. Rev.* **2009**, *38*, 1284. (f) Barea, E. et al. *Chem. Soc. Rev.* **2014**, *43*, 5419. (g) Van de Voorde, B. et al. *Chem. Soc. Rev.* **2014**, *43*, 5766. (h) Qiu, S. et al. *Chem. Soc. Rev.* **2014**, *43*, 6116.

¹⁶ Batten, S. R. et al. *Pure Appl. Chem.* **2013**, *85*, 1715.

¹⁷ (a) Rowsell, J. L. C.; Yaghi, O. M. *Micropor. Mesopor. Mater.* **2004**, *73*, 3. (b) Corma, A. et al. *Chem. Rev.* **2010**, *110*, 4606. (c) Zhou, H.–C.; Kitagawa, S. *Chem. Soc. Rev.* **2014**, *43*, 5415.

¹⁸ Perry IV, J. J. *Chem. Soc. Rev.* **2009**, *38*, 1400.

¹⁹ Pérez–Yáñez, S. *Doctoral Thesis*; Universidad del País Vasco/Euskal Herriko Unibertsitatea, 2012.

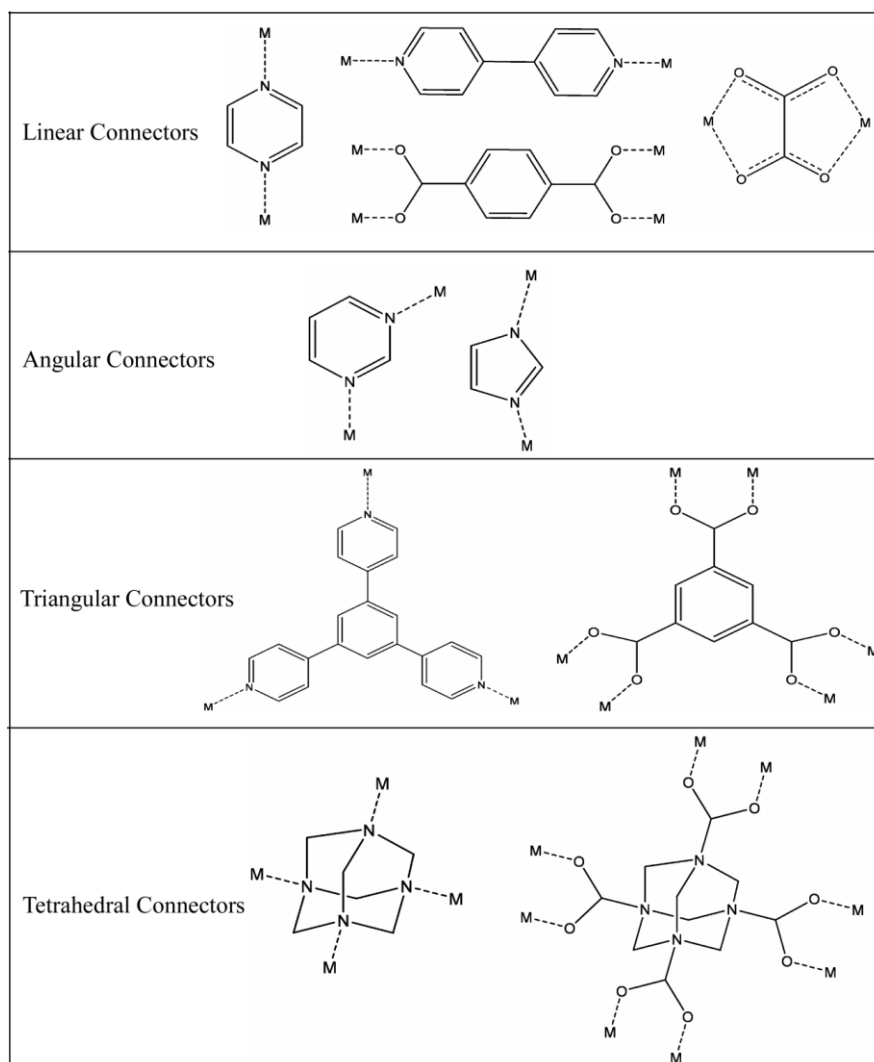


Figure 1.1: Examples of bridging ligands used as linkers in crystal engineering.

To make a coordination polymer, it is only necessary that a potentially bridging ligand reacts with a metal ion which has more than one vacant or labile site. Depending on the systems used, either infinite extended systems (polymers) or discrete closed structures can arise (Figure 1.2). For example, if divergent metal sites like mutually ‘*trans*’ positions or all four sites of a tetrahedron are coordinated, extended polymers are formed.²⁰ The assembly between the metal centres and the ligands is mediated mainly through coordination bonds which determine the geometry, giving rise to a large variety of structurally diverse complexes ranging from discrete units to 1D, 2D and 3D extended systems.

²⁰ James, S. L. *Chem. Soc. Rev.* **2003**, 32, 276.

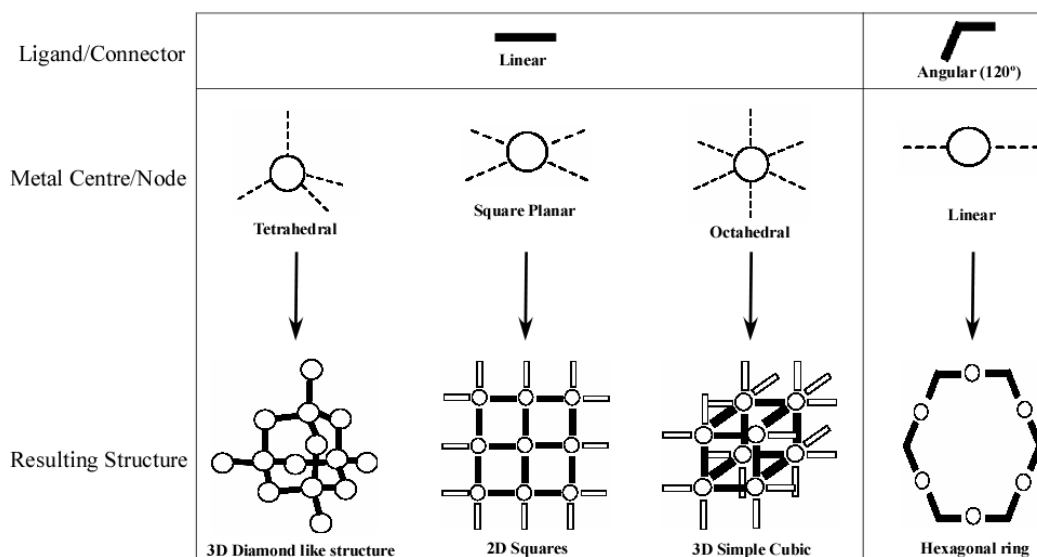


Figure 1.2: Different structural patterns determined by the combination of metal centres (nodes) and ligands (connectors).

In addition to this, the metal centres can be used as nodes with “exotic” geometries that differ from the usual coordination geometries, in cases where some coordination positions of the metal centre have been blocked (Figure 1.3).

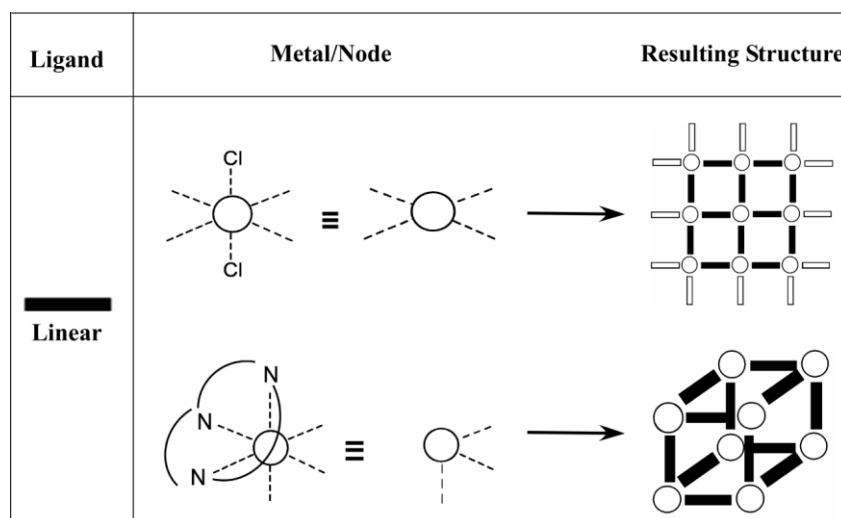


Figure 1.3: Different structures obtained using blocking ligands to create nodes with new geometries.

Yaghi and O’Keeffe expanded the node/connector design concept to exploit the concept of secondary building units (SBUs)²¹ as molecular polygonal or polyhedral

²¹ Eddaoudi, M. et al. *Acc. Chem. Res.* **2001**, *34*, 319.

nodes, for the construction of the MOFs. They called this strategy reticular chemistry.²² The SBUs are formed not only by the metal centers but also by the functional (coordinating) groups of the ligands.

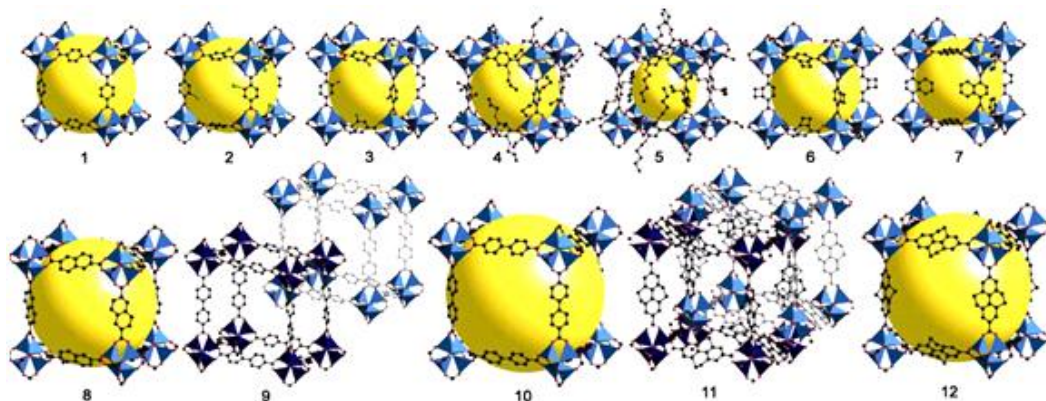


Figure 1.4: Examples of isorecticular MOFs based on Zn_4O clusters and ditopic linkers.²³

The authors demonstrate how the topology of the framework can be rationalized and foretold by the geometrical features of the SBU and of the polytopic linker. Following this concept, a wide variety of diverse architectures with high structural stability have been prepared by connecting the SBUs with rigid organic linkers mediated through strong covalent bonds.²⁴ Figure 1.5 illustrates the structure of the compound $[Zn_4O(bdc)_3]_n$,²⁵ commonly known as IRMOF-1 or MOF-5, wherein the SBU is formed by four atoms of Zn with tetrahedral geometry, connected in the centre with the oxide O^{2-} , and six carboxylate bridging groups giving rise to an octahedral geometry. The connector here is benzene-1,4-diyl, which is a linear connector that connects the SBUs into a 3D cubic structure. The potential of this approach is better depicted in Figure 1.4, where maintaining $[Zn_4O(O_2C)_6]$ as the SBU and varying the length of the ditopic linker, a family of isorecticular MOFs (IRMOFs) can be designed, tuning easily the pore size, surface area and chemical functions. Some other examples of common SBUs are depicted in Figure 1.6.¹⁸

Another factor which affects the final product, to be considered is the synthesis conditions. The choice of solvents, their mixtures or synthesis without solvents,

²² Yaghi, O. M. et al. *Nature* **2003**, 423, 705.

²³ Eddaoudi, M. et al. *Science* **2002**, 295, 469.

²⁴ Reger, D. L. et al. *Inorg. Chem.* **2012**, 51, 1068.

²⁵ Malik, M. A. et al. *Inorg. Chem.* **1995**, 34, 6223.

controlling the pH, temperature, pressure, etc. are crucial in obtaining a specific end product from the same kind of building blocks.

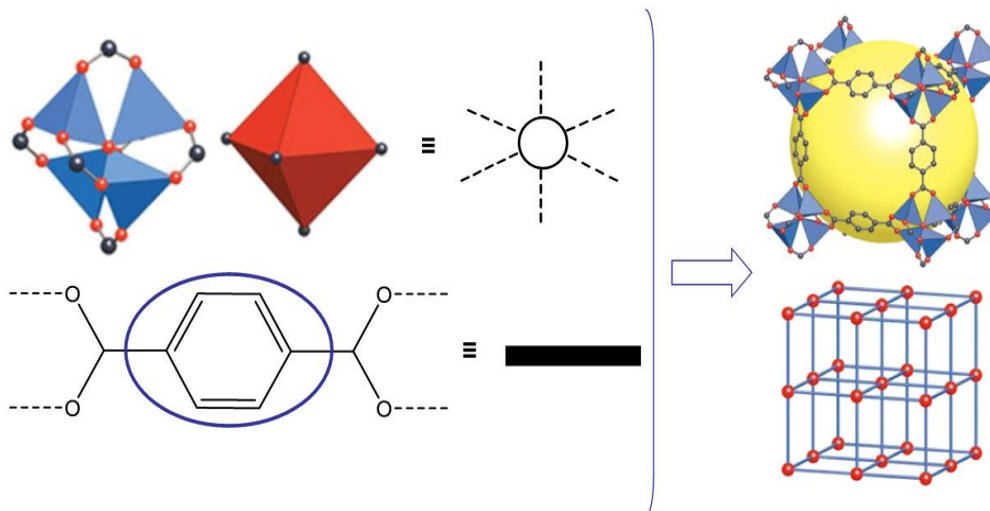


Figure 1.5: Structural breakdown of the compound $[\text{Zn}_4\text{O}(\text{bdc})_3]_n$ (MOF-5, bdc: benzene-1,4-dicarboxylate).

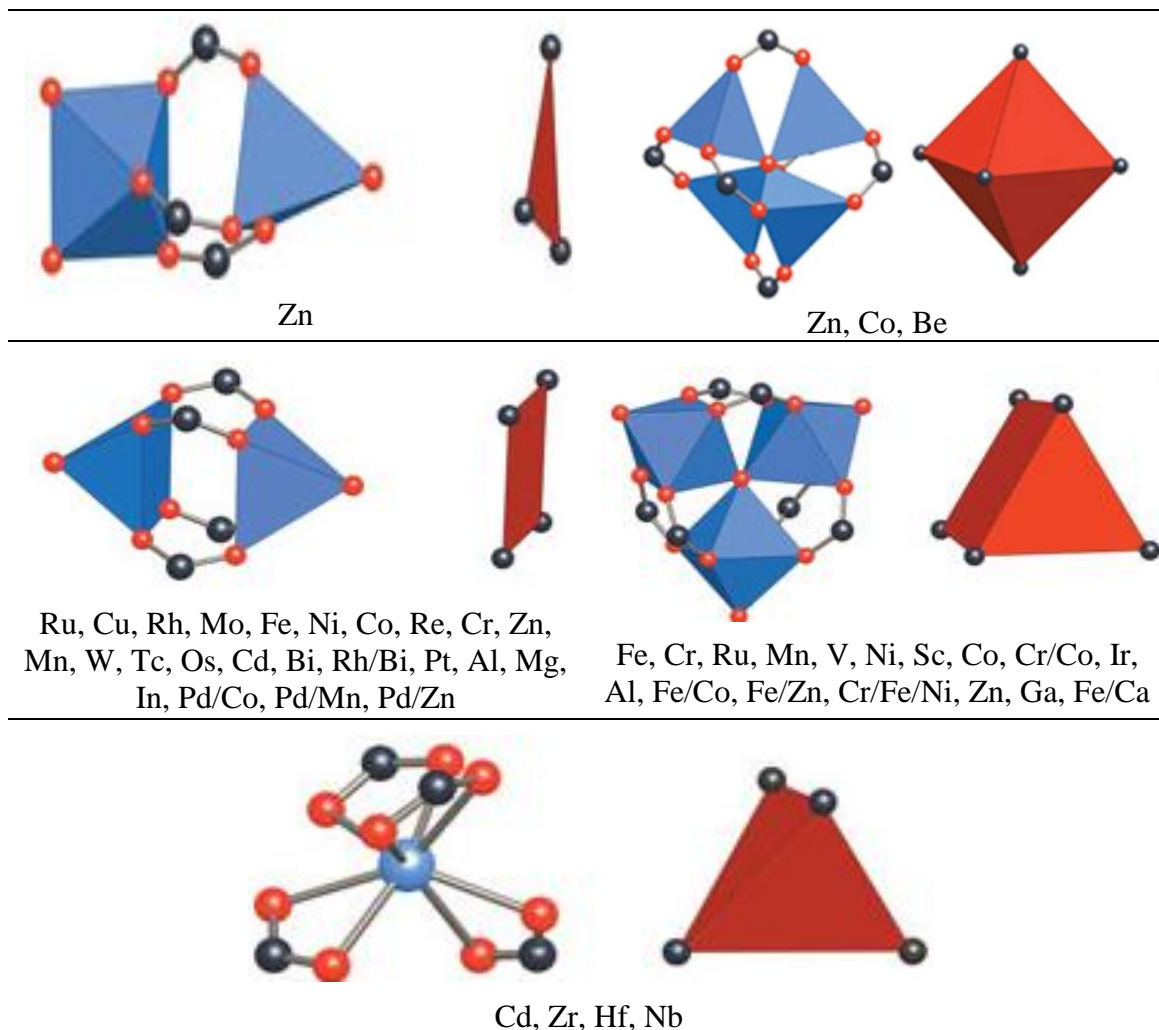


Figure 1.6: Examples of common SBUs.

Porosity is considered as the hallmark physical property of the metal–organic frameworks.²⁶ Nowadays, MOFs possess the highest surface areas ever reported.²⁷ The recently reported MOFs named as NU–109E and NU–110E exhibit the highest surface area ever reported, 7110 and 7140 m²/g, respectively.²⁸ NU–110E consists of dicopper paddle–wheel SBUs connected by the BTTEI (BTTEI = 5,5',5''–(((benzene–1,3,5–triyl–tris(ethyne–2,1–diyl))tris(benzene–4,1–diyl)tris(ethyne–2,1–diyl))trisophthalate) ligand with a solvent accessible volume of 93.0%.²⁹

MOFs are well studied because of their structural beauty, diversity of properties, structural and functional tunability, and large number of applications.^{30–31} Keeping this in mind, currently, researchers are focusing on developing MOFs with high surface areas,³² high hydrogen storage capacity,³³ selective heterogeneous catalysis,³⁴ magnetic sorting,³⁵ channels capable of conducting polymerization,³⁶ selective capture of carbon dioxide,³⁷ host dependent luminescence,³⁸ proton conduction³⁹ and artificial photosynthesis and photo–catalysis.⁴⁰ Their crystalline nature, high and permanent porosity, uniform pore sizes, extraordinary surface areas, and finely tunable pore–surface properties have made these materials an attractive target for further study.⁴¹

²⁶ An, J. et al. *Nat. Commun.* **2012**, *3*, 604.

²⁷ (a) Férey, G. et al. *Science* **2005**, *309*, 2040. (b) Koh, A. et al. *J. Am. Chem. Soc.* **2009**, *131*, 4184. (c) Farha, O. K. et al. *J. Am. Chem. Soc.* **2012**, *134*, 15016.

²⁸ Farha, O. K. et al. *J. Am. Chem. Soc.* **2012**, *134*, 15016.

²⁹ Zhang, M. et al. *CrystEngComm*. **2014**, *16*, 4069.

³⁰ Zhou, H.–C.; Kitagawa, S. *Chem. Soc. Rev.* **2014**, *43*, 5415.

³¹ (a) Chen, C.–T.; Suslick, K. S. *Coord. Chem. Rev.* **1993**, *128*, 293. (b) Janiak, C. *Dalton Trans.* **2003**, 2781. (c) James, S. L. *Chem. Soc. Rev.* **2003**, *32*, 276.

³² (a) Murray, L. J. et al. *Chem. Soc. Rev.* **2009**, *38*, 1294. (b) Farha, O. K. et al. *J. Am. Chem. Soc.* **2012**, *134*, 15016. (c) Martin, R. L.; Haranczyk, M. *Chem. Sci.* **2013**, *4*, 1781.

³³ (a) Han, S. S. et al. *Chem. Soc. Rev.* **2009**, *38*, 1460. (b) Yang, J. et al. *Chem. Soc. Rev.* **2010**, *39*, 656. (c) Goldsmith, J. et al. *Chem. Mater.* **2013**, *25*, 3373.

³⁴ (a) Lee, J. et al. *Chem. Soc. Rev.* **2009**, *38*, 1450. (b) Ma, L. et al. *Chem. Soc. Rev.* **2009**, *38*, 1248. (c) Dakshinamoorthy, A.; Garcia, H. *Chem. Soc. Rev.* **2014**, *43*, 5750. (d) Liu, J. et al. *Chem. Soc. Rev.* **2014**, *43*, 6011.

³⁵ Kurmoo, M. *Chem. Soc. Rev.* **2009**, *38*, 1353.

³⁶ Uemura, T. et al. *Chem. Soc. Rev.* **2009**, *38*, 1228.

³⁷ (a) Li, J.–R. et al. *Chem. Soc. Rev.* **2009**, *38*, 1477. (b) Düren, T. et al. *Chem. Soc. Rev.* **2009**, *38*, 1237. (c) Zhang, Z. J. et al. *Chem. Comm.* **2013**, *49*, 653.

³⁸ (a) Allendorf, M. D. et al. *Chem. Soc. Rev.* **2009**, *38*, 1330. (b) Hu, Z. et al. *Chem. Soc. Rev.* **2014**, *43*, 5815.

³⁹ (a) Yamada, T. et al. *Chem. Soc. Rev.* **2013**, *42*, 6655. (b) Yoon, M. et al. *Angew. Chem. Int. Ed.* **2013**, *52*, 2688. (c) Ramaswamy, P. et al. *Chem. Soc. Rev.* **2014**, *43*, 5913. (d) Taylor, J. M. et al. *J. Am. Chem. Soc.* **2013**, *135*, 1193.

⁴⁰ Zhang, T.; Lin, W. *Chem. Soc. Rev.* **2014**, *43*, 5982.

⁴¹ Furukawa, H. et al. *Science* **2013**, *341*, 1230444.

Moreover, these easily modifiable materials were well studied and new methods has been developed to create novel porous flexible materials (breathing),⁴² and MOF nanoparticles⁴³. Likewise, simple synthetic strategies have been developed to produce these materials in industrial scale and thus boosting their potential impact in the market.^{44,45,46,47}

1.3 SUPRAMOLECULAR CRYSTAL ENGINEERING

A crystal may be comprised of certain repetitive structural units with specific molecular functionalities responsible for the molecular recognition that defines specific interaction patterns between functional groups. These molecular functional groups could be associated with particular packing characteristics, being therefore the basic building units of a crystal structure and so are called as the *supramolecular synthons*. Supramolecular synthons are structural units within crystals that can be formed by known or conceivable synthetic operations.⁵ The identification of synthons is crucial in the designing and analysis of a crystal. The Figure 1.7 lists some common examples of supramolecular synthons.

Supramolecular synthons are kinetically defined structural units that express the core features of the crystal structure and that encapsulate the essence of crystals in terms of molecular recognition. Synthons consist of molecular fragments and the supramolecular association between them is mediated through hydrogen bonds and other directional interactions. In effect, following the synthon theory, a supramolecular synthon can be considered as a reasonable approximation of the entire crystal and the synthon is the device through which information content passes from molecular structure to crystal structure.¹¹

⁴² Zacher, D. et al. *Chem. Soc. Rev.* **2009**, 38, 1418.

⁴³ Spokoyny, A. M. et al. *Chem. Soc. Rev.* **2009**, 38, 1218.

⁴⁴ Czaja, A. U. et al. *Chem. Soc. Rev.* **2009**, 38, 1284.

⁴⁵ Lanchas, M. et al. *Chem. Commun.* **2012**, 48, 9930.

⁴⁶ Lanchas, M. et al. *RSC Adv.* **2014**, 4, 60409.

⁴⁷ Lanchas, M. et al. *Inorg. Chem. Front.* **2015**, 2, 425.

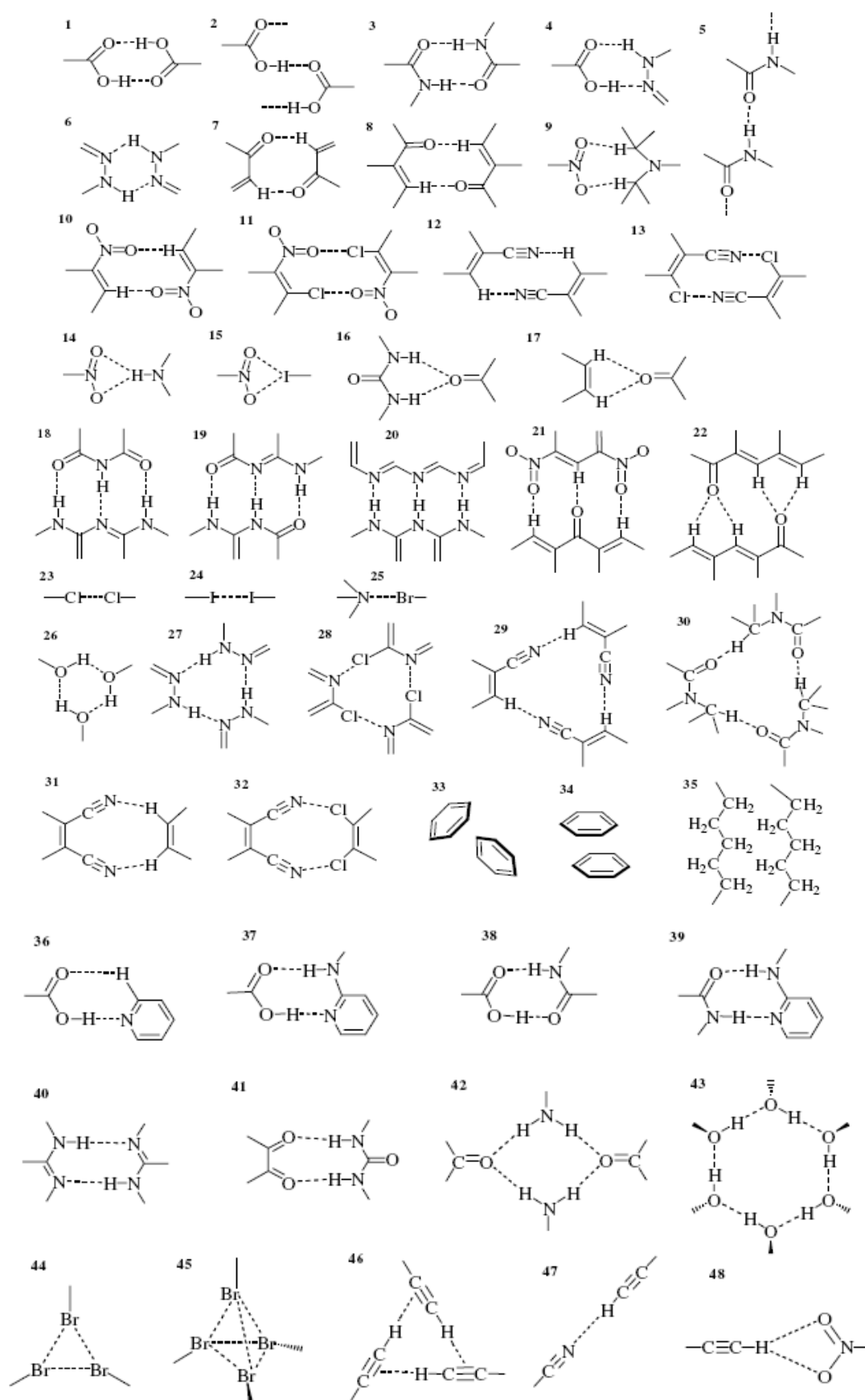


Figure 1.7: Examples of some common representative supramolecular synthons (taken from reference 5).

A detailed analysis of the intermolecular interactions in crystals permits the definition of supramolecular synthons as structural units that more realistically display the recognition process between molecules.⁵ In simple examples like benzoic and terephthalic acids, structural patterns can be represented as networks with the molecules as nodes and the supramolecular synthons as node connections. Figure 1.8¹⁰ depicts the structural rationalization from the molecular recognition of functional groups to the formation of supramolecular synthon and of the crystal structure using the examples of benzoic acid and terephthalic acid.

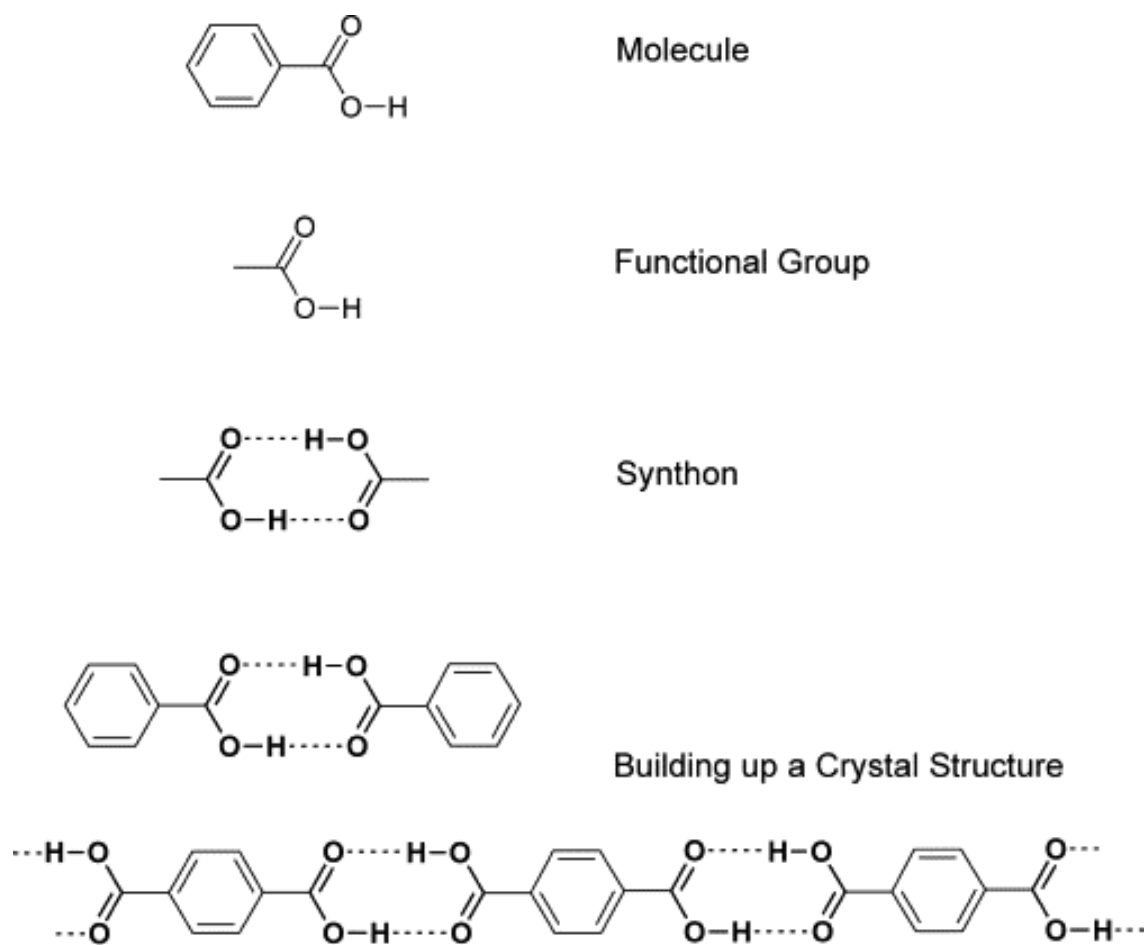


Figure 1.8: The self-assembly from molecule to crystal through supramolecular synthons.

The pioneering works of Etter and his group on the ability of hydrogen bonds to help control molecular crystallisation also revealed that, these hydrogen bonding motifs

are formed by many elementary functional groups frequently found in many simple molecules.⁴⁸ Wuest and coworkers named these special molecules, with multiple peripheral sites of strong directional interactions, that are set apart from molecules by their properties and their inherent suitability for engineering crystals⁴⁹ as ‘tectons’,⁵⁰ which means ‘builder’, that are active building units bearing recognition information and thus capable of recognizing each other. Figure 1.9 shows a schematic representation of the tecton–synthons concept together with an example of the supramolecular net of trimesic acid showing the hydrogen bonded synthons.

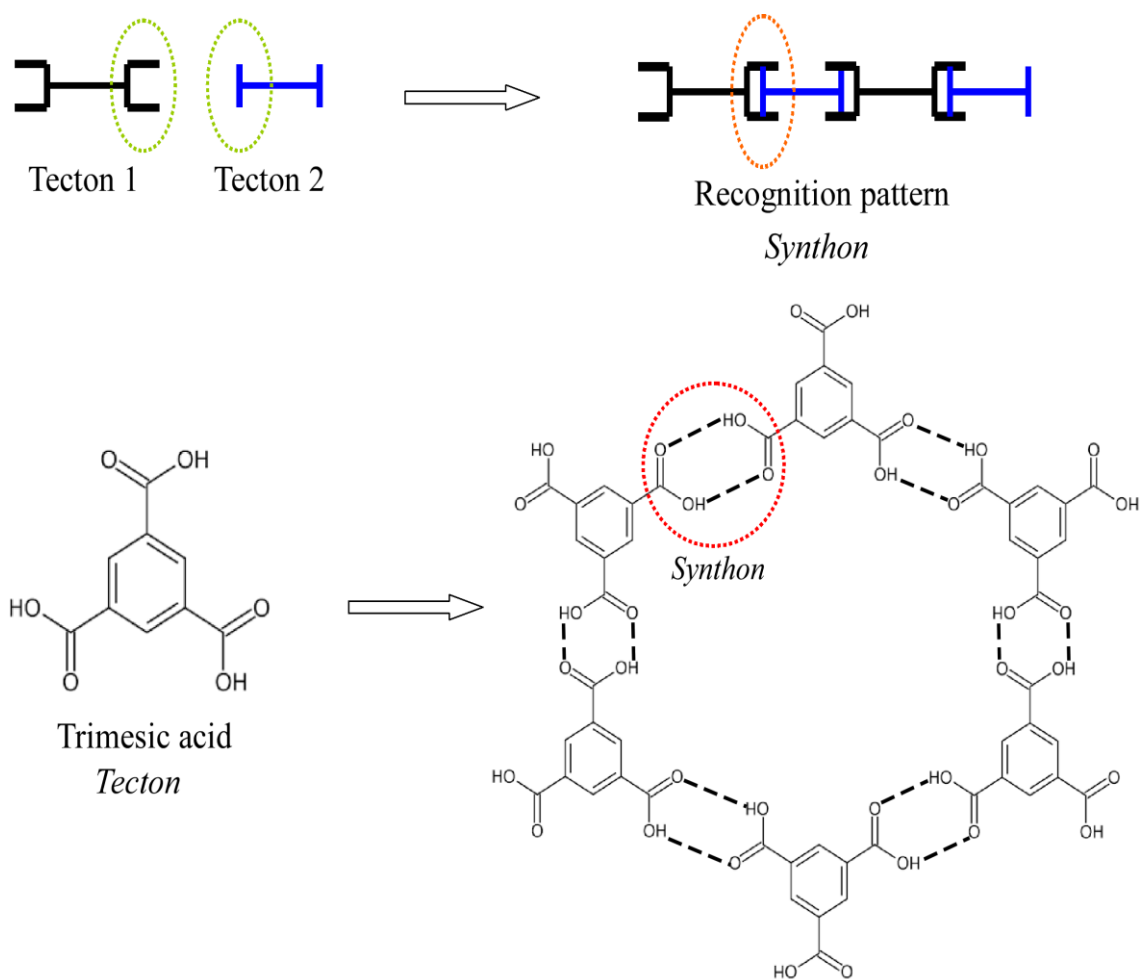


Figure 1.9: Scheme showing the “tecton–synthon” concept using trimesic acid as example.

⁴⁸ (a) Etter, M. C. *Acc. Chem. Res.* **1990**, *23*, 120. (b) Taylor, R.; Kennard, O. *Acc. Chem. Res.* **1984**, *17*, 320.

⁴⁹ Wuest, J. D. *Chem. Commun.* **2005**, 5830.

⁵⁰ Simard, M. et al. *J. Am. Chem. Soc.* **1991**, *113*, 4696.

In line with the principles of crystal engineering, the process of molecular recognition and the so formed repeating units of supramolecular synthons lead to the formation of supramolecular networks. Since supramolecular synthons are the basic building units of any supramolecular architecture, the suitable selection of the synthon with desirable properties permits the desirable tuning of the supramolecular array. So the designing of a crystal structure effectively becomes synthon design and it is possible only with the knowledge of the intermolecular interactions.¹⁰ So crystal engineering can be well defined as the rational design of the functional molecular solids.¹¹

Robustness is one of the important properties of the synthons and their identification facilitates the synthetic aspects of crystal engineering, resulting in high yield supramolecular synthesis.⁵¹ For example, the robust carboxylic dimer synthons are normally used in crystal engineering.

A variety of noncovalent interactions like intermolecular interactions, van der Waals forces, π - π interactions, and other weak interactions were applied to molecular components to construct large entities called supramolecules. So, supramolecular chemistry is a broad field, owing to the myriad of diverse structures that can be formed using a variety of noncovalent intermolecular interactions. The examples include biologically relevant enzyme mimics, molecular devices including light harvesters, sensors, wires, rectifiers, liquid crystals, molecular flasks and many more.⁵² Among these supramolecular interactions, hydrogen bonding is the most predominant organisational synthon in the design of supramolecular arrays due to its clearly defined, reproducible and transferable directional properties⁵³ and predictability.

Figure 1.10 gathers together some examples of supramolecular arrays held together through hydrogen bonded synthons between organic molecules. They include (a) the linear supramolecular chain formed from the self assembly of terephthalic acid, (b) the self-assembled supramolecular hexagonal ring of trimesic acid, (c) the hexagonal 2D network formed between cyanuric acid and melamine⁵⁴ and (d) a

⁵¹ Aakeroy, C. B. et al. *J. Am. Chem. Soc.* **2002**, *124*, 14425.

⁵² Cook, T. R. et al. *Chem. Rev.* **2013**, *113*, 734.

⁵³ (a) Braga, D. et al. *Coord. Chem. Rev.* **2003**, *53*, 246. (b) Desiraju, G. R. *Acc. Chem. Res.* **2002**, *35*, 565.

⁵⁴ Ranganathan, A. et al. *J. Am. Chem. Soc.* **1999**, *121*, 1752.

supramolecular honeycomb grid of trimesate anions and secondary ammonium cations.⁵⁵

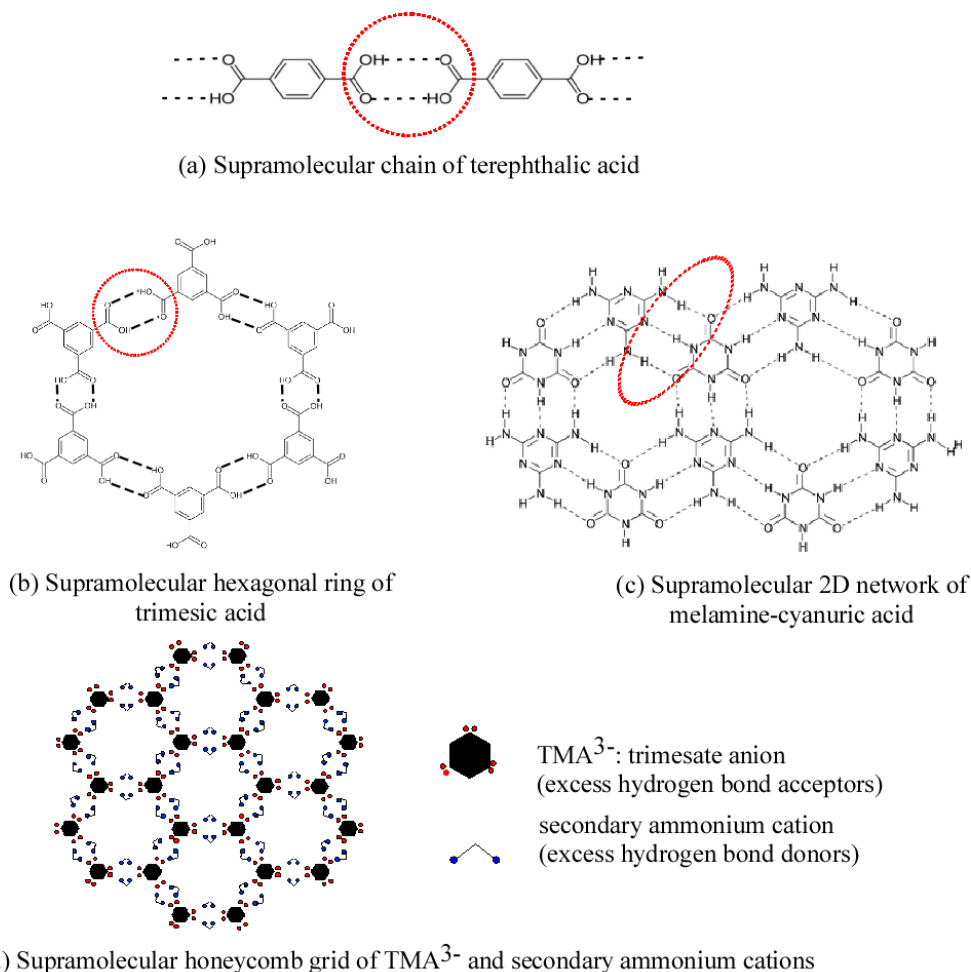


Figure 1.10: Examples of organic synthons formed through hydrogen bonding interaction. Hydrogen bonded synthons are highlighted within the circles.

In similarity to MOFs, Reger et al.⁵⁶ called a three dimensional structure of metal–organic discrete entities sustained by non–covalent interactions, as ‘*Supramolecular Metal–Organic Frameworks*’ (*SMOFs*), where the building blocks are organized partially or completely by robust supramolecular interactions. They reported some examples of this type of compounds mainly based on the π – π stacking between π deficient 1,8–naphthalimide rings (Figure 1.11) which is not as directional as hydrogen

⁵⁵ Melendez, R. E. et al. *Angew. Chem. Int. Engl.* **1996**, 35, 2213.

⁵⁶ Reger, D. L. et al. *Inorg. Chem.* **2011**, 50, 10225.

bonding. These compounds although presenting potential voids in their crystal structure, still do not have proved to present a permanent porosity.

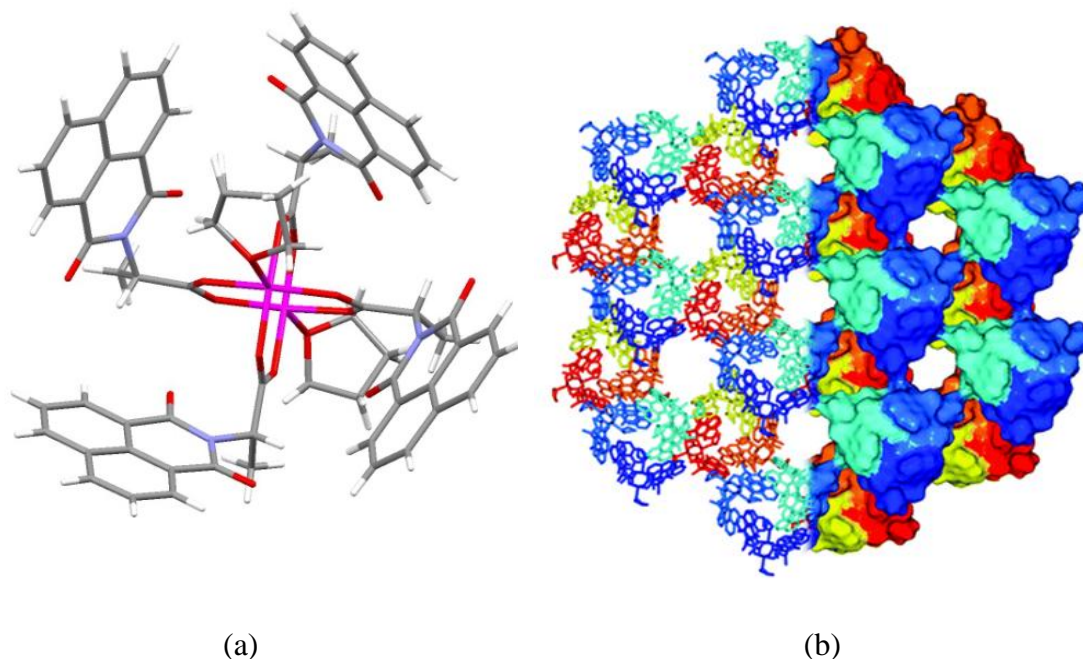


Figure 1.11: (a) The building unit of compound $[\text{Cu}_2((S)\text{-}2\text{-}(1,8\text{-naphthalimido)propanoate})_4(\text{THF})_2]$; (b) The right section of the image represent the van der Waals surface of the structure sustained through $\pi\text{-}\pi$ interactions.

1.4 NUCLEOBASES AS COORDINATION BONDING LINKERS

Rosi et al. put forth many potential applications of MOFs like biological applications including drug delivery, intracellular imaging and many proposed applications may require them to be built from non-toxic building materials and that are biologically and environmentally compatible.⁵⁷ This can be achieved by using biomolecules as the building blocks to construct Metal-Biomolecule Frameworks (MbioFs), which are defined as MOFs constructed from at least one biomolecule which serves as an organic linker.

There are many advantages and applications that arise from the use of biomolecules as building blocks and some of them are mentioned below. Simple biomolecules, including amino acids, nucleobases, sugars and others are readily and naturally available in quantities and prices amenable to preparing bulk quantities of

⁵⁷ Imaz, I. et al. *Chem. Commun.* **2011**, 47, 7287.

materials. Another advantage is that biomolecules can lead to biologically compatible MOFs. Biomolecules are structurally diverse, they can be rigid or flexible and depending on that the functional nature of the MBioFs varies. Biomolecules can have different metal-binding sites and they can exhibit multiple possible coordination modes increasing the potential structural diversity of the MBioFs. Moreover, many biomolecules have intrinsic self-assembly properties which can be used to direct the structure and function of MBioFs. Finally, many chiral biomolecules can be used to construct chiral MBioFs, which may have interesting recognition, separation and catalytic properties. All these characteristics renders biomolecules particularly attractive building blocks for constructing MOFs with new properties and applications that cannot be accessed using the simple organic linkers traditionally used in MOF construction.

Among the bridging biomolecules, nucleobases appear as appealing alternatives since they provide a rigid molecular linker outfitted with many positions able to coordinate to metal centers and additionally are able to establish complementary hydrogen bonding-interactions.⁵⁸ Nucleobases or nitrogenous bases are biological molecules and are key constituents of the nucleic acids, DNA and RNA. The primary nucleobases are, adenine (A), guanine (G), cytosine (C), thymine (T) and uracil (U). In Figure 1.12, the nucleobases are classified into two groups, the purine bases (adenine and guanine) and the pyrimidine bases (thymine, cytosine and uracil). While adenine, guanine, cytosine and thymine are found in the DNA, uracil replaces thymine to form the RNA.

The greater heteroatom number of the purine nucleobases makes them better bridging ligands than the pyrimidinic ones, as it can be derived from the results for bridging puric (adenine: 63 hits, and guanine: 5 hits) and pyrimidinic (thymine: 2 hits, uracil: 17 hits, and cytosine: 15 hits) nucleobases found in the CSD database.⁵⁹ The low number of guanine bridged complexes is not due to an inappropriate geometry disposition of the coordination donor atoms but due to its great insolubility in common solvents.

⁵⁸ Beobide, G. et al. *Coord. Chem. Rev.* **2013**, 257, 2716.

⁵⁹ Allen, F. H. *Acta Crystallogr.* **2002**, B58, 380.

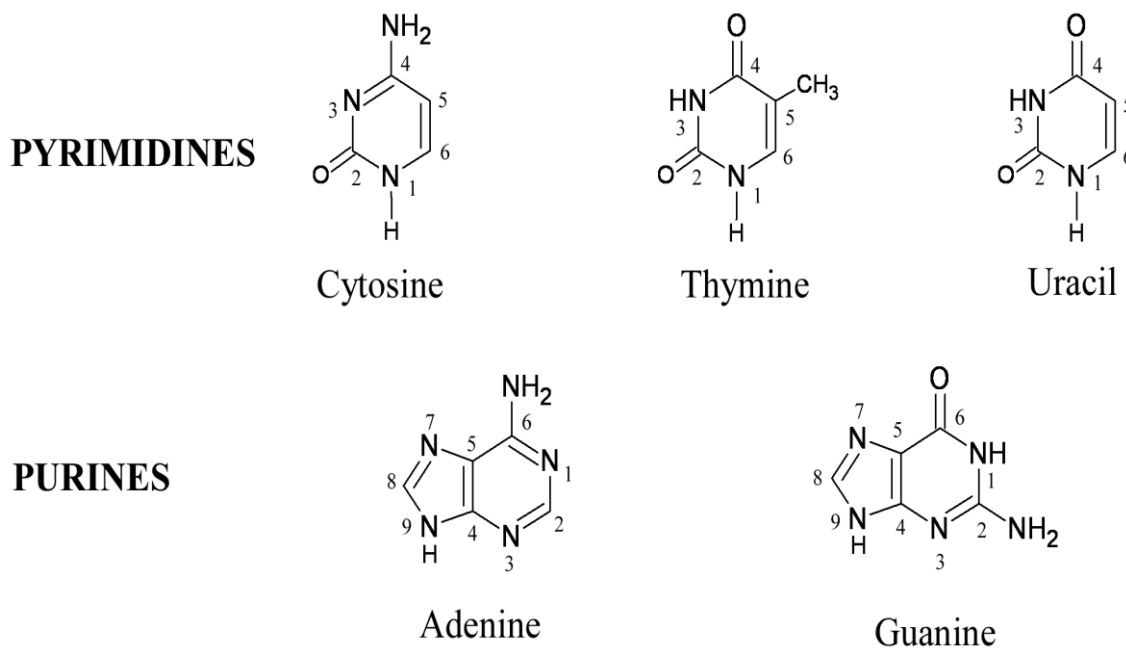


Figure 1.12: Structure and numbering pattern of the nucleobases.

For a long time, nucleobases were evaluated as suitable ligands for the construction of biomimetic compounds,⁶⁰ but recently there has been a substantial increase in their use as pillars for the building up of porous materials.⁵⁸ The first porous polymeric compound of this type was reported by our research group in 2004.⁶¹ It consists of a 3D coordination polymer with formula $[\text{Cu}_4(\mu_3\text{-adeninato-}\kappa\text{N3}:\kappa\text{N7}:\kappa\text{N9})_4(\text{ox})_2(\text{H}_2\text{O})_4]_n$ containing the adenine nucleobase as an anionic *N3,N7,N9*-bridging ligand. The deprotonation of the adenine in the reaction media promotes the polymerization of the framework by sequentially bridging $[\text{Cu}_2(\mu\text{-adeninato})_4(\text{H}_2\text{O})_2]$ paddle-wheel entities through $[\text{Cu}(\text{ox})(\text{H}_2\text{O})]$ units (Figure 1.13) The resulting structure contains one-dimensional (1D) tubular channels with a diameter of about 1.3 nm, that represent around a 40% of the total volume.

⁶⁰ (a) Lippert, B. *Coord. Chem. Rev.* **2000**, 200–202, 487. (b) Verma, S. et al. *Acc. Chem. Res.* **2010**, 43, 79.

⁶¹ García-Terán, J. P. et al. *Inorg. Chem.* **2004**, 43, 4549.

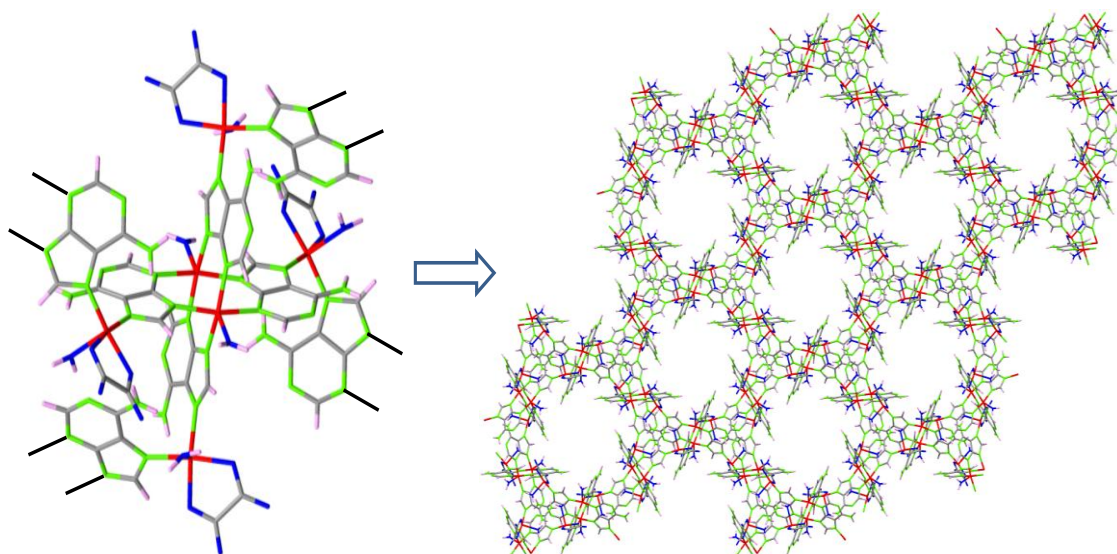


Figure 1.13: Crystal structure of $\{[\text{Cu}_2(\mu\text{-adeninato})_4(\text{H}_2\text{O})_2][\text{Cu}(\text{ox})(\text{H}_2\text{O})]_2\}_n$.

In 2009, Rosi et al. reported a compound with porous network of formula $(\text{Me}_2\text{NH}_2)_2[\text{Zn}_8(\mu_4\text{-adeninato-}\kappa\text{N1}:\kappa\text{N3}:\kappa\text{N7}:\kappa\text{N9})_4(\mu\text{-BPDC-}\kappa^2\text{O},\text{O}':\kappa^2\text{O}'',\text{O}''')_2(\mu_4\text{-O})] \cdot 8\text{DMF} \cdot 11\text{H}_2\text{O}$ (BPDC: biphenyldicarboxylate) obtained under solvothermal conditions at 130 °C.⁶² It consists of infinite zinc–adeninate columnar secondary building units (SBUs) composed of vertex–sharing zinc–adeninate octahedral cages (Figure 1.14a). The zinc–adeninate columns are interconnected via multiple BPDC linkers giving rise to an anionic network that allows the exchange of the cationic counterions. The authors proved that this compound was able to store and release cationic drug molecules. Later, in 2012, they published $(\text{Me}_2\text{NH}_2)_4[\text{Zn}_8(\mu_4\text{-adeninato-}\kappa\text{N1}:\kappa\text{N3}:\kappa\text{N7}:\kappa\text{N9})_4(\mu\text{-BPDC-}\kappa\text{O}:\kappa\text{O}')_6(\mu\text{-O})] \cdot 49\text{DMF} \cdot 31\text{H}_2\text{O}$ compound with the same building blocks but lowering the solvothermal reaction temperature to 85 °C (Figure 1.14b). The same components are arranged in such a way that they could build up a mesoporous material with a high surface area ($4300 \text{ m}^2\text{g}^{-1}$) and one of the largest metal–organic framework pore volume reported till date ($4.3 \text{ cm}^3\text{g}^{-1}$).²⁶

⁶² An, J. et al. *J. Am. Chem. Soc.* **2009**, *131*, 8376.

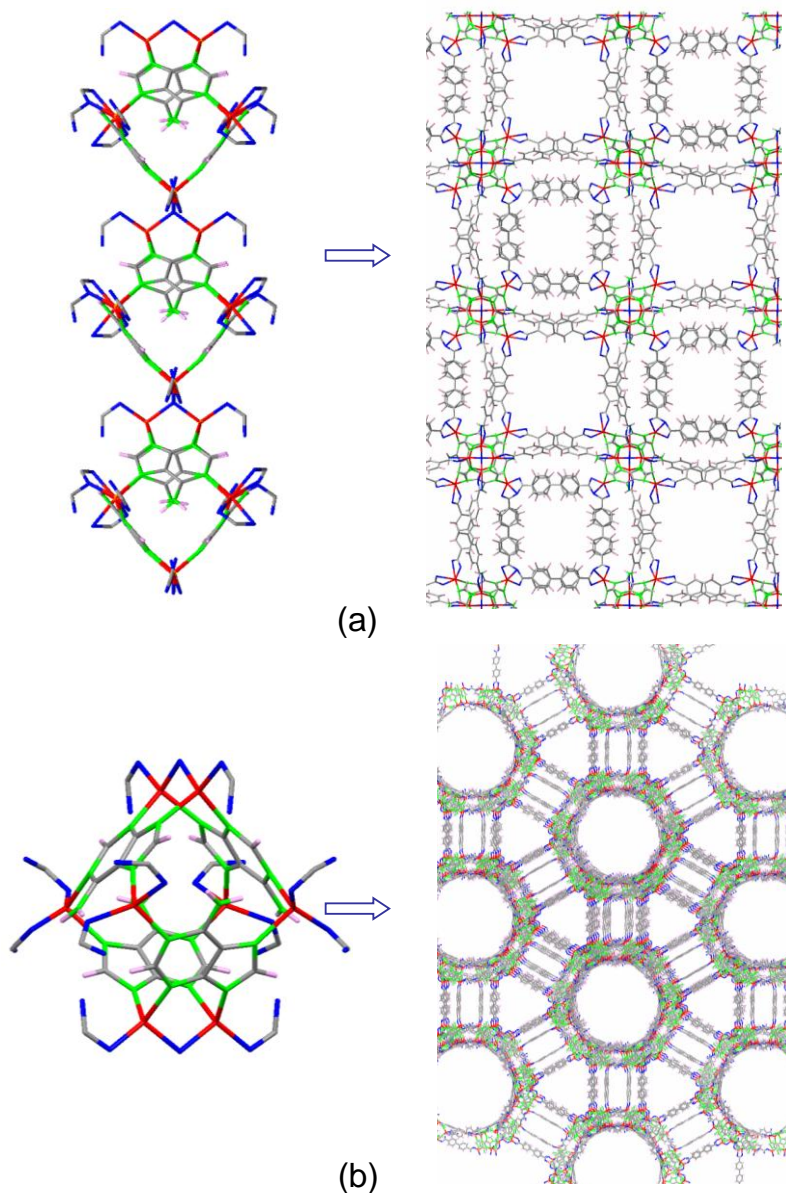


Figure 1.14: SBUs and the resulting crystal structures of compounds (a) $(\text{Me}_2\text{NH}_2)_2[\text{Zn}_8(\mu_4\text{-adeninato})_4(\mu\text{-BPDC})_6(\mu_4\text{-O})] \cdot 8\text{DMF} \cdot 11\text{H}_2\text{O}$, and (b) $(\text{Me}_2\text{NH}_2)_4[\text{Zn}_8(\mu_4\text{-adeninato})_4(\mu\text{-BPDC})_6(\mu\text{-O})] \cdot 49\text{DMF} \cdot 31\text{H}_2\text{O}$.

Another family of metal–adenine–carboxylate compounds that have attracted great interest is that of the formula $[\text{M}_2(\mu_3\text{-adeninato-}\kappa\text{N3}:\kappa\text{N7}:\kappa\text{N9})_2(\mu\text{-OOC}(\text{CH}_2)_x\text{CH}_3\text{-}\kappa\text{O}:\kappa\text{O}')_2]_n$.⁶³ The crystal structure consists of paddle–wheel shaped centrosymmetric dimeric units in which two metal(II) atoms are bridged by two adenine ligands coordinated through their N3 and N9 nitrogen atoms and two carboxylic ligands with a $\mu\text{-}$

⁶³ (a) An, J. et al. *J. Am. Chem. Soc.* **2010**, *132*, 38. (b) Pérez–Yáñez, S. et al. *Inorg. Chem.* **2011**, *50*, 5330. (c) Lanchas, M. et al. *Inorg. Chem. Front.* **2015**, *2*, 425.

O,O' coordination mode. These units are cross-linked through the apical coordination of the imidazole N7 atom of the adeninato ligands in such a way that each paddle-wheel shaped unit is linked to four adjacent entities (Figure 1.15). This self-assembling process generates a 4-connected uninodal net that exhibits a three-dimensional system of intersecting cavities. The accessible effective volume is directly related to the length of the aliphatic chain, which is pointing toward the inner portion of the channels. The free-volume ranges from ca. 40% for the acetate analogues and is negligible for pentanoate and longer carboxylates. It is worthy to mention that the synthetic conditions play a relevant role in obtaining the different members of this last family of compounds. In fact, cobalt(II) analogues are obtained under solvothermal conditions,⁶⁴ the copper(II) ones using room condition aqueous synthesis,⁶⁵ and the nickel(II) and zinc(II) ones employing a less common solvent free approach under conventional oven or microwave assisted heating.⁴⁷

The presence of the highly polar amino groups of the adenines in the pore walls makes these compounds to present a great adsorption selectivity towards CO₂, especially for those with narrower pores.⁶⁶ Related to this great adsorption selectivity and taking advantage of the invariability of the crystal structure even when the carboxylic ligand is changed, core-shell frameworks comprising a porous mixed core (acetato/pentanoato) and a less porous shell (pentanoato) were prepared. Thus, the resulting material exhibited 30% higher CO₂ uptake than the pentanoato analogue and low N₂ uptake in comparison to the core.⁶⁷ These compounds also showed an enhancement of their adsorptive properties by making use of the template effect exerted by butyric acid microemulsions, to define a simple synthetic route that doubled the adsorption capacity of the butanoate analogue.⁶⁸ Moreover, this last 3D crystal structure seems to be so robust that it is obtained even when using long chain aliphatic dicarboxylic acids: HOOC(CH₂)_nCOOH [n from 3 to 5].⁶⁹ Surprisingly, only one of the two carboxylic groups is deprotonated and coordinated to the metal centers, $\mu\text{-}\kappa\text{O1}:\kappa\text{O2}$, while the other remains protonated inside the channels of

⁶⁴ An, J. et al. *J. Am. Chem. Soc.* **2010**, *132*, 38.

⁶⁵ Pérez-Yáñez, S. et al. *Inorg. Chem.* **2011**, *50*, 5330.

⁶⁶ (a) Pérez-Yáñez, S. et al. *Eur. J. Inorg. Chem.* **2012**, 5921. (b) Li, T. et al. *Chem. Sci.* **2013**, *4*, 1746. (c) Xie, Z. et al. *J. Mat. Chem. A*, **2014**, *2*, 1239.

⁶⁷ Li, T. et al. *J. Am. Chem. Soc.* **2013**, *135*, 9984.

⁶⁸ Pérez-Yáñez, S. et al. *Chem. Commun.* **2012**, *48*, 907.

⁶⁹ Pérez-Yáñez, S. et al. *Cryst. Growth Des.* **2012**, *12*, 3324.

the crystal structure in such a way that the dicarboxylic ligands do not join the dimeric fragments as it could in principle be expected. Only when short chain dicarboxylic acids are employed, a different crystal structure is obtained. In this last case, the great tendency of these acids to chelate metal ions hinders the paddle-wheel shaped SBUs providing crystal structures based on discrete complex entities.⁷⁰

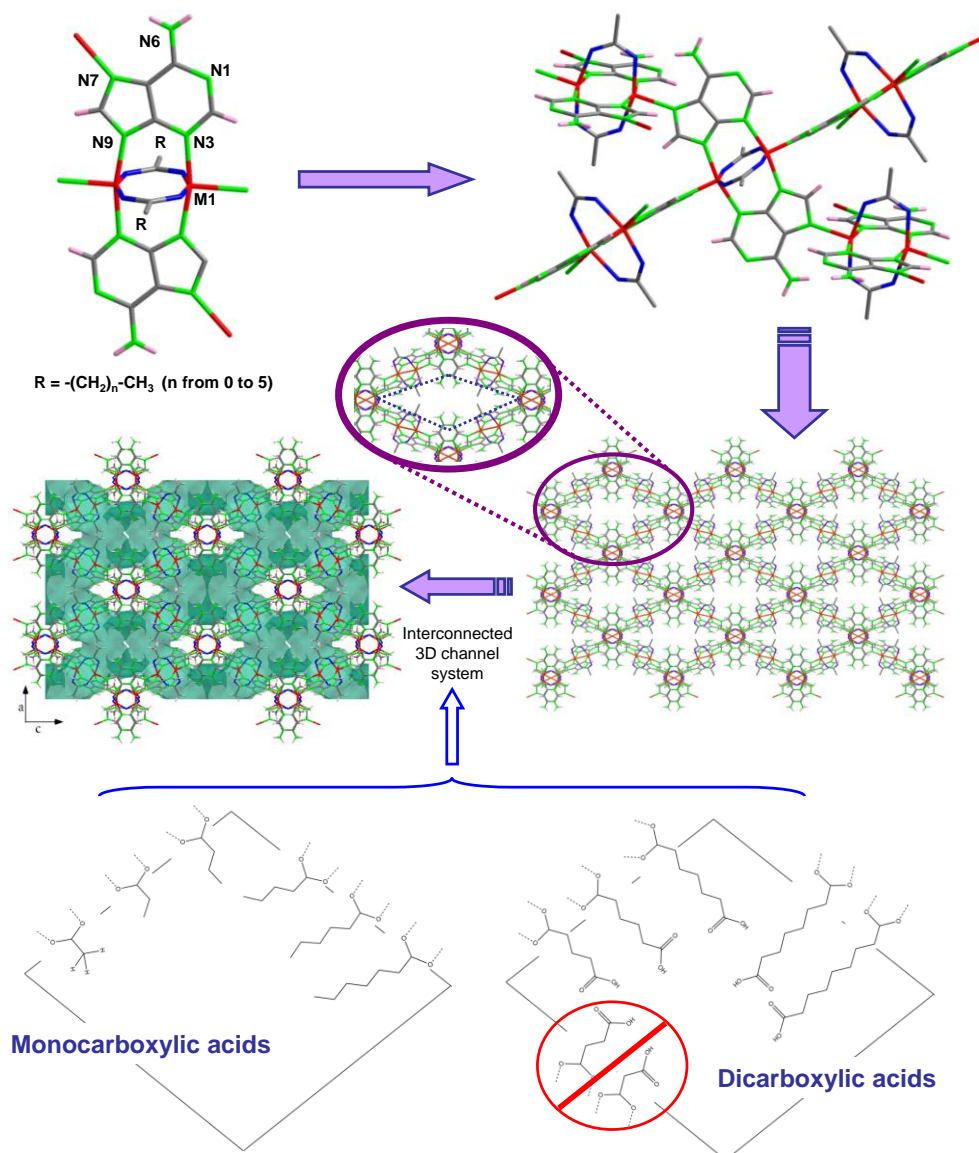


Figure 1.15: Porous crystal structure of $[\text{M}_2(\mu_3\text{-adeninato})_2(\mu_2\text{-carboxylato})_2]_n$ compounds (M being Co^{2+} , Ni^{2+} , Cu^{2+} or Zn^{2+}).

Other examples of collaborative nucleobase/non-nucleobase bridging ligands sustained MOFs are $[\text{Co}_3(\mu\text{-OH})_4(\mu_5\text{-hypoxanthinato-}\kappa\text{N3}:\kappa\text{N7}:\kappa\text{N9}:\kappa\text{O6}:\kappa\text{O6})_2]_n$, with

⁷⁰ Pérez-Yáñez, S. et al. *Eur. J. Inorg. Chem.* **2009**, 3889.

the hypoxanthinato ligand that shows spin canting, metamagnetism, and heterogeneous catalytic ability for the selective oxidation of cis-cyclooctene,⁷¹ and the anionic $[\text{Cd}_4(\mu\text{-Cl})(\mu_4\text{-adeninato-}\kappa\text{N1}:\kappa\text{N3}:\kappa\text{N7}:\kappa\text{N9})_2\text{Cl}_6]_n^{n-}$ network counterbalanced by the presence of $\text{H}^+/\text{H}_3\text{O}^+$ cations in the channels.⁷² All the above examples share in common that the purine nucleobase employs at least N3, N7 and N9 positions to join the metal centers, providing in this way a rigid linker that favors the presence of voids in the resulting structure.

Among nucleobase based MOFs, we can also underline zeolitic type frameworks in which the purine adopts a $\mu\text{-}\kappa\text{N7}:\kappa\text{N9}$ coordination mode (Figure 1.16a). $[\text{M}(\mu\text{-purinato-}\kappa\text{N7}:\kappa\text{N9})_2]_n$ was the first example of a MOF based on this purine nucleobase coordination mode, in which cobalt(II) or zinc(II) tetrahedral nodes are connected through $\text{N7},\text{N9}$ -purinate bridging ligands.⁷³ Similarly, a 2-nitroimidazole and purine mixed ligand zinc(II) ZIF, $[\text{Zn}(\mu\text{-nitroimidazolato-}\kappa\text{N1}:\kappa\text{N3})(\mu\text{-purinato-}\kappa\text{N7}:\kappa\text{N9})]_n$, was later reported.⁷⁴ Furthermore, the use of pyridinecarboxylate ligands together with adenine gave rise as well to zeolitic type metal-organic frameworks (Figure 1.16b). In fact, two compounds showing the same network were achieved with isonicotinato, $[\text{Zn}(\mu\text{-adeninato-}\kappa\text{N7}:\kappa\text{N9})(\mu\text{-isonicotinato-}\kappa\text{N}:\kappa\text{O})]_n$,⁷⁵ and 2-aminoisonicotinato, $[\text{Zn}(\mu\text{-adeninato-}\kappa\text{N7}:\kappa\text{N9})(\mu\text{-2-aminoisonicotinato-}\kappa\text{N}:\kappa\text{O})]_n$.⁷⁶ The functionalization of the isonicotinato ligand with an amino group resulted in a significant enhance of the adsorption selectivity towards CO_2 . Finally, $[\text{Zn}_{1.33}(\text{O},\text{OH})_{0.33}(\mu\text{-nitroimidazolato-}\kappa\text{N1}:\kappa\text{N3})_{1.167}(\mu_3\text{-purinato-}\kappa\text{N1}:\kappa\text{N7}:\kappa\text{N9})]_n$ represents another example of this family in which the usual $\mu\text{-}\kappa\text{N7}:\kappa\text{N9}$ coordination mode is reinforced by the coordination through N1 position.⁷⁴

⁷¹ (a) Zhang, X.-H. et al. *Chem. Eur. J.* **2011**, *17*, 5588. (b) Zhang, G. et al. *Dalton Trans.* **2013**, *42*, 9423.

⁷² Song, Y. et al. *CrystEngComm.* **2014**, *16*, 3082.

⁷³ Hayashi, H. et al. *Nat. Mater.* **2007**, *6*, 501.

⁷⁴ Kahr, J. et al. *Chem. Commun.* **2012**, *48*, 6690.

⁷⁵ (a) Wang, F. et al. *Chem. Commun.* **2011**, *47*, 5828. (b) Wang, F. et al. *J. Mater. Chem.* **2012**, *22*, 19732.

⁷⁶ Yang, E. et al. *CrystEngComm.* **2013**, *15*, 658.

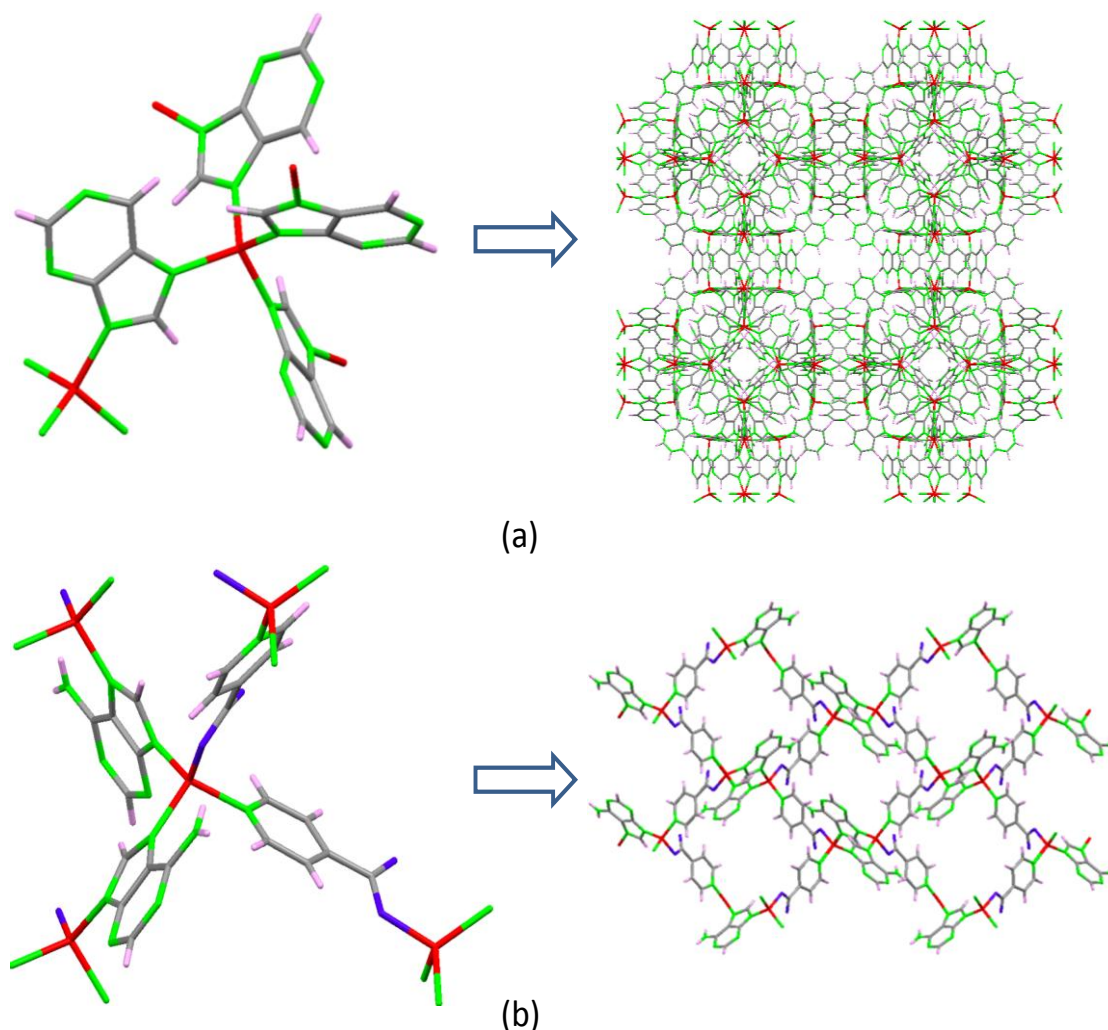


Figure 1.16: Metal coordination environment and final crystal structures of compounds (a) $[\text{Zn}(\mu\text{-purinato-}\kappa\text{N7:}\kappa\text{N9})_2]_n$, and (b) $[\text{Zn}(\mu\text{-adeninato-}\kappa\text{N7:}\kappa\text{N9})(\mu\text{-isonicotinato-}\kappa\text{N:}\kappa\text{O})]_n$.

All above mentioned results emphasize the suitability of purine nucleobases as framework components of MOFs due to their multiple available coordination positions and the stiffness of their molecular structure. In fact the lower coordination positions of the pyrimidinic nucleobases did not yet allow the isolation of a MOF based on these ligands as linkers.

1.5 NUCLEOBASES AS HYDROGEN BONDING LINKERS

The formation of duplex DNA from its single stranded constituents is a result of an assemblage of intermolecular forces including aromatic π -stacking, van der Waals forces and hydrophobic effects.⁷⁷ However, the high constancy observed in the pairing

⁷⁷ Jeffrey, G. A.; Saenger, W. *Hydrogen Bonding in Biological Structures*; Springer: Berlin, 1991.

of complementary DNA sequences is greatly due to the unique molecular recognition capability of naturally occurring nucleobases through Watson–Crick pairing hydrogen bonding interactions,⁷⁸ while triple helix DNA and G–quartets are formed through Hoogsteen base pairing interactions.

In order to have a better understanding of different synthetic structures that can be constructed through nucleobase interactions, a brief note of the various modes of hydrogen bonding interactions between nucleobases are given in the following part. Till date, various naturally occurring hydrogen bonding motifs and additionally many synthetic hydrogen bonding systems have been reported. However, the nucleobases are considered versatile and known for their capability to sustain hydrogen bond mediated self–assembly or to establish the so called complementary base–pairing interactions.⁷⁹ In both DNA and RNA, the purine bases pair with the pyrimidine bases, that is Adenine–Thymine and Cytosine–Guanine in DNA and Adenine–Uracil and Cytosine–Guanine in RNA forming Watson–Crick motifs which are the widely recognised hydrogen bonding interaction in nature. Adenine base has the capacity to form two–point hydrogen bonding either with Thymine or with Uracil, while Guanine forms three–point hydrogen bonding with Cytosine,⁸⁰ being therefore a stronger base–pairing motif (Figure 1.17). Hence, in the broader sense, hydrogen–bonding interactions involving base pairs must be considered as playing a salient role in many critical areas such as genetic coding, biological information storage and protein synthesis.⁸¹

In addition to the conventional G–C and A–T Watson–Crick type base pairing interactions seen in the nucleic acids, the nucleobases are able to establish alternative modes of hydrogen bonding interactions including Hoogsteen and Wobble (mismatched) pairs, two–point homodimers, higher order base–triplets and guanine quartets.⁸² Moreover, nucleobases are able to establish hydrogen bonding interactions among the same type of nucleobases. Figure 1.18 shows the hydrogen bonding interactions established along the Watson–Crick and sugar–edges of two adenine

⁷⁸ Watson, J. D.; Crick, F. H. *Nature* **1953**, *171*, 737.

⁷⁹ Prins, L. J. et al. *Angew. Chem. Int. Ed.* **2001**, *40*, 2382.

⁸⁰ Verma, S. et al. *Acc. Chem. Res.* **2010**, *43*, 79.

⁸¹ (a) Blackburn, G. M. et al. *Nucleic Acids in Chemistry and Biology*; RSC Publishing: Cambridge, UK, 2006, p. 470. (b) Bloomfield, V. A. et al. *Nucleic Acids: Structures, Properties and Functions*; University Science Books: Sausalito, USA, 2000.

⁸² Sessler J. L. et al. *Chem. Soc. Rev.* **2007**, *36*, 314.

moieties. Mimicking the unique ability of DNA to form well-defined assemblies, whose underlying chemistry is governed by the rules of base pairing, is a major area of research in supramolecular chemistry.⁸³ The high fidelity, directionality, and the effectiveness for establishing multiple pairing interactions have resulted in the concept of base pairing being transported out of the biological realm to the field of supramolecular chemistry.⁸²

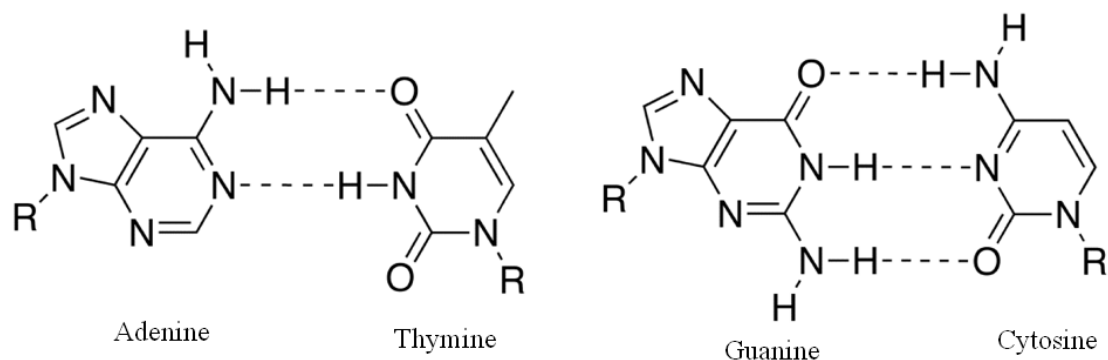


Figure 1.17: Canonical Adenine...Thymine and Guanine...Cytosine complementary base pairing pattern through Watson-Crick faces.

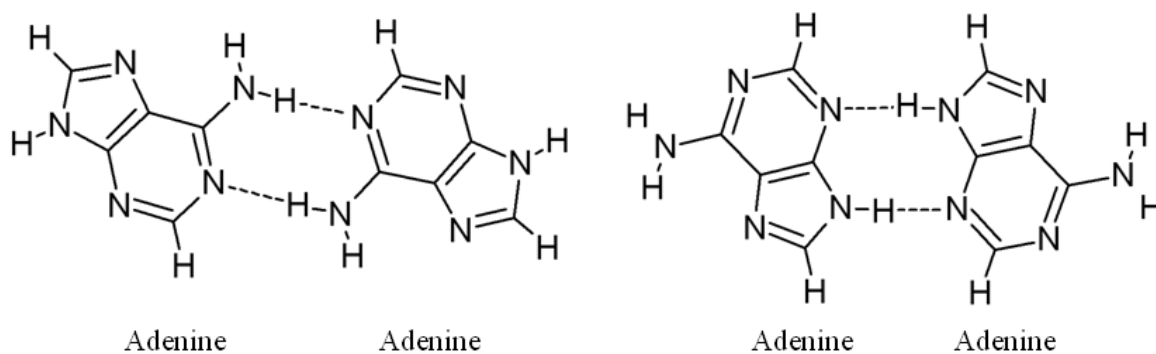


Figure 1.18: The hydrogen bonding interactions established between the same types of nucleobases with adenine as an example.

In addition to these primary nucleobases, there exists other modified nucleobases or nucleobase derivatives. Some examples of them are given in Figure 1.19.

⁸³ (a) Sivakova, S.; Rowan, S. J. *Chem. Soc. Rev.* **2005**, *34*, 9. (b) Sessler, J. L. et al. *J. Chem. Soc. Rev.* **2007**, *36*, 314. (c) Fathalla, M. et al. *J. Chem. Soc. Rev.* **2009**, *38*, 1608.

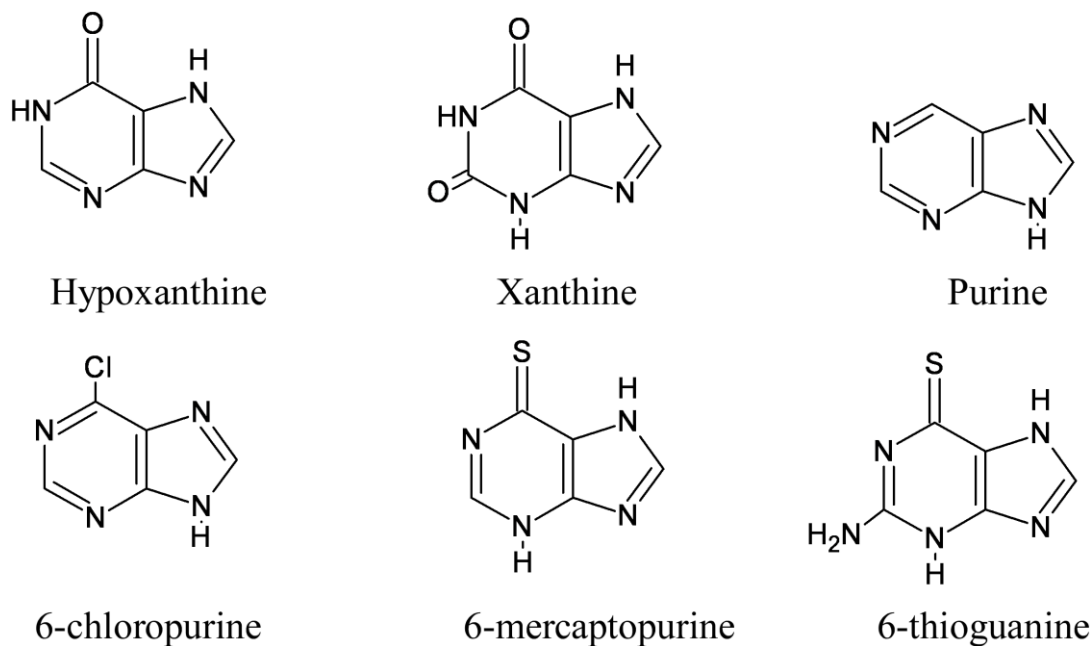


Figure 1.19: Examples of other nucleobases derivatives.

The capacity of the nucleobases to anchor to metal centers through multiple positions at the same time, both acting as bridging or terminal ligand, and their ability to establish complementary interactions makes them suitable for the tailoring of supramolecular arrays based on discrete metal–nucleobase entities. The association patterns between the nucleobases in these discrete entities are directed by a variety of factors like the possible hydrogen bonding scheme, additional stabilization by stacking interactions, the interactions between counterions and also with solvent molecules.⁸⁴ On the other hand, the coordination mode versatility of the nucleobases provides a chart of metal–nucleobase discrete entities with different geometries. It also allows them to form complexes of different nuclearity and among which (a) monomers⁸⁵ and (b) dimers⁸⁶ are very common. However higher nuclearity complexes like (c) trimers,⁸⁷ (d) tetramers,⁸⁸ (e) hexamers⁸⁹ and (f) octamers⁹⁰ are also found (Figures 1.20 and 1.21).

⁸⁴ Amo–Ochoa, P. et al. *J. Biol. Inorg. Chem.* **2007**, *12*, 543.

⁸⁵ de Meester, P.; Skapski, A. C. *J. Chem. Soc. Dalton Trans.* **1973**, 1596.

⁸⁶ Terzis, A. et al. *Inorg. Chem.* **1973**, *12*, 1166.

⁸⁷ de Meester, P. et al. *J. Chem. Soc. Dalton Trans.* **1972**, 2400.

⁸⁸ Sheldrick, W. S. et al. *Inorg. Chim. Acta* **1993**, *206*, 15.

⁸⁹ (a) González–Pérez, J. M. et al. *Inorg. Chem.* **2006**, *45*, 877. (b) An, J. et al. *J. Am. Chem. Soc.* **2009**, *131*, 8401.

⁹⁰ Thomas–Gipson, J. et al. *Cryst. Growth Des.* **2015**, *15*, 975.

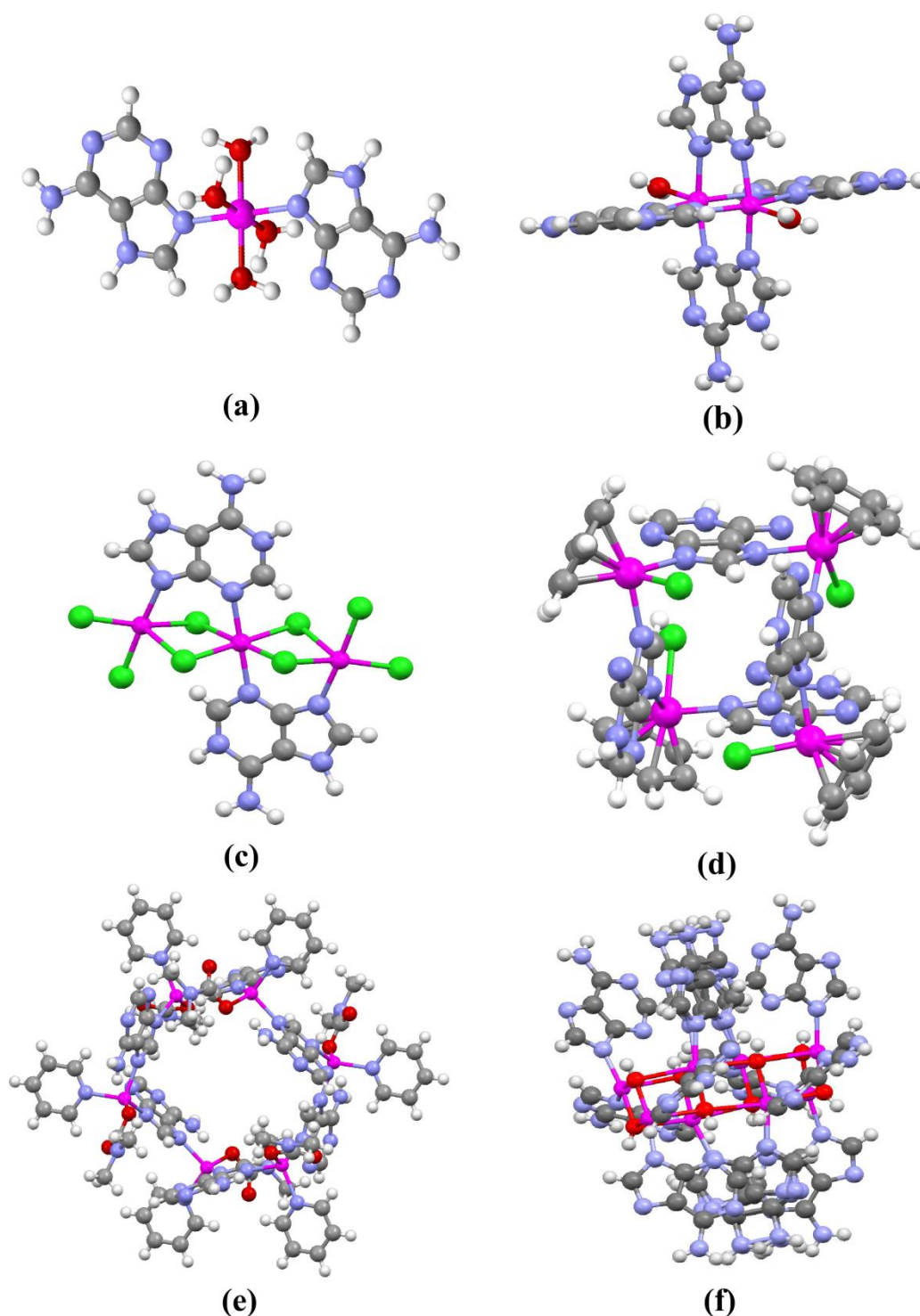


Figure 1.20: Discrete entities of adenine with different nuclearities: (a) monomers,⁸⁵ (b) dimers,⁸⁶ (c) trimers,⁸⁷ (d) tetramers,⁸⁸ (e) hexamers^{89b} and (f) octamers.⁹⁰

One of the appealing applications of the nucleobase self assembly processes involves the generation of supramolecular polymers via hydrogen bonding. Base pairing represents a particularly attractive approach to the construction of supramolecular networks because these hydrogen bonding motifs have the potential to confer both directionality and predictability to the incipient array.

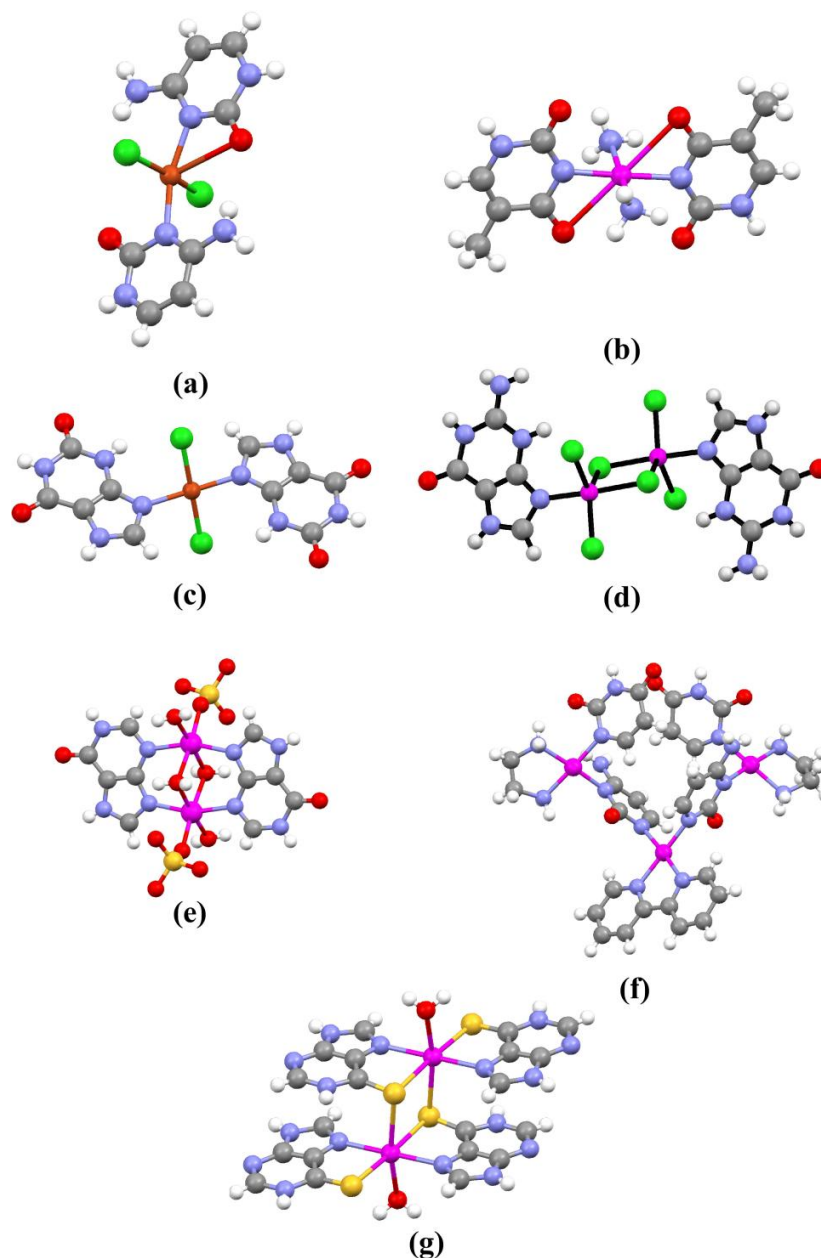


Figure 1.21: Discrete entities of other nucleobases; (a) monomeric compound of cytosine,⁹¹ (b) monomeric compound of thymine,⁹² (c) monomeric compound of xanthine,⁹³ (d) dimeric compound of guanine,⁹⁴ (e) dimeric compound of hypoxanthine,⁹⁵ and (f) trimeric compound of uracil and cytosine⁹⁶ and (g) dimeric compound of 6-mercaptopurine.⁹⁷

⁹¹ Tran Qui, D.; Palacios, E. *Acta Crystallogr. Sect. C: Cryst. Struct. Commun.* **1990**, C46, 1220.

⁹² Parvez, M.; Birdsall, W. J. *Acta Crystallogr. Sect. C, Cryst. Struct. Commun.* **1994**, 50, 540.

⁹³ Dubler, E. et al. *Inorg. Chem.* **1992**, 31, 3728.

⁹⁴ Sundaralingam, M.; Carrabine, J. A. *J. Mol. Bio.* **1971**, 61, 287.

⁹⁵ Hänggi, G. et al. *Acta Crystallogr.* **1992**, C48, 1008.

⁹⁶ Bardají, E. G. et al. *Chem. Eur. J.* **2007**, 13, 6019.

⁹⁷ Amo-Ochoa, P. et al. *Inorg. Chem.* **2006**, 45, 7642.

There are some examples of non-porous supramolecular polymers based on complementary hydrogen bonded base pairing interactions among transition metal-nucleobase supramolecular building units. Figure 1.22 shows some examples of supramolecular polymers where the complementary base pairing interactions are crucial in forming supramolecular arrays. These examples include, (a) trans-bis(adeninato)-bis(tri-n-butylphosphine)-palladium(II) methanol solvate,⁹⁸ (b) (adeninato-N9)-methyl-mercury(II) monohydrate,⁹⁹ (c) tetra-aqua-bis(9-methyladenine)-copper(II) dichloride dehydrate,¹⁰⁰ (d) dichloro-bis(cytosine-N3)-copper(II),⁹¹ (e) bis(9-methylguanine)-tetraaqua-cadmium(II) dinitrate,¹⁰¹ (f) tetrakis(cytosine)-copper(II) diperchlorate dehydrate,¹⁰² and (g) trans-bis(guanine)-aqua-(formato)-copper(II) perchlorate formic acid solvate monohydrate.¹⁰³

Sessler and co-workers⁸² pointed out the relevance of the solvent in designing self assembled structures based on hydrogen bonding interactions. It is to be noted that, in polar protic solvents, monomeric nucleobases do not exist as hydrogen bonded pairs. Rather, they tend to form extended columns as a result of π -stacking and hydrophobic interactions. Thus, the solvent competes with the acceptor and donor sites on the nucleobases leading to decreased hydrogen bonding interactions with the complementary base. Therefore aprotic solvents such as CH_2Cl_2 and CHCl_3 were preferably used to synthesise synthetic self assembled structures as they do not compete appreciably with the donor/acceptor sites needed to establish the base pairing interactions. However, the solubility of the parent nucleobases in these foresaid solvents is still a challenge to be met. Nonetheless, this solvent dependency is rather attractive as the formation and subsequent break-up of such aggregates can be controlled by changing the reaction medium by switching from non-polar to highly competitive hydrogen bonding solvents.

⁹⁸ Beck, W. M. et al. *Inorg.Chem.* **1979**, *18*, 176.

⁹⁹ Prizant, L. et al. *Can. J. Chem.* **1981**, *59*, 1311.

¹⁰⁰ Sletten, E.; Ruud, M. *Acta Crystallogr. Sect. B: Struct. Crystallogr. Cryst. Chem.* **1975**, *B31*, 982.

¹⁰¹ Amo-Ochoa, P. et al. *J. Inorg. Biochem.* **2005**, *99*, 1540.

¹⁰² Palaniandavar, M. et al. *J. Chem. Soc. Dalton Trans.* **1996**, 1333.

¹⁰³ Mastropietro, T. F. et al. *Dalton Trans.* **2008**, 514.

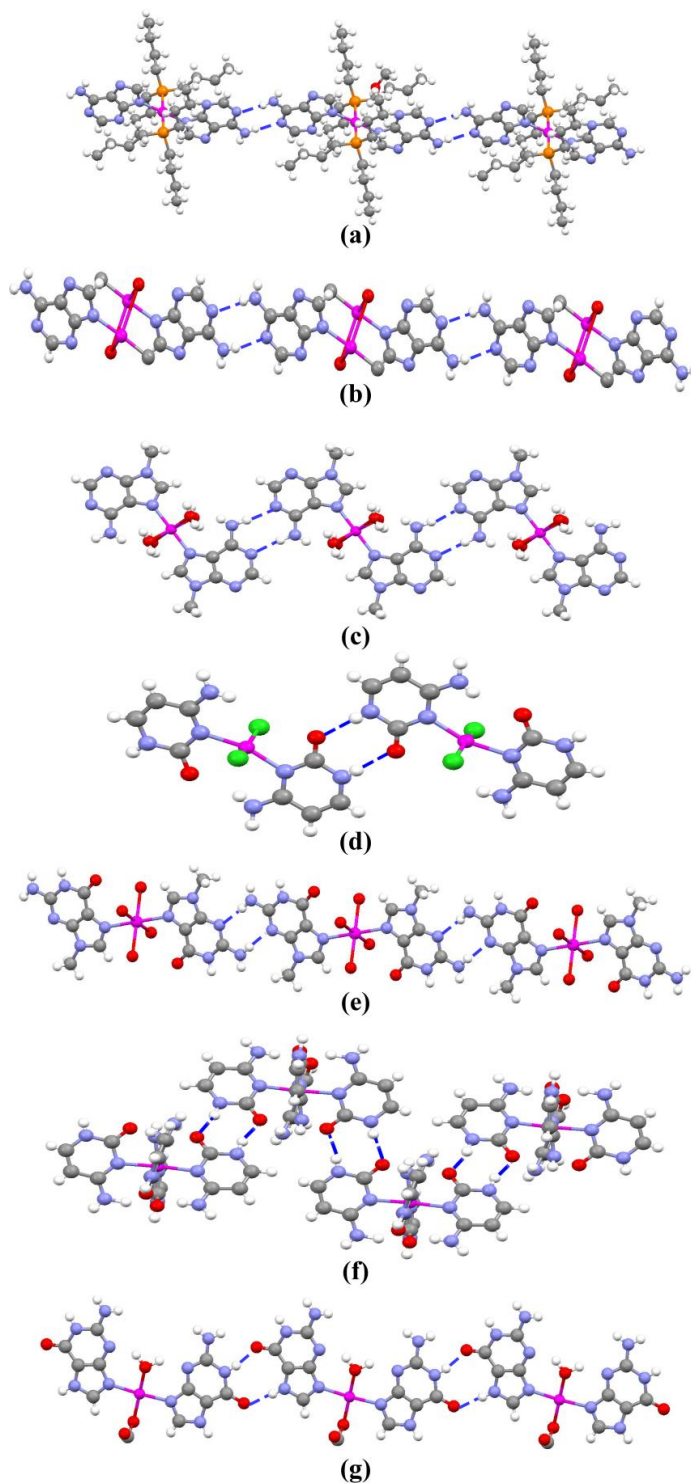


Figure 1.22: Examples of compounds in which base-pairing interactions lead to supramolecular polymerization (a) trans-bis(adeninato)-bis(tri-*n*-butylphosphine)-palladium(II) methanol solvate,⁹⁸ (b) (adeninato-N9)-methyl-mercury(II) monohydrate,⁹⁹ (c) tetra-aqua-bis(9-methyladenine)-copper(II) dichloride dehydrate,¹⁰⁰ (d) dichloro-bis(cytosine-N3)-copper(II),⁹¹ (e) bis(9-methylguanine)-tetraaqua-cadmium(II) dinitrate,¹⁰¹ (f) tetrakis(cytosine)-copper(II) diperchlorate dehydrate,¹⁰² and (g) trans-bis(guanine)-aqua-(formato)-copper(II) perchlorate formic acid solvate monohydrate.¹⁰³

1.6 OBJECTIVE

Taking into account the great potentials of MOFs, herein we decided to explore a novel, but related, type of materials, Supramolecular Metal–Organic Frameworks (*SMOFs*) in which the bridging coordination bonds are replaced with hydrogen bonds, which are also directional and predictable interactions, to sustain the 3D crystal building (Figure 1.23). Although, such kind of alternative materials can arouse an alike fascination to that of MOFs, the crystal engineering principles and the synthetic approach are not yet settled, and examples of this kind of materials have not been yet reported.

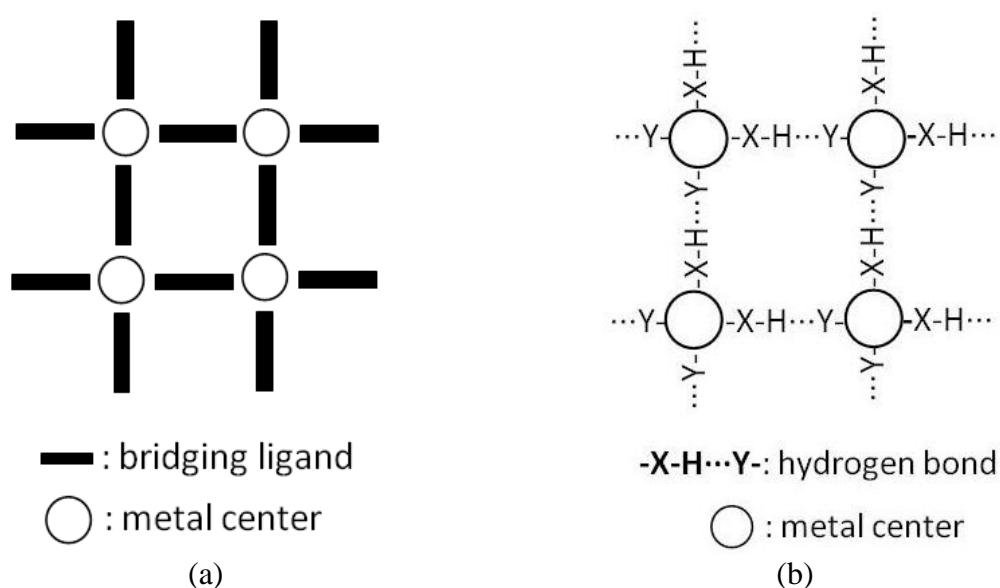


Figure 1.23: Similarity between (a) coordination bonds and (b) hydrogen bonding interactions.

We consider nucleobases as best candidates for this purpose due to their multiple binding positions and capability to establish doubly and triply hydrogen bonded complementary base pairing interactions. Therefore, the original idea is to employ discrete metal–nucleobase complexes in which the nucleobase is tightly anchored to the metal centres but exposing, at the same time, several hydrogen bond donor and acceptor positions to establish base pairing interactions that could sustain a robust supramolecular synthon. It is also expected that the geometrical restraint imposed by the base pairing interactions could led to an inefficient space occupation giving rise to a new family of porous materials.

Chapter 2

Supramolecular architectures based on metal/cytosine systems

2.1 Introduction

2.2 Synthesis and Characterisation

2.3 Results and Discussion

2.4 Conclusions

2.1 INTRODUCTION

The primary objective at the beginning of this work was to develop extended systems of porous supramolecular metal–organic frameworks based on first row transition metal ions and nucleobases. Preference was given to pyrimidine bases due to their high solubility in almost all the solvents and also because there are interesting examples of cytosine derivatives coordinated to transition metal complexes.¹⁰⁴ However, the number of reported examples of such compounds in which unsubstituted neutral cytosine is coordinated to a metal centre is lower.¹⁰⁵

¹⁰⁴ (a) Pacifico, C. et al. *Bioinorg. Chem. Appl.* **2010**, *2010*, 102863. (b) Britten, J. F. et al. *Inorg. Chem.* **1982**, *21*, 1936. (c) Orbell, J. D. et al. *J. Am. Chem. Soc.* **1981**, *103*, 5126. (d) Houlton, A. et al. *J. Chem. Soc. Dalton Trans.* **1999**, 3229. (e) Sabat, M. et al. *J. Am. Chem. Soc.* **1983**, *105*, 976. (f) Cosar, S. et al. *J. Chem. Soc. Dalton Trans.* **1999**, 2329. (g) Amo–Ochoa, P. et al. *J. Inorg. Biochem.* **2008**, *102*, 203. (h) Vijay–Kumar, S. et al. *Nucleic Acids Res.* **1984**, *12*, 3649. (i) Louie, S. et al. *J. Am. Chem. Soc.* **1977**, *99*, 3874. (j) Lippert, B. et al. *Inorg. Chem.* **1981**, *20*, 335. (k) Aoki, K. *Chem. Commun.* **1979**, 589. (l) Aoki, K. *Biochim. Biophys. Acta.* **1976**, *447*, 379. (m) Holowczak, M. S. et al. *J. Am. Chem. Soc.* **1985**, *107*, 5789. (n) Khutia, A. et al. *Chem. Eur. J.* **2011**, *17*, 4195. (o) Miller, S. K. et al. *Inorg. Chem.* **1986**, *25*, 4272. (p) Schollhorn, H. et al. *J. Am. Chem. Soc.* **1986**, *108*, 3680. (q) Jitsukawa, K. et al. *Chem. Lett.* **2004**, *33*, 1302. (r) Grehl, M.; Krebs, B. *Inorg. Chem.* **1994**, *33*, 3877. (s) Djinovic, V. M. et al. *Dalton Trans.* **2010**, *39*, 3633. (t) Miguel, P. J. S. et al. *J. Inorg. Biochem.* **2006**, *100*, 980. (u) Galstyan, A. et al. *Eur. J. Inorg. Chem.* **2011**, 1649. (v) Krumm, M. et al. *Inorg. Chem.* **1991**, *30*, 884. (w) Mastropietro, T. F. et al. *Cryst. Growth Des.* **2007**, *7*, 609. (x) Fusch, E. C.; Lippert, B. *J. Am. Chem. Soc.* **1994**, *116*, 7204. (y) Ruiz, J. et al. *Inorg. Chem.* **2005**, *44*, 7365. (z) De Munno, G. et al. *J. Chem. Soc. Dalton Trans.* **2000**, 1625. (aa) Kistenmacher, T. J. et al. *Inorg. Chem.* **1979**, *18*, 240. (ab) Trovo, G. et al. *Dalton Trans.* **1993**, 669. (ac) Longato, B. et al. *Inorg. Chem.* **2006**, *45*, 8179. (ad) Montagner, D. et al. *Inorg. Chem.* **2008**, *47*, 2688. (ae) Wu, S.–M.; Bau, R. *Biochem. Biophys. Res. Comm.* **1979**, *88*, 1435. (af) Fusch, G. et al. *Inorg. Chim. Acta.* **1996**, *252*, 167. (ag) Holthenrich, D. et al. *Inorg. Chim. Acta* **1996**, *248*, 175. (ah) Freisinger, E. et al. *Proc. Nat. Acad. Sci. USA*, **2003**, *100*, 3748. (ai) Anzellotti, A. I. et al. *Inorg. Chem.* **2006**, *45*, 1638. (aj) Schwarz, F. et al. *Chem. Commun.* **1990**, 1282. (ak) Smith, D. P. et al. *Organometallics* **1993**, *12*, 593. (al) Wienken, M. et al. *J. Chem. Soc. Dalton Trans.* **1993**, 3349. (am) Purohit, P. S. et al. *Appl. Catal. A*, **2007**, *316*, 100. (an) Aoki, K. *Chem. Commun.* **1976**, 748.

¹⁰⁵ (a) Garcia, B. et al. *J. Inorg. Biochem.* **2008**, *102*, 1892. (b) Sundaralingam, M.; Carrabine, J. A. *J. Mol. Biol.* **1971**, *61*, 287. (c) Khutia, A. et al. *Chem. Eur. J.* **2011**, *17*, 4195. (d) Garcia–Raso, A. et al. *Polyhedron* **2006**, *25*, 2295. (e) Panfil, A. et al. *Polyhedron* **1994**, *13*, 2513. (f) Klein, A. et al. *Organometallics* **2007**, *26*, 230. (g) Cervantes, G. et al. *Inorg. Chem.* **1990**, *29*, 5168. (h) Hollis, L. S. et al. *J. Med. Chem.* **1989**, *32*, 128. (i) De Munno, G. et al. *J. Chem. Soc. Dalton Trans.* **2000**, 1625. (j) Capllonch, M. C. et al. *J. Inorg. Biochem.* **2001**, *85*, 173. (k) Aoki, K.; Salam, M. A. *Inorg. Chim. Acta* **2001**, *316*, 50. (l) Brüning, W. et al. *Inorg. Chim. Acta* **2002**, *339*, 400. (m) De Munno, G. et al. *J. Chem. Soc. Dalton Trans.* **1993**, 1113. (n) Kickham, J. E. et al. *J. Am. Chem. Soc.* **1993**, *115*, 7031. (o) Szalda, D. J. et al. *Inorg. Chem.* **1975**, *14*, 2076. (p) Tran Qui, D.; Bagieu, M. *Acta Crystallogr. Sect. C: Cryst. Struct. Commun.* **1990**, *46*, 1645. (q) Bardaji, E. G. et al. *Chem. Eur. J.* **2007**, *13*, 6019. (r) Karthikeyan, A. et al. *Acta Crystallogr. Sect. E: Struct. Rep. Online*, **2010**, *66*, m1693. (s) Brüning, W. et al. *Chem. Eur. J.* **2002**, *8*, 4681. (t) Palaniandavar, M. et al. *J. Chem. Soc. Dalton Trans.* **1996**, 1333.

Neutral cytosine, although presenting different donor positions, shows a relatively predictable coordination mode through N3. In fact, in a search at the CSD database (version February 2015) this coordination mode showed 26 hits from a total of 34 registered crystal structures for neutral cytosine coordinated to a transition metal center. Less common coordination modes involve bonding through the exocyclic O2, N1 or even in two cases it links simultaneously through N3 and O2 both as chelates or bridging ligand. The usually accepted numbering scheme of cytosine is shown in Figure 2.1 altogether with its coordination modes.

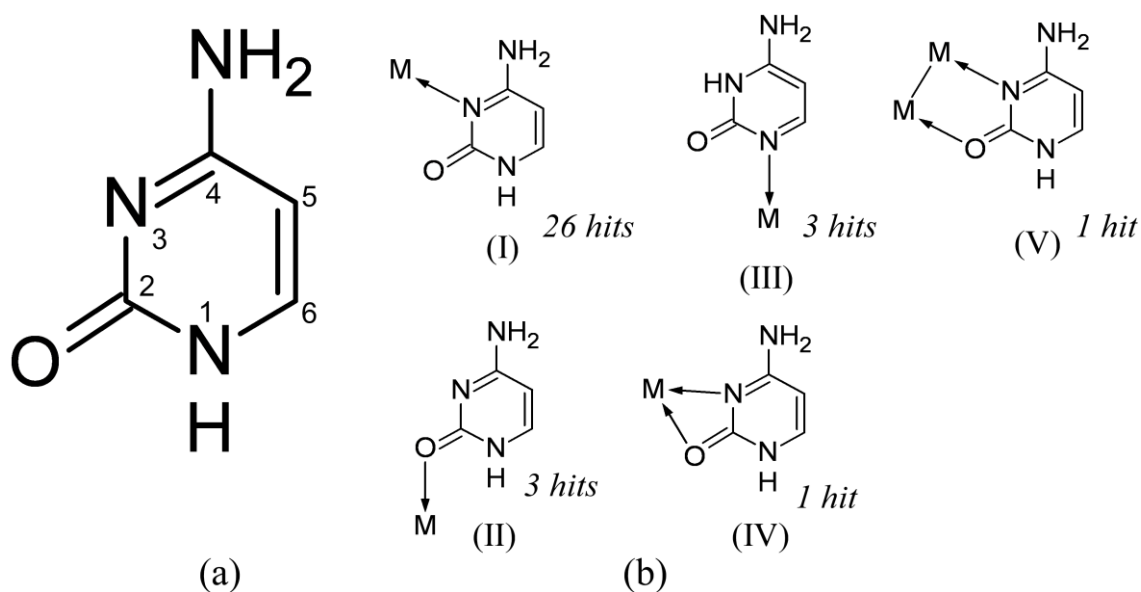


Figure 2.1: (a) The numbering scheme of cytosine and (b) coordination modes of neutral cytosine.

On the other hand, the deprotonation of the cytosine reinforces its coordination capability being relatively common the μ -cytosinato- $\kappa N1: \kappa N3$ (Figure 2.2).

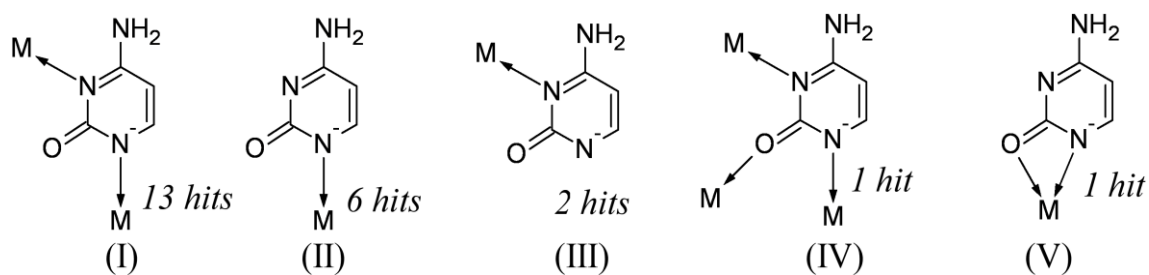


Figure 2.2: Coordination modes of cytosinate anion.

The resulting coordination complexes that emerge from the predominant cytosine- $\kappa N3$ coordination mode, are basically restricted to monomeric entities as those depicted in Figure 2.3, which expose the sugar edge (N1–O2 side) of the nucleobase to

establish complementary hydrogen bonds and therefore they could develop self-assembled *supramolecular MOFs*. Cytosine is able to form three complimentary hydrogen bonds at a time with the guanine molecule, but it is also able to establish cytosine...cytosine self-complementary hydrogen bonding patterns that involves the Watson-Crick and sugar edges (Figure 2.4).¹⁰⁶

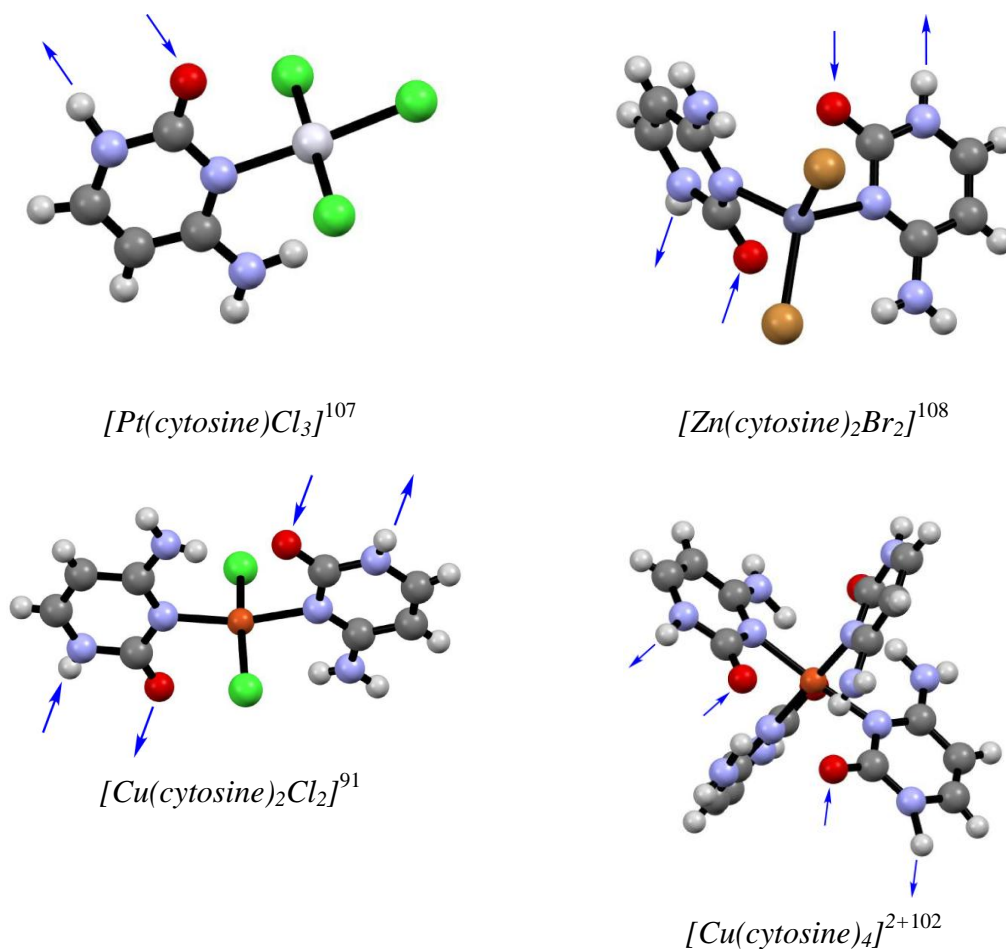


Figure 2.3: Examples of cytosine- $\kappa N3$ coordinated transition metal complexes.

¹⁰⁶ Frey, J. A. et al. *J. Phys. Chem. B*, **2014**, *118*, 682.

¹⁰⁷ Jaworski, S. et al. *Inorg. Chim. Acta* **1988**, *153*, 31.

¹⁰⁸ Karthikeyan, A. et al. *Acta Crystallogr. Sect. E: Struct. Rep. Online*, **2010**, *66*, m1693.

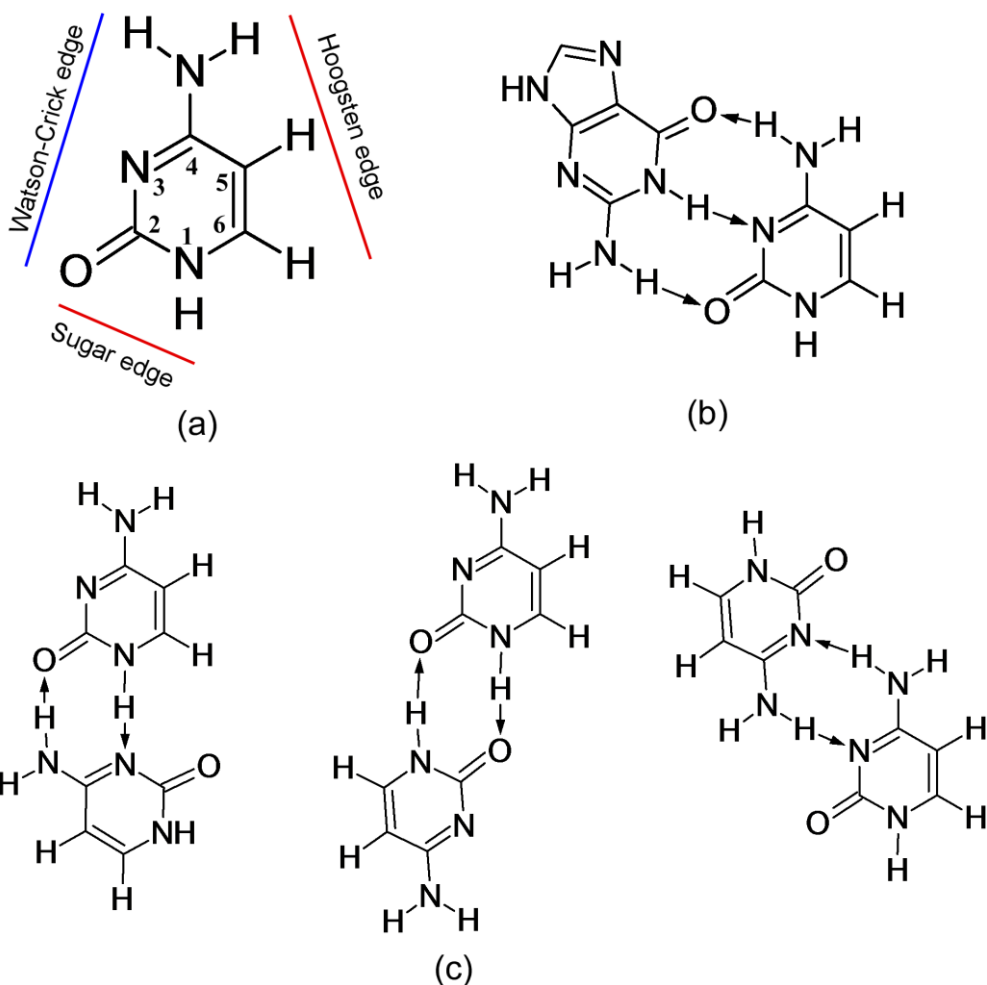


Figure 2.4: (a) Cytosine nucleobase edges, (b) guanine...cytosine triple complementary hydrogen bonds and (c) cytosine...cytosine double complementary hydrogen bonding patterns.

The Figure 2.5 is an example of complementary hydrogen bonding interaction between coordinated cytosine- $\kappa N3$ nucleobases. The objective of this chapter is to explore the use of cytosine as ligand in order to take advantage of its hydrogen bonding capability to form supramolecular networks sustained by noncovalent interactions.

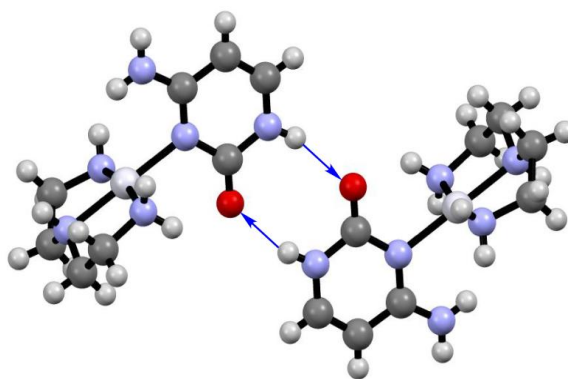


Figure 2.5: Hydrogen bonding interaction between coordinated cytosine- $\kappa N3$ nucleobases.¹⁰⁹

¹⁰⁹ Brüning, W. et al. *Inorg. Chim. Acta* **2002**, 339, 400.

2.2 SYNTHESIS AND CHARACTERISATION

2.2.1 Synthesis

The Table 2.1 shows the compounds obtained for the metal/halide/cytosine system. A common feature of syntheses is the use of alcoholic solvents instead of water to promote the direct hydrogen bonding interactions among the cytosines. The purity of all samples has been checked by means of X-ray diffraction techniques, elemental analysis and ICP analysis.

Table 2.1: Synthesised new compounds.^[a]

Compound ^[a]	Code
(H ₂ Cyt) ₂ [CoCl ₄]·2(HCyt) Cytosinium tetrachloridocobaltate(II)–cytosine (1/2)	<i>COCYTCL</i>
[CoBr ₂ (HCyt) ₂] Dibromidobis(cytosine–κN3)cobalt(II)	<i>COCYTBR</i>
[ZnCl ₂ (HCyt) ₂] Dichloridobis(cytosine–κN3)zinc(II)	<i>ZNCYTCL</i>
[CuCl ₂ (HCyt) ₂] Dichloridobis(cytosine–κN3)copper(II)	<i>CUCYTCL–B</i>
[CuBr ₂ (HCyt) ₂] Dibromidobis(cytosine–κN3)copper(II)	<i>CUCYTBR</i>
[Cu(HCyt) ₄](SO ₄)·2(CH ₃ OH) tetrakis(cytosine–κN3)copper(II) sulphate–methanol (1/2)	<i>CUCYTSO4</i>

^[a] HCyt = C₄H₅N₃O; H₂Cyt = C₄H₆N₃O

2.2.1.1 Synthesis of *COCYTCL*

A solution of 0.1 mmol of CoCl₂·6H₂O (0.0239 g) in 5 mL propanol was added dropwise into a solution of 0.2 mmol of cytosine (0.0237 g) in 35 mL propanol containing 0.2 mmol of hydrochloric acid (37%) and stirred for two hours at 80 °C. A small quantity of a light blue precipitate of *COCYTCL* was obtained and filtered out. The mother liquid was then left evaporating at room temperature and blue good quality single crystals appeared in one week. They were filtered off, washed thoroughly with cold ethanol and left drying under vacuum.

Yield (based on metal): 40%. Anal. Calcd (found) for C₁₆H₂₂Cl₄CoN₁₂O₄: C, 29.69 (29.82); H, 3.43 (3.50); N, 25.97 (26.07), Co, 9.11 (9.08). IR selected data (KBr, cm⁻¹): 3430w, 3076w, 1860m, 1826w, 1796w, 1740vs, 1726sh, 1688vs, 1650vs, 1516m, 1488s, 1455s, 1445sh, 1411w, 1386w, 1372sh, 1294w, 1283sh, 1241vs, 1233sh,

1130w, 1113w, 1091w, 1011m, 988m, 947m, 841w, 808m, 781vs, 758sh, 701m, 668m, 596m, 586s, 570s, 553m, 535s, 471w, 425m.

2.2.1.2 Synthesis of *COCYTBR*

Single crystals were grown by the addition of 0.05 mmol solution of CoBr_2 (0.0120 g) in 10 mL propanol over a 10 mL propanolic solution of 0.1 mmol of cytosine (0.0116 g). The solution was stirred for 2 hours and left evaporating at room temperature. Blue single crystals of *COCYTBR* were obtained after one week.

Yield: 55%. Anal. Calcd (found) for $\text{C}_8\text{H}_{10}\text{Br}_2\text{CoN}_6\text{O}_2$: C, 21.79 (21.87); H, 2.29 (2.34); N, 19.06 (19.03), Co, 13.37 (13.31). IR selected data (KBr, cm^{-1}): 3430m, 3386m, 3313m, 3233m, 3213sh, 3086m, 3016w, 2956w, 2923w, 2883w, 2836w, 1669vs, 1676vs, 1629vs, 1600sh, 1529m, 1500sh, 1475m, 1437m, 1383w, 1362w, 1275m, 1237s, 1216s, 1116w, 1110w, 1004w, 975w, 958w, 850m, 800s, 779s, 750s, 704m, 666w, 640m, 608m, 600w, 578m, 551s, 541s, 530sh, 443m, 436m.

2.2.1.3 Synthesis of *ZNCYTCL*

A solution of 0.1 mmol of ZnCl_2 (0.0140 g) dissolved in 5 mL methanol was added dropwise to a stirring solution of 0.4 mmol of cytosine (0.0450 g) dissolved in 40 mL of methanol. The solution was stirred for one hour and left evaporating at room temperature. Colourless crystals started appearing after one week of evaporation.

Yield: 15%. Anal. Calcd (found) for $\text{C}_8\text{H}_{10}\text{Cl}_2\text{N}_6\text{O}_2\text{Zn}$: C, 26.80 (26.87); H, 2.81 (2.76); N, 23.44 (23.47), Zn, 18.24 (18.21). IR selected data (KBr, cm^{-1}): 3427s, 3367s, 3172s, 3094s, 2922s, 2844s, 2805s, 1672vs, 1633vs, 1505s, 1461s, 1372m, 1288m, 1238m, 1150w, 1105w, 1005w, 977w, 877m, 805s, 788s, 750w, 655m, 600m, 573w, 546m, 433m, 414m.

2.2.1.4 Synthesis of *CUCYTCL-B*

0.1 mmol of $\text{CuCl}_2 \cdot 2\text{H}_2\text{O}$ (0.0170 g) dissolved in 5 mL methanol was added dropwise to a solution of 35 mL methanol containing 0.2 mmol of cytosine (0.0230 g) and 0.2 mmol hydrochloric acid. A blue precipitate appeared on stirring while heating for 10 minutes. The reaction mixture was stirred for one hour at 80 °C. The precipitate was filtered off. X-ray diffraction data showed that this precipitate corresponds to the previously reported compound $[\text{CuCl}_2(\text{C}_4\text{H}_5\text{N}_3\text{O})_2]$.^{91,94} The still blue coloured mother

liquid was left evaporating at room conditions and after one week, purple good quality single crystals of **CUCYTCL-B** started appearing.

Yield: 15%, Anal. Calcd (found) for $C_8H_{10}Cl_2CuN_6O_2$: C, 26.94 (26.99); H, 2.83 (2.75); N, 23.56 (23.62), Cu, 17.82(17.87). IR selected data (KBr, cm^{-1}): 3373s, 3340s, 3163s, 2960w, 2880w, 1720w, 1680m, 1683s, 1630vs, 1519s, 1497s, 1463w, 1441w, 1419w, 1402w, 1383w, 1363m, 1294m, 1261w, 1230s, 1214s, 1136m, 1100s, 861w, 813w, 795m, 776s, 762m, 667m, 616w, 591w, 576w, 564m, 537m, 447s, 434w.

2.2.1.5 Synthesis of CUCYTBR

Single crystals of this compound were grown by the addition of a solution of 0.1 mmol of $CuBr_2$ (0.0248 g) in 5 mL propanol into a 35 mL propanolic solution of 0.2 mmols of cytosine (0.0230 g). Green single crystals were formed on three weeks of slow evaporation.

Yield: 35%, Anal. Calcd (found) for $C_8H_{10}Br_2CuN_6O_2$: C, 21.57 (26.51); H, 2.26(2.34); N, 18.86 (18.97), Cu, 14.26 (14.17). IR selected data (KBr, cm^{-1}): 3448vs, 3377vs, 3177s, 3066w, 2866w, 1627vs, 1515s, 1466w, 1435w, 1380s, 1280w, 1262w, 1217m, 1137w, 1102w, 1022w, 986w, 857w, 791m, 746m, 608w, 560sh, 422m.

2.2.1.6 Synthesis of CUCYTSO4

Single crystals were grown by layering a methanolic solution of 0.2 mmol of cytosine (0.0223 g in 20 mL methanol) over 0.1 mmol $CuSO_4 \cdot 5H_2O$ (0.0270 g) dissolved in 15 mL methanol. Purple single crystals started growing on slow diffusion over one week time. The crystals decomposed upon removal from the mother liquid.

Yield: 20%, Anal. Calcd (found) for $C_{20}H_{36}CuN_{12}O_{12}S$: C, 32.81 (32.76); H, 4.96 (4.91); N, 22.96 (22.99); Cu, 8.68 (8.63). IR selected data (KBr, cm^{-1}): 3372s, 3171s, 1727s, 1651s, 1637s, 1516m, 1496w, 1460w, 1403w, 1383m, 1286w, 1233m, 1196w, 1113s, 1086s, 1013w, 963w, 876w, 780m, 756w, 616m, 601w, 577m, 531m, 484w, 426w.

2.3 RESULTS AND DISCUSSION

2.3.1 Crystallographic analysis

X-ray diffraction data of single crystals were collected at 100(2) K on an Oxford Diffraction Xcalibur diffractometer (Mo-K α λ = 0.71073 Å) and an Agilent

Technologies Supernova (Cu-K α $\lambda = 1.54184$ Å). The data reduction was done with CrysAlis RED¹¹⁰ program. Structures were solved by direct methods using the SIR92 program¹¹¹ and refined by full-matrix least-squares on F² including all reflections (SHELXL97).¹¹² All calculations were performed using the WINGX crystallographic software package.¹¹³ Crystal data and details of the refinement procedure are given in Table 2.2.

¹¹⁰ CrysAlis PRO, version 1.171.33.55; Oxford Diffraction: Wroclaw, Poland, 2010.

¹¹¹ Altomare, A. et. al. *J. Appl. Cryst.* **1993**, 26, 343.

¹¹² Sheldrick, G. M. SHELXL-97, *Programs for X-ray Crystal Structure Refinement*; University of Göttingen: Göttingen, Germany, 1997.

¹¹³ Farrugia, L. J. *J. Appl. Cryst.* **1999**, 32, 837.

Table 2.2: Single crystal data and structural refinement details of metal–cytosine compounds.

Compound	<i>COCYTCL</i>	<i>COCYTBR</i>	<i>ZNCYTCL</i>	<i>CUCYTCL-B</i>	<i>CUCYTBR</i>	<i>CUCYTSO4</i>
Empirical formula	C ₁₆ H ₂₂ Cl ₄ CoN ₁₂ O ₄	C ₈ H ₁₀ Br ₂ CoN ₆ O ₂	C ₈ H ₁₀ Cl ₂ N ₆ O ₂ Zn	C ₈ H ₁₀ Cl ₂ CuN ₆ O ₂	C ₈ H ₁₀ Br ₂ CuN ₆ O ₂	C ₂₀ H ₃₆ CuN ₁₂ O ₁₂ S
Formula weight	647.19	440.97	358.49	356.66	445.58	732.21
λ (Å)	0.71073	0.71073	1.54184	0.71073	0.71073	0.71073
T (K)	100(2)	100(2)	100(2)	100(2)	100(2)	100(2)
Crystal system	monoclinic	triclinic	triclinic	triclinic	monoclinic	tetragonal
Space group	<i>C</i> 2/ <i>c</i>	<i>P</i> $\bar{1}$	<i>P</i> $\bar{1}$	<i>P</i> $\bar{1}$	<i>P</i> 2 ₁ / <i>n</i>	<i>P</i> 4 ₃ 2 2
a (Å)	6.9633(3)	7.1279(7)	7.0087(11)	6.7760(8)	8.4897(2)	10.3967(1)
b (Å)	15.1746(7)	7.7441(8)	7.5786(10)	6.8411(8)	13.8536(4)	10.3967(1)
c (Å)	23.6381(9)	12.3208(12)	12.277(2)	8.0166(9)	10.7710(3)	27.4900(5)
α (°)	90	87.112(8)	85.740(10)	69.905(9)	90.00	90.00
β (°)	93.819(5)	74.907(8)	75.120(10)	87.064(9)	91.842(2)	90.00
γ (°)	90	87.604(8)	87.470(10)	62.633(8)	90.00	90.00
V (Å ³)	2492.18(18)	655.51(11)	628.29(16)	307.38(6)	1266.15(6)	2971.43(7)
Z	4	2	2	1	4	4
ρ_{calcd} (g cm ⁻³)	1.725	2.234	1.895	1.927	2.337	1.637
μ (mm ⁻¹)	1.170	7.411	6.730	2.218	8.044	0.887
Reflections collected	5386	3730	2070	5287	12426	6234
Unique data/parameters	2398/168	2467/172	1460/172	1660/88	3687/172	3145/212
R _{int}	0.0349	0.0745	0.0390	0.0566	0.0379	0.0207
Goodness of fit (S) ^[a]	0.888	0.768	0.967	1.036	0.904	1.060
R1 ^[b] /wR2 ^[c] [I > 2 σ (I)]	0.0337/0.0695	0.0397/0.0660	0.0594/0.1457	0.0375/0.870	0.0262/0.0536	0.0330/0.0780
R1 ^[b] /wR2 ^[c] [all data]	0.0545/0.0719	0.0695/0.0690	0.0728/0.1579	0.0494/0.0900	0.0416/0.0547	0.0355/0.0791

[a] $S = [\sum w(F_o^2 - F_c^2)^2 / (N_{\text{obs}} - N_{\text{param}})]^{1/2}$. [b] $R1 = \sum ||F_o| - |F_c|| / \sum |F_o|$. [c] $wR2 = [\sum w(F_o^2 - F_c^2)^2 / \sum wF_o^2]^{1/2}$; $w = 1/[\sigma^2(F_o^2) + (aP)^2 + bP]$ where $P = (\max(F_o^2, 0) + 2F_c^2)/3$ with $a = 0.0314$ (*COCYTCL*); $a = 0.0021$ (*COCYTBR*); $a = 0.1147$ (*ZNCYTCL*); $a = 0.0536$ (*CUCYTCL*); $a = 0.0229$ (*CUCYTBR*); $a = 0.0352$, $b = 1.7493$ (*CUCYTSO4*).

2.3.2 Structural Description

2.3.2.1 Structure of *COCYTCL*

The crystal structure of this compound consists of $[\text{CoCl}_4]^{2-}$ units, cytosinium counterions (H_2Cyt^+) and neutral cytosine molecules (HCyt). Figure 2.6 depicts the ortep drawing of these building units, showing their labelling scheme. The $[\text{CoCl}_4]^{2-}$ anion, that lies on a two fold axis, presents the usual tetrahedral geometry with Co–Cl bond distances and Cl–Co–Cl bond angles around 2.25–2.28 Å and 106–120°, respectively (Table 2.3). The continuous shape measurements (CSHM) carried out by the program SHAPE¹¹⁴ show a geometry close to an ideal tetrahedron ($S_{\text{tetrahedron}}$: 0.31 and S_{square} : 28.68).

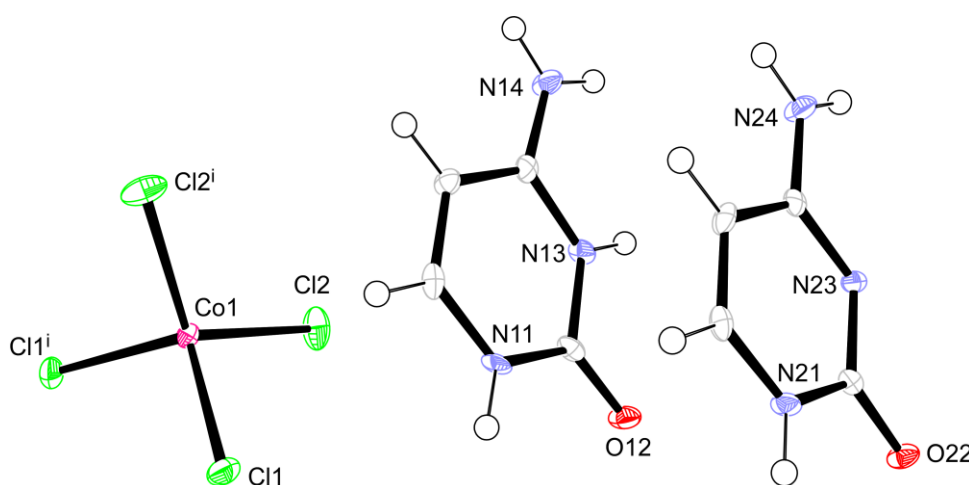


Figure 2.6: Building units of compound *COCYTCL* showing the labelling scheme.

Table 2.3: Selected coordination bond lengths (Å) and angles (°) in compound *COCYTCL*.

Co1–Cl1	2.2813(8)	Cl1–Co1–Cl1 ⁱ	110.80(4)	Cl1–Co1–Cl2i ⁱ	106.46(3)
Co1–Cl2	2.2584(7)	Cl1–Co1–Cl2	106.62(3)	Cl2–Co1–Cl2 ⁱ	119.82(5)

Symmetry code: (i) $-x, y, -z+3/2$.

The overall structure is dominated by electrostatic interactions and by supramolecular hydrogen bonding interactions established between the *1H,3H*-cytosinium cation and the neutral *1H*-cytosine molecule through their Watson–Crick and sugar edges (Figure 2.7, Table 2.4). These complementary interactions give rise to zig–zag supramolecular ribbons in which neutral and cationic cytosine molecules alternate. In fact,

¹¹⁴ Llunell, M. et al. SHAPE v1.7, 2010

the protonation of N3 in cytosinium makes its Watson–Crick edge to be fully complementary (three simultaneous hydrogen bonds) with the non protonated Watson–Crick edge of the neutral cytosine. These cationic ribbons establish additional interactions with the $[\text{CoCl}_4]^{2-}$ entity through N14–H \cdots Cl1, C25–H \cdots Cl1 and C26–H \cdots Cl2 hydrogen bonds. Additionally, adjacent supramolecular ribbons establish off–set face–to–face π – π stacking interactions (Table 2.4) to reinforce the 3D supramolecular structure.

Table 2.4: Supramolecular interactions (Å, °) of *COCYTCL*.

Hydrogen bonding interactions. ^[a]					
<i>D</i> – <i>H</i> \cdots <i>A</i> ^[b]	<i>H</i> \cdots <i>A</i>	<i>D</i> \cdots <i>A</i>	<i>D</i> – <i>H</i> \cdots <i>A</i>		
N11–H11 \cdots O22 ⁱ	1.97	2.818(3)	169		
N13–H13 \cdots N23 ⁱⁱ	2.00	2.857(3)	171		
N14–H14A \cdots O22 ⁱⁱ	1.92	2.783(3)	178		
N14–H14B \cdots Cl1 ⁱⁱⁱ	2.43	3.272(2)	166		
N21–H21 \cdots O12 ⁱ	1.92	2.781(3)	176		
N24–H24A \cdots O12 ⁱⁱ	2.10	2.944(3)	168		

π – π stacking interactions. ^[c]					
Ring \cdots Ring ^[d]	Angle	DC	α	DZ	DXY
H ₂ Cyt1–HCyt2	2.84(12)	3.745(1)	30.5	3.210(1)	1.923
HCyt2–H ₂ Cyt1	2.84(12)	3.745(1)	31.0	3.226(1)	1.902
HCyt2–HCyt2 ^{iv}	0	3.447(2)	21.3	3.213(1)	1.249

[a] Symmetry: (i) $-x+1, -y, -z+1$; (ii) $-x+1/2, -y+1/2, -z+1$; (iii) $-x+1/2, y+1/2, -z+3/2$; (iv) $-x+3/2, -y+1/2, -z+1$. [b] **D**: donor, **A**: acceptor. [c] Angle: Dihedral angle between planes I and J (°), DC: Distance between ring centroids (Å), α : Angle Cg(I) \rightarrow Cg(J) vector and normal to plane I (°), DZ: Perpendicular distance of Cg(I) on ring J (Å), DXY: Slippage. [d] H₂Cyt1: N11, C12, N13, C14, C15, C16; HCyt2: N21, C22, N23, C24, C25, C26.

The analysis of the crystal structure shows that employing an acidic media for the synthesis of materials based on the complementary hydrogen interactions between cytosine coordinated discrete complexes is not a good option. First of all, it promotes the protonation of the cytosine reducing its capability to coordinate metal centre, and secondly the combination of cytosinium cation and cytosine neutral molecule allows establishing a very stable complementary hydrogen bonding interaction that involves Watson–Crick edge which inhibits or at least makes difficult the coordination of the neutral cytosine to the metal center. In other words, the two easy coordinating positions are protonated (N1) or involved in the above mentioned hydrogen bonding interaction (N3). In fact, other previous studies have shown that the direct binding of a *3d* transition metal to the iminic nitrogen atoms of the nucleobases is rather unusual as a result of the competition between

H bonds to form direct cytosine–cytosine base pairing and the Co–cytosine coordination bond.⁹¹

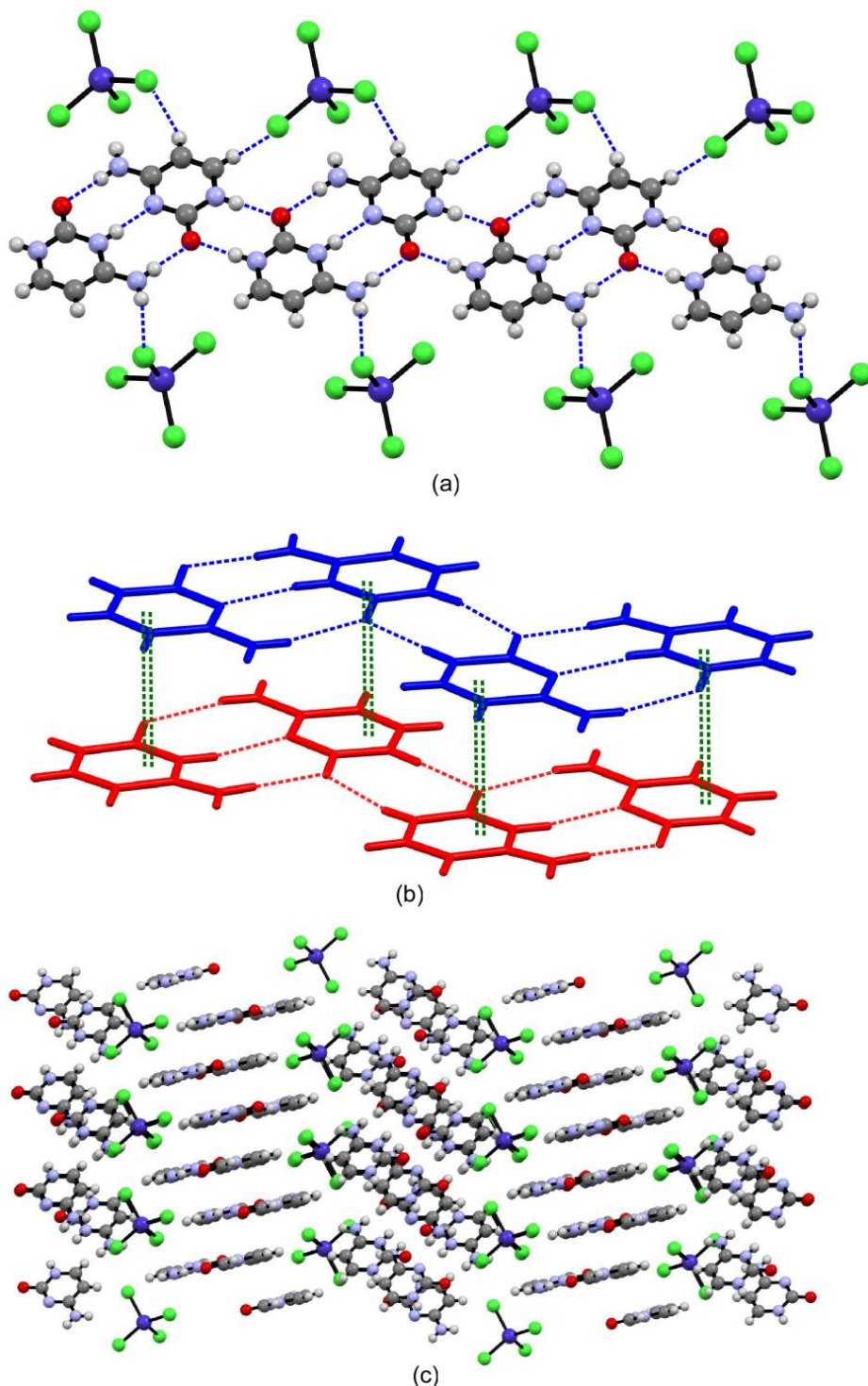


Figure 2.7: (a) Supramolecular ribbons of cytosinium cations and cytosine molecules. (b) π – π stacking interactions among adjacent supramolecular ribbons. (c) Crystal packing of *COCYTCL* viewed along $[1\bar{1}0]$ direction. Single dashed lines indicate H–bonds whereas double dashed ones correspond to π – π stacking interactions.

2.3.2.2 Structures of *COCYTBR* and *ZNCYTCL*

The synthesis in non-acidic media permits the coordination of the cytosines through N3 donor positions to give neutral $[\text{CoBr}_2(\text{C}_4\text{H}_5\text{N}_3\text{O})_2]$ or $[\text{ZnCl}_2(\text{C}_4\text{H}_5\text{N}_3\text{O})_2]$ entities (Figure 2.8). The complex units show a distorted tetrahedral geometry [$S_{\text{tetrahedron}}$: 0.67 and S_{square} : 29.09 for *COCYTBR*; $S_{\text{tetrahedron}}$: 0.46 and S_{square} : 29.23 for *ZNCYTCL*]. The coordination of the cytosine is reinforced by an intramolecular N–H···X hydrogen bond involving the amine group. These structures are isostructural to those of $[\text{CoCl}_2(\text{C}_4\text{H}_5\text{N}_3\text{O})_2]$,¹¹⁵ $[\text{ZnBr}_2(\text{C}_4\text{H}_5\text{N}_3\text{O})_2]$ ¹⁰⁸ and $[\text{CdBr}_2(\text{C}_4\text{H}_5\text{N}_3\text{O})_2]$ ¹¹⁶ complexes.

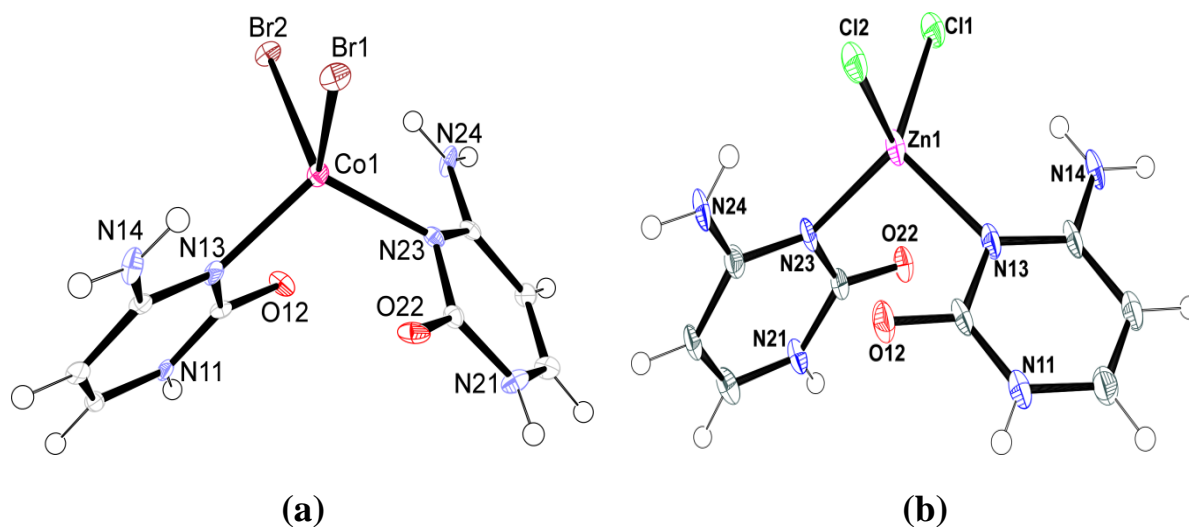


Figure 2.8: Ortep drawing of (a) $[\text{CoBr}_2(\text{C}_4\text{H}_5\text{N}_3\text{O})_2]$ and (b) $[\text{ZnCl}_2(\text{C}_4\text{H}_5\text{N}_3\text{O})_2]$ entities in *COCYTBR* and *ZNCYTCL*, respectively.

The coordination bond distances for Co–N and Zn–N are around 2.037–2.049 Å and 2.045–2.056 Å, respectively, while the Co–Br and Zn–Cl distances are 2.435–2.449 Å and 2.274 and 2.287 Å, respectively. The angles around the metal centre are wider for X–M–X than for N–M–N, which is in agreement with the greater size of halide in comparison with the nitrogen donor atom (Table 2.5).

The cytosine ligands expose the sugar and Hoogsteen edges outwards the monomeric entity, being ready to establish hydrogen bonding interactions. Only one of the coordinated cytosine is able to establish double complementary hydrogen bonds with the sugar edge of an adjacent cytosine. This allows the formation of supramolecular dimers of these discrete

¹¹⁵ Tran Qui, D.; Bagieu, M. *Acta Crystallogr. Sect. C: Cryst. Struct. Commun.* **1990**, *46*, 1645.

¹¹⁶ Muthiah, P. T. et al. *Acta Crystallogr. Sect. E, Struct. Rep. Online*, **2001**, *E57*, m558.

entities (Figure 2.9a), but it is far from the final goal of obtaining a 3D self assembled material through complementary hydrogen bonding interactions. However, taking into account that in compound *COCYTCL*, we could not achieve even a metal–nucleobase discrete entity, compounds *COCYTBR* and *ZNCYTCL* can be considered as a step forward in the intended direction.

Table 2.5: Selected coordination bonds (Å) and angles (°) in compounds *COCYTBR* and *ZNCYTCL*.

<i>COCYTBR</i>				<i>ZNCYTCL</i>			
Co1–Br1	2.4487(12)	Br1–Co1–Br2	102.21(4)	Zn1–Cl1	2.287(2)	Cl1–Zn1–Cl2	105.44(7)
Co1–Br2	2.4353(11)	Br1–Co1–N13	114.39(14)	Zn1–Cl2	2.274(2)	Cl1–Zn1–N13	115.04(17)
Co1–N13	2.049(5)	Br1–Co1–N23	111.41(15)	Zn1–N13	2.056(5)	Cl1–Zn1–N23	111.64(19)
Co1–N23	2.037(5)	Br2–Co1–N13	102.84(15)	Zn1–N23	2.045(5)	Cl2–Zn1–N13	104.09(19)
		Br2–Co1–N23	114.77(14)			Cl2–Zn1–N23	114.33(17)
		N13–Co1–N23	110.78(19)			N13–Zn1–N23	106.3(2)

Anyway, on moving forward with the supramolecular crystal structure of this compound, it can be observed that the 3D cohesiveness is ensured by π – π stacking interactions and a exhaustive network of non complementary hydrogen bonding interactions taking place between the sugar edge of the second cytosine, the amine group of the cytosines and the bromide anions of adjacent complex entities (Figure 2.9b–d; Table 2.6).

Table 2.6: Supramolecular interactions (Å, °) of *COCYTBR/ZNCYTCL*.

Hydrogen bonding interactions.^[a]

<i>D–H...A</i> ^[b]	<i>H...A</i>	<i>D...A</i>	<i>D–H...A</i>
N11–H11...O12 ⁱ	1.89/1.98	2.740(6)/ 2.784(8)	162/151
N14–H14A...Br1/Cl1	2.73/2.56	3.588(5)/ 3.419(6)	165/165
N14–H14B...Br2 ⁱⁱ /Cl2 ⁱⁱ	3.12/3.32	3.877(5)/ 4.024(6)	146/139
N21–H21...Br1 ⁱⁱⁱ /Cl1 ⁱⁱⁱ	2.65/2.54	3.434(5)/ 3.326(6)	150/149
N24–H24A...Br2/Cl2	2.62/2.46	3.455(5)/ 3.281(6)	158/155
N24–H24B...O22 ^{iv}	2.16/2.10	2.995(7)/ 2.928(7)	158/156

π - π stacking interactions.^[c]

Ring...Ring ^[d]	Angle	DC	α	DZ	DXY
HCyt1–HCyt1 ^v (<i>COCYTBR</i>)	0	3.557(3)	23.71	3.257(2)	1.430
HCyt1–HCyt1 ^v (<i>ZNCYTCL</i>)	0	3.576(4)	25.56	3.226(3)	1.543

[a] Symmetry: (i) $-x+1, -y, -z$; (ii) $-x, -y+1, -z$; (iii) $x, y-1, z$; (iv) $x+1, y, z$; (v) $-x, -y, -z$. [b] **D**: donor, **A**: acceptor. [c] Angle: Dihedral angle between planes I and J ($^{\circ}$), DC: Distance between ring centroids (\AA), α : Angle Cg(I) \rightarrow Cg(J) vector and normal to plane I ($^{\circ}$), DZ: Perpendicular distance of Cg(I) on ring J (\AA), DXY: Slippage. [d] HCyt1: N11, C12, N13, C14, C15, C16.

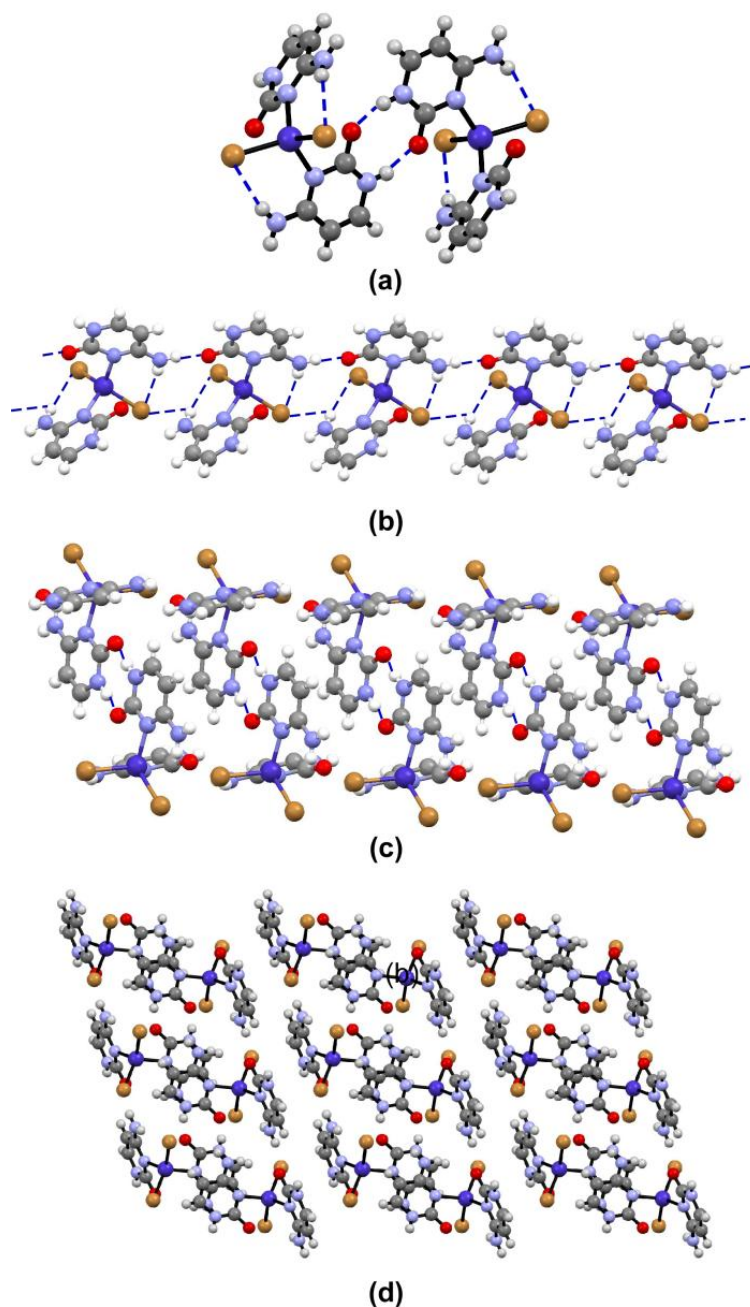


Figure 2.9: (a) Supramolecular dimeric entity. (b) Infinite chains joined by non-complementary supramolecular interactions. (c) Supramolecular ladder like chains as the result of hydrogen bonding interactions. (d) Crystal packing of *COCYTBR* viewed along the crystallographic b axis.

2.3.2.3 Structure of *CUCYTCL-B*

The crystal structure of compound *CUCYTCL-B* contains $[\text{CuCl}_2(\text{C}_4\text{H}_5\text{N}_3\text{O})_2]$ neutral units. Previously, Tran Qui and Palacios reported the crystal structure of a different polymorph of the same compound, $[\text{CuCl}_2(\text{C}_4\text{H}_5\text{N}_3\text{O})_2]$ (*CUCYTCL-A*).⁹¹ The synthesis procedure seems to indicate that *CUCYTCL-A* corresponds to a kinetically preferred crystal structure, as it is obtained immediately after mixing the reagents. The crystal structure of the novel polymorph that is reported here (*CUCYTCL-B*) seems to correspond to the thermodynamically preferred one as it is obtained upon slow evaporation of the mother liquid after filtering out the blue powder belonging to *CUCYTCL-A*. We have also performed several attempts modifying the synthesis temperature but in all cases the result is the same: first *CUCYTCL-A* precipitates out and crystals belonging to *CUCYTCL-B* appears only after subsequent slow evaporation of the filtrate. Additionally, we have performed thermodiffraction measurements to identify any possible phase transition between the two polymorphs but both of them remain unaltered upon cooling or moderate heating. The crystal structure of both polymorphs is comprised of $[\text{CuCl}_2(\text{C}_4\text{H}_5\text{N}_3\text{O})_2]$ complexes in which the central copper(II) ion is coordinated to two chloride ions and to the endocyclic N3 nitrogen atom of two cytosine molecules. However, the space group changes from $P2_1/n$ to $P\bar{1}$. However, both crystal structures show a nearly planar copper(II) coordination environment, the deviation from the ideal geometry is greater for the first polymorph than for *CUCYTCL-B* [*CUCYTCL-A*: S_{square} : 2.37 and $S_{\text{tetrahedron}}$: 27.50; *CUCYTCL-B*: S_{square} : 0.57 and $S_{\text{tetrahedron}}$: 33.71]. In both crystal structures, the cytosine mean plane is twisted with respect to the coordination mean plane, with dihedral angles of 88.38/84.56° for *CUCYTCL-A* and 75.96° for *CUCYTCL-B*. The two coordinated cytosines are strictly coplanar for *CUCYTCL-B* and nearly coplanar for *CUCYTCL-A* (dihedral angle of 7.56°). Additionally, *CUCYTCL-A* presents an intramolecular hydrogen bond, which is not present in *CUCYTCL-B*. This could be probably because of the shortening of the coordination bond distances (Table 2.7; Figure 2.10a–b) that generates a greater steric hindrance which hinders the amine and keto groups of the two coordinated cytosines to get closer enough to establish hydrogen bonding interactions. The presence of the intramolecular hydrogen bond in the compound *CUCYTCL-A*, deviates the N–Cu–N angle from 180° and as a consequence significant differences can also be observed at the semi-coordination contacts: two contacts are found for *CUCYTCL-B* but only one, although shorter, is present in *CUCYTCL-A*. Figure 2.10c

shows a superposition of both crystal structures in which these differences are observable. The cytosine molecules of the compound *CUCYTCL-B* self assemble through complementary hydrogen bonding interactions along the sugar edges, giving rise to a 1D chain (Table 2.8, Figure 2.11).

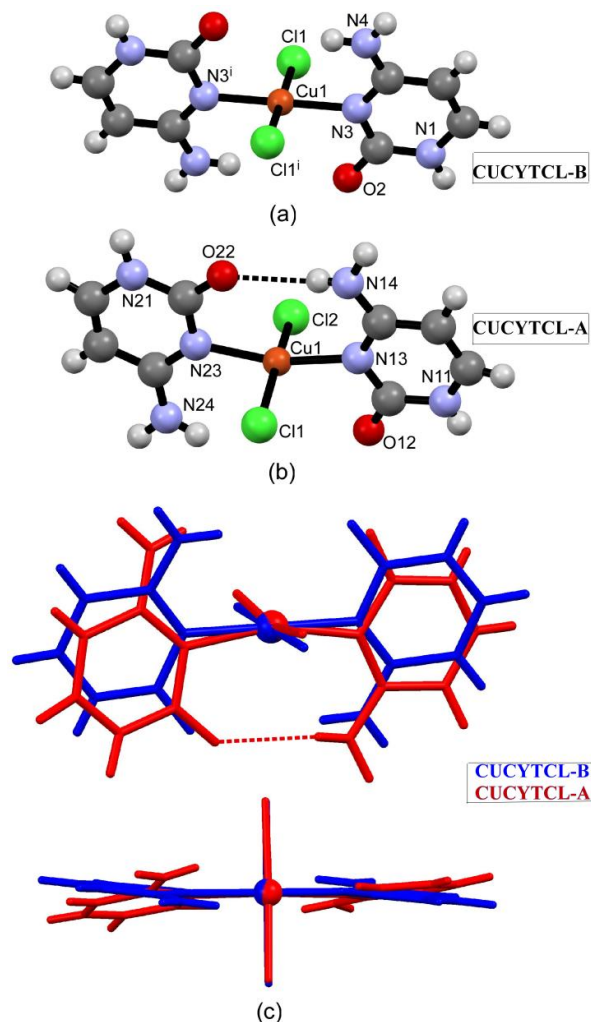


Figure 2.10: Drawing showing the structure of the $[\text{CuCl}_2(\text{C}_4\text{H}_5\text{N}_3\text{O})_2]$ discrete entity of (a) *CUCYTCL-B* and (b) *CUCYTCL-A*. (c) Overlay of both structures.

Table 2.7: Selected coordination bond lengths (\AA) and angles ($^\circ$) in compound *CUCYTCL-A*^[a] and *CUCYTCL-B*^[b]

<i>CUCYTCL-A</i> ^[a]				<i>CUCYTCL-B</i> ^[b]			
Cu1–Cl1	2.299(1)	Cl1–Cu1–Cl2	165.74(6)	Cu1–Cl1	2.2990(7)	Cl1–Cu1–Cl1 ⁱ	180(–)
Cu1–Cl2	2.267(1)	Cl1–Cu1–N13	92.17(12)	Cu1–N3	1.975(2)	Cl1–Cu1–N3 ⁱ	90.26(7)
Cu1–N13	1.985(4)	Cl1–Cu1–N23	89.66(12)	Cu1...O2	2.824(2)	Cl1 ⁱ –Cu1–N3 ⁱ	89.74(7)
Cu1–N23	1.996(3)	Cl2–Cu1–N13	92.40(12)			N3–Cu1–N3 ⁱ	180(–)
Cu1...O22	2.779(5)	Cl2–Cu1–N23	90.14(12)				
		N13–Cu1–N23	162.11(16)				

[a] Data taken from reference ⁹¹. [b] Symmetry: (i) $-x+2, -y, -z+2$.

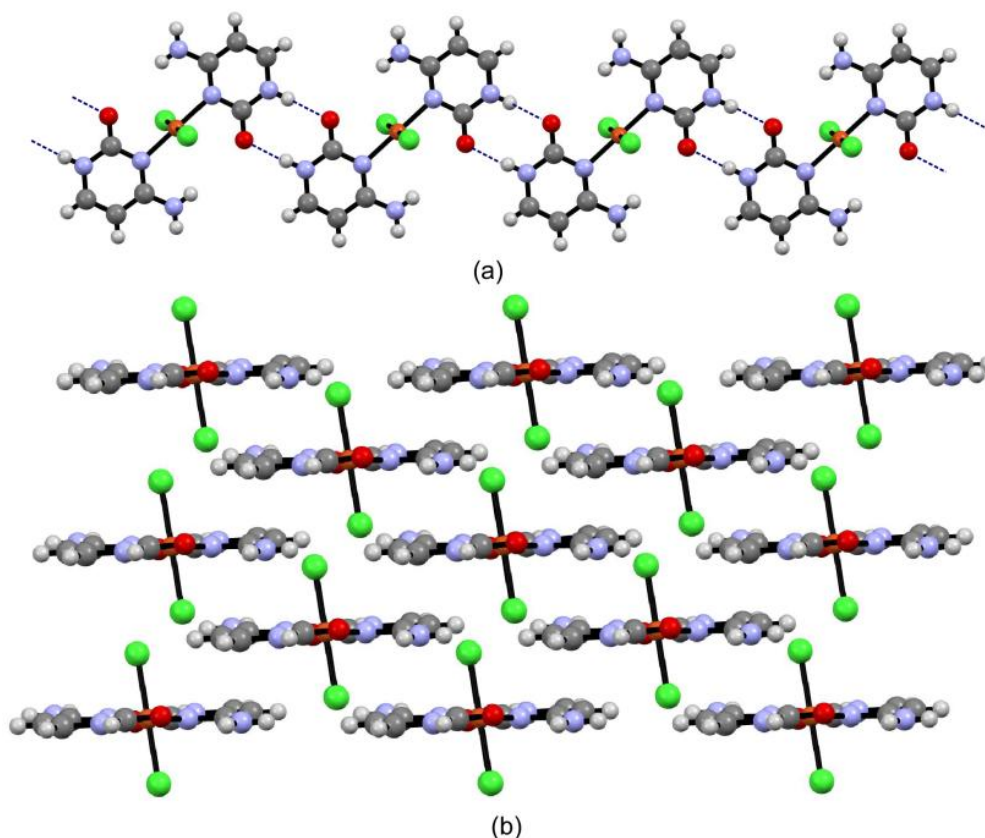


Figure 2.11: (a) Supramolecular chain of cytosine...cytosine complementary hydrogen bonded $[\text{CuCl}_2(\text{C}_4\text{H}_5\text{N}_3\text{O})_2]$ discrete entities and (b) crystal packing in *CUCYTCL-B*.

Table 2.8: Supramolecular interactions (\AA , $^\circ$) of *CUCYTCL*.

Hydrogen bonding interactions. ^[a]					
$D-H\cdots A$ ^[b]	$H\cdots A$	$D\cdots A$	$D-H\cdots A$		
$\text{N1-H1}\cdots\text{O2}^{\text{i}}$	1.93	2.784(3)	175		
$\text{N4-H4B}\cdots\text{C11}^{\text{ii}}$	2.59	3.391(2)	154		
π - π stacking interactions. ^[c]					
Ring...Ring ^[d]	Angle	DC	α	DZ	DXY
$\text{HCyt-HCyt}^{\text{iii}}$	0	3.457(2)	18.22	3.284(1)	1.081

[a] Symmetry: (i) $-x+1, -y+1, -z+1$; (ii) $x, y+1, z$; (iii) $-x+2, -y+1, -z+1$. [b] **D**: donor, **A**: acceptor. [c] Angle: Dihedral angle between planes I and J ($^\circ$), DC: Distance between ring centroids (\AA), α : Angle Cg(I) \rightarrow Cg(J) vector and normal to plane I ($^\circ$), DZ: Perpendicular distance of Cg(I) on ring J (\AA), DXY: Slippage. [d] HCyt: N11, C12, N13, C14, C15, C16.

2.3.2.4 Structure of *CUCYTBR*

The crystal structure of compound *CUCYTBR* is isostructural to the crystal structure of *CUCYTCL-A*. There is no reported case of a second polymorph isostructural to

CUCYTCL-B and the attempts to obtain this polymorph were not successful although many different synthetic conditions were tried. The crystal structure is comprised of $[\text{CuBr}_2(\text{C}_4\text{H}_5\text{N}_3\text{O})_2]$ complexes in which the central copper(II) ion is coordinated to two bromide ions and to the endocyclic N3 nitrogen atom of two cytosine molecules (Figure 2.12). Selected bond angles and bond lengths are given in Table 2.9. Due to the greater steric hindrance of the bromide ions in comparison to chloride, the coordination geometry is more distorted but still closer to a square planar one than to a tetrahedron [S_{square} : 2.54 and $S_{\text{tetrahedron}}$: 23.14]. The two coordinated cytosines are nearly coplanar (dihedral angle of 7.45°) but almost perpendicular to the coordination mean plane with dihedral angles of 84.13° and 88.72° . An intramolecular hydrogen bond is established between the amino and keto groups of the two coordinated cytosine molecules at one side of the complex but not at the other. The supramolecular crystal structure is like that of the previously described example *CUCYTCL-A*. The hydrogen bonding parameters are given in Table 2.10.

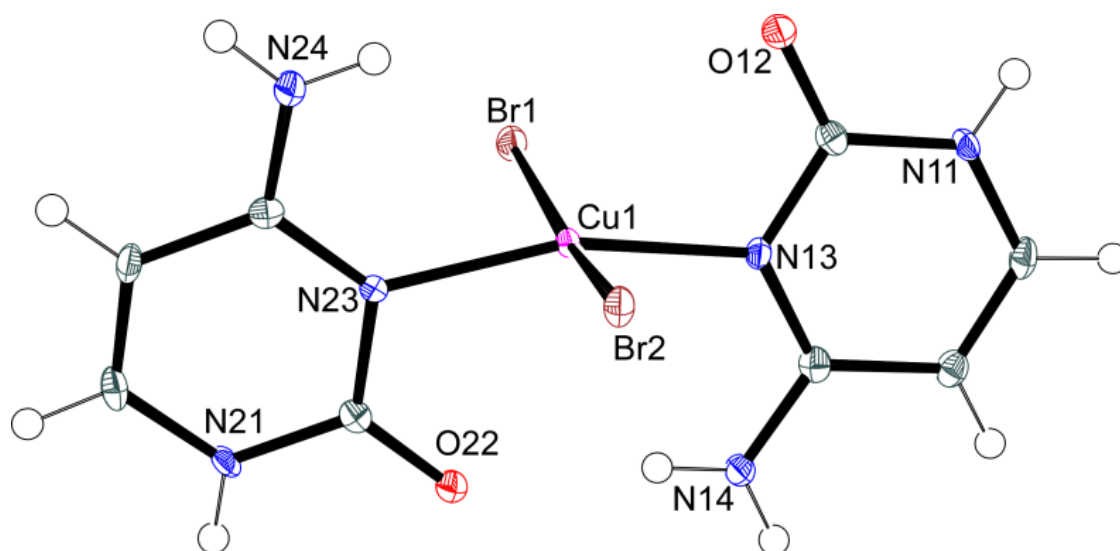


Figure 2.12: Ortep drawing of $[\text{CuBr}_2(\text{C}_4\text{H}_5\text{N}_3\text{O})_2]$ complex with labelling scheme.

Table 2.9: Selected coordination bond lengths (Å) and angles ($^\circ$) in compound *CUCYTBR*.^[a]

Cu1–Br1	2.4024(5)	Br1–Cu1–Br2	168.03(2)
Cu1–Br2	2.4294(5)	Br1–Cu1–N13	92.62(7)
Cu1···O22	2.761(2)	Br1–Cu1–N23	89.92(7)
Cu1–N13	1.970(2)	Br2–Cu1–N13	91.80(7)
Cu1–N23	1.985(2)	Br2–Cu1–N23	89.12(7)
		N13–Cu1–N23	162.86(10)

Table 2.10: Supramolecular interactions (Å, °) of *CUCYTBR*.

Hydrogen bonding interactions. ^[a]					
<i>D–H</i> ⋯ <i>A</i> ^[b]	<i>H</i> ⋯ <i>A</i>	<i>D</i> ⋯ <i>A</i>	<i>D–H</i> ⋯ <i>A</i>		
N11–H⋯O12 ⁱ	2.01	2.843(3)	162		
N14–H⋯O22	2.12	2.976(3)	173		
N14–H⋯Br1 ⁱⁱ	2.75	3.520(2)	150		
N21–H⋯Br2 ⁱⁱⁱ	2.47	3.245(2)	150		
N24–H⋯Br2 ^{iv}	2.61	3.388(2)	151		
N24–H⋯O22	2.12	2.971(3)	170		

π – π stacking interactions. ^[c]					
Ring⋯Ring ^[d]	Angle	DC	α	DZ	DXY
HCyt1–HCyt2 ^v	6.66(14)	3.609(2)	22.62	3.439	1.388
HCyt2–HCyt1 ^{vi}	6.66(14)	3.609(2)	17.65	3.311	1.094

[a] Symmetry: (i) $-x+2, -y+1, -z$; (ii) $-x+3/2, y-1/2, -z+1/2$; (iii) $x-1/2, -y+1/2, z+1/2$; (iv) $-x+1, -y+1, -z$; (v) $1+x, y, z$; (vi) $1+x, y, z$; [b] **D**: donor, **A**: acceptor. [c] Angle: Dihedral angle between planes I and J (°), DC: Distance between ring centroids (Å), α : Angle Cg(I)→Cg(J) vector and normal to plane I (°), DZ: Perpendicular distance of Cg(I) on ring J (Å), DXY: Slippage. [d] HCyt1: N11, C12, N13, C14, C15, C16; HCyt2: N21, C22, N23, C24, C25, C26.

2.3.2.5 Structure of *CUCYTSO4*

The crystal structure of *CUCYTSO4* $\{[\text{Cu}(\text{C}_4\text{H}_5\text{N}_3\text{O})_4](\text{SO}_4) \cdot 2(\text{MeOH})\}$ consists of $[\text{Cu}(\text{HCyt})_4]^{2+}$ cationic units where the N3 nitrogen atoms of the four cytosines are coordinated to the equatorial positions of the central copper atom. These four nitrogen atoms define the equatorial plane with a maximum deviation of 0.014 Å from planarity. The metal atom is placed over a binary rotation axis and show no deviation from the equatorial mean plane. The oxygen atoms of the cytosine keto group establishes four additional short contacts of 2.6037(18) and 2.9543(17) Å to provide a relatively unusual (4 + 2) + 2 coordination surrounding (Figure 2.13; Table 2.11).

The molecular structure of the $[\text{Cu}(\text{C}_4\text{H}_5\text{N}_3\text{O})_4]^{2+}$ discrete entity is reinforced by the presence of bifurcated intramolecular hydrogen bonds among the amine and keto groups of the cytosines (Figure 2.14), which increases its rigidity with the presence of four cytosines able to establish complementary hydrogen bonding interactions through their sugar edges in four non-coplanar directions (Figure 2.15). Therefore, if the predicted supramolecular interactions would take place, the resulting material probably would be porous because of

an inefficient occupation of the space due to the rigidity of both the secondary building unit and the synthons.

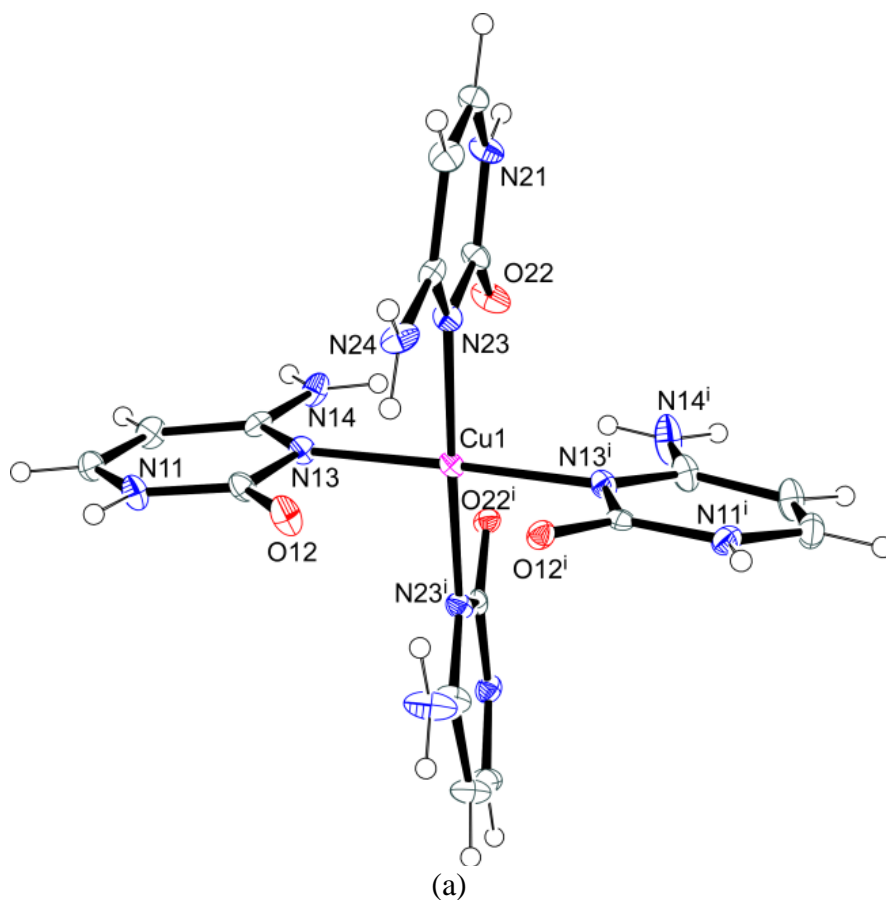


Figure 2.13: Ortep drawing of $[\text{Cu}(\text{C}_4\text{H}_5\text{N}_3\text{O})_4]^{2+}$ complex entity in *CUCYTSO4*.

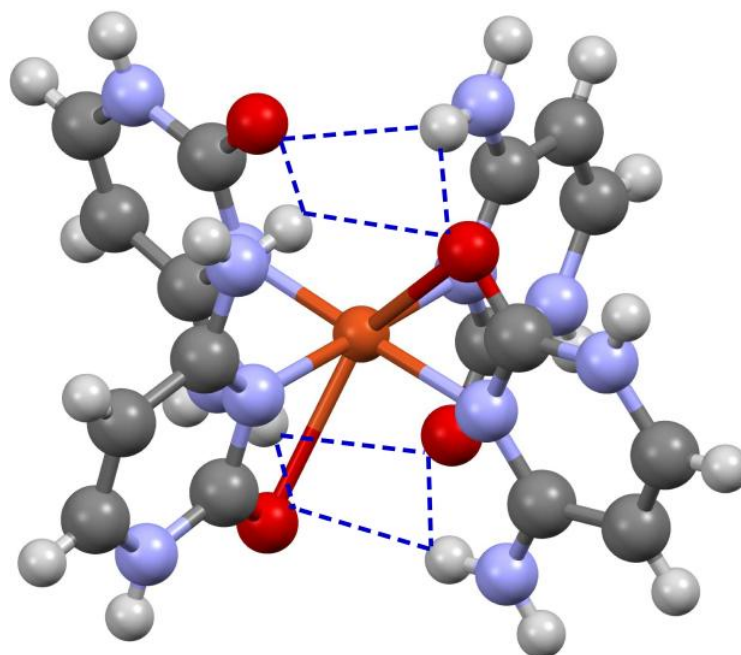


Figure 2.14: Intramolecular bifurcated hydrogen bonding.

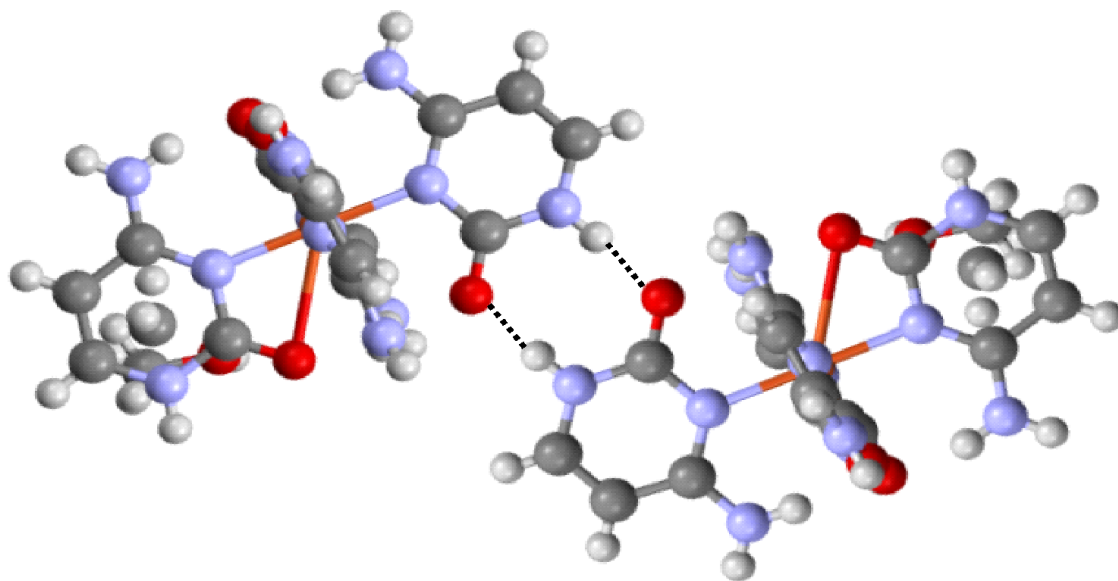


Figure 2.15: Hypothetical complementary base pairing interactions between the sugar edges of cytosine moieties in *CUCYTSO4*.

However, the presence of solvent molecules or counterions can disrupt the complementary base pairing interactions that we are trying to use as the structure directing agents. This could be especially relevant when strong hydrogen bond donor or acceptor molecules/ions are present. This happens in the case of the compound *CUCYTSO4* in which, instead of establishing the predicted cytosine...cytosine interaction, the sulphate counterion interacts with the sugar edge of the nucleobase giving rise to a different crystal structure. As a result, the interactions between adjacent cytosines follow a non conventional hydrogen bonding pattern as shown in Figure 2.16, that involves the presence of an, otherwise repulsive, close contact between keto...keto groups. This interaction gives rise to supramolecular ribbons of $[\text{Cu}(\text{C}_4\text{H}_5\text{N}_3\text{O})_4]^{2+}$ discrete entities. Methanol solvent molecules and sulphate counterions occupy the voids within the packing of the supramolecular ribbons, establishing hydrogen bonding interactions by acting as acceptors with the iminium and amine groups of the cytosine.

In addition to this complex network, there exists hydrogen bonding interactions between the oxygen atoms of the sulphate anion and solvated methanol molecule as acceptors and the N4-H and N1-H of cytosines as donors. Further, there are intermolecular interactions occurring between adjacent $[\text{Cu}(\text{C}_4\text{H}_5\text{N}_3\text{O})_4]^{2+}$ complexes in a head to tail arrangement. Hydrogen bonding parameters are given in Table 2.12.

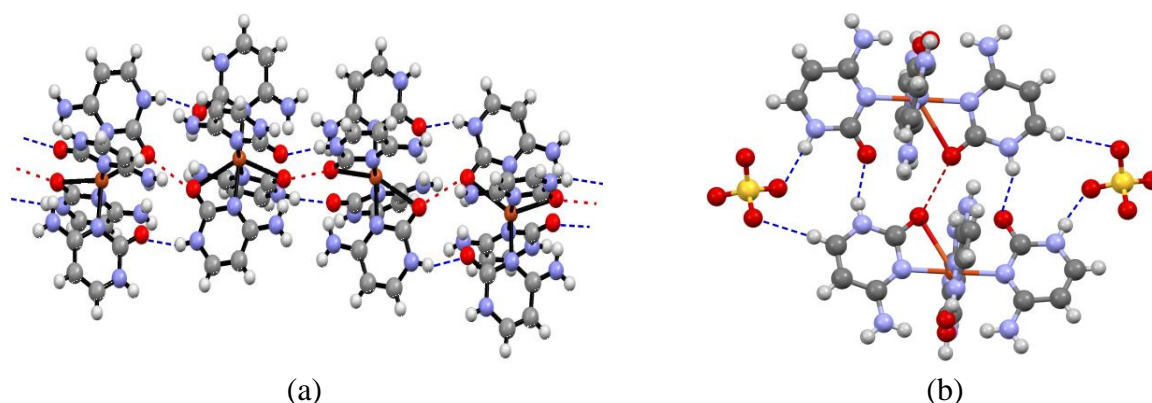


Figure 2.16: (a) Hydrogen bonding interactions between the $[\text{Cu}(\text{C}_4\text{H}_5\text{N}_3\text{O})_4]^{2+}$ complex entity in *CUCYTSO4*. (b) Hydrogen bonding interactions of the $[\text{Cu}(\text{C}_4\text{H}_5\text{N}_3\text{O})_4]^{2+}$ units with the sulphate counterions.

Table 2.11: Selected coordination bond lengths (\AA) and angles ($^\circ$) in compound *CUCYTSO4*.^[a]

Cu1–N13	2.029(2)	N13–Cu1–N13 ⁱ	90.89(13)
Cu1–N23	2.021(2)	N13–Cu1–N23	90.59(9)
Cu1···O12	2.604(2)	N13–Cu1–N23 ⁱ	178.32(9)
Cu1···O22	2.954(2)	N23–Cu1–N23 ⁱ	87.94(13)

[a]Symmetry codes: (i) $-x+2, y, -z+2$.

Table 2.12: Hydrogen bonding interactions (\AA , $^\circ$) of *COCYTSO4*.^[a]

$D-H\cdots A$ ^[b]	$H\cdots A$	$D\cdots A$	$D-H\cdots A$
N11–H11···O22 ⁱ	2.03	2.847(3)	159
N14–H14B···O3 ⁱⁱ	2.03	2.866(3)	164
N14–H14A···O12 ⁱⁱⁱ	2.30	3.000(3)	138
N14–H14A···O22	2.38	2.928(3)	122
N21–H21···O2	1.98	2.833(3)	170
N21–H21···S1	2.82	3.593(2)	151
N24–H24A···O22 ⁱⁱⁱ	2.32	2.956(3)	131
N24–H24A···O12	2.32	2.991(4)	135
N24–H24B···O4 ^{iv}	1.99	2.843(3)	172
O3–H3···O1	2.00	2.850(3)	162
O3–H3···S1	2.72	3.428(2)	138
O4–H4···O2 ^v	1.86	2.788(3)	171

[a]Symmetry codes: (i) $y, -x+2, z+1/4$; (ii) $-y+1, -x+2, -z+7/4$; (iii) $-x+2, y, -z+2$; (iv) $y, x, -z+9/4$; (v) $-x+1, y, -z+2$. [b] **D**: donor, **A**: acceptor.

As briefly described in previous paragraph, the hydrogen bonding scheme depicts that, the neighbouring monomeric units are sequentially bound by a double hydrogen bond

among the pyrimidinic proton and the exocyclic oxygen atom (N11–H11...O22). However, these array of monomers present oxygen...oxygen distances of 2.719 Å between neighbouring entities, which is relatively short and accounts for a repulsive interaction that would make the supramolecular strip unstable unless other interactions coming from the array itself or from the crystal packing overcome it. Thus, in order to determine the structural features that make these array stable in the crystal structure, geometry optimization calculations were performed on a finite structural model consisting of two interacting monomers by using dispersion-corrected density-functional theory calculations with the code DMOL3.¹¹⁷ The PBE exchange-correlation functional was used in the calculations,¹¹⁸ together with the “D2” flavour of the dispersion correction scheme proposed by Grimme.¹¹⁹ Figure 2.17 shows the computed structural model together with the numbering scheme and monitored intermolecular interactions.

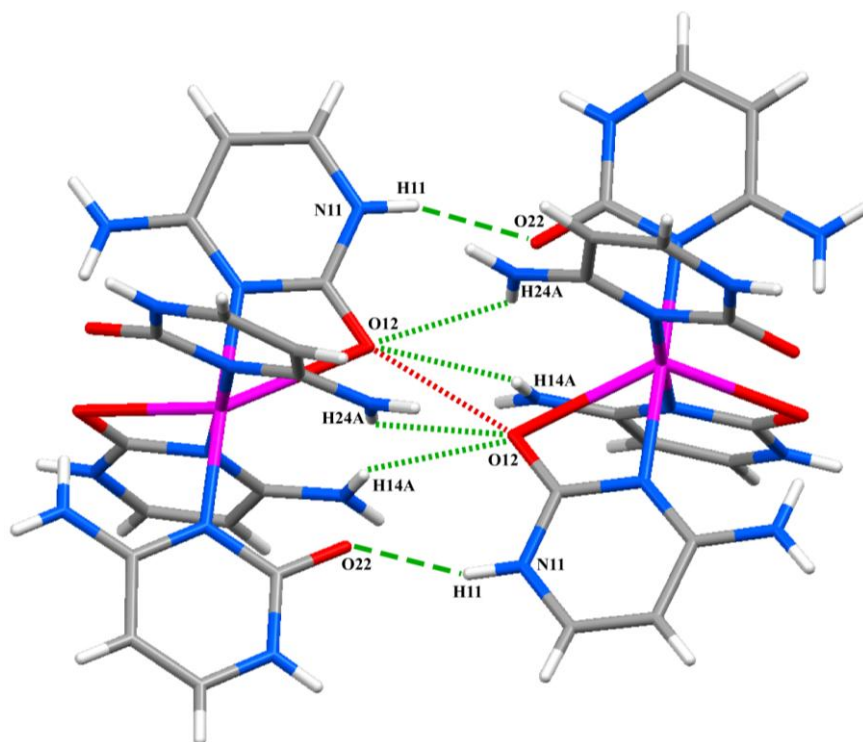


Figure 2.17: Structural model for the DFT–D geometry optimization showing the numbering scheme.

Table 2.13 shows a comparison between relevant distances belonging to the pristine crystal structure and to the computed structure. The similarity among the coordination

¹¹⁷ (a) Delley, B. J. *Chem. Phys.* **1990**, 92, 508. (b) Delley, B. J. *Chem. Phys.* **2000**, 113, 7756.

¹¹⁸ Perdew, J. P. et al. *Phys. Rev. Lett.* **1996**, 77, 3865.

¹¹⁹ Grimme, S. J. *Comput. Chem.* **2006**, 27, 1787.

bond distances (along with all the intra–monomer distances) of the optimized model and of the experimental structure supports the suitability of the employed computational method. As depicted in Figure 2.17 and Table 2.13, to assess the stability of the these supramolecular aggregates, a hydrogen bonding interaction (N11–H11···O22), three interactions of electrostatic nature (O12···O12, H14A···O12, H24A···O12) and Cu···Cu distances were considered. Figure 2.18 shows the electrostatic potential (ESP) surface and charges on selected atoms.

Table 2.13: Distances for coordination bonds and intermolecular interaction between two $[\text{Cu}(\text{Hcyt})_4]^{2+}$ in the optimized structure and crystal structure.

	Coordination bond distances (Å)		Intermolecular interactions (Å)		
	Optimized structure	Crystal structure		Optimized structure	Crystal structure
Cu1–N13	2.132	2.029	O12···O12	2.828	2.719
Cu1–N23	2.134	2.021	N11–H11···O22 ⁱ	1.875	2.029
Cu1–O12	2.650	2.604	N14–H14A···O12	2.859	2.916
Cu1–O22	2.925	2.954	N14–H24A···O12	2.409	2.717
			Cu···Cu	6.851	6.942

Symmetry code: $y, -x+2, z+1/4$

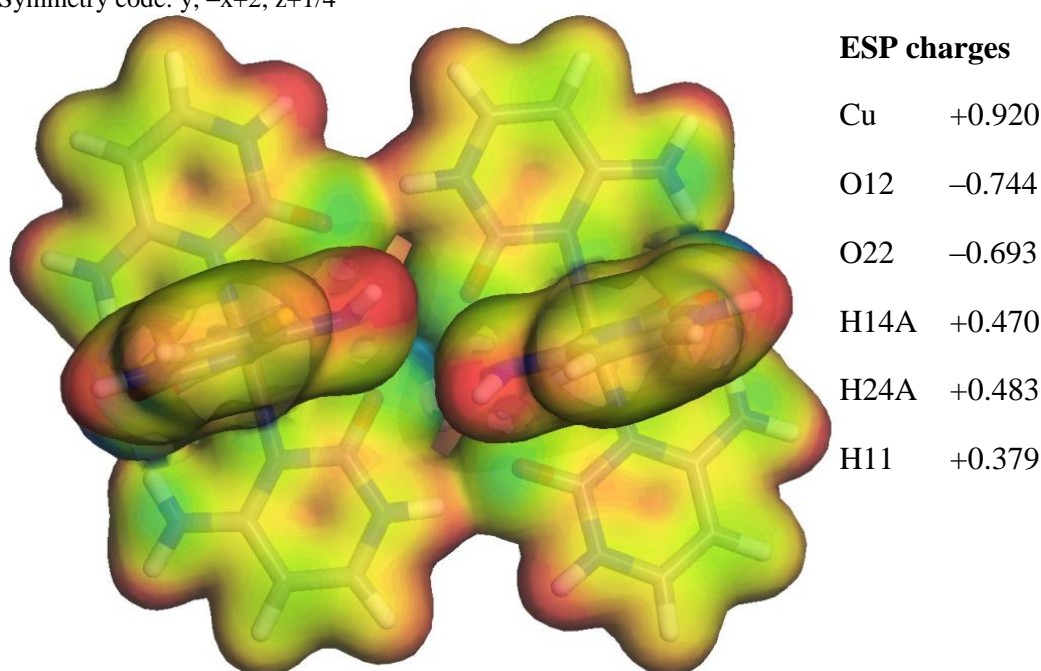


Figure 2.18: (Left) Electrostatic potential upon an electronic isosurface of 0.01 a.u. (Right) Electrostatic potential (ESP) charges for metal center and for atoms implied in the intermolecular interactions.

According to the results, the repulsive ‘oxygen···oxygen’ interaction leads to a slight increase (*ca.* 0.1 Å) of the O12···O12 distance, while the distances between all the atom pairs involved in attractive interactions are shortened by 0.1–0.3 Å. Moreover, in

agreement with Cu...Cu distance, both the entities get 0.1 Å closer when the supramolecular aggregate is relaxed, which stands for the stability of the 1D array.

2.3.3 Thermal analysis

Figure 2.19 and Table 2.14 show the thermal behaviour (TG/DTA) of the *COCYTBR*, *CUCYTCL-B* and *CUCYTBR*, performed upon synthetic air atmosphere (79% N₂, 21% O₂).

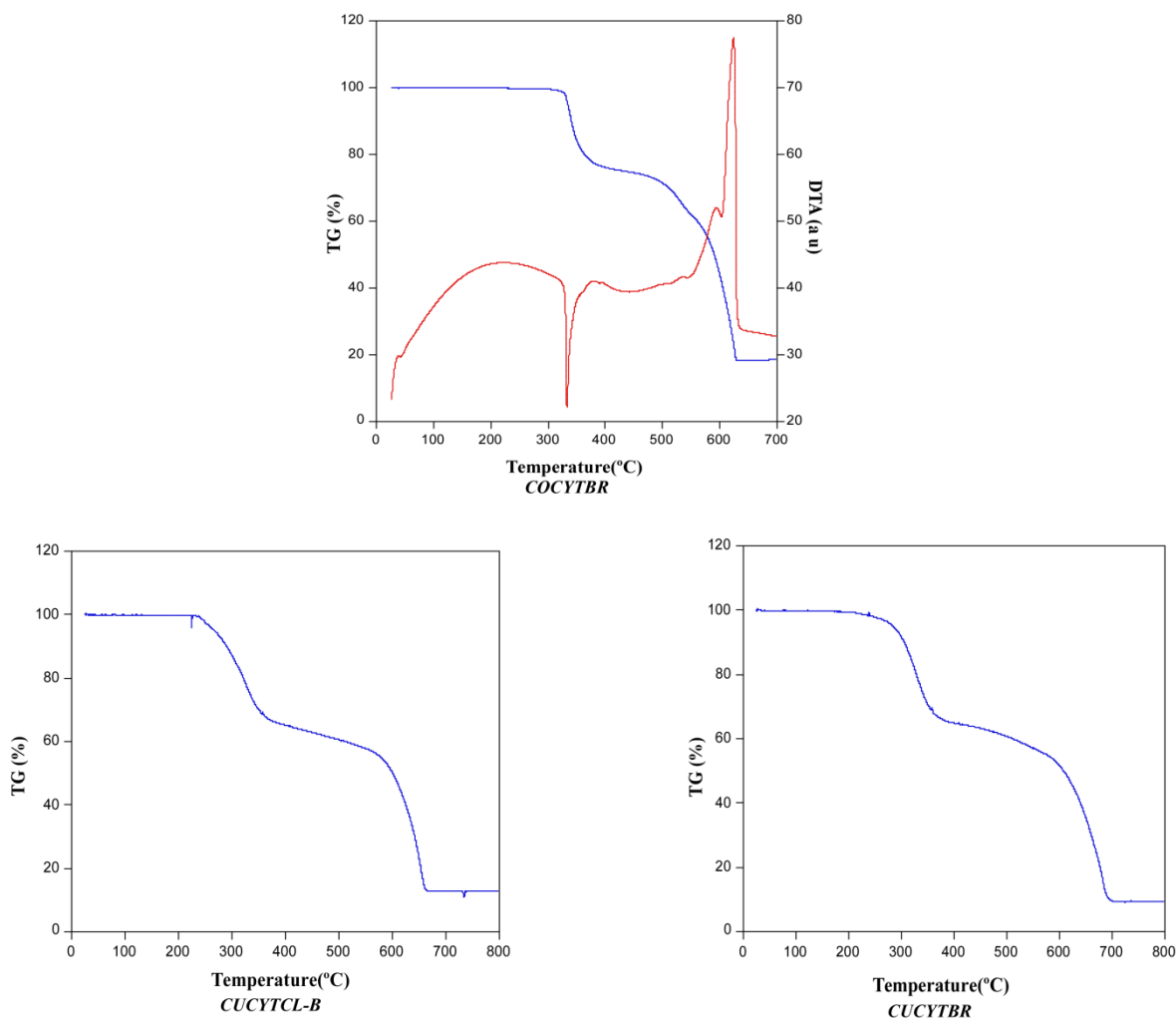


Figure 2.19: Thermogravimetric analysis of *COCYTBR*, *CUCYTCL*, *CUCYTBR*.

All three compounds present a relatively high thermal stability and start decomposing at temperatures above 250–315°C. This is a relevant aspect because although these crystal structures do not present the desired porous structure, the crystal structures of *COCYTBR*, *CUCYTCL-B* and *CUCYTBR* are composed of neutral metal–nucleobase entities that are assembled together by hydrogen bonding interactions. Therefore, these compounds could advance the thermal stability of the supramolecular porous materials that we are pursuing. On the other hand, the first decomposition stage correspond to an

endothermic process for **COCYTBR**, that may indicate it is not due to a combustion reaction, that are usually exothermic, but to an internal reaction that implies the release of some of the components of the corresponding compound probably as volatile hydrogen halide. For compounds **CUCYTCL-B** and **CUCYTBR**, a similar explanation can be assumed for this first decomposition stage. However the explanation is unsure as this step corresponds to an exothermic process for **CUCYTCL-B** and overlapped exo–endothermic processes for **CUCYTBR**. After this first stage, the thermal decomposition continues further in several, and usually overlapped, processes to provide Co_3O_4 or CuO as final residues.

Table 2.14: Thermoanalytic data for **COCYTBR**, **CUCYTCL** and **CUCYTBR**.

Step	T_i	T_f	T_{peak}	$\Delta m(\%)$	ΔH	$\Sigma \Delta m(\%)$	$\Sigma \Delta m(\%)_{theor}$
COCYTBR							
1	325	420	331	24.7	Endo	24.7	25.19(–1 $\text{C}_4\text{N}_3\text{H}_5\text{O}$)
2	440	660	624	56.97	Exo	81.67	81.79 (1/3 Co_3O_4)
CUCYTCL-B							
1	25	365	–	33	–	33.00	31.15 (–1 $\text{C}_4\text{H}_5\text{N}_3\text{O}$)
2	530	665	–	45.98	–	78.98	77.60 (CuO)
CUCYTBR							
1	25	400	–	35.17	–	35.17	36.30 (–2 HBr)
2	540	700	–	48.76	–	83.93	82.15 (CuO)

[a] T_i = initial temperature; T_f = final temperature; T_{peak} = DTA peak temperature; $\Delta m(\%)$ = mass loss percentage for each process; ΔH = process type in the basis of DTA; $\Sigma \Delta m(\%)$ = total mass loss percentage; $\Sigma \Delta m(\%)_{theor}$ = theoretical total mass loss percentage. [b] Released fragments and final residue per formula.

2.4 CONCLUSIONS

In order to achieve the first step towards our goal: a porous 3D supramolecular network sustained by complementary hydrogen bonding interactions between discrete metal–nucleobase entities, it is mandatory to use a non–acidic reaction media for cytosine. This is easy understandable as protonation reduces the cytosine coordination capabilities; but even if not all cytosines are protonated, the cytosine···cytosinium complementary hydrogen bonding interactions preclude the coordination of the remaining neutral cytosines to the metal center (**COCYTCL**). On the other hand, when cytosine is coordinated, it uses N3 position to bind metal center and therefore complementary hydrogen bonding

interactions can only take place through the sugar–edge of the cytosine (2 x N1–H and O2).

Under these conditions, if only two cytosines are coordinated, at the most 1D infinite supramolecular chains are obtained through cytosine···cytosine complementary hydrogen bonds. Depending on the coordination sphere geometry, these chains would change from zig–zag ones for tetrahedral geometry (Co^{II} metal center) to linear ones for *trans* arranged square planar geometry (Cu^{II}, *CUCYTCL–B*). Apart from that, in many cases other supramolecular interactions such as N–H···X (halide) can disrupt these complementary hydrogen bond interactions as seen in compounds *COCYTBR*, *ZNCYTCL*, *CUCYTCL–A* and *CUCYTBR*.

Taking all these previous results into account, it becomes evident that in order to achieve a 3D supramolecular material it would be necessary to increase the number of coordinated cytosines, preferably to four of them in a non–coplanar disposition. This goal was achieved with the synthesis of *CUCYTSO4*, comprised of cationic [Cu(cytosine)₄]²⁺ complexes and SO₄^{2–} counterions. However, the crystal structure of this compound did not show the predicted complementary hydrogen bonding interactions between adjacent cytosines because of the presence of the strong hydrogen bond acceptor SO₄^{2–} anions which disrupt these complementary hydrogen bonding interactions. This result shows that not only the design of the supramolecular secondary building units are important but also the presence of other hydrogen bonding competitors in the reaction media, such as counterions or even solvent molecules that could disrupt the direct hydrogen bonding interactions between the nucleobases. Therefore, it becomes clear that in order to achieve the corresponding porous 3D supramolecular network we must design not only the supramolecular building unit but also the synthetic conditions.

Other fact that has become evident is that, each cytosine molecule anchored to the metal centre through N3 (it's preferred coordination position) can only establish complementary hydrogen bonding interactions with just one adjacent cytosine, that limits connectivity and dimensionality of the resulting hydrogen bonding network. This fact makes purine nucleobases specially appealing to meet our objective, because they present more than one edge capable of establishing complementary hydrogen bonding interactions and therefore they can be connected to more than one adjacent nucleobases through hydrogen bonding. It would make easier to achieve the goal of obtaining 3D

supramolecular networks as the number of required coordinated nucleobases per metal centre is reduced.

Chapter 3

Supramolecular metal– organic frameworks based on metal/purine systems

3.1 Introduction

3.2 Synthesis and chemical characterization

3.3 Results and discussion

3.4 Conclusions

3.1 INTRODUCTION

As it was concluded in the previous chapter, using purine nucleobases as ligands take the advantage of their multiple binding and hydrogen bonding positions. It means that the nucleobase can be anchored to the metallic centres through different positions giving rise to extended systems or discrete complex entities. The first case has been previously exploited by our research group to provide MOFs sustained by coordination bonds, usually called as MBioFs.¹²⁰ There are many reported examples for discrete complex entities as those depicted in Figure 3.1.¹²¹ Those entities are able to establish complementary hydrogen bonding interactions between adjacent units as it has been seen for the cytosine analogues. However, at one hand they provide the advantage of the increased rigidity of the supramolecular building blocks, because of the coordination through multiple positions, and on the other, they present more edges capable of establishing complementary hydrogen bonding interactions. Therefore, the correct selection of the metal–nucleobase discrete entities in such a way that they provide a non coplanar disposition of the nucleobases could provide the desired supramolecular porous materials that we are looking for.

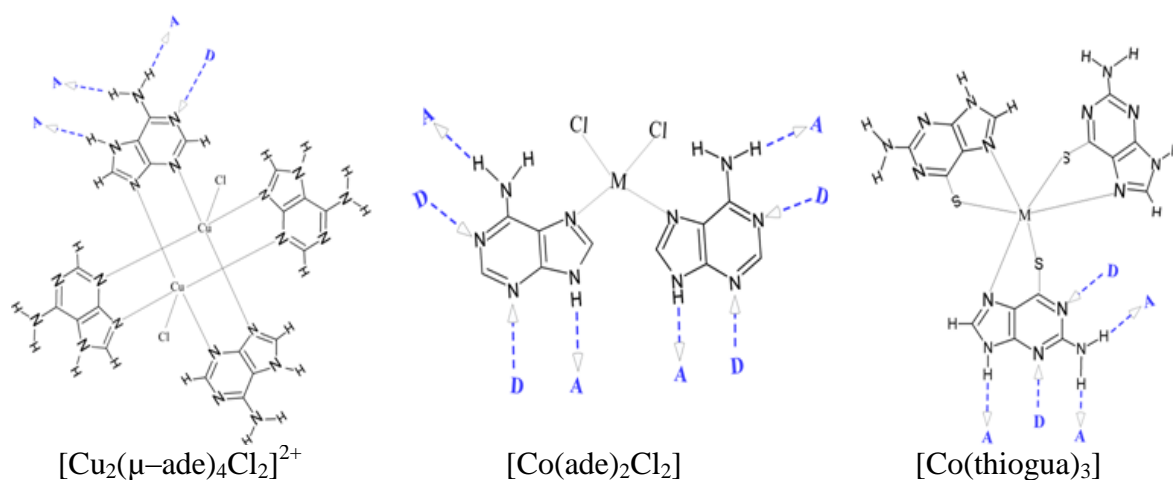


Figure 3.1: Metal–nucleobase discrete entities suitable for the synthesis of *SupraMOFs*.

¹²⁰ (a) Pérez–Yáñez, S. et al. *Chem. Commun.* **2012**, 48, 907. (b) Pérez–Yáñez, S. et al. *Cryst. Growth Des.* **2013**, 13, 3057.

¹²¹ (a) de Meester, P.; Skapski, A. C. *J. Chem. Soc. A*, **1971**, 2167. (b) Lee, C. F. et al. *J. Chem. Soc. Dalton Trans.* **1993**, 1, 467. (c) Schmalle, H. W. et al. *Acta Crystallogr. Section C, Cryst. Struct. Commun.* **2000**, 56, 957.

Adenine (Figure 3.2) is ideal for building up MOFs because it has an imidazole ring which can imitate the imidazole derivatives, it is rigid which helps the formation of permanent porous materials, and it has also multiple possible coordination sites allowing the construction of a topologically diverse family of materials.^{122,64} As mentioned above, adenine has a wide range of binding possibilities through the endocyclic imino nitrogens, N9, N7, N3, N1 and exocyclic amino nitrogen atom N6, as donor sites.¹²³ The order of basicity of these five coordinating N atoms are N9 > N1 > N7 > N3 > N6 making adenine a versatile ligand.¹²⁴ All the five nitrogen coordination sites are available in a deprotonated adeninate which allows the formation of vast number of coordination polymers. Moreover, adenine can adopt different binding patterns like monodentate N9,¹²⁵ N7,¹²⁶ and N3,¹²⁷ bidentate bridging or chelating through μ -N7,N9;¹²⁸ μ -N3,N9;¹²⁹ μ -N3,N7;¹³⁰ μ -N1,N9;¹³¹ and μ -N6,N7¹³² (with 9-ethyladenine) and also as tridentate μ_3 -N3,N7,N9¹³³. There are

¹²² Wang, F.; Kang, Y. *Inorg. Chem. Comm.* **2012**, *20*, 266.

¹²³ (a) Tornita, K. et al. *Biochem. Biophys. Res. Commun.* **1973**, *54*, 96. (b) de Meester, P.; Skapski, A. C. *J. Chem. Soc. A*, **1971**, 2167. (c) Terzis, A. et al. *Inorg. Chem.* **1973**, *12*, 1166. (d) Brown, D. B. et al. *Inorg. Chem.* **1977**, *16*, 2675. (e) Sletten, E. *Acta Crystallogr. Sect. B*, **1969**, *25*, 1480. (f) Marzotto, A. et al. *J. Chem. Soc. Dalton Trans.* **1995**, 1461. (g) Prizant, L. et al. *Can. J. Chem.* **1981**, *59*, 1311. (h) Charland, J.-P. et al. *Croat. Chem. Acta* **1984**, *57*, 679. (i) Charland, J.-P.; Beauchamp, A. L. *Inorg. Chem.* **1986**, *25*, 4870. (j) Korn, S.; Scheldrick, W. S. *Inorg. Chim. Acta* **1997**, *254*, 85. (k) Kickham, J. E. et al. *Chem. Eur. J.* **1997**, *3*, 1203. (l) Salam, M. A.; Aoki, K. *Inorg. Chim. Acta* **2000**, *311*, 15.

¹²⁴ (a) Lippert, B. *Prog. Inorg. Chem.* **2005**, *54*, 385. (b) de Meester, P.; Skapski, A. C. *J. Chem. Soc. Dalton Trans.* **1973**, 424. (c) Choquesillo-Lazarte, D. et al. *J. Coord. Chem. Rev.* **2008**, *252*, 1241.

¹²⁵ (a) Tornita, K. et al. *Biochem. Biophys. Res. Commun.* **1973**, *54*, 96. (b) Brown, D. B. et al. *Inorg. Chem.* **1977**, *16*, 2675. (c) de Meester, P.; Skapski, A. C. *J. Chem. Soc. Dalton Trans.* **1973**, 424. (d) Sakaguchi, H. et al. *Chem. Pharm. Bull.* **1978**, *26*, 2465. (e) Marzotto, A. et al. *J. Chem. Soc. Dalton Trans.* **1995**, 1461. (f) de Meester, P.; Skapski, A. C. *J. Chem. Soc. Dalton Trans.* **1973**, 1596. (g) Kistenmacher, L. G. et al. *J. Am. Chem. Soc.* **1973**, *95*, 5817. (h) Gagnon, C. et al. *Inorg. Chem.* **1977**, *16*, 2469. (i) Rosopulos, Y. et al. *Chem. Ber.* **1985**, *118*, 931. (j) Prizant, L. et al. *Can. J. Chem.* **1981**, *59*, 1311. (k) Charland, J.-P.; Beauchamp, A. L. *Croat. Chem. Acta* **1984**, *57*, 679.

¹²⁶ (a) Taylor, M. R. *Acta Crystallogr. Sect. B* **29**, **1973**, 884. (b) Muthiah, P. T. et al. *J. Inorg. Biochem.* **1983**, *19*, 237. (c) Taylor, M. R.; Westphalen, J. A. *Acta Crystallogr. Sect. A* **37** (S), **1981**, C63.

¹²⁷ (a) Marzotto, A. et al. *J. Crystallogr. Spectrosc. Res.* **1993**, *23*, 119. (b) Kickham, J. E. et al. *Chem. Eur. J.* **1997**, *3*, 1203.

¹²⁸ (a) Prizant, L. et al. *Acta Crystallogr. Sect. B* **38**, **1982**, 88. (b) Scheldrick, W. S. et al. *Inorg. Chim. Acta* **1993**, *206*, 15.

¹²⁹ (a) de Meester, P.; Skapski, A. C. *J. Chem. Soc. A*, **1971**, 2167. (b) Terzis, A. et al. *Inorg. Chem.* **1973**, *12*, 1166. (c) de Meester, P.; Skapski, A. C. *J. Chem. Soc. Dalton Trans.* **1972**, 2400. (d) Sletten, E. *Acta Crystallogr. Sect. B*, **1969**, *25*, 1480.

¹³⁰ (a) Bugella-Altamirano, E. et al. *Inorg. Chim. Acta* **2002**, *339*, 160. (b) Brandi-Blanco, M. P. et al. *J. Inorg. Biochem.* **2013**, *127*, 211.

¹³¹ Das, S. et al. *Inorg. Chim. Acta* **2005**, *358*, 3236.

¹³² Day, E. F. et al. *J. Am. Chem. Soc.* **1994**, *116*, 9339.

¹³³ (a) Wang, F.; Kang, Y.: *Inorg. Chem. Commun.* **2012**, *20*, 266. (b) Song, Y. et al. *CrystEngComm.* **2014**, *16*, 3082. (c) García-Terán, J. P. et al. *Inorg. Chem.* **2004**, *43*, 4549. (d) An, J. et al. *J. Am. Chem. Soc.* **2010**, *132*, 38.

also reported compounds where all the four imino N atoms are coordinated to the metal centre at the same time.¹³⁴

A large number of metal organic complexes of adenine in which adenine is coordinated to one or more metal centres have been reported. Due to the highly versatile nature of adenine, it can adopt different coordination modes and thirteen such coordination modes are represented in Figure 3.3.

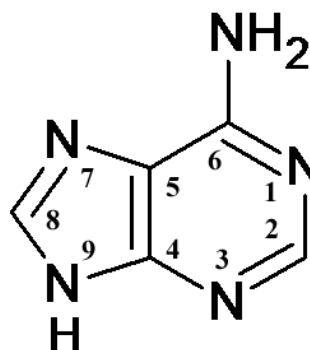


Figure 3.2: Numbering pattern of the atoms in adenine molecule.

Another benefit of using adenine as ligand in the supramolecular synthesis is the presence of the exocyclic primary 6–amino group which enables adenine as a potential connector in the network formation, since the 6–amino group acts as a hydrogen donor in intermolecular hydrogen–bonding interactions and thus spreading the resulting complex into more extended architectures.¹³⁵

Adenine can be found in neutral or ionic forms according to the pH of the medium and thereby modifying its coordinative properties. The pKa values of adenine are 4.2 and 9.8,¹³⁶ respectively (Figure 3.4). Adenine in neutral form is capable of forming different types of compounds like, monomers,⁸⁵ discrete polynuclear species⁸⁶ or one dimensional (1D) polymeric chains.¹³⁷ Being a strong base, the adeninate anion has the capacity to form compounds varying from monomeric,⁹⁸ polynuclear^{138–139} to three dimensional (3D) networks.⁸⁶

¹³⁴ (a) Yang, E.–C. et al. *Inorg. Chem.* **2009**, *48*, 3511. (b) Song, Y. et al. *CrystEngComm.* **2014**, *16*, 3082 (c) Li, T. et al. *J. Am. Chem. Soc.* **2013**, *135*, 11688.

¹³⁵ Choquesillo–Lazarte, D. et al. *J. Coord. Chem. Rev.* **2008**, *252*, 1241.

¹³⁶ Taqui–Khan, M. M.; Krishnamoorthy, C. R. *J. Inorg. Nucl. Chem.* **1971**, *33*, 1417.

¹³⁷ García–Terán J. P. et al. *Inorg Chem.* **2004**, *43*, 5761.

¹³⁸ Hubert, J.; Beauchamp, A. L. *Acta Crystallogr.* **1980**, *B36*, 2613.

¹³⁹ (a) Prizant, L. et al. *Acta Crystallogr.* **1982**, *B38*, 88. (b) Beauchamp, A. L. *J. Cryst. Mol. Struct.* **1980**, *10*, 149.

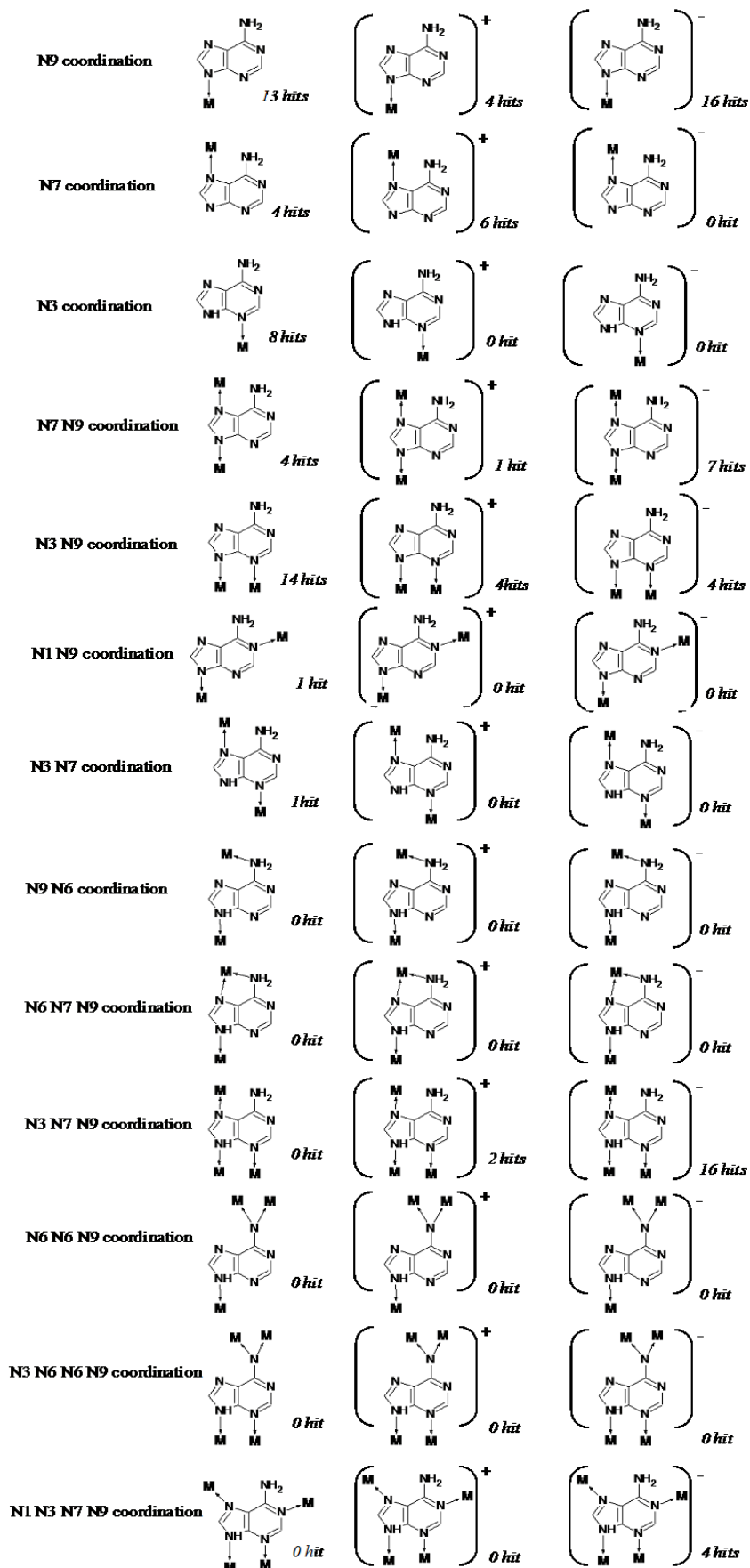


Figure 3.3: Coordination modes of the adenine ligand with the number of examples for each mode found in the CSD.

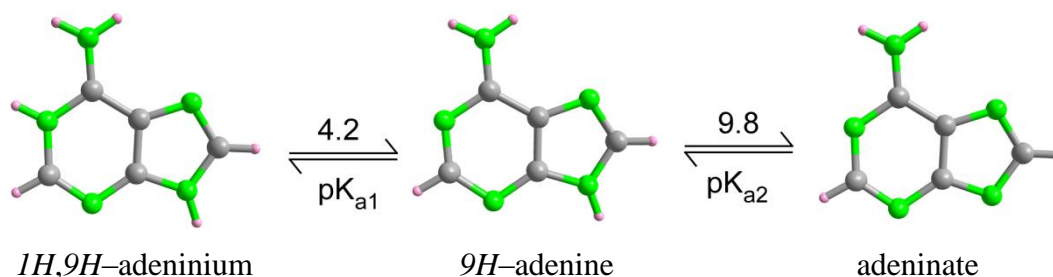


Figure 3.4: The pKa values of adenine.

Guanine nucleobase has the highest number of tautomers among the purine nucleobases.¹⁴⁰ Among which 1H,9H-keto form is the most abundant in the solid state¹⁴¹ while 1H,7H-keto form is most abundant in the gas phase.¹⁴² In the literature there exist a very large number of structural reports of substituted guanine nucleobase coordinated to a transition metal. However, because of the insoluble nature of guanine in most solvents, only few structures are reported in which guanine itself acts as a ligand.¹⁴³ Figure 3.5, shows the usually accepted numbering scheme and the coordination modes found for the guanine nucleobase (as found in the CSD data base version February 2015). In the case of unsubstituted guanine the most preferred binding position is N9 with 6 examples found.¹⁴⁴ The other possible binding modes are through $\mu\text{-N7:N9}$ (2 examples),¹⁴⁵ $\mu\text{-N3:N7}$ (2 examples)¹⁰³ and $\mu\text{-N3:N9}$ (1 example).¹⁴⁶

Crystal engineering through the design of supramolecular network structures is a well known practice in the solid-state supramolecular chemistry.¹⁴⁷ The key to success in such supramolecular network designing is to choose tectons with proper geometry and robust synthons.¹⁴⁸ Adenine fulfils the above requirements as can be observed in Figure 3.6. Similarly, guanine is also able to establish complementary hydrogen bonds with a second

¹⁴⁰ Gupta, D. et. al. *Dalton Trans.* **2010**, 39, 73.

¹⁴¹ Thewalt, U. et. al. *Acta Crystallogr. Sect. B: Struct. Crystallogr. Cryst. Chem.* **1971**, 27, 2358.

¹⁴² Lippert, B.; Gupta, D. *Dalton Trans.* **2009**, 4619.

¹⁴³ (a) Mastropietro, T. F. et. al. *Dalton Trans.* **2008**, 514. (b) Gupta, D. et al. *Dalton Trans.* **2010**, 39, 73. (c) Turel, I. et. al. *J. Inorg. Biochem.* **2004**, 98, 393. (d) Gaballa, A. S. et al. *Inorg. Chim. Acta* **2008**, 361, 2070. (e) Sundaralingam, M.; Carrabine J. A. *J. Mol. Biol.* **1971**, 61, 287. (f) Colacio, E. et al. *J. Inorg. Biochem.* **2004**, 98, 595. (g) Declercq, J. P. et. al. *Bull. Soc. Chim. Belg.* **1971**, 80, 527.

¹⁴⁴ (a) Gupta, D. et al. *Dalton Trans.* **2010**, 39, 73. (b) Mastropietro, T. F. et al. *Dalton Trans.* **2008**, 514. (c) Turel, I. et al. *J. Inorg. Biochem.* **2004**, 98, 393. (d) Declercq, J. P. et al. *Bull. Soc. Chim. Belg.* **1971**, 80, 527. (e) Sundaralingam, M.; Carrabine, J. A. *J. Mol. Biol.* **1971**, 61, 287. (f) Gaballa, A. S. et al. *Inorg. Chim. Acta* **2008**, 361, 2070.

¹⁴⁵ (a) Gupta, D. et al. *Dalton Trans.* **2010**, 39, 73. (b) Annen, P. et al. *Inorg. Chim. Acta* **2000**, 307, 115.

¹⁴⁶ Colacio, E. et al. *J. Inorg. Biochem.* **2004**, 98, 595.

¹⁴⁷ Han, L. et al. *Cryst. Growth Des.* **2009**, 9, 660.

¹⁴⁸ Saha, B. K.; Bhattacharya, S. *CrystEngComm.* **2010**, 12, 2369.

guanine (Figure 3.7). However, some recognition patterns requires the simultaneous presence of neutral and protonated guanines. Additionally, there is a relatively common interaction between the guanines that involves keto group as acceptor and N2–H + N3–H or N1–H + N2–H as donor to form a $R_2^1(6)$. These last interactions does not provide a rigid synthon as the second guanine can rotate retaining this interaction. There are many other purine derivatives not involved in the DNA structure but still retaining most of the hydrogen bonding self–recognition capacities. A brief selection of these purine based molecules has been depicted in Figure 1.19.

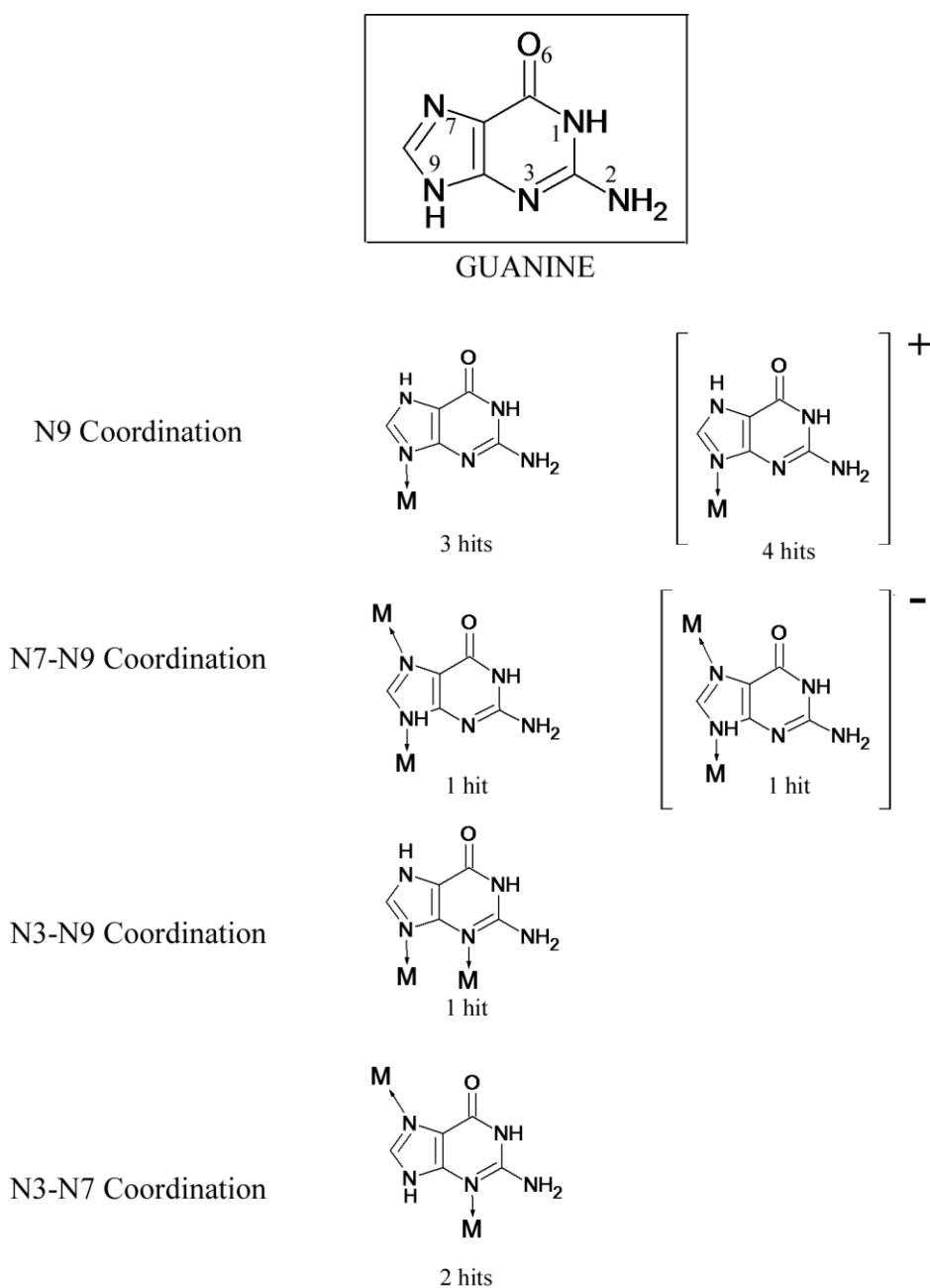


Figure 3.5: (a) Structure and numbering pattern of guanine. (b) Different coordination modes as found in the CSD database.

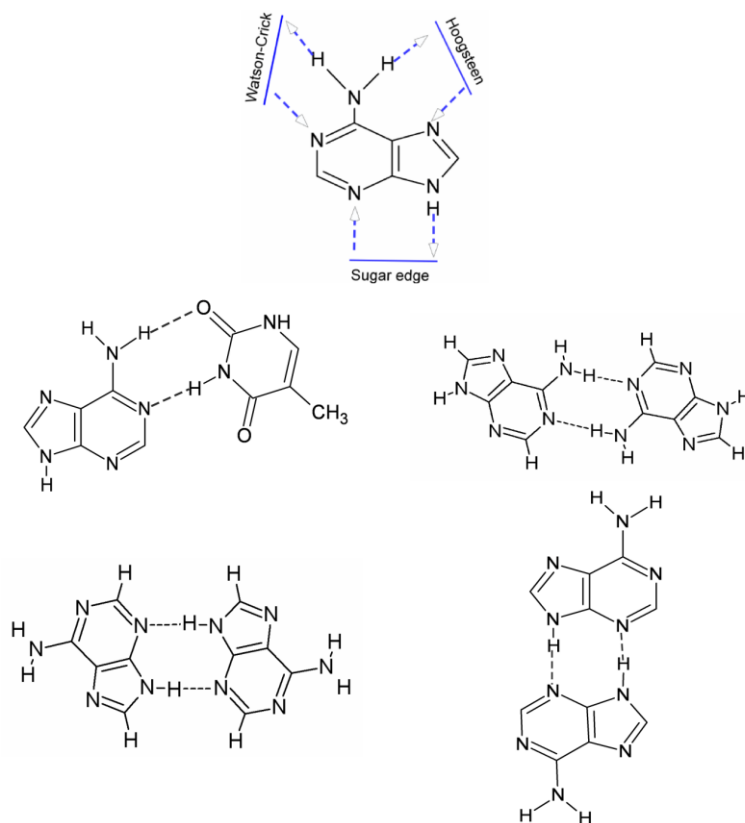


Figure 3.6: Complementary hydrogen bonds between adenines.

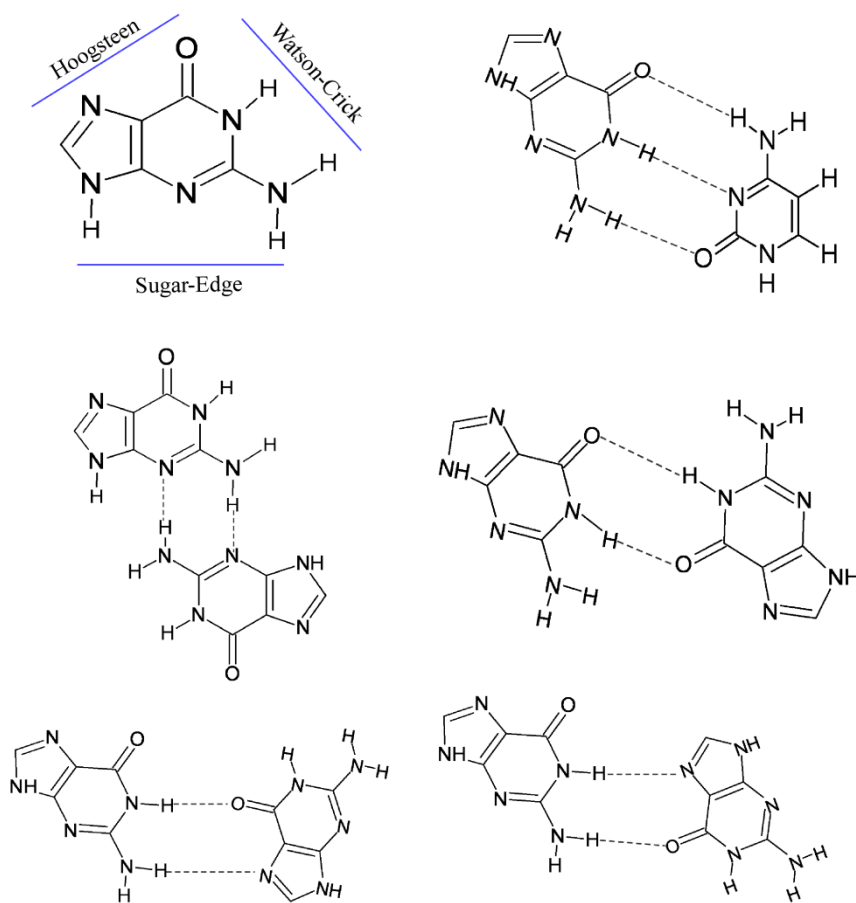


Figure 3.7: Complementary hydrogen bonds between guanines.

3.2 SYNTHESIS AND CHEMICAL CHARACTERISATION

3.2.1 Synthesis

Taking into account the above mentioned ideas, we report herein the synthesis and crystal structures of fifteen compounds with purine derivatives (Table 3.1). Apart from compounds *CUADECL-A*, *CO-6-CLPUR* and *CO-6-THIOG*, all other compounds were obtained using alcohols as solvent to avoid the instability of the 3D supramolecular architectures due to the presence of water mediated hydrogen bonds between the nucleobases.

Table 3.1: Compounds synthesised^[a]

<i>Compound</i> ^[a]	<i>Code</i>
[Cu ₂ (μ-Hade) ₄ Cl ₂]Cl ₂ ·8H ₂ O Tetrakis(μ-adenine-κN3:κN9)bis(chlorido)dicopper(II) chloride-water (1/8)	<i>CUADECL-A</i>
[Cu ₂ (μ-Hade) ₄ (Cl) ₂]Cl ₂ ·2MeOH Dichloridotetrakis(μ-adenine-κN3:κN9)dicopper(II) chloride-methanol (1/2)	<i>CUADECL-B</i> (<i>SMOF-1</i>)
[Cu ₂ (μ-Hade) ₄ (Br) ₂]Br ₂ ·~2MeOH Dibromidotetrakis(μ-adenine-κN3:κN9)dicopper(II) bromide-methanol (1/2)	<i>CUADEBR-A</i> (<i>SMOF-2</i>)
[Cu ₂ (μ-Hade) ₂ (Cl) ₄]·2MeOH Dichloridobis(μ-chlorido)bis(μ-adenine-κN3:κN9)dicopper(II)-methanol(1/2)	<i>CUADECL-C</i> (<i>SMOF-3</i>)
[Cu ₂ (μ-Hade) ₂ (Br) ₄]·2PrOH Dibromidobis(μ-bromido)bis(μ-adenine-κN3:κN9)dicopper(II)-propanol (1/2)	<i>CUADEBR-B</i>
[Cu ₄ (μ ₃ -ade) ₂ (μ ₂ -ade) ₂ (pentylNH ₂) ₂ (CH ₃ OH) ₂ (CO ₃) ₂ (H ₂ O) ₂]·n(solvent) Tetrakis(μ ₃ -adeninato-κN3:κN7:κN9)(μ ₂ -adeninato-κN3:κN9)diaquabis(carbonato-κO:κO)dimethanolbis(pentylamine)tetracopper(II)]-n(solvent)	<i>CUADECOS</i> (<i>SMOF-8</i>)
[Cu ₂ (μ-ade) ₃ (μ-OH)(H ₂ O)(CH ₃ OH)] _n ·n(solvent) <i>catena</i> -poly[Bis(μ-adeninato-κN3:κN9)(μ-adeninato-κN7:κN9)aqua(μ-hydroxido)methanoldicopper(II)]-solvent(1/n)	<i>CUADEOH</i> (<i>SMOF-9</i>)
[Co ₃ (μ-Hade) ₂ (μ-Cl) ₄ Cl ₂ (H ₂ O) ₄]·2H ₂ O (μ-adenine-1κN3:3κN9)(μ-adenine-2κN3:3κN9)bis(μ-chlorido-1κCl:3κCl)bis(μ-chlorido-2κCl:3κCl)di(chlorido-1κCl,2κCl)tetra(aqua-1κ2O,2κ2O)tricobalt(II)-water (1/2)	<i>CO3ADECL</i>
[Co(Hade) ₂ Cl ₂] Dichloridobis(adenine-κN7)cobalt(II)	<i>COADECL</i> (<i>SMOF-5</i>)
[Co(Hade) ₂ Br ₂] Dibromidobis(adenine-κN7)cobalt(II)	<i>COADEBR</i> (<i>SMOF-6</i>)
[Co(9-MeAde) ₂ (H ₂ O) ₄]Cl ₂ ·2(H ₂ O). Tetraaquabis(9-methyladenine-κN7)cobalt(II) chloride-water (1/2)	<i>CO-9-MEADECL</i>
[Cu ₂ (μ-CH ₃ COO) ₄ (μ-9-MeAde)] _n ·nCH ₃ OH <i>catena</i> -poly[tetrakis(μ-acetato-κO:κO)(μ-9-methyladenine-κN1:κN7)dicopper(II)]-methanol (1/1)	<i>CU-9-MEADEACE</i>
[Co(6-ClPur) ₂ (H ₂ O) ₄]·4H ₂ O Tetraaquabis(6-chloropurinato-κN9)cobalt(II)-water (1/4)	<i>CO-6-CLPUR</i>
[Cu ₂ (Hgua) ₂ (H ₂ gua) ₂ (μ-Cl) ₂ Cl ₂][CuCl ₄] Bis(guanine-κN9)bis(guaninium-κN9)bis(μ-chlorido)bis(chlorido)dicopper(II) tetrachloridocuprate(II)	<i>CUGUACL</i>
[Co(Thiogua) ₃]·nH ₂ O Tris(6-thioguaninato-κN7, κS6)cobalt(III)-water (1/n)	<i>CO-6-THIOG</i> (<i>SMOF-4</i>)

[a] Hade = adenine (C₅H₅N₅); ade = adeninate (C₅H₄N₅); Hgua = guanine (C₅H₅N₅O); H₂gua = guaninium (C₅H₆N₅O); 9-MeAde = 9-methyladenine (C₆H₇N₅); 6-ClPur = 6-chloropurinato (C₅H₂ClN₄); Thiogua = 6-thioguaninato (C₅H₄N₅S); MeOH = CH₃OH; PrOH = 1-propanol; pentylNH₂ = pent-1-amine.

3.2.1.1 Synthesis of compound *CUADECL-A*

0.0852 g of $\text{CuCl}_2 \cdot 2\text{H}_2\text{O}$ (0.5 mmol) dissolved in 5 mL water was added dropwise to the stirring solution of 0.0682 g of adenine (0.5 mmol) dissolved in 30 mL water. After stirring for 30 minutes, a dark blue precipitate corresponding to *CUADECL-A* appeared. It was filtered off and washed thoroughly with water. The filtrate was left evaporating at room temperature for two weeks and good quality blue single crystals were formed.

Yield: 80%. Anal. Calcd (Found) for $\text{C}_{20}\text{H}_{36}\text{Cl}_4\text{Cu}_2\text{N}_{20}\text{O}_8$: C, 25.19 (25.13); H, 3.81 (3.75); N, 29.38 (29.42); Cu, 13.33 (13.27) %. Main IR features (cm^{-1} ; KBr pellets): 3440s, 3191s, 2362w, 2338w, 1646vs, 1463m, 1400m, 1343w, 1310w, 1280w, 1203m, 1143m, 1110m, 993w, 906, 791m, 738m, 655m, 619m, 569m, 461m.

3.2.1.2 Synthesis of compound *CUADECL-B (SMOF-1)*

0.0171 g of $\text{CuCl}_2 \cdot 2\text{H}_2\text{O}$ (0.1 mmol) dissolved in 5 mL of methanol was added dropwise to a warm stirring solution (50 °C) of 0.0277 g of adenine (0.2 mmol) dissolved in 30 mL methanol. The blue precipitate was formed immediately on the addition of the CuCl_2 solution. It was filtered, washed with methanol and dried. Single crystals of *CUADECL-B* were obtained by the following diffusion technique. A methanolic solution of 0.0138 g of adenine (0.1 mmol) in 10 mL was layered slowly over a propanolic solution of 0.0086 g of $\text{CuCl}_2 \cdot 2\text{H}_2\text{O}$ (0.05 mmol) in 10 mL in a test tube. Blue crystals suitable for the single crystal X-ray analysis were formed in one week.

Yield: 80%. Anal. Calcd (found) for $\text{C}_{22}\text{H}_{28}\text{Cl}_4\text{Cu}_2\text{N}_{20}\text{O}_2$: C, 30.25 (30.35); H, 3.23 (3.14); N, 32.07 (32.09), Cu, 14.55 (14.62) %. Main IR features (cm^{-1} ; KBr pellets): 3360s, 3170s, 1650vs, 1515w, 1460m, 1400m, 1350w, 1210m, 1320m, 1110w, 785w, 740w, 550m.

3.2.1.3 Synthesis of compound *CUADECL-C (SMOF-3)*

0.0702 g of $\text{CuCl}_2 \cdot 2\text{H}_2\text{O}$ (0.4 mmol) dissolved in 10 mL of methanol was added dropwise to the hot stirring solution (50 °C) of 0.0128 g of adenine (0.1 mmol) dissolved in 20 mL methanol. The light green precipitate formed was filtered, washed with methanol and dried. Diffusion technique was used again to obtain crystals but using a methanolic solution of 0.0136 g of adenine (0.1 mmol in 10 mL) slowly layered over a propanolic solution of 0.0086 g of $\text{CuCl}_2 \cdot 2\text{H}_2\text{O}$ (0.05 mmol in 10 mL) in a diffusion tube. Good

quality green crystals were formed along with blue crystals of the compound **CUADECL-B**, in one week.

Yield: 70%. Anal. Calcd (found) for $C_{12}H_{18}Cl_4Cu_2N_{10}O_2$: C, 23.89 (23.92); H, 3.01 (3.14); N, 23.22 (23.18), Cu, 21.07 (21.03) %. Main IR features (cm^{-1} ; KBr pellets): 3387s, 3142sh, 3103sh, 1666vs, 1611m, 1580m, 1520m, 1478m, 1450s, 1404vs, 1383w, 1356sh, 1347sh, 1318vs, 1262w, 1244w, 1215m, 1291w, 1170m, 1111vs, 1016w, 976sh, 970sh, 931m, 788m, 737sh, 722sh, 680m, 633w, 597m, 573w, 548s.

3.2.1.4 Synthesis of compound **CUADEBR-A** (SMOF-2)

0.0112 g of $CuBr_2$ (0.05 mmol) dissolved in 5 mL methanol was added dropwise to the hot stirring solution of 0.0270 g adenine (0.2 mmol) dissolved in 30 mL of methanol at 50 °C. Precipitation started immediately and the solution was kept stirring for 20 minutes. The blue precipitate corresponds to **CUADEBR-A**. Crystals suitable for single-crystal X-ray diffraction studies were obtained by diffusion of a methanolic solution of adenine (0.0136 g, 0.1 mmol in 10 mL) slowly layered over a propanolic solution of $CuBr_2$ (0.0116 g, 0.05 mmol in 10 mL). Within one week, **CUADEBR-A** crystallized as deep blue colored crystals along with some red crystals corresponding to **CUADEBR-B**.

Yield: 80%. Anal. Calcd (found) for $C_{23}H_{32}Br_4Cu_2N_{20}O_3$: C, 25.13 (25.24); H, 2.68 (2.81); N, 26.65 (26.53), Cu, 12.09 (11.97) %. Main IR features (cm^{-1} ; KBr pellets): 3330s, 3170s, 1650vs, 1515w, 1460m, 1348w, 1320m, 1260w, 1215m, 1182w, 1148w, 1117m, 1022w, 970w, 934sh, 922sh, 790m, 738m, 683w, 610w, 563w, 545m.

3.2.1.5 Synthesis of compound **CUADEBR-B**

As mentioned above, single crystals of **CUADEBR-B** were obtained in the diffusion tube along with the crystals of **CUADEBR-B** (SMOF-2). The compound **CUADEBR-B** was obtained in pure form by adding 0.0273 g of adenine (0.2 mmol) dissolved in 40 mL methanol over the solution of 0.0226 g of $CuBr_2$ (0.1 mmol) dissolved in 15 mL of propanol. Red coloured crystals started appearing on evaporating the brown coloured mother liquid for one week.

Yield: 60%. Anal. Calcd (found) for $C_{16}H_{26}Br_4Cu_2N_{10}O_2$: C, 22.96 (22.91); H, 3.13 (3.09); N, 16.73 (16.78); Cu, 15.18 (15.15) %. Main IR features (cm^{-1} ; KBr pellets): 3380s, 3226s, 3293s, 3240s, 3193s, 3130s, 2953s, 1666vs, 1612m, 1476w, 1460w, 1405m, 1384w, 1357w, 1344w, 1320s, 1262w, 1220m, 1175w, 1112m, 1050w, 1002s, 972w, 930w, 875m, 802w, 876m, 736m, 711w, 677w, 663w, 613m, 569m, 538w, 472w, 463w.

3.2.1.6 Synthesis of compound *CUADEOH* (SMOF-9)

Single crystals of this compound were obtained by the slow addition of a 10 mL methanolic solution of 0.0199 g of $\text{Cu}(\text{OOCCH}_3)_2 \cdot \text{H}_2\text{O}$ (0.1 mmol) into a cold methanolic solution (50 mL) of 0.0546 g of adenine (0.4 mmol) mixed with 0.59 mL of pentylamine stirring in an ice-bath. The green solution was stirred in the ice-bath for 1 hour and left evaporating at room temperature. Blue needle like crystals appeared in one week.

Yield: 5%. Anal. Calcd (found) for $\text{C}_{16}\text{H}_{19}\text{Cu}_2\text{N}_{15}\text{O}_3$: C, 33.87 (33.77); H, 6.15 (6.08); N, 24.18 (24.09); Cu, 14.63 (14.74) %. Main IR features (cm^{-1} ; KBr pellets): 3446s, 3356vs, 3123s, 1671s, 1418m, 1398m, 1385m, 1333m, 1308s, 1268m, 1251w, 1191m, 1149m, 1123w, 1022w, 979w, 939m, 910w, 875w, 845w, 797m, 738w, 723s, 641m, 620w, 570w, 541m.

3.2.1.7 Synthesis of compound *CUADEC03* (SMOF-8).

The synthesis was performed similarly as that of compound *CUADEOH*, but using 0.0206 g of adenine (0.15 mmol) dissolved in 20 mL of cold methanol. On evaporating, the colour of the solution changed to blue-violet and violet prismatic shaped crystals appeared after one week. The crystals were unstable outside the mother liquid. Main IR features (cm^{-1} ; KBr pellets): 3444s, 2961m, 2930m, 2872w, 1644s, 1506w, 1489w, 1465m, 1397w, 1382m, 1343w, 1308w, 1265w, 1238w, 1191m, 1113m, 991w, 941w, 731w, 657w, 618m, 575w, 556w.

3.2.1.8 Synthesis of compound *CO3ADECL*

Pink coloured single crystals of compound *CO3ADECL* were obtained using diffusion techniques by layering a methanolic solution of 0.0135 g of adenine (0.1 mmol in 10 mL) over an aqueous solution of 0.0119 g of $\text{CoCl}_2 \cdot 6\text{H}_2\text{O}$ (0.05 mmol in 10 mL). Pink crystals were formed with in one week.

Yield: 10%. Anal. Calcd (found) for $\text{C}_{10}\text{H}_{22}\text{Cl}_6\text{Co}_3\text{N}_{10}\text{O}_6$: C, 15.64 (15.67); H, 2.89 (2.83); N, 18.24 (18.27); Co, 23.02 (22.98) %. Main IR features (cm^{-1} ; KBr pellets): 3444s, 2360vs, 2340s, 2266w, 1650m, 1633m, 1311w, 1244m, 1186w, 1147w, 983w, 719w, 680w, 668m, 649m, 614w, 536w.

3.2.1.9 Synthesis of compound *COADECL* (SMOF-5)

This compound was obtained as deep blue polycrystalline sample by the dropwise addition of a propanolic solution 0.0270 g of adenine (0.2 mmol 40 mL) into a stirring

solution of 0.0238 g of $\text{CoCl}_2 \cdot 6\text{H}_2\text{O}$ (0.1 mmol) dissolved in 5 mL propanol. When the synthesis was performed in methanol low quality crystals were obtained. Then single crystals of good quality were obtained by layering a methanolic solution of 0.0135 g of adenine (0.1 mmol, 10 mL) over a solution of 0.0119 g of $\text{CoCl}_2 \cdot 6\text{H}_2\text{O}$ (0.05 mmol, 10 mL) in propanol. Blue crystals appeared after two weeks. Polycrystalline sample of this compound was obtained through solvent-free synthesis by heating a 1:2 mixture of $\text{CoCl}_2 \cdot 6\text{H}_2\text{O}$ and adenine in a closed container up to 130 °C.

Yield: 70%. Anal. Calcd (found) for $\text{C}_{10}\text{H}_{10}\text{Cl}_2\text{CoN}_{10}$: C, 30.02 (30.09); H, 2.52 (2.47); N, 35.01 (34.93); Cu, 14.73 (14.82) %. Main IR features (cm^{-1} ; KBr pellets): 3391vs, 3258vs, 3133vs, 3058vs, 2346w, 2280w, 2186w, 2016w, 1943w, 1790w, 1696vs, 1611s, 1498m, 1459w, 1397s, 1327m, 1237m, 1171m, 1105w, 1066w, 1016w, 942m, 895m, 856w, 778m, 712m, 631w, 610m, 530m.

3.2.1.10 Synthesis of compound COADEBR (SMOF-6)

This compound was obtained as deep blue polycrystalline sample by the dropwise addition of a propanolic solution 0.0270 g of adenine (0.2 mmol) dissolved in 40 mL into a stirring solution of 0.0240 g of CoBr_2 (0.1 mmol) in 5 mL propanol. All the attempts to grow single-crystals were unsuccessful.

Yield: 60%. Anal. Calcd (found) for $\text{C}_{10}\text{H}_{10}\text{Br}_2\text{CoN}_{10}$: C, 24.56 (24.49); H, 2.06 (2.09); N, 28.68 (28.57); Cu, 12.05 (12.01) %. Main IR features (cm^{-1} ; KBr pellets): 3450s, 3341vs, 3066s, 2817w, 2671w, 2284w, 1951w, 1663vs, 1596vs, 1513w, 1480s, 1416s, 1360w, 1343s, 1306s, 1246s, 1170w, 1120w, 1020w, 1063w, 1030w, 973m, 910m, 870w, 791m, 763m, 722s, 680w, 638m, 627m, 557s, 545m, 532s.

3.2.1.11 Synthesis of compound CO-9-MEADECL

0.0298 g (0.2 mmol) of 9-methyladenine dissolved in 20 mL of methanol was added dropwise to the stirring solution of 0.0237 g (0.1 mmol) of $\text{CoCl}_2 \cdot 6\text{H}_2\text{O}$ dissolved in 5 mL of methanol at room temperature. The pink coloured clear solution formed was stirred at room temperature for 2 hours and left for evaporation. Orange-yellow good quality single crystals were formed within one week.

Yield: 40%. Anal. Calcd (found) for $\text{C}_{12}\text{H}_{26}\text{Cl}_2\text{CoN}_{10}\text{O}_6$: C, 26.88 (26.81); H, 4.88 (4.79); N, 26.12 (26.17); Co, 10.99 (11.03) %. Main IR features (cm^{-1} ; KBr pellets): 3417s, 2740w, 2760w, 2275w, 1947m, 1886w, 1793m, 1663vs, 1600vs, 1576vs, 1500s, 1467s, 1426s, 1416s, 1390w, 1373w, 1346s, 1326m, 1300s, 1266m, 1256s, 1230m,

1196m, 1086w, 1063m, 1047m, 1019m, 978w, 945m, 921m, 898s, 843m, 795m, 760w, 742w, 717m, 684w, 641w, 602w, 585w, 542m.

3.2.1.12 Synthesis of compound CU-9-MEADACE

0.0298 g (0.2 mmol) of 9-methyladenine dissolved in 20 mL of methanol was added dropwise to the stirring solution of 0.0199 g (0.1 mmol) of $\text{Cu}(\text{OOCCH}_3)_2 \cdot \text{H}_2\text{O}$ dissolved in 5 mL of methanol at room temperature. A green coloured precipitate was obtained immediately. Single crystals were obtained using diffusion techniques. A methanolic solution of 9-methyladenine (0.1 mmol, 0.1490 g in 10 mL) was layered over a methanolic solution of copper(II) acetate monohydrate (0.05 mmol, 0.0099 g in 10 mL). Good quality green crystals were obtained within one week.

Yield: 50%. Anal. Calcd (found) for $\text{C}_{15}\text{H}_{23}\text{Cu}_2\text{N}_5\text{O}_9$: C, 33.09 (33.01); H, 4.26 (4.39); N, 12.86 (12.77); Cu, 23.34 (23.51) %. Main IR features (cm^{-1} ; KBr pellets): 3395s, 3288m, 3195s, 1666s, 1626s, 1603vs, 1530w, 1508w, 1475w, 1433s, 1421s, 1385m, 1336m, 1310m, 1258w, 1230s, 1197m, 1083w, 1067w, 1050m, 1020m, 945w, 902w, 880w, 841w, 795m, 760w, 742w, 720m, 685m, 642w, 626w, 603w, 561w, 540w, 530w.

3.2.1.13 Synthesis of compound CO-6-CLPUR

0.0464 g (0.3 mmol) of 6-chloropurine dissolved in 30 mL of water was mixed with 0.59 mL (0.4 mmol) of pentylamine and the mixture was stirred in an ice bath for 1 hour. 0.0291 g (0.1 mmol) of $\text{Co}(\text{NO}_3)_2 \cdot 6\text{H}_2\text{O}$ dissolved in 5 mL of water was added dropwise to the cold stirring solution of 6-chloropurine. The orange coloured solution formed was stirred in ice bath for 2 hours more and kept for evaporating. Orange coloured single crystals were formed in three days.

Yield: 60%. Anal. Calcd (found) for $\text{C}_{10}\text{H}_{20}\text{Cl}_2\text{CoN}_8\text{O}_8$: C, 23.54 (23.63); H, 3.95 (3.87); N, 21.96 (21.99); Co, 11.55 (11.51) %. Main IR features (cm^{-1} ; KBr pellets): 3442s, 1717w, 1624s, 1593w, 1511w, 1482w, 1451w, 1384vs, 1330w, 1286w, 1250w, 1230w, 1144m, 1100m, 1064w, 990w, 933w, 920w, 855m, 939m, 785w, 750w, 630w, 606w, 595w, 537w, 500w.

3.2.1.14 Synthesis of compound CUGUACL

Good quality green crystals of compound **CUGUACL** were obtained by mixing methanolic solutions of 0.0173 g of $\text{CuCl}_2 \cdot 2\text{H}_2\text{O}$ (0.1 mmol in 5 mL) and an acidified

methanolic solution of 0.0337 g of guanine, dissolved in 40 mL methanol, with 34 μl (0.4 mmol) of concentrated HCl (purity: 37%).

Yield: 30%. Anal. Calcd (found) for $\text{C}_{20}\text{H}_{24}\text{Cl}_8\text{Cu}_3\text{N}_{20}\text{O}_5$: C, 21.96 (21.84); H, 2.21 (2.28); N, 25.63 (25.54); Cu, 17.27 (17.36) %. Main IR features (cm^{-1} ; KBr pellets): 3450s, 1750vs, 1666vs, 1400m, 1383s, 1361m, 1316w, 1196w, 1160w, 1116w, 1073w, 1046w, 993m, 820w, 800w, 763w, 660w, 593w, 543w, 506m, 426w.

3.2.1.15 Synthesis of compound CO-6-THIOG (SMOF-4)

0.59 mL (0.4 mmol) of pentylamine was added dropwise to a 0.0685 g (0.4 mmol) of 6-thioguanine dissolved in 20 mL of water and the mixture was stirred in an ice bath for 1 hour. To this mixture a 10 mL aqueous solution of 0.0291 g (0.1 mmol) of $\text{Co}(\text{NO}_3)_2 \cdot 6\text{H}_2\text{O}$ was added. The brown coloured solution was then stirred for 2 hours in ice bath and then left for evaporation. Brown coloured single crystals were obtained after two weeks. The same compound was obtained on replacing $\text{Co}(\text{NO}_3)_2 \cdot 6\text{H}_2\text{O}$ with $\text{CoSO}_4 \cdot 7\text{H}_2\text{O}$.

Yield: 60%. Anal. Calcd (found) for $\text{C}_{15}\text{H}_{12}\text{CoN}_{15}\text{S}_3$: C, 26.56 (26.68); H, 3.78 (3.70); N, 30.98 (31.29), Co, 14.18 (14.21). IR selected data (KBr, cm^{-1}): 3422s, 1611m, 1498w, 1459w, 1385m, 1306w, 1243vs, 1190m, 1146s, 983s, 933w, 893w, 836w, 803w, 743w, 716w, 680w, 630w, 523w.

3.3 RESULTS AND DISCUSSION

3.3.1 Crystallographic analysis

The crystallographic data and the refinement conditions are given in Table 3.2–4. Diffraction data of single crystals were collected on Oxford Diffraction Xcalibur and STOE IPDS II diffractometers. The data reduction was done with CrysAlis RED¹¹⁰ and X-Area¹⁴⁹ programs, respectively. Structures were solved by direct methods using the SIR92 program¹¹¹ and refined by full-matrix least-squares on F^2 including all reflections (SHELXL97).¹¹² All calculations were performed using the WINGX crystallographic software package.¹¹³

During the data acquisition of some of these compounds, it became evident that some of them were non-merohedrally twinned: *CO3ADECL*, *CUADECL-C* and

¹⁴⁹ Stoe & Cie. X-Area, Main Menu Version 1.15, 2001, Stoe & Cie GmbH, Darmstadt, Germany.

CUADEC03. The corresponding twin laws and percentage of the minor domain are listed below:

CO3ADECL: (0.997 0.007 0.002 0.579 -0.998 0.001 0.942 0.003 -0.999) 47.43%

CUADECL-C: (1.000 0.000 1.986 0.000 -1.000 0.000 0.000 0.000 -1.000) 14.37%

CUADEC03: (1.026 -0.077 0.038 0.070 0.963 0.012 -0.023 -0.000 1.003) 24.32%

Additionally, some other ones presented great voids within the crystal structure that were occupied by solvent molecules in a very disordered manner. Their contribution to the diffraction pattern has been removed using the SQUEEZE subroutine as implemented in PLATON: **CUADEBR-A**, **CUADECL-B**, **CUADEC03** and **CUADEOH**.¹⁵⁰

CUGUACL compound shows a disorder related to the orientation of the Jahn-Teller effect on the dimeric unit. It implies the terminal and bridging chlorido ligands that are disordered over two positions with short and significantly longer Cu-Cl distances. This disorder also implies the presence of a coordination water molecule with an occupation factor of 0.50.

The hydrogen atoms were geometrically positioned or fixed at the position of a maximum of the Fourier difference map. However, for compounds **CUADECL-C** and **CUADEOH** it was impossible to locate the hydrogen atoms attached to the H₂O, OH⁻ and MeOH molecules.

¹⁵⁰ Spek, A. L. *J. Appl. Crystallogr.* **2003**, *36*, 7.

Table 3.2: Single crystal data and structural refinement details of compounds *CUADECL-A*, *CUADECL-B (SMOF-1)*, *CUADEBR-A (SMOF-2)*, *CUADECL-C (SMOF-3)* and *CUADEBR-B*.

Compound	<i>CUADECL-A</i>	<i>CUADECL-B_100K</i>	<i>CUADECL-B_293K</i>	<i>CUADEBR-A</i>	<i>CUADECL-C</i>	<i>CUADEBR-B</i>
Empirical formula	C ₂₀ H ₃₆ Cl ₄ Cu ₂ N ₂₀ O ₈	C ₂₂ H ₂₈ Cl ₄ Cu ₂ N ₂₀ O ₂	C ₂₂ H ₂₈ Cl ₄ Cu ₂ N ₂₀ O ₂	C ₂₂ H ₂₈ Br ₄ Cu ₂ N ₂₀ O ₂	C ₁₂ H ₁₈ Cl ₄ Cu ₂ N ₁₀ O ₂	C ₁₆ H ₂₆ Br ₄ Cu ₂ N ₁₀ O ₂
Formula weight	953.553	873.49	873.49	1051.229	603.24	837.19
λ (Å)	0.71073	0.71073	0.71073	0.71073	0.71073	0.71073
T (K)	293(2)	100(2)	293(2)	100(2)	100(2)	100(2)
Diffractometer	IPDS II	IPDS II	IPDS II	Xcalibur	Xcalibur	IPDS II
Crystal system	orthorhombic	trigonal	trigonal	trigonal	monoclinic	monoclinic
Space group	<i>Pbam</i>	R $\bar{3}m$	R $\bar{3}m$	R $\bar{3}m$	C2/c	P21/c
a (Å)	13.7405(7)	26.9032(17)	26.820(1)	27.1979(9)	22.2245(18)	9.1344(7)
b (Å)	10.3343(6)	26.9032(17)	26.820(1)	27.1979(9)	13.8069(10)	11.0778(10)
c (Å)	12.1024(7)	15.4298(10)	15.528(1)	15.4999(4)	7.0204(6)	13.0778(11)
α (°)	90	90	90	90	90	90
β (°)	90	90	90	90	108.280(6)	103.873(7)
γ (°)	90	120	120	120	90	90
V (Å ³)	1718.52(17)	9671.6(11)	9673(1)	9929.6(5)	2045.5(3)	1284.7(2)
Z	2	9	9	9	4	2
ρ_{calcd} (g cm ⁻³)	1.843	1.350	1.349	1.582	1.959	2.164
μ (mm ⁻¹)	1.627	1.284	1.284	4.630	2.636	7.912
Reflections collected	7022	11165	20165	31767	9439	18741
Unique data/parameters	2073/132	2035/109	2029/109	2837/109	9439/127	3059/161
R _{int}	0.0721	0.0536	0.0598	0.0465	0.0695	0.0942
Goodness of fit (S) ^[a]	0.918	0.960	1.050	1.234	1.089	1.119
R1 ^[b] /wR2 ^[c] [I>2 σ (I)]	0.0519/0.1040	0.0337/0.0822	0.0798/0.2501	0.0927/0.2997	0.0778/0.2048	0.0504/0.0927
R1 ^[b] /wR2 ^[c] [all data]	0.1113/0.1115	0.0500/0.0872	0.1002/0.2601	0.1112/0.3107	0.1119/0.2342	0.0688/0.1005

[a] $S = [\sum w(F_0^2 - F_c^2)^2 / (N_{\text{obs}} - N_{\text{param}})]^{1/2}$. [b] $R1 = \sum ||F_0| - |F_c|| / \sum |F_0|$. [c] $wR2 = [\sum w(F_0^2 - F_c^2)^2 / \sum wF_0^2]^{1/2}$; $w = 1/[\sigma^2(F_0^2) + (aP)^2 + bP]$ where $P = (\max(F_0^2, 0) + 2F_c^2)/3$ with $a = 0.0447$ (*CUADECL-A*); $a = 0.0548$ (*CUADECL-B_100K*); $a = 0.1794$ (*CUADECL-B_293K*); $a = 0.2000$ (*CUADEBR-A*); $a = 0.1437$ (*CUADECL-C*); $a = 0.0235$, $b = 9.0683$ (*CUADEBR-B*).

Table 3.3: Single crystal data and structural refinement details of compounds *CUADEOH (SMOF-9)*, *CUADEC03 (SMOF-8)*, *CO3ADECL*, *COADECL (SMOF-5)* and *CUGUACL*.

Compound	<i>CUADEOH</i>	<i>CUADEC03</i>	<i>CO3ADECL</i>	<i>COADECL</i>	<i>CUGUACL</i>
Empirical formula	C ₁₆ H ₁₉ Cu ₂ N ₁₅ O ₃	C _{30.85} H _{46.80} Cu _{3.55} N _{21.55} O _{8.20}	C ₁₀ H ₂₂ Cl ₆ Co ₃ N ₁₀ O ₆	C ₁₀ H ₁₀ Cl ₂ CoN ₁₀	C ₂₀ H ₂₄ Cl ₈ Cu ₃ N ₂₀ O ₅
Formula weight	596.54	1076.37	767.87	400.11	1098.81
λ (Å)	1.54184	0.71073	0.71073	1.54184	1.54184
T (K)	100(2)	293(2)	100(2)	100(2)	100(2)
Diffractometer	Xcalibur	Xcalibur	Xcalibur	IPDS II	Xcalibur
Crystal system	monoclinic	triclinic	triclinic	monoclinic	triclinic
Space group	C2/c	P $\bar{1}$	P $\bar{1}$	C2/c	P $\bar{1}$
a (Å)	23.472(7)	12.646(5)	7.203(2)	11.2442(18)	7.8461(5)
b (Å)	16.398(3)	13.136(5)	9.520(3)	6.9401(7)	8.7590(5)
c (Å)	18.803(5)	13.158(5)	9.659(4)	18.760(2)	13.1716(8)
α (°)	90.00	73.784(5)	82.49(2)	90.00	79.157(5)
β (°)	112.30(3)	81.840(5)	69.47(2)	95.000(13)	77.230(5)
γ (°)	90.00	62.368(5)	77.59(4)	90.00	78.526(5)
V (Å ³)	6696(3)	1859.2(12)	604.7(3)	1458.4(3)	855.28(9)
Z	8	1	1	4	1
ρ_{calcd} (g cm ⁻³)	1.184	0.961	2.109	1.822	2.133
μ (mm ⁻¹)	1.899	1.047	2.748	12.758	8.550
Reflections collected	5529	6909	4885	5201	5856
Unique data/parameters	5529/325	6909/269	4885/161	1462/109	3346/264
R _{int}	0.0972	0.1840	0.0602	0.0656	0.0391
Goodness of fit (S) ^[a]	0.741	0.773	0.959	1.045	1.048
R1 ^[b] /wR2 ^[c] [I>2 σ (I)]	0.0800/0.1840	0.1044/0.2691	0.0288/0.0666	0.0606/0.1560	0.0638/0.1704
R1 ^[b] /wR2 ^[c] [all data]	0.1519/0.2091	0.2330/0.2882	0.0388/0.0681	0.0664/0.1606	0.0820/0.1886

[a] $S = [\sum w(F_o^2 - F_c^2)^2 / (N_{\text{obs}} - N_{\text{param}})]^{1/2}$. [b] $R1 = \sum ||F_o| - |F_c|| / \sum |F_o|$. [c] $wR2 = [\sum w(F_o^2 - F_c^2)^2 / \sum wF_o^2]^{1/2}$; $w = 1/[\sigma^2(F_o^2) + (aP)^2 + bP]$ where $P = (\max(F_o^2, 0) + 2F_c^2)/3$ with $a = 0.0584$ (*CUADEOH*); $a = 0.1283$ (*CUADEC03*); $a = 0.0897$, $b = 4.8645$ (*CO3ADECL*); $a = 0.1437$ (*COADECL-A*); $a = 0.1110$, $b = 2.2530$ (*CUGUACL*).

Table 3.4: Single crystal data and structural refinement details of compounds *CO-9-MEADECL*, *CU-9-MEADEACE*, *CO-6-CLPUR*, *CO-6-THIOG (SMOF-4)*.

Compound	<i>CO-9-MEADECL</i>	<i>CU-9-MEADEACE</i>	<i>CO-6-CLPUR</i>	<i>CO-6-THIOG</i>
Empirical formula	C ₁₂ H ₂₆ Cl ₂ CoN ₁₀ O ₆	C ₁₅ H ₂₃ Cu ₂ N ₅ O ₉	C ₁₀ H ₂₀ Cl ₂ CoN ₈ O ₈	C ₁₅ H ₁₂ CoN ₁₅ S ₃
Formula weight	536.26	544.46	510.17	557.51
λ (Å)	0.71073	0.71073	0.71073	0.71073
T (K)	100(2)	100(2)	100(2)	100(2)
Crystal system	monoclinic	triclinic	monoclinic	trigonal
Space group	<i>I2/m</i>	P $\bar{1}$	<i>P2₁/c</i>	<i>P$\bar{3}$</i>
a (Å)	11.3880(14)	7.3349(8)	10.6365(2)	16.7297(14)
b (Å)	6.7307(7)	8.5513(8)	13.20990(10)	16.7297(14)
c (Å)	14.9009(19)	16.8119(12)	7.33780(10)	6.5245(4)
α (°)	90	94.649(7)	90.00	90.00
β (°)	109.960(14)	93.046(7)	110.057(2)	90.00
γ (°)	90	99.041(8)	90.00	120.00
V (Å ³)	1073.5(2)	1035.64(17)	968.48(2)	1581.4(2)
Z	2	2	2	2
ρ_{calcd} (g cm ⁻³)	1.659	1.746	1.749	1.171
μ (mm ⁻¹)	1.101	2.112	1.221	0.769
Reflections collected	3999	6694	6770	4690
Unique data/parameters	1263/93	3849/287	2104/135	2300/103
R _{int}	0.0216	0.0522	0.0210	0.1278
Goodness of fit (S) ^[a]	1.084	1.083	1.064	1.033
R1 ^[b] /wR2 ^[c] [I>2 σ (I)]	0.0254/0.0600	0.0635/0.1085	0.0244/0.0592	0.0646/0.1585
R1 ^[b] /wR2 ^[c] [all data]	0.0278/0.0618	0.1018/0.1237	0.0268/0.0607	0.0924/0.1673

[a] $S = [\sum w(F_o^2 - F_c^2)^2 / (N_{\text{obs}} - N_{\text{param}})]^{1/2}$. [b] $R1 = \sum ||F_o| - |F_c|| / \sum |F_o|$. [c] $wR2 = [\sum w(F_o^2 - F_c^2)^2 / \sum wF_o^2]^{1/2}$; $w = 1/[\sigma^2(F_o^2) + (aP)^2 + bP]$ where $P = (\max(F_o^2, 0) + 2F_c^2)/3$ with $a = 0.0244$, $b = 1.3486$ (*CO-9-MEADECL*); $a = 0.0341$ (*CU-9-MEADEACE*); $a = 0.0246$, $b = 0.6946$; (*CO-6-CLPUR*); $a = 0.0691$, $b = 1.2150$ (*CO-6-THIOG*).

3.3.2 Structural Description

3.3.2.1 Structural Description of $[\text{Cu}_2(\mu\text{-Hade})_4\text{Cl}_2]\text{Cl}_2\cdot 8\text{H}_2\text{O}$; (*CUADECL-A*)

The crystal structure of *CUADECL-A*, consists of paddle-wheel shaped $[\text{Cu}_2(\mu\text{-adenine})_4\text{Cl}_2]^{2+}$ complex cations, chloride counterions and disordered water molecules. The structure of the dimeric complex cation is shown in Figure 3.8. The two copper(II) centers are bridged by four adenine moieties through their N3 and N9 nitrogen atoms resulting in a paddle-wheel like structure. The copper(II) centers exhibit a distorted square pyramidal geometry with the N3,N9 atoms of the adenine placed in the basal plane and the chloride ligands in the apical position. The dimeric complex is seated on a 2/m crystallographic position and shows a UDD conformation, referring the terms U(up) or D(down) to the coordination of each pyrimidinic N3 atoms to the upper or lower metal centre. The dimeric entity resembles the structure of the previously published complex $[\text{Cu}_2(\mu\text{-ade})_4\text{Cl}_2]\text{Cl}_2\cdot 6\text{H}_2\text{O}$,¹⁵¹ but its crystal structure differs by the number of entrapped water molecules ($[\text{Cu}_2(\mu\text{-ade})_4(\text{Cl})_2]\text{Cl}_2\cdot 8\text{H}_2\text{O}$ for *CUADECL-A*). These subtle changes on the number of crystallization water molecules have been also described for other systems and they have been attributed to a difference on the crystallization temperature: lowering the temperature helps increasing the amount of entrapped water molecules.¹⁵² The selected coordination bond lengths and angles are given in Table 3.5.

In this attempt, though we had been successful in obtaining paddle-wheel shaped discrete entity, we had still been away from the final goal of obtaining rigid synthons that could lead to robust supramolecular arrays as water molecules disrupt the desired direct hydrogen bonding interactions between the nucleobases. The $[\text{Cu}_2(\mu\text{-adenine})_4\text{Cl}_2]^{2+}$ units are held together by hydrogen bonding interactions mediated through the crystallization water molecules, that are in fact disordered altogether with the chloride counterions, giving rise to a complex network of hydrogen bonds. The crystal structure can also be described as layers of dimeric entities held together by means of water mediated $\text{Cl1}\cdots\text{O}_w\cdots\text{O}_w\cdots\text{Cl1}$ and weaker $\text{C8-H}\cdots\text{N1}$ hydrogen bonds. Among these complex sheets, disordered chloride and crystallization water molecules are placed. Figure 3.9 provides a better insight into the crystal structure of compound *CUADECL-A*.

¹⁵¹ de Meester, P.; Skapski, A. C. *J. Chem. Soc. (A)*, **1971**, 2167.

¹⁵² García-Couceiro, U. et al. *Inorg. Chim. Acta* **2004**, 357, 339.

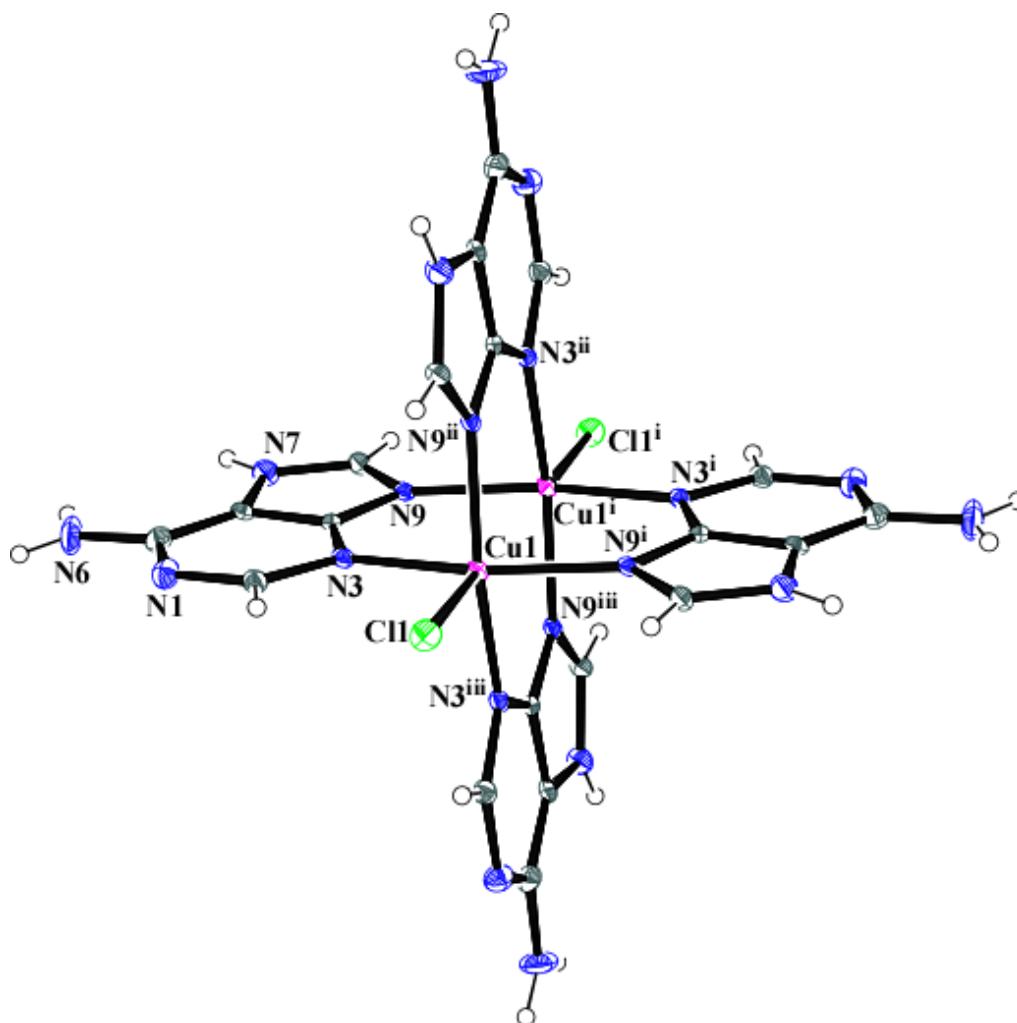


Figure 3.8: Structure of the dimeric complex cation $[\text{Cu}_2(\mu\text{-adenine})_4\text{Cl}_2]^{2+}$ present in *CUADECL-A* together with labeling scheme.

Table 3.5: Selected bond lengths (Å) and angles (°) of the compound *CUADECL-A*.^[a]

Cu1–N3	2.025(4)	N3–Cu1–N3 ⁱⁱⁱ	90.2(2)	N3 ⁱⁱⁱ –Cu1–Cu1 ⁱ	79.99(10)
Cu1–N9 ⁱ	2.020(4)	N3–Cu1–N9 ⁱ	87.90(13)	N9 ⁱ –Cu1–N9 ⁱⁱ	89.90(13)
Cu1–Cl1	2.4017(17)	N3–Cu1–N9 ⁱⁱ	163.14(15)	N9 ⁱ –Cu1–Cl1	97.52(11)
Cu1⋯Cu1 ⁱ	3.0346(15)	N3–Cu1–Cl1	99.32(11)	N9 ⁱ –Cu1–Cu1 ⁱ	79.99(10)
		N3–Cu1–Cu1 ⁱ	79.99(10)	N9 ⁱⁱ –Cu1–Cl1	97.52(11)
		N3 ⁱⁱⁱ –Cu1–N9 ⁱ	163.14(15)	N9 ⁱⁱ –Cu1–Cu1 ⁱ	79.99(10)
		N3 ⁱⁱⁱ –Cu1–N9 ⁱⁱ	87.90(13)	Cl1–Cu1–Cu1 ⁱ	176.47(6)
		N3 ⁱⁱⁱ –Cu1–Cl1	99.32(11)		

[a]Symmetry codes: (i) $-x, -y, z$; (ii) $-x, -y, -z+1$; (iii) $x, y, -z+1$.

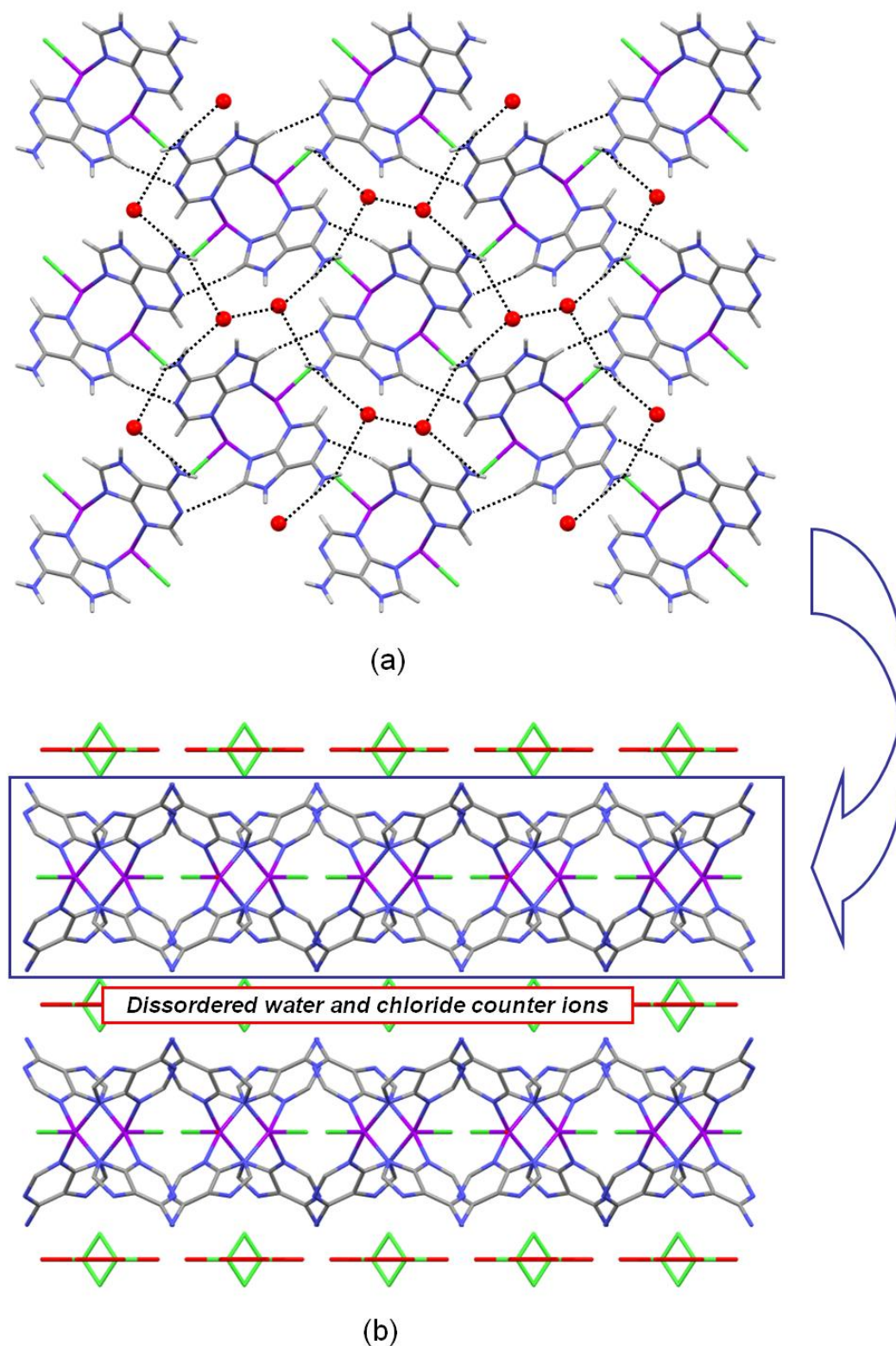


Figure 3.9: Graphical insight into the crystal structure of *CUADECL-A*. (a) Complex layer of $[\text{Cu}_2(\mu\text{-adenine})_4\text{Cl}_2]^{2+}$ units and water molecules. (b) Projection along the crystallographic *a* axis. Notice that the chloride counterions and interlayer water molecules are disordered.

Not only considering this specific example but also other reported examples¹⁵³ with solvated water or any other strong hydrogen bond acceptors shows a general trend of reduced rigidity of the overall network due to solvent mediated flexible hydrogen bonds. From these observations we assume that the presence of strong hydrogen bonding solvents in the reaction media can disrupt the desired direct complementary base pairing interactions between the adenine moieties. Therefore, we focused to avoid the presence of water molecules during the following syntheses and, instead of water, alcohols were employed as solvent.

3.3.2.2 Structural description of $[\text{Cu}_2(\mu\text{-Hade})_4(\text{Cl})_2]\text{Cl}_2 \cdot 2\text{MeOH}$; (**CUADECL-B/SMOF-1**) and $[\text{Cu}_2(\mu\text{-Hade})_4(\text{Br})_2]\text{Br}_2 \cdot \sim 2\text{MeOH}$; (**CUADEBR-A/SMOF-2**)

The compounds **CUADECL-B** (**SMOF-1**) and **CUADEBR-A** (**SMOF-2**) are isostructural and their crystal structure consists of windmill-like $[\text{Cu}_2(\mu\text{-adenine})_4\text{X}_2]^{2+}$ complex cations, along with chloride or bromide counterions respectively, and disordered methanol molecules. Figure 3.10 shows a perspective view of the dimeric entity together with the labelling scheme which is conventionally accepted for the adenine nucleobase for chemical and biological purposes (where, X = chlorido or bromido), while coordination bond lengths and angles are gathered in Table 3.6. Four bridging adenine molecules are linked to the copper(II) centers through their N3 and N9 nitrogen atoms to provide the core of the windmill shaped dinuclear entity.¹⁵⁴ Two halide anions occupy the apical positions resulting in an elongated square pyramidal coordination environment of the metal centers. As discussed for **CUADECL-A**, the dimeric complex is seated on a $2/m$ crystallographic position and shows a UDD conformation. The structural parameters listed in Table 3.6 are similar to those reported for dimeric compounds containing $\mu\text{-}\kappa\text{N}3:\kappa\text{N}9$ bridging purine ligands.¹⁵⁵ The shape and structural features of the dimeric cation resembles those reported for the analogous compounds $[\text{Cu}_2(\mu\text{-adenine})_4\text{Cl}_2]\text{Cl}_2 \cdot 6\text{H}_2\text{O}$ ¹⁵¹ and the previously mentioned **CUADECL-A** which were obtained using a similar synthesis method but employing water as solvent.

¹⁵³ (a) de Meester, P.; Skapski, A. C. *J. Chem. Soc(A)*, **1971**, 2167. (b) de Meester, P.; Skapski, A. C. *J. Chem. Soc. Dalton Trans.* **1972**, 2400. (c) González-Pérez, J. M. et al. *Inorg. Chem.* **2006**, *45*, 877. (d) Bugella-Altamirano, E. et al. *Inorg. Chim. Acta* **2002**, *339*, 160.

¹⁵⁴ (a) Cepeda, J. et al. *Eur. J. Inorg. Chem.* **2009**, 2344. (b) González-Pérez, J. M. et al. *Inorg. Chem.* **2006**, *45*, 877.

¹⁵⁵ (a) Suggs, J. W. et al. *J. Chem. Soc. Chem. Commun.* **1993**, 307. (b) Sonnenfroh, D.; Kreilick, R. W. *Inorg. Chem.* **1980**, *19*, 1259. (c) Sletten, E. *Acta Crystallogr.* **1969**, *B25*, 1480.

However, the dissimilar features of the solvation molecules afford dramatic changes in the resulting crystal buildings. In the hydrated compounds the interactions between the complex entities are mediated by water molecules to give a non-porous crystal structure maintained by an intricate network of adenine···water and chloride···water/bromide···water interactions. On the contrary, the weaker ability of methanol to establish hydrogen bonds implies that the crystal packing of *CUADECL-B* and *CUADEBR-A* are essentially sustained by the assembling of the windmill dimeric $[\text{Cu}_2(\mu\text{-adenine})_4\text{X}_2]^{2+}$ entities through rigid direct intermolecular hydrogen bonds between the adenine molecules, without involving the solvent methanol molecules, together with interactions taking place between the halide anions and the adenine moieties of the cationic complexes. These direct hydrogen bonding interactions provides extra stability and rigidity to the 3D porous supramolecular network and, as a consequence, increasing the robustness of the crystal building.

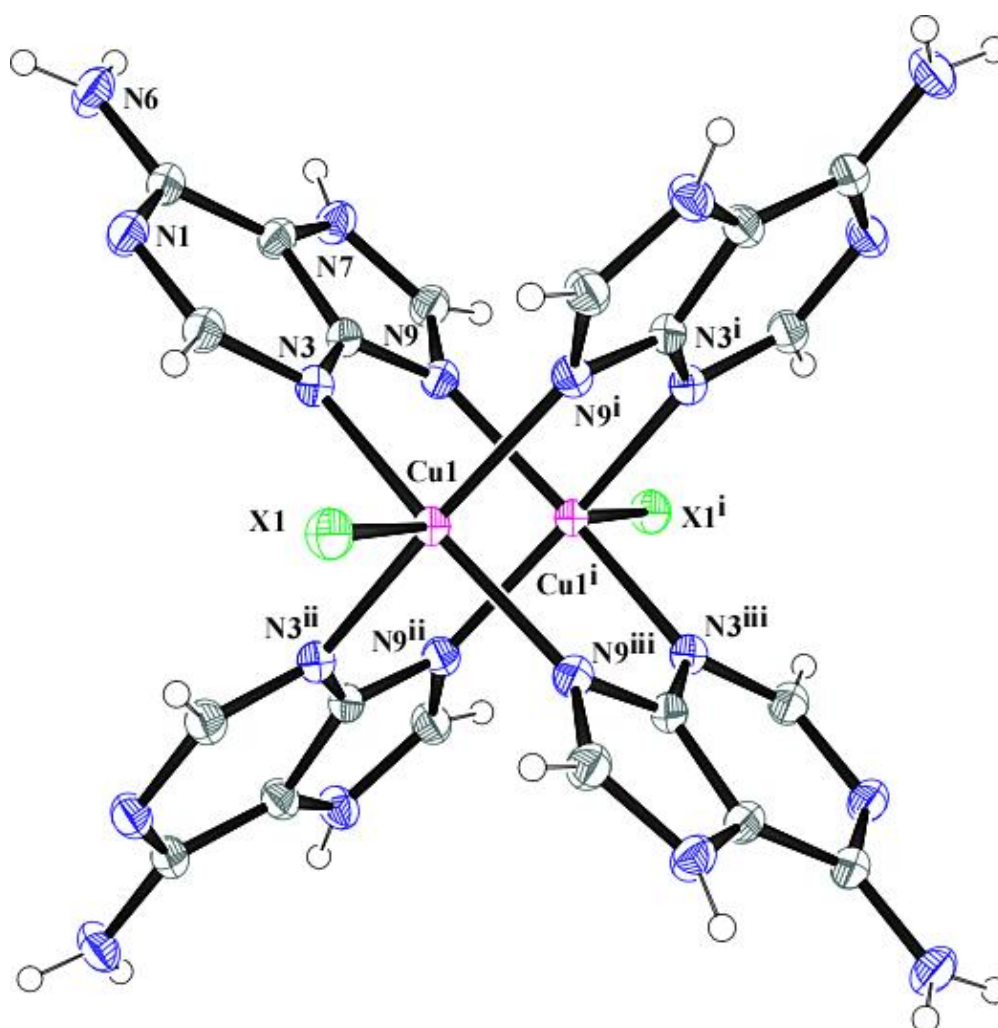


Figure 3.10: Structural unit of *CUADECL-B* and *CUADEBR-A* with the atomic numbering scheme (where X = Cl^- or Br^-).

Table 3.6: Selected bond lengths (Å) and angles (°) for *CUADECL-B* and *CUADEBR-A*.^[a]

	CUADECL-B (SMOF-1)		CUADEBR-A (SMOF-2)	
	100K	293K	100K	
Cu–N3	2.009(2)	2.002(6)	Cu–N3	1.994(5)
Cu–N9 ⁱ	2.027(2)	2.031(5)	Cu–N9 ⁱ	2.016(6)
Cu–Cl1	2.445(1)	2.466(3)	Cu–Br1	3.080(2)
Cu···Cu ⁱ	3.0761(9)	3.064(2)	Cu···Cu ⁱ	3.082(1)
N3–Cu–N3 ⁱⁱ	87.01(13)	86.9(3)	N3–Cu–N3 ⁱⁱ	88.1(3)
N3–Cu–N9 ⁱ	87.45(9)	87.7(2)	N3–Cu–N9 ⁱ	86.5(2)
N3–Cu–N9 ⁱⁱⁱ	161.49(9)	162.5(3)	N3–Cu–N9 ⁱⁱⁱ	161.6(3)
N3–Cu–Cl1	100.57(7)	99.8(2)	N3–Cu–Br1	100.2(2)
N9 ⁱ –Cu–N9 ⁱⁱⁱ	92.27(12)	92.5(3)	N9 ⁱ –Cu–N9 ⁱⁱⁱ	93.1(3)
N9 ⁱ –Cu–Cl1	97.80(7)	97.5(2)	N9 ⁱ –Cu–Br1	98.0(2)

[a] Symmetry codes: (i) $x-y, -y, -z+2$; (ii) $-x+y+1, y, z$; (iii) $-x+1, -y, -z+2$.

This synthon involving the Watson–Crick faces yields by itself a four-connected uninodal 3 dimensional net with *nbo* topology and $(6^4.8^2)$ point symbol.¹⁵⁶ However, the cohesion of the structure is further strengthened by $R_2^1(7)$ type hydrogen bonding interaction established among the free halide counterions and the Hoogsteen faces of two adenines of neighboring complexes. Considering both types of interactions (Watson–Crick base pairing and Hoogsteen···halide) the supramolecular network can be alternatively described as an eight-connected uninodal with *reo* topology and $(3^8.4^8.5^8.6^4)$ point symbol.

On analysing the supramolecular hydrogen bonding interactions of *CUADECL-B* (*SMOF-1*) (as can be seen in Figure 3.11), the dinuclear entities of *CUADECL-B* (*SMOF-1*) are cross-linked together by pairs of symmetry-related N6–H···N1 hydrogen bonding interactions between the Watson–Crick faces of two adjacent nucleobases to give a $R_2^2(8)$ ring, a well-known structural synthon involved in the supramolecular recognition processes which determines the self-assembling pattern of the adenine moieties to form supramolecular aggregates in a great diversity of metal–nucleobase systems.^{80,157} Furthermore, coordination

¹⁵⁶ Blatov, V. A. *IUCR CompComm. Newsletter* **2006**, 7, 4, (accessed jan. 2012), TOPOS Main Page. <http://www.topos.ssu.samara.ru>.

¹⁵⁷ See for example: (a) Byres, M. et al. *CrystEngComm*. **2009**, 11, 135. (b) Galindo, M. A. et al. *Chem. Commun.* **2009**, 2833. (c) Peacock, A. F. A. et al. *J. Am. Chem. Soc.* **2007**, 129, 3348 (d) Morel, A. C. et al. *Inorg. Chem. Commun.* **2003**, 6, 1354.

of the adenine through the N9 atom of the pyridine ring produce the proton transfer to the imidazole N7 site to give the non-canonical 7H-adenine tautomer¹⁵⁸ which favours the formation of a hydrogen-bonded $R_2^1(7)$ ring between the Hoogsteen face [N6H, N7H] of the nucleobase as donor and the chloride anion as acceptor.¹⁵⁹ Structural parameters for the supramolecular interactions are listed in Table 3.7. Each chloride counterion is joined to two adenine ligands from adjacent dimeric complexes forming a distorted tetrahedral hydrogen bonding environment.

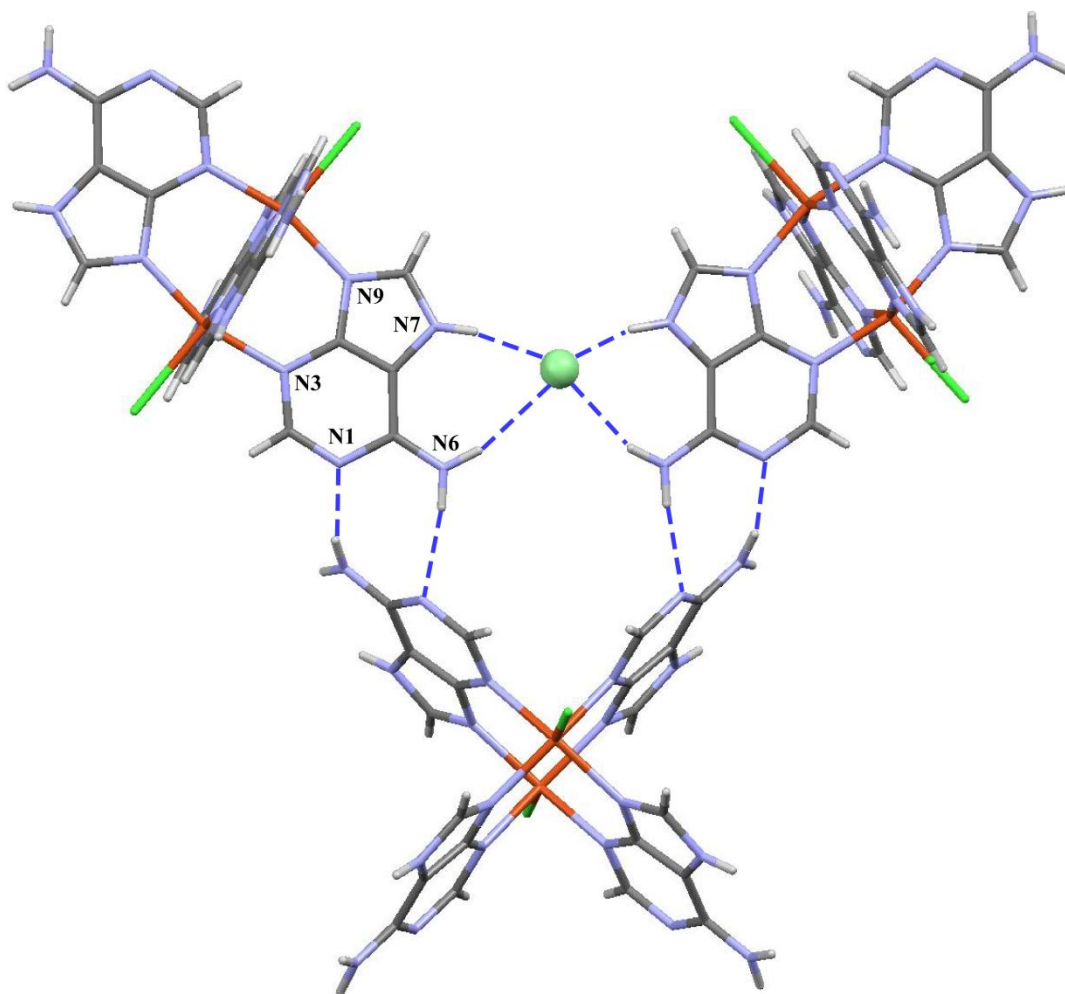


Figure 3.11: Details of the adenine...adenine and adenine...chloride interactions in the crystal packing of *CUADECL-B (SMOF-1)*.

¹⁵⁸ García-Terán, J. P. et al. *Dalton Trans.* **2006**, 902.

¹⁵⁹ See for example: (a) Garcia-Raso, A. et al. *Polyhedron* **2007**, 26, 949. (b) Mastropietro, T. F. et al. *Polyhedron* **2007**, 26, 4945. (c) Suzuki, T. et al. *Inorg. Chem.* **2004**, 43, 6435. (d) de Meester, P.; Skapski, A. C. *J. Chem. Soc. Dalton Trans.* **1973**, 424.

Table 3.7: Hydrogen bonding interactions (Å, °) in *CUADECL-B (SMOF-1)*.^[a]

<i>D-H...A</i> ^[b]	<i>D-H</i>	<i>H...A</i>	<i>D-H...A</i>
<i>100K</i>			
N6-H6A...N1 ⁱ	2.19	3.015(3)	161.1
N6-H6A...Cl2 ⁱⁱ	2.66	3.466(3)	156.4
N7-H7...Cl2 ⁱⁱ	2.24	3.034(2)	154.2
<i>293K</i>			
N6-H6A...N1 ⁱ	2.20	3.032(8)	163.3
N6-H6A...Cl2 ⁱⁱ	2.69	3.505(8)	157.5
N7-H7...Cl2 ⁱⁱ	2.23	3.032(7)	156.3

[a] Symmetry codes: (i) $x-y, -y, -z+1$; (ii) $y, -x+y, -z$; [b] **D**: donor; **A**: acceptor.

The self-assembling process driven by the above-described rigid interactions results in a supramolecular 3D structure containing very large channels along the crystallographic *c* axis with a diameter of ~6.3 Å (Figure 3.12). These channels represent a 36% of the total volume of the unit cell and they are occupied by solvent methanol molecules in a highly disordered manner.

The hydrogen bonding parameters of *CUADEBR-A (SMOF-2)* shown in Table 3.8 and Figure 3.13, depict the hydrogen bonding interactions involving the nucleobases and the bromide anions and the resulting porous supramolecular network.

Table 3.8: Hydrogen bonding interactions (Å, °) in *CUADEBR-A (SMOF-2)*.^[a]

<i>D-H...A</i> ^[b]	<i>D-H</i>	<i>H...A</i>	<i>D...A</i>	<i>D-H...A</i>
N6-H6A...N1 ⁱ	0.86	2.23	3.060(9)	162.4
N6-H6B...Br2 ⁱ	0.86	2.76	3.572(8)	158.7
N7-H7...Br2	0.86	2.35	3.140(6)	152.3

[a] Symmetry codes: (i) $-x+2/3, -x+y+1/3, -z+4/3$. [b] **D**: donor; **A**: acceptor.

As it is depicted in Figure 3.13, the synthon involving the Watson-Crick faces of the adenine nucleobases yields by itself a four-connected uninodal 3 dimensional net with *nbo* topology and $(6^4.8^2)$ point symbol¹⁵⁶ same as in the case of the previously mentioned chloride analogue *CUADECL-B (SMOF-1)*. Similarly, the cohesion of the structure is further

strengthened by the hydrogen bonding interaction established among the free bromide counterions and the Hoogsteen faces of two adenines of neighbouring complexes. A $R_2^1(7)$ hydrogen bonded ring is established for each bromide...Hoogsteen face interaction. Considering both types of interactions (Watson–Crick base pairing and Hoogsteen...bromide) the supramolecular network can be alternatively described as an eight-connected uninodal with *reo* topology and $(3^8.4^8.5^8.6^4)$ point symbol. Representations of the hydrogen bonding nets are shown in Figure 3.14.

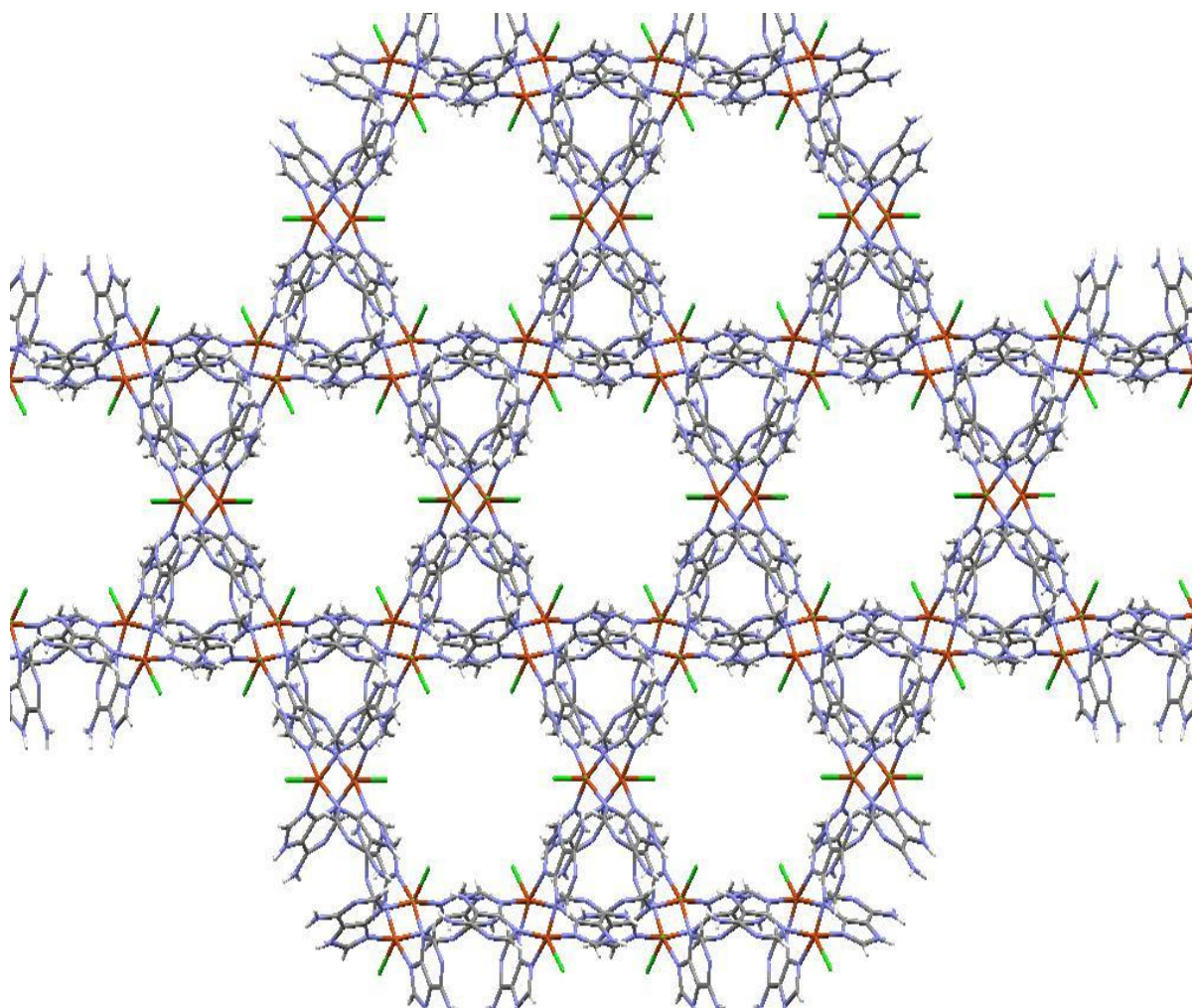


Figure 3.12: Perspective view of the 3D framework along the *c*-axis showing the pores in compound *CUADDECL-B* (*SMOF-1*). Solvated methanol molecules are omitted for clarity.

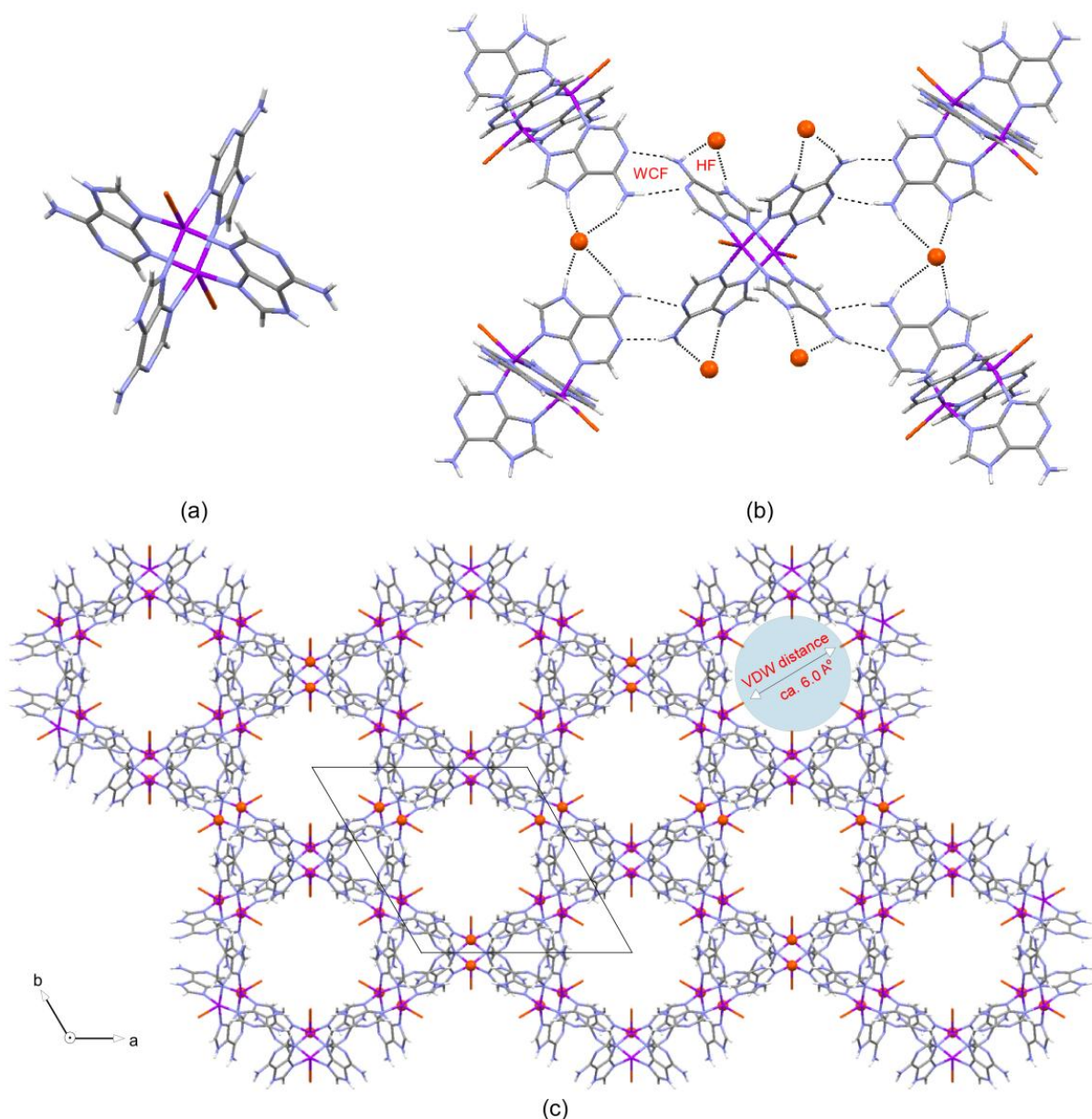


Figure 3.13: Crystal structure features of *CUADEBR-A (SMOF-2)*: (a) Structural unit. (b) Details of the adenine base pairing interaction through the Watson–Crick face (WCF) and of the Hoogsteen Face (HF) mediated adenine...bromide interaction (free bromide anions are represented as orange spheres). (c) Perspective view of the 3D framework along the c -axis showing the pores.

The resulting porous structure consists of 1D tubular channels that run along the crystallographic c axis with a diameter of ~ 6.0 Å (distance between van der Waals surfaces of opposite bromide anions). These channels represent 30% of the total crystal volume¹⁵⁰ and they are occupied by solvent methanol molecules in a highly disordered manner. Due to the greater size of bromide anion these values are somewhat lower than those found in the case of *CUADECL-B (SMOF-1)* where the pore diameter is 6.3 Å and the accessible volume is 36%.

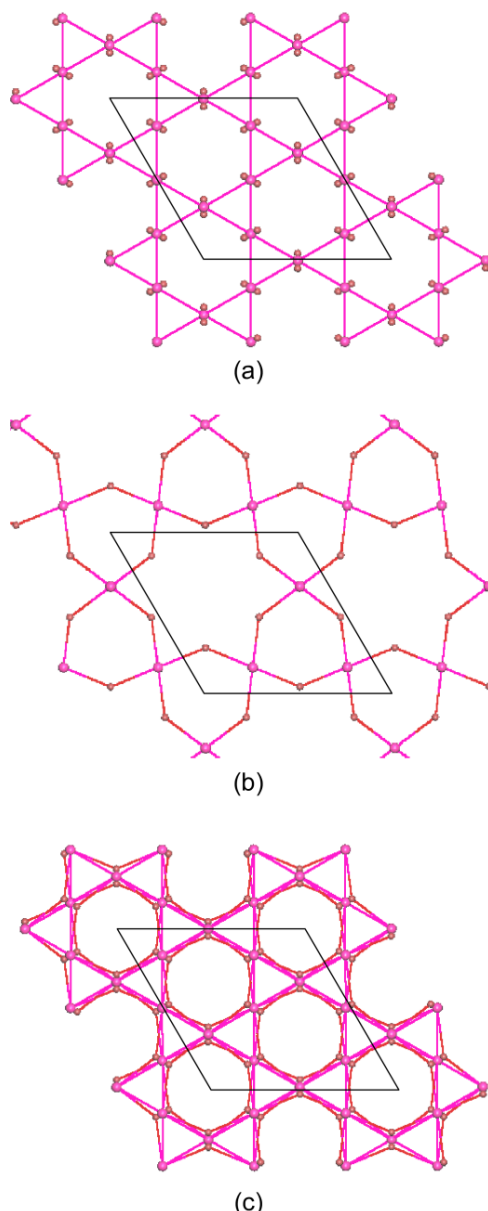


Figure 3.14: (a) Watson-Crick base pairing generated four-connected uninodal 3D net, (b) Hoogsteen edge···bromide hydrogen bond generated net and (c) supramolecular network considering both interactions in **CUADEBR-A** (**SMOF-2**).

3.3.2.2.1 Thermogravimetric analysis of **CUADECL-B** (**SMOF-1**) and **CUADEBR-A** (**SMOF-2**)

The thermal stability of the two compounds was assessed by means of thermogravimetric analysis. Figures 3.15–16 and Table 3.9 show the thermogravimetric and thermodiffractometric data of **CUADECL-B** (**SMOF-1**) and **CUADEBR-A** (**SMOF-2**). According to the thermogravimetric data of both compounds, the release of the solvent molecules hosted in the channels takes place between room temperature and 100 °C, and it involves a weight loss of *ca.* 7.0% (calcd.: 7.32% for two methanol molecules per formula

unit). In both cases the resulting compound remains stable up to 240 °C and the XRPD patterns at different temperatures (Figure 3.16) do not differ substantially from that corresponding to the starting material, suggesting that the 3D open framework is retained after the removal of the methanol molecules. Above this temperature it undergoes successive exothermic processes leading to CuO as final residue above 500°C.

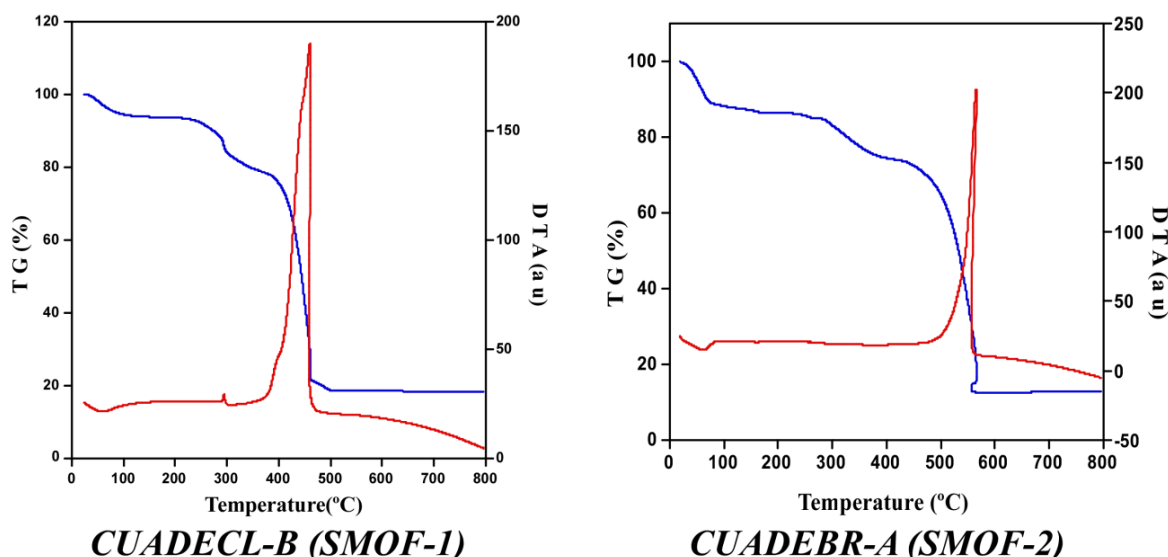


Figure 3.15: Thermoanalytic data for compounds *CUADECL-B* (*SMOF-1*) and *CUADEBR-A* (*SMOF-2*) performed upon synthetic air atmosphere (79% N₂, 21% O₂).

Table 3.9: Thermogravimetric data of *CUADECL-B* (*SMOF-1*) and *CUADEBR-A* (*SMOF-2*).^[a, b]

Step	T_i	T_f	T_{peak}	$\Delta m(\%)$	ΔH	$\Sigma \Delta m(\%)$	$\Sigma \Delta m(\%)_{theor}$
<i>CUADECL-B</i>							
1	25	155	58	7	Endo	7	7.32 (-2 CH ₃ OH)
2	205	375	294	15.2	Exo	22.2	12.77 (-1 C ₅ H ₅ N ₅)
3	375	500	460	60	Exo	82.2	81.8 (2 CuO)
<i>CUADEBR-A</i>							
1	25	100	63	11.67	Endo	11.67	12.12 (-4 CH ₃ OH)
2	100	215	–	2.33	–	14	15.26 (-1 CH ₃ OH)
3	215	415	–	12.27	–	26.27	28.24 (-1 C ₅ H ₅ N ₅)
4	415	555	566	60.50	Exo	86.77	84.88 (2 CuO)

[a] T_i = initial temperature; T_f = final temperature; T_{peak} = DTA peak temperature; $\Delta m(\%)$ = mass loss percentage for each process; ΔH = process type in the basis of DTA; $\Sigma \Delta m(\%)$ = total mass loss percentage; $\Sigma \Delta m(\%)_{theor}$ = theoretical total mass loss percentage. [b] Released molecules/fragments and final residue by formula.

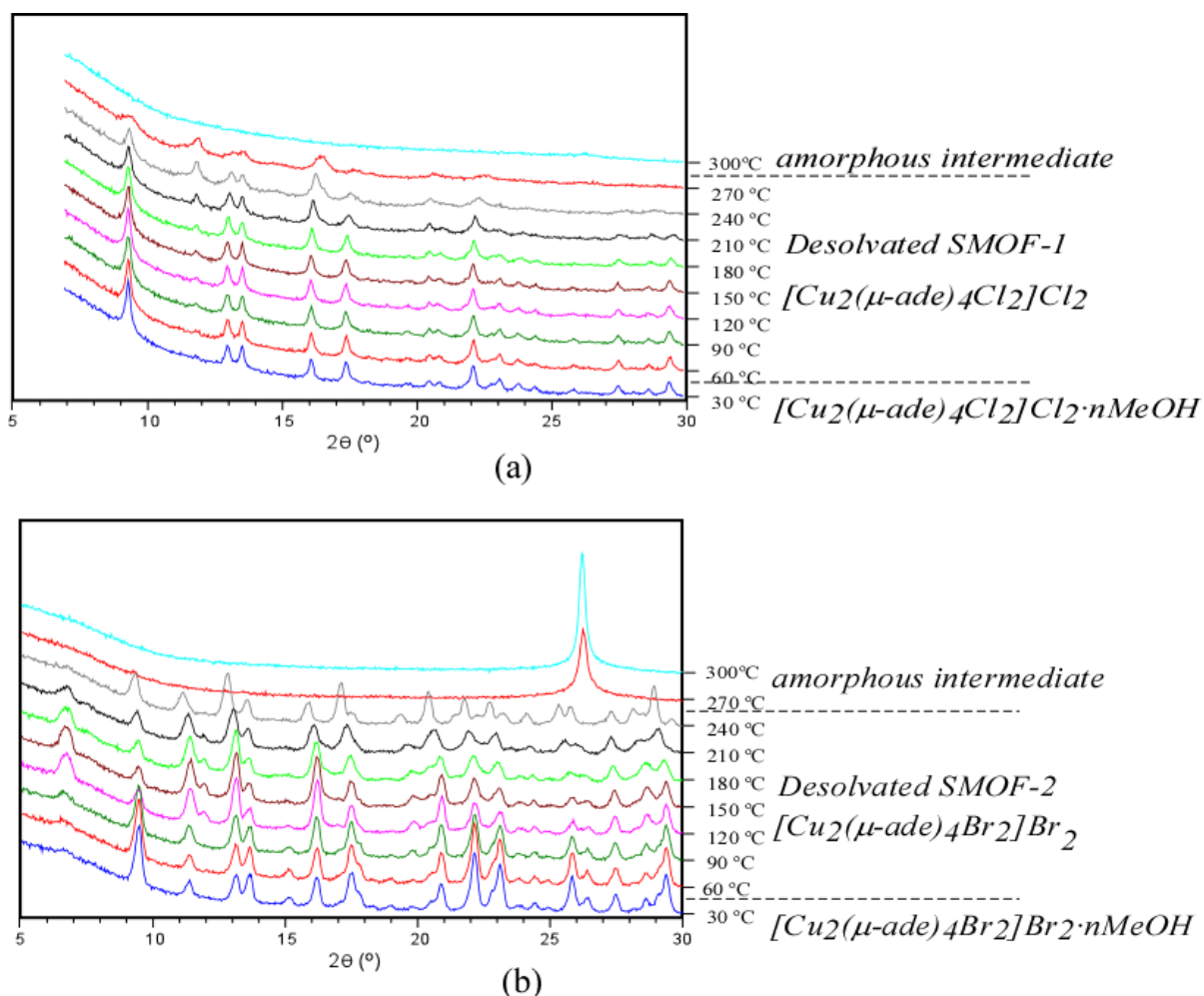


Figure 3.16: Thermodiffractometric plots of (a) *CUADECL-B* (SMOF-1) and (b) *CUADEBR-A* (SMOF-2).

3.3.2.2.2 Gas adsorption experiments on *CUADECL-B* (SMOF-1) and *CUADEBR-A* (SMOF-2).

Freshly synthesized single crystals of *CUADECL-B* (SMOF-1) and *CUADEBR-A* (SMOF-2) were used for gas adsorption experiments and they were activated under vacuum at temperatures ranging from 100 to 180°C during 6–24 h to eliminate solvent guest molecules prior to measurements. Different outgassing conditions did not exert significant changes in N₂ uptake capacity. For clarity only the results of samples outgassed at 150 °C during 12 h are shown in subsequent figures. The adsorption curve collected at 77 K exhibits features resulting from multilayer adsorption. The fitting of the adsorption area to BET equation lead to surface area values of 26 and 14 m²/g, respectively. These values are substantially smaller than the accessible surface area calculated from the crystal structure (789

and 658 m²/g) by a Monte Carlo integration technique, where a probe molecule with a diameter equal to the Lennard–Jones parameter for N₂ (3.681 Å) is “rolled” over the framework.¹⁶⁰ Thereafter, H₂ adsorption experiments were also carried out by collecting isotherms at 77 K. Similarly to N₂, a negligible adsorption is observed for both compounds. A common explanation for such difference between the experimental and expected porosity includes incomplete solvent removal, crystal collapse or a massive presence of impurities. However, the weight loss of the outgassed sample fits the one expected from the compound formula which suggests a quantitative removal of the solvent. The XRPD data confirms that the outgassed sample retains its crystallinity and therefore, its bulk porous framework. Finally, the comparison of XRPD, chemical analysis and scanning electron microscopy data on the fresh and outgassed samples allowed ruling out the presence of a substantial amount of impurities.

In a recent work, Matzger and coworkers explained the discrepancies between crystallographic porosity and experimental gas uptake for *Zn–HKUST–1* based on positron annihilation lifetime spectroscopy.¹⁶¹ The authors state that the lack of gas uptake is due to the inherent surface instability after solvent removal which renders the material impermeable to molecular guests irrespective of the handling and activation methods used in the gas adsorption experiments. However, according to the later work, the surface collapse is overcome when the sample is immersed in a solvent and thus, the porous network is well accessible.

Nonetheless, preliminary experiments have shown that the desolvated product of *CUADECL–B (SMOF–1)* is able to adsorb in few minutes the humidity of the surrounding atmosphere to fill the empty channels with water molecules undergoing a weight increase of around 8% (*ca.* 4 water molecules per formula unit) and retaining the initial porous crystal structure without substantial changes in the X–ray diffraction powder pattern. Upon heating, the hydrated compound releases again the water molecules which are reabsorbed at room temperature. However, a suspension of the *CUADECL–B (SMOF–1)* in water affords an amorphous material after 24 hours. These facts suggest that the title compound is able to accept some amount of water molecules without any remarkable change in its crystal structure

¹⁶⁰ Düren, T. et al. *J. Phys. Chem. C*, **2007**, *111*, 15350

¹⁶¹ Feldblyum, J. I. et al. *J. Am. Chem. Soc.* **2011**, *133*, 18257.

but when the water is used as solvent, it acts as disruptor of the direct hydrogen bonds established between the adenine molecules and the crystal building collapses. With further experiments, the present compounds have shown to behave as an adsorbent not only for humidity but also when it was exposed to the vapours of methanol, acetone, dichloromethane, tetrachloromethane.¹⁶² Thus it seems that the above described diffusion barrier resulting from the surface instability, it is not only overcome in solution but also when guest molecules in gas phase have enough interaction energy to pass through. In order to get further evidence on the later statement, we have carried out gas adsorption measurements at greater temperatures by collecting the isotherms for CO₂ at 273 K and CH₄ at 298 K (Figure 3.17).

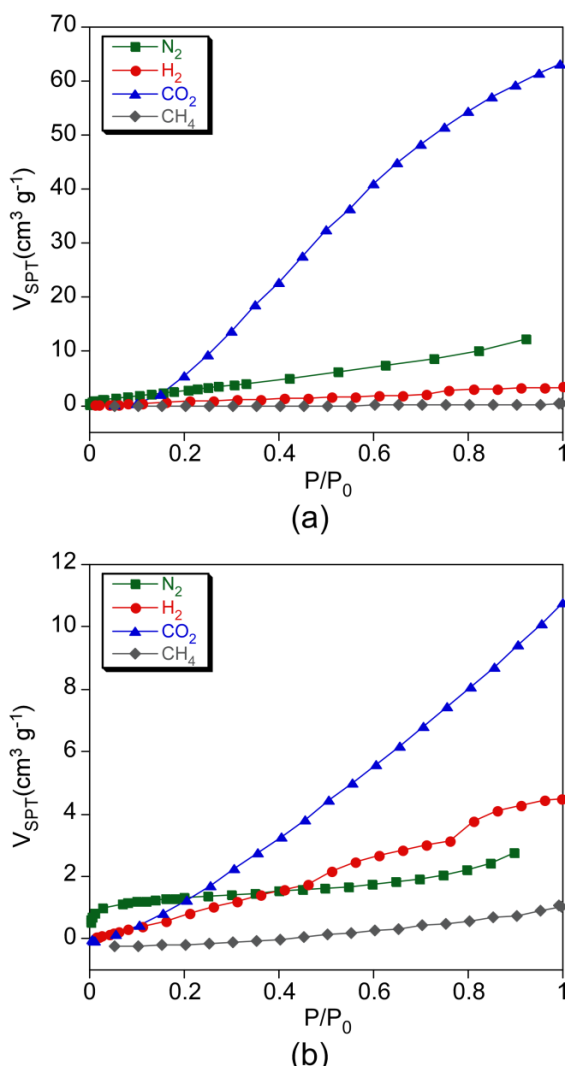


Figure 3.17: Adsorption isotherms for N₂ (77 K), H₂ (77 K), CO₂ (273 K), and CH₄ (298 K) for fresh samples of compounds **CUADDECL-B (SMOF-1)** (a) and **CUADEBR-A (SMOF-2)** (b).

¹⁶² Thomas-Gipson, J. et al. *CrystEngComm*. **2011**, *13*, 3301.

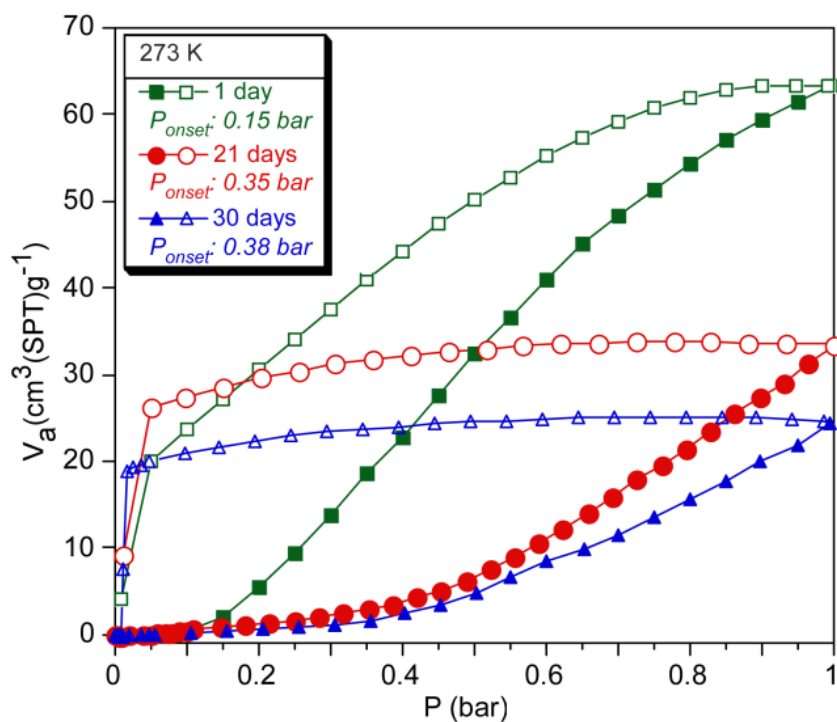
Similar to the previous adsorbates, no methane adsorption is observed. However the CO₂ uptake shows a notable increase in both compounds. In fact while at pressures close to saturation, the N₂ uptake is of 0.54 and 0.12 mmol/g for compounds **CUADECL-B (SMOF-1)** and **CUADEBR-A (SMOF-2)**, the CO₂ uptake increases about four times to reach values of 2.81 and 0.48 mmol/g, respectively. Considering the later results this behavior can be rationalized on the basis of the thermal energy and of the polar nature of the adsorbate. The apolar CH₄ lacks of quadrupole moment, while CO₂ presents a relatively strong quadrupole moment ($-0.8908 \text{ e}\cdot\text{\AA}^2$), substantially greater than that for N₂ or H₂ (-0.2946 and $+0.1288 \text{ e}\cdot\text{\AA}^2$, respectively).¹⁶³ Methane has not been able to permeate the surface even with the increase of the adsorption temperature. Nonetheless, the greater measurement temperature and the stronger quadrupole moment of CO₂ confer the ability to diffuse through the surface barrier and permeate the porous network.

An additional proof that supports the surface instability of these compounds is obtained from the gas adsorption study of the sample ageing. In this regard, CO₂ measurements were carried out periodically during a month on samples of **CUADECL-B (SMOF-1)** stored at room conditions (Figure 3.18a). It becomes clear that the CO₂ uptake capacity decreases progressively as the sample becomes older, and after a month the uptake at P = 1 bar is depleted to a *ca.* 60% when compared to its initial value ($V_{\text{STP}} = 63.3$ and $24.4 \text{ cm}^3 \text{ g}^{-1}$ for the initial and one month aged sample). A second phenomenon related with the sample ageing lies on the adsorption onset pressure calculated from the intersection between the tangents at the low pressure region and at the region of maximum slope of the adsorption branch (Table 3.10).

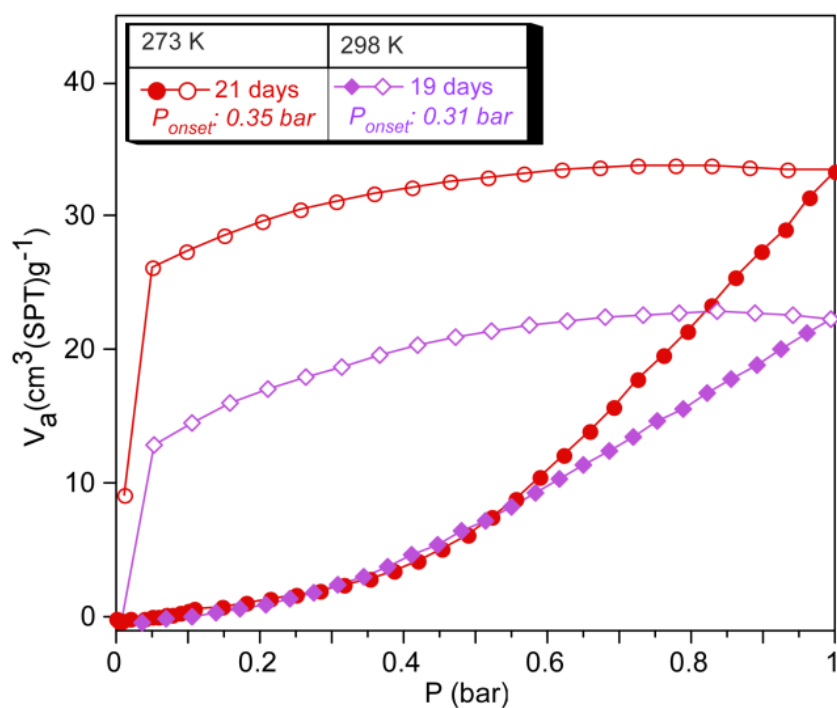
Table 3.10: Calculated onset point values for **CUADECL-B (SMOF-1)**.

Sample	Aging (days)	Adsorption Temp. (K)	Onset value (bar)
SMOF-1	1	273	0.15
	21	273	0.35
	30	273	0.38
	21	298	0.31

¹⁶³ NIST Computational Chemistry Comparison and Benchmark Database NIST Standard Reference Database Number 101. Release 16a, August 2013, Editor: Johnson, R. D. III. <http://cccbdb.nist.gov/>.



(a)



(b)

Figure 3.18: (a) CO₂ adsorption/desorption isotherms measured at 273 K showing the aging of *CUADCL-B (SMOF-1)*. (b) CO₂ isotherms at 273 and 298 K. The onset pressure value is indicated for each case.

The adsorption of the initial sample shows a plateau with a negligible CO₂ uptake at pressures below 0.1 bar, and it requires a minimum breakthrough pressure (P_{onset} : 0.15 bar) to

permeate the surface and reach the porous network. Moreover, the breakthrough pressure has increased to higher values as the sample gets older, to reach an onset value of $P_{\text{onset}} = 0.38$ bar for the sample aged during 1 month. This progressive increase of the breakthrough pressure is related with an increase of the thickness of the collapsed surface which acts as a surface permeation barrier. Another feature that supports the presence of a surface barrier that hinders the diffusion of the molecules is related to the hysteresis cycle enclosed by desorption branch and its trend with the ageing of the sample (Figure 3.18a). It is noteworthy that despite different equilibration times were used the hysteresis cycle was not affected, and as a consequence, this hysteresis seems to be induced by structural features of the sample. In fact, the hysteresis becomes more acute as the sample is aged and its end-pressure is also delayed progressively (P_{end} : 0.05 and 0.02 bar for fresh and one month aged samples, respectively). This behavior is also congruent with an increasing thickness of the collapsed surface (or diffusion barrier) as the storage time goes on, which would also obstruct the release of the adsorbed molecules during the desorption process.

On the other hand, comparison between adsorption experiments carried out at 273 K and 298 K on similarly aged samples (Figure 3.18b), shows that the onset pressure (0.35 and 0.31 bar, respectively) is reduced with the increase of the experiment temperature, as the potential energy of the molecules to permeate the surface is increased.

In order to analyze the bulk crystal stability during CO₂ adsorption PXRD patterns were collected in a sample subjected to a CO₂ atmosphere with pressure ranging between 0.5 and 6 bar. Prior to the experiment the sample was outgassed at 150 °C during several hours. As it can be observed (Figure 3.19) all the experimental reflections match the ones corresponding to the simulated patterns of *CUADECL-B (SMOF-1)*, *CUADEBR-A (SMOF-2)*, and in any case no shift in 2θ positions is observed which stands for stability of the bulk crystallinity and for the bulk framework rigidity during the CO₂ adsorption process (i.e. reversible structural changes caused by CO₂ uptake can be disregarded, as for example, the so-called breathing effect).¹⁶⁴

¹⁶⁴ (a) Ramsahye, N. A. et al. *Chem. Commun.* **2007**, 3261. (b) Serre, C. et al. *Adv. Mater.* **2007**, *19*, 2246.

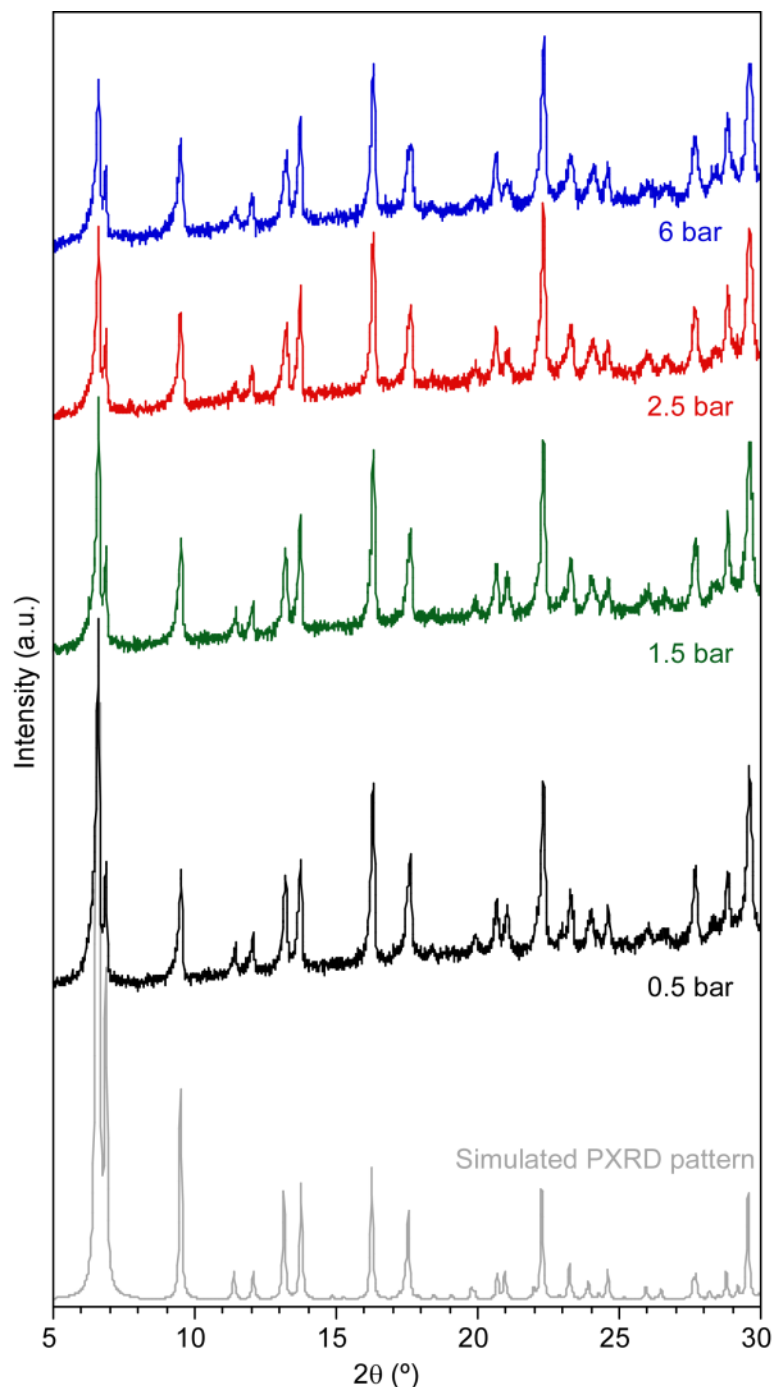


Figure 3.19: Comparison between experimental PXRD patterns collected at different CO₂ pressures and simulated PXRD pattern for the pristine crystal structure of *CUADDECL-B* (*SMOF-1*).

Regarding to the peak intensity, despite most of the peaks show no changes, the intensities of certain reflections are significantly affected. Figure 3.20a shows the trend of three reflections within the 6–10° 2θ range. As it can be observed [2 0 $\bar{1}$] reflection remains unvarying while the intensity of [2 $\bar{1}$ 0] and [1 0 1] decay continuously with the increasing CO₂ pressure, which seems to be related with the CO₂ uptake within the structural pores.

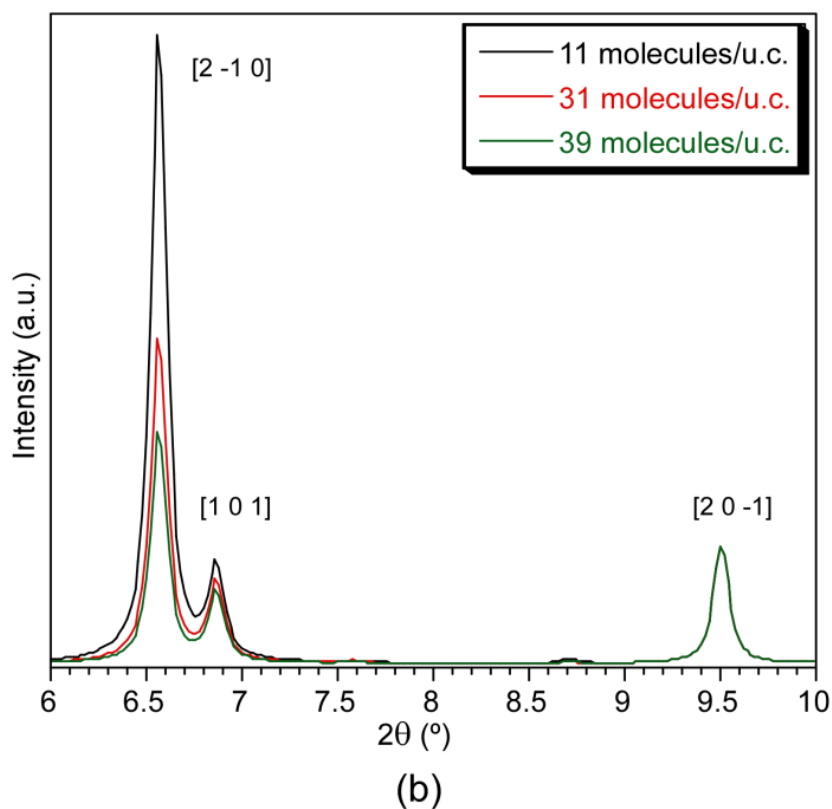
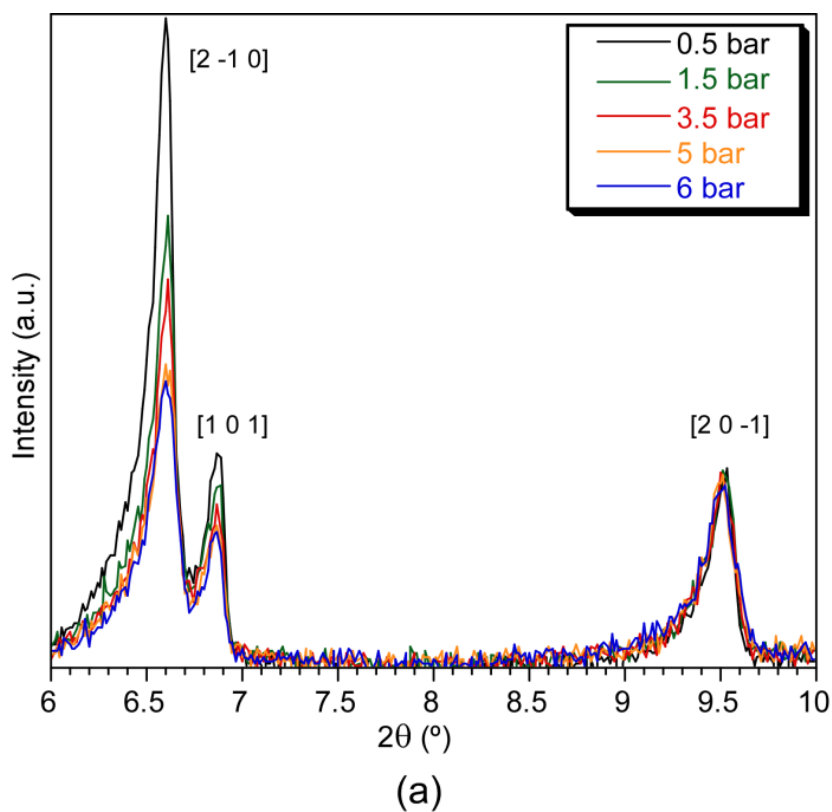


Figure 3.20: PXRD data for *CUADDECL-B* (*SMOF-1*) within 6–10°: (a) experimental patterns with increasing CO₂ pressure. (b) Simulated PXRD patterns from GCMC low energy configurations with increasing CO₂ uptake per unit cell.

In order to confirm the later proposal, Grand Canonical Monte Carlo (GCMC) calculations were carried out in which the porous framework of *CUADECL-B (SMOF-1)* was loaded with different amounts of CO₂. Low energy configurations of the adsorbed molecules were used to model how the PXRD patterns are affected by the CO₂ (Figure 3.20b). The trend derived from the GCMC simulations matches the observed one for experimental PXRD patterns, which allows to state that intensity decay of the cited reflections ($[2 \bar{1} 0]$ and $[1 0 1]$) is due to the presence of CO₂ within the 1D pores. When coordinates of CO₂ molecules are considered non symmetry relation is found in any of the GCMC calculations. However, there is a periodicity of the preferential sites of adsorption (most sites derived from probability density distribution for the center of mass of CO₂ molecule) in which electron density coming from adsorbed gas is accumulated (Figure 3.21). As a consequence, the decay of the mentioned reflections can be attributed to this periodically distributed averaged electron density of the adsorbed molecules.

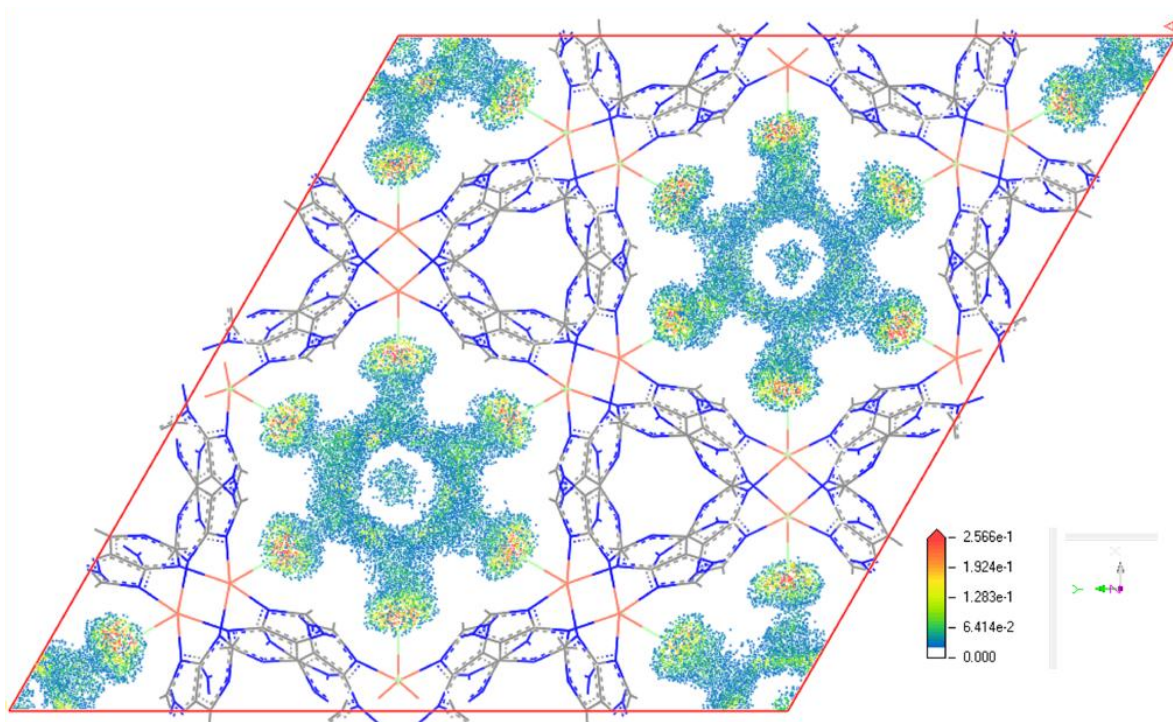


Figure 3.21: Average occupation profiles for CO₂ at 298 K in *CUADECL-B (SMOF-1)*.

3.3.2.3 Structural description of $[\text{Cu}_2(\mu\text{-Hade})_2(\mu\text{-Cl})_2(\text{Cl})_2] \cdot 2\text{MeOH}$; *CUADECL-C (SMOF-3)* and $[\text{Cu}_2(\mu\text{-Hade})_2(\mu\text{-Br})_2(\text{Br})_2] \cdot 2\text{PrOH}$; *CUADEBR-B*

Both compounds are comprised of neutral centrosymmetric dimeric $[\text{Cu}_2(\mu\text{-adenine})_2(\mu\text{-X})_2(\text{X})_2]$ entities (X: Cl⁻, Br⁻) (Figure 3.22). They present some resemblances with the previously described $[\text{Cu}_2(\mu\text{-adenine})_4\text{X}_2]^{2+}$ dimeric entity of *CUADECL-B*

(*SMOF-1*) and *CUADEBR-A (SMOF-2)*. The overall paddle-wheel shape is retained but two opposite adenine ligands have been replaced by two bridging halido ligands giving rise to a neutral dimeric entity showing a UD conformation with regard to the adenine bridges and capped by two additional terminal halido ligands. The intradimeric Cu...Cu distances (2.942(1) and 2.902(1) Å, for chloride and bromide analogues) are slightly shorter than that of *CUADECL-B (SMOF-1)* and *CUADEBR-A (SMOF-2)* (3.064(1) and 3.082(1) Å). Each copper atom is penta-coordinated by a N₂X₃ donor set which resembles a compressed trigonal bipyramid. The equatorial plane consists of three halido ligands implying longer bond distances than the apical ones (Table 3.11) and X–Cu–X angles within the range of 106–144° and a deviation of *ca.* 0.05 Å for the Cu(II) centre. The apical positions are occupied by the N3 and N9 donor sites of two symmetry related adenine molecules with a N–Cu–N angle of *ca.* 165° and an angle between equatorial plane and Cu–N bond of 83–86°. The coordination bond distances of the bridging halide anions are slightly longer than those of the terminal ones as usually happens.⁸⁷

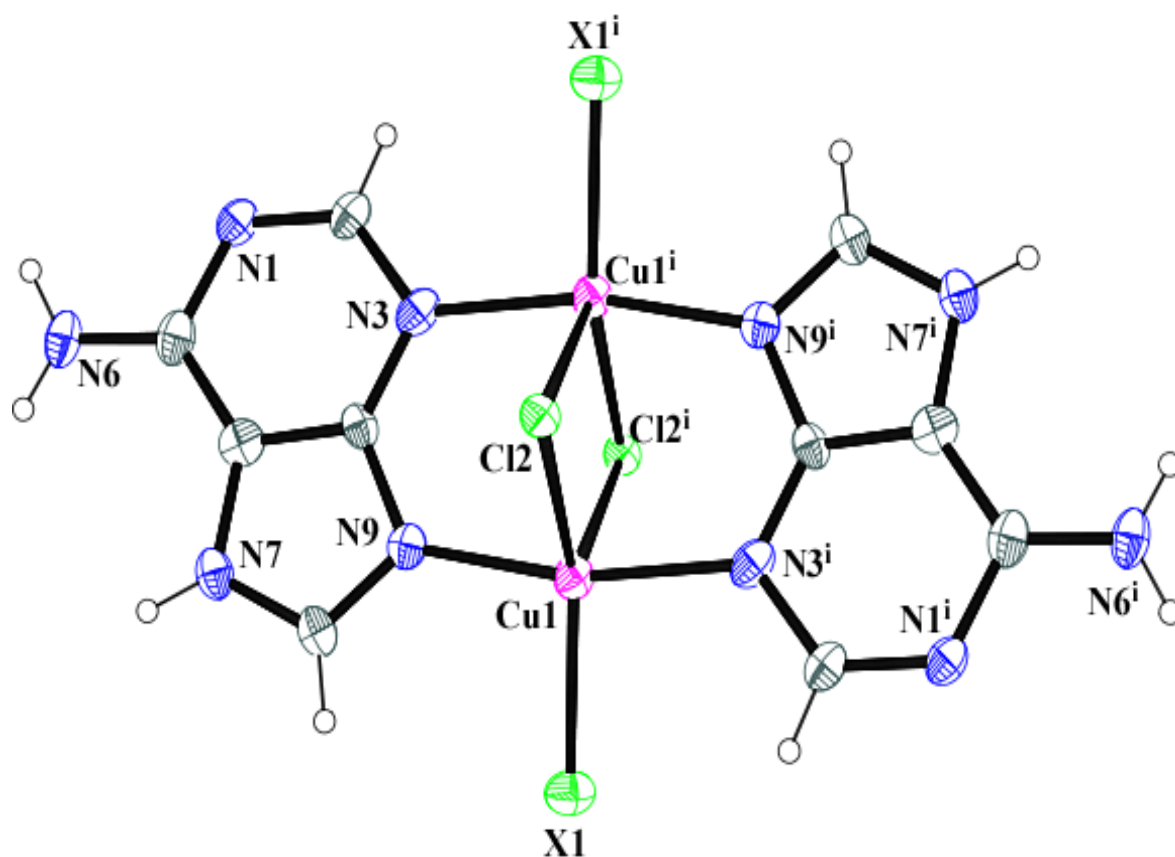


Figure 3.22: Ortep representation of the $[\text{Cu}_2(\mu\text{-ade})_2(\mu\text{-X})_2\text{X}_2]$ units in *CUADECL-C (SMOF-3)* and *CUADEBR-B*.

Table 3.11: Selected bond lengths (Å) and angles (°) for the coordination polyhedron of *CUADECL-C (SMOF-3)* and *CUADEBR-B*.^[a]

CUADECL-C		CUADEBR-B	
Cu–N3 ⁱ	2.006(4)	Cu–N3 ⁱ	1.963(5)
Cu–N9	1.983(4)	Cu–N9	1.962(5)
Cu–Cl1	2.241(1)	Cu–Br1	2.378(1)
Cu–Cl2	2.342(1)	Cu–Br2	2.540(1)
Cu–Cl2 ⁱ	2.757(1)	Cu–Br2 ⁱ	2.656(1)
Cu···Cu ⁱ	2.942(1)	Cu···Cu ⁱ	2.902(1)
N3 ⁱ –Cu–N9	164.83(17)	N3 ⁱ –Cu–N9	165.8(2)
N3 ⁱ –Cu–Cl1	96.71(13)	N3 ⁱ –Cu–Br1	98.02(14)
N3 ⁱ –Cu–Cl2	87.19(14)	N3 ⁱ –Cu–Br2	87.23(14)
N3 ⁱ –Cu–Cl2 ⁱ	83.77(13)	N3 ⁱ –Cu–Br2 ⁱ	86.58(13)
N9–Cu–Cl1	94.32(13)	N9–Cu–Br1	95.56(14)
N9–Cu–Cl2	87.19(14)	N9–Cu–Br2	86.78(14)
N9–Cu–Cl2 ⁱ	83.21(13)	N9–Cu–Br2 ⁱ	83.73(14)
Cl1–Cu–Cl2	144.00(6)	Br1–Cu–Br2	132.35(3)
Cl1–Cu–Cl2 ⁱ	105.81(6)	Br1–Cu–Br ⁱ	115.45(3)
Cl2–Cu–Cl2 ⁱ	110.07(4)	Br2–Cu–Br2 ⁱ	112.12(3)

[a]Symmetry codes: (i) $-x+1/2, -y+1/2, -z+1$.

Obviously, in the case of *CUADECL-C (SMOF-3)*, the coplanar arrangement and the lower amount of adenines in the dimeric $[\text{Cu}_2(\mu\text{-ade})_2(\mu\text{-Cl})_2\text{Cl}_2]$ entity in comparison to the secondary building unit found in compounds *CUADECL-B (SMOF-1)* and *CUADEBR-A (SMOF-2)*, does not preclude the polymerization through direct complementary hydrogen bonding interactions between the nucleobases. However, it reduces the dimensionality of the resulting supramolecular network polymerized through direct complementary hydrogen bonding interactions between the nucleobases. The hydrogen bonding parameters of *CUADECL-C (SMOF-3)* are given in Table 3.12. In fact, in the case of *CUADECL-C (SMOF-3)*, the base pairing interaction between the Watson–Crick faces of $[\text{Cu}_2(\mu\text{-ade})_2(\mu\text{-Cl})_2(\text{Cl})_2]$ units gives rise to linear 1D supramolecular ribbons that spread along two different

crystallographic directions $[1\ 1\ 0]$ and $[1\ \bar{1}\ 0]$ as it can be observed in Figure 3.23. These supramolecular ribbons are further crosslinked by means of both the hydrogen-bonding interactions between the Hoogsteen face and the bridging chlorido ligands and π - π stacking interactions between adjacent adenines. The combination of the later two types of interactions leads also to a relatively rigid synthon that extends the connectivity towards a robust supramolecular 3D network and, at the same time, precludes an efficient occupation of the space. Considering both types of synthons (Watson-Crick base pairing and Hoogsteen...chlorido/ π - π stacking) the supramolecular network can be described as a six-connected uninodal with *rob* topology and $(4^8.6^6.8)$ point symbol. This packing generates 1D channels along the crystallographic *c* axis with an elliptical cross-section of *ca.* 5.5×7.5 Å, that are filled by solvation methanol molecules that represent a 21% of the total volume. Again, the combination of rigid metal-nucleobase building unit and geometrically restricted supramolecular synthons leads to an ineffective space occupation providing accessible space within the crystal structure of this material. It is worthy to mention that the hydrogen bonding interaction between the Hoogsteen side of the adenine and the chlorido ligands is reinforced by an indirect hydrogen bond mediated by a solvation methanol molecule that will cause, as it is discussed later, a relatively significant unit cell change upon the removal of the solvent molecules.

Table 3.12: Supramolecular interactions (Å, °) in *CUADECL-C (SMOF-3)*.

Hydrogen bonding interactions. ^[a]					
<i>D-H...A</i> ^[b]	<i>D-H</i>	<i>H...A</i>	<i>D...A</i>	<i>D-H...A</i>	
N6-H6B...O1	0.86	2.19	2.811(8)	128.7	
N6-H6B...N1 ⁱ	0.86	2.14	2.999(6)	175.0	
N7-H7...Cl2 ⁱⁱ	0.86	2.45	3.180(5)	143.5	
π - π stacking interactions. ^[c]					
Ring...Ring ^[d]	Angle	DC	α	DZ	DXY
Ring(1)...Ring(2) ⁱⁱⁱ	2.1(3)	3.656(3)	26.93	3.298(2)	1.58
Ring(2)...Ring(1) ^{iv}	2	4.216(3)	37.52	3.260(2)	2.67

[a] Symmetry: (i) $-x+1, -y, -z+1$; (ii) $-x+1/2, y-1/2, -z+1/2$; (iii) $x, -y, z+1/2$; (iv) $x, -y, z-1/2$. [b] **D**: donor; **A**: acceptor. [c] Angle: Dihedral Angle between Planes I and J (°), DC: Distance between ring centroids (Å), α : Angle Cg(I)—>Cg(J) vector and normal to plane I (°), DZ: Perpendicular distance of Cg(I) on ring J (Å), DXY: Slippage. [d] Ring 1: N7, C5, C4, N9, C8; Ring 2: N1, C2, N3, C4, N9, C6.

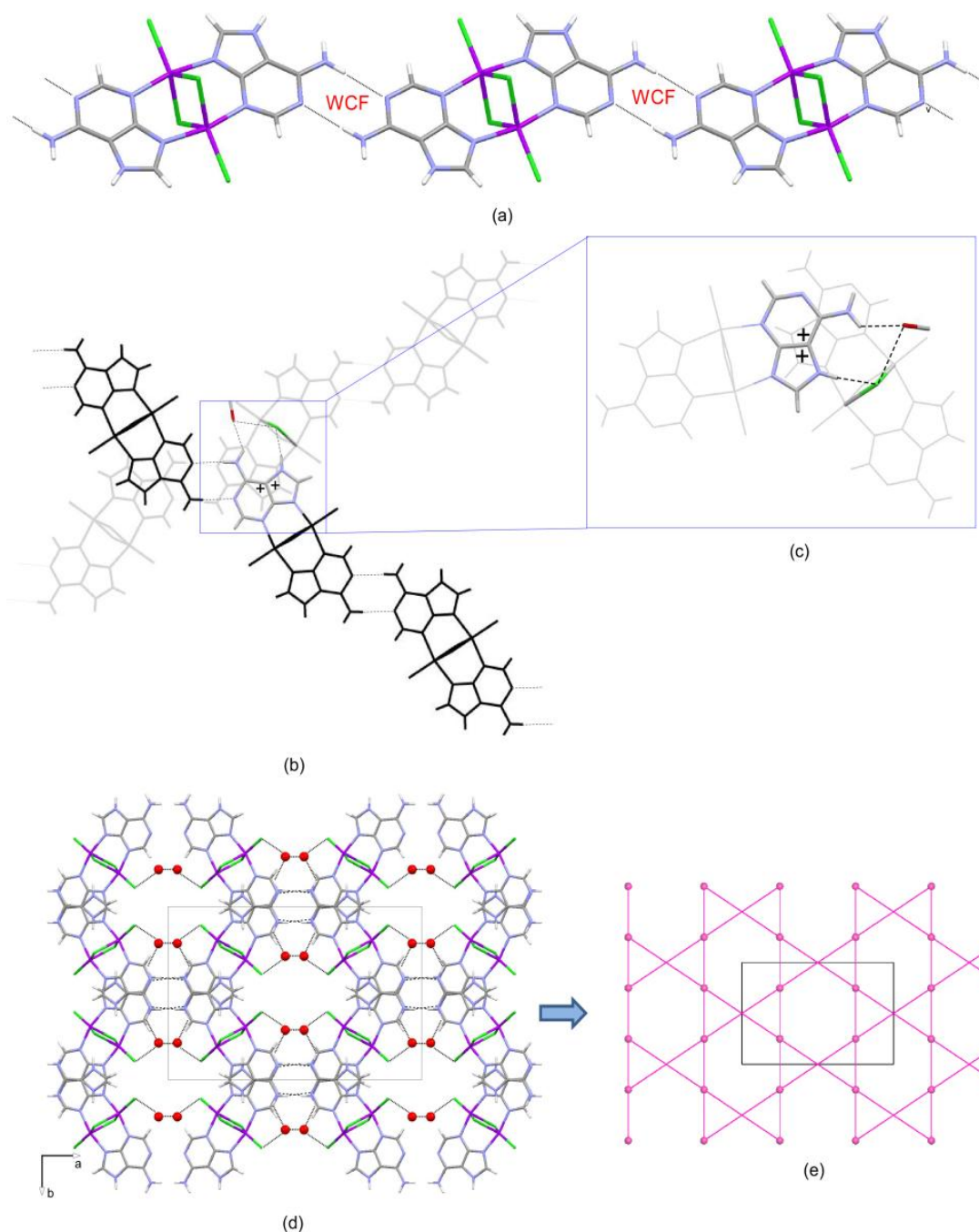


Figure 3.23: Crystal packing features in *CUADECL-C* (*SMOF-3*): (a) Strips of $[\text{Cu}_2(\mu\text{-adenine})_2(\mu\text{-Cl})_2(\text{Cl})_2]$ dinuclear complexes grown by Watson-Crick base pairing interactions. (b, c) Dinuclear entities interacting through $\text{Cl}\cdots\text{Hoogsteen face}$ and $\pi\text{-}\pi$ interactions. (d, e) View of the crystal packing through $[1\ 0\ 0]$ direction and overall supramolecular connectivity. Dashed lines indicate hydrogen bonds, while double plus signals represent $\pi\text{-}\pi$ stacking interactions.

The weaker hydrogen bond accepting nature of the bromido ligand in comparison to chlorido makes the crystal packing features of *CUADEBR-B*, $[\text{Cu}_2(\mu\text{-ade})_2(\mu\text{-Br})_2(\text{Br})_2]\cdot\text{PrOH}$ (Figure 3.24) to be essentially different from that of its chloride analogue *CUADECL-C* (*SMOF-3*). It does not present neither base pairing interactions nor any other

direct hydrogen bonding interactions between the adenine moieties and coordinated bromides. In fact, the dinuclear entities are held together by the hydrogen bonding interactions mediated through the entrapped propan-1-ol molecules with the Hoogsteen and Watson-Crick faces of adjacent paddle-wheel entities. The Hoogsteen face of the nucleobase is hydrogen bonded to the oxygen atom of the propan-1-ol molecule ($R_2^1(7)$ hydrogen bonded ring), while the Watson-Crick face of the adenine establishes a single hydrogen bond by means of the interaction of N1 with H atom of the alcohol group. The hydrogen bonding parameters are given in Table 3.13. The supramolecular network is further reinforced by halido $\cdots\pi$ type interactions established between the terminal Br1 atoms and C5 carbon of the (Br1 \cdots C5: 3.489(1) Å). The lack of direct hydrogen bonding interactions among the rigid adenine moieties and the solvent mediated disruption of the hydrogen bonding network results in a non-porous crystal structure which collapses at temperatures close to 50 °C rendering an amorphous product, according to the thermogravimetric and temperature variable XRPD measurements.

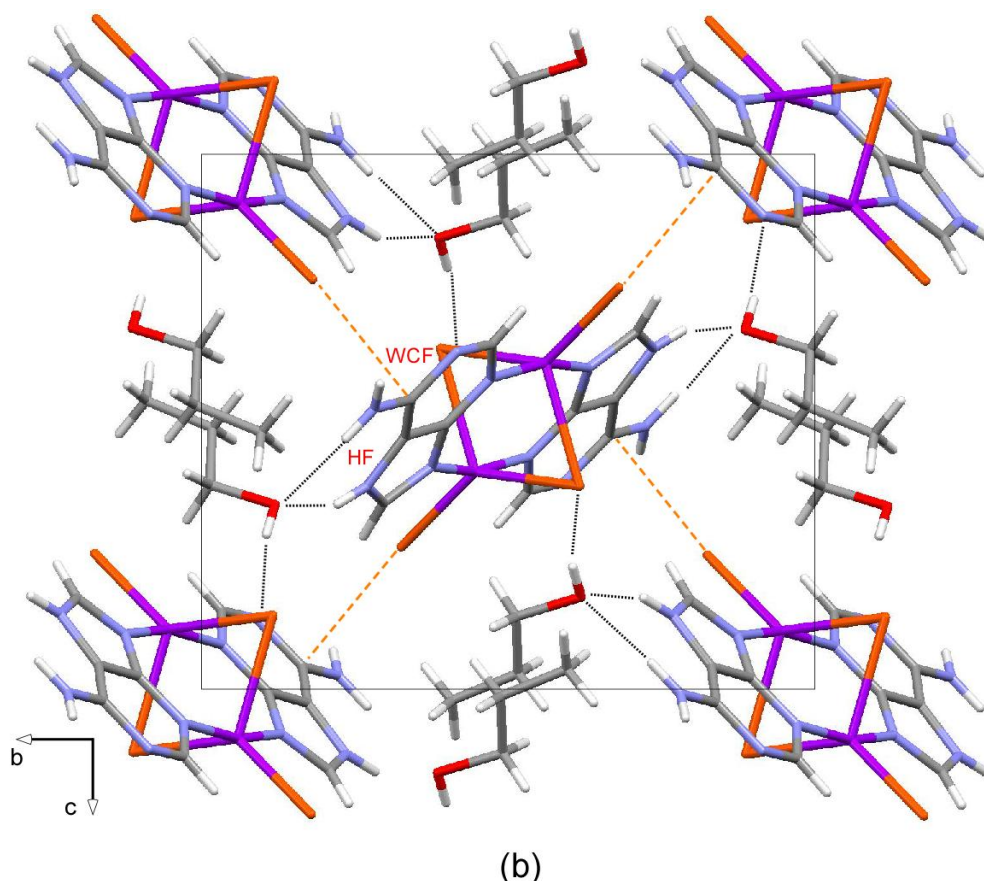


Figure 3.24: A view of the crystal packing through [1 0 0] direction in *CUADEBR-B*. Black dotted lines indicate hydrogen bonding interactions, while orange dashed lines indicate halido $\cdots\pi$ contacts.

Table 3.13: Hydrogen bonding interactions (Å, °) in the compound *CUADEBR-B*.^[a]

<i>D-H...A</i> ^[b]	<i>D-H</i>	<i>H...A</i>	<i>D...A</i>	<i>D-H...A</i>
N6-H6A...Br2 ⁱ	0.86	2.63	3.424(5)	153.1
N6-H6B...O1 ⁱⁱ	0.86	2.10	2.931(6)	162.1
N7-H7...O1 ⁱⁱ	0.93(9)	1.89(9)	2.776(6)	159(8)
O1-H1...N1 ⁱ	0.77(10)	2.02(10)	2.775(6)	171(10)

[a] Symmetry codes: (i) $-x+2, -y, -z+2$; (ii) $x, -y+1/2, z-1/2$. [b] **D**: donor; **A**: acceptor.

3.3.2.3.1 Thermogravimetric analysis of *CUADECL-C (SMOF-3)* and *CUADEBR-B*

In order to assess the stability of the unsolvated *CUADECL-C (SMOF-3)* thermogravimetric (Figure 3.25 and Table 3.14) and temperature variable XRPD experiments were carried out (Figure 3.26). Thermogravimetric analysis shows that the solvent molecules are released easily at temperatures below 140 °C. Afterwards, the TGA curve shows a stable plateau that extends up to 245 °C. At higher temperatures the compound decomposes in successive exothermic steps to yield CuO as the final residue at temperatures above 500 °C. The compound *CUADEBR-B* is also stable up to 200 °C and then it decomposes to the final residue CuO above 600 °C.

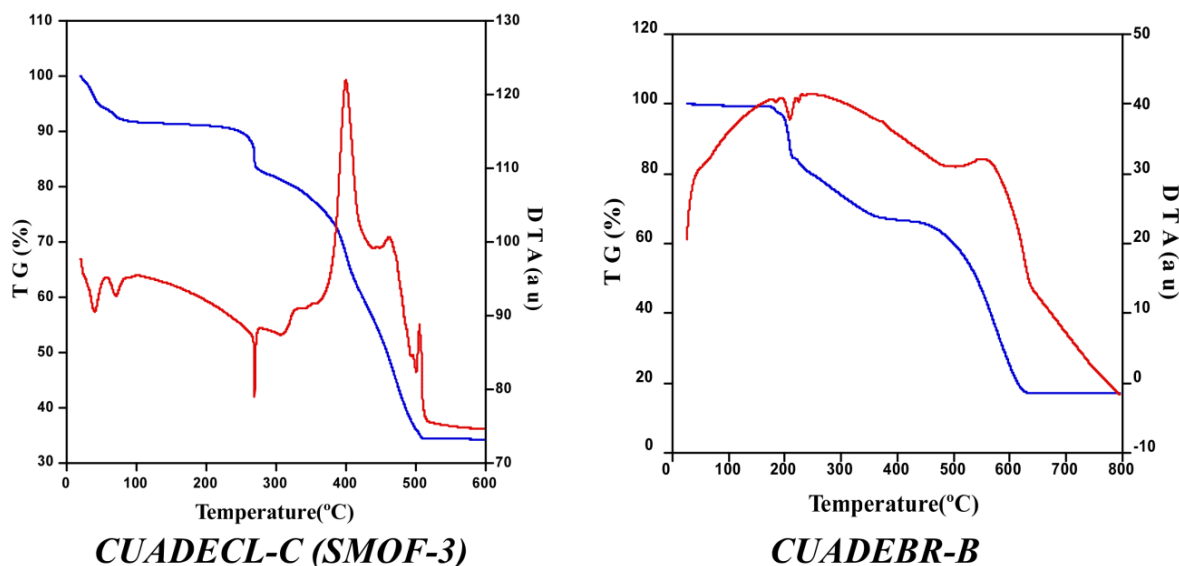


Figure 3.25: Thermogravimetric data for compounds *CUADECL-C (SMOF-3)* and *CUADEBR-B*

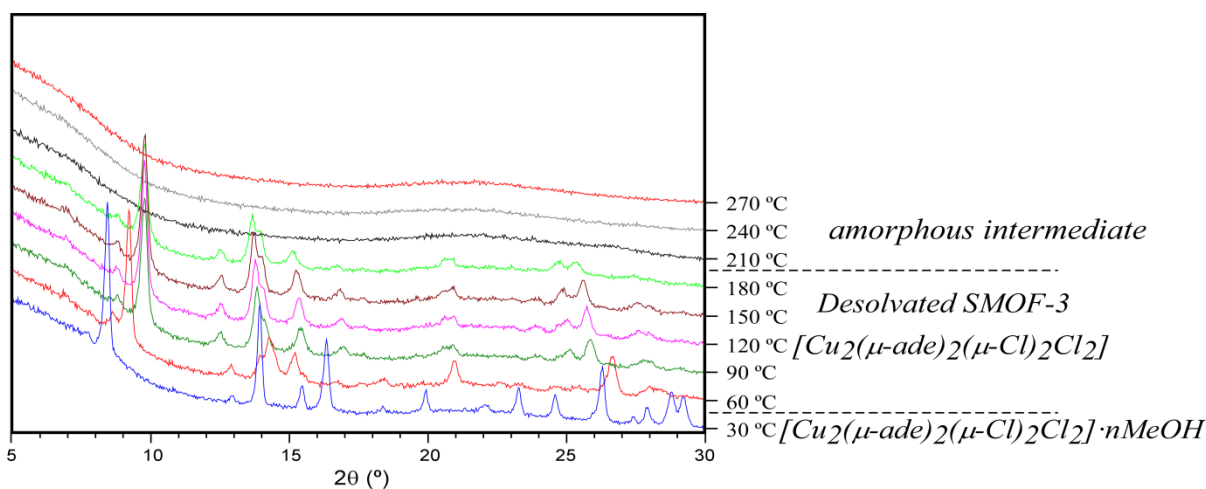
Table 3.14: Thermogravimetric data for compounds *CUADECL-C (SMOF-3)* and *CUADEBR-B*^[a,b]

Step	T_i	T_f	T_{peak}	$\Delta m(\%)$	ΔH	$\Sigma \Delta m(\%)$	$\Sigma \Delta m(\%)_{theor}$
<i>CUADECL-C (SMOF-3)</i>							
1	25	140	40/70	9.44	Endo	9.44	10.06(-2 CH ₃ OH)
2	245	320	270	7.37	Endo	16.81	16.10 (-HCl)
3	320	510	400/462/505	48.75	Exo	65.56	67.05 (2 CuO)
<i>CUADEBR-B</i>							
1	25	215	185/210	15.12	Endo	15.12	14.36 (-2 PrOH)
2	220	375	–	18.26	Exo	33.38	33.68 (-2 HBr)
4	430	630	555	49.48	Exo	82.86	81.00 (2 CuO)

[a] T_i = initial temperature; T_f = final temperature; T_{peak} = DTA peak temperature; $\Delta m(\%)$ = mass loss percentage for each process; ΔH = process type in the basis of DTA; $\Sigma \Delta m(\%)$ = total mass loss percentage; $\Sigma \Delta m(\%)_{theor}$ = theoretical total mass loss percentage. [b] Released molecules/fragments and final residue per formula.

As it is evident from the Figure 3.26, the thermodiffractometric measurements of *CUADECL-C (SMOF-3)* show a significant difference between the diffractogram performed at 30 °C and those performed between 90–180 °C. The cell parameters indexed for the PXRD pattern collected at 30 °C match the ones corresponding to the single crystal structure. However, the PXRD pattern change observed at temperatures above 60 °C lead to new unit cell parameters closely related to the previous ones but with a significant change in the unit cell transforming it to a non standard monoclinic setting with $\gamma \neq 90^\circ$. This transformation is related to a rearrangement of the synthon established between the Hoogsteen face and the chloride anion once the methanol molecule is released.¹⁶⁵ A scheme of this rearrangement is given in the Figure 3.26. It indicates that although the supramolecular structure has suffered a moderate change, its overall supramolecular crystal structure remains essentially stable up to 180 °C.

¹⁶⁵ Thomas–Gipson, J. et al. *Cryst. Growth Des.* **2014**, *14*(8), 4019.



T (°C)	a (Å)	b (Å)	c (Å)	α (°)	β (°)	γ (°)	V (Å ³)
30	22.962(1)	13.668(1)	7.184(1)	90	108.47(1)	90	2138.5(1)
60	21.657(1)	13.393(1)	7.096(1)	90	90	107.65(1)	1961.3(1)
90	21.643(1)	12.859(1)	7.391(1)	90	90	101.16(1)	2018.0(1)
120	21.631(1)	12.935(1)	7.440(1)	90	90	101.51(1)	2040.0(1)
150	21.559(1)	12.915(1)	7.135(1)	90	90	101.69(1)	1945.4(1)
180	21.639(1)	12.764(1)	7.725(1)	90	90	100.95(1)	2094.8(1)

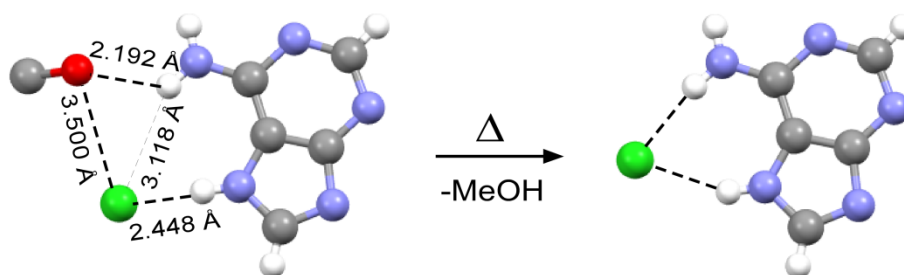


Figure 3.26: Thermodiffractometric data of *CUADECL-C* (*SMOF-3*) and proposed rearrangement scheme for the structural phase transition.

3.3.2.3.2 Gas Adsorption studies of *CUADECL-C* (*SMOF-3*)

In order to assess the permanent porosity inferred from thermodiffractometric measurement, gas adsorption isotherms were measured on freshly synthesized sample of *CUADECL-C* (*SMOF-3*) which was activated under vacuum at 140 °C during 12 h to eliminate solvent guest molecules. The results and conclusions derived from the study of the gas adsorption behavior of *CUADECL-B* (*SMOF-1*) and *CUADEBR-A* (*SMOF-2*), suggest that the surface feebleness of this kind of supramolecular compounds can make routine nitrogen adsorption isotherms not suitable for the study of their porosity features. In fact, *CUADECL-C* (*SMOF-3*) presents a computed surface area of 361 m²g⁻¹, but the experimental N₂ adsorption isotherm corresponds to a non-porous material. *CUADECL-C* (*SMOF-3*) adsorbs a significant amount of CO₂ as depicted by Figure 3.27, but comparatively smaller than *CUADECL-B* (*SMOF-1*) and *CUADEBR-A* (*SMOF-2*), due to

the greater free volume and surface area of the later ones. Similar to the precedent supramolecular microporous compounds, *CUADECL-C* (*SMOF-3*) presents a breakthrough pressure close to $P = 0.31$ bar.

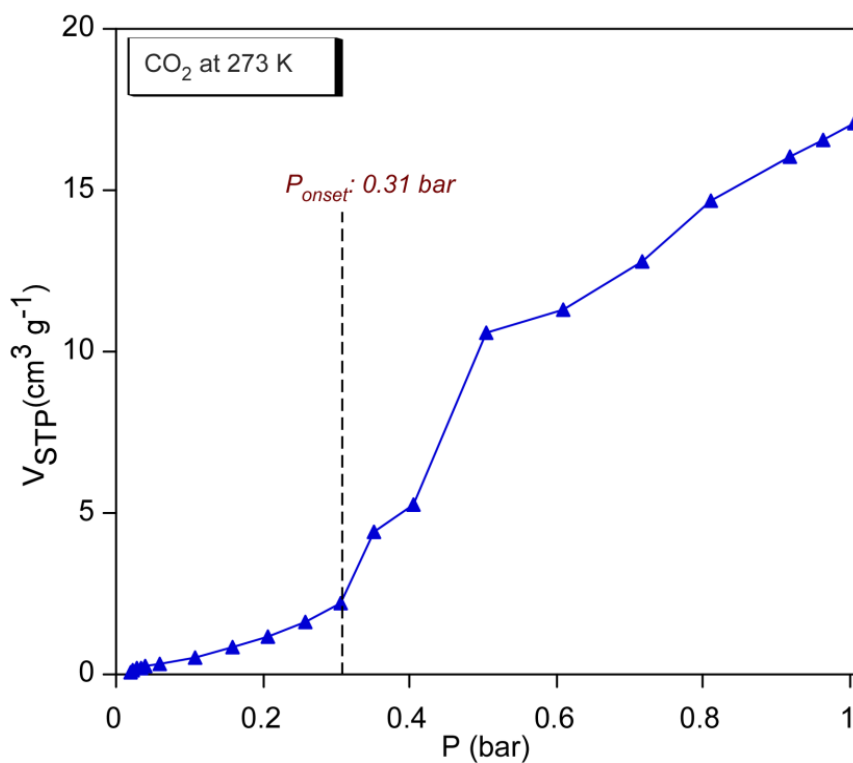


Figure 3.27: CO₂ adsorption isotherm *CUADECL-C* (*SMOF-3*) at 273 K.

3.3.2.4 Structural description of $[\text{Cu}_2(\mu\text{-ade})_3(\mu\text{-OH})(\text{H}_2\text{O})(\text{CH}_3\text{OH})]_n \cdot n(\text{solvent});$ *CUADEOH* (*SMOF-9*)

The basic structural unit of this compound consists of 1D infinite coordination polymers held together by complementary hydrogen bonding interactions in a 3D supramolecular porous structure. Table 3.15 and Table 3.16 display the most relevant coordination and hydrogen bonding structural parameters. The coordination polymer is composed of non-centrosymmetric dinuclear units (Figure 3.28) in which two Cu(II) centers are bridged by two adeninate moieties through the N3 and N9 nitrogen atoms and also by one oxygen atom of a hydroxyl group (Figure 3.29). One of the metal centers is also coordinated to a terminal water molecule while the other to the oxygen atom of a methanol molecule. These dinuclear units are connected by additional bridging adeninates that are coordinated to the Cu(II) centers through the N7 and N9 to provide a 1D coordination chain (Figure 3.29). An interesting structural feature is that the bridging adeninates inside the dinuclear units are tilted 22°, but they present wider tilt angle with respect to those connecting the dimeric units (56 and 78°,

respectively) in the polymeric chain. This fact together with the complementary hydrogen bonding interactions of the nucleobases promotes a three-dimensional propagation of the supramolecular structure sustained by the complementary hydrogen bonding interactions. The $\mu\text{-}\kappa\text{N}3\text{:}\kappa\text{N}9$ -adeninates are able to establish double WC \cdots WC and H \cdots H synthons leading to $R_2^2(8)$ and $R_2^2(10)$ hydrogen bonding rings, respectively. On the other hand, the $\mu\text{-}\kappa\text{N}7\text{:}\kappa\text{N}9$ -adeninates are hydrogen bonded to the bridging hydroxide and the coordinated water molecule of an adjacent polymeric chain through N1 and N6 positions of the Watson-Crick face. The resulting supramolecular crystal structure shows the presence of large channels along the *b* axis with a calculated surface area of 295 m²/g and 44% of void space.

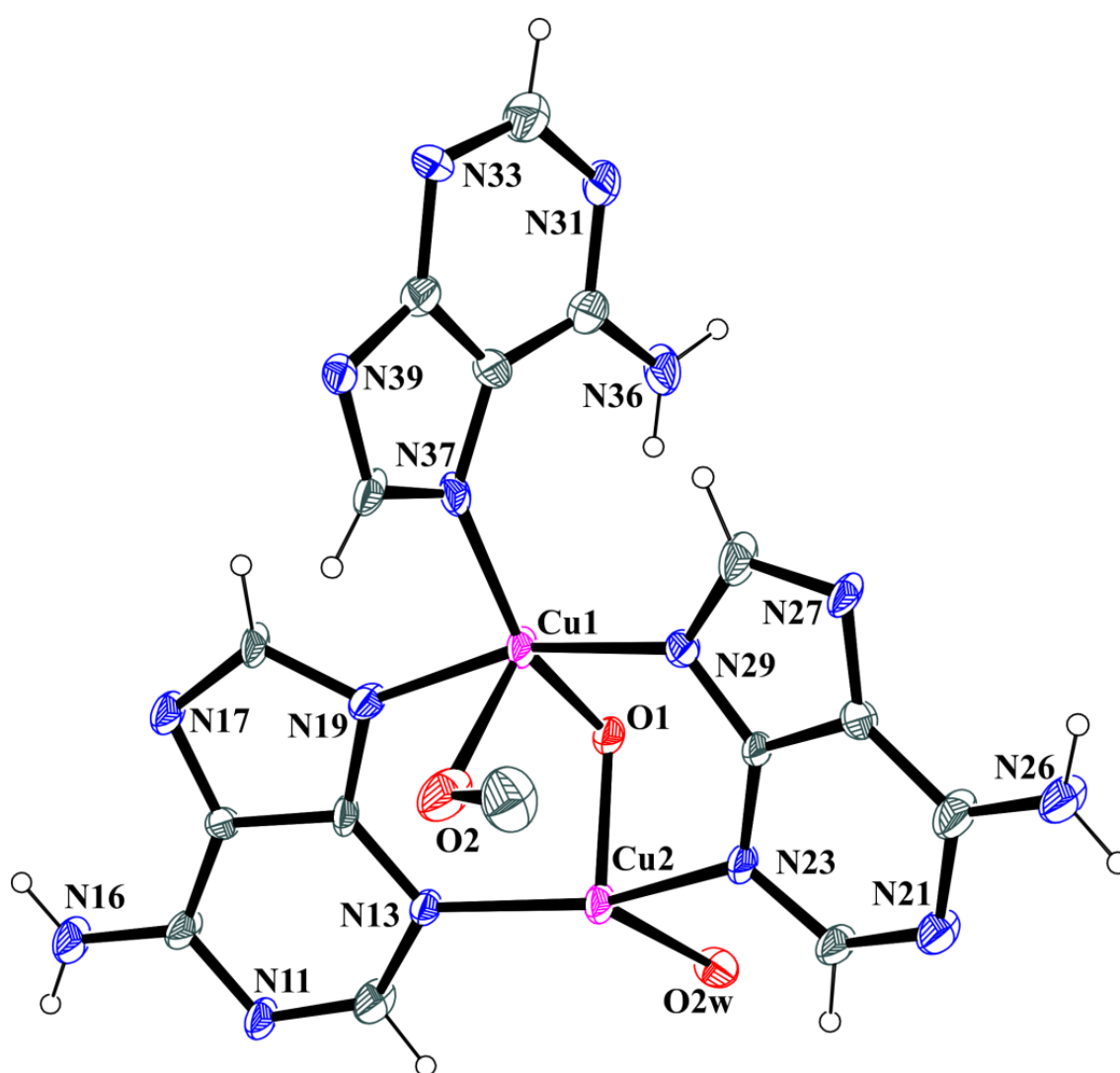
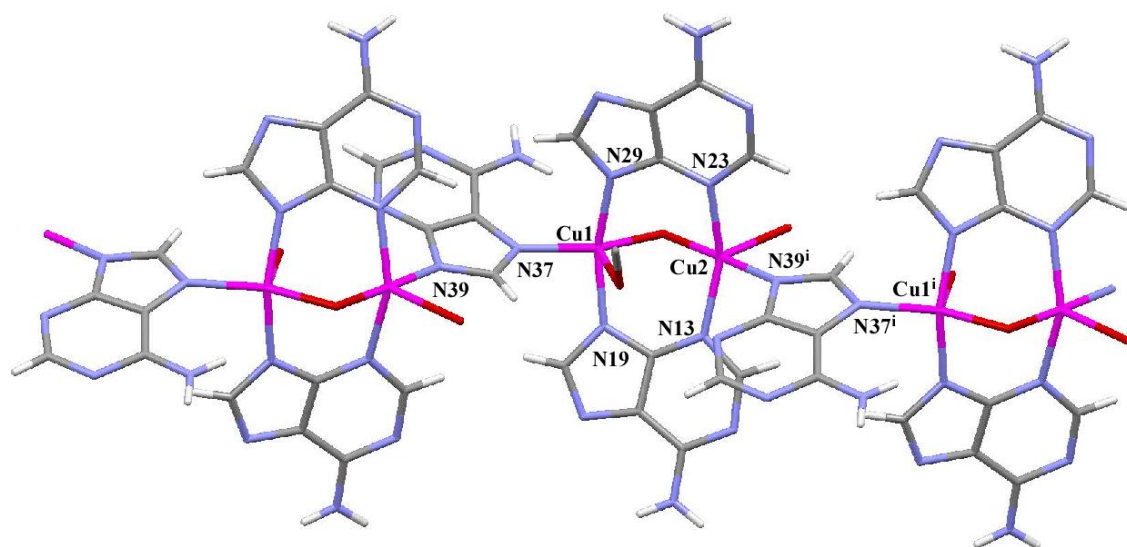
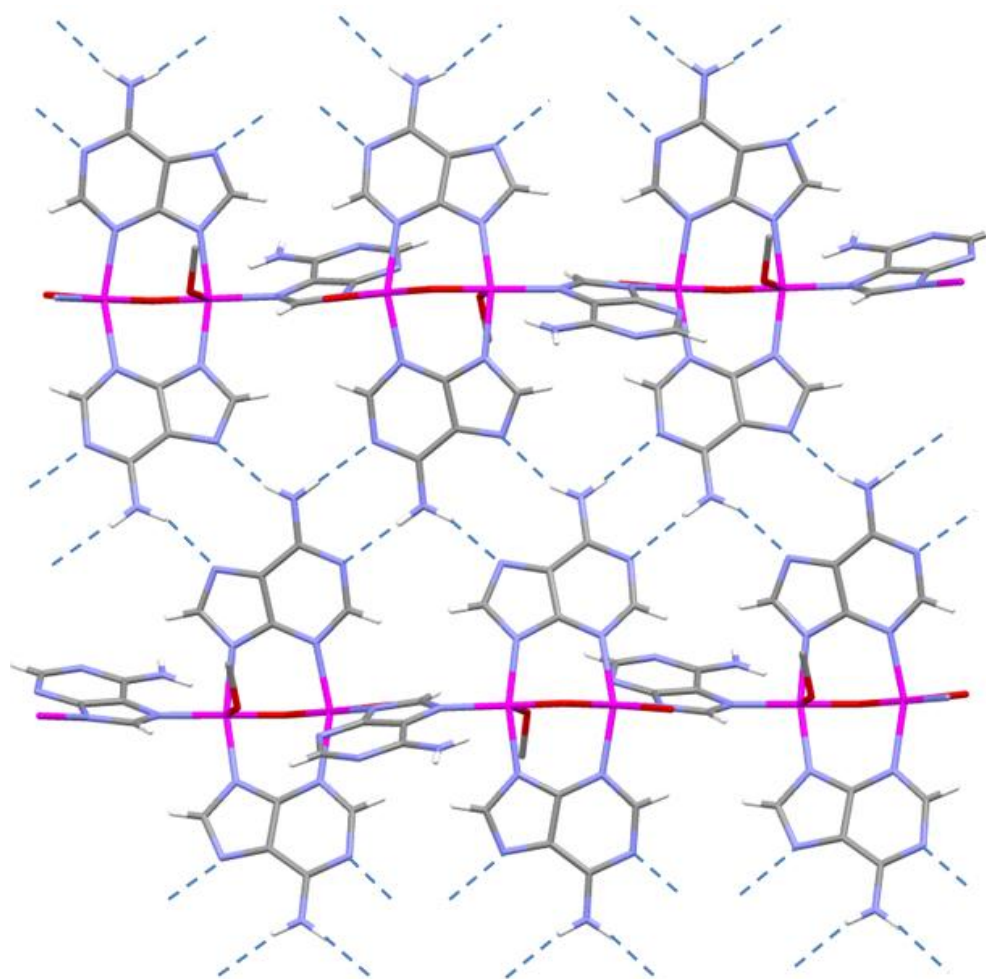


Figure 3.28: Ortep representation of the the asymmetric unit of *CUADEOH* (*SMOF-9*) together with the numbering scheme.



(a)



(b)

Figure 3.29: (a) The coordination polymeric chain and (b) supramolecular complementary base pairing interactions among the adeninate entities in compound *CUADEOH (SMOF-9)*.

Table 3.15: Selected bond lengths (Å) and angles (°) of the coordination sphere of *CUADEOH (SMOF-9)*.^[a]

Cu1–N19	1.954(6)	N19–Cu1–N37	96.7(3)	N39 ⁱ –Cu2–N13	91.1(3)
Cu1–N29	1.972(7)	O1–Cu1–N29	86.3(3)	N23–Cu2–N13	157.0(3)
Cu1–O1	1.940(6)	N19–Cu1–N29	161.2(3)	O1–Cu2–O2w	92.8(3)
Cu1–N37	1.969(8)	N37–Cu1–N29	95.2(3)	N39 ⁱ –Cu2–O2w	89.6(3)
Cu2–N13	2.031(6)	O1–Cu1–Cu2	39.1(2)	N23–Cu2–O2w	95.9(3)
Cu2–N23	2.017(7)	N19–Cu1–Cu2	82.2(2)	N13–Cu2–O2w	106.8(3)
Cu2–O1	1.936(7)	N37–Cu1–Cu2	166.5(3)	O1–Cu2–Cu1	39.2(2)
Cu2–O2w	2.264(7)	N29–Cu–Cu2	82.8(2)	N39 ⁱ –Cu2–Cu1	138.4(3)
Cu2–N39 ⁱ	1.952(8)	O1–Cu2–N39 ⁱ	177.6(3)	N23–Cu2–Cu1	80.7(2)
Cu1–Cu2	3.0046(18)	O1–Cu2–N23	86.9(3)	N13–Cu2–Cu1	81.5(2)
O1–Cu1–N19	89.1(3)	N39 ⁱ –Cu2–N23	92.7(3)	O2W–Cu2–Cu1	131.80(19)
O1–Cu1–N37	154.3(4)	O1–Cu2–N13	88.4(3)		

[a] Symmetry codes: (i) $-x+1/2, y+1/2, -z+1/2$.

Table 3.16: Hydrogen bonding interactions (Å, °) in *CUADEOH (SMOF-9)*.^[a]

<i>D–H...A</i> ^[b]	<i>D–H</i>	<i>H...A</i>	<i>D...A</i>	<i>D–H...A</i>
N16–H16A...N11 ⁱ	0.86	2.23	3.075(10)	169.6
N26–H26A...N21 ⁱⁱ	0.86	2.06	2.920(11)	179.2
N26–H26B...N17 ⁱⁱⁱ	0.86	2.08	2.904(11)	160.9
N36–H36B...O1 ^{iv}	0.86	2.12	2.884(9)	148.1

[a] Symmetry codes: (i) $-x+1, -y+2, -z+1$; (ii) $-x, -y+2, -z$; (iii) $x-1/2, -y+3/2, z-1/2$; (iv) $-x+1/2, -y+3/2, -z$.

[b] **D**: donor; **A**: acceptor.

This compound is an interesting case because it is in between pure *MOFs* and *SMOFs* as it polymerizes into 1D through coordination bonds and further extends to supramolecular array through complementary hydrogen bonding interactions resulting in a 3D porous network (Figure 3.30).

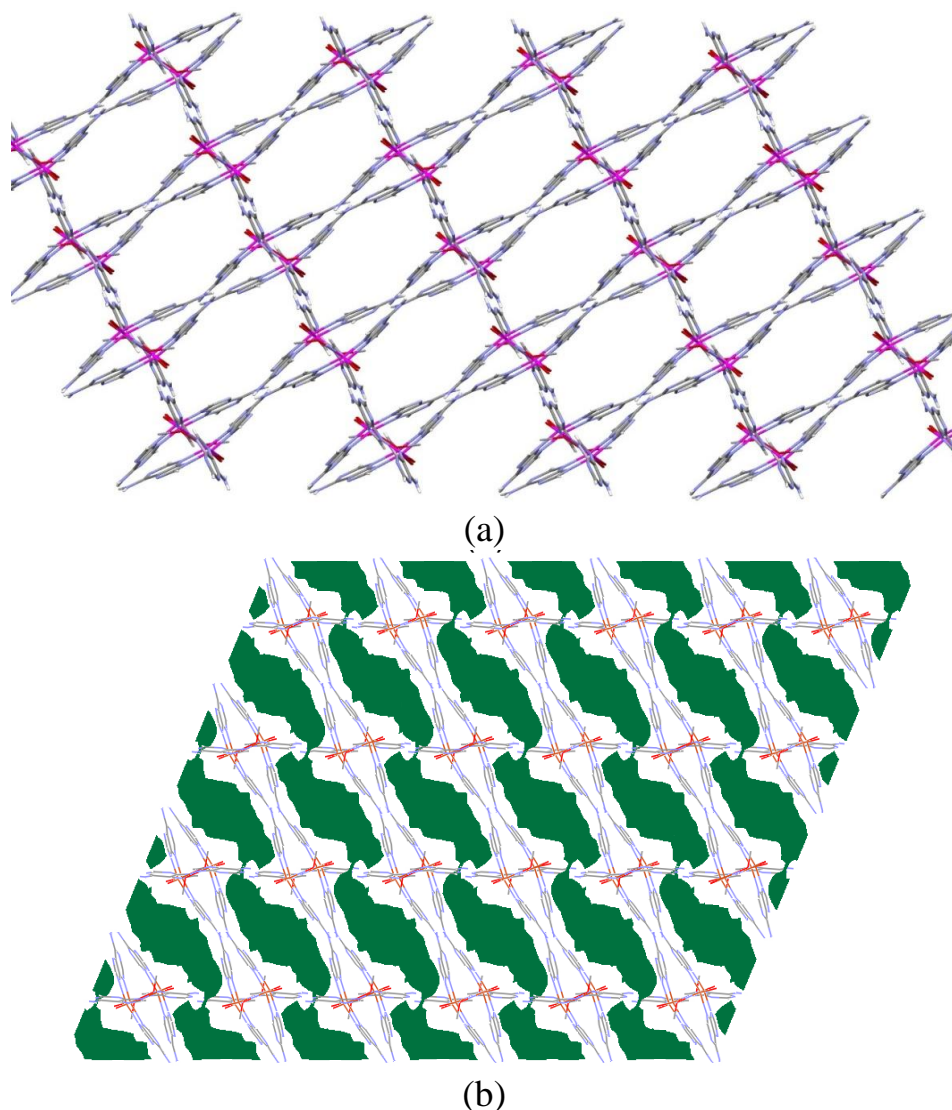


Figure 3.30: (a) Porous supramolecular architecture of *CUADEOH* (*SMOF-9*) (b) the available void space shown in green colour.

3.3.2.5 Structural description of $[\text{Co}_3(\mu\text{-Hade})_2(\mu\text{-Cl})_4\text{Cl}_2(\text{H}_2\text{O})_4] \cdot 2\text{H}_2\text{O}$; (*CO3ADECL*)

The crystal structure consists of linear trinuclear units of formula $[\text{Co}_3(\mu\text{-Hade})_2(\mu\text{-Cl})_4\text{Cl}_2(\text{H}_2\text{O})_4]$ and solvated water molecules. The metal centres are held together by two neutral 7H-adenines showing a $\mu\text{-}\kappa\text{N}3:\kappa\text{N}9$ coordination mode and four bridging $\mu\text{-}$ chloridos. Every cobalt(II) atom presents an octahedral coordination environment, with Cl_4N_2 atoms around the cobalt atom placed at the centre of the trimeric entity and $\text{Cl}_3\text{N}_1\text{Ow}_2$ atoms around the terminal cobalt centres. Figure 3.31 provides a structural representation of the trimeric entity of compound *CO3ADECL*. The coordination bond lengths and angles are gathered in Table 3.17.

The 7H-tautomeric form of the adenine precludes the Hoogsteen side from establishing complementary hydrogen bond interactions because both N6 and N7 behaves as hydrogen bonding donor atoms but the Watson-Crick side remains available (N1: acceptor, N6: donor). However, the synthesis was performed in a water/methanol mixture and, as it happens in *CUADECL-A*, the water molecules disrupt the direct hydrogen bonding interaction between the adenines. In fact, the trimeric units interact through hydrogen bonds between the N1 nitrogen of the adenines and the coordinated water molecules of the neighbouring units in a head to tail manner, leading to a 1D chain along the [0 1 0] direction (Figure 3.32). Additionally, the N6 and N1 donor positions of the Hoogsteen face are pointing towards a solvated water molecule that acts as acceptor of the two hydrogen bonds. This solvation water molecule is further hydrogen bonded as donor to a terminal chloride and a coordinated water molecule from adjacent trimers giving rise to a 3D non porous structure (Figure 3.33). Table 3.18 shows the hydrogen bonding interaction parameters.

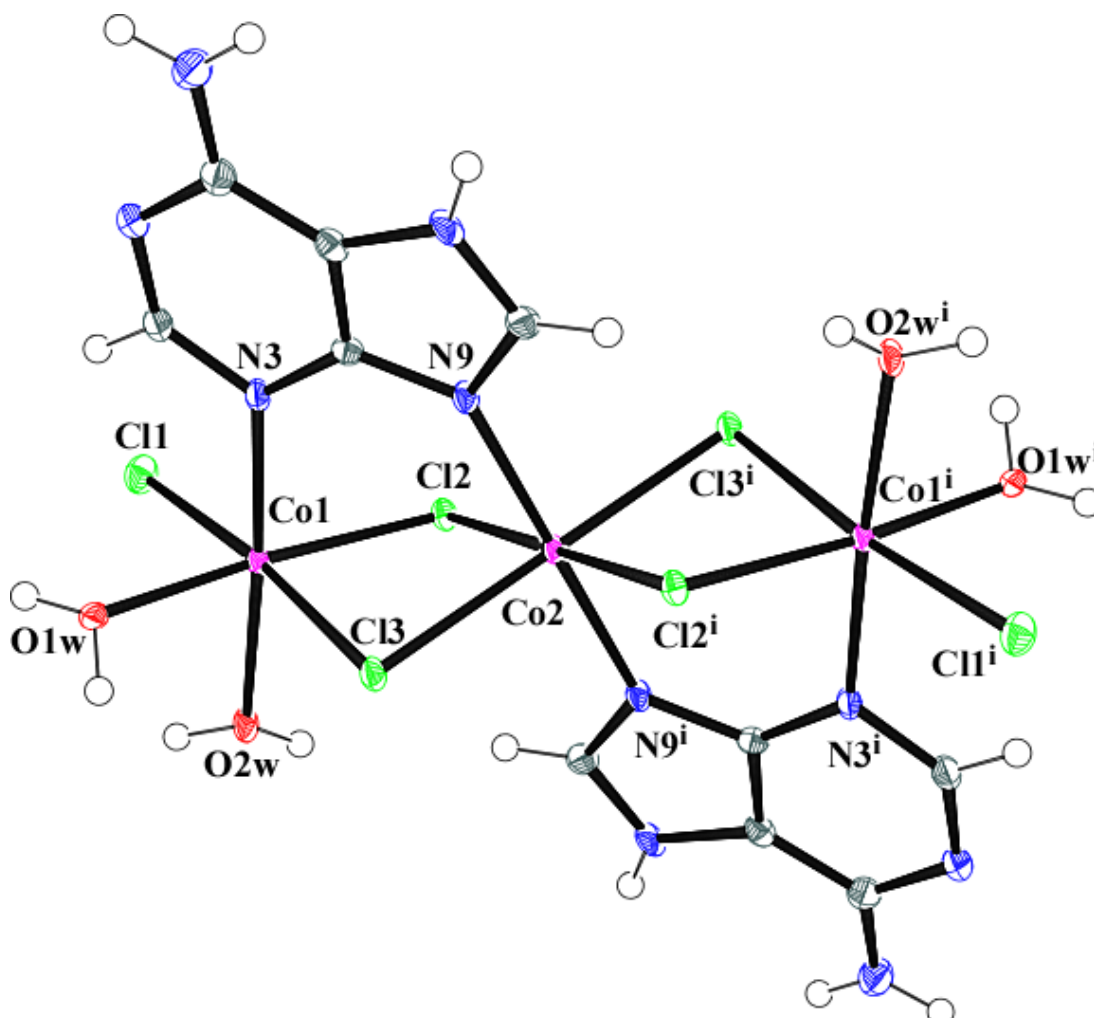


Figure 3.31: Ortep representation of $[\text{Co}_3(\mu\text{-Hade})_2(\mu\text{-Cl})_4\text{Cl}_2(\text{H}_2\text{O})_4]$ trimeric unit in *CO3ADECL*.

Table 3.17: Selected coordination bond lengths (Å) and angles (°) in *CO3ADECL*.^[a]

Co1–N3	2.115(2)	N3–Co1–O1w	91.00(7)	Cl1–Co1–Cl3	174.15(2)
Co1–O1w	2.1217(16)	N3–Co1–O2w	175.45(6)	Cl2–Co1–Cl1	96.42(3)
Co1–O2w	2.1544(17)	N3–Co1–Cl1	90.92(6)	Cl2–Co1–Cl3	87.35(3)
Co1–Cl1	2.4356(11)	N3 Co1 Cl2	91.37(6)	N9–Co2–N9 ⁱ	180.00(1)
Co1–Cl2	2.4106(10)	N3–Co1–Cl3	93.47(6)	N9–Co2–Cl2 ⁱ	89.04(6)
Co1–Cl3	2.4823(11)	O1w–Co1–Cl1	87.79(5)	N9–Co2–Cl2	90.96(6)
Co2–N9	2.105(2)	O1w–Co1–Cl2	175.13(4)	N9–Co2–N9 ⁱ	180.00(1)
Co2–Cl2	2.5108(11)	O1w–Co1–Cl3	88.26(5)	N9–Co2–Cl3 ⁱ	93.01(5)
Co2–Cl3	2.4744(10)	O1w–Co1–O2w	84.45(6)	N9–Co2–Cl3 ⁱ	86.99(5)
Co1...Co2	3.476(2)	O2w–Co1–Cl1	88.73(5)	Cl2–Co2–Cl2	180.00
		O2w–Co1–Cl2	93.18(5)	Cl3–Co2–Cl2 ⁱ	94.65(3)
		O2w–Co1–Cl3	86.59(5)	Cl3–Co2–Cl2 ⁱ	85.35(3)
				Cl3–Co2–Cl3 ⁱ	180.00

[a] Symmetry code: (i) $-x+2, -y, -z+2$.**Table 3.18:** Hydrogen bonding interactions (Å, °) in *CO3ADECL*.^[a]

<i>D–H...A</i> ^[b]	<i>D–H</i>	<i>H...A</i>	<i>D...A</i>	<i>D–H...A</i>
N7–H7...O3w	0.86	1.92	2.731(3)	157.1
N6–H6A...Cl3 ⁱ	0.86	2.70	3.435(2)	144.6
N6–H6B...O3w	0.86	2.23	3.054(3)	161.6
O1w–H11...N1 ⁱⁱ	0.86	1.93	2.785(3)	176.4
O2w–H21...Cl1 ⁱⁱⁱ	0.87	2.20	3.055(2)	168.8
O1w–H12...O2w ^{iv}	0.84	2.08	2.859(2)	153.6
O3w–H31...O1w ^v	0.92	2.30	3.071(2)	141.4
O3w–H31...N3 ^v	0.92	2.59	3.365(2)	142.0
O3w–H32...Cl1 ^{vi}	0.93	2.24	3.1437(19)	163.5

[a] Symmetry code: (i) $x, y-1, z$; (ii) $-x+2, -y-1, -z+3$; (iii) $-x+1, -y, -z+3$ (iv); $-x+2, -y, -z+3$; (v) $-x+3, -y-1, -z+2$; (vi) $-x+2, -y-1, -z+2$. [b] **D**: donor; **A**: acceptor.

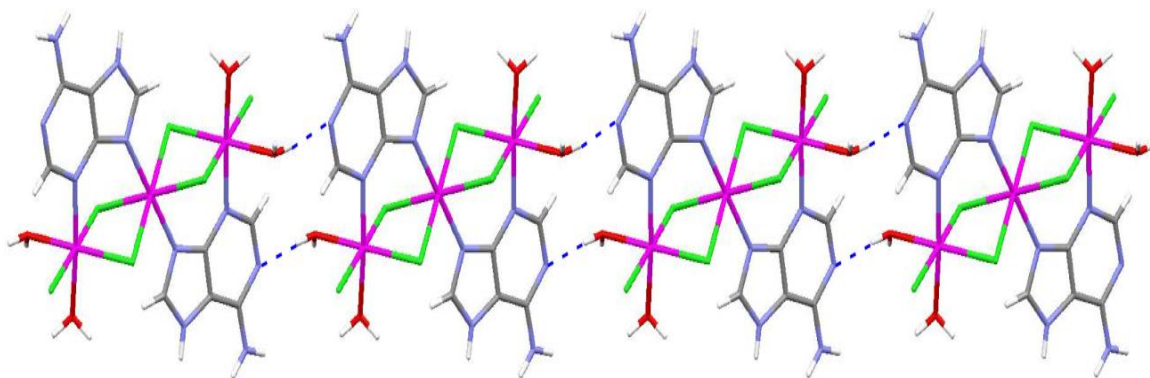
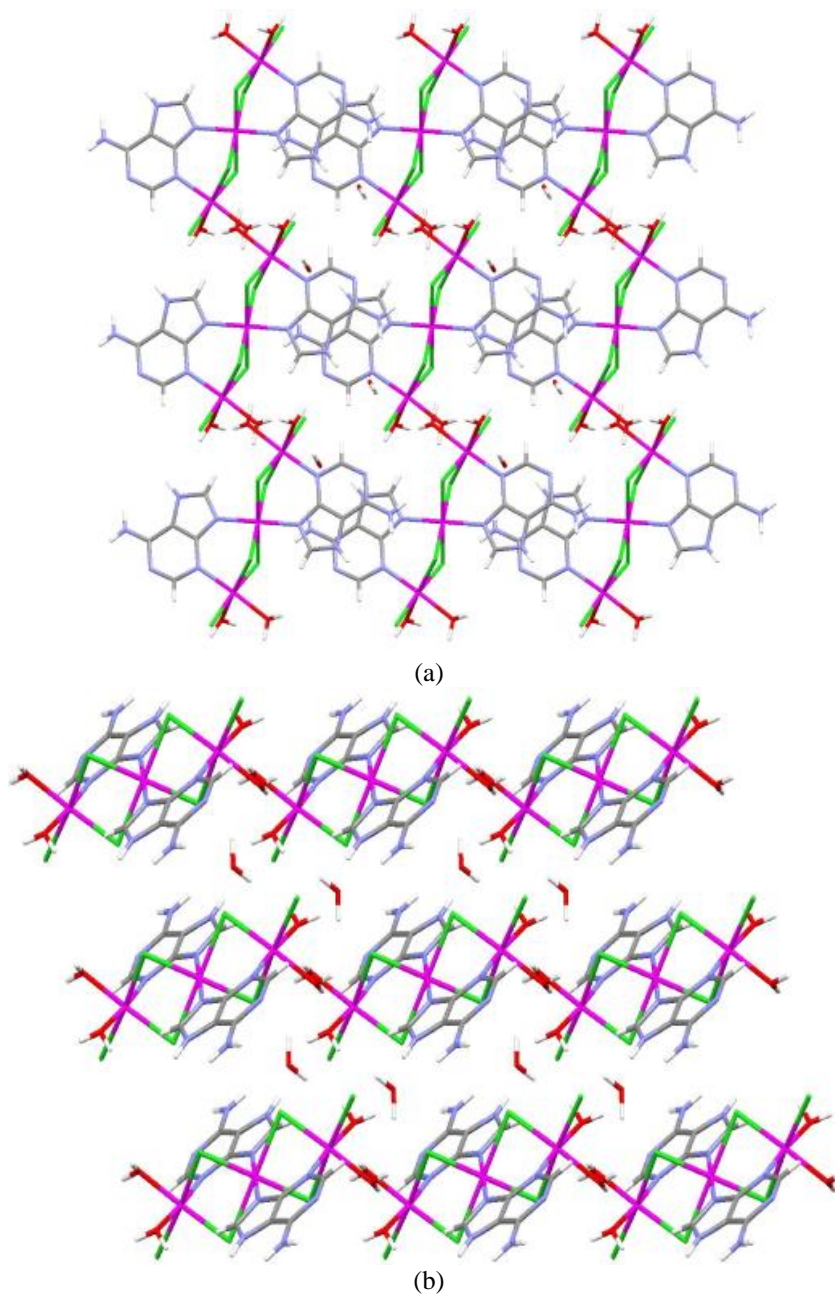


Figure 3.32: The head to tail hydrogen bonding interactions between the neighbouring trimeric units in *CO3ADECL*.



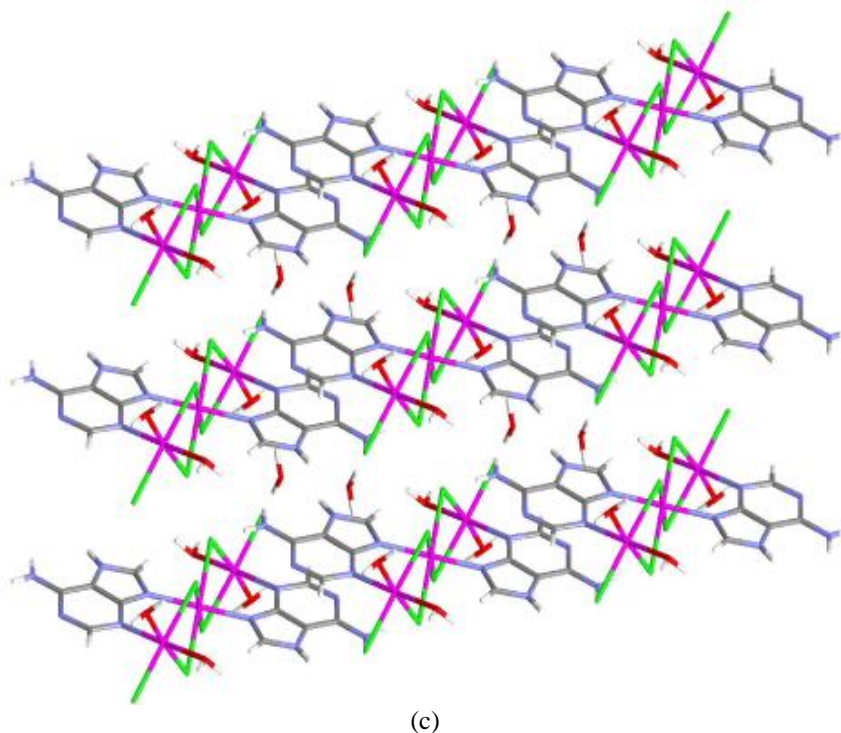


Figure 3.33: Projection of the crystal structure of compound *CO3ADECL* along the crystallographic *a* (a), *b* (b) and *c* (c) axes.

3.3.2.6 Structural description of compound $[\text{Cu}_4(\mu_3\text{-ade})_2(\mu_2\text{-ade})_2(\text{pentylNH}_2)_2(\text{CH}_3\text{OH})_2(\text{CO}_3)_2(\text{H}_2\text{O})_2] \cdot n(\text{solvent})$ *CUADEC03 (SMOF-8)*

Compound *CUADEC03 (SMOF-8)* is built up by tetranuclear units of $[\text{Cu}_4(\mu_3\text{-ade})_2(\mu_2\text{-ade})_2(\text{pentylNH}_2)_2(\text{CH}_3\text{OH})_2(\text{CO}_3)_2(\text{H}_2\text{O})_2]$ in which coexist two types of neutral building units: a dimeric $[\text{Cu}_2(\mu\text{-ade})_4(\text{H}_2\text{O})_2]$ entity and two monomeric $[\text{Cu}(\text{pentylNH}_2)(\text{CH}_3\text{OH})(\text{CO}_3)]$ entities with a partial occupation factor of 0.775 (Figure 3.34). The presence of the carbonate has been attributed to the diffusion of CO_2 into the basic media of the reaction. In fact, this compound is obtained only if the reaction media is exposed to the open atmosphere. Similar behavior has been previously reported for some other compounds.¹⁶⁶

The dimeric fragment is centrosymmetric and is made of two Cu(II) atoms bridged by four $\mu\text{-N3:N9}$ -adeninate anions in a paddle-wheel shaped arrangement. The apical position of the distorted square pyramidal coordination around Cu1 atom is completed with a water

¹⁶⁶ (a) Sertucha, J. et al. *Inorg. Chem. Commun.* **1999**, 2, 14. (b) Kitajima, N. et al. *J. Am. Chem. Soc.* **1993**, 115, 5496. (c) Verdejo, B. et al. *Inorg. Chem.* **2006**, 45, 3803.

molecule. Each dimeric entity is linked to two neighboring monomeric entities via the N7 imidazolic atoms of two adeninato ligands. Therefore, two adeninate anions behave as tridentate μ_3 -N3:N7:N9 bridging ligands, whereas the other two act as bidentate μ -N3:N9. Two oxygen atoms from a carbonato ligand, an oxygen atom of a methanol molecule and the nitrogen atom of a pentylamine molecule define the basal plane of the square pyramidal chromophore around Cu2 atom, whereas N7 atom of the adenine occupies the apical position with a slightly longer coordination bond distance.

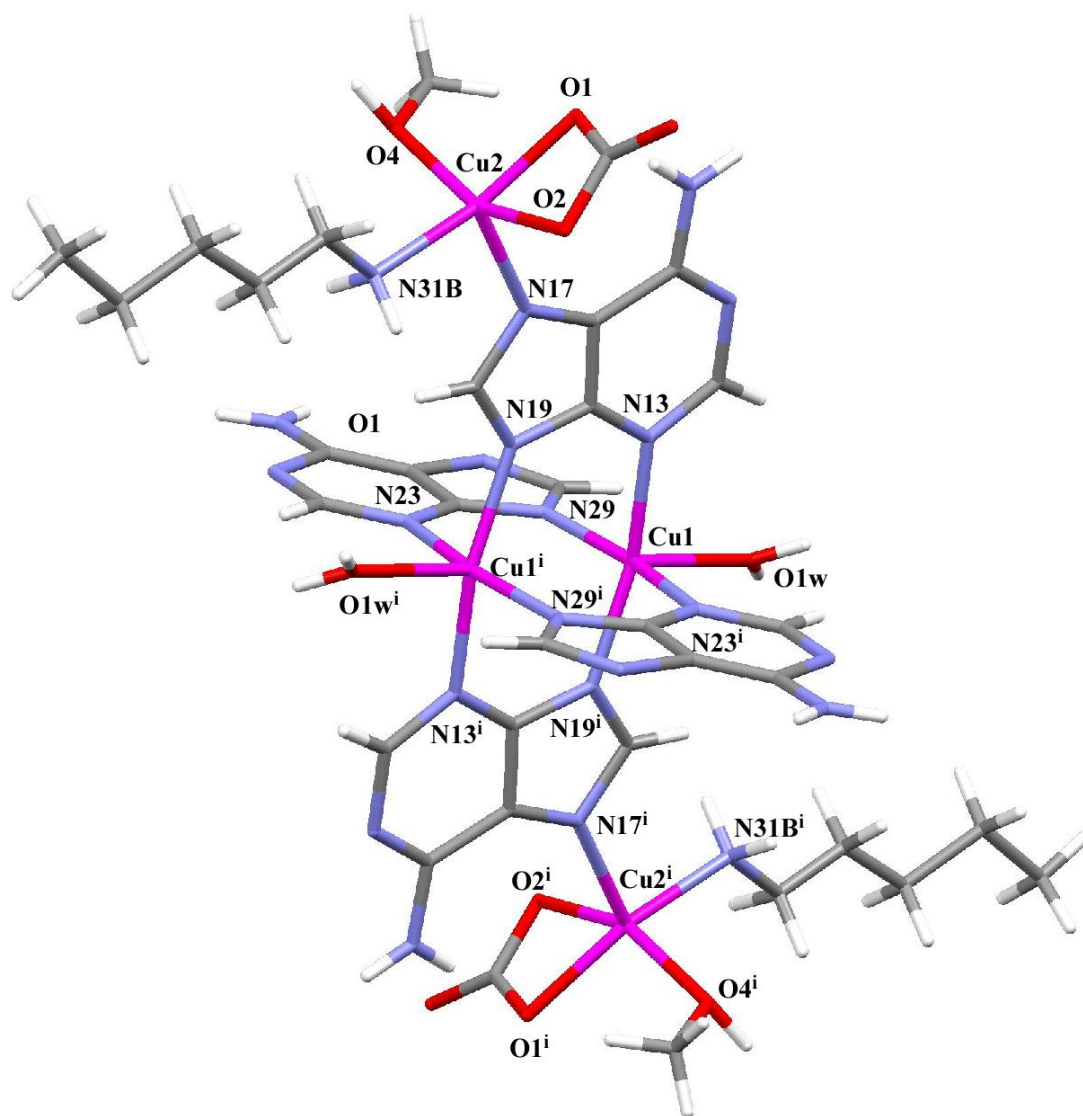


Figure 3.34: Structural unit of *CUADeco3* (*SMOF-8*) with the atomic numbering scheme.

Each tetranuclear entity is linked to four adjacent ones via doubly N6-H \cdots N1 hydrogen bonding interactions between the Watson–Crick faces of neighboring entities to give a $R_2^2(8)$ ring. The linkage of these tetrameric entities by the Watson–Crick faces gives rise to layers that can be described as a four-connected uninodal net with Shubnikov tetragonal **sql** topology and $(4^4.6^2)$ point symbol (Figure 3.35). The layers are further connected by means of

hydrogen bonding interactions involving the coordination water molecule, the carbonato ligand and the pentylamine molecule (Figure 3.36) leading to an α -Po **pcu** topology with a 42.9% of accessible volume (highlighted in green colour in Figure 3.36b). The selected coordination bond angles and bond lengths are given in Table 3.19 and the selected hydrogen bond lengths and angles are given in Table 3.20.

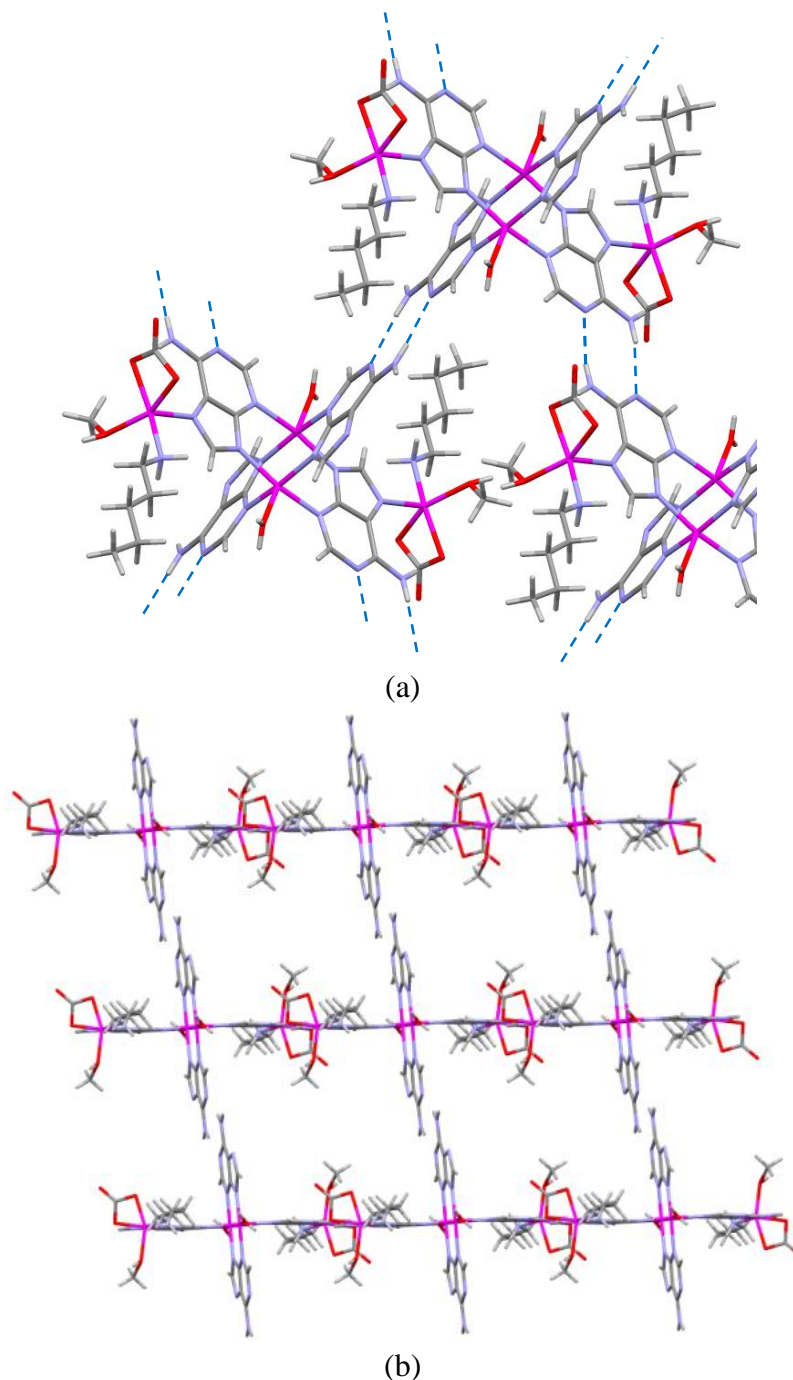


Figure 3.35: (a) Complementary hydrogen bonding interaction through the Watson–Crick faces of the adenines. (b) Supramolecular sheets sustained through Watson–Crick faces interaction *CUADECO3* (*SMOF-8*).

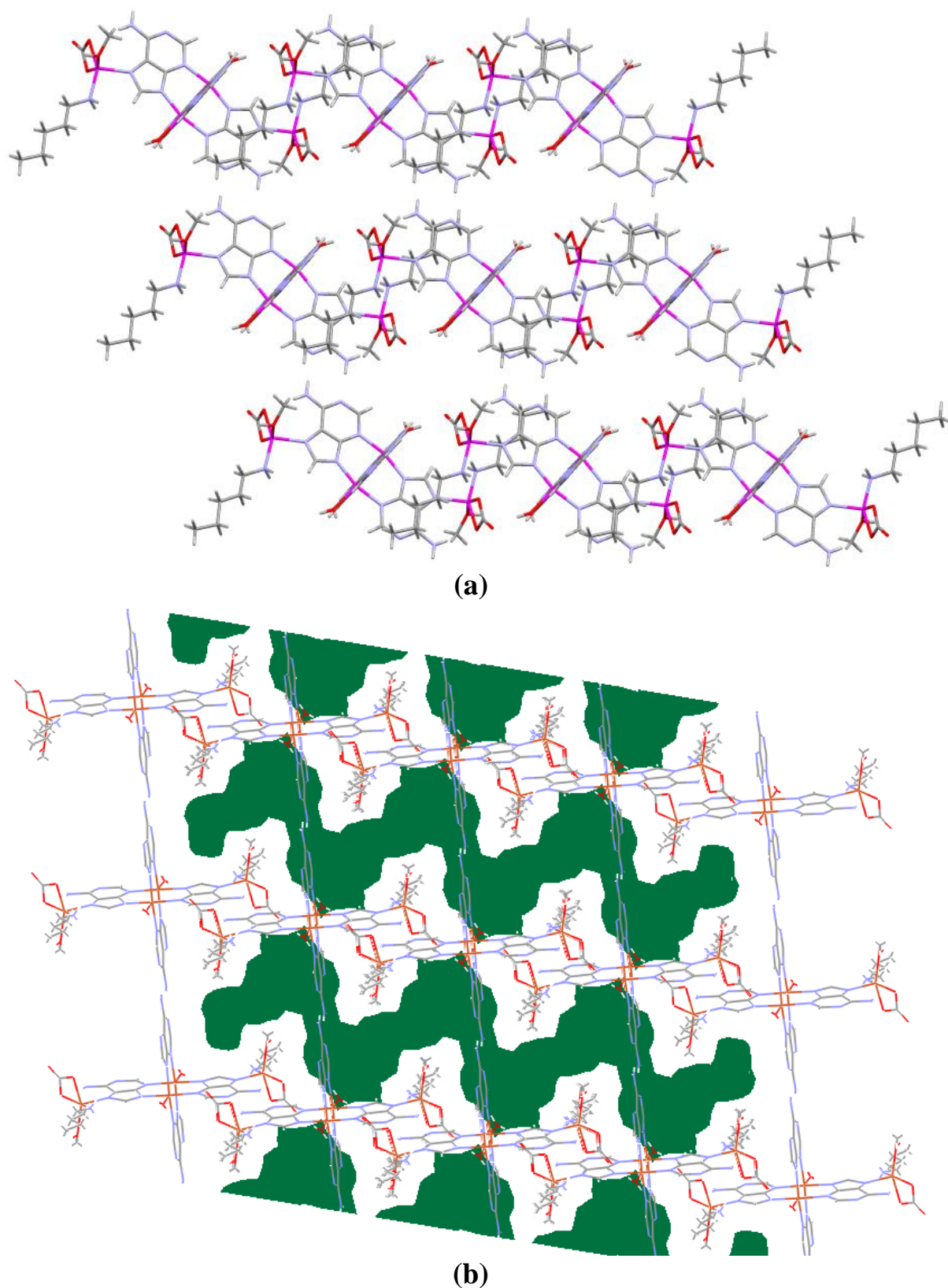


Figure 3.36: (a) Projection of the crystal structure of compound *CUADeco3* (*SMOF-8*) along the crystallographic *c* axis and (b) green coloured regions representing the solvent accessible void.

Table 3.19: The coordination bond lengths (Å) and angles (°) for *CUADEC03 (SMOF-8)*.^[a]

Cu1–N29	1.952(10)	N29–Cu1–N19 ⁱ	90.0(3)	N13–Cu1–Cu1 ⁱ	84.5(2)
Cu1–N23 ⁱ	1.989(9)	N23 ⁱ –Cu1–N19 ⁱ	89.5(3)	O1w–Cu1–Cu1 ⁱ	176.69(19)
Cu1–N19 ⁱ	1.993(7)	N29–Cu1–N13	89.6(3)	O2–Cu2–O1	66.4(3)
Cu1–N13	2.010(7)	N23 ⁱ –Cu1–N13	87.2(3)	O2–Cu2–N31	94.9(5)
Cu1–O1w	2.235(7)	N19 ⁱ –Cu1–N13	165.2(3)	O1–Cu2–N31	149.5(4)
Cu1...Cu1 ⁱ	2.945(3)	N29–Cu1–O1w	97.2(3)	O2–Cu2–O4	156.2(6)
Cu2–O2	1.953(14)	N23 ⁱ –Cu1–O1w	97.2(4)	O1–Cu2–O4	94.6(6)
Cu2–O1	1.997(9)	N19 ⁱ –Cu1–O1w	96.5(3)	N31–Cu2–O4	95.6(7)
Cu2–N31	2.057(12)	N13–Cu1–O1w	98.2(3)	O2–Cu2–N17	96.3(6)
Cu2–O4	2.08(2)	N29–Cu1–Cu1 ⁱ	80.9(3)	O1–Cu2–N17	105.2(4)
Cu2–N17	2.185(10)	N23 ⁱ –Cu1–Cu1 ⁱ	84.8(3)	N31–Cu2–N17	100.4(4)
N29–Cu1–N23 ⁱ	165.5(4)	N19 ⁱ –Cu1–Cu1 ⁱ	80.8(3)	O4–Cu2–N17	102.8(6)

[a] Symmetry codes: (i) $-x+2, -y, -z+1$.

Table 3.20: Hydrogen bonding interactions (Å, °) in *CUADEC03 (SMOF-8)*.^[a]

<i>D–H...A</i> ^[b]	<i>D–H</i>	<i>H...A</i>	<i>D...A</i>	<i>D–H...A</i>
N16–H16A...N11 ⁱ	0.86	2.13	2.978(11)	167.1
N16–H16B...O1	0.86	2.11	2.965(13)	174.7
N26–H26B...N21 ⁱⁱ	0.86	2.08	2.935(17)	172.4
O1W–H12W...O3 ⁱⁱⁱ	0.86	1.94	2.790(13)	169.0
N31–H31A...O2 ^{iv}	0.90	1.94	2.843(18)	176.1

[a] Symmetry codes: (i) $-x+2, -y+1, -z+1$; (ii) $-x+2, -y, -z$; (iii) $x-1, y, z$; (iv) $-x+3, -y, -z+1$. [b] **D**: donor; **A**: acceptor.

3.3.2.7 Structural description of [Co(Hade)₂Cl₂] *COADECL (SMOF-5)* and [Co(Hade)₂Br₂] *COADEBR (SMOF-6)*

Both compounds are isostructural (Figure 3.37) but only single crystals of *COADECL* were obtained. Its crystal structure is comprised of neutral monomeric [Co(Hade)₂Cl₂] building units (Figure 3.38a). In this compound 9H-adenine acts as a monodentate ligand and it is coordinated to the Co(II) metal centre through the N7 position. This N7 coordination is very common in the case of unsubstituted adenine moieties, but it requires a second anchoring position of the nucleobase to be stiff enough for our requirements. It is achieved by the

presence of intramolecular hydrogen bonding interactions between the amino hydrogen and chlorido ligand. Most relevant coordination bond lengths and angles are given in Table 3.21.

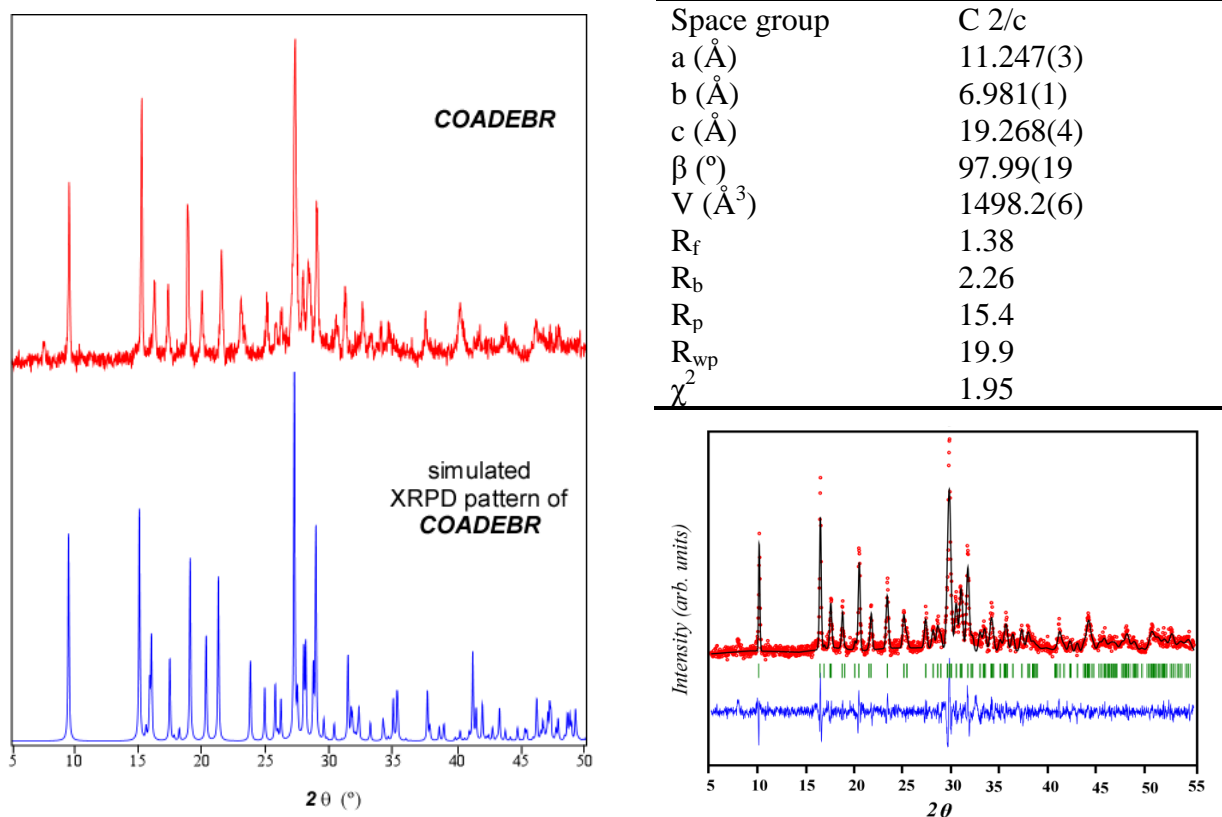


Figure 3.37: X-ray powder diffractograms of *COADEBR* (*SMOF-6*) and simulated pattern resulting from the replacement of chloride by bromide in the crystal structure of *COADECL* (*SMOF-5*).

Table 3.21: Coordination bond lengths (Å) and angles (°) in *COADECL-A* (*SMOF-5*).^[a]

Co1–N7	2.047	N7–Co1–Cl1	106.85(11)
Co1–Cl1	2.2560(13)	N7–Co1–Cl1	115.77(12)
N7–Co1–N7	104.2(2)	Cl1–Co1–Cl1	107.75(8)

[a].Symmetry codes: (i) $-x, y, -z+1/2$.

The adenine exposes its Watson–Crick and sugar–edges to establish intermolecular complementary hydrogen bonding interactions with other adenine molecules (Figure 3.38). It gives rise to two rigid synthons involving WC···WC and sugar···sugar edges that build up a four–connected uninodal supramolecular net with **dia** topology and (6⁶) point symbol. This supramolecular framework would represent a new porous material with an estimated internal surface area of 3600 m²/g and 66.7 % of void space (Figure 3.39a). The structural parameters for hydrogen bonding are given in the Table 3.22.

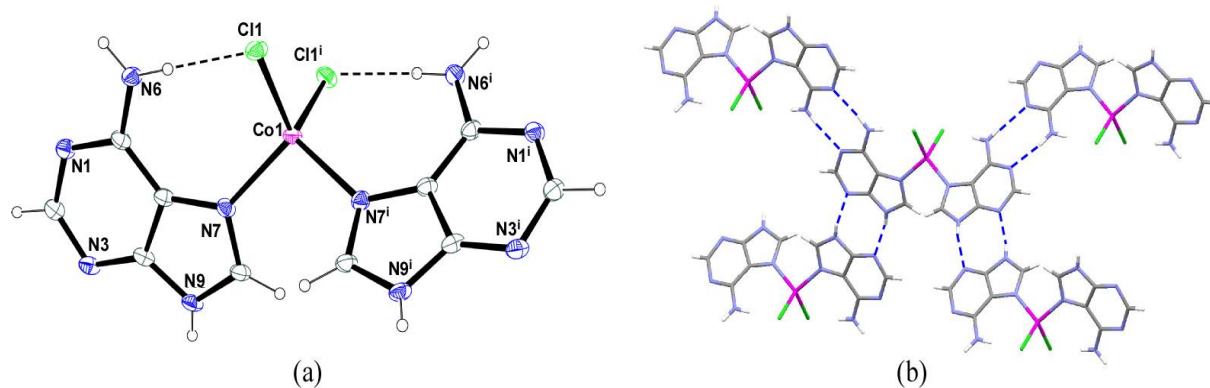


Figure 3.38: (a) Ortep representation of the monomeric entity $[\text{Co}(\text{Hade})_2\text{Cl}_2]$ together with the labelling scheme and (b) Complementary hydrogen bonding interactions taking place between the $[\text{Co}(\text{Hade})_2\text{Cl}_2]$ units.

Table 3.22: Hydrogen bonding interactions (\AA , $^\circ$) in *COADECL (SMOF-5)*.^[a]

$D-H\cdots A$ ^[b]	$D-H$	$H\cdots A$	$D\cdots A$	$D-H\cdots A$
$N6-H6A\cdots N1^i$	0.86	2.06	2.912(6)	173.3
$N6-H6B\cdots C11$	0.86	2.39	3.237(4)	167.3
$N9-H9\cdots N3$	0.74(7)	2.11(7)	2.833(6)	165(6)

[a] Symmetry codes: (i) $-x+1/2, -y+1/2, -z+1$; (ii) $-x, -y-1, -z+1$. [b] D: donor; A: acceptor.

Nevertheless, it would contain so huge channels that the real crystal structure involves three fold interpenetrated networks that occupy all the available space providing a non-porous material. This entanglement problem is also common in MOFs.¹⁶⁷ Huge pore sizes usually give rise to a fundamental complication, namely called interpenetration that consist on the inclusion of additional sublattices occupying the void space left by the first one. This interpenetration greatly reduces the pore size and thus the available space¹⁶⁸ and is a challenge in designing compounds with potential porosities. Porous materials try to minimize the systematic energy through optimal filling of void space, but structural interpenetration may occur only if the pore space of an individual net is sufficiently large to accommodate an additional net. Moreover, various weak supramolecular forces such as H-bonding, π - π aromatic stacking interactions, and van der Waals forces are believed to play vital roles in the formation of interpenetrated structures. *COADECL (SMOF-5)* follows the same pattern,

¹⁶⁷ (a) Hoskins, B. F.; Robson, R. *J. Am. Chem. Soc.* **1990**, *112*, 1546. (b) Alexandrov, E. V. et al. *Acta Crystallogr. Sect. A*, **2012**, 484.

¹⁶⁸ Shekhah, O. et al. *Nat. Mater.* **2009**, *8*, 481.

provided that it contains comparatively bigger voids. Thus the resulting structure can be described as a 3-fold interpenetrated network as shown in Figure 3.39b.

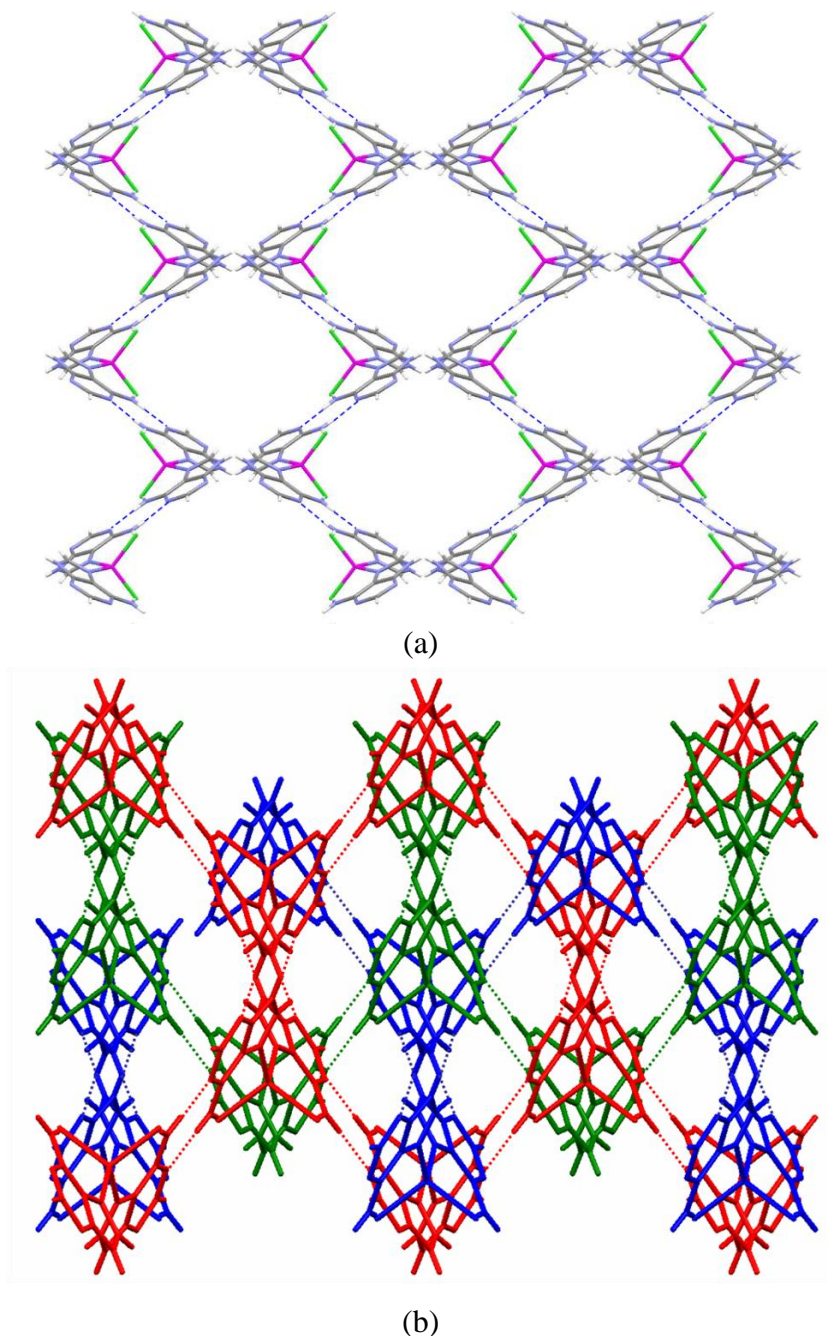


Figure 3.39: (a) Crystal structure of an individual supramolecular subnet of *COADECL* (*SMOF-5*) and (b) real crystal structure resulting from the interpenetration of three individual subnets depicted using different colours.

The stability of *COADECL* (*SMOF-5*) and *COADEBR* (*SMOF-6*) has been measured using thermogravimetric techniques (TG/DTA) under synthetic air (Figure 3.40 and Table 3.23). The *COADECL* remains stable up to 260 °C and then undergoes a mass loss that ends at 390 °C by a strong endothermic process. The intermediate is not stable and decomposes in several consecutive exothermic processes to afford Co_3O_4 at 620 °C. The results obtained

from *COADEBR* (*SMOF-6*) show a small mass loss below 100°C, that could be attributed to humidity but we believe that it could imply a small portion of the non-interpenetrated phase. Around 300 °C the compound suffers a second endothermic mass loss that agrees with the release of HBr acid. The intermediate remains relatively stable up to 425 °C after which it suffers several consecutive exothermic processes to afford Co_3O_4 at 590 °C.

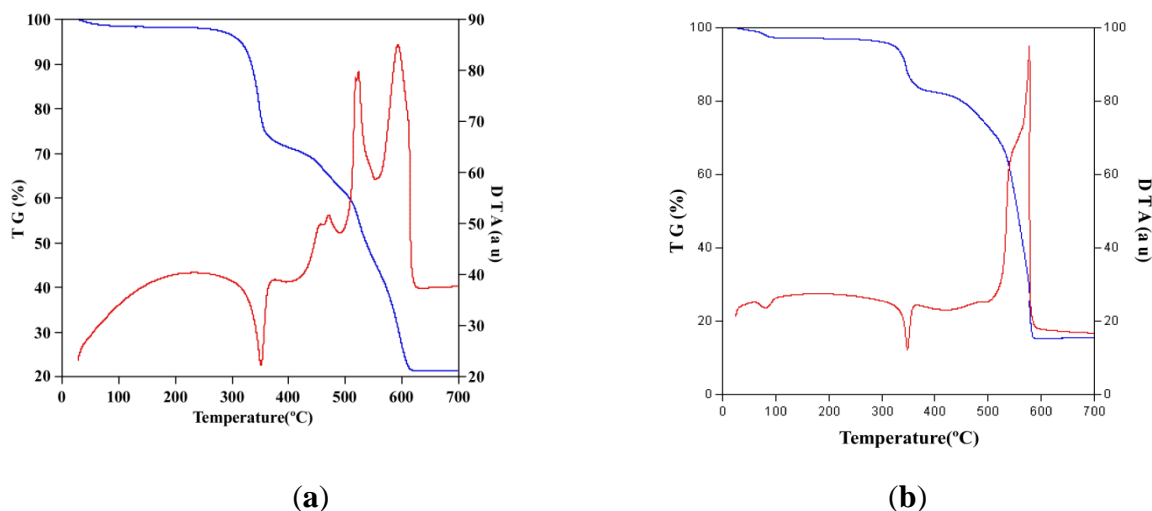


Figure 3.40: TG and DTA curves of the *COADECL* (*SMOF-5*) and *COADEBR* (*SMOF-6*) under synthetic air atmosphere.

Table 3.23: Thermogravimetric data for *COADECL* (*SMOF-5*) and *COADEBR* (*SMOF-6*).^[a,b]

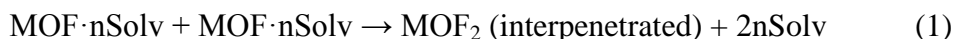
Step	T_i	T_f	T_{peak}	$\Delta m(\%)$	ΔH	$\Sigma \Delta m(\%)$	$\Sigma \Delta m_{theor}^{[b]}$
<i>COADECL</i> (<i>SMOF-5</i>)							
1	25	390	352	28.32	Endo	28.32	–
3	390	620	524,590	50.40	Exo	78.72	79.93 (1/3 Co_3O_4)
<i>COADEBR</i> (<i>SMOF-6</i>)							
1	25	95	82	2.8	Endo	2.8	2.9 (–0.8 H_2O)
2	270	395	347	14.72	Endo	17.52	16.54 (–1 HBr)
3	425	590	577	66.95	Exo	84.47	83.57 (1/3 Co_3O_4)

[a] T_i = initial temperature; T_f = final temperature; T_{peak} = DTA peak temperature; $\Delta m(\%)$ = mass loss percentage for each process; ΔH = process type in the basis of DTA; $\Sigma \Delta m(\%)$ = total mass loss percentage; $\Sigma \Delta m(\%)_{theor}$ = theoretical total mass loss percentage. [b] Released fragments and final residue per formula.

Although interpenetration usually provides robustness to the MOFs, it negatively affects the porosity of open frameworks by reducing the size of open pores and hence poses low surface area and high density which negatively affects the potential applications of such

materials because high surface area and porosity are generally most desired in porous material.¹⁶⁹ Therefore it is important to find some methods to avoid interpenetration. Many new strategies have been developed to suppress the interpenetration in order to construct highly porous MOFs with high surface area and some of them are explained below in detail. In this work we have adopted many of such strategies to avoid the interpenetration of compounds *COADECL* (*SMOF-5*) and *COADEBR* (*SMOF-6*).

Reaction parameters such as temperature and concentration play vital role in the determination of framework interpenetration of MOFs. For example, in the case of IRMOFs (isoreticular MOF) longer organic linkers leads to 2-fold interpenetrated networks but lowering the concentration of reaction solution has been found effective in affording non-interpenetrated MOFs with larger pores²³ and specific surface areas ranging from 570 to 3800 m²/g.¹⁶⁹ To better understand the effect of concentration on the interpenetration, it is convenient to consider this phenomena as two or more crystals growing in the same point of the space. At lower concentration, the chances for several crystals growing at the same place is smaller than when using higher concentration of the reagents. Therefore, diluting the reaction media hinders the interpenetration phenomena. On the other hand, the [Cd(4,4'-bpy)(bdc)] system showed that not only the concentration but also the temperature plays a relevant role in determining the presence of interpenetration. The interpenetrated isomer was preferentially produced at elevated temperatures and hence temperature control was the key factor in obtaining the non-interpenetrated form of this compound together with concentration control.¹⁷⁰ To better understand this fact, we must consider a hypothetical equilibrium reaction between the non-interpenetrated and interpenetrated forms of a compound (equation 1). It is easy to understand that due to entropic effects, reaction (1) would be displaced towards the interpenetrated form at high temperatures, being more probable to isolate the non-interpenetrated one at lower temperatures.



The use of templates has been widely used for the construction of porous materials. It is also reasonable to introduce a template in order to construct non-interpenetrated MOFs with larger pores on assuming that the MOF will grow around the surface of the template and thus

¹⁶⁹ Jiang, H.-L. et al. *Coord. Chem. Rev.* **2013**, 257, 2232.

¹⁷⁰ Zhang, J. et al. *J. Am. Chem. Soc.* **2009**, 131, 17040.

prevent the interpenetration of multiple nets.¹⁶⁹ The Zhou research group with the synthesis of non interpenetrated PCN-6' has proven that in this specific case only template control could determine the presence or absence of interpenetration where temperature and concentration controls were not fruitful.¹⁷¹ The template effect can be also exerted by the solvent molecules.¹⁷² A relatively similar approach consist of modifying/designing the ligand to incorporate bulky substituents, although they do not occupy the total accessible volume of the MOF, avoids the interpenetration of additional nets.¹⁶⁹

Finally, layer-by-layer assembly-liquid phase epitaxy provides another way to achieve the interpenetration suppression. It is done through liquid-phase epitaxy on an organic monolayer modified surface followed by a layer-by-layer growth approach.¹⁶⁸ The surface is modified with functional groups able to anchor the metal centers. Later on, using a dip coating strategy the MOFs are grown by consecutive immersion in a solution containing only the bridging ligand or metal. This strategy completely avoids the interpenetration phenomena as the presence of a second net is completely precluded.

However, although we have made great efforts to avoid the interpenetration of compounds *COADECL* (*SMOF-5*) and *COADEBR* (*SMOF-6*), it has been unsuccessful. Probably because the hydrogen-bonding nature of the connections established between the building units makes this issue more difficult to overcome.

3.3.2.8 Structural Description of $[\text{Co}(\text{9-MeAde})_2(\text{H}_2\text{O})_4]\text{Cl}_2 \cdot 2\text{H}_2\text{O}$;

CO-9-MEADECL

After exploring the possibilities that adenine offers as a ligand and a hydrogen-bond donor/acceptor molecule, we tried to analyze the effects on the resulting crystal structures by methylating this nucleobase. The 9-methyladenine was selected for this purpose because it somehow mimics the behaviour of the adenosine/deoxyadenosine where the adenine is bonded through N9 to a ribose or deoxyribose, respectively. The alkylation of adenine at N9 position prevents N3,N9-bidentate coordination mode which was essential for it to act as a bridging ligand in forming windmill shaped dimeric entities. A search in the CSD database of transition metal complexes of 9-methyladenine shows the prevalence of N7 coordination mode, because of the steric hindrance imparted by the methyl group on the neighbouring N3

¹⁷¹ Sun, D. et al. *J. Am. Chem. Soc.* **2006**, *128*, 3896.

¹⁷² Ma, L.; Lin, W. *J. Am. Chem. Soc.* **2008**, *130*, 13834.

nitrogen atom makes its coordination difficult. The different coordination modes of 9-methyladenine are shown in Figure 3.41 with the frequency of their appearance as found in the CSD data base.

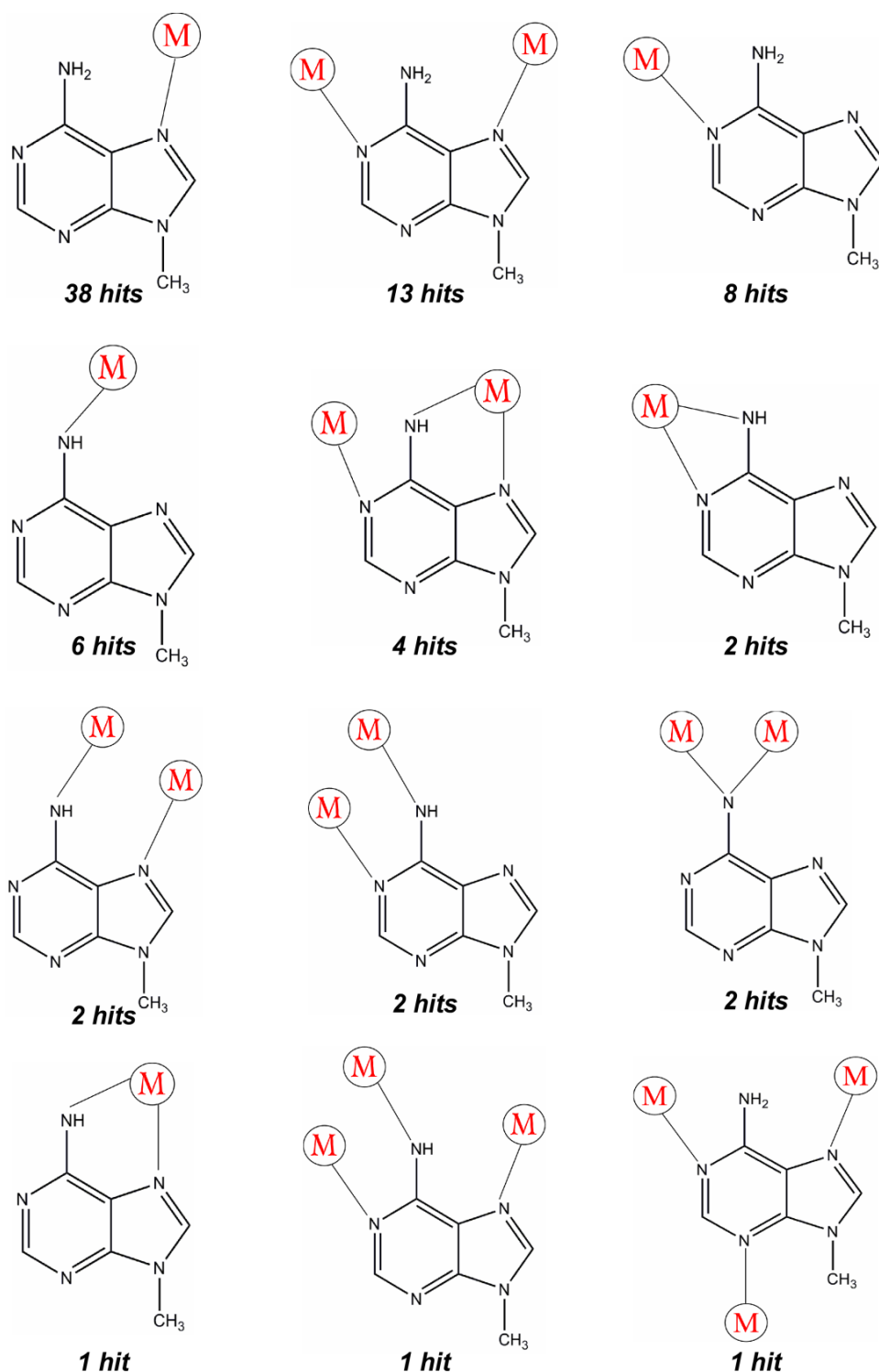


Figure 3.41: Coordination modes of 9-methyladenine and their appearance frequency.

The crystal structure of the compound resulting from the reaction of two equivalents of 9-methyladenine with one equivalent of $\text{CoCl}_2 \cdot 6\text{H}_2\text{O}$ in methanol consist of complex

monomeric $[\text{Co}(9\text{-MeAde})_2(\text{H}_2\text{O})_4]^{2+}$ cations, chloride counterions and crystallization water molecules. The cobalt(II) centre is octahedrally coordinated to four water molecules in the equatorial plane and to two 9-methyladenine molecules occupying the axial positions (Figure 3.42). The methylated nucleobase is anchored to the metal centre through N7 providing a distorted octahedral environment around the metal centre with slightly longer coordination bond distances for Co–N bonds than for Co–O ones (Table 3.24).

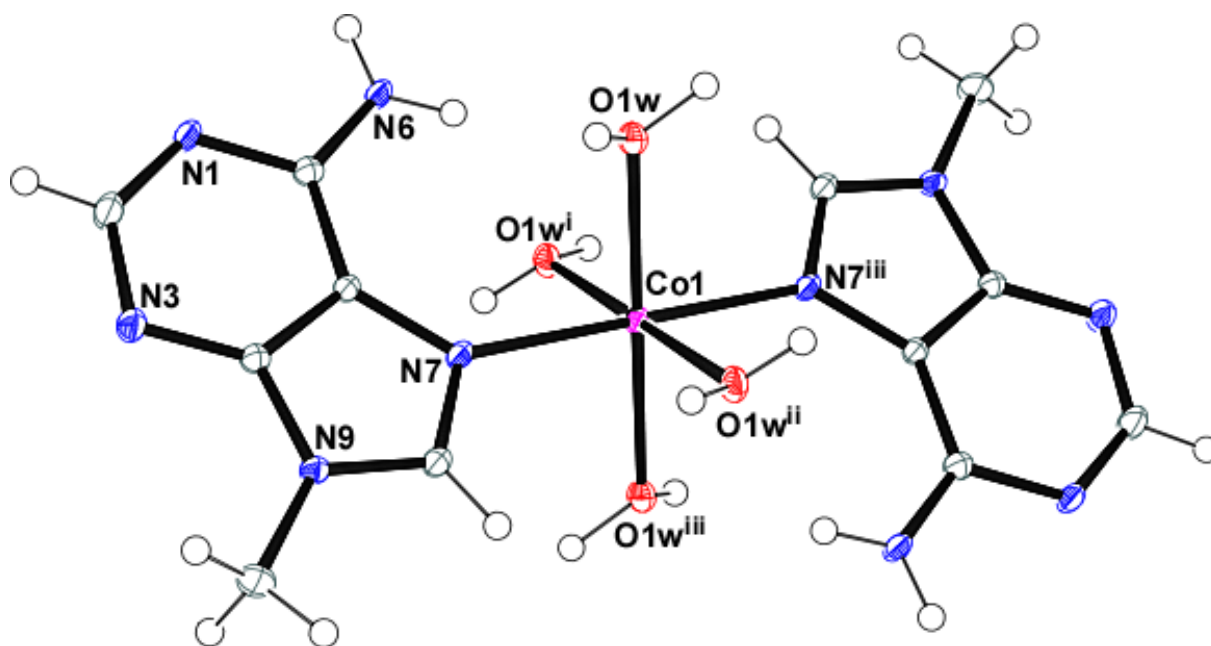


Figure 3.42: Ortep view of the complex cation present in compound *CO-9-MEADECL*.

Table 3.24: Coordination bond lengths (Å) and angles (°) for compound *CO-9-MEADECL*.^[a]

Co1–O1w	2.0912(11)	O1w ⁱ –Co1–O1w ⁱⁱⁱ	89.06(6)
Co1–N7	2.1488(18)	O1w ⁱ –Co1–N7	91.09(4)
N7–Co1–N7 ⁱⁱⁱ	180.000(1)	O1w ⁱ –Co1–N7 ⁱⁱⁱ	88.91(4)
O1w–Co1–N7	88.91(4)	O1w ⁱⁱ –Co1–O1w ⁱⁱⁱ	90.94(6)
O1w–Co1–N7 ⁱⁱⁱ	91.09(4)	O1w ⁱⁱ –Co1–N7 ⁱⁱⁱ	91.09(4)
O1w–Co1–O1w ⁱ	90.94(6)	O1w ⁱⁱ –Co1–N7	88.91(4)
O1w–Co1–O1w ⁱⁱⁱ	180.0	O1w ⁱⁱⁱ –Co1–N7	88.91(4)
O1w–Co1–O1w ⁱⁱ	89.06(6)	O1w ⁱⁱⁱ –Co1–N7	91.09(4)
O1w ⁱ –Co1–O1w ⁱⁱ	180.0		

[a] Symmetry codes: (i) $-x+2, y, -z$; (ii) $x, -y+1, z$; (iii) $-x+2, -y+1, -z+1$.

The crystal architecture is dominated by the hydrogen-bonding complementary interactions taking place between the Watson–Crick faces that connect the cationic complex

entities in supramolecular 1D chains (Figure 3.43 and Table 3.25). The N6–H of each 9-methyladenine moieties further establishes intramolecular hydrogen bonds with coordinated water molecules. The supramolecular chains are held together not only by the electrostatic interactions taking place between the cationic complex and the chloride counterions but also by a complex network of hydrogen bonding interactions between the water molecules, the N3 position of the 9-methyladenine and the chloride counterions. There are also some structural evidences of weak π – π stacking interactions between the pyrimidine rings of the 9-methyladenines with a perpendicular distance of 3.365 Å between the mean planes and a slippage of 2.07 Å.

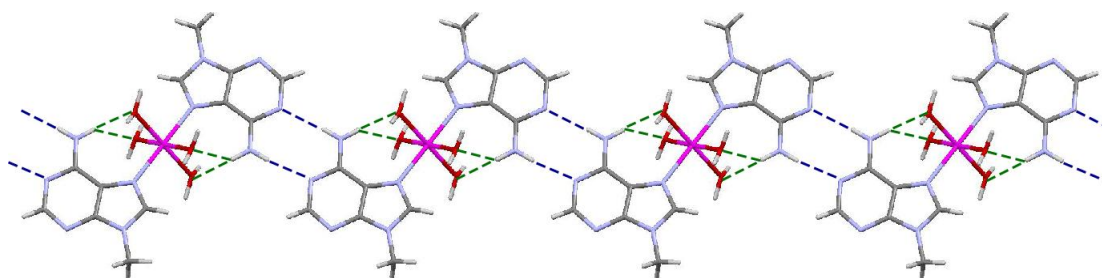


Figure 3.43: Supramolecular chain of $[\text{Co}(9\text{-MeAde})_2(\text{H}_2\text{O})_4]^{2+}$ complex cations.

Table 3.25: Supramolecular interactions (Å, °) in *CO-9-MEADECL*.

Hydrogen bonding interactions. ^[a]					
<i>D</i> – <i>H</i> ⋯ <i>A</i> ^[b]	<i>D</i> – <i>H</i>	<i>H</i> ⋯ <i>A</i>	<i>D</i> ⋯ <i>A</i>	<i>D</i> – <i>H</i> ⋯ <i>A</i>	
N6–H6A⋯N1 ⁱ	0.86	2.12	2.974(3)	175.6	
N6–H6B⋯O1w	0.86	2.31	2.980(2)	135.3	
N6–H6B⋯O1w ⁱⁱ	0.86	2.31	2.980(2)	135.3	
O1w–H1A⋯Cl1 ⁱⁱⁱ	0.96	2.13	3.073(1)	167.2	
O1w–H1B⋯O2w	0.85	1.93	2.771(2)	171.2	
O2w–H2A⋯N3 ^{iv}	0.91	2.06	2.920(2)	156.6	
O2w–H2B⋯Cl1	0.87	2.35	3.209(2)	171.4	
π – π stacking interactions. ^[c]					
Ring⋯Ring ^[d]	Angle	DC	α	DZ	DXY
Ring(1)⋯Ring(1) ^v	0	3.9521(8)	31.62	3.3654(1)	2.072

[a] Symmetry: (i) $-x+1, -y+1, -z+1$; (ii) $x, -y+1, z$; (iii) $-x+2, -y+1, -z+1$; (iv) $-x+3/2, -y+3/2, -z+3/2$; (v) $-x+3/2, y-1/2, -z+3/2$. [b] **D**: donor; **A**: acceptor. [c] Angle: Dihedral Angle between Planes I and J (°), DC: Distance between ring centroids (Å), α : Angle Cg(I)–>Cg(J) vector and normal to plane I (°), DZ: Perpendicular distance of Cg(I) on ring J (Å), DXY: Slippage. [d] Ring 1: N1, C2, N3, C4, N9, C6.

As it was expected, the methyl group at N9 position reduces the capacity of the adenine to both coordinate and to establish hydrogen-bond interactions. The adenine molecule could provide three faces able to establish complementary hydrogen bonding interactions (Figure 3.44): Watson-Crick face (N1/N6), Hoogsteen side (N6/N7) and sugar edge (N3/N9). The methylation at N9 precludes the sugar-edge for this purpose and the coordination at N7 does the same for the Hoogsteen side. Therefore only the Watson-Crick face is available to establish complementary hydrogen bonding interaction. Taking into account that there are only two nucleobases per cobalt(II) center, the generation of supramolecular 1D chains though double hydrogen-bond interactions would be expected, as it has been the case.

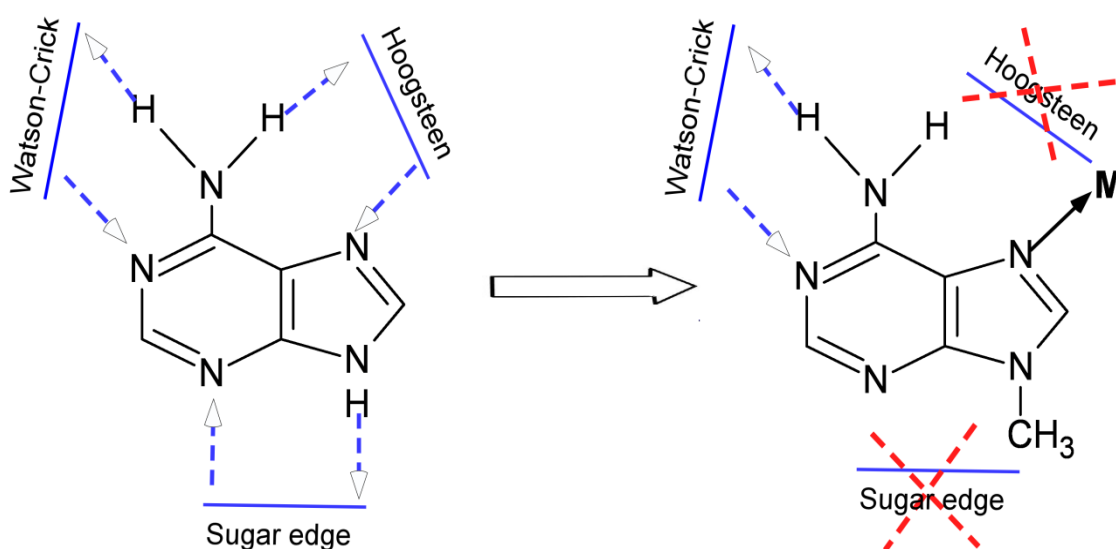


Figure 3.44: The availability of hydrogen bonding faces for free adenine and *N*7-coordinated 9-methyladenine.

Details of the thermogravimetric studies are given in Figure 3.45 and Table 3.26. According to the thermogravimetric analysis, the first mass loss occurs below 55 °C. Then the compound remains stable upto 75 °C. After that it undergoes consecutive decomposition to the final residue Co_3O_4 above 630 °C.

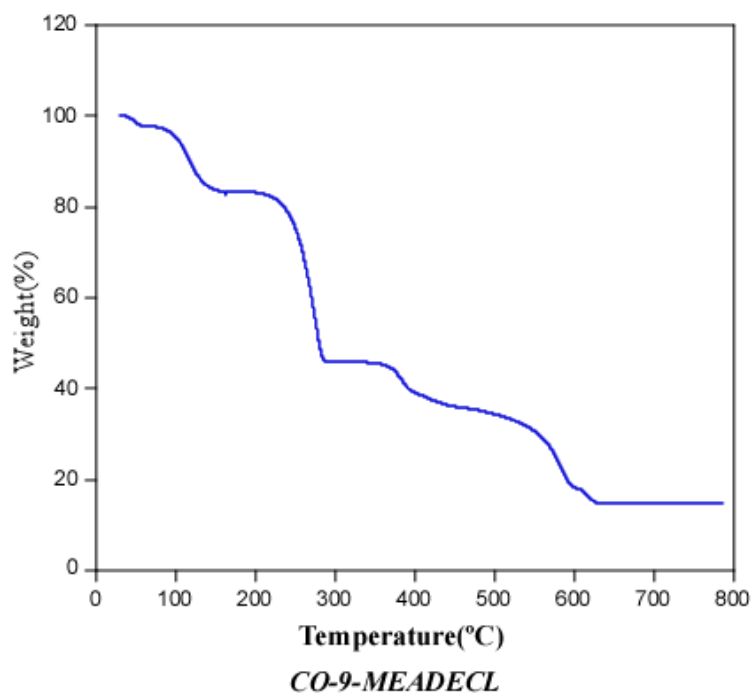


Figure 3.45: Thermogravimetric analysis of *CO-9-MEADECL*.

Table 3.26: The thermogravimetric data of *CO-9-MEADECL*.^[a,b]

Step	T_i	T_f	$\Delta m(\%)$	$\Sigma \Delta m(\%)$	$\Sigma \Delta m(\%)_{theor}$
<i>CO-9-MEADECL</i>					
1	25	55	2.16	2.16	3.36 (–1 H ₂ O)
2	75	155	14.32	16.48	16.78 (–4 H ₂ O)
3	205	285	37.4	53.88	–
4	330	630	31.17	85.05	85.03 (1/3 C ₃ O ₄)

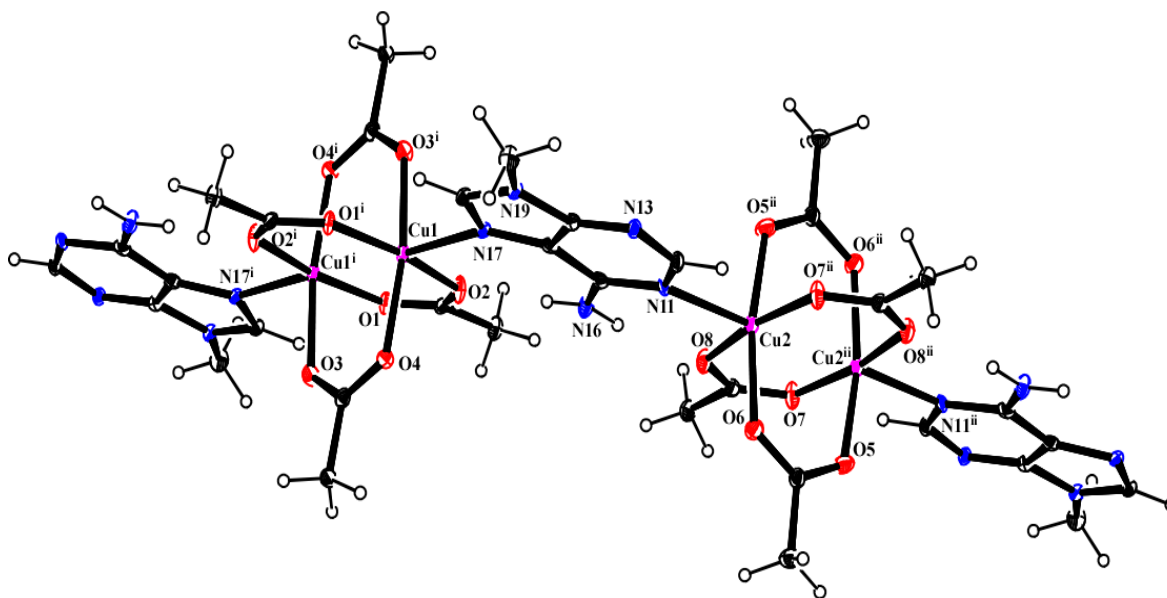
[a] T_i = initial temperature; T_f = final temperature; T_{peak} = DTA peak temperature; $\Delta m(\%)$ = mass loss percentage for each process; ΔH = process type in the basis of DTA; $\Sigma \Delta m(\%)$ = total mass loss percentage; $\Sigma \Delta m(\%)_{theor}$ = theoretical total mass loss percentage. [b] Released molecules and final residue per formula.

3.3.2.9 Structural Description of $[\text{Cu}_2(\mu\text{-CH}_3\text{COO})_4(\mu\text{-9-MeAde})]_n \cdot n\text{CH}_3\text{OH}$; *CU-9-MEADEACE*

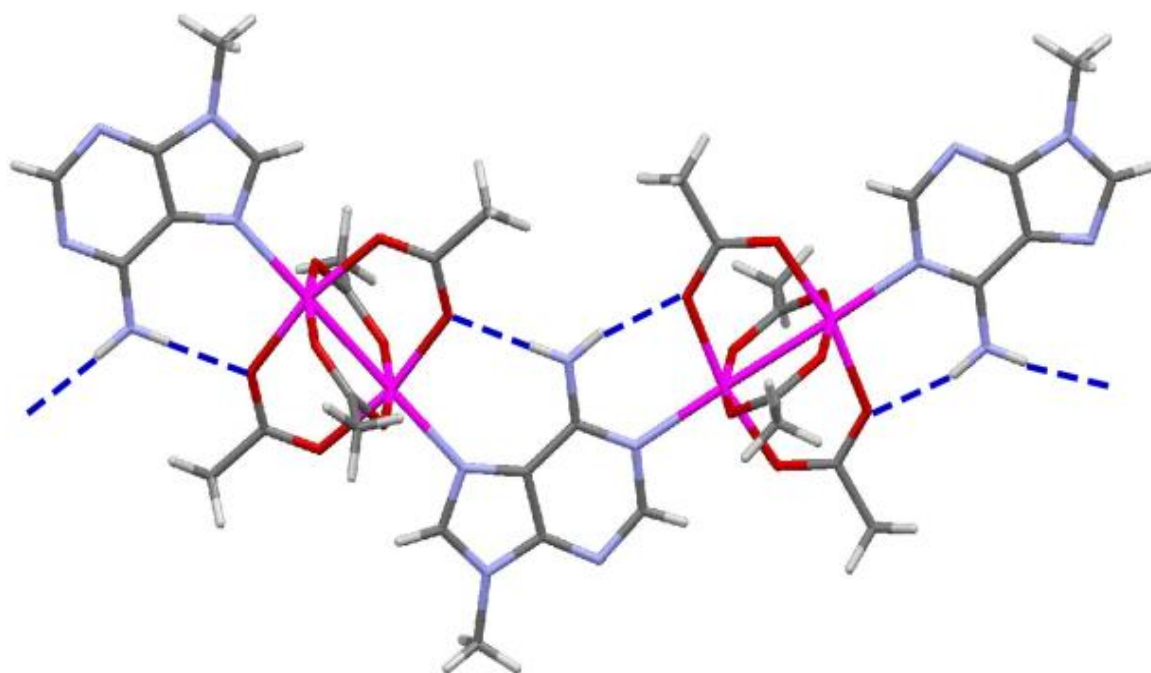
The reaction between 9-methyladenine and $\text{Cu}(\text{OOCCH}_3)_2 \cdot \text{H}_2\text{O}$ in methanol at room temperature provided a green compound that retains the usual $[\text{Cu}_2(\mu\text{-OOCCH}_3)_4]$ paddle-wheel shaped entities but bridged by $\mu\text{-9-methyladenine-}\kappa\text{N1}:\kappa\text{N7}$ molecules that are anchored to the apical positions of the dimeric entities (Figure 3.46a). This coordination mode is the second most probable one for the 9-methyladenine and it is reinforced by the intramolecular hydrogen bonding interactions implying the exocyclic amino group as donor

and the oxygen atoms from two acetates as acceptors (Figure 3.46b). The copper(II) coordination environment can be described as an elongated square pyramid with the apical bond distances (Cu–N) longer than the equatorial ones (Cu–O). The coordination bond network extends into *zig-zag* infinite chains that propagate along the [0 1 1] direction with acetate anions and 9-methyladenine moieties bridging alternatively the copper(II) atoms. The metal···metal distances are shorter through the four-fold acetate bridge (2.64 and 2.66 Å) than through the μ -9-methyladenine- $\kappa N1:\kappa N7$ molecule (7.08 Å). Table 3.27 list the most relevant coordination bond distances and angles.

The μ - $\kappa N1:\kappa N7$ coordination mode of the 9-methyladenine precludes any possible complementary hydrogen-bonding interaction along either its Watson-Crick or Hoogsteen sides. Therefore, the supramolecular crystal structure is dominated by weak van der Waals interactions and the hydrogen-bonding interactions between the methanol solvation molecules and the oxygen atoms of the carboxylato ligands that does not provide any accessible void (Figure 3.47 and Table 3.28). No structural evidence of π - π interactions has been observed. An interesting result coming from this compound is that the 9-methyladenine does not coordinate strong enough to the metal center as to displace the carboxylato ligands from the paddle-wheel shaped building unit, instead being only able to occupy the more labile apical positions.



(a)



(b)

Figure 3.46: (a) A fragment of the polymeric chain of *CU-9-MEADACE* (b) and the intramolecular hydrogen bond between N6-H and oxygen atoms of the carboxylate anions.

Table 3.27: Selected bond lengths (Å) and angles (°) of compound *CU-9-MEADACE*.^[a]

Cu1–O2 ⁱ	1.952(4)	O1–Cu1–O3	90.48(17)	O5–Cu2–O7	89.33(18)
Cu1–O1	1.955(4)	O1–Cu1–O4 ⁱ	89.73(17)	O5–Cu2–Cu2 ⁱⁱ	83.96(12)
Cu1–O3	1.967(4)	O1–Cu1–N17	94.12(17)	O5–Cu2–O7	89.33(18)
Cu1–O4 ⁱ	1.977(4)	O2–Cu1–O1 ⁱ	168.08(16)	O6–Cu2–O7 ⁱⁱ	88.79(19)
Cu1–N17	2.211(5)	O2–Cu1–O3 ⁱ	89.38(17)	O6–Cu2–N11 ⁱⁱ	96.13(17)
Cu2–O5	1.957(4)	O2–Cu1–O4 ⁱ	87.91(16)	O6–Cu2–Cu2 ⁱⁱ	83.31(13)
Cu2–O8 ⁱⁱ	1.959(4)	O2–Cu1–N17 ⁱ	97.69(16)	O7–Cu2–N11	99.25(17)
Cu2–O6 ⁱⁱ	1.962(4)	O3–Cu1–O4 ⁱ	167.79(17)	O7–Cu2–Cu2 ⁱⁱ	82.13(12)
Cu2–O7	1.982(4)	O3–Cu1–N17	98.19(17)	O8–Cu2–N11 ⁱⁱ	93.61(17)
Cu2–N11	2.211(5)	O4–Cu1–N17 ⁱ	93.97(16)	O8–Cu2–O7 ⁱⁱ	167.13(16)
Cu1…Cu1 ⁱ	2.6434(14)	O5–Cu2–O8 ⁱⁱ	89.32(19)	O8–Cu2–Cu2 ⁱⁱ	85.00(12)
Cu1…Cu2	7.0797(11)	O5–Cu2–O6 ⁱⁱ	167.27(17)	O8–Cu2–O6 ⁱⁱ	89.7(2)
Cu2…Cu2 ⁱⁱ	2.6616(14)	O5–Cu2–N11	96.60(17)	O8–Cu2–O6 ⁱⁱ	89.7(2)

[a] Symmetry codes: (i) $-x+1, -y, -z$; (ii) $-x+1, -y+1, -z+1$.

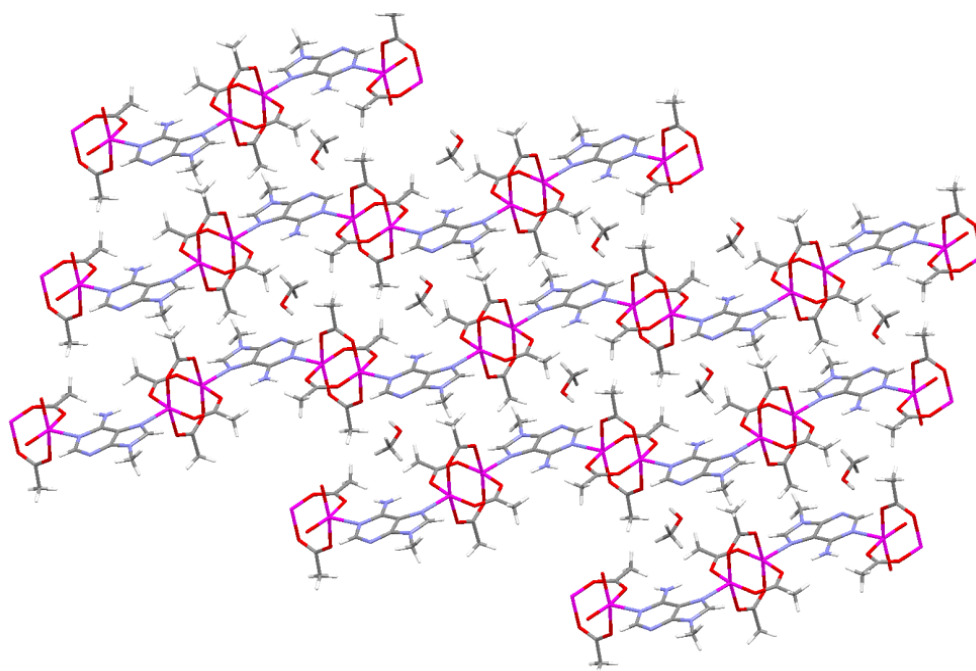


Figure 3.47: Crystal packing of *CU-9-MEADACE* viewed along the crystallographic *b* axis.

Table 3.28: Hydrogen bonding interactions (\AA , $^\circ$) in *CU-9-MEADACE*.^[a]

$D-H\cdots A$ ^[b]	$D-H$	$H\cdots A$	$D\cdots A$	$D-H\cdots A$
N16-H16A \cdots O7	0.86	1.96	2.793(6)	162.3
N16-H16B \cdots O3	0.86	1.94	2.801(6)	178.1
O9-H9 \cdots O5 ⁱ	0.82	2.04	2.835(6)	161.8

[a] Symmetry code: (i) $-x+1, -y+1, -z+1$. [b] **D**: donor; **A**: acceptor.

The thermogravimetric analysis of the compound *CU-9-MEADACE* (Figure 3.48 and Table 3.29) shows that the solvent removal occurs below 135 $^\circ\text{C}$, then the compound remains stable up to 185 $^\circ\text{C}$ and further decomposes in different steps to CuO as final residue, above 475 $^\circ\text{C}$.

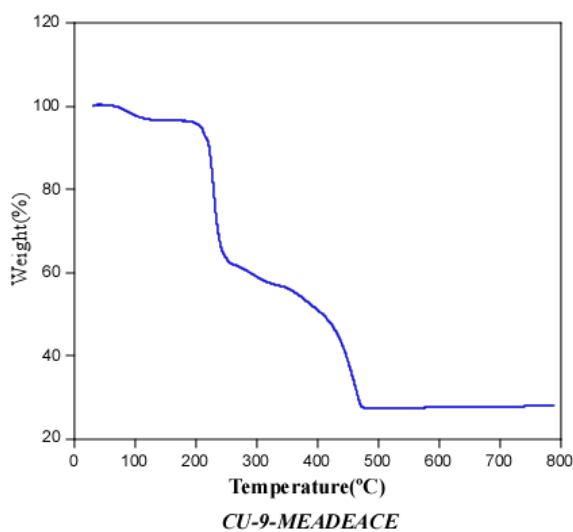


Figure 3.48: Thermogravimetric analysis of *CU-9-MEADACE*.

Table 3.29: Thermogravimetric data of **CU-9-MEADEACE**.^[a,b]

Step	T_i	T_f	$\Delta m(\%)$	$\Sigma \Delta m(\%)$	$\Sigma \Delta m(\%)_{theor}$
CO-9-MEADEACE					
1	25	135	3.4	3.4	3.31 (-1 H ₂ O)
2	185	260	34.54	37.94	–
3	260	475	34.61	72.35	70.8 (2 CuO)

[a] T_i = initial temperature; T_f = final temperature; T_{peak} = DTA peak temperature; $\Delta m(\%)$ = mass loss percentage for each process; ΔH = process type in the basis of DTA; $\Sigma \Delta m(\%)$ = total mass loss percentage; $\Sigma \Delta m(\%)_{theor}$ = theoretical total mass loss percentage. [b] Released water molecules and final residue per formula.

3.3.2.10 Structural description of $[\text{Cu}_2(\text{Hgua})_2(\text{H}_2\text{gua})_2(\mu\text{-Cl})_2\text{Cl}_2(\text{H}_2\text{O})][\text{CuCl}_4]$; **CUGUACL**

There are few examples of unsubstituted guanines coordinated to a metal centre because it is highly insoluble in most solvents. Herein, a very acidic media has been employed in order to promote its solubility and reaction with the copper(II) metal centres. **CUGUACL** compound contains two disordered copper(II) cationic dimeric entities and $[\text{CuCl}_4]^{2-}$ counterions. The centrosymmetric dimeric entities are based on double chloride bridged copper(II) metal centers that complete their coordination sphere with two *1H,3H,7H*-guaninium/*1H,7H*-guanine in *trans*-arrangement and coordinated through N9. Crystallographically there is no way to distinguish between the guaninium and guanine ligand because the hydrogen atom placed at N3 position is disordered over the two ligands with 50% occupation factor. The coordination of a cationic molecule to a metal centre is not usual but there have been some reported examples.¹⁷³ The difference between the two dimeric entities relies on the orientation of the Jahn–Teller effect and the presence of a coordination water molecule (Figure 3.49). The $[\text{Cu}_2(\text{C}_5\text{H}_5\text{N}_5\text{O})_2(\text{C}_5\text{H}_6\text{N}_5\text{O})_2(\mu\text{-Cl})_2\text{Cl}_2]^{2+}$ entity, with an occupation factor of 50%, presents a square–pyramidal coordination geometry around the metal centers, whereas $[\text{Cu}_2(\text{C}_5\text{H}_5\text{N}_5\text{O})_2(\text{C}_5\text{H}_6\text{N}_5\text{O})_2(\mu\text{-Cl})_2\text{Cl}_2(\text{OH}_2)]^{2+}$ dimer (occupation factor: 50%) provides a tetragonally elongated octahedral geometry. The N3 nitrogens of all guaninium cations are held additionally through an intramolecular hydrogen bonding with the coordinated water molecule. Table 3.30 lists the coordination bond lengths and angles.

¹⁷³ (a) Turel, I. et al. *J. Inorg. Biochem.* **2004**, 98, 393. (b) Gaballa, A. S. et al. *Inorg. Chim. Acta* **2008**, 361, 2070. (c) Sundaralingam, M.; Carrabine J. A. *J. Mol. Biol.* **1971**, 61, 287. (d) Declercq, J. P. et al. *Bull. Soc. Chim. Belg.* **1971**, 80, 527.

The copper(II) dimeric entities are linked together through direct nucleobase–nucleobase base pairing interactions involving the Hoogsteen face to provide a double–ladder like supramolecular structure, as shown in Figure 3.50. It becomes clear that the protonation of the guanine does not preclude the formation of complementary hydrogen–bonding interactions among these nucleobases (Table 3.31). In fact, a detailed inspection of the hydrogen–bond donor/acceptor position at the 1H,7H–guaninium molecule indicate that both O6/N1 (Watson–Crick face) and O6/N7 (Hoogsteen face) are available for this purpose. However, the parallel arrangement of the coordinated nucleobases precludes their supramolecular polymerization into a 3D structure.

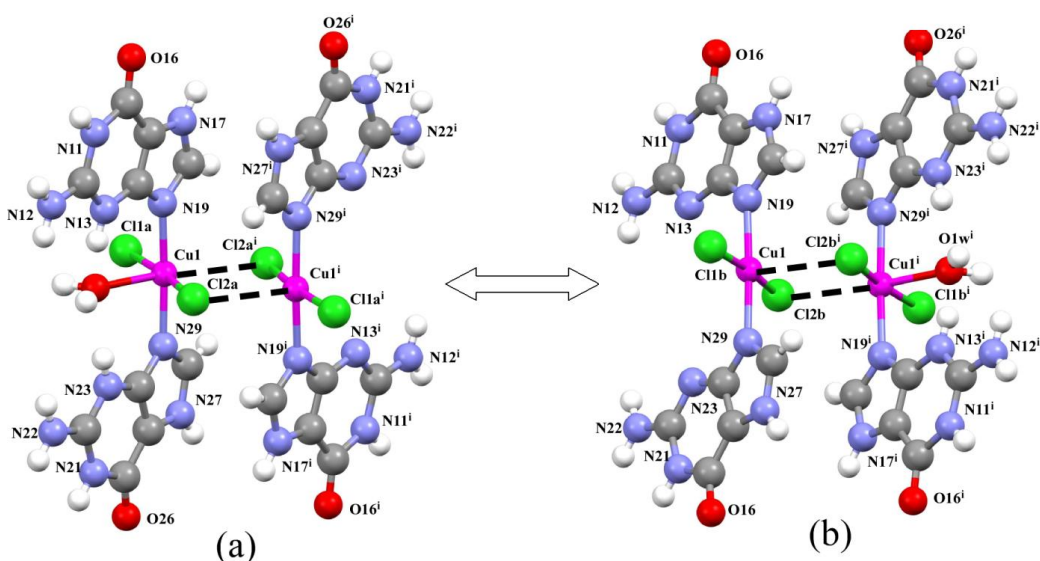


Figure 3.49: Disordered dimeric $[\text{Cu}_2(\text{Hgua})_2(\text{H}_2\text{gua})_2(\mu\text{-Cl})_2\text{Cl}_2]^{2+}$ and $[\text{Cu}_2(\text{Hgua})_2(\text{H}_2\text{gua})_2(\mu\text{-Cl})_2\text{Cl}_2(\text{H}_2\text{O})]^{2+}$ cations of compound *CUGUACL*.

Table 3.30: Coordination bond lengths (Å) and angles (°) of *CUGUACL*.^[a]

Cu1–N29	1.987(4)	N19–Cu1–O1w	88.38(17)
Cu1–N19	1.991(5)	N29–Cu1–Cl2B ⁱ	92.59(15)
Cu1–O1w	2.134(5)	N19–Cu1–Cl2B ⁱ	91.34(16)
Cu1–Cl2A	2.242(3)	O1w–Cu1–Cl2B ⁱ	179.48(17)
Cu1–Cl1A	2.350(3)	N29–Cu1–Cl2A	88.13(16)
Cu1–Cl2B ⁱ	2.260(4)	N19–Cu1–Cl2A	88.88(18)
Cu1⋯Cu1	3.658(4)	N29–Cu1–Cl1A	89.94(16)
N29–Cu1–N19	175.50(2)	N19–Cu1–Cl1A	92.72(18)
N29–Cu1–O1w	87.70(16)	Cl2A–Cu1–Cl1A	174.17(12)

[a] Symmetry code: (i) $-x+1, -y, -z+1$.

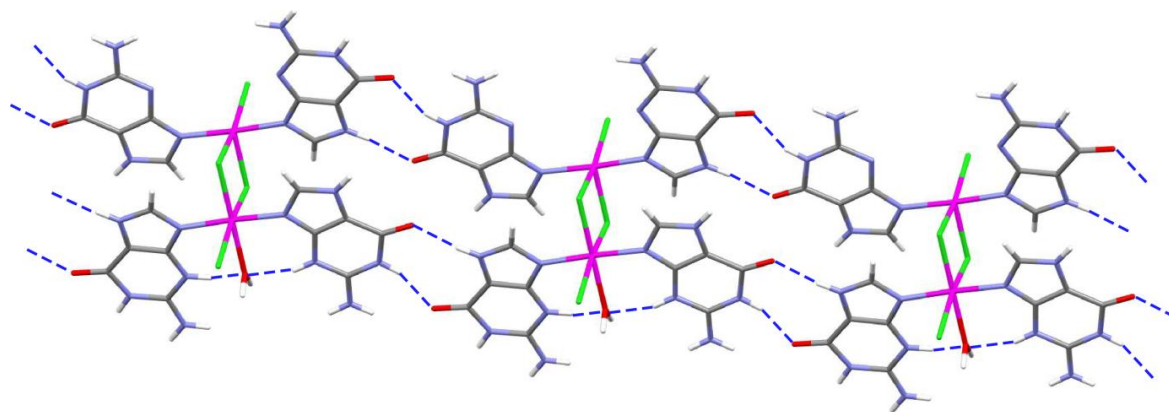


Figure 3.50: Hydrogen bonding interaction in the crystal structure of *CUGUACL*. Only the water coordinated dimeric entities are depicted here for clarity purposes.

Table 3.31: Hydrogen bonding interactions (Å, °) for compound *CUGUACL*.^[a]

$D-H\cdots A$ ^[b]	$D-H$	$H\cdots A$	$D\cdots A$	$D-H\cdots A$
O1w–H2w \cdots Cl1B ⁱ	0.94	1.92	2.786(10)	153.9
N13–H13 \cdots O1w	0.86	1.86	2.576(6)	139.4
N23–H23 \cdots O1w	0.86	1.93	2.604(6)	133.9
N13–H13 \cdots Cl1B ⁱ	0.86	2.66	3.389(6)	143.8
N23–H23 \cdots Cl1B ⁱ	0.86	2.68	3.393(6)	141.8
N11–H11 \cdots O26 ⁱⁱ	0.86	1.90	2.723(6)	161.1
N12–H12A \cdots Cl1A ⁱ	0.86	2.60	3.421(6)	161.1
N12–H12A \cdots Cl1B ⁱ	0.86	2.37	3.182(6)	158.4
N12–H12B \cdots O26 ⁱⁱ	0.86	2.42	3.105(6)	137.5
N17–H17 \cdots Cl4 ⁱⁱⁱ	0.86	2.27	3.118(5)	170.0
N21–H21 \cdots Cl3 ^{iv}	0.86	2.31	3.123(5)	156.8
N22–H22A \cdots Cl1A ⁱ	0.86	2.62	3.429(7)	156.4
N22–H22A \cdots Cl1B ⁱ	0.86	2.36	3.172(7)	156.7
N22–H22B \cdots Cl3 ^{iv}	0.86	2.52	3.274(6)	147.5
N27–H27 \cdots O16 ^v	0.86	1.90	2.754(6)	174.7

[a] Symmert code: (i) $-x+1, -y+1, -z+1$; (ii) $x, y, z+1$; (iii) $x+1, y, z+1$; (iv) $x, y+1, z$; (v) $x, y, z-1$. [b] **D**: donor; **A**: acceptor.

The supramolecular structure further extends into a 3D network through hydrogen-bonding interactions involving the Watson–Crick faces of the nucleobases, the coordinated chlorido ligands of the $[\text{CuCl}_4]^{2-}$ counterions and adjacent cationic dimers resulting in a compact crystal packing (Figure 3.51).

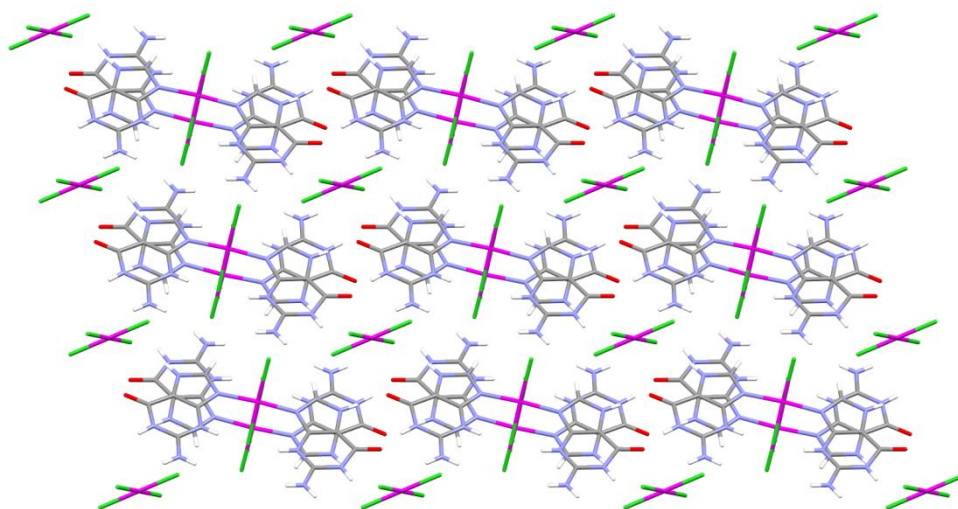


Figure 3.51: Packing of compound *CUGUACL*.

3.3.2.11 Structural description of $[\text{Co}(6\text{-ClPur})_2(\text{H}_2\text{O})_4]\cdot 4\text{H}_2\text{O}$; *CO-6-CLPUR*

We have also tried to obtain supramolecular porous materials using non-natural nucleobases such as 6-chloropurine by its reaction with $\text{Co}(\text{NO}_3)_2\cdot 6\text{H}_2\text{O}$ in a pentylamine containing aqueous media. The presence of pentylamine in the reaction media promotes the deprotonation of the nucleobase increasing the options of obtaining a neutral complex entity but it also could play a templating effect on the resulting crystal structure. The crystal structure of *CO-6-CLPUR* consist of $[\text{Co}(6\text{-ClPur})_2(\text{H}_2\text{O})_4]$ monomeric entities (6-ClPur being 6-chloropurinate) and crystallization water molecules (Figure 3.52). The cobalt centers are coordinated to two 6-chloropurinato ligands through N9 positions occupying axial positions and the equatorial positions are coordinated by four water molecules forming an octahedral environment (Table 3.32).

The coordination of the 6-chloropurinato ligands is reinforced by the presence of an intramolecular hydrogen bond between a coordinated water molecule as donor and N3 position of the nucleobase as acceptor. It is worthy to denote that, as far as we know, this is the first example of this coordination mode for the 6-chloropurine/6-chloropurinato ligand (Figure 3.53).¹⁷⁴ The deprotonation of the chloropurine ligands leads to a situation that avoids any chance to promote a robust supramolecular structure by means of complementary hydrogen bond interactions between the nucleobases as it only contains donor groups. In fact

¹⁷⁴(a) Dalby, C. et al. *Angew. Chem. Int. Ed.* **1993**, 32, 1696. (b) Cepeda, J. et al. *Eur. J. Inorg. Chem.* **2009**, 2344.

the supramolecular structure seems to be dominated by the π - π stacking interactions between the nucleobases to provide a corrugated supramolecular sheet of monomeric complexes. There are also many hydrogen bond interactions involving the coordination and crystallization water molecules that reinforce the supramolecular sheet and also provide cohesion between adjacent sheets giving rise to a non porous structure (Figure 3.54 and Table 3.33).

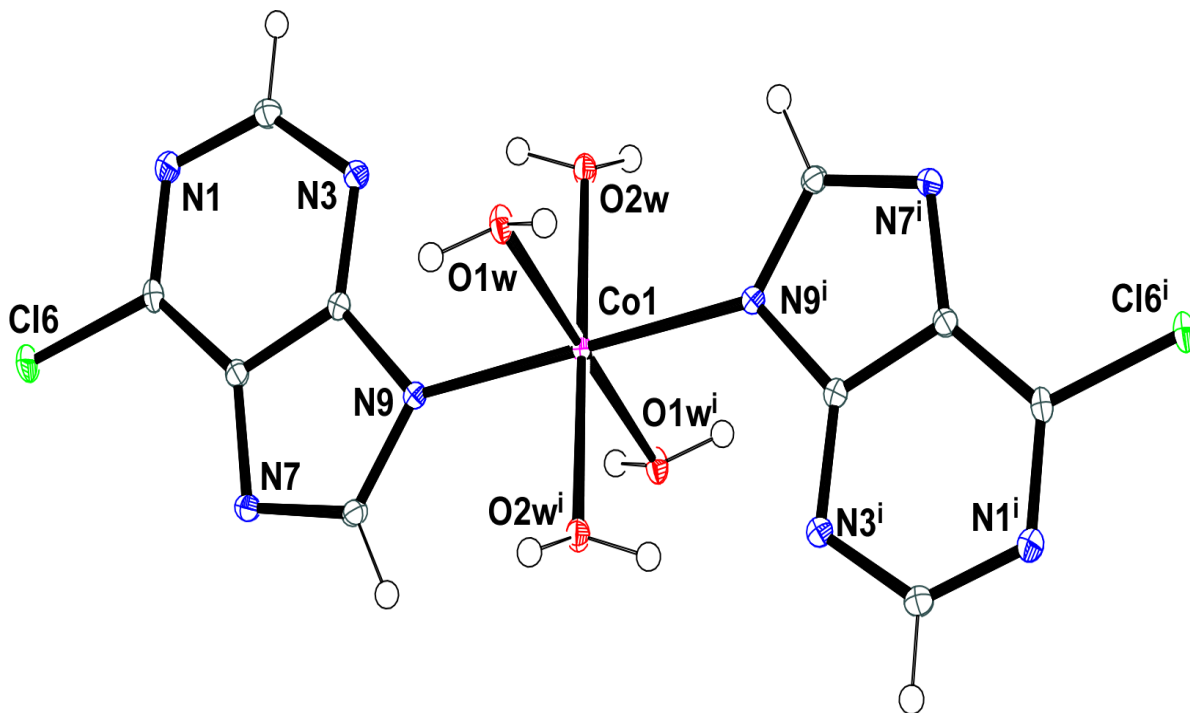


Figure 3.52: The monomeric entity of *CO-6-CLPUR*.

Table 3.32: Selected coordination bond lengths (Å) and angles (°) for compound *CO-6-CLPUR*.^[a]

Co1–O2w ⁱ	2.0860(11)	O2w–Co1–O1w ⁱ	94.74(4)	O1w–Co1–N9	88.16(4)
Co1–O2w	2.0860(11)	O2w–Co1–O1w ⁱ	85.26(4)	O2w–Co1–N9 ⁱ	88.33(5)
Co1–O1w ⁱ	2.1215(11)	O2w–Co1–O1w	94.74(4)	O2w–Co1–N9 ⁱ	91.67(5)
Co1–O1w	2.1215(11)	O1w–Co1–O1w ⁱ	180.0	O1w–Co1–N9 ⁱ	88.16(4)
Co1–N9	2.1284(13)	O2w–Co1–N9 ⁱ	91.67(5)	O1w–Co1–N9 ⁱ	91.84(4)
Co1–N9 ⁱ	2.1284(13)	O2w–Co1–N9	88.33(5)	N9–Co1–N9 ⁱ	180.0
O2w–Co1–O2w ⁱ	180.0	O1w–Co1–N9 ⁱ	91.84(4)		

[a] Symmetry code: (i) $-x+2, -y+1, -z+1$.

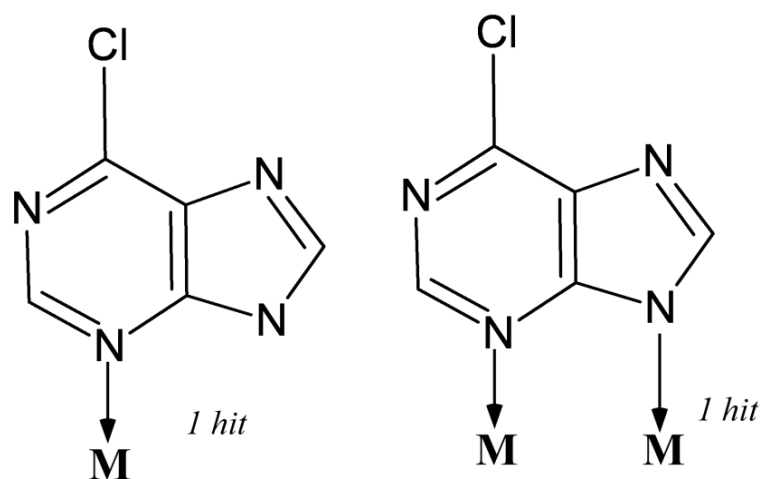


Figure 3.53: Coordination modes of 6-chloropurine/6-chloropurinate as found in the CSD data base.

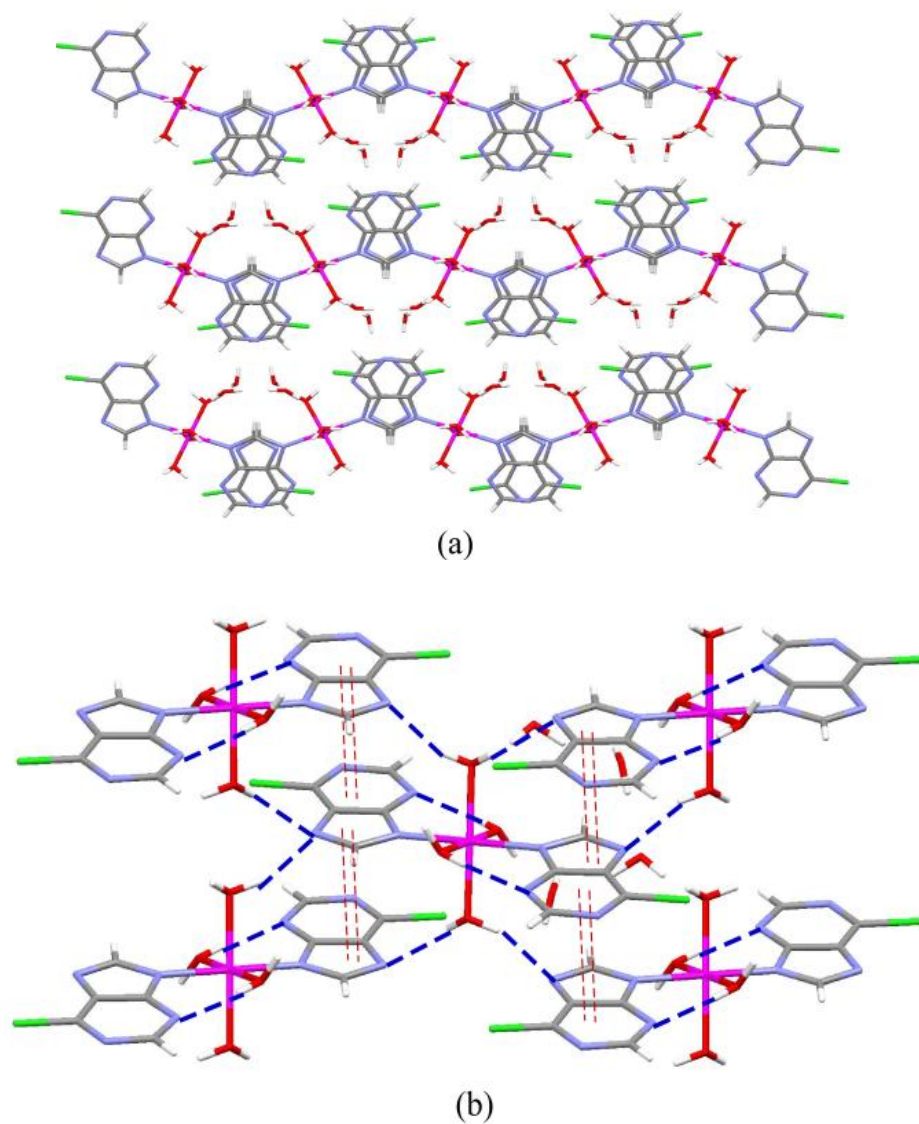


Figure 3.54: (a) Packing of compound *CO-6-CLPUR* and (b) hydrogen bonding (blue dashed lines) and π - π stacking interactions (red double dashed lines).

Table 3.33: Supramolecular interactions (Å, °) in *CO-6-CLPUR*.

Hydrogen bonding interactions. ^[a]					
<i>D-H</i> ... <i>A</i> ^[b]	<i>D-H</i>	<i>H</i> ... <i>A</i>	<i>D</i> ... <i>A</i>	<i>D-H</i> ... <i>A</i>	
O1w-H11...N7 ⁱ	0.87	2.24	3.020(2)	149.8	
O1w-H12...N7 ⁱⁱ	0.87	2.11	2.902(2)	151.1	
O2w-H21...N3 ⁱⁱⁱ	0.86	1.94	2.737(2)	153.4	
O2w-H22...O4w ^{iv}	0.91	1.81	2.709(2)	169.4	
O3w-H31...O1w	0.85	2.19	2.979(2)	153.7	
O4w-H41...N1	0.95	1.90	2.827(2)	164.0	
O4w-H42...O3w ^v	0.85	1.82	2.673(2)	175.5	
π - π stacking interactions. ^[c]					
Ring...Ring ^[d]	Angle	DC	α	DZ	DXY
Ring1-Ring1 ^{vi}	2	3.6908(9)	19.22	3.4987(6)	1.1752
Ring1-Ring1 ^{vii}	2	3.6908(9)	18.56	3.4851(6)	1.2149
Ring1-Ring2 ^{vi}	1.79(8)	3.6505(8)	18.26	3.4958(6)	1.1434
Ring2-Ring1 ^{vii}	1.79(8)	3.6506(8)	16.74	3.4668(6)	1.1438
Ring2-Ring2 ^{vi}	1	3.7471(8)	22.24	3.4857(6)	1.3750
Ring2-Ring2 ^{vii}	1	3.7472(8)	21.53	3.4684(6)	1.4183

[a] Symmetry: (i) $-x+2, y-1/2, -z+3/2$; (ii) $x, -y+3/2, z+1/2$; (iii) $-x+2, -y+1, -z+1$; (iv) $x+1, -y+3/2, z+1/2$; (v) $-x+1, y+1/2, -z+3/2$; (vi) $x, 3/2-y, -1/2+z$; (vii) $x, 3/2-y, 1/2+z$; [b] **D**: donor; **A**: acceptor. [c] Angle: Dihedral Angle between Planes I and J (°), DC: Distance between ring centroids (Å), α : Angle Cg(I)→Cg(J) vector and normal to plane I (°), DZ: Perpendicular distance of Cg(I) on ring J (Å), DXY: Slippage. [d] Ring1: N7, C5, C4, N9, C8; Ring 2: N1, C2, N3, C4, C5, C6.

The thermogravimetric analysis of the compound *CO-6-CLPUR* (Figure 3.55 and Table 3.34) shows that the solvent removal occurs in two steps at moderately low temperatures, below 80 °C. Then the compound remains stable up to 370 °C and further decomposes to Co₃O₄ as final residue above 610 °C.

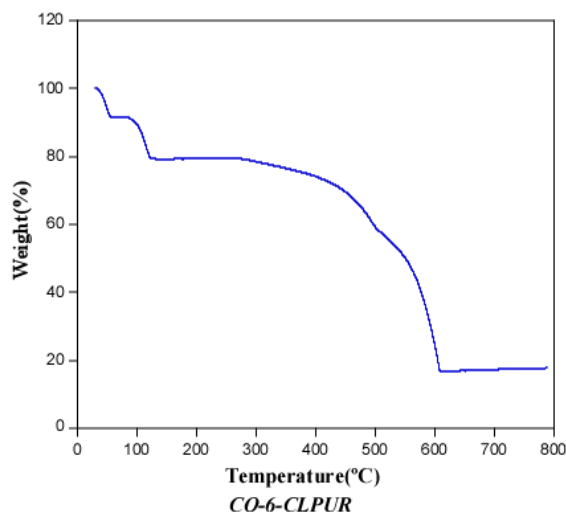


Figure 3.55: Thermogravimetric studies of *CO-6-CLPUR*.

Table 3.34: Thermogravimetric data of *CO-6-CLPUR*.^[a,b]

Step	T_i	T_f	$\Delta m(\%)$	$\Sigma \Delta m(\%)$	$\Sigma \Delta m(\%)_{theor}$
<i>CO-6-CLPUR</i>					
1	25	60	8.35	8.35	7.05 ($-2 \text{ H}_2\text{O}$)
2	80	130	12.39	20.74	21.16 ($-4 \text{ H}_2\text{O}$)
3	370	610	62.63	83.37	84.27 ($1/3 \text{ Co}_3\text{O}_4$)

[a] T_i = initial temperature; T_f = final temperature; T_{peak} = DTA peak temperature; $\Delta m(\%)$ = mass loss percentage for each process; ΔH = process type in the basis of DTA; $\Sigma \Delta m(\%)$ = total mass loss percentage; $\Sigma \Delta m(\%)_{theor}$ = theoretical total mass loss percentage. [b] Released water molecules and final residue per formula.

3.3.2.12 Structural description of $[\text{Co}(\text{ThioG})_3] \cdot n\text{H}_2\text{O}$; *CO-6-THIOG (SMOF-4)*

The analysis of the previous compounds enabled us to select a more appropriate ligand which even when deprotonated can promote complementary hydrogen-bonding interactions. The selected non-natural nucleobase was 6-thioguanine. There are not many examples of transition metal coordination complexes of 6-thioguanine in the literature but the preferred coordination mode seems to involve the chelation through 6-thione and N7 as it is found in the Ru, Rh and Ir complexes of 6-thioguanine.¹⁷⁵ There are also examples of 6-thioguanine acting as bridging ligands to provide 1D chains using a $\mu\text{-}\kappa\text{N7},\kappa\text{S6}:\kappa\text{S6}$ coordination mode.¹⁷⁶ Figure 3.56 represents the possible complementary hydrogen bonding scheme for the different tautomers of the anionic form of this molecule when chelating a metal centre through S6 and N7 positions.

¹⁷⁵ Yamanari, K. et al. *Inorg. Chem.* **2002**, *41*, 6824.

¹⁷⁶ Amo-Ochoa, P. et al. *Inorg. Chem.* **2013**, *52*, 5290.

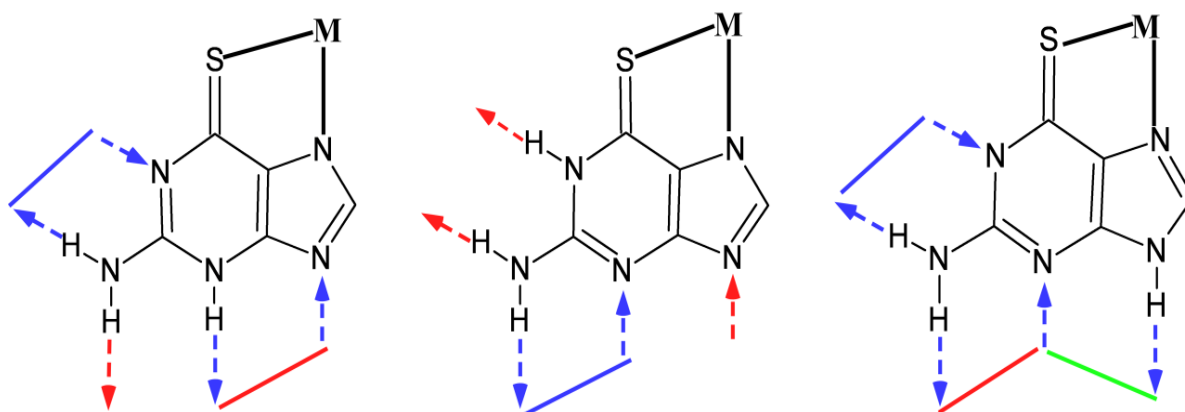


Figure 3.56: 6-thiopurinate sides available for complementary hydrogen bonding interaction when chelating to a metal centre through S6 and N7.

The reaction between 6-thioguanine and $\text{Co}(\text{NO}_3)_2 \cdot 6\text{H}_2\text{O}$ in a basic media of pentylamine containing aqueous solution favoured the oxidation to Co(III), as assured by its diamagnetic nature, gave rise to neutral monomeric $[\text{Co}(\text{ThioG})_3]$ entities (Figure 3.57). Three thioguaninato ligands, in its *9H*-tautomeric form, are coordinated in a bidentate chelating mode to the Co(III) metal centers by their N7 and S6 atoms affording an octahedral coordination environment (Table 3.35).

Table 3.35: Selected bond lengths (Å) and angles (°) for *CO-6-THIOG (SMOF-4)*.^[a]

Co1–N17	1.950(3)	N17–Co1–N17 ^{i,ii}	90.01(14)	N17–Co1–S16 ⁱⁱ	92.12(10)
Co1–N17 ⁱ	1.950(3)	N17–Co1–N17 ⁱⁱ	90.01(14)	S16–Co1–S16 ⁱ	88.73(5)
Co1–N17 ⁱⁱ	1.950(3)	N17–Co1–S16 ⁱ	89.17(10)	N17–Co1–S16 ^{i,ii}	92.12(10)
Co1–S16	2.2979(12)	N17–Co1–S16 ⁱ	92.12(10)	N17–Co1–S16 ⁱⁱ	177.72(10)
Co1–S16 ⁱ	2.2979(12)	N17–Co1–S16 ⁱⁱ	177.72(10)	N17–Co1–S16 ⁱⁱ	89.17(10)
Co1–S16 ⁱⁱ	2.2979(12)	N17–Co1–S16 ⁱ	177.72(10)	S16–Co1–S16 ^{i,ii}	88.73(5)
N17–Co1–N17 ⁱ	90.01(14)	N17–Co1–S16	89.17(10)	S16–Co1–S16 ⁱⁱ	88.73(5)

[a] Symmetry codes: (i) $-x+y, -x+1, z$; (ii) $-y+1, x-+1, z$.

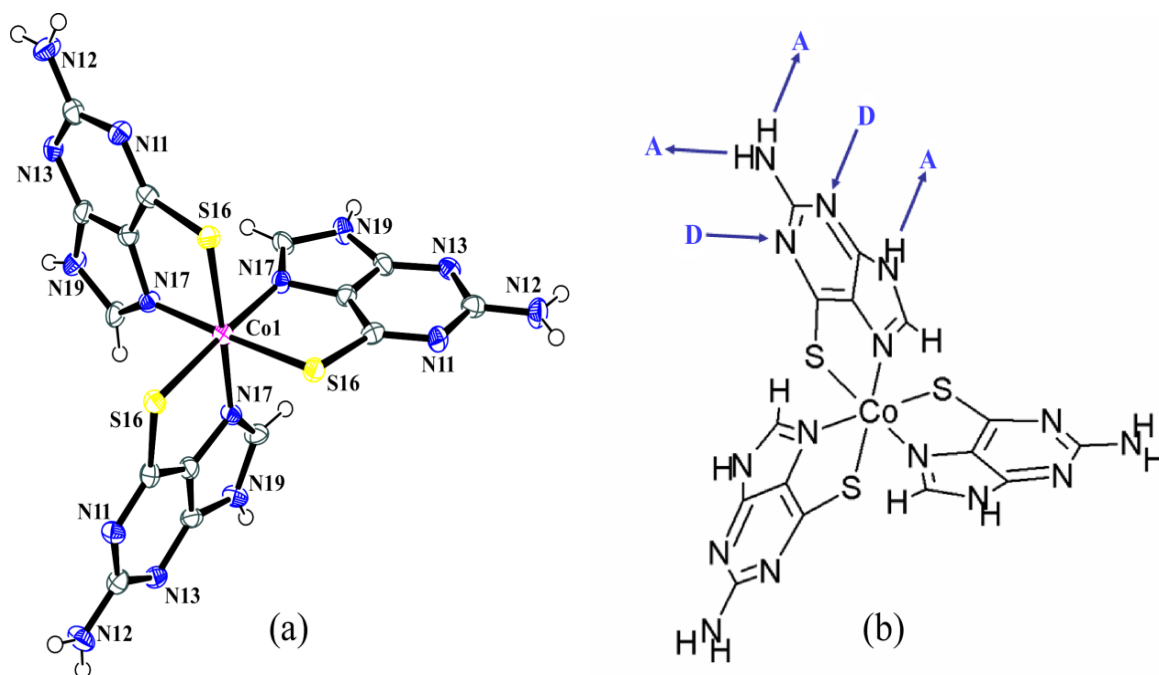


Figure 3.57: [Co(ThioG)₃] entity (a) of *CO-6-THIOG* (*SMOF-4*) and (b) available supramolecular hydrogen bonding scheme.

The coordination mode of the nucleobase analogue renders a rigid metal complex, and, at the same time, exposes its Watson–Crick (N1, N2) and sugar edges (N3, N9) that are both able to establish complementary hydrogen bonding interactions in non-coplanar directions. Therefore, this discrete complex entity seems to fulfill the requirements for the successful development of a supramolecular porous material.⁹⁰ In fact, there is a previous result based on similar discrete entities but using 6-thioguanosine that provides a complementary hydrogen bonding interaction involving only the Watson–Crick face (N1, N2) as the sugar edge is blocked by the sugar residue. It affords a supramolecular assembly containing great voids that are occupied by the sugar residue of the thioguanosine.¹⁷⁶ In compound *CO-6-THIOG* (*SMOF-4*) both sides of the 6-thioguaninato ligands are available to contribute to the supramolecular assembly. The sugar edge (N3, N9) of the nucleobases establish a double hydrogen bonding interaction with the nucleobases of three neighboring entities to give a $R_2^2(8)$ ring (Figure 3.58 and Table 3.36). This rigid synthon, based on direct thioguaninato⋯thioguaninato pairing interactions, leads to layers in the *ab* plane in which Δ and Λ isomers of the trischelate complex are sequentially arranged similarly to what happens

in layered $[M(\text{ox})_3]^{n-}$ compounds.¹⁷⁷ The resulting arrangement corresponds to the Shubnikov hexagonal **hcb** topology with a (6^3) point symbol (Figure 3.59).¹⁷⁸

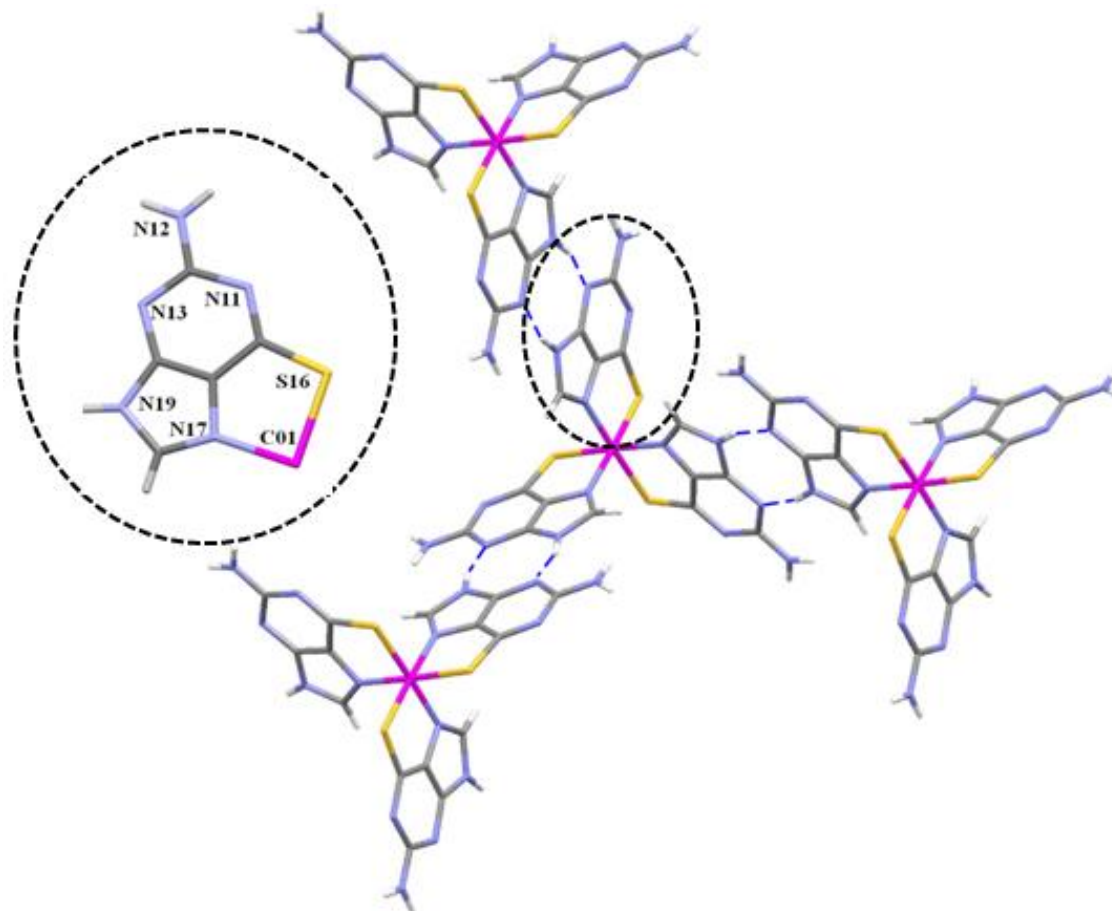


Figure 3.58: Nucleobase...nucleobase base pairing interactions.

Table 3.36: Supramolecular interactions (Å, °) in *CO-6-THIOG (SMOF-4)*.

Hydrogen bonding interactions.^[a]

$D-H\cdots A$ ^[b]	$D-H$	$H\cdots A$	$D\cdots A$	$D-H\cdots A$
N19-H19...N13 ⁱ	0.86	2.03	2.875(5)	167
N12-H12...S16 ⁱⁱ	0.86	2.69	3.467(4)	151
C18-H18...S16 ⁱⁱⁱ	0.86	2.67	3.415(4)	138

[a] Symmetry Code: (i) $-x, -y+1, -z+2$; (ii) $x-y, x, -z+1$; (iii) $-x+y, -x+1, z+1$. [b] **D**: donor; **A**: acceptor.

¹⁷⁷ (a) García-Couceiro, U. et al. *Inorg. Chem.* **2010**, *49*, 11346. (b) Coronado, E. et al. *Nature* **2000**, *408*, 447.

¹⁷⁸ (a) Blatov, V. A. *IUCR CompComm. Newsletter* **2006**, *7*, 4, (accessed Apr. 2014), TOPOS Main Page. <http://www.topos.ssu.samara.ru>. (b) O’Keeffe, M.; Yaghi, O. M. *Chem. Rev.* **2012**, *112*, 675.

π - π interactions.^[c]

Ring...Ring ^[d]	Angle	DC	α	DZ	DXY
Ring1...Ring2 ^{iv}	0.0	3.46	18.5	3.28	1.10

[a] Symmetry: (i) $-x, -y+1, -z+2$; (ii) $x-y, x, -z+1$; (iii) $-x+y, -x+1, z+1$; (iv) $-x, 1-y, 1-z$. [b] **D**: donor; **A**: acceptor. [c] Angle: Dihedral Angle between Planes I and J ($^\circ$), DC: Distance between ring centroids (\AA), α : Angle Cg(I) \rightarrow Cg(J) vector and normal to plane I ($^\circ$), DZ: Perpendicular distance of Cg(I) on ring J (\AA), DXY: Slippage. [d] Ring 1: N17, C15, C14, N19, C18; Ring 2: N11, C12, N13, C14, N19, C16.

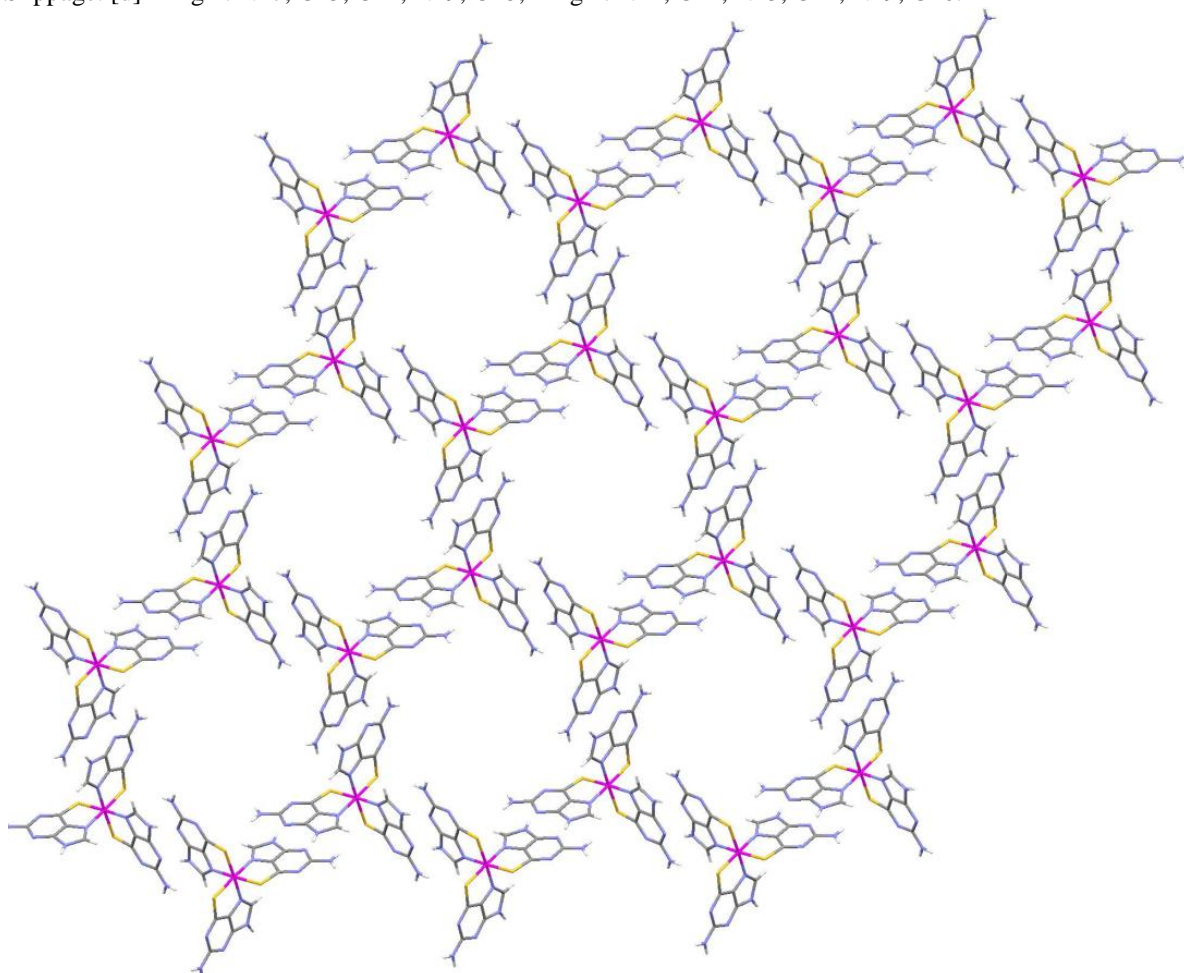


Figure 3.59: 2D supramolecular sheet assembled by means of base pairing interactions among the 6-thioguanine nucleobases with a Shubnikov hexagonal **hcb** topology in *CO-6-THIOG (SMOF-4)*.

The interactions among the three-connected uninodal two-dimensional (2D) nets are linked via weaker hydrogen bonds (N2-H \cdots S6 and C8-H \cdots S6) and reinforced with π - π interactions, (Table 3.36) leading to an **acs** topology and $(4^9.6^6)$ point symbol that corresponds to a porous crystal structure with an estimated surface area of $887 \text{ m}^2/\text{g}$ and 43% of void space

based on theoretical calculations.¹⁷⁹ The resulting porous structure consists of 1D channels that run along the crystallographic *c* axis with a diameter of 8.2–9.4 Å (Figure 3.60).

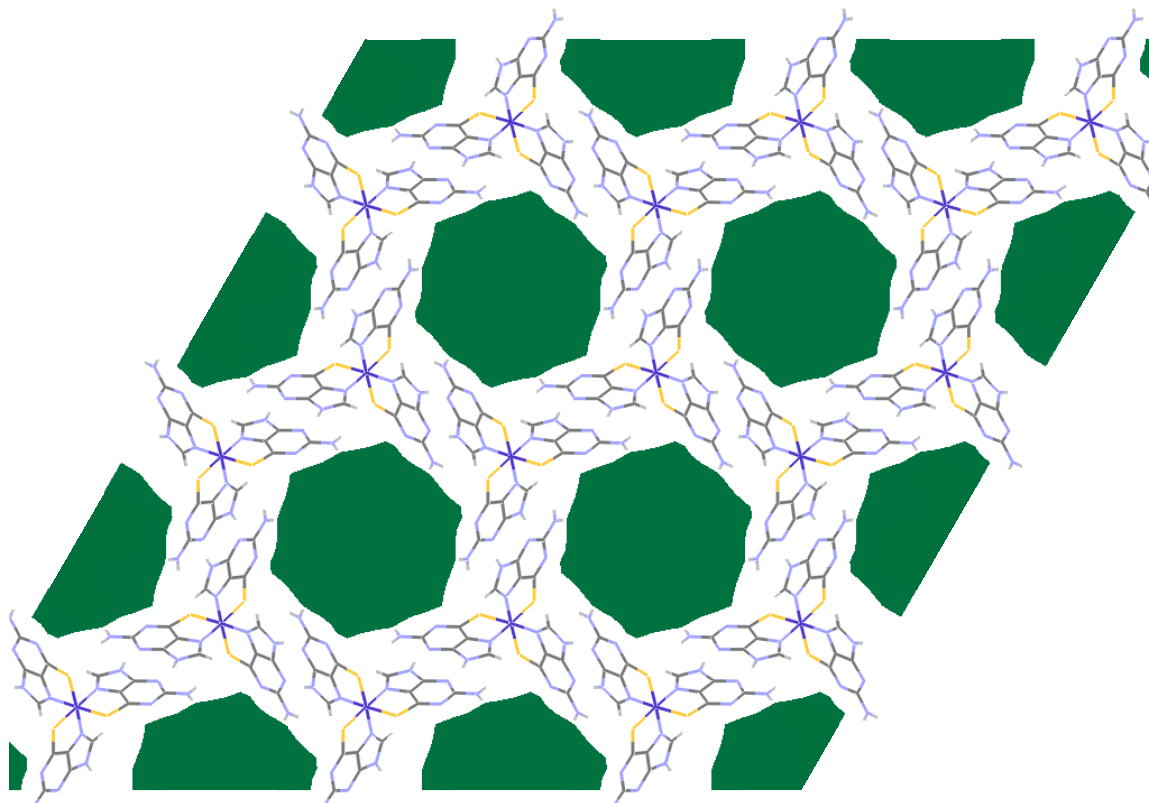


Figure 3.60: Projection of the crystal packing of *SMOF-4* along the crystallographic *c* axis. Green coloured regions represent the solvent accessible void.

It is worth to mention the template effect exerted by pentylamine. This molecule provides the basic media that this reaction requires and, at the same time, the tendency of the aliphatic tails to form aggregates in water promotes the growth of the supramolecular structure around them. In fact, the same synthesis but using different amines with shorter aliphatic tails does not provide this compound.

The thermogravimetric analysis (Figure 3.61 and Table 3.37) shows that, the solvent molecules are released below 100 °C. After the solvent removal, the compound remains stable up to almost 280 °C and then get decomposed in different exothermic steps to the final residue Co_3O_4 above 545 °C.

¹⁷⁹ (a) Sarkisov, L.; Harrison, A. *Mol. Simul.* **2011**, *37*, 1248. (b) Spek, A. L. *J. Appl. Crystallogr.* **2003**, *36*, 7.

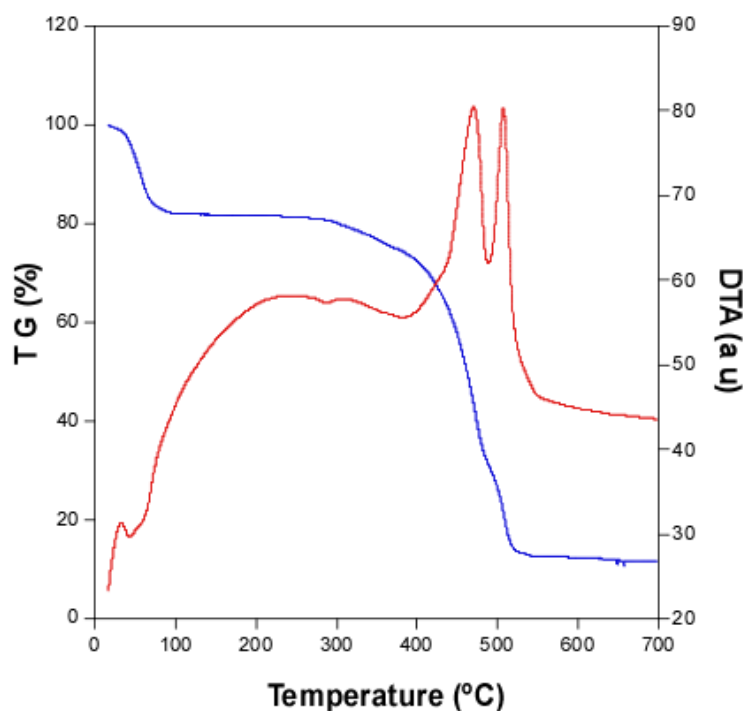


Figure 3.61: Thermogravimetric studies of *CO-6-THIOG (SMOF-4)*.

Table 3.37: Thermogravimetric data of *CO-6-THIOG (SMOF-4)*.

Step	T_i	T_f	T_{peak}	$\Delta m(\%)$	ΔH	$\Sigma \Delta m(\%)$	$\Sigma \Delta m(\%)_{theor}$
<i>CO-6-THIOG</i>							
1	25	100	43	18.25	Endo	18.25	19.37 ($-6H_2O$)
2	280	545	470, 507	69.12	Exo	87.37	85.60 ($1/3Co_3O_4$)

[a] T_i = initial temperature; T_f = final temperature; T_{peak} = DTA peak temperature; $\Delta m(\%)$ = mass loss percentage for each process; ΔH = process type in the basis of DTA; $\Sigma \Delta m(\%)$ = total mass loss percentage; $\Sigma \Delta m(\%)_{theor}$ = theoretical total mass loss percentage. [b] Released water molecules and final residue per formula.

3.3.2.12.1 Adsorption studies of *CO-6-THIOG (SMOF-4)*

According to N_2 (77 K) and CO_2 (273 K) adsorption studies this compound is highly selective towards CO_2 adsorption (Figure 3.62). The N_2 adsorption curve exhibits features of a non-porous material and, accordingly, the fitting of the adsorption area to BET equation leads to a negligible value. However, it shows a significant CO_2 uptake with a non-saturating curve reaching a value of 1.4 mmol/g at 1 bar. This behaviour has been described in the introduction section for *CUADECL-B (SMOF-1)*, *CUADEBR-A (SMOF-2)*, and *CUADECL-C (SMOF-3)* and its explanation for *CO-6-THIOG (SMOF-4)* probably would also be related to a crystal surface instability.

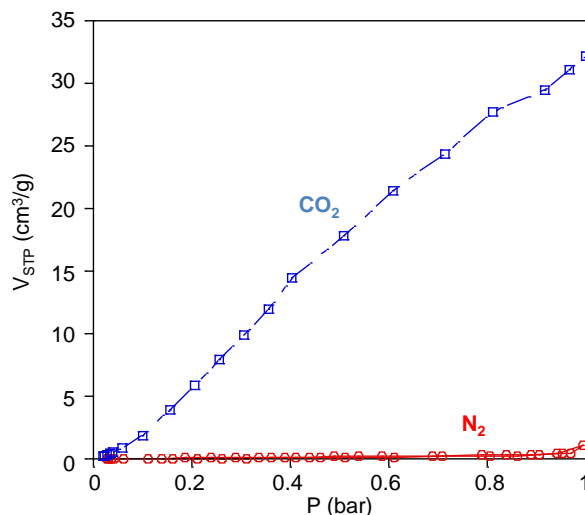


Figure 3.62: Adsorption isotherms for N₂ (77 K) and CO₂ (273 K), of a fresh sample of *CO-6-THIOG (SMOF-4)*.

3.4 CONCLUSIONS

On examining the above discussed structures, it becomes clear how a combination of rigid tectons with rigid synthons spreading at least in three non-coplanar directions is a well suited route to obtain porous supramolecular networks. In this context, the metal–nucleobase complexes can be good candidates to fulfill both requirements when the nucleobase is anchored to the discrete entity by at least two positions to provide a rigid building unit. This anchoring and the aromatic nature of the nucleobase provide rigid supramolecular building units. On the other hand, the well known complementary hydrogen bonding established between the nucleobases ensures the necessary rigidity of these synthons. Therefore, as it has been proved here the chances to obtain 3D supramolecular metal–organic frameworks based on metal–nucleobase systems are high. However, it is necessary to take care of the synthetic conditions in order to ensure the presence of the required direct hydrogen bonding interactions between the nucleobases. Related to this later issue, the presence of water molecules can disrupt these direct adenine···adenine hydrogen bonding interactions, leading to non porous materials as evidenced by the crystal structure of [Cu₂(μ-adenine)₄Cl₂]Cl₂·8H₂O (*CUADECL-A*). The direct hydrogen bonding disrupting capacity of the water molecule seems also to be responsible of the surface instability observed in *CUADECL-B (SMOF-1)*, *CUADEBR-A (SMOF-2)*, *CUADECL-C (SMOF-3)* and *CO-6-THIOG (SMOF-4)*.

Chapter 4

Conclusions and future perspectives

4.1 Conclusiones

4.2 Future perspectives

(iii) the non-coplanarity of functional groups involved in the predictable synthons. The rigidity of the building units (discrete complexes) can be achieved using rigid ligands bonded through multiple positions. It means, in most common cases, a double anchoring of the ligand by means of double coordination bonds or the combination of a coordination bond and an intramolecular hydrogen bond. The predictability and rigidity of the synthons requires the presence of adjacent functional groups, incorporated into the rigid ligands, able to establish complementary hydrogen bonding interactions. Finally, the requisite of non-coplanar arrangement of the synthons comes from our objective of obtaining three-dimensional extended systems that are achieved by the presence of at least three non-coplanar synthons. The use of complexes with non-planar coordination geometries makes this last condition easy to accomplish.

It has become clear that a suitable system that would fulfil all the above described requirements for obtaining *SMOFs* are the discrete metal-nucleobase systems, especially those based on purine nucleobases. These ligands provide, at one hand, the advantage of the increased rigidity of the supramolecular building block due to the coordination through multiple positions, and, on the other hand, they present more edges capable of establishing complementary hydrogen bonding interactions.

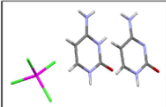




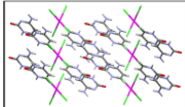
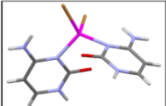




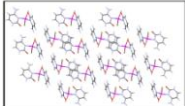
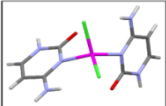




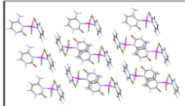
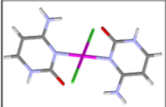




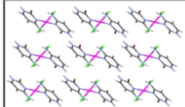
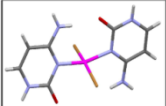




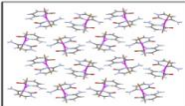
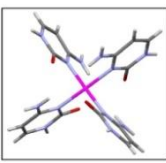




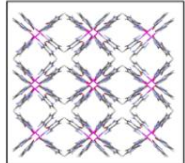
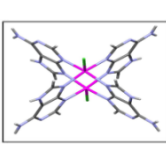




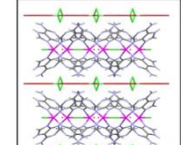
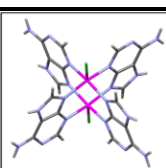




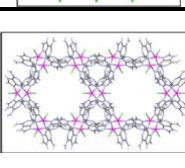
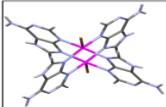




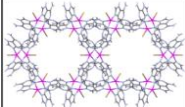
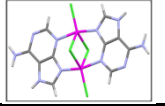




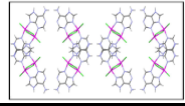
Additionally, the results achieved employing $[\text{Cu}_2(\mu\text{-adenine})_4(\text{X})_2]^{2+}$ ($\text{X} = \text{Cl}^-, \text{Br}^-$) as supramolecular building blocks (*CUADECL-B/SMOF-1* and *CUADEBR-A/SMOF-2*) show that these compounds present a surface instability because of the ambient humidity that creates a diffusion barrier than can be permeated only by strong interacting adsorbate molecules with high kinetic energy such as CO_2 but not by N_2 , H_2 , and CH_4 , that makes them attractive for selective gas adsorption and separation technologies. More recently, Zaworotko et al. reported an analogous compound, based on the $[\text{Cu}_2(\mu\text{-adenine})_4(\text{X})_2]^{2+}$ dinuclear entity, replacing the halides by bulkier TiF_6^{2-} anions improving the chemical stability of the supramolecular network toward humidity, thus avoiding the surface instability, and therefore, being able to adsorb CO_2 , CH_4 and N_2 .¹⁸¹ These studies also pointed out the relevance of the solvent selection because strong hydrogen bond donor and acceptor solvents such as water

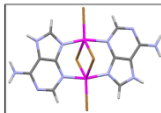




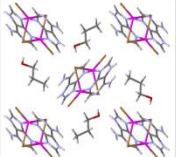
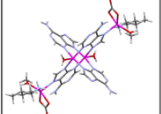




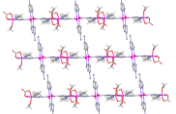
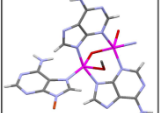




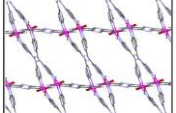
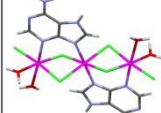




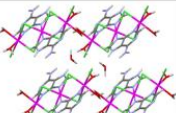
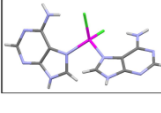




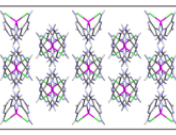





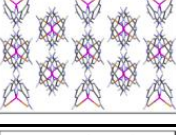
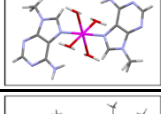




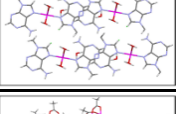
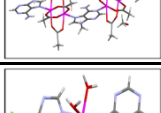




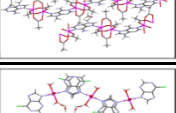
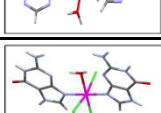
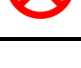

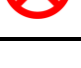

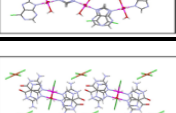
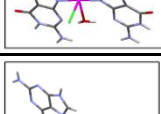




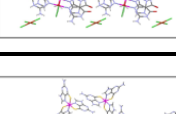
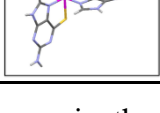




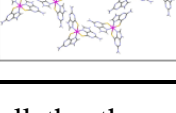
¹⁸¹ Nugent, P. S. et al. *J. Am. Chem. Soc.* **2013**, *135*, 10950.

could disrupt the direct hydrogen bonding interactions between the nucleobases that are the key factor to achieve these compounds.

In Table 4.2, we make a summary of all the 21 compounds reported in this thesis, accounting for the above mentioned key factors for obtaining supraMOFs. It demonstrates the suitability of this synthetic strategy to afford supramolecular porous materials with eight new *SMOFs* involving different metal centers, nucleobases and complex entities.

Table 4.1: A summary table showing the effect of the key factors determining the formation of porous *SMOFs*.

Compound	Building unit	Rigidity	Rigid synthons	Non-coplanar synthons (≥ 3)	Porosity / structure	
<i>COCYTCL</i>						
<i>COCYTBR</i>						
<i>ZNCYTCL</i>						
<i>CUCYTCL</i>						
<i>CUCYTBR</i>						
<i>CUCYTSO4</i>			 <i>counterions</i>			
<i>CUADECL-A</i>			 <i>water</i>			
<i>CUADECL-B SMOF-1</i>						
<i>CUADEBR-A SMOF-2</i>						
<i>CUADECL-C SMOF-3</i>						

CUADEBR-B			 <i>Propanol</i>			
CUADEC03 SMOF-8						
CUADEC0H SMOF-9						
CO3ADECL						
COADECL SMOF-5					 <i>Interpenetration</i>	
COADEBR SMOF-6					 <i>Interpenetration</i>	
CO-9- MEADECL						
CU-9- MEADEACE						
CO-6-CLPUR						
CUGUACL						
CO-6-THIOG SMOF-4						

As shown in the table above, porous *SMOFs* were formed only when all the three criteria were met. In the case of *COCYTBR*, *ZNCYTCL*, and *CUCYTBR* even though they establish direct base pairing interactions and also are non-coplanar, the lack of rigidity of the building unit, because of the monodentate anchoring of the nucleobase, hinders it from developing porosity. In the case of *CUCYTCL*, the synthons are planar. *CUCYTSO4*,

CUADECL-A, *CUADEBR-B*, *CUGUACL* and *CU-9-MEAEACE* could have been porous as they provide rigid building units and establish non-coplanar synthons, however in all these cases the direct base pairing interactions were blocked by other competitive groups such as counter ions or solvent molecules. In similar situations, it has been successful to design *SMOFs* by selecting solvents with less hydrogen bonding affinity. It demonstrates that the wise selection of solvents is also a key factor for the synthesis of *SMOFs*.

4.2 FUTURE WORK

Although this thesis contains a research work that can be considered as accomplished, there arised many ideas and suggestions during this research activity. These could be developed and implemented as the key points for the future research projects. Some of the future objectives are listed below.

1. Apply the strategies adopted in this work to other metal centres and nucleobase derivatives (hypoxanthine, 6-mercaptapurine) or similar systems with hydrogen bonding ability, to develop more *SMOFs*.
2. Experiment different synthetic modifications to avoid interpenetration of compounds like *COADECL* and *COADEBR* and hence to achieve *SMOFs* with high pore volume and surface area.
3. Adopt these strategies to design and develop *SMOFs* based on other polynuclear building units as a trial to increase the porosity.
4. Apply solvent-free synthesis as a synthetic approach to different metal nucleobase systems to develop *SMOFs*, since *COADECL* was obtained through solvent free synthesis as well.
5. Try to overcome the surface instability of these *SMOFs* by growing more stable *MBioFs* outside the *SMOF* core, protecting it from the atmospheric humidity and related surface thickening and hence increasing the gas uptaking capacity of these *SMOFs*.

Chapter 5

References

5.1 Introduction

5.2 References

5.1 INTRODUCTION:

In this work, the references are given as footnotes in all the chapters. In this section, the full references are listed in alphabetical order according to the name of the first author and, then, in ascending order of the year of publication. In cases, where the same author has more than one publication in the same year, the names of the rest of the authors are considered for hierarchy. When this criterion is not enough, the publication name and the first page number are taken into account. The reference style followed is that recommended by the American Chemical Society. Additionally, the title of the article is included for better identification.

5.2 REFERENCES:

- AAKEROY, C. B.; BEATTY, A. M.; HELFRICH, B. A.: A High-yielding supramolecular reaction. *J. Am. Chem. Soc.* **2002**, *124*, 14425–14432.
- ALEXANDROV, E. V.; BLATOV, V. A.; PROSERPIO, D. M.: A topological method for the classification of entanglements in crystal networks. *Acta Crystallogr. Sect. A*, **2012**, *A68*, 484–493.
- ALLEN, F. H.: The Cambridge Structural Database: a quarter of a million crystal structures and rising. *Acta Crystallogr.* **2002**, *B58*, 380–388.
- ALLEN, M. P.; TILDESLEY, D. J.: Computer simulation of liquids. Clarendon Press, Oxford, UK, 1st edn, 1987.
- ALLENDORF, M. D.; BAUER, C. A.; BHAKTA, R. K.; HOUK, R. J. T.: Luminescent metal-organic frameworks. *Chem. Soc. Rev.* **2009**, *38*, 1330–1352.
- ALTOMARE, A.; CASCARANO, M.; GIACOVAZZO, C.; GUAGLIARDI, A.: A program for crystal structure solution. *J. Appl. Cryst.* **1993**, *26*, 343–350.
- AMO-OCHOA, P.; RODRIGUEZ-TAPIADOR, M. I.; ALEXANDRE, S. S.; PASTOR, C.; ZAMORA, F.: Structural models for the interaction of Cd(II) with DNA: trans-[Cd(9-RGH-N7)₂(H₂O)₄]²⁺. *J. Inorg. Biochem.* **2005**, *99*, 1540–1547.
- AMO-OCHOA, P.; RODRIGUEZ-TAPIADOR, M. I.; CASTILLO, O.; OLEA, D.; GUIJARRO, A.; ALEXANDRE, S. S.; GÓMEZ-HERRERO, J.; ZAMORA, F.: Assembling of dimeric entities of Cd(II) with 6-Mercaptopurine to afford one-dimensional coordination polymers: synthesis and scanning probe microscopy characterization. *Inorg. Chem.* **2006**, *45*, 7642–7650.
- AMO-OCHOA, P.; SANZ-MIGUEL, P. J.; CASTILLO, O.; SABAT, M.; LIPPERT, B.; ZAMORA, F.: Interguanine hydrogen bonding patterns in adducts with water and Zn-purine

complexes (purine = 9-methyladenine and 9-methylguanine). Unexpected preference of Zn(II) for adenine-N7 over guanine-N7. *J. Biol. Inorg. Chem.* **2007**, *12*, 543–555.

AMO-OCHOA, P.; CASTILLO, O.; MIGUEL, P. J. S.; ZAMORA, F.: Unusual dimeric Zn(II)-cytosine complexes: new models of the interaction of Zn(II) with DNA and RNA. *J. Inorg. Biochem.* **2008**, *102*, 203–208.

AMO-OCHOA, P.; ALEXANDRE, S. S.; HRIBESH, S.; GALINDO, M. A.; CASTILLO, O.; GOMEZ-GARCÍA, C. J.; PIKE, A. R.; SOLER, J. M.; HOULTON, A.; ZAMORA, F.: Coordination chemistry of 6-thioguanine derivatives with cobalt: towards formation of electrical conductive one-dimensional coordination polymers. *Inorg. Chem.* **2013**, *52*, 5290–5299.

AN, J.; FIORELLA, R. P.; GEIB, S. J.; ROSI, N. L.: Synthesis, structure, assembly, and modulation of the CO₂ adsorption properties of a zinc-adeninate macrocycle. *J. Am. Chem. Soc.* **2009**, *131*, 8401–8403.

AN, J.; GEIB, S. J.; ROSI, N. L.: Cation-triggered drug release from a porous zinc-adeninate metal-organic framework. *J. Am. Chem. Soc.* **2009**, *131*, 8376–8377.

AN, J.; GEIB, S. J.; ROSI, N. L.: High and selective CO₂ uptake in a cobalt adeninate metal-organic framework exhibiting pyrimidine- and amino-decorated pores. *J. Am. Chem. Soc.* **2010**, *132*, 38–39.

AN, J.; FARHA, O. K.; HUPP, J. T.; POHL, E.; YEH, J. I.; ROSI, N. L.: Metal-adeninate vertices for the construction of an exceptionally porous metal-organic framework. *Nature Commun.* **2012**, *3*, 604.

ANNEN, P.; SCHILDBERG, S.; SHELDRIK, W. S.: (η^5 -Pentamethylcyclopentadienyl)iridium(III) complexes of purine nucleobases and nucleotides: a comparison with (η^6 -arene)ruthenium(II) and (η^5 -pentamethylcyclopentadienyl)rhodium(III) species. *Inorg. Chim. Acta* **2000**, *307*, 115–124.

ANTHONY, A.; DESIRAJU, G. R.; JETTI, R. K. R.; KUDUVA, S. S.; MADHAVI, N. N. L.; NANGIA, A.; THAIMATTAM, R.; TALLADI, V. R.: Crystal engineering: some further strategies. *Cryst. Eng.* **1998**, *1*, 1–18.

ANZELLOTTI, A. I.; SABAT, M.; FARRELL, N.: Covalent and noncovalent interactions for [metal(dien)nucleobase](2+) complexes with L-tryptophan derivatives: formation of palladium-tryptophan species by nucleobase substitution under biologically relevant conditions. *Inorg. Chem.* **2006**, *45*, 1638–1645.

AOKI, K.: The Crystal and Molecular Structure of the Polymeric Complex of Zinc (II) with Cytosine 5'-Phosphate: Metal Bonding to Both N (3) and Phosphate. *Biochim. Biophys. Acta* **1976**, *447*, 379–381.

AOKI, K.: X-Ray crystal structure of the 1:1 manganese-cytosine 5'-phosphate complex: metal bonding to both O(2) of the base and phosphate. *J. Chem. Soc. Chem. Commun.* **1976**, 748–749.

- AOKI, K.: X-Ray crystal structures of the ternary complexes $[\text{Cd}(5'\text{-UMP})(\text{dpa})(\text{H}_2\text{O})_2]_n(5'\text{-UMP}=\text{uridine } 5'\text{-phosphate, dpa}=2,2'\text{-dipyridylamine})$: metal ion bridged stacking between nucleotide bases and aromatic amine rings, and $[\text{Cu}(5'\text{-CMP})(\text{dpa})(\text{H}_2\text{O})_2]_2(5'\text{-CMP}=\text{cytidine } 5'\text{-phosphate})$: phosphate only metal bonding. *Chem. Commun.* **1979**, 589–591.
- AKOI, K.; SALAM, M. A.: Interligand interactions affecting specific metal bonding to nucleic acid bases: the tetrakis(μ -trifluoroacetamido)dirhodium(II)-cytosine system. Crystal structures of $[\text{Rh}_2(\text{CF}_3\text{CONH})_4(\text{cytosine})]$ and $[\text{Rh}_2(\text{CF}_3\text{CONH})_4(1\text{-methylcytosine})_2] \cdot 2\text{H}_2\text{O}$. *Inorg. Chim. Acta* **2001**, 316, 50–58.
- BARDAJÍ, E. G.; FREISINGER, E.; COSTISELLA, B.; SCHALLEY, C. A.; BRÜNING, W.; SABAT, M.; LIPPERT, B.: Mixed-metal (platinum, palladium), mixed-pyrimidine (uracil, cytosine) self-assembling metallacalix[*n*]arenes: dynamic combinatorial chemistry with nucleobases and metal species. *Chem. Eur. J.* **2007**, 13, 6019–6039.
- BAREA, E.; MONTORO, C.; NAVARRO, J. A. R.: Toxic gas removal-metal-organic frameworks for the capture and degradation of toxic gases and vapours. *Chem. Soc. Rev.* **2014**, 43, 5419–5430.
- BASU, S.; CANO-ODENA, A.; VANKELECOM, I. F. J.: MOF-containing mixed-matrix membranes for CO_2/CH_4 and CO_2/N_2 binary gas mixture separations. *J. Sep. Purif. Technol.* **2011**, 81, 31–40.
- BATTEN, S. R.; CHAMPNESS, N. R.; CHEN, X. -M.; GARCIA-MARTINEZ, J.; KITAGAWA, S.; ÖHRSTRÖM, L.; O'KEEFFE, M.; SUH, M. P.; REEDIJK, J.: Terminology of metal-organic frameworks and coordination polymers (IUPAC Recommendations 2013). *Pure Appl. Chem.* **2013**, 85, 1715–1724.
- BECK, W. M.; CALABRESE, J. C.; KOTTMAYER, N. D.: Palladium(II) and Platinum (II) complexes with nucleobases and nucleosides. Crystal structure of trans-bis(Adeninato)-bis(tri-*n*-butylphosphine)-palladium(ii) methanol solvate. *Inorg. Chem.* **1979**, 18, 176–182.
- BEOBIDE, G.; CASTILLO, O.; CEPEDA, J.; LUQUE, A.; PÉREZ-YÁÑEZ, S.; ROMÁN, P.; THOMAS-GIPSON, J.: Metal-carboxylato-nucleobase systems: From supramolecular assemblies to 3D porous materials. *Coord. Chem. Rev.* **2013**, 257, 2716–2736.
- BLACKBURN, G. M.; GAIT, M. J.; LOAKES, D.; WILLIAMS, D. M.: Nucleic Acids in Chemistry and Biology. *RSC Publishing*: Cambridge, UK, 2006, p.470.
- BLATOV, V. A.: Multipurpose crystallochemical analysis with the program package TOPOS. *IUCr CompComm Newsletter* **2006**, 7, 4–38. TOPOS is available at <http://www.topos.ssu.samara.ru>. (accessed Jan. 2012).
- BLATOV, V. A.: Multipurpose crystallochemical analysis with the program package TOPOS. *IUCr CompComm Newsletter* **2006**, 7, 4–38. TOPOS is available at <http://www.topos.ssu.samara.ru>. (accessed Apr. 2014).
- BLOOMFIELD, V. A.; CROTHERS, D. M.; TINOCO, I. JR.: Nucleic acids: Structures, properties and functions. *University Science Books*: Sausalito, USA, 2000.

- BRAGA, D.; MAINI, L.; POLITO, M.; TAGLIAVINI, E.; GREPIONI, F.: Design of hydrogen bonded networks based on organometallic sandwich compounds. *Coord. Chem. Rev.* **2003**, *246*, 53–71.
- BRANDI-BLANCO, M. P.; CHOQUESILLO-LAZARTE, D.; MATILLA-HERNÁNDEZ, A.; GONZÁLEZ-PÉREZ, J. M.; CASTIÑEIRAS, A.; NICLÓS-GUTIÉRREZ, J.: Molecular recognition modes between adenine or adeninium(1+) ion and binary MII(pdc) chelates (M = Co–Zn; pdc = pyridine–2, 6–dicarboxylate(2–) ion). *J. Inorg. Biochem.* **2013**, *127*, 211–219.
- BRITTEN, J. F.; LIPPERT, B.; LOCK, C. J. L.; PILON, P.: Platinum(II) complexes with terminal hydroxo and aqua groups: crystal structures of hydroxo–cis–diammine(1–methylcytosine–N3)platinum(II) nitrate dihydrate, $[\text{Pt}(\text{OH})(\text{NH}_3)_2(\text{C}_5\text{H}_7\text{N}_3\text{O})]\text{NO}_3 \cdot 2\text{H}_2\text{O}$, and cis–diammineaqua(1–methylcytosine–N3)platinum(II) dinitrate hydrate, $[\text{Pt}(\text{NH}_3)_2(\text{H}_2\text{O})(\text{C}_5\text{H}_7\text{N}_3\text{O})](\text{NO}_3)_2 \cdot \text{H}_2\text{O}$. *Inorg. Chem.* **1982**, *21*, 1936–1941.
- BROWN, D. B.; HALL, J. W.; HELIS, H. M.; WALTON, E. G.; HODGSON, D. J.; HATFIELD, W. E.: The preparation and magnetic and structural examination of monomeric, dimeric, and polymeric adenine complexes of copper(II). *Inorg. Chem.* **1977**, *16*, 2675–2680.
- BRUNAUER, S.; EMMET, P. H.; TELLER, E.: Adsorption of gases in multimolecular layers. *J. Am. Chem. Soc.* **1938**, *60*, 309–319.
- BRUNAUER, S.; DEMING, L. S.; DEMING, W. E.; TELLER, E.: On a theory of the van der Waals adsorption of gases. *J. Am. Chem. Soc.* **1940**, *62*, 1723–1732.
- BRÜNING, W.; ASCASO, I.; FREISINGER, E.; SABAT, M.; LIPPERT, B.: Metal–stabilized rare tautomers of nucleobases. 8. Promotion of rare cytosine tautomer upon complex formation with (dien)M₂⁺ (M = Pt, Pd). *Inorg. Chim. Acta* **2002**, *339*, 400–410.
- BRÜNING, W.; FREISINGER, E.; SABAT, M.; SIGEL, R. K. O.; LIPPERT, B.: Metal–stabilized rare tautomers of nucleobases. 7. N1 and N3 linkage isomers of neutral and deprotonated cytosine with trans–(CH₃NH₂)₂Pt(II). *Chem. Eur. J.* **2002**, *8*, 4681–4692.
- BUGELLA-ALTAMIRANO, E.; CHOQUESILLO-LAZARTE, D.; GONZALEZ-PEREZ, J. M.; SANCHEZ-MORENO, M. J.; MARIN-SANCHEZ, R.; MARTIN-RAMOS, J. D.; COVELO, B.; CARBALLO, R.; CASTINEIRAS, A.; NICLOS-GUTIERREZ, J.: Three new modes of adenine–copper(II) coordination: interligand interactions controlling the selective N3, N7 and bridging μ -N3,N7 metal–bonding of adenine to different N–substituted iminodiacetato–copper(II) chelates. *Inorg. Chim. Acta* **2002**, *339*, 160–170.
- BYRES, M.; COX, P. J.; KAY, G.; NIXON, E.: Supramolecular structures of six adenine–carboxylic acid complexes. *CrystEngComm.* **2009**, *11*, 135–142.
- CAPLLONCH, C.; GARCIA-RASO, A.; TERRON, A.; APELLA, M. C.; ESPINOSA, E.; MOLINS, E.: Interactions of d(10) metal ions with hippuric acid and cytosine. X–ray structure of the first cadmium (II)–amino acid derivative–nucleobase ternary compound. *J. Inorg. Biochem.* **2001**, *85*, 173–178.
- CEPEDA, J.; CASTILLO, O.; GARCÍA-TERAN, J. P.; LUQUE, A.; PÉREZ –YÁÑEZ, S.; ROMÁN, P.: Supramolecular architectures and magnetic properties of self assembled

windmill like dinuclear copper (II) complex with purine ligands. *Eur. J. Inorg. Chem.* **2009**, 2344–2353.

CERVANTES, G.; FIOL, J. J.; TERRON, A.; MORENO, V.; ALABART, J. R.; AGUILO, M.; GOMEZ, M.; SOLANS, X.: Synthesis and characterization of nickel(II) complexes of purine and pyrimidine bases. Crystal and molecular structure of trans-bis(cytosine-O2)bis(ethylenediamine)nickel(II) bis(tetraphenylborate). An unusual metal binding mode of cytosine. *Inorg. Chem.* **1990**, 29, 5168–5173.

CHARLAND, J. P.; BEAUCHAMP, A. L.: Preparation and structural studies of methylmercury compounds containing amino-deprotonated adenine. *Inorg. Chem.* **1986**, 25, 4870–4876.

CHEN, B.; XIANG, S.; QIAN, G.: Metal-organic frameworks with functional pores for recognition of small molecules. *Acc. Chem. Res.* **2010**, 43, 1115–1124.

CHEN, C.-T.; SUSLICK, K. S.: One-dimensional coordination polymers: applications to material science. *Coord. Chem. Rev.* **1993**, 128, 293–322.

CHOQUESILLO-LAZARTE, D.; BRANDI-BLANCO, M. P.; GARCIA-SANTOS, I.; GONZALEZ-PEREZ, J. M.; CASTINEIRAS, A.; NICLOS-GUTIERREZ, J.: Interligand interactions involved in the molecular recognition between copper(II) complexes and adenine or related purines. *J. Coord. Chem. Rev.* **2008**, 252, 1241–1256.

COLACIO, E.; CRESPO, O.; CUESTA, R.; KIVEKAS, R.; LAGUNA, A. J.: [Au(2)(micro-G)(micro-dmpe)].(KBr)(0.75) 2H(2)O, a cyclic dinuclear gold(I) complex with an N3,N9-bridging coordination mode of guanine and aurophilic interactions: synthesis, X-ray crystal structure and luminescence properties (dmpe=1,2-bis(dimethylphosphino)ethane and G=guaninato dianion). *J. Inorg. Biochem.* **2004**, 98, 595–600.

COOK, T. R.; ZHENG, Y. R.; STANG, P. J.: Metal-organic frameworks and self-assembled supramolecular coordination complexes: Comparing and contrasting the design, synthesis, and functionality of metal-organic materials. *Chem. Rev.* **2013**, 113, 734–777.

CORMA, A.; GARCÍA, H.; LLABRÉS I XAMENA, F. X.: Engineering metal-organic frameworks for heterogeneous catalysis. *Chem. Rev.* **2010**, 110, 4606–4655.

CORONADO, E.; GALÁN-MASCARÓS, J. R.; GÓMEZ-GARCÍA, C. J.; LAUKHIN, V.: Coexistence of ferromagnetism and metallic conductivity in a molecule-based layered compound. *Nature* **2000**, 408, 447–449.

COSAR, S.; JANIK, M. B. L.; FLOCK, M.; FREISINGER, E.; FARKAS, E.; LIPPERT, B.: Mono- and di-nuclear complexes of (trpy)MII (M = Pd, Pt) with the model nucleobase 1-methylcytosine. Crystal structure and NMR solution studies. *J. Chem. Soc. Dalton Trans.* **1999**, 2329–2336.

CrysAlis PRO, version 1.171.33.55; Oxford Diffraction: Wroclaw, Poland, 2010.

CZAJA, A. U.; TRUKHAN, N.; MÜLLER, U.: Industrial applications of metal-organic frameworks. *Chem. Soc. Rev.* **2009**, 38, 1284–1293.

- DHAKSHINAMOORTHY, A.; ALVARO, M.; CORMA, A.; GARCIA, H.: Delineating similarities and dissimilarities in the use of metal organic frameworks and as heterogeneous for organic reactions. *Dalton Trans.* **2011**, 40, 6344–6360.
- DHAKSHINAMOORTHY, A.; GARCIA, H.: Metal–organic Frameworks as solid catalysis for the synthesis of nitrogen–containing heterocycles. *Chem. Soc. Rev.* **2014**, 43, 5750–5765.
- DALBY, C.; BLEASDALE, C.; CLEGG, W.; ELSEGOOD, M. R. J.; GOLDING, B. T.; GRIFFIN, R. J.: Regiospecific alkylation of 6–chloropurine and 2,6–dichloropurine at N–7 via transient protection of N–3/N–9 by methylcobaloxime. *Angew. Chem. Int. Ed.* **1993**, 32, 1696–1697.
- DAS, S.; MADHAVIAIAH, C.; VERMA, S.; BHARADWAJ, P. K.: A reusable zigzag copper(II) coordination polymer with bio–essential constituents as a facile DNA scission agent. *Inorg. Chim. Acta* **2005**, 358, 3236–3240.
- DAY, E. F.; CRAWFORD, C. A.; FOLTING, K.; DUNBAR, K. R.; CHRISTAU, G.: New metal–binding mode for adenine: A bidentate (N6,N7) bridging mode in the complex $[\text{Mo}_2(\text{O}_2\text{CCHF}_2)_2(9\text{-EtAH})_2(\text{MeCN})_2](\text{BF}_4)_2 \cdot 2\text{MeCN}$. *J. Am. Chem. Soc.* **1994**, 116, 9339–9340.
- DECLERCQ, J. P.; DEBBAUDT, M.; VAN MEERSSCHE, M.: Confirmation de la Structure Cristalline et Moléculaire du Complexe Guanine. $\text{CuCl}_2 \cdot \text{HCl} \cdot \text{H}_2\text{O}$. *Bull. Soc. Chim. Belg.* **1971**, 80, 527–532.
- DELLEY, B.: An all–electron numerical method for solving the local density functional for polyatomic molecules. *J. Chem. Phys.* **1990**, 92, 508–517.
- DELLEY, B.: From molecules to solids with the DMol3 approach. *J. Chem. Phys.* **2000**, 113, 7756–7764.
- DE MEESTER, P.; SKAPSKI, A. C.: Crystal structure of dichlorotetra– μ –adenine–dicopper(II) chloride hexahydrate. *J. Chem. Soc. A*, **1971**, 2167–2169.
- DE MEESTER, P.; SKAPSKI, A. C.: Crystal structure of octachloro bis(adeninium)tricopper(II) tetra hydrate: A trinuclear complex with bridging adenine. *J. Chem. Soc. Dalton Trans.* **1972**, 2400–2404.
- DE MEESTER, P.; SKAPSKI, A. C.: Crystal structure of dibromodiadeniniumcopper(II) dibromide: a complex with unidentate adenine. *J. Chem. Soc. Dalton Trans.* **1973**, 424–427.
- DE MEESTER, P.; SKAPSKI, A. C.: X–Ray crystal structure of bis(adeninium) trans–bis(adenine)tetra–aquo bis(sulphate) hexahydrate: A complex of unidentate adenine containing adenine–adeninium hydrogen bonded pairs. *J. Chem. Soc. Dalton Trans.* **1973**, 1596–1601.
- DE.MUNNO, G.; MAURO, S.; PIZZINO, T.; VITERBO, D.: Synthesis, characterization and unusual crystal structures of two cytosine cadmium(II) chloride compounds. *J. Chem. Soc. Dalton Trans.* **1993**, 1113–1119.
- DE MUNNO, G.; MEDAGLIA, M.; ARMENTANO, D.; ANASTASSOPOULOU, J.; THEOPHANIDES, T.: New supramolecular complexes of manganese(II) and cobalt(II) with

nucleic bases. Crystal structures of $[M(H_2O)_6(1-Mecyt)_6][ClO_4]_2 \cdot H_2O$, $[Co(1-Mecyt)_4][ClO_4]_2$ and $[M(H_2O)_4(cyt)_2][ClO_4]_2 \cdot 2cyt \cdot 2H_2O$ [$M = CoII$ or $MnII$; $cyt =$ cytosine; $1-Mecyt = 1$ -methylcytosine]. *J. Chem. Soc. Dalton Trans.* **2000**, 1625–1629.

- DESIRAJU, G. R.: Crystal Engineering: The design of organic solids, *Amsterdam: Elsevier*, 1989.
- DESIRAJU, G. R.: Supramolecular synthons in crystal engineering—A new organic synthesis. *Angew. Chem. Int. Ed. Engl.* **1995**, *34*, 2311–2327.
- DESIRAJU, G. R.: Hydrogen bridges in crystal engineering: Interactions without borders. *Acc. Chem. Res.* **2002**, *35*, 565–573.
- DESIRAJU, G. R.: Crystal engineering. From molecules to materials. *J. Mol. Struct.* **2003**, *656*, 5–15.
- DESIRAJU, G. R.: Crystal engineering: A holistic view. *Angew. Chem. Int. Ed.* **2007**, *46*, 8342–8356.
- DESIRAJU, G. R.: Crystal engineering: A brief overview. *J. Chem. Sci.* **2010**, *122*, 667–675.
- DJINOVIC, V. M.; GALANSKI, M.; ARION, V. B.; KEPPLER, B. K.: Synthesis and structures of novel 1-methylcytosinato-bridged (ethylenediamine)platinum(II) and platinum(III) dinuclear complexes. *Dalton Trans.* **2010**, *39*, 3633–3643.
- DUBLER, E.; HAENGGI, G.; SCHMALLE, H.: Crystallographic evidence of preferred N(9)-coordination of xanthine: structures of $Cu(II)(xan)_2(NO_3)_2 \cdot 2H_2O$, $Cu(II)(xan)_2Cl_2 \cdot 2H_2O$, and $Zn(II)(xan)_2Cl_2$ ($xan =$ xanthine). *Inorg. Chem.* **1992**, *31*, 3728–3736.
- DUNITZ, J. D.: Phase transitions in molecular crystals from a chemical point of view. *Pure Appl. Chem.* **1991**, *63*, 177–185.
- DÜREN, T.; MILLANGE, F.; FÉREY, G.; WALTON, K. S.; SNURR, R.: Calculating geometric surface areas as a characterization tool for metal-organic frameworks. *J. Phys. Chem. C*, **2007**, *111*, 15350–15356.
- DÜREN, T.; BAE, Y.-S.; SNURR, R. Q.: Using molecular simulation to characterise metal-organic frameworks for adsorption applications. *Chem. Soc. Rev.* **2009**, *38*, 1237–1247.
- EDDAOUDI, M.; MOLIER, D. B.; LI, H.; CHEN, B.; REINEKE, T. M.; O'KEFFE, M.; YAGHI, O. M.: Modular chemistry: secondary building units as a basis for the design of highly porous and robust metal-organic carboxylate frameworks. *Acc. Chem. Res.* **2001**, *34*, 319–330.
- EDDAOUDI, M.; KIM, J.; ROSI, N.; VODAK, D.; WACHTER, J. B.; O'KEEFFE, M.; YAGHI, O. M.: Systematic design of pore size and functionality in isorecticular MOFs and their application in methane storage. *Science* **2002**, *295*, 469–472.
- ETTER, M. C.: Encoding and decoding hydrogen-bond patterns of organic compounds. *Acc. Chem. Res.* **1990**, *23*, 120–126.

- FALCARO, P.; RICCO, R.; DOHERTY, C. M.; LIANG, K.; HILL, A. J.; STYLES, M. J.: MOF positioning technology and device fabrication. *Chem. Soc. Rev.* **2014**, *43*, 5513–5560.
- FARHA, O. K.; ERYAZICI, I.; JEONG, N. C.; HAUSER, B. G.; WILMER, C. E.; SARJEANT, A. A.; SNURR, R. Q.; NGUYEN, S. T.; YAZAYDIN, A. O.; HUPP, J. T.: Metal–organic framework materials with ultrahigh surface areas: Is the sky the limit? *J. Am. Chem. Soc.* **2012**, *134*, 15016–15021.
- FARRUGIA, L. J.: *WINGX–1.63 Integrated System of Windows Programs for the Solution, Refinement and Analysis of Single Crystal X–Ray Diffraction Data*. *J. Appl. Cryst.* **1999**, *32*, 837–838.
- FARRUSSENG, D.; AGUADO, S.; PINEL, C.: Metal–organic frameworks: opportunities for catalysis. *Angew. Chem. Int. Ed.* **2009**, *48*, 7502–7513.
- FATHALLA, M.; LAWRENCE, C. M.; ZHANG, N.; SESSLER, J. L.; JAYAWICKRAMARAJAH: Base–pairing mediated non–covalent polymers. *J. Chem. Soc. Rev.* **2009**, *38*, 1608–1620.
- FELDBLYUM, J. I., LIU, M.; GIDLEY, D. W.; MATZGER, A. J.: Reconciling the discrepancies between crystallographic porosity and guest access as exemplified by Zn–HKUST–1. *J. Am. Chem. Soc.* **2011**, *133*, 18257–18263.
- FÉREY, G.; MELLOTT–DRAZNIÉKS, C.; SERRE, C.; MILLANGE, F.; DUTOUR, J.; SURBLE, S.; MARGIOLAKI, I.: A chromium terephthalate–based solid with unusually large pore volumes and surface area. *Science* **2005**, *309*, 2040–2042.
- FISHER, M.; HOFFMANN, F.; FRÖBA, M.: New microporous materials for acetylene storage and C₂H₂/CO₂ separation: insights from molecular simulations. *Chem. Phys. Chem.* **2010**, *11*, 2220–2229.
- FREISINGER, E.; ROTHER, I. B.; LUTH, M. S.; LIPPERT, B.: Canonical and unconventional pairing schemes between bis(nucleobase) complexes of trans–a2PtII: artificial nucleobase quartets and C–H···N bonds. *Proc. Nat. Acad. Sci. USA*, **2003**, *100*, 3748–3753.
- FRENKEL, D.; SMIT, B.: *Understanding molecular simulation: from algorithms to applications*. Academic Press, San Diego, California, USA, 2002.
- FREY, J. A.; OTTIGER, P.; LEUTWYLER, S.: Watson–Crick and Sugar–Edge base pairing of cytosine in the gas phase: UV and Infrared spectra of cytosine·2–pyridone. *J. Phys. Chem. B*, **2014**, *118*, 682–691.
- FURUKAWA, H.; CORDOVA, K. E.; O´KEEFFE, M.; YAGHI, O. M.: The chemistry and applications of metal–organic frameworks. *Science* **2013**, *341*, 1230444 (1–12).
- FUSCH, E. C.; LIPPERT, B.: [Zn₃(OH)₂(1–MeC–N₃)₅(1–MeC–O₂)₃]₄⁺ (1–MeC = 1–Methylcytosine): Structural model for DNA crosslinking and DNA rewinding by Zn(II)? *J. Am. Chem. Soc.* **1994**, *116*, 7204–7209.

- FUSCH, G.; FUSCH, E. C.; ERXLEBEN, A.; HUTTERMAN, J.; SCHOLL, H.-J.; LIPPERT, B.: Heteronuclear μ -1-methylcytosinato- N_3,N_4 complexes containing short Pt-Cu dative bonds. *Inorg. Chim. Acta* **1996**, 252, 167-178.
- GABALLA, A. S.; SCHMIDT, H.; WAGNER, C.; STEINBORN, D.: Structure and characterization of platinum(II) and platinum(IV) complexes with protonated nucleobase ligands. *Inorg. Chim. Acta* **2008**, 361, 2070-2080.
- GAGNON, C.; HUBERT, J.; RIVERT, R.; BEAUCHAMP, A. L.: Crystal structure of di- μ -adeninium-disilver(I) perchlorate monohydrate. *Inorg. Chem.* **1977**, 16, 2469-2473.
- GALINDO, M. A.; AMANTIA, D.; CLEGG, W.; HARRINGTON, R. W.; EYRE, R. J.; GOSS, J. P.; BRIDDON, P. R.; MCFARLANE, W.; HOULTON, A.: Self-assembly of a bis(adeninyl)-Cu(I) complex: a cationic nucleobase duplex mimic. *Chem. Commun.* **2009**, 2833-2835.
- GALSTYAN, A.; MIGUEL, P. J. S.; WOLF, J.; FREISINGER, E.; LIPPERT, B.: Discrete molecular squares $\{[(en)M(CN)_4]_4\}^{4+}$ derived from $[(en)M(CN)_2]$ (with M = PtII, PdII). *Eur. J. Inorg. Chem.* **2011**, 1649-1656.
- GARCIA, B.; GARCIA-TOJAL, J.; RUIZ, R.; GIL-GARCIA, R.; IBEAS, S.; DONNADIEU, B.; LEAL, J. M.: Interaction of the DNA bases and their mononucleotides with pyridine-2-carbaldehyde thiosemicarbazone copper(II) complexes. Structure of the cytosine derivative. *J. Inorg. Biochem.* **2008**, 102, 1892-1900.
- GARCÍA-COUCERO, U.; CASTILLO, O.; LUQUE, A.; BEOBIDE, G.; ROMÁN, P.: One-dimensional oxalato-bridged metal(II) complexes with 4-amino-1,2,4-triazole as apical ligand. *Inorg. Chim. Acta* **2004**, 357, 339-344.
- GARCÍA-COUCERO, U.; CASTILLO, O.; CEPEDA, J.; LANCHAS, M.; LUQUE, A.; PÉREZ-YÁÑEZ, S.; ROMÁN, P.; VALLEJO SANCHEZ, D.: Influence of the synthetic conditions on the structural diversity of extended manganese-oxalato-1,2-bis(4-pyridyl)ethylene systems. *Inorg. Chem.* **2010**, 49, 11346-11361.
- GARCIA-RASO, A.; FIOL, J. J.; LOPEZ-ZAFRA, A.; TASADA, A.; MATA, I.; ESPINOSA, E.; MOLINS, E.: Different ways of interaction between binary copper(II)-Schiff bases (Cu-N-salicylideneserinato) and pyrimidine derivatives. *Polyhedron* **2006**, 25, 2295-2302.
- GARCIA-RASO, A.; FIOL, J. J.; TASADA, A.; ALBERTI, F. M.; BADENAS, F.; SOLANS, X.; FONT-BARDIA, M.: $N^9,N^{9'}$ -polymethylene-bisadenine complexes with d^{10} metal ions. *Polyhedron* **2007**, 26, 949-957.
- GARCÍA-SÁNCHEZ, A.; ANIA, C. O.; PARRA, J. B.; DUBBELDAM, D.; VLUGT, T. J. H.; KRISHNA, R.; CALERO, S.: Transferable force field for carbon dioxide adsorption in zeolites. *J. Phys. Chem. C*, **2009**, 113, 8814-8820.
- GARCÍA-TERÁN, J. P.; CASTILLO, O.; LUQUE, A.; GARCÍA-COUCERO, U.; ROMÁN, P.; LEZAMA, L.: An unusual 3D coordination polymer based on bridging interactions of the nucleobase adenine. *Inorg. Chem.* **2004**, 43, 4549-4551.

- GARCÍA-TERÁN, J. P.; CASTILLO, O.; LUQUE, A.; GARCÍA-COUCERO, U.; ROMÁN, P.; LLORET, F.: One-dimensional oxalato-bridged Cu(II), Co(II), and Zn(II) complexes with purine and adenine as terminal ligands. *Inorg. Chem.* **2004**, *43*, 5761–5770
- GARCÍA-TERÁN, J. P.; CASTILLO, O.; LUQUE, A.; GARCÍA-COUCERO, U.; BEOBIDE, G.; ROMÁN, P.: Supramolecular architectures assembled by the interaction of purine nucleobases with metal-oxalato frameworks. Non-covalent stabilization of the 7H-adenine tautomer in the solid-state. *Dalton Trans.* **2006**, 902–911.
- GOLDSMITH, J.; WONG-FOY, A. G.; CAFARELLA, M. J.; SIEGEL, D. J.: Theoretical limits of hydrogen storage in Metal-Organic Frameworks: Opportunities and trade-offs. *Chem. Mater.* **2013**, *25*, 3373–3382.
- GONZÁLEZ-PÉREZ, J. M.; ALARCÓN-PAYER, C.; CASTINEIRAS, A.; PIVETTA, T.; LEZAMA, L.; CHOQUESILLO-LAZARTE, D.; CRISPONI, G.; NICLOS-GUTIERREZ, J.: A windmill-shaped hexacopper (II) molecule built up by template core-controlled expansion of diaqua μ_2 -adeninato N3, N9)dicopper(II) with aqua (oxydiacetato)copper(II). *Inorg. Chem.* **2006**, *45*, 877–882.
- GREEN, M. A.: Crystal engineering in two dimensions: surface attraction. *Nat. Mater.* **2010**, *9*, 539–540.
- GREHL, M.; KREBS, B.: Reaction of model nucleobases with the diaqua(bis(N-methylimidazol-2-yl)ketone)platinum(II) dication. synthesis and structure of the head-to-tail isomers of bis(9-methylguanine-N7)(bis(N-methylimidazol-2-yl)ketone)-platinum(II) perchlorate, bis(1-methylcytosine-N3)(bis(N-methylimidazol-2-yl)ketone)platinum(II) perchlorate, bis(-1-methylthyminato-N3,O4)bis-[(bis(N-methylimidazol-2-yl)ketone)platinum(II)] perchlorate, Bis(-1-methyluracilato-N3,O4)bis[(bis(N-methylimidazol-2-yl)ketone)-platinum(II)] nitrate. *Inorg. Chem.* **1994**, *33*, 3877–3885.
- GRIMME, S.: Semiempirical GGA-type density functional constructed with a long-range dispersion correction. *J. Comput. Chem.* **2006**, *27*, 1787–1799.
- GUPTA, D.; NOWAK, R.; LIPPERT, B.: Pt(II) complexes of unsubstituted guanine and 7-methylguanine. *Dalton Trans.* **2010**, *39*, 73–84.
- HAN, L.; ZHOU, Y.; ZHAO, W. N.; LI, X.; LIANG, Y. X.: Assembly of metal-organic frameworks with helical layer: from 2D parallel interpenetrated layer to 3D self-penetrating network. *Cryst. Growth Des.* **2009**, *9*, 660–662.
- HAN, S. S.; MENDOZA-CORTÉS, J. L.; GODDARD, W. A.: Recent advances on simulation and theory of hydrogen storage in metal-organic frameworks and covalent organic frameworks. *Chem. Soc. Rev.* **2009**, *38*, 1460–1476.
- HÄNGGI, G.; SCHMALLE, H.; DUBLER, E.: Structure of $[\text{Co}_2(\mu_2\text{-hypoxanthine})(\text{SO}_4)_2(\mu\text{-H}_2\text{O})_2(\text{H}_2\text{O})_2]$. *Acta Crystallogr.* **1992**, *C48*, 1008–1112.
- HAYASHI, H.; CÔTÉ, A. P.; FURUKAWA, H.; Ó KEEFFE, M.; YAGHI, O. M.: Zeolite a imidazolate frameworks. *Nat. mater.* **2007**, *6*, 501–506.

- HE, Y.; ZHOU, W.; QUIAN, G.; CHEN, B.: Methane storage in metal–organic frameworks. *Chem. Soc. Rev.* **2014**, *43*, 5657–5678.
- HOLDEN, A. *Shapes, Space, and Symmetry*. New York: Dover, 1991, p.154–163.
- HOLLIS, L. S.; AMUNDSEN, A. R. STERN, E. W.: Chemical and biological properties of a new series of cis–diammineplatinum(II) antitumor agents containing three nitrogen donors: cis–[Pt(NH₃)₂(N–donor) Cl]⁺. *J. Med. Chem.* **1989**, *32*, 128–136.
- HOLLOWCZAK, M. S.; STANCL, M. D.; WONG, G. B.: Trichloro(1–methylcytosinato)gold(III). model for gold–DNA interactions. *J. Am. Chem. Soc.* **1985**, *107*, 5789–5790.
- HOLTHENRICH, D.; ZANGRANDO, E.; PICHIERRI, F.; RANDACCIO, L.; LIPPERT, B.: Palladium –1–methylcytosine compounds – crystal structure of the tris(nucleobase) complex [(NH₃)PD(1–MEC–N₃)₃](ClO₄)₂. H₂O–role of intramolecular H bonding in stabilising the head–tail–head rotamer. *Inorg. Chim. Acta* **1996**, *248*, 175–179.
- HOULTON, A.; ISAAC, C. J.; GIBSON A. E.; HORROCKS B.R.; CLEGG W.; ELSEGOOD M. R. J.: Synthesis, structure and redox properties of ferrocenyl methyl nucleobases. *J. Chem. Soc. Dalton Trans.* **1999**, 3229–3234.
- HOSKINS, B. F.; ROBSON, R.: Design and construction of a new class of scaffolding–like materials comprising infinite polymeric frameworks of 3–D–linked molecular rods. A reappraisal of the zinc cyanide and cadmium cyanide structures and the synthesis and structure of the diamond–related frameworks [N(CH₃)₄][Cu^IZn^{II}(CN)₄] and Cu^I[4,4',4'',4'''–tetracyanotetraphenylmethane]BF₄·xC₆H₅NO₂. *J. Am. Chem. Soc.* **1990**, *112*, 1546–1554.
- HU, Z.; DEIBERT, B. J.; LI, J.: Luminescent metal–organic frameworks for chemical sensing and explosive detection. *Chem. Soc. Rev.* **2014**, *43*, 5815–5840.
- IMAZ, I.; RUBIO–MARTÍNEZ, M.; AN, J.; SOLÉ–FONT, I.; ROSI, N. L.; MASPOCH, D.: Metal–biomolecule frameworks (MBioFs). *Chem. Commun.* **2011**, *47*, 7287–7302.
- JAMES, S. L.: Metal–organic frameworks. *Chem. Soc. Rev.* **2003**, *32*, 276–288.
- JANIAK, C.: Engineering coordination polymers towards applications. *Dalton Trans.* **2003**, 2781–2804.
- JAWORSKI, S.; SCHOLLHORN, H.; EISENMANN, P.; THEWALT, U.; LIPPERT, B.: Trichloroamine complexes of platinum: preparation, crystal structure and solution behavior of cytosinium trichlorocytosineplatin(II). *Inorg. Chim. Acta* **1988**, *153*, 31–38.
- JEFFREY, G. A.; SAENGER, W.: Hydrogen bonding in biological structures. *Springer*: Berlin, 1991.
- JIANG, H.–L.; MAKAL, T. A.; ZHOU, H.–C.: Interpenetration control in metal–organic frameworks for functional applications. *Coord. Chem. Rev.* **2013**, *257*, 2232–2249.

- JITSUKAWA, K.; MIZUTANI, M.; ARII, H.; KUBO, I.; IZU, Y.; OZAWA, T.; MASUD, H.: Characteristics of pyrimidine nucleobases through inter-base interactions on the crystals of the ternary copper(II) complexes. *Chem. Lett.* **2004**, *33*, 1302–1303.
- KAHR, J.; MOWAT, J. P.; SLAWIN, A. M.; MORRIS, R. E.; FAIREN-JIMENEZ, D.; WRIGHT, P. A.: Synthetic control of framework zinc purinate crystallisation and properties of a large pore, decorated, mixed-linker RHO-type ZIF. *Chem. Commun.* **2012**, *48*, 6690–6692.
- KARTHIKEYAN, A.; EBENEZER, S.; MUTHIAH, P.T.: Metal-nucleobase inter-action: bis[4-amino-pyrimidin-2(1H)-one- κ N³]dibromidozinc(II). *Acta Crystallogr. Sect. E: Struct. Rep. Online*, **2010**, *66*, m1693.
- KHUTIA, A.; MIGUEL, P. J. S.; LIPPERT, B.: Directed assembly of metallacalix[n]arenes with pyrimidine nucleobase ligands of low symmetry: metallacalix[n]arene derivatives of cis-[a₂M(cytosine-N₃)₂]²⁺ (M=Pt(II), Pd(II); n=4 and 6). *Chem. Eur. J.* **2011**, *17*, 4195–4204.
- KICKHAM, J. E.; LOEB, S. J.; MURPHY, S. L.: Molecular recognition of nucleobases via simultaneous first- and second-sphere coordination. *J. Am. Chem. Soc.* **1993**, *115*, 7031–7032.
- KICKHAM, J. E.; LOEB, S. J.; MURPHY, S. L.: Molecular receptors for adenine and guanine employing metal coordination, hydrogen-bonding and π -stacking interactions. *Chem. Eur. J.* **1997**, *3*, 1203–1213.
- KISTENMACHER, T. J.; MARZILLI, L. G.; CHANG, C.-H.: Crystal and molecular structure of a cobalt(III) complex containing adenine as a unidentate ligand. *J. Am. Chem. Soc.* **1973**, *95*, 5817–5819.
- KISTENMACHER, T. J.; ROSSI, M.; MARZILLI, L. G.: Crystal and molecular structure of (nitrate)(1-methylcytosine)silver(I): an unusual crosslinked polymer containing a heavy metal and a modified nucleic acid constituent. *Inorg. Chem.* **1979**, *18*, 240–244.
- KITAJIMA, N.; HIKICHI, S.; TANAKA, M.; MOROOKA, Y.: Fixation of atmospheric carbon dioxide by a series of hydroxo complexes of divalent metal ions and the implication for the catalytic role of metal ion in carbonic anhydrase. Synthesis, characterization, and molecular structure of [LM(OH)]_n (n = 1 or 2) and LM(μ -CO₃)ML (M(II) = Mn, Fe, Co, Ni, Cu, Zn; L = HB(3,5-iso-Pr₂pz)₃). *J. Am. Chem. Soc.* **1993**, *115*, 5496–5508.
- KLEIN, A.; SCHURR, T.; SCHERER, H.; GUPTA, N. S.: Cytosine binding in the novel organoplatinum(II) complex [(COD)PtMe(cytosine)](SbF₆). *Organometallics* **2007**, *26*, 230–233.
- KOH, A.; WONG-FOY, A. G.; MATZGER, A. J.: A porous coordination copolymer with over 5000 m²/g BET surface area. *J. Am. Chem. Soc.* **2009**, *131*, 4184–4185.
- KORN, S.; SCHELDRIK, W. S.: Oligomeric (η^6 -arene) ruthenium(II) complexes of adenine and adenosine with N₆,N₇ coordination. *Inorg. Chim. Acta* **1997**, *254*, 85–91.

- KRUMM, M.; MUTIKAINEN, I.; LIPPERT, B.: Palladium–1–methylcytosine chemistry: N3 and N3, N4 metal binding to 1–methylcytosine and an unexpected trans \rightarrow cis isomerization of two diamminepalladium(II) entities. *Inorg. Chem.* **1991**, *30*, 884–890.
- KURMOO, M.: Magnetic metal–organic frameworks. *Chem. Soc. Rev.* **2009**, *38*, 1353–1379.
- LAN, A.; LI, K.; WU, H.; OLSON, D. H.; EMGE, T. J.; KI, W.; HONG, M.; LI, J.: A luminescent microporous metal–organic framework for the fast and reversible detection of high explosives. *Angew. Chem. Int. Ed.* **2009**, *48*, 2334–2338.
- LANCHAS, M.; VALLEJO–SÁNCHEZ, D.; BEOBIDE, G.; CASTILLO, O.; AGUAYO, A. T.; LUQUE, A.; ROMÁN, P.: A direct reaction approach for the synthesis of zeolitic imidazolate frameworks: template and temperature mediated control on network topology and crystal size. *Chem. Commun.* **2012**, *48*, 9930–9932.
- LANCHAS, M.; ARCEDIANO, S.; AGUAYO, A. T.; BEOBIDE, G.; CASTILLO, O.; CEPEDA, J.; VALLEJO–SÁNCHEZ, D.; LUQUE, A.: Two appealing alternatives for MOFs synthesis: solvent–free oven heating vs. microwave heating. *RSC Adv.* **2014**, *4*, 60409–60412.
- LANCHAS, M.; ARCEDIANO, S.; BEOBIDE, G.; CASTILLO, O.; LUQUE, A.; PÉREZ–YÁÑEZ, S.: Towards multicomponent MOFs via solvent–free synthesis under conventional oven and microwave assisted heating. *Inorg. Chem. Front.* **2015**, *2*, 425–433.
- LANGMUIR, I.: The construction and fundamental properties of solids and liquids. Part I. Solids. *J. Am. Chem. Soc.* **1916**, *38*, 2221–2295.
- LEE, C. F.; CHIN, K. F.; PENG, S. M.; CHE, C. M.: A Luminescent Tetrameric Zinc(ii) Complex containing the 7–Azaindolate Ligand. Photophysical Properties and Crystal Structure. *J. Chem. Soc. Dalton Trans.* **1993**, *1*, 467–470.
- LEE, H.; ZONES, S. I.; DAVIS, M. E.: A combustion–free methodology for synthesizing zeolites and zeolite–like materials. *Nature* **2003**, *425*, 385–388.
- LEE, J.; FARHA, O. K.; ROBERTS, J.; SCHEIDT, K. A.; NGUYEN, S. T.; HUPP, J. T.: Metal–organic framework materials as catalysts. *Chem. Soc. Rev.* **2009**, *38*, 1450–1459.
- LI, J.–R.; KUPPLER, R. J.; ZHOU, H.–C.: Selective gas adsorption and separation in metal–organic frameworks. *Chem. Soc. Rev.* **2009**, *38*, 1477–1504.
- LI, T.; CHEN, D.–L.; SULLIVAN, J. E.; KOZLOWSKI, M. T.; JOHNSON, J. K.; ROSI, N. L.: Systematic modulation and enhancement of CO₂: N₂ selectivity and water stability in an isorecticular series of bio–MOF–11 analogues. *Chem. Sci.* **2013**, *4*, 1746–1765.
- LI, T.; KOZLOWSKI, M. T.; DOUD, E. A.; BLAKELY, M. N.; ROSI, N. L.: Stepwise ligand exchange for the preparation of a family of mesoporous MOFs. *J. Am. Chem. Soc.* **2013**, *135*, 11688–11691.
- Li, T.; SULLIVAN, J. E.; ROSI, N. L.: Design and preparation of a core–shell metal–organic framework for selective CO₂ capture. *J. Am. Chem. Soc.* **2013**, *135*, 9984–9987.

- LIPPERT, B.; LOCK, C. J. L.; SPERANZINI, R. A.: Triamine complexes containing 1-methylcytosine. *Inorg. Chem.* **1981**, *20*, 335–342.
- LIPPERT, B.: Multiplicity of metal ion binding patterns to nucleobases. *Coord. Chem.Rev.* **2000**, *200–202*, 487–516.
- LIPPERT, B.: Alterations of nucleobase pKa values upon metal coordination: origins and consequences. *Prog. Inorg. Chem.* *54*, in Karlin, K. D., John Wiley & Sons: NJ, 2005, 385–447.
- LIPPERT, B.; GUPTA, D.: Promotion of rare nucleobase tautomers by metal binding. *Dalton Trans.* **2009**, 4619–4934.
- LIU, J.; CHEN, L.; CUI, H.; ZHANG, J.; ZHANG, L.; SU, C–Y.: Applications of metal–organic frameworks in heterogeneous supramolecular catalysis. *Chem. Soc. Rev.* **2014**, *43*, 6011–6061.
- LIU, S.; LI, J.; LUO, F.: The first transition–metal metal–organic framework showing cation exchange for highly selective sensing of aqueous Cu(II) ions. *Inorg. Chem. Commun.* **2010**, *13*, 870–872.
- LLUNELL, M.; CASANOVA, D.; CIRERA, J.; BOFILL, J. M.; ALEMANY, P.; ALVAREZ, S.; PINSKY, M.; AVNIR, D.: *SHAPE–2, program for the calculation of continuous shape measures of molecular fragments*, Universitat de Barcelona: Barcelona, 2010.
- LONGATO, B.; MONTAGNER, D.; ZANGRANDO, E.: Mono– and polynuclear complexes of the model nucleobase 1–methylcytosine. Synthesis and characterization of cis–[(PMe₂Ph)₂Pt{(1–MeCy(–H))₃(NO₃)₃} and cis–[(PPh₃)₂Pt{(1–MeCy(–H))(1–MeCy)}]NO₃. *Inorg. Chem.* **2006**, *45*, 8179–8197.
- LOUIE, S.; BAU, R.: Structure of [Pt(en)(5'–CMP)]₂.2H₂O. An example of direct platinum–phosphate bonding. *J. Am. Chem. Soc.* **1977**, *99*, 3874–3876.
- MA, L.; LIN, W.: Chirality–controlled and solvent–templated catenation isomerism in Metal–Organic Frameworks. *J. Am. Chem. Soc.* **2008**, *130*, 13834–13835.
- MA, L.; ABNEY, C.; LIN, W.: Enantioselective catalysis with homochiral metal–organic frameworks. *Chem. Soc. Rev.* **2009**, *38*, 1248–1256.
- MALIK, M. A.; MOTEVALLI, M.; O'BRIEN, P.: Structural diversity in the carbamate chemistry of zinc: X–ray single–crystal structures of ((Me₂NCH₂)₂Zn(O₂CN(C₂H₅)₂)₂) and (C₅H₅NZn₂Me(O₂CN(C₂H₅)₂)₃). *Inorg. Chem.* **1995**, *34*, 6223–6225.
- MANOS, M. J.; IYER, R. G.; QUAREZ, E.; LIAO, J. H.; KANATZIDIS, M. G.: {Sn[Zn₄Sn₄S₁₇]}^{6–}: A robust open framework based on metal–linked penta–supertetrahedral [Zn₄Sn₄S₁₇]^{10–} clusters with ion–exchange properties. *Angew. Chem. Intl. Ed.* **2005**, *44*, 3552–3555.
- MARTIN, R. L.; HARANCZYK, M.: Exploring frontiers of high surface area metal–organic frameworks. *Chem. Sci.* **2013**, *4*, 1781–1785.

- MARZOTTO, A.; CLEMENTE, D. A.; CICCARESE, A.; VALLE, G.: New selective nickel(II)–N₃ nitrogen bond in adenine: Synthesis and structure of [(tren) (adenine) (monochloro)nickel(II)] chloride and [(tren)(imidazole)(monoaqua)nickel(II)] dichloride. *J. Crystallogr. Spectrosc. Res.* **1993**, 23, 119–131.
- MARZOTTO, A.; CICCARESE, A.; CLEMENTE, D. A.; VALLE, G.: Co-ordination chemistry of adenine (HAde): synthesis and characterization of [CuII(tren)(nucleobase)]X₂[tren = tris-(2-aminoethyl)amine, X = Cl or NO₃] complexes and crystal structure of [CuII(tren)(Ade)]Cl·2H₂O. *J. Chem. Soc. Dalton Trans.* **1995**, 1461–1448.
- MASTROPIETRO, T. F.; ARMENTANO, D.; MARINO, N.; DE MUNNO, G.; ANASTASSOPOULOU, J.; THEOPHANIDES, T.: Supramolecular assemblies of nucleobase derivative 1-Mecyt with Mg(II) and Ni(II) and solid-state transformation of Ni(II) phase: a comprehensive evidence of their different reactivity toward 1-mecyt [1-Mecyt]1-methylcytosine]. *Cryst. Growth Des.* **2007**, 7, 609–612.
- MASTROPIETRO, T. F.; ARMENTANO, D.; MARINO, N.; DE MUNNO, G.: Metal–nucleobase interactions in magnesium(II) and manganese(II) complexes with adenine: influence of the anion on the non-covalent stabilization of 7H–adenine tautomer. *Polyhedron* **2007**, 26, 4945–4954.
- MASTROPIETRO, T. F.; ARMENTANO, D.; GRISOLIA, E.; ZANCHINI, C.; LLORET, F.; JULVE, M.; DE MUNNO, G.: Guanine–containing copper(II) complexes: synthesis, X-ray structures and magnetic properties. *Dalton Trans.* **2008**, 514–520.
- Materials Studio v. 5.5*; Accelrys Inc.: San Diego, 2011.
- MELLENDEZ, R. E.; SHARMA, C. V. K.; ZAWOROTKO, M. J.; BAUER, C.; ROGERS, R. D.: Toward the design of porous organic solids: modular honey comb grids sustained by anions of trimesic acid. *Angew. Chem. Int. Engl.* **1996**, 35, 2213–2215.
- MIGUEL, P. J. S.; LAX, P.; LIPPERT, B.: (Dien)MII (M = Pd, Pt) and (NH₃)₃PtII complexes of 1-methylcytosine: Linkage and rotational isomerism, metal–promoted deamination, and pathways to dinuclear species. *J. Inorg. Biochem.* **2006**, 100, 980–991.
- MILLER, S. K.; MARZILLI, L. G.; DORRE, S.; KOLLAT, P.; STIGLER, R.–D.; STEZOWSKI, J. J.: Models for the interaction of zinc(2+) with DNA. Syntheses and x-ray structural characterizations of two polymeric tetrahedral zinc complexes of monomethyl phosphate esters of cytidine and deoxycytidine 5'-monophosphate nucleotides. *Inorg. Chem.* **1986**, 25, 4272–4277.
- MONTAGNER, D.; ZANGRANDO, E.; LONGATO, B.: Role of the phosphine ligands on the stabilization of monoadducts of the model nucleobases 1-methylcytosine and 9-methylguanine in platinum(II) complexes. *Inorg. Chem.* **2008**, 47, 2688–2695.
- MOREL, A. C.; CHOQUECILLO–LASARTE, D.; ALARCÓN–PAYER, C.; GONZÁLEZ–PÉREZ, J. M.; CASTINEIRAS, A.; NICLÓS–GUTIÉRREZ, J.: An aqua–adenine H-bonding interaction controlling the formation of the rare Zn(II)–N₉(adenine) bond in crystal structure of diaqua(adenine)(iminodiacetato)zinc(II). *Inorg. Chem. Commun.* **2003**, 6, 1354–1357.

- MULLER, U.; SCHUBERT, M.; TEICH, F.; PUETTER, H.; SCHIERLE-ARNDT, K.; PASTRÉ, J.: Metal-organic-frameworks-prospective industrial applications. *J. Mater. Chem.* **2006**, *38*, 626-636.
- MUNDWILER, S., SPINGLER, B.; KURZ, P.; KUNZE, S.; ALBERTO, R.: Cyanide-bridged vitamin B12-cisplatin conjugates. *Chem. Eur. J.* **2005**, *11*, 4089-4095.
- MURRAY, L. J.; DINCĂ, M.; LONG, J. R.: Hydrogen storage in metal-organic frameworks. *Chem. Soc. Rev.* **2009**, *38*, 1294-1314.
- MUTHIAH, P. T.; MAZUMDAR, S. K.: Metal ions-nucleobases interactions: preparation and crystal structures of trichloroadeninium zinc(II) (form II) and a similar zinc complex of arprinocid [6-amino-9-(2-chloro-6-fluorobenzyl)purine]. *J. Inorg. Biochem.* **1983**, *19*, 237-246.
- MUTHIAH, P. T.; ROBERT, J. J.; RAJ, S. B.; BOCELLI, G.; OLLÁ, R.: Metal-nucleobase interaction: dibromobis(cytosine)-cadmium(II). *Acta Crystallogr. Sect. E, Struct. Rep. Online*, **2001**, E57, m558-m560.
- NIST Computational Chemistry Comparison and Benchmark Database NIST Standard Reference Database Number 101. Release 16a, August 2013, Editor: Johnson, R. D. III. <http://cccbdb.nist.gov/>.
- NUGENT, P. S.; RHODUS, V. L.; PHAM, T.; FORREST, K.; WOTJAS, L.; SPACE, B.; ZAWOROTKO, M. J.: A robust molecular porous material with high CO₂ uptake and selectivity. *J. Am. Chem. Soc.* **2013**, *135*, 10950-10953.
- O'KEEFFE, M.; YAGHI, O. M.: Deconstructing the crystal structures of metal-organic frameworks and related materials into their underlying nets. *Chem. Rev.* **2012**, *112*, 675-702.
- ORBELL, J. D.; MARZILLI, L. G.; KISTENMACHER, T. J.: Preparation, H NMR spectrum and structure of cis-diammine bis(1-methylcytosine)platinum(II) nitrate-1-methylcytosine. Cis steric effects in pyrimidine ring-bound cis-bis(nucleic acid base)- platinum(II) compounds. *J. Am. Chem. Soc.* **1981**, *103*, 5126-5133.
- PACIFICO, C.; INTINI, F. P.; NUSHI, F.; NATILE, G.: "Lantern-shaped" platinum(III) complexes with axially bound 9-ethylguanine or 1-methylcytosine (L) of general formula [Pt₂{HN=C(Bu¹)O}₄L₂](NO₃)₂. *Bioinorg. Chem. Appl.* **2010**, *2010*, 102863-102870.
- PALANIANDAVAR, M.; SOMASUNDARAM, I.; LAKSHMINARAYANAN, M.; MANOHAR, H.: Stabilisation of unusual simultaneous binding of four cytosine nucleobases to copper(II) by a novel network of bifurcated hydrogen bonding. *J. Chem. Soc. Dalton Trans.* **1996**, 1333-1340.
- PANFIL, A.; TERRON, A.; FIOL, J. J.; QUIROS, M.: Synthesis and characterization of a novel copper(II)-cytosine complex-tetrakis(cytosine)copper(II)chloridebis(dimethylacetamide) solvate. *Polyhedron* **1994**, *13*, 2513-2518.

- PARVEZ, M.; BIRDSALL, W. J.: Diamminebis[5-methylpyrimidine-2,4(1H,3H)dionato(1-)-N3]copper(II) trihydrate. *Acta Crystallogr. Sect. C, Cryst. Struct. Commun.* **1994**, *50*, 540–542.
- PEACOCK, A. F. A.; PARSONS, S.; SADLER, P. J.: Tuning the hydrolytic aqueous chemistry of osmium arene complexes with N, O-chelating ligands to achieve cancer cell cytotoxicity. *J. Am. Chem. Soc.* **2007**, *129*, 3348–3357.
- PEPINSKY, R.: Crystal engineering: New concepts in crystallography. *Phys. Rev.* **1955**, *100*, 971–971.
- PERDEW, J. P.; BURKE, K.; ERNZERHOF, M.: Generalised gradient approximation made simple. *Phys. Rev. Lett.* **1996**, *77*, 3865–3868.
- PÉREZ-YÁÑEZ, S.; CASTILLO, O.; CEPEDA, J.; GARCÍA-TERÁN, J. P.; LUQUE, A.; ROMÁN, P.: Analysis of the interaction between adenine nucleobase and metal-malonato complexes. *Eur. J. Inorg. Chem.* **2009**, *26*, 3889–3899.
- PÉREZ-YÁÑEZ, S.; BEOBIDE, G.; CASTILLO, O.; CEPEDA, J.; LUQUE, A.; AGUAYO, A. T.; ROMÁN, P.: Open-framework copper adeninate compounds with three dimensional microchannels tailored by aliphatic monocarboxylic acids. *Inorg. Chem.* **2011**, *50*, 5330–5332.
- PÉREZ-YÁÑEZ, S. Tesis Doctoral, Universidad del País Vasco/Euskal Herriko Unibertsitatea: Leioa, 2012.
- PÉREZ-YÁÑEZ, S.; BEOBIDE, G.; CASTILLO, O.; FISCHER, M.; HOFFMANN, F.; FRÖBA, M.; CEPEDA, J.; LUQUE, A.: Gas adsorption properties and selectivity in Cu^{II}/adeninato/carboxylato metal-biomolecule framework. *Eur. J. Inorg. Chem.* **2012**, 5921–5933.
- PÉREZ-YÁÑEZ, S.; BEOBIDE, G.; CASTILLO, O.; CEPEDA, J.; LUQUE, A.; ROMÁN, P.: Directing the formation of adenine coordination polymers from tunable copper(II) / dicarboxylato/adenine paddle-wheel building blocks. *Cryst. Growth Des.* **2012**, *12*, 3324–3334.
- PÉREZ-YÁÑEZ, S.; BEOBIDE, G.; CASTILLO, O.; CEPEDA, J.; FRÖBA, M.; HOFFMANN, F.; LUQUE, A.; ROMÁN, P.: Improving the performance of a poorly adsorbing porous material: Template mediated addition of microporosity to a crystalline submicroporous MOF. *Chem. Commun.* **2012**, 907–909.
- PÉREZ-YÁÑEZ, S.; BEOBIDE, G.; CASTILLO, O.; CEPEDA, J.; LUQUE, A.; ROMÁN, P.: Structural diversity in a copper(II)/isophthalato/9-methyladenine system. From one- to three-dimensional metal-biomolecule frameworks. *Cryst. Growth Des.* **2013**, *13*, 3057–3067.
- PERRY IV, J. J.; PERMAN, J. A.; ZAWOROTKO, M. J.: Design and synthesis of metal-organic frameworks using metal-organic polyhedra as supermolecular building blocks. *Chem. Soc. Rev.* **2009**, *38*, 1400–1417.

- PHAN, A.; CZAJA, A. U.; GÁNDARA, F.; KNOBLER, C. B.; YAGHI, O. M.: Metal–organic frameworks of vanadium as catalyst for conversion of methane to acetic acid. *Inorg. Chem.* **2011**, *50*, 7388–7390.
- POTOFF, J. J.; SIEPMANN, J. I.: Vapor–liquid equilibria of mixtures containing alkanes, carbon dioxide, and nitrogen. *AIChE Journal* **2001**, *47*, 1676–1682.
- PRINS, L. J.; REINHOUDT, D. N.; TIMMERMAN, P.: Noncovalent synthesis using hydrogen bonding. *Angew. Chem. Int. Ed.* **2001**, *40*, 2382–2426.
- PRIZANT, L.; OLIVIER, M. J.; RIVEST, R.; BEAUCHAMP, A. L.: Reactions of the methylmercury(II) ion with adenine and crystal structure of (adeninato–N9)methylmercury (II) monohydrate. *Can. J. Chem.* **1981**, *59*, 1311–1317.
- PRIZANT, L.; OLIVIER, M. J.; RIVEST, R.; BEAUCHAMP, A. L.: Structure of μ –(adeninato–N7,N9)–bis[methylmercury(II)]nitrate dihydrate. *Acta Crystallogr.* **1982**, *B38*, 88–91.
- PUROHIT, C. S.; PARVEZ, M.; VERMA, S.: Kinetic characterization of a bioinspired, heterogeneously active macromolecular catalyst for phenol oxidation and coupling reactions. *Appl. Catal. A–Gen.* **2007**, *316*, 100–106.
- QIU, S.; ZHU, G.: Molecular engineering for synthesizing novel structures of metal–organic frameworks with multifunctional properties. *Coord. Chem. Rev.* **2009**, *253*, 2891–2911.
- QIU, S.; XUE, M.; ZHU, G.: Metal–organic framework membranes: from synthesis to separation application. *Chem. Soc. Rev.* **2014**, *43*, 6116–6140.
- RAMASWAMY, P.; WONG, N. E.; SHIMIZU, G. K.: MOFs as proton conductors–challenges and opportunities. *Chem. Soc. Rev.* **2014**, *43*, 5913–5932.
- RAMSAHYE, N. A.; MAURIN, G.; BOURRELLY, S.; LLEWELLYN, P. L.; LOISEAU, T.; SERRE, C.; FÉREY, G.: On the breathing effect of a metal–organic framework upon CO₂ adsorption: Monte Carlo compared to microcalorimetry experiments. *Chem. Commun.* **2007**, 3261–3261.
- RANGANATHAN, A.; PEDIREDDI, V. R.; RAO, C. N. R.: Hydrothermal synthesis of organic channel structures: 1:1 hydrogen bonded adducts of melamine with cyanuric acid trithiocyanuric acid. *J. Am. Chem. Soc.* **1999**, *121*, 1752–1753.
- RAPPE, A. K.; CASEWIT, C. J.; COLWELL, K. S.; GODDARD, W. A.; SKIFF, W. M.: UFF, a full periodic table force field for molecular mechanics and molecular dynamics simulations. *J. Am. Chem. Soc.* **1992**, *114*, 10024–10035.
- REGER, D. L.; HORGER, J. J.; DEBRECZENI, A.; SMITH, M. D.: Synthesis and characterisation of copper (II) carboxylate dimers formed from enantiopure ligands containing a strong $\pi \cdots \pi$ stacking synthon: Enantioselective single–crystal to single–crystal gas/solid–mediated transformations. *Inorg. Chem.* **2011**, *50*, 10225–10240.
- REGER, D. L.; DEBRECZENI, A.; SMITH, M. D.; JEZIEWSKA, J.; OZAROWSKI, A.: Copper(II) carboxylate dimers prepared from ligands designed to form a robust π – π stacking

stacking synthon: supramolecular structures and molecular properties. *Inorg. Chem.* **2012**, *51*, 1068–1083.

RODRÍGUEZ–CARVAJAL, J. *FULLPROF*, a Program for Rietveld Refinement and Pattern Matching Analysis, Abstracts of the Satellite Meeting on Powder Diffraction of the XVth Congress of the IUCr.: Toulouse, France, 1990, p.127.

RODRÍGUEZ–CARVAJAL, J. *FULLPROF 2000*, version 2.5d, Laboratoire Léon Brillouin (CEA–CNRS), Centre d'Études de Saclay, Gif sur Yvette Cedex: France, 2003.

ROMÁN, P.; GUTIÉRREZ–ZORRILLA, J. M.: A quick method for determining the density of single crystals. *J. Chem. Educ.* **1985**, *62*, 167–168.

ROSOPULOS, Y.; NAGEL, U.; BECK, W.: Metal complexes with biologically important ligands. XXXIV. Allylpalladium(II) and triphenylphosphinegold(I) complexes with nucleobases and nucleosides. *Chem. Ber.* **1985**, *118*, 931–942.

ROUQUEROL, J.; AVNIER, D.; FAIRBRIDGE, C. W.; EVERETT, D. H.; HAYNES, J. H.; PERNICONE, N.; RAMSAY, J. D. F.; SING, K. S. W.; UNGER, K. K.: Recommendations for the characterization of porous solids. *Pure Appl. Chem.* **1994**, *66*, 1739–1758.

ROUSELL, J. L. C.; YAGHI, O. M.: *Micropor. Mesopor. Mater.* **2004**, *73*, 3–14.

RUIZ, J.; CUTILLAS, N.; VICENTE, C.; VILLA, M. D.; LOPEZ, G.; LORENZO, J.; AVILES, F. X.; MORENO, V.; BAUTISTA, D.: New palladium(II) and platinum(II) complexes with the model nucleobase 1–methylcytosine: Antitumor activity and interactions with DNA. *Inorg. Chem.* **2005**, *44*, 7365–7376.

SABAT, M.; SATYSHUR, K. A.; SUNDARALINGAM, M.: Ternary complexes as models for protein–metal–nucleic acid interactions: structure of palladium(II) complex with glycyl–L–tyrosine and cytidine. *J. Am. Chem. Soc.* **1983**, *105*, 976–980.

SAHA, B. K.; BHATTACHARYA, S.: Hydrogen–bond networks in the binary complexes of trigonal molecules with 4,4'–bipyridine. *CrystEngComm.* **2010**, *12*, 2369–2373.

SAKAGUCHI, H.; ANZAI, H.; FURUHATA, K.; OGURA, H.; IITAKA, Y.; FUJITA, T.; SAKAGUCHI, T.: Studies on metal complexes of amino acids and nucleotide base. Part IV. Crystal structure of facial–[bis(adeninato)(diethylenetriamine)copper(II)] monohydrate. *Chem. Pharm. Bull.* **1978**, *26*, 2465–2474.

SALAM, M. A.; AOKI, K.: Interligand interactions affecting specific metal bonding to nucleic acid bases: the tripodal nitrilotriacetato (nta) ligand–system. Crystal structures of [(nta)(adeninium)(aqua)nickel(II)] hydrate, [(nta)(diaqua)nickel(II)]·(cytosinium) hydrate, and [(nta)(diaqua)nickel(II)]·(cytosinium)·(cytosine) hydrate. *Inorg. Chim. Acta* **2000**, *311*, 15–24.

SARKISOV, L.; HARRISON, A.: Computational structure characterisation tools in application to ordered and disordered porous materials. *Mol. Simul.* **2011**, *37*, 1248–1257.

- SCHMALLE, H.W.; GYR, E.; DUBLER, E.: A mixed-valence iron complex of the antitumour drug 6-mercaptopurine: tris(6-mercaptopurine)iron(II) tetrachloroferrate(III) chloride. *Acta Crystallogr. Section C, Cryst. Struct. Commun.* **2000**, *56*, 957–959.
- SCHMDT, G. M. J.: Photodimerization in the solid state. *Pure Appl. Chem.* **1971**, *27*, 647–678.
- SCHMDT, G. M. J.; GERDARD, M. J.: Solid State Photochemistry. *D. Ginsburg(ed), Verlag Chemie*, Weinheim, 1976.
- SCHOLLHORN, H.; BEYERLE-PFNUR, R.; THEWALT, U.; LIPPERT, B.: Unusual four-membered chelate rings of platinum(IV) with a cytosine nucleobase. *J. Am. Chem. Soc.* **1986**, *108*, 3680–3688.
- SCHWARZ, F.; SCHOLLHORN, H.; THEWALT, U.; LIPPERT, B.: Unusual dehydrogenation of a diethylenetriamine ligand to a schiff base ligand in the coordination sphere of platinum (iv). *Chem. Commun.* **1990**, 1282–1284.
- SERRE, C.; BOURRELLY, S.; VIMONT, A.; RAMSAHYE, N. A.; MAURIN, G.; LLEWELLYN, P. L.; DATURI, M.; FILINCHUK, Y.; LEYNAUD, O.; BARNES P.; FÉREY, G.: An explanation for the very large breathing effect of a metal-organic framework during CO₂ adsorption. *Adv. Mater.* **2007**, *19*, 2246–2251.
- SERTUCHA, J.; LUQUE, A.; CASTILLO, O.; ROMÁN, P.; LLORET, F.; JULVE, M.: Ferromagnetic coupling through a carbonate bridge in the copper(II) chain [Cu(CO₃)(4-apy)₂] × H₂O (4-apy = 4-aminopyridine). *Inorg. Chem. Commun.* **1999**, *2*, 14–16.
- SESSLER, J. L.; LAWRENCE, C. M.; JAYAWICKRAMARAJAH: Molecular recognition via base-pairing. *J. Chem. Soc. Rev.* **2007**, *36*, 314–325.
- SHARMA, C V K.: Crystal engineering—where do we go from here? *Cryst. Growth Des.* **2002**, *2*, 465–474.
- SHEKHAH, O.; WANG, H.; PARADINAS, M.; OCAL, C.; SCHÜPBACH, B.; TERFORT, A.; ZACHER, D.; FISCHER, R. A.; WÖLL, C.: Controlling interpenetration in metal-organic frameworks by liquid-phase epitaxy. *Nat. Mater.* **2009**, *8*, 481–484.
- SHELDRIK, G. M.: SHELXL-97, Programs for X-ray crystal structure refinement. University of Göttingen: Göttingen, Germany, 1997.
- SHELDRIK, W. S.; HAGEN-ECKHARD, H. S.; HEEB, S.: Preparation and structural characterization of tetranuclear (η⁶-benzene)ruthenium(II) complexes with bridging N-donor ligands. *Inorg. Chim. Acta* **1993**, *206*, 15–21.
- SING, K.: The use of nitrogen adsorption for the characterisation of porous materials. *Colloids and Surfaces A: Physicochem. Eng. Aspects* **2001**, *187–188*, 3–9.
- SING, K. S. W.; EVERETT, D. H.; HAUL, R. A. W.; MOSCOU, L.; PIEROTTI, R. A.; ROUQUÉROL, J.; SIEMIENIEWSKA, T.: Reporting physisorption data for gas/solid systems with special reference to the determination of surface area and porosity. *Pure Appl. Chem.* **1985**, *57*, 603–619.

- SINGH, U. C.; KOLLMAN, P.A.: An approach to computing electrostatic charges for molecules. *J. Comput. Chem.* **1984**, *5*, 129–145.
- SIVAKOVA, S.; ROWAN, S. J.: Nucleobases as supramolecular motifs. *Chem. Soc. Rev.* **2005**, *34*, 9–21.
- SLETTEN, E.: Crystallographic studies of metal–nucleotide base complexes. I. Triclinic bis–(6–aminopurine)copper(II) tetrahydrate. *Acta Crystallogr.* **1969**, *B25*, 1480–1491.
- SLETTEN, E.; RUUD, M.: Crystallographic studies on metal–nucleotide base complexes. V. Tetraaquo–bis–(9–methyladenine)–copper(II) dichloride dehydrate. *Acta Crystallogr. Sect. B: Struct. Crystallogr. Cryst. Chem.* **1975**, *B31*, 982–985.
- SMITH, D. P.; OLMSTEAD, M. M.; NOLL, B. C.; MAESTRE, M. F.; FISH, R. H.: Bioorganometallic chemistry. 2. Synthesis and structural studies of the reactions of a nucleobase 1–methylcytosine with a (η^5 –pentamethylcyclopentadienyl)rhodium aqua complex. *Organometallics* **1993**, *12*, 593–596.
- SIMARD, M.; SU, D.; WUEST, J. D.: Use of hydrogen bonds to control molecular aggregation. Self–assembly of three–dimensional networks with large chambers. *J. Am. Chem. Soc.* **1991**, *113*, 4696–4698.
- SONG, Y.; YIN, X.; TU, B.; PANG, Q.; LI, H.; REN, X.; WANG, B.; LI, Q.: Metal–organic frameworks constructed from mixed infinite inorganic units and adenine. *CrystEngComm.* **2014**, *16*, 3082–3085.
- SONNENFROH, D.; KREILICK, R. W.: Exchange coupling in copper dimers with purine ligands. *Inorg. Chem.* **1980**, *19*, 1259–1262.
- SPEK, A. L.: Single–crystal structure validation with the program PLATON. *J. Appl. Crystallogr.* **2003**, *36*, 7–13.
- SPEK, A. L.: Structure validation in chemical crystallography. *Acta Crystallogr.* **2009**, *D65*, 148–155.
- SPOKOYNY, A. M.; KIM, D.; SUMREIN, A.; MIRKIN, C. A.: Infinite coordination polymer nano– and microparticle structures. *Chem. Soc. Rev.* **2009**, *38*, 1218–1227.
- STOE & CIE ,X–AREA, Main Menu Version 1.15, Stoe & Cie GmbH, Darmstadt, Germany, 2001.
- SUGGS, J. W., DUBE, M. J.; NICHOLS, M.: Synthesis and structure of a product, formed during DNA nicking with a cyclometallated nuclease, consisting of an adenine bridging two palladium(II) complexes. *J. Chem. Soc. Chem. Commun.* **1993**, 307–309.
- SUN, D.; MA, S.; KE, Y.; COLLINS, D. J.; ZHOU, H.–C.: An interweaving MOF with high hydrogen uptake. *J. Am. Chem. Soc.* **2006**, *128*, 3896–3897.
- SUNDARALINGAM, M.; CARRABINE, J. A.: Stereochemistry of nucleic acids and their constituents: XIX. Copper binding sites and mechanism of G·C selective denaturation of

DNA. Crystal and molecular structures of guanine·copper(II) chloride and cytosine·copper(II) chloride complexes. *J. Mol. Biol.* **1971**, *61*, 287–309.

SUZUKI, T., IRÍA, Y.; MONJUSHIRO, H, KAIZAKI, S.: Cobalt(III) complexes of monodentate N9-bound adeninate (ade⁻), [Co(ade- κ N9)Cl(en)2]⁺ (en = 1,2-diaminoethane): syntheses, crystal structures, and protonation behaviors of the geometrical isomers. *Inorg. Chem.* **2004**, *43*, 6435–6444.

SZALDA, D. J.; MARZILLI, L. G.; KISTENMACHER, T. J.: Secondary interactions and their role in the molecular conformation of transition metal–pyrimidine complexes. Semichelation and interligand hydrogen bonding involving O(2) of cytosine in the complex [(N-salicylidene-N'-methylethylenediamine)(cytosine)copper(II)] nitrate monohydrate. *Inorg. Chem.* **1975**, *14*, 2076–2081.

TAQUI-KHAN, M. M.; KRISHNAMOORTHY, C. R.: Interaction of metal ions with monosubstituted purines. *J. Inorg. Nucl. Chem.* **1971**, *33*, 1417–1425.

TAYLOR, M. R.: Metal binding to nucleic acid constituents. The crystal structure of trichloroadeniniumzinc(II). *Acta Crystallogr. Sect. B* **29**, **1973**, 884–890.

TAYLOR, M. R.; WESTPHALEN, J. A.: A crystal structure containing the N(7)-H isomer of adenine. *Acta Crystallogr. Sect. A* **37** (S), **1981**, C63.

TAYLOR, R.; KENNARD, O.: Hydrogen-bond geometry in organic crystals. *Acc. Chem. Res.* **1984**, *17*, 320–326.

TAYLOR, J. M.; DAWSON, K. W.; SHIMIZU, G. K. H.: A water-stable Metal–Organic Framework with highly acidic pores for proton-conducting applications. *J. Am. Chem. Soc.* **2013**, *135*, 1193–1196.

TERZIS, A.; BEACUCHAMP, A. L.; RIVEST, R.: Crystal and molecular structure of diaquotetra- μ -adenine diaquodicopper(I) perchlorate dihydrate. [Cu₂(C₅N₅H₅)₄(H₂O)₂](ClO₄)₄ · 2H₂O. *Inorg. Chem.* **1973**, *12*, 1166–1170.

THEWALT, U.; BUGG, C. E.; MARSH, R. E.: The crystal structure of guanine monohydrate. *Acta Crystallogr. Sect. B: Struct. Crystallogr. Cryst. Chem.* **1971**, *27*, 2358–2362.

THOMAS-GIPSON, J.; BEOBIDE, G.; CASTILLO, O.; CEPEDA, J.; LUQUE, A.; PÉREZ-YÁÑEZ, S.; AGUAYO, A. T.; ROMÁN, P.: Porous supramolecular compound based on paddle-wheel shaped copper(II)-adenine dinuclear entities. *CrystEngComm.* **2011**, *13*, 3301–3305.

THOMAS-GIPSON, J.; BEOBIDE, G.; CASTILLO, O.; FRÖBA, M.; HOFFMANN, F.; LUQUE, A.; PÉREZ-YÁÑEZ, S.; ROMÁN, P.: Paddle-wheel shaped copper (II) adenine discrete entities as supramolecular building blocks to afford porous supramolecular metal-organic frameworks. *Cryst. Growth Des.* **2014**, *14*, 4019–4029.

- THOMAS–GIPSON, J.; PÉREZ–AGUIRRE, R.; BEOBIDE, G.; CASTILLO, O.; LUQUE, A.; PÉREZ–YÁÑEZ, S.; ROMÁN, P.: Unravelling the growth of supramolecular metal–organic frameworks based on metal–nucleobase entities. *Cryst. Growth Des.* **2015**, *15*, 975–983.
- TORNITA, K.; IZUNO, T.; FUJIWARA, T.: Biologically important ternary coordination complex. Crystal and molecular structures of adenine–glycylglycine–copper (II) complex. *Biochem. Biophys. Res. Commun.* **1973**, *54*, 96–99.
- TRAN QUI, D.; PALACIOS, E.: Syntheses and structure of cytosine dichloride cuprate: Direct bonding of copper to cytosine. *Acta Crystallogr. Sect. C: Cryst. Struct. Commun.* **1990**, *C46*, 1220–1223.
- TRAN QUI, D.; BAGIEU, M.: Synthesis and structure of cytosine cobalt dichloride. *Acta Crystallogr. Sect. C: Cryst. Struct. Commun.* **1990**, *46*, 1645–1647.
- TROVO, G.; VALLE, G.; LONGATO, B.: 1–Methylcytosine and cytidine complexes of platinum(II) stabilized by trimethylphosphine. Synthesis and characterization. *Dalton Trans.* **1993**, 669–673.
- TUREL, I.; PECANAC, M.; GOLOBIC, A.; ALESSIO, E.; SERLI, B.; BERGAMO, A.; SAVA, G.: Solution, solid state and biological characterization of ruthenium(III)–DMSO complexes with purine base derivatives. *J. Inorg. Biochem.* **2004**, *98*, 393–401.
- UEMURA, T.; YANAI, N.; KITAWAGA, S.: Polymerization reactions in porous coordination polymers. *Chem. Soc. Rev.* **2009**, *38*, 1228–1236.
- VAN DE VOORDE, B.; BUEKEN, B.; DENAYER, J.; DE VOS, D.: Adsorptive separation on metal–organic frameworks in the liquid phase. *Chem. Soc. Rev.* **2014**, *43*, 5766–5788.
- VAN NIEKERK, J. N.; SCHOENING, F. R. L.: A new type of copper complex as found in the crystal structure of cupric acetate, $\text{Cu}_2(\text{CH}_3\text{COO})_4 \cdot 2\text{H}_2\text{O}$. *Acta Crystallogr.* **1953**, *6*, 227–232.
- VERDEJO, B.; AGUILAR, J.; GARCÍA–ESPAÑA, E.: CO_2 Fixation by Cu^{2+} and Zn^{2+} complexes of a terpyridinophane aza receptor. Crystal structures of Cu^{2+} complexes, pH–metric, spectroscopic, and electrochemical studies. *Inorg. Chem.* **2006**, *45*, 3803–3815.
- VERMA, S.; MISHRA, A. K.; KUMAR, A.: The many facets of adenine: Coordination, crystal patterns, and catalysis. *Acc. Chem. Res.* **2010**, *43*, 79–91.
- VIJAY–KUMAR, S.; SAKORE, T. D.; SOBELL, H. M.: A crystalline end product produced by the hydrolytic cleavage of an RNA–like fragment by an organometallointercalator: 1,10–phenanthroline–platinum(II)–ethylenediamine–cytidine 3' monophosphate. *Nucleic Acids Res.* **1984**, *12*, 3649–3657.
- WANG, F.; TAN, Y. X.; ZANG, H.; ZHANG, H. X.; KANG, Y.; ZHANG, J.: A new approach towards tetrahedral imidazolate frameworks for high and selective CO_2 uptake. *Chem. Commun.* **2011**, *47*, 5828–5830.
- WANG, F.; KANG, Y.: Unusual cadmium(II)–adenine paddle–wheel units for the construction of a metal–organic framework with mog topology. *Inorg. Chem. Commun.* **2012**, *20*, 266–286.

- WANG, F.; XANG, H.; KANG, Y.; ZHANG, J.: Guest selectivity of a porous tetrahedral imidazolate framework material during self-assembly. *J. Mater. Chem.* **2012**, *22*, 19732–19737.
- WATSON, J. D.; CRICK, F. H.: Molecular structure of nucleic acids. *Nature* **1953**, *171*, 737–738.
- WIENKEN, M.; ZANGRANDO, E.; RANDACCIO, L.; MENZER, S.; LIPPERT, B.: Structural and solution study on binary peptide and ternary peptide–nucleobase complexes of palladium(II). *J. Chem. Soc. Dalton Trans.* **1993**, 3349–3357.
- WU, S.-M.; BAU, R. The structure of a platinum(II) complex of cytidine-3'-monophosphate. *Biochem. Biophys. Res. Commun.* **1979**, *88*, 1435–1442.
- WUEST, J. D.: Engineering crystals by the strategy of molecular tectonics. *Chem. Commun.* **2005**, 5830–5837.
- XIE, Z.; LI, T.; ROSI, N. L.; CARREON, M. A.: Alumina-supported cobalt-adeninate MOF membranes for CO₂/CH₄ separation. *J. Mater. Chem. A* **2014**, *2*, 1239–1241.
- YAGHI, O. M.; O'KEEFFE, M.; OCKWIG, N. W.; CHAE, H. K.; EDDAOUDI, M.; KIM, J.: Reticular synthesis and the design of new materials. *Nature* **2003**, *423*, 705–714.
- YAMADA, T.; OTSUBO, K.; MAKIURA, R.; KITAWAGA, H.: Designer coordination polymers: Dimensional crossover architectures and proton conduction. *Chem. Soc. Rev.* **2013**, *42*, 6655–6669.
- YAMANARI, K.; ITO, R.; YAMAMOTO, S.; KONNO, T.; FAYUHIRO, A.; FUJIOKA, K.; ARAKAWA, R.: Cyclic tetramers composed of rhodium(III), iridium(III) or ruthenium(II) half-sandwich and 6-purinethiones. *Inorg. Chem.* **2002**, *41*, 6824–6830.
- YANG, E.; LI, H.-Y.; WANG, F.; YANG, H.; ZHANG, J.: Enhancing CO₂ adsorption enthalpy and selectivity via amino functionalization of a tetrahedral framework material. *CrystEnggComm.* **2013**, *15*, 658–661.
- YANG, E.-C.; ZHAO, H.-K.; FENG, Y.; ZHAO, X.-J.: A Tetranuclear Cu(II)-based 2D aggregate with an unprecedented tetradentate μ_4 -N₁,N₃,N₇,N₉-adeninate nucleobase. *Inorg. Chem.* **2009**, *48*, 3511–3513.
- YANG, J.; SUDIK, A.; WOLVERTON, C.; SIEGEL, D. J.: High capacity hydrogen storage materials: attributes for automotive applications and techniques for materials discovery. *Chem. Soc. Rev.* **2010**, *39*, 656–675.
- YOON, M.; SUH, K.; NATARAJAN, S.; KIM, K.: Proton conduction in metal-organic frameworks and related modularly built porous solids. *Angew. Chem. Int. Ed.* **2013**, *52*, 2688–2700.
- ZACHER, D.; SKEKHAH, O.; WÖLL, C.; FISCHER, R. A.: Thin films of metal-organic frameworks. *Chem. Soc. Rev.* **2009**, *38*, 1418–1429.

- ZHANG, G.; LI, H.; ZHAO, F.; HU, H.; HUANG, H.; LI, H.; HAN, X.; LIU, R.; DONG, H.; LIU, Y.; KANG, Y.: A cobalt-based 3D porous framework with excellent catalytic ability for the selective oxidation of *cis*-cyclooctene. *Dalton Trans.* **2013**, 42, 9423–9427.
- ZHANG, J.; WOJTAS, L.; LARSEN, R. W.; EDDAOUDI, M.; ZAWOROTKO, M. J.: Temperature and concentration control over interpenetration in a metal–organic material. *J. Am. Chem. Soc.* **2009**, 131, 17040–17041.
- ZHANG, M.; BOSCH M.; GENTLE, T.; ZHOU, H.–C.: Rational design of metal–organic frameworks with anticipated porosities and functionalities. *CrystEnggComm.* **2014**, 16, 4069–4083.
- ZHANG, T.; LIN, W.: Metal–organic frameworks for artificial photosynthesis and photocatalysis. *Chem. Soc. Rev.* **2014**, 43, 5982–5993.
- ZHANG, X.–H.; HAO, Z.–M.; ZHANG, X.–M.: Spin canting and metamagnetism in the first hybrid cobalt–hypoxanthine open framework with umr topology. *Chem. Eur. J.* **2011**, 17, 5588–5594.
- ZHANG, Z. J.; ZHAO, Y. G.; GONG, Q. H.; LI, Z.; LI, J.: MOFs for CO₂ capture and separation from flue gas mixtures: The effect of multifunctional sites on their adsorption capacity and selectivity. *Chem. Comm.* **2013**, 49, 653–661.
- ZHAO, D.; TIMMONS, D. J.; YUAN, D.; ZHOU, H. C.: Tuning the topology and functionality of metal–organic frameworks by ligand design. *Acc. Chem. Res.* **2011**, 44, 123–133.
- ZHOU, H.–C.; KITAGAWA, S.: Metal–Organic Frameworks (MOFs). *Chem. Soc. Rev.* **2014**, 43, 5415–5418.

Chapter 6

Appendices

A.1 Chemicals

A.2 Instrumental techniques

A.3 IR Spectra

A.4 Thermogravimetric analysis

A.5 Experimental and theoretical adsorption measurements

A.6 Articles published from this work

APPENDICES

A.1. CHEMICALS

All chemicals employed for the synthesis of the compounds were of reagent grade and used as commercially obtained. Tables A.1.1 and A.1.2 gather the reactants, formula, commercial supplier (CS), assay (AS), molecular weight (MW), Chemical Abstracts Service number (CAS), and risk (R) and safety (S) statements for their manipulation.

Table A.1.1 Reactants used.

Name	Formula	CS	AS	MW (g/mol)	CAS	R	S
Cobalt(II) bromide	CoBr ₂	Aldrich	≥99%	218.75	7789–43–7	36–37–38	26–37–39–45–28A
Cobalt(II) chloride hexahydrate	CoCl ₂ ·6H ₂ O	Merck	≥99%	237.93	7791–13–1	49–60–22–42/43–68–50/53	53–45–60–61
Cobalt(II) nitrate hexahydrate	Co(NO ₃) ₂ ·6H ₂ O	Fluka	≥99%	291.03	10026–22–9	8–22–40–43–50/53	17–36/37–60–61
Cobalt(II) sulphate heptahydrate.	Co(SO ₄) ₇ ·7H ₂ O	Aldrich	≥99%	281.1	10026–24–1	49–60–22–42/43–68–50/53	–
Copper(II) acetate monohydrate	Cu(CH ₃ COO) ₂ ·H ₂ O	Scharlau	≥99%	199.65	6046–93–1	22.41–50/53	26–39–46–61
Copper(II) bromide	CuBr ₂	Fluka	≥99%	223.36	7789–45–9	–	–
Copper(II) chloride dihydrate	CuCl ₂ ·2H ₂ O	Merck	≥99%	170.48	10125–13–0	24/25	20–37–44
Copper(II) sulphate pentahydrate	CuSO ₄ ·5H ₂ O	Merck	≥99%	249.68	7758–99–8	22–36/38–50/53	2–22–60–61
Hydrochloric acid	HCl	Fluka	≥37%	36.46	7647–01–0	280–314–339	261–280–305+351+338–310–410+403
n-Pentyl amine	C ₅ H ₁₃ N	Fluka	≥98%	87.17	110–58–7	11–20/21/22–34	16–26–33–36/37/39–45
Potassium bromide	KBr	Aldrich	≥99%	119.00	7758–02–3	20–21–22–36/37/38	22–36
Zinc(II) chloride	ZnCl ₂	Merck	≥98%	136.28	7646–85–7	22–34–50/53	1/2–26–36/37/39–45–60–61

Table A.1.2 Ligands used

Name	Formula	CS	AS	MW (g/mol)	CAS	R	S
6-chloropurine	C ₅ H ₃ ClN ₄	Aldrich	≥99%	154.6	87–42–3	22	
6-thioguanine	C ₅ H ₅ N ₅ S	Aldrich	≥98%	167.19	154–42–7		
9-methyl adenine	C ₆ H ₇ N ₅	Aldrich	≥97%	149.16	700–00–5	22	
Adenine	C ₅ H ₅ N ₅	Aldrich	≥99%	135.13	73–24–5	22	²⁶ –36
Cytosine	C ₄ H ₅ N ₃ O	Aldrich	≥97%	111.1	71–30–7		24/25

A.2 INSTRUMENTAL TECHNIQUES

A.2.1. Density measurements

Density measurements of the synthesized compounds have been performed on single-crystals by means of the flotation method.¹⁸² The preparation of the mixtures was made employing trichloromethane (CHCl_3 : $\rho = 1.48 \text{ g cm}^{-3}$), carbon tetrachloride (CCl_4 : $\rho = 1.59 \text{ g cm}^{-3}$), and bromoform (CHBr_3 : $\rho = 2.89 \text{ g cm}^{-3}$).

A.2.2. Quantitative analysis

Elemental analyses (C, H, N) were performed on a Euro EA Elemental Analyzer, whereas the metal content was determined by inductively coupled plasma (ICP–AES) performed on a Horiba Yobin Yvon Activa spectrometer, provided by the SGIker of the University of the Basque Country (UPV/EHU).

A.2.3. Infrared spectroscopy

The IR spectra were recorded on a FTIR 8400S Shimadzu spectrometer of the Inorganic Department of the Science and Technology Faculty of the UPV/EHU in the $4000\text{--}400 \text{ cm}^{-1}$ spectral region. KBr pellets were prepared, with an approximate concentration of 2–3%. The potassium bromide was of spectroscopic quality and was previously dried at $130 \text{ }^\circ\text{C}$. The pellets were obtained at a pressure of 10 Tm.



Figure A.2.1: FTIR spectrophotometer 8000S Shimadzu.

¹⁸² Román, P.; Gutiérrez–Zorrilla, J. M. *J. Chem. Educ.* **1985**, *62*, 167.

A.2.4. Thermal analysis

The thermogravimetric studies (TG, DTG, and DTA) were carried out in a TA Instruments SDT 2960 thermobalance of the Inorganic Department of the Science and Technology Faculty of the UPV/EHU. The measures were performed in an atmosphere of synthetic air (79% N₂ / 21% O₂) with a flow rate of 150 cm³ min⁻¹, between 25 and 800 °C, with a heating rate of 5 °C min⁻¹.



Figure A.2.2: Thermobalance TA instrument SDT 2960.

A.2.6. Single-crystal X-ray diffraction

The single crystal X-ray diffraction data collections were done at 293(2) K and at 100(2) K on an Oxford Diffraction Xcalibur ($\lambda_{\text{Mo-K}\alpha} = 0.71073 \text{ \AA}$), STOE IPDS ($\lambda_{\text{Mo-K}\alpha} = 0.71073 \text{ \AA}$), and on an Agilent Technologies Supernova ($\lambda_{\text{Mo-K}\alpha} = 0.71073 \text{ \AA}$ and $\lambda_{\text{Cu-K}\alpha} = 1.5418 \text{ \AA}$) diffractometers of the SGIKer of the UPV/EHU.



(a)



(b)

Figure A.2.3: Single crystal X-ray diffractometer (a) Oxford Diffraction Xcalibur and (b) Stoe IPDS 2T.

The data reduction was done with the CrysAlis PRO¹⁸³ and X-RED programs. Most of the structures were solved by direct methods using the SIR92¹⁸⁴ program and refined by full-matrix least-squares on F^2 including all reflections (SHELXL97),¹⁸⁵ with all calculations performed using the WINGX crystallographic software package.¹⁸⁶ Geometrical calculations were performed with the program PLATON.¹⁸⁷

A.2.7. X-ray powder diffraction

The X-ray powder diffraction patterns were collected on a Philips X'PERT powder diffractometer of the SGIker of the UPV/EHU with Co-K α radiation ($\lambda = 1.5418 \text{ \AA}$) over the range $5 < 2\theta < 50^\circ$ with a step size of 0.02° and an acquisition time of 2.5 S per step at 25°C . Indexation of the diffraction profiles were made by means of the FULLPROF program (pattern-matching analysis)¹⁸⁸ on the basis of the space group and the cell parameters found for isostructural compounds by single crystal X-ray diffraction. The calculated and observed diffraction patterns are shown in Figures A.3.1–11.

A Bruker D8 Advance Vario powder diffractometer of the SGIker of the UPV/EHU with Cu-K α ($\lambda = 1.5406 \text{ \AA}$) was used to perform the variable-temperature X-ray powder diffraction measurements, heating the samples from room temperature with a heating rate of $5^\circ\text{C}\cdot\text{min}^{-1}$ and measuring a complete diffractogram every 20 or 30 $^\circ\text{C}$ as appropriate.

A.2.8. Adsorption measurements

Micromeritics ASAP 2020 surface area and porosity analyser was used for carbon dioxide at 298 K and 273 K (Grant GR150 thermostatic refrigerated bath) and carbon monoxide (273 K) adsorption experiments. Hiden IGA automatic gravimetric porosimeter was used to collect adsorption isotherms at 196 K (ethanol/dry ice mixture) up to 900 mbar. Adsorption isotherms of N_2 were measured at 77 K using a Micromeritics Tristar II 3020.

¹⁸³ CrysAlis PRO, version 1.171.33.55; Oxford Diffraction: Wroclaw, Poland, 2010.

¹⁸⁴ Altomare, A. et al. *J. Appl. Cryst.* **1993**, 26, 343.

¹⁸⁵ Sheldrick, G. M. *SHELXL-97, Programs for X-ray Crystal Structure Refinement*; University of Göttingen: Göttingen, Germany, 1997.

¹⁸⁶ Farrugia, L. J. *J. Appl. Cryst.* **1999**, 32, 837.

¹⁸⁷ Spek, A. L. *Acta Crystallogr.* **2009**, D65, 148.

¹⁸⁸ (a) Rodríguez-Carvajal, J. *FULLPROF, a Program for Rietveld Refinement and Pattern Matching Analysis*; Abstracts of the Satellite Meeting on Powder Diffraction of the XVth Congress of the IUCr.: Toulouse, France, 1990, 127. (b) Rodríguez-Carvajal, J. *FULLPROF 2000*, version 2.5d, Laboratoire Léon Brillouin (CEA-CNRS), Centre d'Études de Saclay, Gif sur Yvette Cedex: France, 2003.

Approximately 0.1 g of sample was used for analysis and placed in a glass bulb which is sealed with a rubber seal frit to prevent exposure to the atmosphere. Generally, the material is activated to remove all solvent from the pores by heating and under vacuum for 12 hours prior to adsorption.

A3: IR SPECTRA

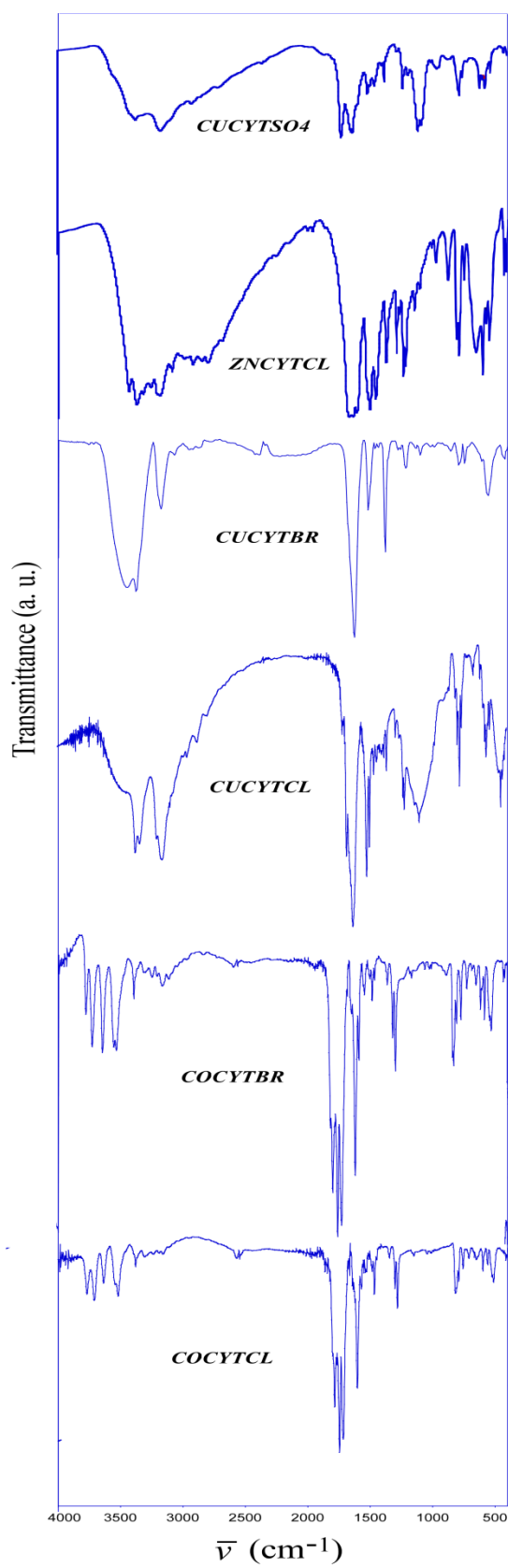


Figure A.3.1: IR spectra of Metal-Cytosine compounds.

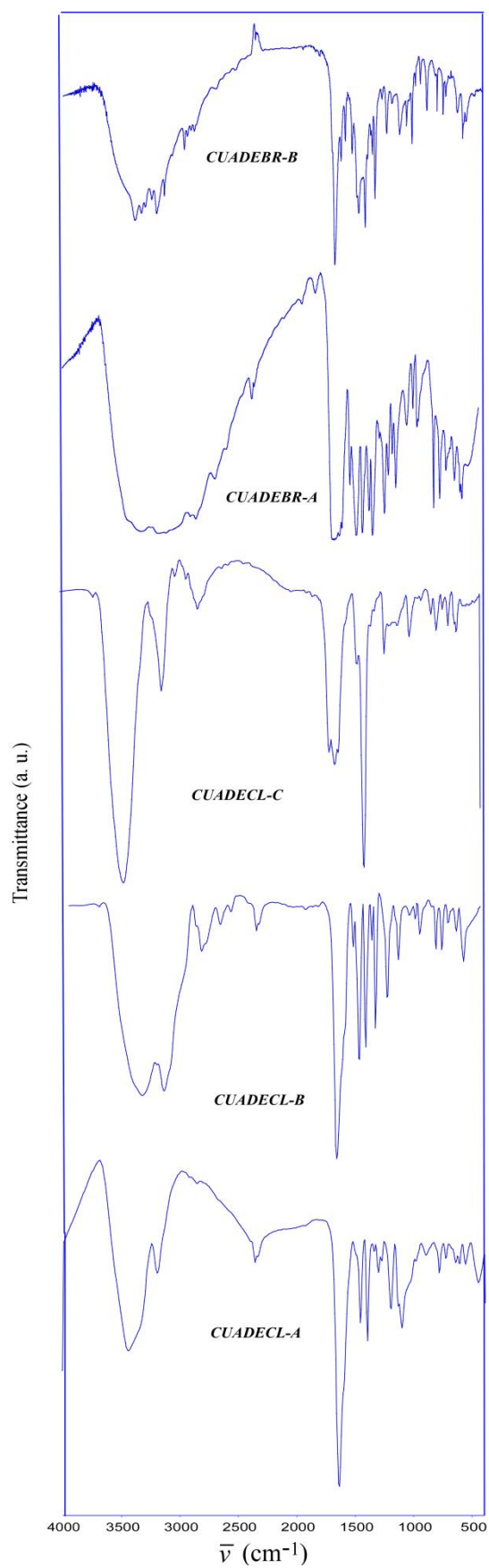


Figure A.3.2: IR spectra of Metal-Adenine compounds.

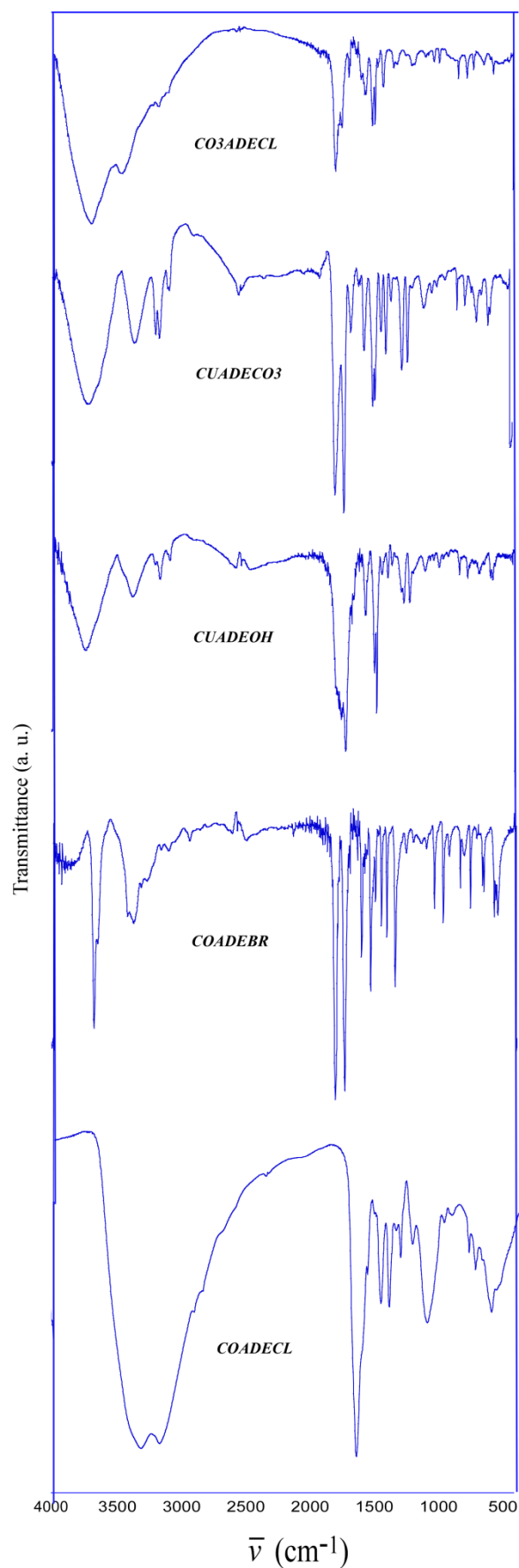


Figure A.3.3: IR spectra of Metal-Adenine compounds.

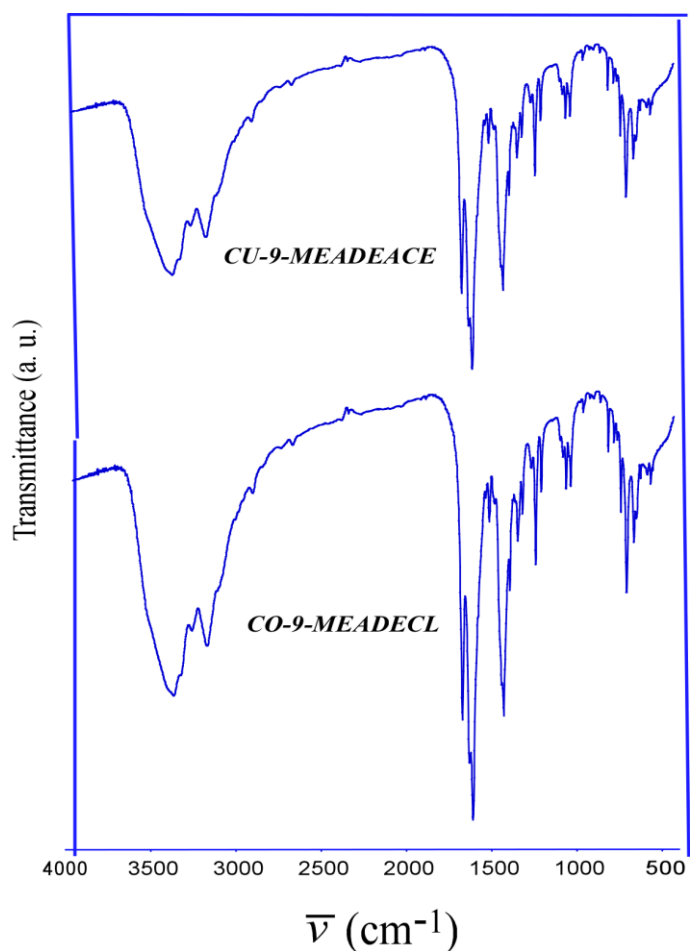


Figure A.3.4: IR spectra of *CU-9-MEADEACE* and *CO-9-MEADECL*.

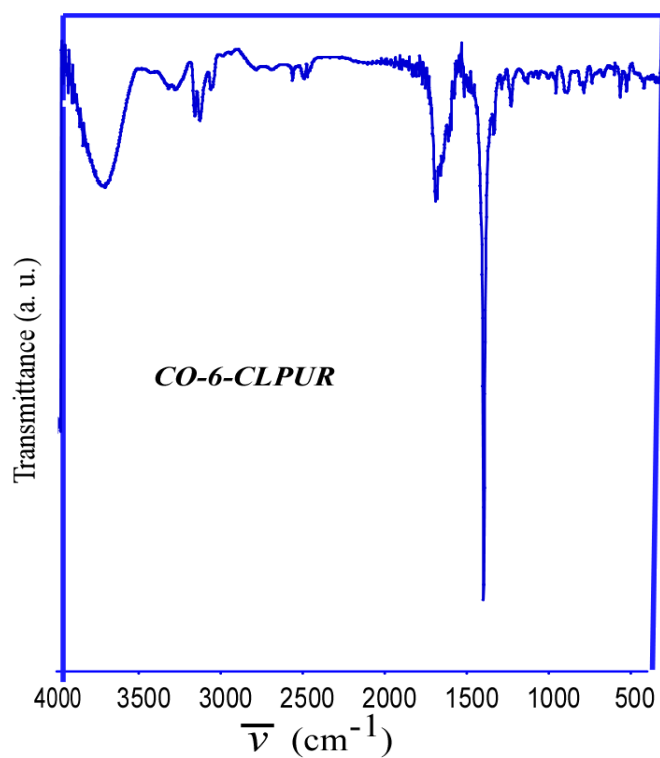


Figure A.3.5: IR spectra of *CO-6-CLPUR*.

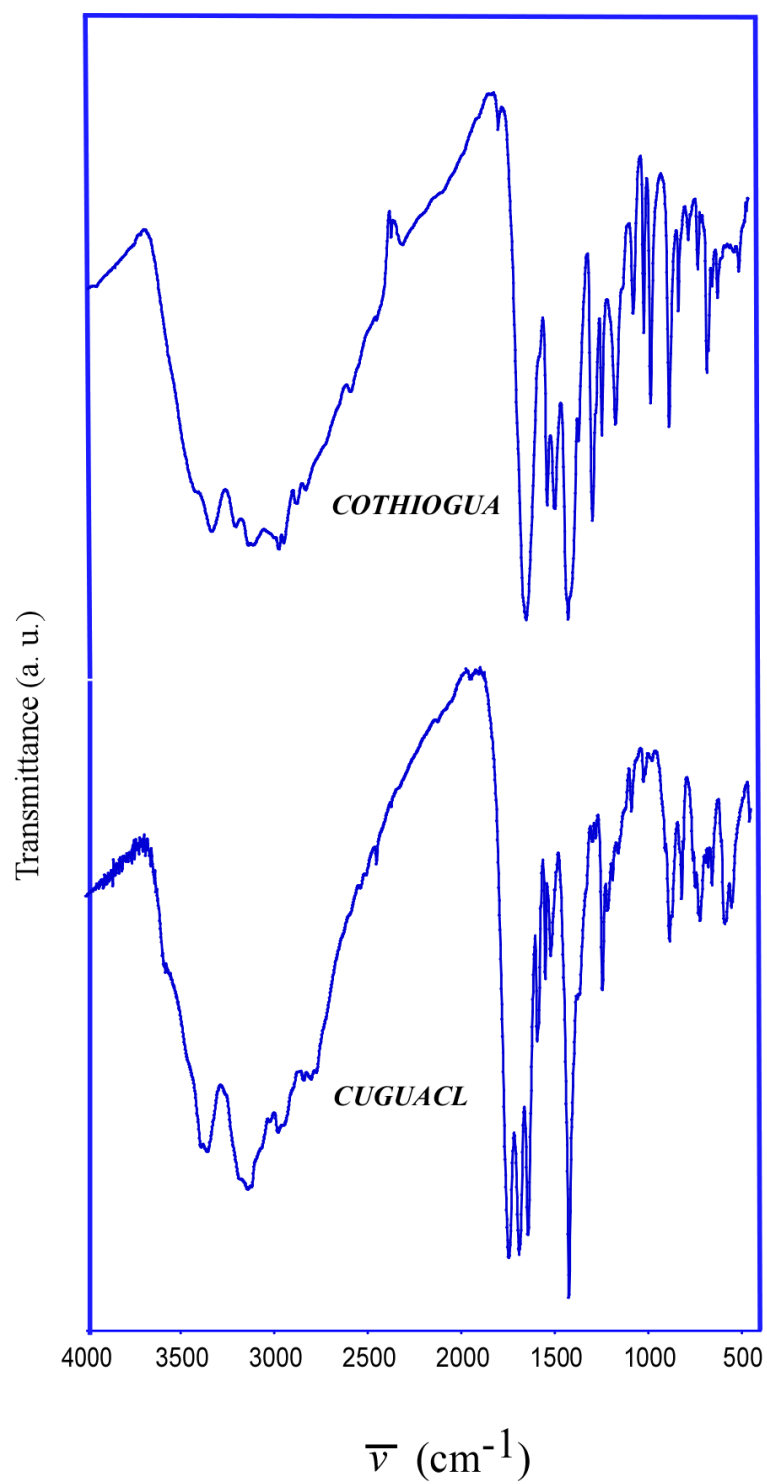


Figure A.3.6: IR spectra of *CUGUACL* and *CO-6-THIOG*.

A4: THERMOGRAVIMETRIC ANALYSIS

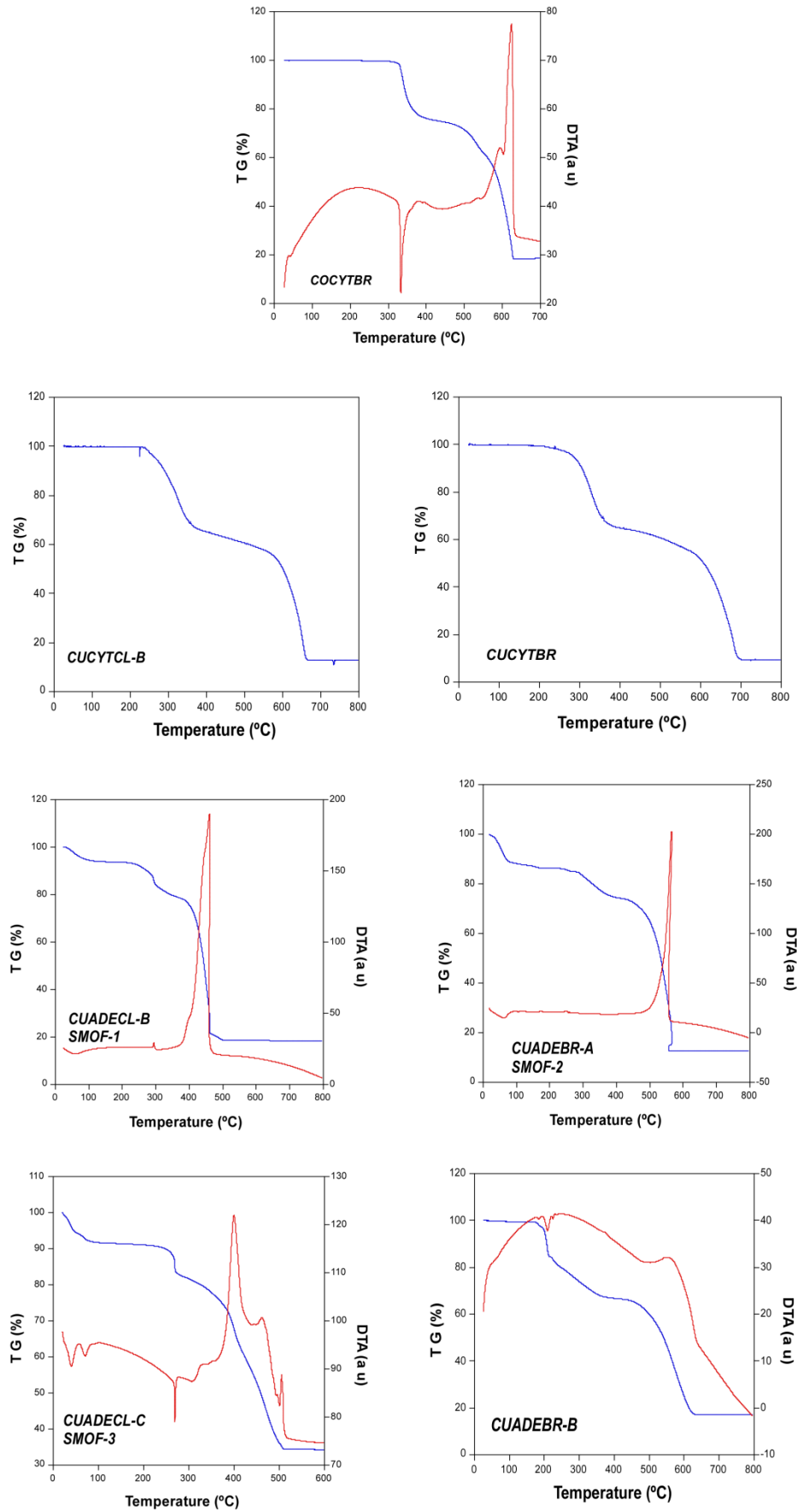


Figure A.4.1: Thermogravimetric analysis.

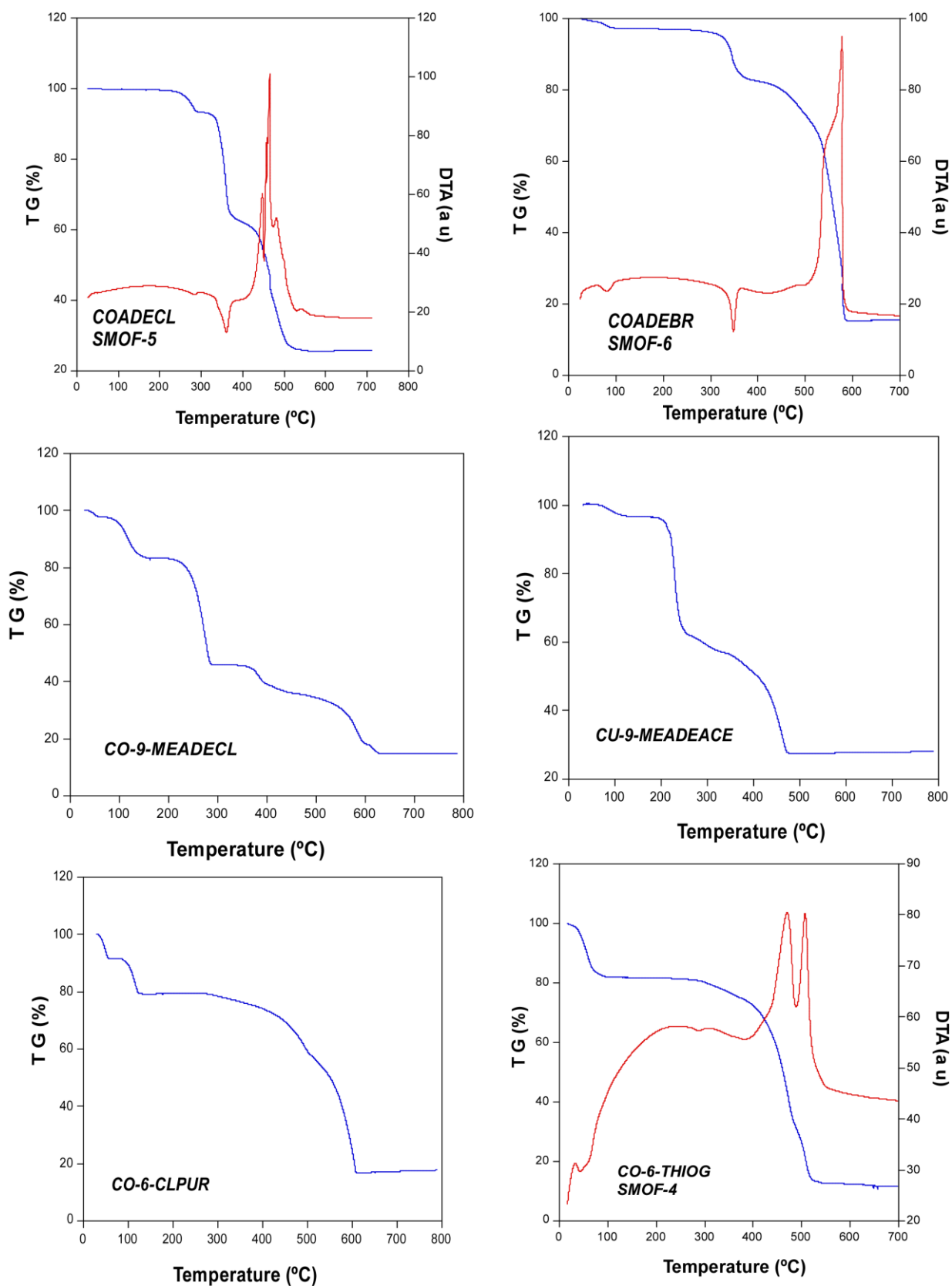


Figure A.4.1 (contd.): Thermogravimetric analysis.

A5: EXPERIMENTAL AND THEORETICAL ADSORPTION MEASUREMENTS

A.5.1. Introduction

The measurement of the adsorption of gases is widely used to determine the surface area, pore volume and pore size distribution of porous solids.¹⁸⁹ The use of selected molecules can also provide information on the pore connectivity and surface chemistry. Adsorption is performed at a constant temperature while the pressure is varied, and it can be measured volumetrically (the amount of adsorption is inferred from pressure measurements made before and after the measurement) or gravimetrically (the sample is weighted as the pressure of the adsorbate is increased, correlating the increase in weight of the sample to the uptake). The uptake of gas can be expressed as an equivalent volume at standard pressure, as a true volume or mass, or as moles per gram. This is plotted against the equilibrium pressure (p/p_0) at a constant temperature, and the plot is an isotherm of the adsorbate uptake. Figure A.5.1 shows the different types of adsorption isotherms which complete the IUPAC classification.¹⁹⁰

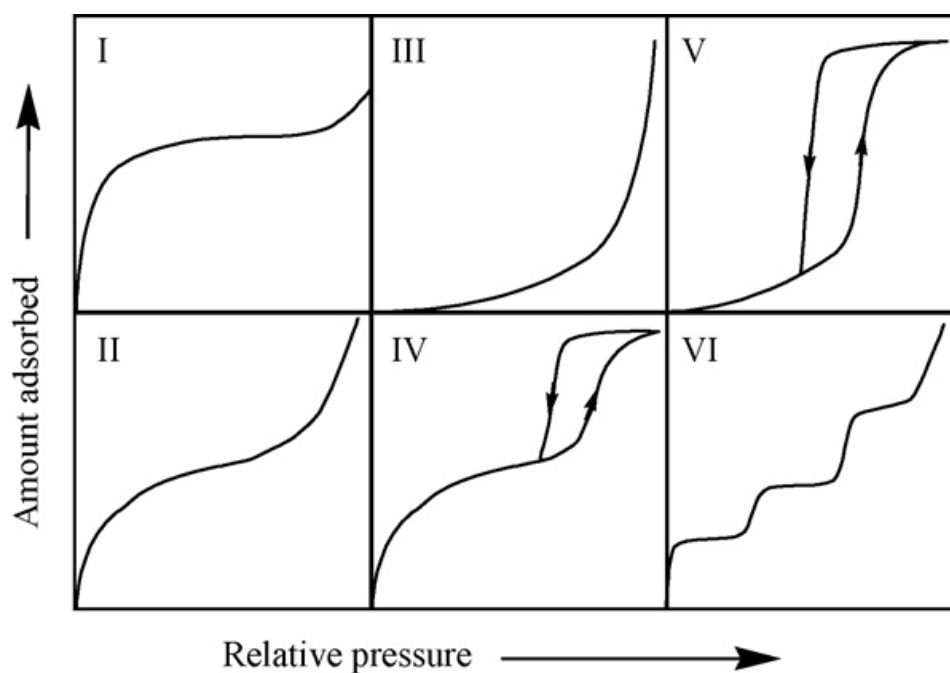


Figure A.5.1: Different types of adsorption isotherms

Type I isotherms are characteristic of microporous materials. The initial step section of the isotherm corresponds to monolayer deposition inside the micropores. Once the pores are

¹⁸⁹ Sing, K. *Colloids and Surfaces A: Physicochem. Eng. Aspects*, **2001**, 187–188, 3.

¹⁹⁰ (a) Brunauer, S. et al. *J. Am. Chem. Soc.* **1940**, 62, 1723. (b) Sing, K. S. W. et al. *Pure Appl. Chem.* **1985**, 57, 603. (c) Rouquerol, J. et al. *Pure Appl. Chem.* **1994**, 66, 1739.

filled, there is little extra room for adsorption and so the isotherm reaches a saturation value quickly. Condensation of the gas at high partial pressures results in an increase in uptake. Type II and IV isotherms are found from non-porous materials or mesoporous structures. Type II characterises monolayer coverage at low pressures, a plateau when all energetically favourable sites have been covered, and multilayers at higher pressures. The hysteresis effect in type IV isotherms is due to the different energetics of condensation on the surface of the pore and evaporation away from the pore (the curvature of the surfaces is different in the forward and reverse direction). When molecules in a gas have a stronger affinity for each other than for the surface of the adsorbant, type III and V isotherms are found. Type VI isotherms result from distinct monolayers being built up on a surface. For this it requires a material with a very uniform surface and no preferential adsorbant sites.

A.5.2. Langmuir theory

Langmuir theory¹⁹¹ assumes that all sites on the surface are energetically equivalent and considers only the interactions between gas and surface (assuming that the interaction between gas molecules is negligible). The theory also assumes that during adsorption the collision of the gas with the surface is inelastic. Assuming that the gas forms only a monolayer on the surface gives V_a , volume adsorbed at a certain pressure, P :

$$V_a = \frac{V_m bP}{1 + bP} \quad (\text{A.5.1})$$

where V_m is the quantity of gas that covers the whole surface in a monolayer and b is an empirical constant. Manipulation of this equation gives:

$$\frac{P}{V_a} = \frac{1}{V_m P} + \frac{P}{V_m} \quad (\text{A.5.2})$$

A plot of P/V_a vs. P should give a straight line in situations where the Langmuir equation applies, with a gradient equal to $1/V_m$ and a y-intercept of $1/V_m b$. The surface area of the adsorbant can be estimated by using the calculated value of V_m in the equation:

$$s = \frac{V_m \sigma N_A}{mV_0} \quad (\text{A.5.3})$$

¹⁹¹ Langmuir, I. *J. Am. Chem. Soc.* **1916**, 38, 2221.

where s is the area of the surface covered by a single gas molecule, m is the mass of the adsorbing sample, N_A is the Avogadro constant and V_0 is the molar volume of the gas. Where nitrogen is used, the surface area covered by a molecule is 16.2 \AA^2 so the expression becomes:

$$s \left(\frac{m^2}{g} \right) = \frac{4.35 V_m (cm^3 @ STP)}{m(g)} \quad (\text{A.5.4})$$

A.5.3. BET Theory

BET (Brunauer, Emmett and Teller) theory¹⁹² advances Langmuir theory by incorporating the effect of multilayer gas adsorption. It assumes that the force behind the binding of the gas to a surface is the same as those forces accounting for condensation of gases. The BET method equates the rate of condensation of the gas onto a monolayer with the evaporation of the gas away from the monolayer and then sums this effect over an infinite number of layers to give the BET equation.

$$V_a = \frac{V_m C P}{(P_0 - P) \left[1 + (C - 1) \frac{P}{P_0} \right]} \quad (\text{A.5.5})$$

Where C is a constant and P_0 is the saturation pressure of the gas. C relates to the heat of adsorption of the first layer, q_1 , and the heat of liquifaction, q_L , by the relationship:

$$C \propto \exp \frac{q_1 - q_L}{RT} \quad (\text{A.5.6})$$

Where R is the gas constant and T is the absolute temperature of the measurement. This equation can be written in the linear form:

$$\frac{P}{V_a (P_0 - P)} = \frac{1}{V_m C} + \frac{C - 1}{V_m C} \left(\frac{P}{P_0} \right) \quad (\text{A.5.7})$$

A plot of $P/[V_a(P_0 - P)]$ vs. (P/P_0) can determine V_m and C from the intercept and slope of a regression line. The surface area can be calculated from the volume of the monolayer, by assuming that gas molecules at the surface are close packed and by using the formula:

¹⁹² Brunauer, S. et. al. *J. Am. Chem. Soc.* **1938**, *60*, 309.

$$\sigma = (4) (0.866) \left[\frac{M}{4(2N_A \ell)^{1/2}} \right]^{2/3} \quad (\text{A.5.8})$$

where σ is the mean area per molecule, M is the molecular weight, N_A is Avogadro's number and ρ is the density of the liquid adsorbate. Pore volume per unit mass can be assessed from the maximum uptake by assuming that the nitrogen adsorbed on the surface at 77 K will have the same density as liquid nitrogen.

A.5.4. Atomistic simulations for the determination of the adsorption properties.

A.5.4.1. Computational method details.

Force-field based Grand Canonical Monte Carlo (GCMC) simulations of single component (N_2 , CO_2 and H_2) adsorption were carried out using the SORPTION module included in the Accelrys "Materials Studio" package.¹⁹³ The theoretical background of GCMC simulations is described in detail elsewhere.¹⁹⁴ For comparison with experimental data, simulations of single-component isotherms were carried out under the same conditions for each adsorbate ($P < 1$ bar; N_2 at 77 K, CO_2 at 196, 273, and 298 K; H_2 at 77K). The simulations of adsorption isotherms involved 4 million equilibration steps and 6 million production steps.

A.5.4.2. Models of fluid molecules

In all simulations, dispersive and electrostatic interactions were taken into account. Dispersive interactions were modelled using a Lennard-Jones 12-6 potential. Parameters to represent the interaction between different atom types were calculated using Lorentz-Berthelot mixing rules. A cutoff radius of 12.5 Å was employed for dispersive interactions. Electrostatic interactions were modelled by assigning point charges to the atomic sites, and an Ewald summation was used to account for the periodicity of the simulation box. The representation of the models and parameters used for the fluid molecules are gathered in Figure A.5.2 and Table A.5.1, respectively.

¹⁹³ *Materials Studio v. 5.5*; Accelrys Inc. 2011.

¹⁹⁴ (a) Allen, M. P.; Tildesley, D. J. *Computer simulation of liquids*, 1987. (b) Frenkel, D.; Smit, B. *Understanding molecular simulation: from algorithms to applications*, 2002.

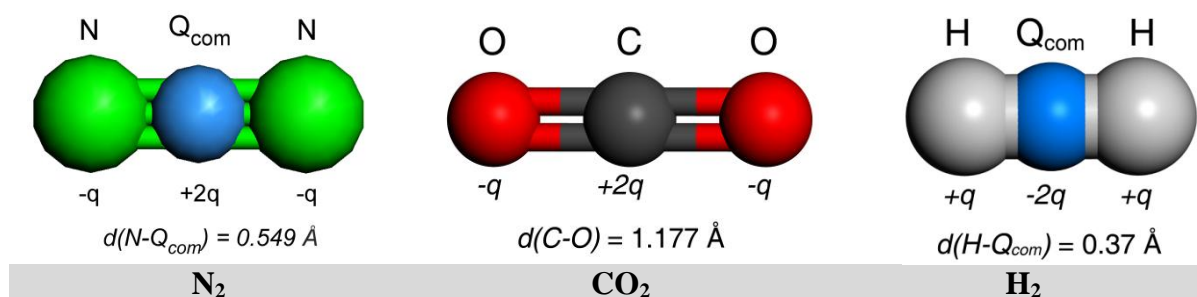


Figure A.5.2. Models for N₂, CO₂ and H₂.

The selection of the models and parameters used to define the fluid molecules have been done based on previous studies. For the N₂ molecule, the LJ parameters were taken from the TraPPE model.¹⁹⁵ This model simulates the quadrupolar moment of the N₂, placing two negative charges (−0.482) in the positions of the nitrogen atoms and a positive one in the centre of mass (+0.964). The LJ parameters used to represent the CO₂ interactions were taken from the work of García–Sánchez and coworkers,¹⁹⁶ and consist of a modified version of the TraPPE potential model. The combination of these parameters with the distribution of the charges calculated in a previous work has proved to be suitably adjusted to experimental data of different MOFs.¹⁹⁷

Table A.5.1. Lennard–Jones parameters and point charges.

	$r_0 / \text{Å}$	$D_0 / \text{kJ mol}^{-1}$	q / e
N₂			
N	3.7153	0.2993	−0.482
Q _{com}	—	—	+0.964
CO₂			
C	3.0811	0.2444	+0.5810
O	3.3865	0.7121	−0.2905
H₂(77K)			
H	3.4394	2.0503	—
H₂(298K)			
H	—	—	−0.4705
Q _{com}	3.3225	0.2844	−0.9410
CO			
C	—	—	−0.75
Q _{com}	4.2238	0.8330	1.60
O	—	—	−0.85

¹⁹⁵ Potoff, J. J.; Siepmann, J. I. *AIChE J.* **2001**, *47*, 1676.

¹⁹⁶ García–Sánchez, A. et al. *J. Phys. Chem. C*, **2009**, *113*, 8814

¹⁹⁷ Fischer, M. et al. *Chem. Phys. Chem.* **2010**, *11*, 2220.

A.5.4.3. Details on GCMC calculations

Calculation details: Force-field based GCMC simulations of N₂ and CO₂ were carried out using the SORPTION module included in the Accelrys “Materials Studio” package.¹⁹⁸ The theoretical background of GCMC simulations is described in detail many articles.¹⁹⁹ The selection of the models and parameters used to define the fluid molecules have been done based on previous studies. For the N₂ molecule, the LJ parameters were taken from the TraPPE model.¹⁹⁵ This model simulates the quadrupolar moment of the N₂, placing two negative charges (−0.482) in the positions of the nitrogen atoms and a positive one in the center of mass (+0.964). The LJ parameters used to represent the CO₂ interactions were taken from the work of García-Sánchez and coworkers²⁰⁰ and consist of a modified version of the TraPPE potential model. The structure of *CUADECL-B (SMOF-1)*., *CUADEBR-A (SMOF-2)* and *CUADECL-C (SMOF-3)* was taken from experimental data, for which all solvent molecules were removed. GCMC calculations were performed using 2x2x2-supercells. The LJ parameters for all the atoms of the adsorbents were taken from the Universal Force Field (UFF).²⁰¹ The partial charges to represent the electrostatic potential inside the pores were derived from DFT calculations, using the ESP method as described by Singh and Kollman,²⁰² which is implemented in the DMOL3 code.²⁰³ For this calculation the DNP basis set and the PBE exchange–correlation functional were selected²⁰⁴ and a dinuclear entity was used the finite cluster model.

Table A.5.2: Lennard–Jones parameters and partial charges

	$r_0 / \text{Å}$	$D_0 / \text{kJ mol}^{-1}$	q / e
N₂			
N	3.7153	0.2993	−0.482
Q _{com}	—	—	+0.964
CO₂			
C	3.0811	0.2444	+0.5810
O	3.3865	0.7121	−0.2905

¹⁹⁸ Materials studio version 5.5, **2011**, Accelrys Inc., San Diego,

¹⁹⁹ (a) Allen, M. P.; Tildesley, D. J. *Computer simulation of liquids*, Clarendon Press, Oxford, UK, 1st edn, 1987. (b) Frenkel, D.; Smit, B. *Understanding molecular simulation: from algorithms to applications*, Academic Press, San Diego, California, USA, 2nd edn. 2002.

²⁰⁰ García-Sánchez, A. et al. *J. Phys. Chem. C*, **2009**, *113*, 8814.

²⁰¹ Rappe, A. K. et al. *J. Am. Chem. Soc.* **1992**, *114*, 10024.

²⁰² Singh, U. C.; Kollman, P. A. *J. Comput. Chem.* **1984**, *5*, 129.

²⁰³ (a) Delley, B. *J. Chem. Phys.* **1990**, *92*, 508. (b) Delley, B. *J. Chem. Phys.* **2000**, *113*, 7756.

²⁰⁴ Perdew, J. P. et al. *Phys. Rev. Lett.* **1996**, *77*, 3865.

Table A.5.3: Resulting ESP charges upon the atoms of the structural models of the *CUADECL-B (SMOF-1)*, *CUADEBR-A (SMOF-2)*, *CUADECL-C (SMOF-3)* adsorbents.

Atom	q / e	Atom	q / e
<i>CUADECL-B (SMOF-1)</i>			
Cu	+0.7570	H61	+0.485
N1	-0.6520	H62	+0.497
C2	+0.5300	N7	-0.105
H2	+0.0620	H7	+0.134
N3	-0.6500	C8	+0.079
C4	+0.719	H8	+0.158
C5	-0.477	N9	-0.442
N6	-0.994	C11	-0.536
		C12	-1.000
<i>CUADEBR-A (SMOF-2)</i>			
Cu1	+0.451	H61	+0.340
N1	-0.289	H62	+0.336
C2	+0.089	N7	-0.357
H2	+0.265	H7	+0.309
N3	-0.454	C8	+0.142
C4	+0.392	H8	+0.245
C5	+0.140	N9	-0.373
N6	-0.550	Br1	-0.576
		Br2	-1.000
<i>CUADECL-C (SMOF-3)</i>			
Cu1	+0.638	H61	+0.491
N1	-0.730	H62	+0.489
C2	+0.645	N7	-0.018
H2	+0.027	H7	+0.297
N3	-0.813	C8	-0.008
C4	+1.010	H8	+0.182
C5	-0.633	N9	-0.497
N6	-1.093	C11	-0.467
		C12	-0.436

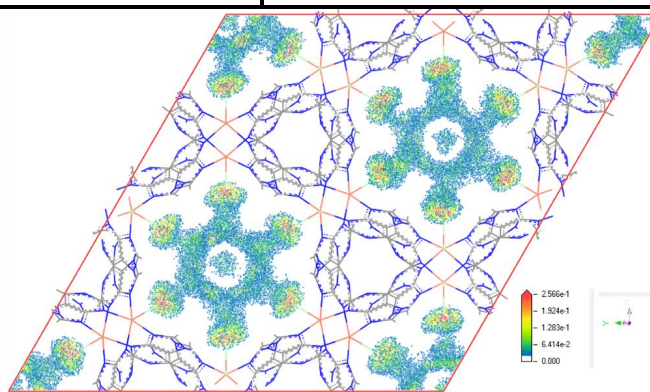


Figure A.5.3: Average occupation profiles for CO₂ at 298 K in *CUADECL-B (SMOF-1)*.

A6: ARTICLES PUBLISHED FROM THIS WORK

This work has led to the publication of several articles in international scientific journals which are listed below:

1. *Porous supramolecular compound based on paddle-wheel shaped copper(II)-adenine dinuclear entities*. Thomas-Gipson, J.; Beobide, G.; Castillo, O.; Cepeda, J.; Luque, A.; Perez-Yañez, S.; Aguayo, A. T.; Roman, P. *CrystEngComm*. **2011**, *13*, 3301–3305.
2. *Metal-carboxylato-nucleobase systems: From supramolecular assemblies to 3D porous materials*. Beobide, G.; Castillo, O.; Cepeda, J.; Luque, A.; Pérez-Yañez, S.; Román, P.; Thomas-Gipson, J.: *Coord. Chem. Rev.* **2013**, *257*, 2716–273.
3. *Paddle-wheel shaped copper (II) adenine discrete entities as supramolecular building blocks to afford porous supramolecular metal-organic frameworks*. Thomas-Gipson, J.; Beobide, G.; Castillo, O.; Fröba, M.; Hoffmann, F.; Luque, A.; Pérez-Yañez, S.; Román, P. *Cryst. Growth Des.* **2014**, *14*, 4019–4029.
4. *Unravelling the growth of supramolecular metal-organic frameworks based on metal-nucleobase entities*. Thomas-Gipson, J.; Pérez-Aguirre, R.; Beobide, G.; Castillo, O.; Luque, A.; Perez-Yañez, S.; Roman, P. *Cryst. Growth Des.* **2015**, *15*, 975–983.

Cite this: *CrystEngComm*, 2011, **13**, 3301

www.rsc.org/crystengcomm

Porous supramolecular compound based on paddle-wheel shaped copper(II)–adenine dinuclear entities†

J. Thomas-Gipson,^a G. Beobide,^a O. Castillo,^{*a} J. Cepeda,^a A. Luque,^a S. Pérez-Yáñez,^a A. T. Aguayo^b and P. Román^a

Received 11th February 2011, Accepted 28th February 2011

DOI: 10.1039/c1ce05195d

The reaction between CuCl₂ and adenine in a non-aqueous solvent provides a 3D porous structure based on paddle-wheel [Cu₂(μ-adenine)₄Cl₂]²⁺ cations and Cl[−] anions that are held together by a robust supramolecular hydrogen bonding network. The desolvated compound is able to host different guest molecules within the ~6 Å diameter 1D channels.

Crystal engineering comprises an understanding of intermolecular interactions that govern crystal packing.¹ Unfortunately, most of the supramolecular networks based on these non-covalent interactions lack the necessary stability required for many potential applications.² The ability to create permanent pores in supramolecular solids is considered as one of the biggest challenges in crystal engineering.³ Usually, formation of a porous solid requires that the network sustaining interactions are of sufficient strength to pay the energetic penalty for existence of the pores themselves.⁴ On the other hand, for these porous supramolecular frameworks to have technological relevance in gas storage, separation, catalysis or for the development of smart materials by combining other functionalities,⁵ it is highly desired to be thermally stable and robust enough to retain the porous structure even after the removal of guest molecules.⁶ There are few examples of molecular organic compounds that exhibit permanent porosity,⁷ but the number of examples of porous molecular crystal structures based on coordination complexes as building units is ever increasing, as the investigations into these molecular based porous materials are an up-and-coming field of research.⁸

At first sight, a reasonable strategy to obtain stable porous crystal structures is to use polynuclear coordination complexes as rigid tectons which can only establish hydrogen bonding interactions along specific directions by means of predictable supramolecular synthons.⁹ As a consequence of the rigidity of the tectons, in many cases, the resulting network is unable to occupy the whole space and presents

voids or channels that are usually occupied by solvent molecules. However, there are still many challenges to realize on these tailor-made porous materials because the pursued structural control is often thwarted by the delicate balance of all covalent and noncovalent forces present in the crystal framework, and a slight structural modification may result in the failure to achieve the desired supramolecular interaction scheme or even the overall three-dimensional (3D) architecture.¹⁰ For example, most of the syntheses methods are performed in aqueous media and the water molecule, a powerful donor and acceptor site of hydrogen bonds,¹¹ interferes with the desired hydrogen bonding network leading to indirect, water mediated, hydrogen bonds between the tectons affording a non-porous crystal framework. Sometimes the porous 3D structure is achieved but it is thermally unstable because of the well-known flexibility of the hydrogen bond orientation around the water molecules which allows the displacement of the rigid tectons without the rupture of the hydrogen bonds. So that the involvement of water molecules in the supramolecular assembly weakens the stability of the crystal building due to two effects: (a) the water molecules can be easily removed leading to the collapse of the overall crystal structure, as they are involved in the hydrogen bond network and (b) in the case of a hypothetical porous supramolecular network not based on water mediated hydrogen bonds, even the removal of only those solvent molecules placed in the channels may lead to the collapse of the crystal structure due to the flexibility of the remaining hydrogen bonding network.

Taking into account the above-mentioned ideas, we report herein the synthesis‡ and crystal structure§ of a robust supramolecular porous compound of Cu(II) and adenine with the formula [Cu₂(μ-adenine)₄Cl₂]₂·~2CH₃OH (**1**) which shows a high thermal stability. It has been obtained using methanol as solvent to avoid the instability of the 3D supramolecular architectures due to the presence of crystallization water molecules. Although a handful of covalent 2D and 3D coordination compounds have been reported^{12–14} exploiting the ability of the nucleobases to act as polydentate bridging ligands, as far as we are aware, compound **1** represents the first example of a robust porous 3D architecture based on adenine-containing complexes in which the self-assembling of the structural units is only driven by non-covalent interactions.

At room temperature crystals of compound **1** exhibit a blue colour but they undergo a gradual thermochromic transformation to give

^aDepartamento de Química Inorgánica, Facultad de Ciencia y Tecnología, Universidad del País Vasco, Apartado 644, E-48080 Bilbao, Spain. E-mail: oscar.castillo@ehu.es

^bDepartamento de Ingeniería Química, Facultad de Ciencia y Tecnología, Universidad del País Vasco, Apartado 644, E-48080 Bilbao, Spain

† Electronic supplementary information (ESI) available. CCDC reference numbers 785522 and 785523. For ESI and crystallographic data in CIF or other electronic format see DOI: 10.1039/c1ce05195d

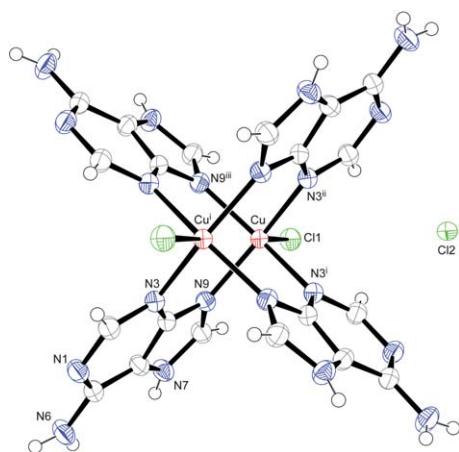


Fig. 1 Structural units of compound 1.

violet specimens at 100 K. The X-ray analysis at 293 K and 100 K revealed similar crystallographic parameters and the same crystal building so that the thermochromic properties can be probably attributed to subtle changes in the coordination polyhedron around the metallic centre.

The crystal structure is composed of paddle-wheel $[\text{Cu}_2(\mu\text{-adenine})_4\text{Cl}_2]^{2+}$ complexes, chloride counterions, and disordered methanol molecules. Fig. 1 shows a perspective view of the dimeric entity together with the labelling scheme which is conventionally accepted for the adenine nucleobase for chemical and biological purposes. Four bridging adenine molecules are linked to the copper(II) atoms through their N3 and N9 nitrogen atoms to provide the core of the paddle-wheel shaped dinuclear entity¹⁵ and two chloride anions occupy the apical positions of the elongated square pyramidal coordination environment of the metal centers. The complex is sited on a $2/m$ crystallographic position and shows a UDD conformation, referring the terms U(up) or D(down) to the coordination of each pyrimidinic N3 atoms to the upper or lower metal centre. The structural parameters listed in Table 1 are similar to those reported for dimeric compounds containing $\mu\text{-}\kappa\text{N3}:\kappa\text{N9}$ bridging purine ligands.^{15,16}

The shape and structural features of the dimeric cation resemble those reported for the analogous $[\text{Cu}_2(\mu\text{-adenine})_4\text{Cl}_2]\text{Cl}_2 \cdot 6\text{H}_2\text{O}$ compound obtained using a similar synthesis method but employing

Table 1 Selected bond lengths and angles (\AA , deg) for the coordination polyhedron of compound 1^a

	100 K	293 K
Cu–N3 ⁱ	2.009(2)	2.002(6)
Cu–N9	2.027(2)	2.031(5)
Cu–Cl1	2.445(1)	2.466(3)
Cu···Cu ⁱ	3.0761(9)	3.064(2)
N3 ⁱ –Cu–N3 ⁱⁱ	87.01(13)	86.9(3)
N3 ⁱ –Cu–N9 ⁱⁱⁱ	161.49(9)	162.5(3)
N3 ⁱⁱ –Cu–N9 ⁱⁱⁱ	87.45(9)	87.7(2)
N9–Cu–N9 ⁱⁱⁱ	92.27(12)	92.5(3)
N3 ⁱ –Cu–Cl1	100.57(7)	99.8(2)
N9–Cu–Cl1	97.80(7)	97.5(2)

^a Symmetry codes: (i) $-x + 2/3, -x + y + 1/3, -z + 1/3$; (ii) $-x + 2/3, -y + 1/3, -z + 1/3$; (iii) $x, x - y, z$.

water as solvent.¹⁷ However, the dissimilar features of the solvation molecules afford drastic changes in the resulting crystal framework. In the hydrated compound the interactions between the complex entities are mediated by water molecules to give a non-porous crystal structure maintained by an intricate network of adenine···water and chloride···water interactions. On the contrary, the weaker ability of methanol to establish hydrogen bonds implies that the crystal packing of 1 is essentially sustained by the assembling of the paddle-wheel dimeric $[\text{Cu}_2(\mu\text{-adenine})_4\text{Cl}_2]^{2+}$ entities through rigid direct intermolecular hydrogen bonds between the adenine molecules, without involving the solvent methanol molecules, together with interactions between the chloride anions and the adenine moieties of the cationic complexes providing extra stability and rigidity to the 3D porous supramolecular network and, as a consequence, increasing the robustness of the crystal framework.

As it can be observed in Fig. 2, the dinuclear entities are cross-linked together by pairs of symmetry-related N6–H···N1 hydrogen bonding interactions between the Watson–Crick faces of two adjacent nucleobases to give a $R_2^2(8)$ ring, a well-known structural synthon involved in the supramolecular recognition processes which determines the self-assembling pattern of the adenine moieties to form supramolecular aggregates in a great diversity of metal-nucleobase systems.^{13,18} Furthermore, coordination of the adenine through the N9 atom of the imidazole ring produces the proton transfer to the imidazole N7 site to give the non-canonical 7*H*-adenine tautomer¹⁹ which favours the formation of a hydrogen-bonded $R_2^1(7)$ ring between the Hoogsteen face [N6H, N7H] of the nucleobase as donor and the chloride anion as acceptor.²⁰ Structural parameters for the supramolecular interactions are listed in Table 2. Each chloride counterion is joined to two adenine ligands from adjacent dimeric complexes to form a distorted tetrahedral hydrogen bonding environment.

The self-assembling process driven by the above-described rigid interactions results in a supramolecular 3D structure (Fig. 3) containing very large channels along the crystallographic c axis with a diameter of 6.3 \AA (distance among van der Waals surfaces of

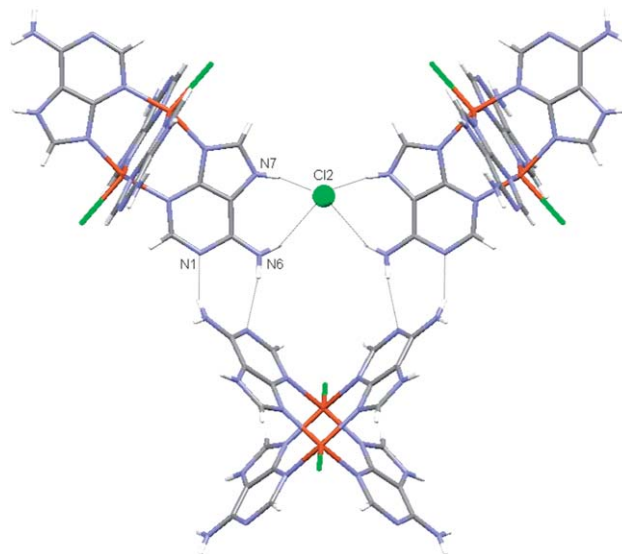


Fig. 2 Details of the adenine···adenine and adenine···chloride interactions in the crystal packing of compound 1.

Table 2 H-bond parameters (Å, deg) in compound **1**^a

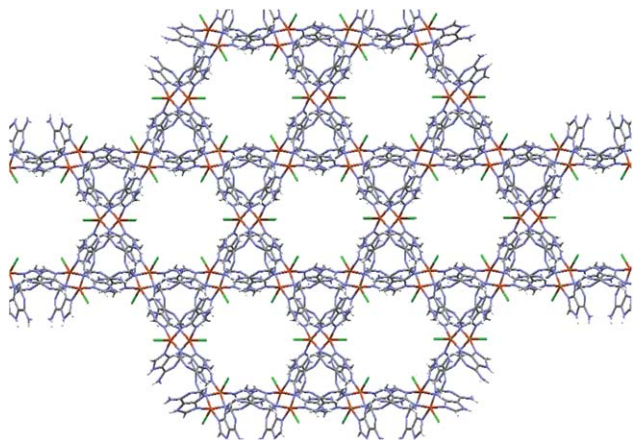
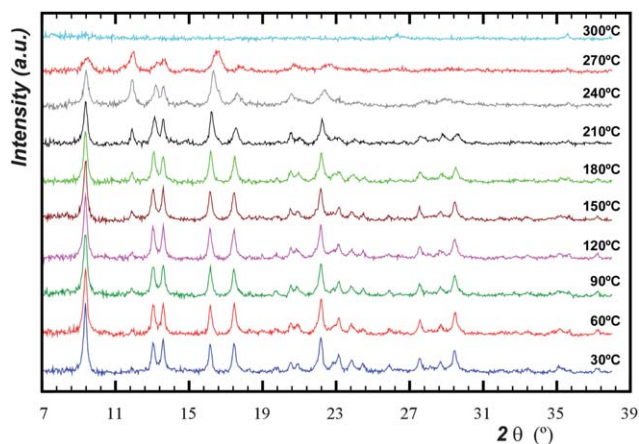
	H...A	D...A	D-H...A ^b
100 K			
N6-H6A...N1 ^{iv}	2.19	3.015(3)	161
N6-H6B...Cl2 ^v	2.66	3.466(3)	156
N7-H7...Cl2 ^v	2.24	3.034(2)	154
293 K			
N6-H6A...N1 ^{iv}	2.20	3.032(8)	163
N6-H6B...Cl2 ^v	2.69	3.505(8)	158
N7-H7...Cl2 ^v	2.23	3.032(7)	156

^a Symmetry codes: (iv) $x - y, -y, -z + 1$; (v) $y, -x + y, -z$. ^b D: donor and A: acceptor.

opposite chlorine atoms). These channels represent the 36% of the total volume of the unit cell²¹ and they are occupied by solvent methanol molecules in a highly disordered manner.

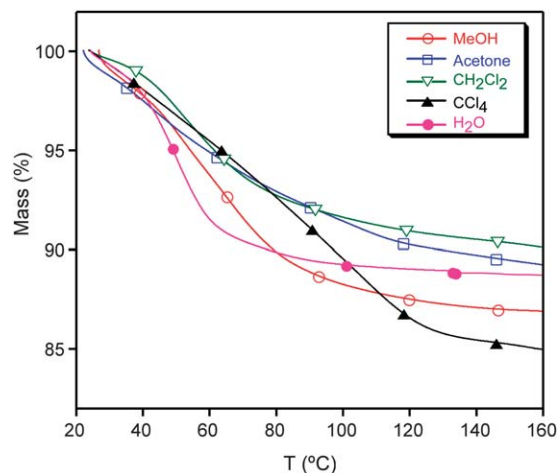
Thermal degradation of compound **1** (see ESI†) starts with an initial well-separated endothermic weight loss of 7.0% from room temperature to 100 °C corresponding to the release of the methanol molecules trapped inside the channels (calcd: 7.3% for two methanol molecules per formula unit). The resulting compound remains stable up to 240 °C and the XRPD patterns at different temperatures (Fig. 4) do not differ substantially from that corresponding to the starting material, suggesting that the 3D open framework is retained after the removal of the methanol molecules. Above this temperature it undergoes successive exothermic processes leading to CuO as final residue above 500 °C.

The thermal stability of the porous 3D crystal structure and the features of its channels, where the coordinated Cl1 chloride atoms are projected inward, suggest that the title compound may provide a suitable opportunity for host-guest interactions in solid-state.²² In this field, extended metal-organic frameworks containing biological moieties (so-called bio-MOF) are extensively studied to obtain information about a great diversity of molecular recognition processes which play a key role in biological systems,²³ to analyse their efficiency in the selective gas capture,¹⁴ and to advance in the design of artificial systems suitable for the releasing of adsorbed bioactive molecules from the pores at the cellular level.²⁴

**Fig. 3** Perspective view of the 3D framework along the *c*-axis showing the pores. Solvation methanol molecules are omitted for clarity.**Fig. 4** Variable-temperature X-ray diffraction powder patterns performed during the thermal degradation of compound **1**.

Preliminary experiments have shown that the desolvated product of compound **1** is able to adsorb in few minutes the humidity of the surrounding atmosphere to fill the empty channels with water molecules undergoing a weight increase of around 8% (*ca.* 4 water molecules per formula unit) and retaining the initial porous crystal structure without substantial changes in the X-ray diffraction powder pattern. Upon heating, the hydrated compound releases again the water molecules which are readsorbed at room temperature. The sample can undergo cycles of sorption and desorption without any loss in capacity or crystallinity. However, a suspension of the compound **1** in water affords an amorphous material after 24 hours. These facts suggest that the title compound is able to accept some amount of water molecules without any remarkable change in its crystal structure, but when the water is used as solvent, it acts as disruptor of the direct hydrogen bonds established between the adenine molecules and, as a consequence, the crystal building collapses.

Compound **1**, following evacuation at 150 °C, was exposed to the vapours of several solvents (methanol, acetone, dichloromethane, tetrachloromethane, and water), as reported for other porous compounds.²⁵ TGA curves (Fig. 5) show that in all cases the

**Fig. 5** TGA curves for evacuated compound **1** after exposure to different vapours.

adsorption of the vapour molecules takes place, showing dissimilar mass losses as expected for the different molecular weights and volumes. It is interesting to note that in the case of water and methanol, the amount of guest molecules placed in the channels is greater than that adsorbed in a non-saturated atmosphere of these solvents (for water: 8 and 11%, respectively). For tetrachloromethane and dichloromethane solvents, the TGA data show very different mass loss (15 vs. 10%) but the calculated guest molecule amount in the channels is almost the same (~0.5 molecules per dimeric entity), which may suggest a similar anchorage of both guest molecules to the channel surface.

The permanent porosity of the metal–organic framework was also studied by means of N₂ adsorption measurements (see ESI†). Freshly synthesized single crystals of compound **1** were dried under vacuum at 150 °C during 24 h to eliminate solvent guest molecules prior to measurements. The adsorption curve collected at 77 K exhibits features resulting from multilayer adsorption. The fitting of the adsorption area to Langmuir and BET equations leads to surface area values of 30 and 26 m² g⁻¹, respectively. These values are substantially smaller than the accessible surface area calculated from the crystal structure (790 m² g⁻¹) by a Monte Carlo integration technique where a probe molecule with a diameter equal Lennard-Jones parameter for N₂ (3.681 Å) is “rolled” over the framework.²⁶ This method has demonstrated to be very appropriate for characterization of microporous metal–organic frameworks fitting rather well the experimental surface areas.²⁷ Generally, such difference between the experimental surface area and calculated accessible area is attributed to incomplete solvent removal, crystal collapse or a massive presence of impurities. However, the weight loss of the outgassed sample fits the one expected from the compound formula which suggests a quantitative removal of the solvent. Additionally, the XRPD data confirm that the desolvated sample retains its crystal structure and therefore, its bulk porous framework, without any sign of other crystalline phases or amorphous contaminants that may cause the depletion of the surface area. It deserves to note that the minimum pore diameter (6.3 Å) is fairly greater than the molecular and kinetic diameters of N₂ (3.1 and 3.6 Å). This kind of reduced nitrogen adsorption has also been observed in other microporous hydrogen-bonded coordination frameworks (effective pore diameter: 4.0 Å).²⁸ This behaviour has been attributed to the strong quadrupole interaction between N₂ molecules and the electrostatic-field gradients around the pore window, thus blocking the diffusion of other N₂ molecules into the pores.²⁹ The relative narrowness of the pore of compound **1** together with the low dimensionality of the pore network (1D channels without connectivity among them) seems to support the latter statement. Another possible explanation is the relative flexibility of the supramolecular structure at the surface that could lead to a temperature induced superficial rearrangement that involves a closure of the pore window.

In conclusion, the adenine molecules in the dimeric units that are rigidly coordinated to the metal centers allow them to establish direct hydrogen bonds only along specific directions, so as to form the rigid supramolecular porous network. In addition to this, the use of methanol instead of water, with very weak hydrogen bonding ability has helped to avoid solvent mediated interactions between the dimeric units. So the robustness of the direct hydrogen bonding interactions between the Watson–Crick edges of the adenine nucleobases in the [Cu₂(μ-adenine)₄Cl₂]Cl₂·~2CH₃OH compound allows crystal framework to maintain its integrity even after the removal of

solvent molecules from the channels. Hence, the use of solvents with weak hydrogen bonding interactions and the resulting absence of solvent mediated interactions can be considered as a good strategy for the synthesis of robust 3D porous metal–organic frameworks sustained only by non-covalent interactions among the building blocks.

Financial support from the Ministerio de Ciencia e Innovación (Project MAT2008-05690/MAT) and the Gobierno Vasco (IT477-10) is gratefully acknowledged. We also thank Universidad del País Vasco/Euskal Herriko Unibertsitatea for predoctoral fellowships (PIFA01/2007/021). Technical and human support provided by SGIker (UPV/EHU, MICINN, GV/EJ, ESF) is gratefully acknowledged.

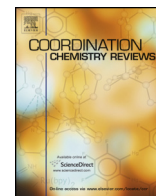
Notes and references

† *Synthesis and characterization of [Cu₂(μ-adenine)₄Cl₂]Cl₂·~2CH₃OH*: a highly insoluble polycrystalline powder of the title compound, in almost quantitative yield, was obtained by the slow addition of a methanolic solution of adenine (0.2 mmol, 30 mL) into a warm stirring solution of CuCl₂ in methanol (0.1 mmol, 5 mL) at 40 °C. Well-formed single crystals in 20–25% yield (based on copper) were obtained after one week by the slow diffusion of a solution of 0.2 mmol adenine in 40 mL of methanol layered over a solution of 0.1 mmol CuCl₂ in 15 mL propanol. The X-ray powder pattern of both the single-crystals and the polycrystalline samples matched the calculated pattern generated from the single-crystal structure data. Anal. Calcd (found) for C₂₂H₂₈Cl₄Cu₂N₂₀O₂: C, 30.25 (30.35); H, 3.23 (3.14); N, 32.07 (32.09), Cu, 14.55 (14.62). IR (KBr, cm⁻¹): 3360s; 3170s; 1650vs; 1515w; 1460m; 1400m; 1350w; 1320m; 1210m; 1110w; 785w; 740w; 550m.

‡ Diffraction data were collected at 100(2) and 293(2) K with a Stoe IPDS diffractometer with graphite-monochromated Mo-Kα radiation (λ = 0.71073). Structures were solved by direct methods and refined by full-matrix least-squares on *F*² including all reflections. All non-hydrogen atoms were refined anisotropically and hydrogen atoms by a riding model. The solvent molecules present in the channels are highly disordered and their contribution to the diffraction pattern has been removed using the SQUEEZE subroutine as implemented in PLATON.²¹ Crystal data: C₂₂H₂₈Cl₄Cu₂N₂₀O₂, *M*_r = 873.49, trigonal, space group *R*3̄m. At 293 K: *a* = *b* = 26.820(1), *c* = 15.528(1) Å, *V* = 9673(1) Å³, *Z* = 9, ρ = 1.349 g cm⁻³, 20 165 reflections, 2029 unique (*R*_{int} = 0.0598), *R*₁ = 0.0793, *wR*₂ = 0.2601 (all data). At 100 K: *a* = *b* = 26.903(2), *c* = 15.430(1) Å, *V* = 9672(3) Å³, *Z* = 9, ρ = 1.350 g cm⁻³, 11 165 reflections, 2035 unique (*R*_{int} = 0.0536), *R*₁ = 0.0337, *wR*₂ = 0.0872 (all data).

- 1 B. Moulton and M. J. Zaworotko, *Chem. Rev.*, 2001, **101**, 1629.
- 2 G. R. Desiraju, in *Crystal Engineering: the Design of Organic Solids*, Elsevier, New York, 1989.
- 3 H. Dodziuk, in *Introduction to Supramolecular Chemistry*, Kluwer Academic Publishers, New York, 2002.
- 4 S. A. Dalrymple and G. K. H. Shimizu, *J. Am. Chem. Soc.*, 2007, **129**, 12114.
- 5 X. N. Cheng, W. Xue, J. B. Lina and X.-M. Chen, *Chem. Commun.*, 2010, **46**, 246.
- 6 L. J. Barbour, *Chem. Commun.*, 2006, 1163.
- 7 (a) J. J. Jiang, L. Li, M. H. Lan, M. Pan, A. Eichhöfer, D. Fenske and C. Y. Su, *Chem.–Eur. J.*, 2010, **16**, 1841; (b) T. Tozawa, J. T. A. Jones, S. I. Swamy, S. Jiang, D. J. Adams, S. Shakespeare, R. Clowes, D. Bradshaw, T. Hasell, S. Y. Chong, C. Tang, S. Thompson, J. Parker, A. Trewin, J. Bacsá, A. M. Z. Slawin, A. Steiner and A. I. Cooper, *Nat. Mater.*, 2009, **8**, 973; (c) S. Lim, H. Kim, N. Selvapalam, K. J. Kim, S. J. Cho, G. Seo and K. Kim, *Angew. Chem., Int. Ed.*, 2008, **120**, 3400; (d) S. J. Dalgarno, P. K. Thallapally, L. J. Barbour and J. L. Atwood, *Chem. Soc. Rev.*, 2007, **36**, 236; (e) P. K. Thallapally, L. Dobranska, T. R. Gingrich, T. B. Wirsig, L. J. Barbour and J. L. Atwood, *Angew. Chem., Int. Ed.*, 2006, **45**, 6506; (f) P. K. Thallapally, G. O. Lloyd, J. L. Atwood and L. J. Barbour, *Angew. Chem., Int. Ed.*, 2005, **44**, 3848; (g) N. Malek, T. Maris, M. Simard and J. D. Wuest, *J. Am. Chem. Soc.*, 2005, **127**, 5910; (h) K. J. Ooms,

- K. Campbell, R. R. Tykwinski and R. E. Wasylshen, *J. Mater. Chem.*, 2005, **15**, 4318; (i) J. A. Riddle, J. C. Bollinger and D. Lee, *Angew. Chem., Int. Ed.*, 2005, **44**, 6689; (j) C. Tedesco, I. Immediata, L. Gregoli, L. Viragilano, A. Immizi and P. Neri, *CrystEngComm*, 2005, **7**, 449; (k) D. V. Soldatov, I. L. Moudrakovski and J. A. Ripmeester, *Angew. Chem., Int. Ed.*, 2004, **43**, 6308; (l) J. L. Atwood, L. J. Barbour and A. Jerga, *Angew. Chem., Int. Ed.*, 2004, **43**, 2948; (m) J. L. Atwood, L. J. Barbour and A. Jerga, *Angew. Chem., Int. Ed.*, 2004, **43**, 2948; (n) J. L. Atwood, L. J. Barbour, A. Jerga and B. L. Schottel, *Science*, 2002, **298**, 1000.
- 8 (a) Z. Huang, P. S. White and M. Brookhart, *Nature*, 2010, **465**, 598; (b) T. Jacobs, J.-A. Gertenbach, D. Dinabandhu and L. J. Barbour, *Aust. J. Chem.*, 2010, **63**, 573; (c) L. Dobrzanska, G. O. Lloyd, H. G. Raubenheimer and L. J. Barbour, *J. Am. Chem. Soc.*, 2006, **128**, 698; (d) K. Uemura, K. Saito, S. Kitagawa and H. Kita, *J. Am. Chem. Soc.*, 2006, **128**, 16122; (e) L. Dobrzanska, G. O. Lloyd, C. Esterhuysen and L. J. Barbour, *Angew. Chem., Int. Ed.*, 2006, **45**, 5856; (f) A. W. Kleij, M. Kuil, D. M. Tooke, M. Lutz, A. L. Spek and J. N. H. Reek, *Chem.–Eur. J.*, 2005, **11**, 4743; (g) L. Dobrzanska, G. O. Lloyd, H. G. Raubenheimer and L. J. Barbour, *J. Am. Chem. Soc.*, 2005, **127**, 13134; (h) B. Chatterjee, J. C. Noveron, M. J. E. Resendiz, J. Liu, T. Yamamoto, D. Parker, M. Cinke, C. V. Nguyen, A. M. Arif and P. J. Stang, *J. Am. Chem. Soc.*, 2004, **126**, 10645; (i) S.-S. Sun and A. J. Lees, *J. Am. Chem. Soc.*, 2000, **122**, 8956; (j) M. Albrecht, M. Lutz, A. L. Spek and G. van Koten, *Nature*, 2000, **406**, 970; (k) S. Belanger, J. T. Hupp, C. L. Stern, R. V. Slone, D. F. Watson and T. G. Carrell, *J. Am. Chem. Soc.*, 1999, **121**, 557; (l) C. B. Aakeröy, A. M. Beatty and D. S. Leinen, *Angew. Chem., Int. Ed.*, 1999, **38**, 1815.
- 9 (a) C. B. Aakeroy, N. R. Champness and C. Janiak, *CrystEngComm*, 2010, **12**, 22; (b) R. Zou, A. I. Abdel-Fattah, H. Xu, Y. Zhao and D. D. Hickmott, *CrystEngComm*, 2010, **12**, 1337; (c) A. D. Naik, M. M. Dirtu, A. Leonard, B. Tinaut, J. Marchand-Brynaert, B. L. Su and Y. García, *Cryst. Growth Des.*, 2010, **10**, 1798.
- 10 (a) J. P. García-Terán, O. Castillo, A. Luque, U. García-Couceiro, G. Beobide and P. Román, *Cryst. Growth Des.*, 2007, **7**, 2594; (b) A. M. Beatty, B. A. Helfrich, G. A. Hogan and H. A. Reed, *Cryst. Growth Des.*, 2006, **6**, 122.
- 11 G. V. Oshovsky, D. N. Reinhoudt and W. Verboom, *Angew. Chem., Int. Ed.*, 2007, **46**, 2366.
- 12 (a) E. C. Yang, H. K. Zhao, Y. Feng and X. J. Zhao, *Inorg. Chem.*, 2009, **48**, 3511; (b) E. C. Yang, H. K. Zhao, B. Ding, X. G. Wang and X. J. Zhao, *New J. Chem.*, 2007, **31**, 1887; (c) J. P. García-Terán, O. Castillo, A. Luque, U. García-Couceiro, P. Román and L. Lezama, *Inorg. Chem.*, 2004, **43**, 4549.
- 13 S. Verma, A. Kumar-Mishra and J. Kumar, *Acc. Chem. Res.*, 2010, **43**, 79.
- 14 (a) J. An, S. J. Geib and N. L. Rosi, *J. Am. Chem. Soc.*, 2010, **132**, 38; (b) J. An, R. P. Fiorella, S. J. Geib and N. L. Rosi, *J. Am. Chem. Soc.*, 2009, **131**, 8401.
- 15 (a) J. Cepeda, O. Castillo, J. P. García-Terán, A. Luque, S. Pérez-Yáñez and P. Román, *Eur. J. Inorg. Chem.*, 2009, 2344; (b) J. M. González-Pérez, C. Alarcón-Payer, A. Castineiras, T. Pivetta, L. Lezama, D. Choquesillo-Lazarte, G. Crisponi and J. Niclós-Gutiérrez, *Inorg. Chem.*, 2006, **45**, 877.
- 16 (a) J. W. Suggs, M. J. Dube and M. Nichols, *J. Chem. Soc., Chem. Commun.*, 1993, 307; (b) D. Sonnenfroh and R. W. Kreilick, *Inorg. Chem.*, 1980, **19**, 1259; (c) E. Sletten, *Acta Crystallogr., Sect. B: Struct. Crystallogr. Cryst. Chem.*, 1969, **25**, 1480.
- 17 P. De Meester and A. C. Skapski, *J. Chem. Soc. A*, 1971, 2167.
- 18 For examples see (a) M. Byres, P. J. Cox, G. Kay and E. Nixon, *CrystEngComm*, 2009, **11**, 135; (b) M. A. Galindo, D. Amantia, W. Clegg, R. W. Harrington, R. J. Eyre, J. P. Goss, P. R. Briddon, W. McFarlane and A. Houlton, *Chem. Commun.*, 2009, 2833; (c) A. F. A. Peacock, S. Parsons and P. J. Sadler, *J. Am. Chem. Soc.*, 2007, **129**, 3348; (d) A. C. Morel, D. Choquesillo-Lazarte, C. Alarcón-Payer, J. M. González-Pérez, A. Castineiras and J. Niclós-Gutiérrez, *Inorg. Chem. Commun.*, 2003, **6**, 1354.
- 19 J. P. García-Terán, O. Castillo, A. Luque, U. García-Couceiro, G. Beobide and P. Román, *Dalton Trans.*, 2006, 902.
- 20 For examples see (a) A. Garcia-Raso, J. J. Fiol, A. Tasada, F. M. Alberti, F. Badenas, X. Solans and M. Font-Bardia, *Polyhedron*, 2007, **26**, 949; (b) T. F. Mastropietro, D. Armentano, N. Marino and G. De Munno, *Polyhedron*, 2007, **26**, 4945; (c) T. Suzuki, Y. Hirai, H. Monjushiro and S. Kaizaki, *Inorg. Chem.*, 2004, **43**, 6435; (d) P. de Meester and A. C. Skapski, *J. Chem. Soc., Dalton Trans.*, 1973, 424.
- 21 A. L. Spek, *J. Appl. Crystallogr.*, 2003, **36**, 7.
- 22 J. Kumar and S. Verma, *Inorg. Chem.*, 2009, **48**, 6350.
- 23 C. S. Purohit and S. Verma, *J. Am. Chem. Soc.*, 2006, **128**, 400.
- 24 J. An, S. J. Geib and N. L. Rosi, *J. Am. Chem. Soc.*, 2009, **131**, 8376.
- 25 (a) R. Yang, L. Lee, Y. Xiong, J.-R. Lee, H.-C. Zhou and C.-Y. Su, *Chem.–Asian J.*, 2010, **5**, 2358; (b) C. E. Willans, S. French, L. J. Barbour, J.-A. Gertenbach, P. C. Junk, G. O. Lloyd and J. W. Steed, *Dalton Trans.*, 2009, 6480.
- 26 T. Düren, F. Millange, G. Férey, K. S. Walton and R. Snurr, *J. Phys. Chem. C*, 2007, **111**, 15350.
- 27 B. Assfour and G. Seifert, *Microporous Mesoporous Mater.*, 2010, **133**, 59.
- 28 J. J. Jiang, M. Pan, J. M. Liu, W. Wang and C. Y. Su, *Inorg. Chem.*, 2010, **49**, 10166.
- 29 (a) K. M. Ok, J. Sung, G. Hu, R. M. J. Jacobs and D. O'Hare, *J. Am. Chem. Soc.*, 2008, **130**, 3762; (b) T. K. Maji, R. Matsuda and S. Kitagawa, *Nat. Mater.*, 2007, **6**, 142; (c) W. Steele, *Chem. Rev.*, 1993, **93**, 2355.



Review

Metal–carboxylato–nucleobase systems: From supramolecular assemblies to 3D porous materials



Garikoitz Beobide, Oscar Castillo*, Javier Cepeda, Antonio Luque, Sonia Pérez-Yáñez, Pascual Román, Jintha Thomas-Gipson

Departamento de Química Inorgánica, Facultad de Ciencia y Tecnología, Universidad del País Vasco/Euskal Herriko Unibertsitatea, UPV/EHU, Apartado 644, E-48080 Bilbao, Spain

Contents

1. Introduction	2716
2. Paddle-wheel shaped secondary building units	2717
2.1. Composition control	2717
2.2. Magnetic properties	2717
2.3. Polymerization strategies	2718
3. [Cu ₂ (μ-adenine) ₄] secondary building unit	2719
3.1. Porous MBioFs based on [Cu ₂ (μ-adenine) ₄] units	2720
3.2. Porous supraMBioFs based on [Cu ₂ (μ-adenine) ₄] units	2720
4. [Cu ₂ (μ-adenine) ₂ (μ-carboxylato) ₂] secondary building unit	2722
4.1. Porous MBioFs based on [Cu ₂ (μ-adenine) ₂ (μ-carboxylato) ₂] units	2722
4.2. Fine tuning of the adsorptive properties	2724
4.3. Overtaking gas uptake capacity limited by the crystal structure	2726
5. [Cu ₂ (μ-carboxylato) ₄] secondary building unit	2727
6. Other metal–carboxylato–adenine systems	2728
6.1. Metal-malonato–adenine discrete systems. Magnetic properties	2728
6.2. Metal-oxalato–adenine extended systems	2729
6.3. Hybrid systems based on metal-oxalato entities and protonated nucleobases	2732
7. Summary and perspective	2734
Acknowledgements	2735
References	2735

ARTICLE INFO

Article history:

Received 29 November 2012

Accepted 4 March 2013

Available online 29 March 2013

Keywords:

Metal-biomolecule-frameworks
Supramolecular porous materials
Crystal engineering
Porous materials
Adsorption properties
Magnetic properties

ABSTRACT

A complete overview of the preparation of metal–carboxylato–nucleobase architectures that range from supramolecular assemblies to 3D porous materials is reported. The basic building units of these materials consist of metal–nucleobase fragments which link together through coordination bonding or by means of supramolecular assembling among the nucleobases anchored to metal centres. In the case of extended systems based on coordination bonds, the connectivity among the metal centres can be achieved through bridging nucleobases and/or by auxiliary organic linkers such as carboxylate and dicarboxylate anions. The latter bridging mode confers to the nucleobases a greater capacity to involve in molecular recognition processes with other biologically relevant species by means of the establishment of non-covalent interactions such as hydrogen bonding and/or π – π stacking among aromatic groups. On the other hand, the geometrical rigidity imposed by several metal–nucleobase fragments and the base pairing interactions through complementary hydrogen bonding, lead to structural restraints that preclude an effective filling of the space, and as a consequence, it favours the growth of tailor-made open-frameworks based either on coordination bonds (MBioFs) or on non-covalent interactions (*supra*MBioFs).

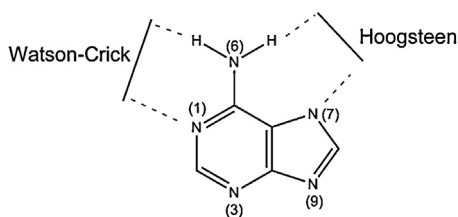
© 2013 Elsevier B.V. All rights reserved.

1. Introduction

Metal-organic frameworks (MOFs) encompass an area of chemistry that has experienced awesome growth during the last decades, as indicated by not only the sheer number of research

* Corresponding author. Tel.: +34 946 015 991.

E-mail address: oscar.castillo@ehu.es (O. Castillo).



Scheme 1. Adenine nucleobase showing the numbering scheme and the Watson–Crick and Hoogsteen faces.

papers published but also the ever-expanding scope of the research [1]. The combination of the metallic nodes and the linkers provides endless possibilities, so that the judicious selection of the metal atom and the ligands employed, together with the coordination features of both, allows rational design of the resulting compounds and, therefore, their physical and chemical properties can be tuned at will. However, many applications of the MOFs require them to be both biologically and environmentally compatible. In this sense, the biomolecules are suitable to act as building units in the formation of metal–biomolecule frameworks, called MBioFs or BioMOFs. This kind of building block offers several advantages as stated by Maspoeh et al.: (i) biomolecules are easily and naturally available, so they can be used to prepare bulk quantities of materials at amenable prices, (ii) biomolecules can lead to biologically compatible MOFs, (iii) biomolecules are structurally diverse, (iv) biomolecules can have many different metal binding sites, (v) many of them have intrinsic self-assembly properties, (vi) some of them are chiral [2].

Among the variety of biomolecules we have focused our research work in the use of nucleobases. Nucleobases are suitable ligands for the construction of MBioFs since they present several heteroatoms allowing them acting as multidentate organic ligands, as well as being able to establish large hydrogen bonding networks. The nucleobase most employed in these kinds of compound is adenine (Scheme 1), which presents five nitrogen atoms that allow a variety of coordination modes, and further, its non coordinated positions remain accessible to interact through hydrogen bonds with other structural units, especially, the Watson–Crick (N1, N6H) and Hoogsteen (N7, N6H) faces. The acid–base balance of the adenine molecule also makes it usable as a cationic, neutral or anionic species [3].

In this review we summarize the preparation of metal–carboxylato–nucleobase architectures that range from supramolecular assemblies to 3D porous materials. In particular, we have focused on the chances that the paddle-wheel shaped SBU (Secondary Building Unit) gives for the construction of porous compounds, based on the synthetic control over the three dicopper paddle-wheel entities built up from the adenine nucleobase and carboxylato ligands. The geometrical rigidity imposed by these fragments and the base pairing interactions through complementary hydrogen bonding, lead to structural restraints that preclude an effective filling of the space, and as a consequence, it favours the growth of tailor-made open-frameworks based either on coordination bonds (MBioFs) or on non-covalent interactions (*supra*MBioFs).

2. Paddle-wheel shaped secondary building units

The design of coordination frameworks via deliberate selection of metals and multifunctional ligands, including biologically relevant molecules such as nucleobases [3], is one of the most attractive topical areas of chemistry due to the fascinating structural diversity and the development as new materials with tunable properties [4]. An essential part of coordination polymer design, and of the

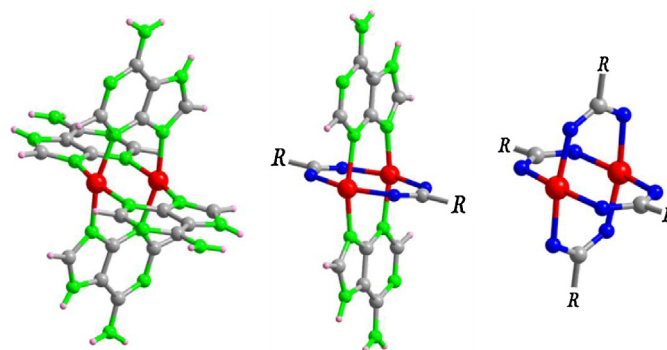


Fig. 1. Paddle-wheel entities for the metal/carboxylato/adenine system. Reproduced from Ref. [37]. Copyright (2012) American Chemical Society.

wider field of crystal engineering, is the use of building blocks that combine the flexibility and the necessary interconnection capability to achieve the required dimensionality, but also enough strength to permit a predictable core which maintains its structural integrity throughout the construction of the solid. In this sense, $[M_2(\mu-L)_4X_2]$ entities have been known for a long time since the crystal structure of the $[Cu_2(\mu\text{-acetato})_4(H_2O)_2]$ compound was reported [5]. The attractiveness of the paddle-wheel (PW) motif is that structural and functional changes can be achieved, almost at will, by simply varying the metal cores, the bridging moieties, or the apical X-ligands [6]. This functional versatility of the dinuclear PW motifs makes them particularly suitable as secondary building units (SBUs) for the design and synthesis of numerous crystalline materials ranging from zero-dimensional (0D) species to three-dimensional (3D) coordination polymers with interesting properties in areas such as magnetism, medicine, catalysis, and gas storage [4,7,8].

2.1. Composition control

The nitrogen donor atoms disposition of the adenine molecule makes possible to replace carboxylato bridging ligands of the $[Cu_2(\mu\text{-carboxylato})_4]$ dimeric entity retaining the paddle-wheel shaped morphology of the dinuclear unit. Apart from that, it is possible to obtain synthetic control over the three dicopper paddle-wheel entities built up from the adenine nucleobase and carboxylato ligands (Fig. 1).

The first building unit, $[M_2(\mu\text{-adenine})_4]$, in which the metal centres are bridged by the adenine nucleobase acting as N3,N9-bridging ligand, is obtained in the absence of the carboxylic ligand in the reaction media. The second one, $[M_2(\mu\text{-adenine})_2(\mu\text{-carboxylato})_2]$, appears with the simultaneous presence of adenine and carboxylic acid in the reaction media. The last one, $[M_2(\mu\text{-carboxylato})_4]$, where the metal centres are bridged exclusively by carboxylato ligands, is obtained in the absence of adenine or when the nucleobase is functionalized in the N3 or N9 positions.

2.2. Magnetic properties

It is well known that non-linear OCO or NCN bridges cause antiferromagnetic coupling with J values ranging from -210 to -320 cm^{-1} [9] and -250 to -325 cm^{-1} [9a,10], respectively. However, the coexistence of these two types of bridges requires a more exhaustive analysis than when there is only one type. In fact, when the bridging ligands are different, the two bridges may either add or counterbalance their effects. This problem has been treated by Nishida and Kida [11] and McKee et al. [12], and these phenomena are known as orbital complementarity and countercomplementarity, respectively. In the case of $[M_2(\mu\text{-adenine})_2(\mu\text{-carboxylato})_2]$,

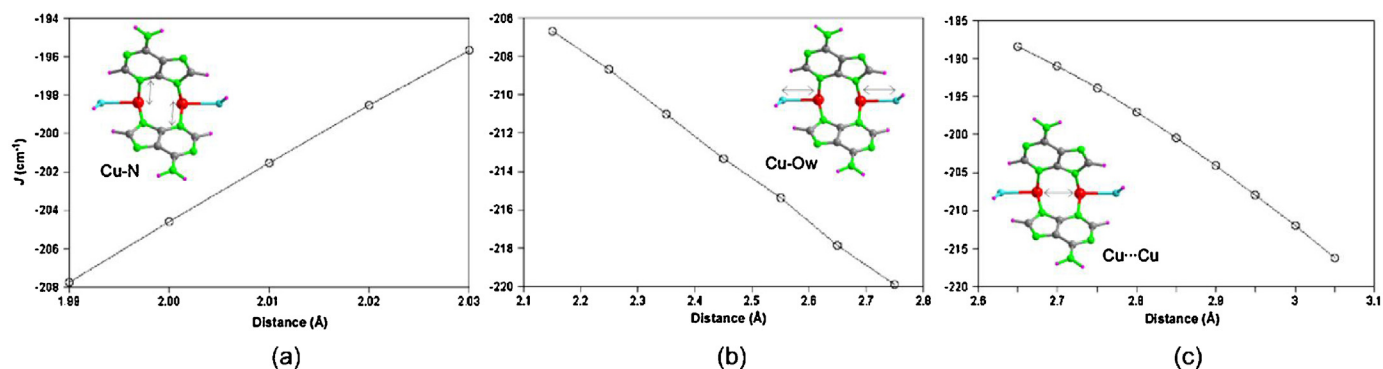
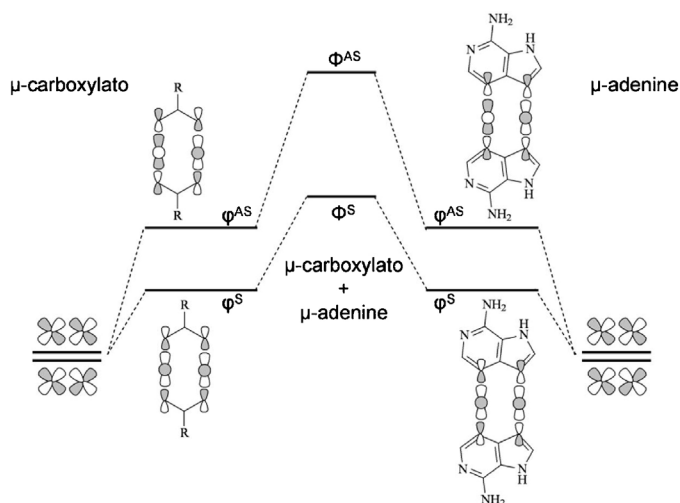


Fig. 2. Variation in the magnetic coupling constant value as a function of (a) the Cu–N bond equatorial distance, (b) the Cu–Ow bond axial distance and (c) the Cu···Cu distance.

Reproduced from Ref. [10b]. Copyright (2009) WILEY-VCH Verlag GmbH & Co. KGaA, Weinheim.

the splitting order of the molecular magnetic orbitals is the same for each type of bridging ligand leading as a consequence to J values intermediate between the values found for the nonmixed paddle-wheels (Scheme 2).

Moreover, our research group reported, based on DFT calculations, that for $[\text{Cu}_2(\mu\text{-adenine})_4]$ entities the magnitude of the antiferromagnetic coupling is governed by both structural and chemical parameters [10b]. Three main structural parameters were considered: copper–nitrogen, copper–water molecule and copper···copper distances (Fig. 2). The decrease in the Cu–N distances favours the interaction between the magnetic orbitals of the metal and the ligands and reinforces the antiferromagnetism. On the contrary, a shorter Cu–Ow distance brings a decrease in the antiferromagnetism as a result of the increase in the d_{z^2} character of the magnetic orbitals (decreasing the $d_{x^2-y^2}$ character), as previously reported by Sonnenfroh and Kreilick [10a]. In contrast, longer metal···metal distances cause an increase in the antiferromagnetic interactions. To explain this latter behaviour, it is necessary to pay attention to the orbitals of the bridging ligand, whose lobes positioned on the N3 and N9 atoms further overlap in the vicinity of the central carbon atom as the copper···copper distance increases. Consequently, the energy difference between the resulting magnetic orbitals is enhanced (Scheme 3). As the effect of these structural parameters on the magnetic coupling is of the same order of magnitude, any attempt to obtain experimental magnetostructural correlations on the basis of just one parameter is precluded.



Scheme 2. Orbital complementarity of the $\mu\text{-carboxylato-}\kappa\text{O}:\kappa\text{O}'$ and $\mu\text{-adenine-}\kappa\text{N3}:\kappa\text{N9}$ bridging ligands.

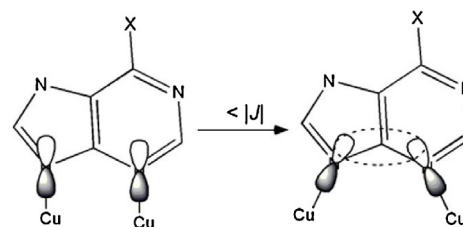
A similar trend is also observed for $[\text{Cu}_2(\mu\text{-carboxylato})_4]$ entities [10c].

The charge of the bridging ligand and its substituents also play an important role in the magnitude of the antiferromagnetic interaction. DFT calculations for different models maintaining the same structural parameters but modifying the bridging ligand by adding different substituents in the C6-position left to antiferromagnetic J values with the following relative order: $7H\text{-adenine} > 7H\text{-hypoxanthine} > 6\text{-chloro-}7H\text{-purine} > \text{adeninato} > \text{hypoxanthinato} > 6\text{-chloropurinato}$ (Scheme 4). This order can be related to the increase in the number of electron lone pairs in the bridging ligand (by means of the deprotonation or by substitution of the exocyclic amine group by a chlorine atom). This fact increases the extension of the molecular orbitals of the bridging ligands and the N3 and N9 atoms contribute to a lesser extent, so they overlap less efficiently with the metal-centred magnetic orbitals and a weaker antiferromagnetic interaction is observed.

2.3. Polymerization strategies

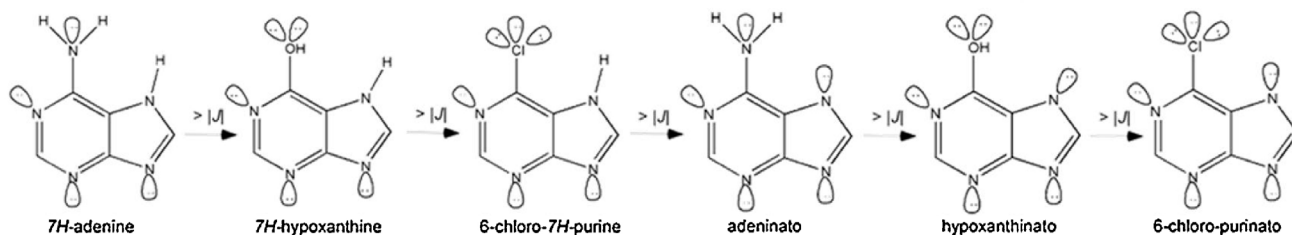
Any of the previously stated paddle-wheel shaped dimeric entities can further polymerize to obtain extended systems. There are two main options to achieve this purpose: to make use of polycarboxylato ligands that are able to connect the PW motifs through the equatorial positions and/or to make use of the axial positions of the PW motifs (Fig. 3).

The latter option is not always available because of the steric hindrance exerted by the equatorial ligands over the axial position. Taking into account the van der Waals radii, we have carried out a simple estimation of the closest axial-approach of a pyridine ligand to assess the accessibility of the axial position of each PW motif (Fig. 4). The results indicate that the axial positions are only available for bulky ligands (such as pyridine and other



Scheme 3. Increase in the magnetic coupling constant as a result of a greater overlap around the central carbon atom.

Reproduced from Ref. [10b]. Copyright (2009) WILEY-VCH Verlag GmbH & Co. KGaA, Weinheim.



Scheme 4. Calculated order of the bridging ligands according to their ability to transmit magnetic interactions by the superexchange pathway. Reproduced from Ref. [10b]. Copyright (2009) WILEY-VCH Verlag GmbH & Co. KGaA, Weinheim.

aromatic amines) in the case of $[M_2(\mu\text{-adenine})_2(\mu\text{-carboxylato})_2]$ and $[M_2(\mu\text{-carboxylato})_4]$ entities. The $[M_2(\mu\text{-adenine})_4]$ moiety only allows the coordination to the axial positions of small molecules or ions, such as water molecules or halides but not of more sterically hindered molecules.

In this way, the polymerization of the $[M_2(\mu\text{-adenine})_4]$ entity is promoted by means of the deprotonation of the nucleobase, but since the coordination of an adjacent PW entity to the axial position is forbidden, the presence of a second less hindered metal centre becomes requisite for the polymerization.

With the well-known $[M_2(\mu\text{-carboxylato})_4]$ entities, the resulting crystal structure can be directed by means of the correct selection of the polycarboxylato ligand towards a great variety of architectures ranging from polynuclear discrete entities to 3D

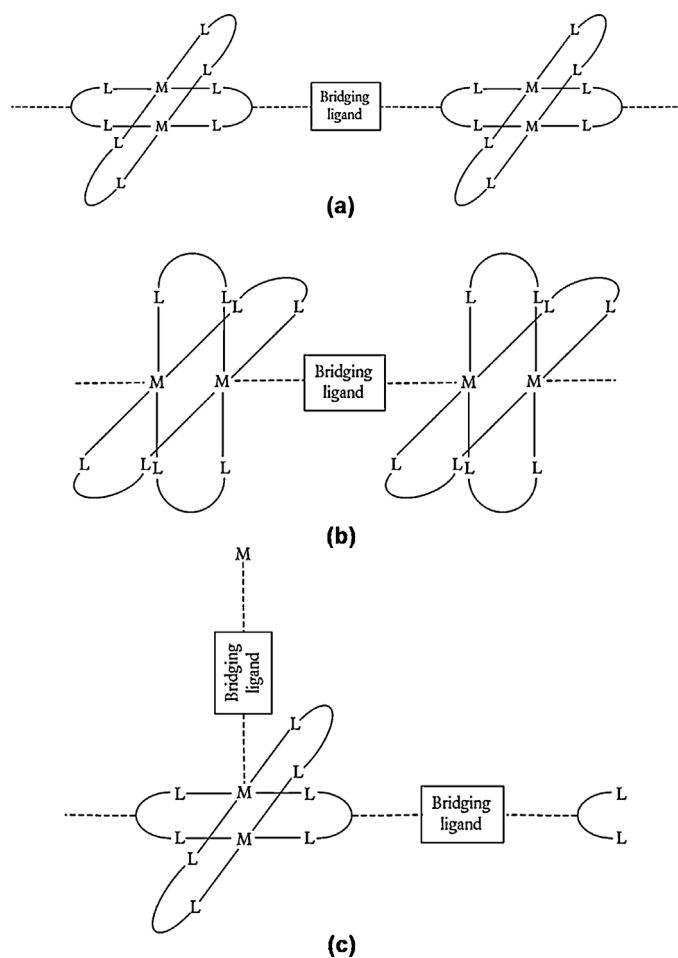


Fig. 3. Different polymerization strategies for paddle-wheel shaped entities: (a) through the equatorial positions, (b) through the axial ones and (c) through both of them.

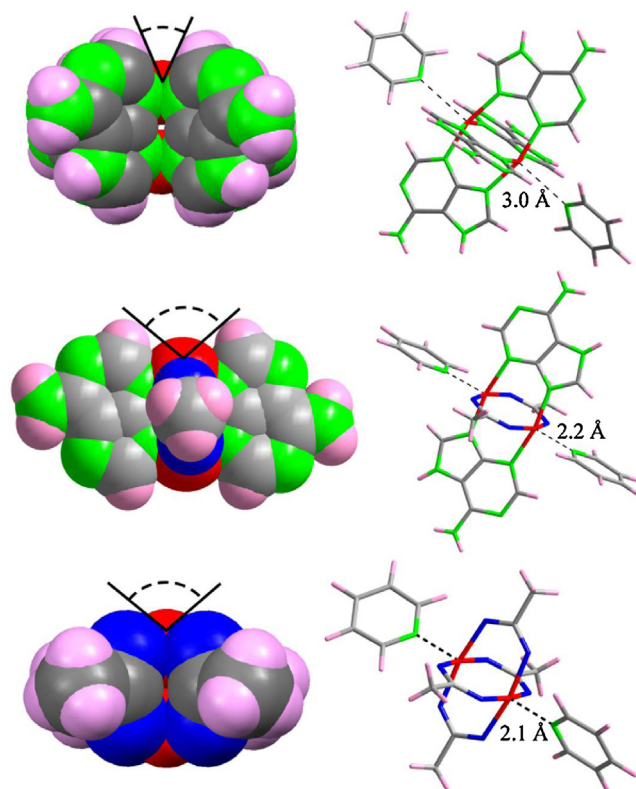


Fig. 4. Accessibility of the axial position of each PW motif for aromatic amines. Reproduced from Ref. [37]. Copyright (2012) American Chemical Society.

crystal structures [13]. In these entities, the axial positions, usually occupied by solvent molecules, can be replaced by nucleobase ligands, thus increasing the ability of the systems to establish molecular recognition processes.

In the $[M_2(\mu\text{-adenine})_2(\mu\text{-carboxylato})_2]$ unit, both approaches are possible: (i) polymerization through the deprotonation of the nucleobase and its further coordination, and (ii) polymerization by using polycarboxylato ligands.

3. $[Cu_2(\mu\text{-adenine})_4]$ secondary building unit

The first crystal-structure containing a $[Cu_2(\mu\text{-adenine})_4]$ unit was reported by de Meester and Skapski in 1971: $[Cu_2(\mu\text{-adenine})_4Cl_2]Cl_2 \cdot 6H_2O$ [14]. A few years later the crystal structure of the analogous perchlorate compound was published: $[Cu_2(\mu\text{-adenine})_4(OH_2)_2](ClO_4)_4 \cdot 2H_2O$ [15]. In both compounds the adenine molecule remains neutral. However, early studies of Sletten showed the possibility of obtaining the same dimeric unit based on deprotonated adenine: $[Cu_2(\mu\text{-adeninato})_4(OH_2)_2] \cdot 5H_2O$, but

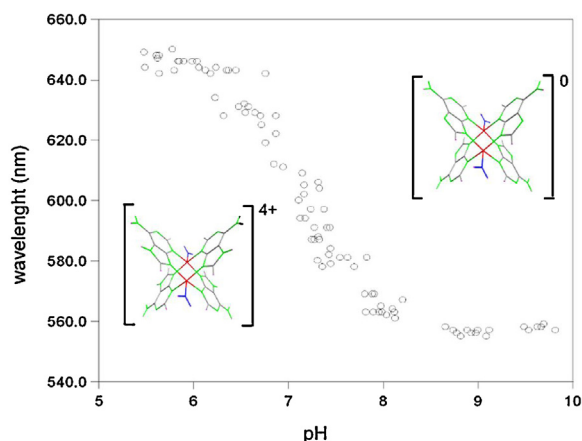


Fig. 5. Position of the absorbance maximum at different pH values for $[\text{Cu}_2(\mu\text{-adenine/adeninate})_4]$.

the author was not aware of its potential to obtain extended frameworks [16]. This work remained more or less forgotten as its coordinate data are not available in the Cambridge Structural Database (CSD) [17] and the assigned structure scheme is also incorrect. Since then, there was no further evidence to decide if the paddle wheel shaped entity would retain its structure upon the deprotonation of the adenine, until the structures of $\{[\text{Cu}_2(\mu\text{-adeninato})_4(\text{H}_2\text{O})_2][\text{Cu}(\text{ox})(\text{H}_2\text{O})_2]\}_n$ and $[\text{Cu}_2(\mu\text{-adeninato})_4(\text{OH})_2] \cdot 7\text{H}_2\text{O}$ were reported. These confirmed that the dimeric entity was robust enough to allow the deprotonation of the adenine and offering the opportunities to use it as a secondary building unit (SBU) [18,19].

UV–vis spectroscopy was employed to obtain information on the acid–base behaviour of the $[\text{Cu}_2(\mu\text{-adenine})_4(\text{H}_2\text{O})_2]^{4+}$ dimeric entity, because the acid–base balance of the neat adenine molecule ($\text{p}K_{\text{a}1} = 4.2$ and $\text{p}K_{\text{a}2} = 9.8$) is affected by its coordination to the metal centres. The dimeric entity in its cationic form (with adenine ligands) shows a characteristic band at 650 nm which is displaced towards shorter wavelengths as the pH increases reaching values close to 555 nm. This fact is indicative of the deprotonation of the adenine ligand. Fig. 5 shows two plateaux, the first one corresponding with the predominance of the cationic $[\text{Cu}_2(\mu\text{-adenine})_4(\text{H}_2\text{O})_2]^{4+}$ at pH values below 6 and the second one corresponding with the neutral $[\text{Cu}_2(\mu\text{-adeninato})_4(\text{H}_2\text{O})_2]$ at pH values above 9. It can be inferred from the graph that the $\text{p}K_{\text{a}}$ value is shifted to a value around 7.2–7.4. There is no evidence of an intermediate species.

Naturally, this information about the pH speciation is crucial in order to fix the synthetic conditions appropriate for the polymerization of the dimeric entities.

3.1. Porous MBioFs based on $[\text{Cu}_2(\mu\text{-adenine})_4]$ units

As previously stated the paddle wheel $[\text{Cu}_2(\mu\text{-adenine})_4]$ units can be polymerized by establishing new coordination bonds to obtain extended systems. For this purpose we need to deprotonate the adenine ligand in order to increase its coordinative capacity. However, the steric hindrance that the four adenine bridging molecules set at the apical positions, requires the presence of a less sterically hindered second node for the polymerization to proceed. The first polymeric compound of this type was reported by us in 2004. It consists of a 3D coordination polymer with formula $\{[\text{Cu}_2(\mu\text{-adeninato})_4(\text{H}_2\text{O})_2][\text{Cu}(\text{ox})(\text{H}_2\text{O})_2]\}_n$ containing the adenine nucleobase as an anionic N3,N7,N9-bridging ligand. The deprotonation of the adenine at the reaction media promotes the polymerization of the framework by sequentially bridging $[\text{Cu}_2(\mu\text{-adeninato})_4]$ units through the less sterically hindered $[\text{Cu}(\text{ox})(\text{H}_2\text{O})_2]$ units (Fig. 6). The resulting structure contains one-dimensional (1D) tubular channels with a diameter of about 13 Å and that represent around a 40% of the total volume [18].

The same strategy was employed later on by Nicolás-Gutiérrez et al. to obtain a discrete hexanuclear complex of formula $\{[(\text{H}_2\text{O})_2\text{Cu}_2(\mu\text{-adeninato})_4][\text{Cu}(\text{oda})(\text{H}_2\text{O})_4]_2\} \cdot 6\text{H}_2\text{O}$ (oda: oxydiacetato(2-)ligand) [19]. In these two examples the adenine adopts a $\mu_3\text{-N}3,\text{N}7,\text{N}9$ bridging tridentate mode that it is reinforced by a simultaneous hydrogen bonding interaction of the exocyclic amino group. There are many examples of this kind of reinforcement in the coordination chemistry of the nucleobases [20]. The magnetic behaviour of this compound is dominated by the intradimer exchange pathway that provides strong antiferromagnetic coupling as previously mentioned. The references show that the interdimeric exchange pathway through the imidazolic ring provides very weak antiferromagnetic coupling between the Cu(II) ions [20b,21].

3.2. Porous supraMBioFs based on $[\text{Cu}_2(\mu\text{-adenine})_4]$ units

The neutral adenine presents a well-known capacity to establish strong complementary hydrogen bonding interactions that can lead to generation of robust supramolecular porous materials. In fact, the Watson–Crick and Hoogsteen faces of the adenine ligands are accessible in the $[\text{Cu}_2(\mu\text{-adenine})_4]$ units opening a new way to polymerize the dimeric entities just by means of non-covalent interactions. At first sight, a reasonable strategy to obtain stable porous crystal structures is to use discrete mononuclear or polynuclear coordination complexes as rigid tectons which can only establish hydrogen bonding interactions along specific directions by means of predictable supramolecular synthons [22]. As a consequence of the rigidity of the tectons, in many cases, the resulting network is unable to occupy the whole space and presents

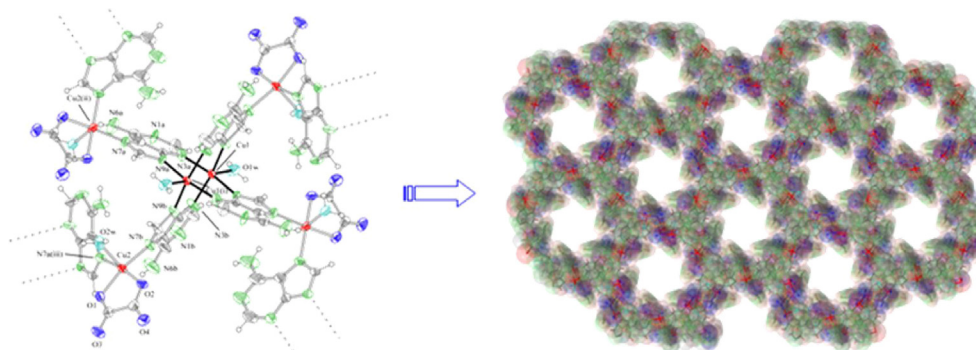


Fig. 6. Crystal structure of compound $\{[\text{Cu}_2(\mu\text{-adeninato})_4(\text{H}_2\text{O})_2][\text{Cu}(\text{ox})(\text{H}_2\text{O})_2]\}_n$ [18].

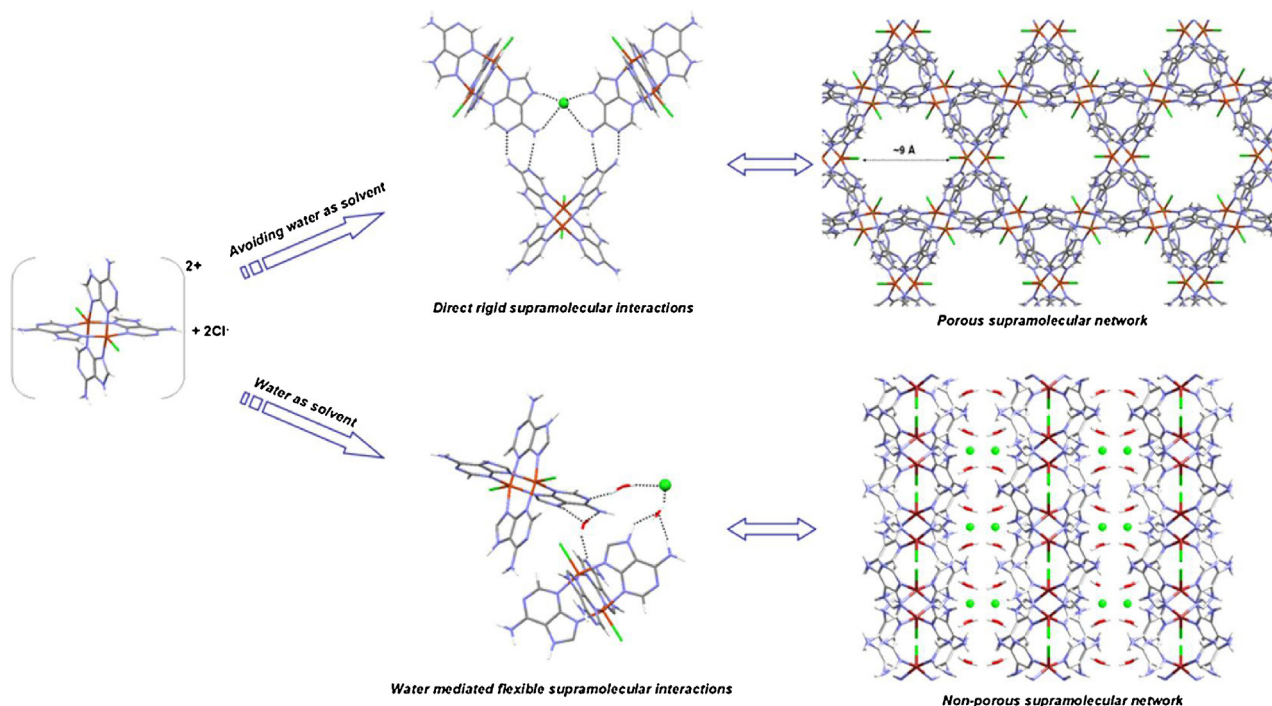


Fig. 7. Solvent influence on the crystal packing of $[\text{Cu}_2(\mu\text{-adenine})_4\text{Cl}_2]\text{Cl}_2$ [14,24].

voids or channels that are usually occupied by solvent molecules. However, there are still many challenges to realize on these tailor-made porous materials because the pursued structural control is often thwarted by the delicate balance of all covalent and non-covalent forces present in the crystal building, and a slight change in the synthetic approach may result in the failure to achieve the desired supramolecular interaction scheme and thus, in the overall three-dimensional architecture [23].

Proceeding in this way, we obtained a robust supramolecular porous compound of Cu(II) and adenine with the formula $[\text{Cu}_2(\mu\text{-adenine})_4\text{Cl}_2]\text{Cl}_2 \cdot 2\text{CH}_3\text{OH}$ which shows a high thermal stability (stable up to 220 °C) [24]. De Meester and Skapski reported many years ago, a similar but non-porous compound crystallized in water: $[\text{Cu}_2(\mu\text{-adenine})_4\text{Cl}_2]\text{Cl}_2 \cdot 6\text{H}_2\text{O}$ [14]. The apparently striking difference is due to hydrogen bonding characteristics of the water molecule, a powerful donor and acceptor site of hydrogen bonds [25]. It therefore can interfere, as is the case, with the predicted hydrogen bonding network leading to indirect, water mediated, hydrogen bonds between the tectons that produces the crystal structure collapse upon their removal (Fig. 7).

The weaker ability of methanol to establish hydrogen bonds implies that the crystal packing of the supramolecular porous compound $[\text{Cu}_2(\mu\text{-adenine})_4\text{Cl}_2]\text{Cl}_2 \cdot 2\text{CH}_3\text{OH}$, is essentially commanded by the assembling of the windmill dimeric $[\text{Cu}_2(\mu\text{-adenine})_4\text{Cl}_2]^{2+}$ entities through rigid direct hydrogen bonding pairing interactions between the adenine molecules. Moreover, interactions between the chloride anions and the adenine moieties of the cationic complexes provide extra stability and rigidity to the 3D porous supramolecular network and, as a consequence, increase the robustness of the crystal building. The dinuclear entities are cross-linked together by pairs of symmetry-related N6–H...N1 hydrogen bonding interactions between the Watson–Crick faces of two adjacent nucleobases to give a $R_2^2(8)$ ring, a well-known structural synthon involved in the supramolecular recognition processes which determines the self-assembling pattern of the adenine moieties in a great diversity of metal–nucleobase systems [26]. Furthermore, coordination of the adenine through the N9 atom of the

pyridine ring produces the proton transfer to the imidazole N7 site to give the non-canonical 7H-adenine tautomer which favours the formation of a hydrogen-bonded $R_2^1(7)$ ring between the Hoogsteen face [N6H, N7H] of the nucleobase as donor and the chloride counterion as acceptor in such a way that each counterion is joined to two adenine ligands from adjacent dimeric complexes.

The self-assembling process driven by the rigid interactions described above, results in a supramolecular 3D structure containing 1D cylindrical channels along the crystallographic *c* axis with a diameter of $\sim 9 \text{ \AA}$, that are occupied by the solvent molecules and that represent 36% of the total volume. This supramolecular network remains stable after the release of the methanol molecules and only collapses at temperatures above 240 °C. The compound is also stable against the surrounding humidity and only when immersed in water for several hours, does the crystal structure collapse leading to an amorphous material. This fact is also further evidence of the direct adenine–adenine hydrogen bonding disruptor effect of the water molecules. The permanent porosity of this material was ensured by the adsorption of several vapour molecules, finding that almost 0.5 molecules of dichloromethane and tetrachloromethane were adsorbed per dimeric entity. However, the N_2 adsorption isotherm measurements at 77 K showed very low adsorption capability and accessible surface area, just 3% of what would be expected ($790 \text{ m}^2 \text{ g}^{-1}$). This kind of reduced nitrogen adsorption has also been observed in other microporous hydrogen-bonded coordination frameworks [27]. This behaviour has been attributed to the strong quadrupole interaction between N_2 molecules and the electrostatic-field gradients around the pore window, thus blocking the diffusion of other N_2 molecules into the pores [28]. However, another possible explanation is the relative flexibility of the supramolecular structure at the surface that could lead to a temperature or humidity induced superficial rearrangement that involves a closure of the pore window. In fact, a recent paper of Matzger et al. proves, by means of positron annihilation lifetime spectroscopy (PALS), that the surface instability of several MOFs after solvent removal can render an impermeable barrier that hinders the adsorption of gas molecules [29].

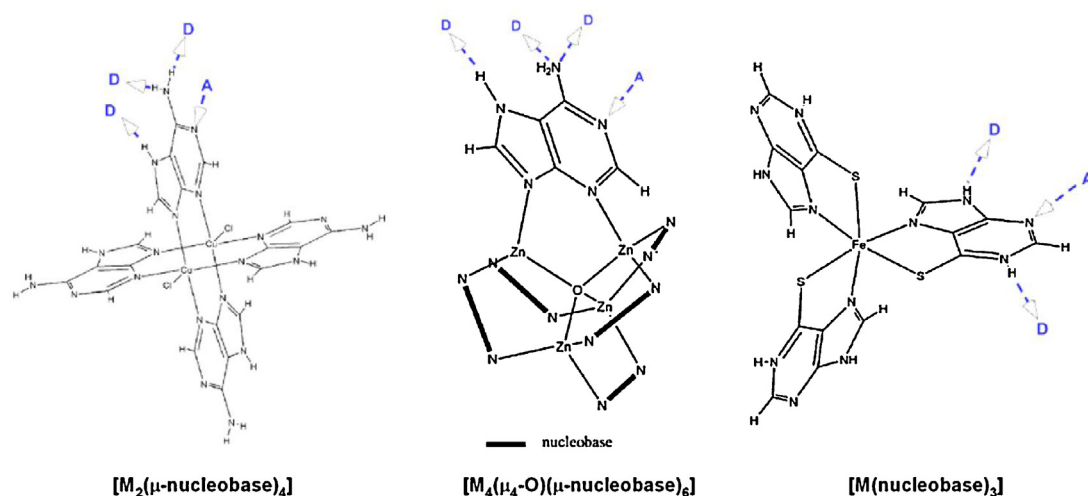


Fig. 8. Metal–nucleobase discrete entities suitable for the synthesis of *supra*MOFs.

This compound represents one of the first members of a new family of porous materials based on supramolecular interactions that differ from the extended supramolecular materials based on organic molecules because in this case the building units are coordination complexes or clusters that are connected through non-covalent interactions. Focusing on the synthons that imply the metal–nucleobase systems (Fig. 8), the opportunities to grow novel supramolecular metal–organic frameworks (*supra*MOFs), as named by Reger et al., are many [30]. A special feature of these systems is the geometrical angles set between the synthons, which are otherwise difficult to achieve in organic molecules.

4. [Cu₂(μ-adenine)₂(μ-carboxylato)₂] secondary building unit

There are few examples of the simultaneous presence and cooperation of μ-carboxylato and μ-adenine bridges (Fig. 9). The first example of this type corresponds with a 2D compound $\{[\text{Cd}_3(\mu_3\text{-adeninato-}\kappa\text{N3:}\kappa\text{N7:}\kappa\text{N9})_2(\mu_3\text{-adipate-}\kappa^2\text{O, O':}\kappa^2\text{O', O'':}\kappa^2\text{O', O'''})_2(\text{H}_2\text{O})_2] \cdot 1.5\text{H}_2\text{O}\}_n$ composed of trimeric entities in which both the adenine ligand and the adipate ligand cooperatively bridge the same metal centres [31]. More recently Rosi et al. provided new examples of this successful strategy. The first one corresponds with a porous network of formula $(\text{Me}_2\text{NH}_2)_2[\text{Zn}_8(\mu_4\text{-adeninato-}\kappa\text{N1:}\kappa\text{N3:}\kappa\text{N7:}\kappa\text{N9})_4(\mu\text{-BPDC-}\kappa\text{O:}\kappa\text{O}')_4(\mu\text{-BPDC-}\kappa^2\text{O, O':}\kappa^2\text{O', O'':}\kappa^2\text{O'})_2(\mu_4\text{-O})] \cdot 8\text{DMF} \cdot 11\text{H}_2\text{O}$ (BPDC: biphenyldicarboxylate) and commonly named bio-MOF-1 [32]. It consists of an anionic network that allows the exchange of the cationic counterions to provide a way to storage and release cationic drug molecules. The second one, $(\text{Me}_2\text{NH}_2)_4[\text{Zn}_8(\mu_4\text{-adeninato-}\kappa\text{N1:}\kappa\text{N3:}\kappa\text{N7:}\kappa\text{N9})_4(\mu\text{-BPDC-}\kappa\text{O:}\kappa\text{O}')_6(\mu\text{-O})] \cdot 49\text{DMF} \cdot 31\text{H}_2\text{O}$, corresponds with a novel topology using the same components that are arranged in such a way that they build up a mesoporous material with a high surface area ($4300\text{ m}^2\text{ g}^{-1}$) and one of the largest metal–organic framework pore volume reported to date ($4.3\text{ cm}^3\text{ g}^{-1}$) [33]. Almost at the same time, additional examples of this strategy appeared but using 2,6-diaminopurine instead of adenine [34]. These pioneer compounds envisaged the possibility to develop porous metal–organic frameworks based on the combined action of deprotonated adenine and carboxylate ligands.

There has been some other different approaches to synthesize these kinds of adeninate and carboxylate mixed compounds as it is the case for a series of compounds based on carboxylate functionalized adenines [9-(carboxypropyl)adenine] reported by Kumar and

Verma [35]. This strategy increases the coordination capacity of the adenine molecule, which is able to coordinate five different silver ions providing a polymeric crystal structure composed of hexameric silver–adenine rings.

In all the examples described above, the adenine and carboxylato ligands although they cooperate in the polymerization process, do not present the expected coordination mode similarity (Scheme 5). This fact is mainly due to the use of SBUs in which both ligands play different roles. In our case, due to the similarities between the μ-carboxylato-κO:κO' and μ-adenine-κN3:κN9 coordination modes it was possible to foresee the formation of mixed rigid paddle-wheel shaped $[\text{Cu}_2(\mu\text{-adenine})_x(\mu\text{-carboxylato})_y]$ entities (where $x+y=4$) that can be later used as SBUs, to provide extended porous systems as will be described below.

4.1. Porous MBioFs based on [Cu₂(μ-adenine)₂(μ-carboxylato)₂] units

Using the strategy described above we obtained a family of 3D metal–organic compounds, $\{[\text{Cu}_2(\mu_3\text{-adeninato-}\kappa\text{N3:}\kappa\text{N7:}\kappa\text{N9})_2(\mu_2\text{-OOC}(\text{CH}_2)_x\text{CH}_3\text{-}\kappa\text{O:}\kappa\text{O}')_2] \cdot y\text{H}_2\text{O}\}_n$ [x from 0 (acetate) to 5 (heptanoate)], whose adsorption measurements have demonstrated that the length of the aliphatic chain of the carboxylate ligands modifies the porosity of the open-framework structures [36]. The synthesis of this family of compounds is relatively simple as they can be obtained as green polycrystalline powder just by the addition of carboxylic acid to an aqueous solution containing the nucleobase and a copper(II) salt at room or near room temperature. The crystal structure, as predicted, consists of paddle-wheel shaped centrosymmetric dimeric units in which two copper(II) atoms are bridged by two adenine ligands coordinated by their N3 and N9 nitrogen atoms and two carboxylic ligands with a μ-O, O' coordination mode. These units are cross-linked (Fig. 10) through the apical coordination of the imidazole N7 atom of the adeninato ligands in such a way that each PW is linked to four adjacent entities with a Cu...Cu separation across the imidazole N9/N7 bridge of ca. 6.0 Å. This self-assembling process directed by the metal–adeninate linkages generates a 4-connected uninodal net with a *1vt* topology and a ($4^2.8^4$) point symbol, using as a node the dinuclear building unit. The net exhibits a three-dimensional system of intersecting cavities (Fig. 10) whose effective volume comprises 37% and 25% of the unit cell volume for the acetate and butanoate compounds, respectively. The free volume is directly related to the length of the aliphatic chain, which is pointing

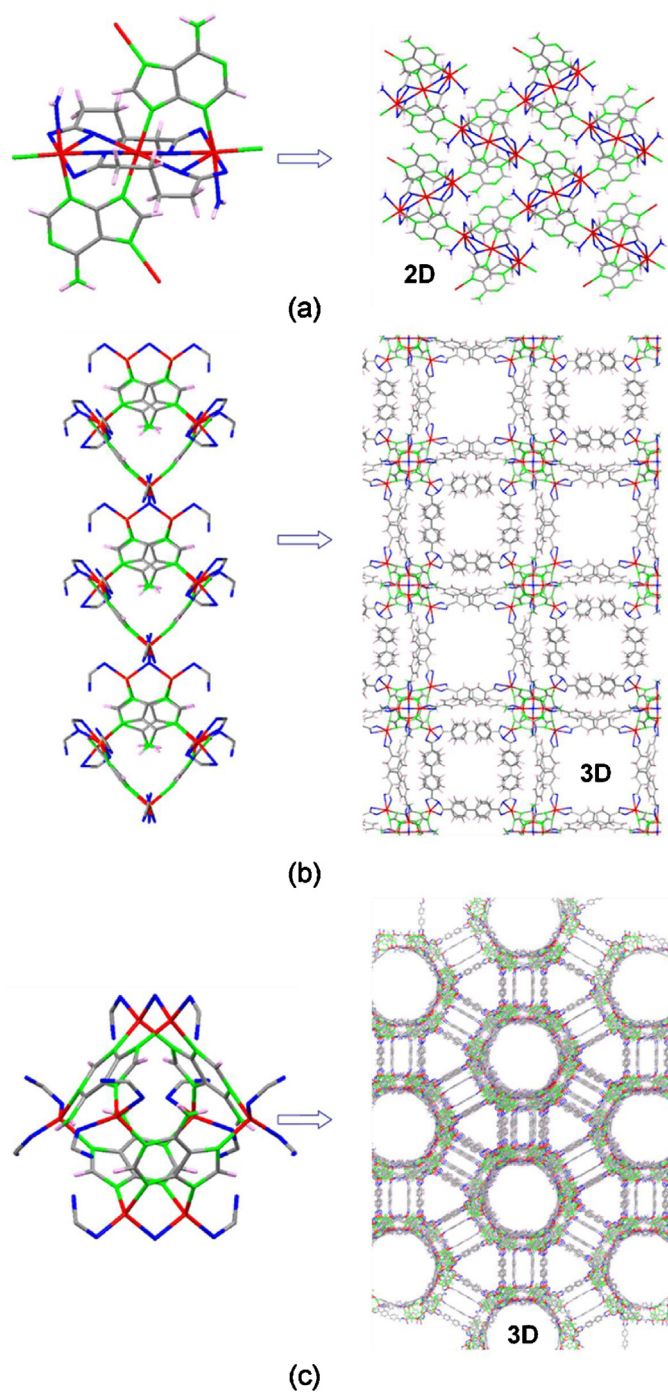
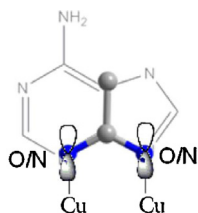


Fig. 9. SBUs and the resulting crystal structures of compounds (a) $\{[\text{Cd}_3(\mu_3\text{-adeninato})_2(\mu_3\text{-adipate})_2(\text{H}_2\text{O})_2] \cdot 1.5\text{H}_2\text{O}\}_n$ [31], (b) $(\text{Me}_2\text{NH}_2)_2[\text{Zn}_8(\mu_4\text{-adeninato})_4(\mu\text{-BPDC})_6(\mu_4\text{-O})] \cdot 8\text{DMF} \cdot 11\text{H}_2\text{O}$ [32], and (c) $(\text{Me}_2\text{NH}_2)_4[\text{Zn}_8(\mu_4\text{-adeninato})_4(\mu\text{-BPDC})_6(\mu\text{-O})] \cdot 49\text{DMF} \cdot 31\text{H}_2\text{O}$ [33].



Scheme 5. Coordination similarities between the $\mu\text{-carboxylato-}\kappa\text{O}:\kappa\text{O}'$ and $\mu\text{-adenine-}\kappa\text{N3}:\kappa\text{N9}$ coordination modes.

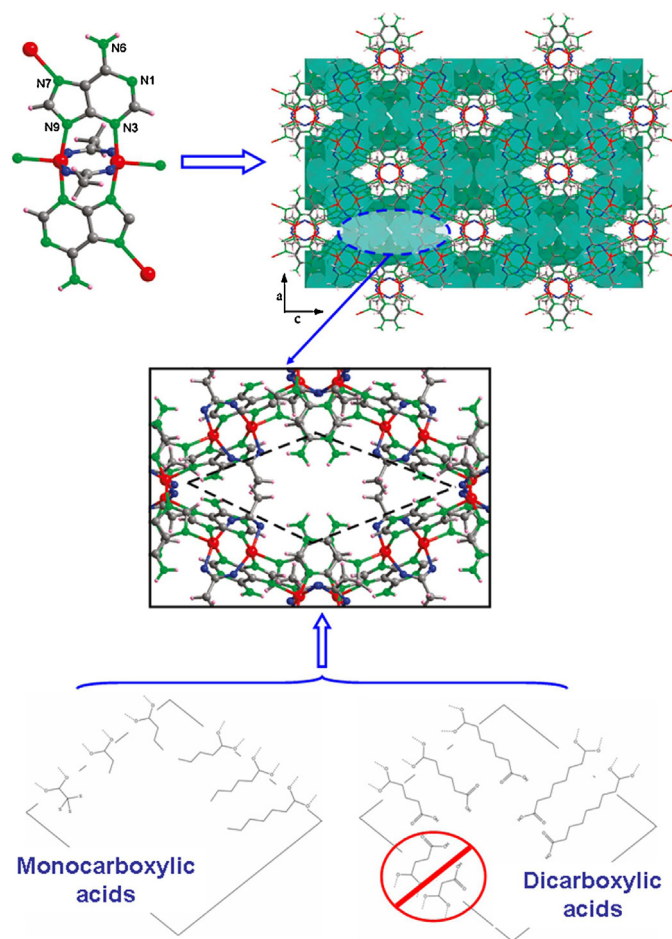


Fig. 10. Top: $[\text{Cu}_2(\mu_3\text{-adeninato})_2(\mu_2\text{-OOCCH}_3)_2]_n$ compound, showing the paddle-wheel core, the crystal packing and the cavity with the Watson–Crick face and the aliphatic chains pointing towards it. Bottom: monocarboxylic and dicarboxylic acids of different length employed in the preparation of the compounds [36,37].

towards the inner portion of the channels, so that a longer chain implies less free volume.

Moreover, the 3D crystal structure seems to be so robust that it is obtained even when using long chain aliphatic dicarboxylic acids: $\text{HOOC}(\text{CH}_2)_n\text{COOH}$ [n from 3 to 5] [37]. Surprisingly, only one of the two carboxylic groups is deprotonated and coordinated to the metal centres, $\mu\text{-}\kappa\text{O1}:\kappa\text{O2}$, while the other remains protonated inside the channels of the crystal structure in such a way that the dicarboxylic ligands do not join the dimeric fragments as could in principle be expected. Only when short chain dicarboxylic acids are employed a different crystal structure is obtained. In this last case the great tendency of these acids to chelate metal ions disturbs the paddle-wheel shaped SBUs providing crystal structures based on discrete complex entities that will be further discussed in Section 6. Almost at the same time that we reported this new family, Rosi et al. reported the synthesis of the analogous $[\text{Co}_2(\mu_3\text{-adeninato-}\kappa\text{N3}:\kappa\text{N7}:\kappa\text{N9})_2(\mu_2\text{-OOCCH}_3\text{-}\kappa\text{O}:\kappa\text{O}')_2] \cdot 2\text{DMF} \cdot 0.5\text{H}_2\text{O}$ (Bio-MOF-11) [3d]. The synthesis of this last compound is more exigent than that of copper(II) based ones, as it requires a prior lyophilization of the reagent mixture, the use of solvothermal conditions and DMF solvent. All attempts to obtain this analogous compound and others (using Zn^{2+} , Ni^{2+} and Mn^{2+} as metal centres) by means of simple aqueous solvent synthesis were unsuccessful. The reason for this failure seems to be a subtle balance of the acid constants when coordinated to the metal centres that allows the deprotonation of the adenine when coordinated to copper(II) ions but not for the other metal centres. In the case of

the cobalt(II) analogous it becomes clear that the presence of the alkylamines generated during the partial decomposition of the DMF solvent at the solvothermal condition is necessary to deprotonate the adenine.

4.2. Fine tuning of the adsorptive properties

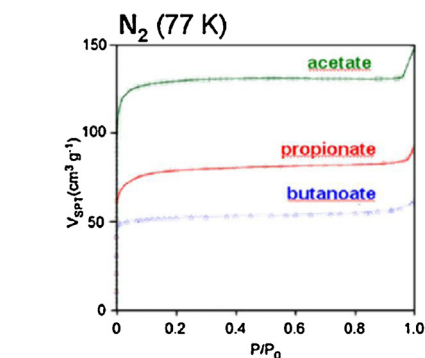
All the compounds of this family of porous MBioFs are relatively highly thermally stable. They are able to release the solvent molecules without the collapse of the crystal structure, after which they remain stable up to around 250 °C. This behaviour offered the opportunity to use them as adsorptive materials.

The permanent porosity of the MBioFs with formula $[\text{Cu}_2(\mu_3\text{-adeninato-}\kappa\text{N3:}\kappa\text{N7:}\kappa\text{N9})_2(\mu_2\text{-OOC}(\text{CH}_2)_x\text{CH}_3\text{-}\kappa\text{O:}\kappa\text{O}')_2]_n$ was studied by means of measuring N_2 (77 K), CO_2 (273 K) and H_2 (77 K) isotherms (Fig. 11) [38]. Compounds containing acetate, propionate and butanoate showed a type I isotherm with a sharp knee at low relative pressures ($p/p_0 \sim 0.01$), followed by a plateau, which is characteristic of a crystalline microporous solid with uniform pore-size distribution. On the other hand, the pentanoate compound exhibited an isotherm corresponding with an essentially non-adsorbing solid. The results also showed that the permanent porosity of guest-free compounds is easily tunable by means of the length of the aliphatic chains. Longer tails reduce the accessible space decreasing accordingly the amount of adsorbed gas molecules. It must be emphasized that the amount of CO_2 adsorbed in the acetate compound exceeds the values reported for many other well-known MOFs.

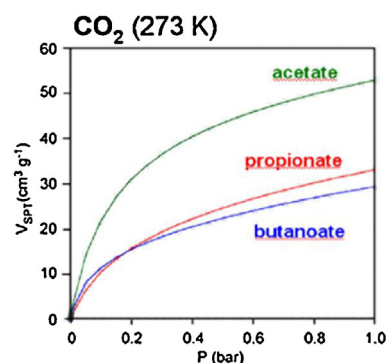
Their microporous nature, the presence of the Watson–Crick face in the pore walls and the tunability of the channels by means of the length of the aliphatic chain makes them good candidates for studying their behaviour in gas capture and separation technologies [39] where a high adsorptive selectivity towards a specific species is fundamental. In relation to the latter, the suitability of the MOFs in CO_2 capture and sequestration (CCS, Carbon Capture and Sequestration) technologies is remarkable, where compared with the existing methods thus far the CO_2 capture by means of adsorption in porous materials presents a higher energetic efficiency [40]. Nowadays, CO_2 capture is of special interest in combined cycle power plants with integrated gasification [41] or in the H_2 production by means of fuel or biomass gasification processes [42], where the syngas (mixture mainly composed by CO and H_2) is converted by the water gas shift reaction to a mixture composed of H_2 and CO_2 . Furthermore, the purification of H_2 destined for catalytic hydrogenation reactions or to fuel cells, where impurities such as CO can be harmful, is also relevant.

Considering all the aspects mentioned above the presence of MBioFs is vital as they decorate the pore walls with the Watson–Crick faces of the adenine, which facilitates these coordination polymers to selectively capture CO/CO_2 based on the basicity of this site and also the H-bonding interactions with polar CO and quadrupolar CO_2 [3c,43]. Therefore, we have carried out the study of the adsorption selectivity of binary mixtures of CO_2/H_2 and CO/H_2 [38]. Owing to the experimental complexity of this kind of analysis and the good fits that Grand Canonical Monte Carlo (GCMC) calculations have shown in previous works, the estimation of the selectivity values was performed by computing the values of the Henry constants and the adsorption isotherms of the binary gas mixtures (Fig. 12).

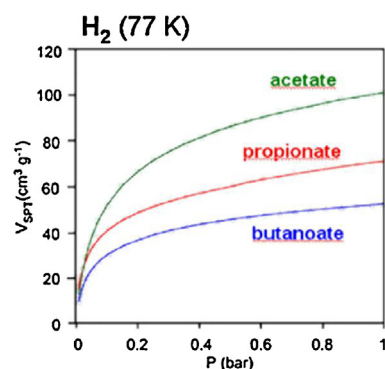
In general, the selectivity towards CO_2 and CO increases as the pore gets smaller and as the temperature is lowered. In fact, at the lower temperature boundary noticeably greater values are estimated for compound containing butanoate. In all cases, with increasing temperature the selectivity falls exponentially and the selectivity values of each compound tend to be comparable. This fall is more pronounced for butanoate, which at 373 K reaches



Compound	Area _{BET} (m ² /g)	N ₂ (mmol/g)	V _{t-plot} (cm ³ /g)
acetate	505	5.8	0.173
propionate	301	3.4	0.107
butanoate	202	2.4	0.073
pentanoate	8.9	--	--



Compound	CO ₂ (mmol/g)	V _{t-plot} (cm ³ /g)
acetate	2.3	52.90
propionate	1.5	33.04
butanoate	1.3	29.41



Compound	H ₂ (mmol/g)	H ₂ (wt.-%)	V _{t-plot} (cm ³ /g)
acetate	4.51	0.9	98
propionate	3.17	0.6	67
butanoate	2.33	0.5	46

Fig. 11. N_2 (77 K), CO_2 (273 K) and H_2 (77 K) experimental adsorption isotherms. Reproduced from Ref. [38]. Copyright (2012) WILEY-VCH Verlag GmbH & Co. KGaA, Weinheim.

selectivity values only slightly above that of acetate and propionate containing compounds. The adsorption selectivity values match the Henry's selectivity at low pressure values.

In acetate and propionate compounds, the CO_2 vs. H_2 adsorption selectivity shows a comparable evolution as a function of pressure.

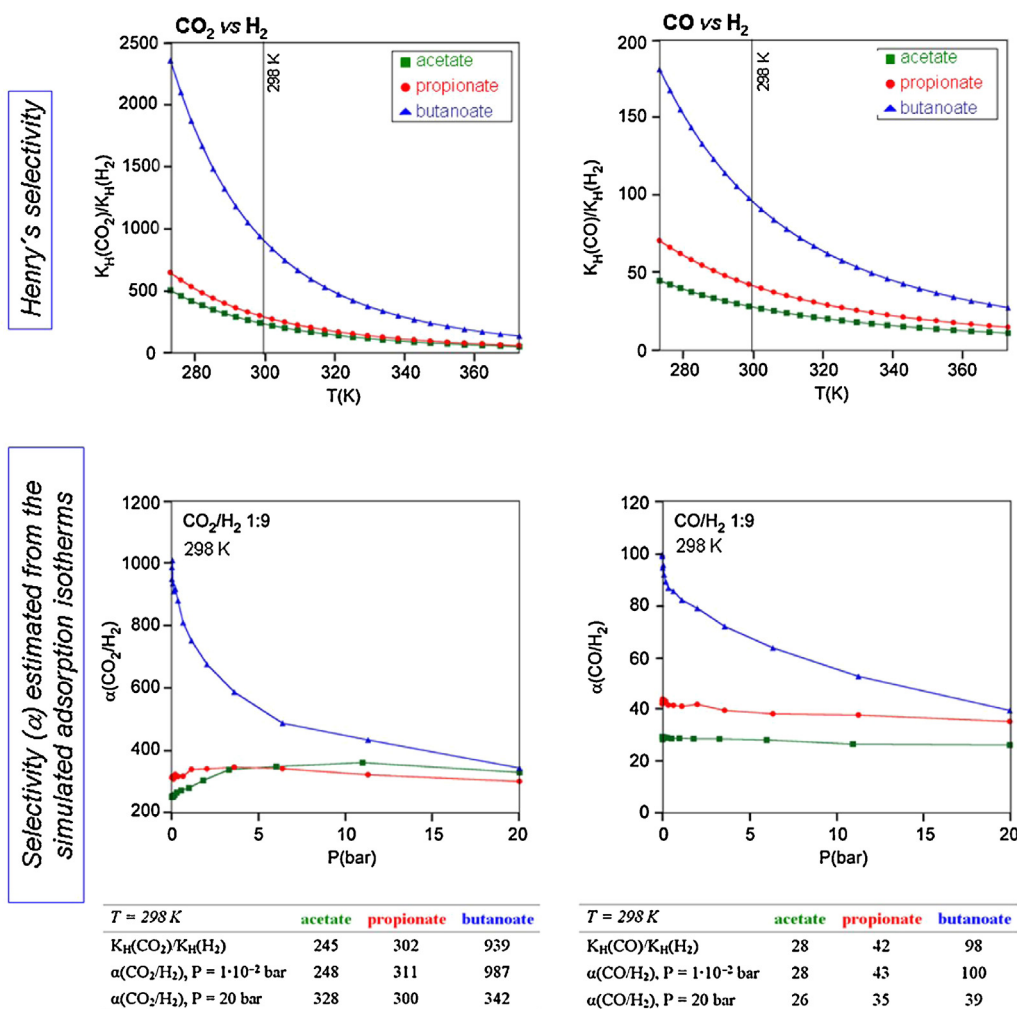


Fig. 12. Adsorption selectivities for binary CO₂/H₂ and CO/H₂ mixtures: Henry's selectivity, $K_H(A)/K_H(B)$, and selectivity (α) estimated from the simulated adsorption isotherms at 298 K.

Reproduced from Ref. [38]. Copyright (2012) WILEY-VCH Verlag GmbH & Co. KGaA, Weinheim.

As the pressure increases these values undergo a slight rise, which after reaching a maximum remain stable or decrease slightly. The selectivity of these compounds is intermediate with respect to other microporous materials [44]. On the contrary, the butanoate analogue shows comparatively high selectivity values (ca. 1000) over the low-pressure range. The pressure increment produces an exponential fall reaching the selectivity values described for the acetate and propionate compounds at high pressure. On the other hand, in the case of the CO/H₂ binary mixture, the initial selectivity values for acetate and propionate (α : 28 and 43 at $P = 1 \times 10^{-2}$ bar) show a slight fall with increasing pressure, stabilizing at somewhat lower values (26 and 35) at ca. 5 bar. These values can be considered as intermediate and comparable to those described for other microporous materials [45]. In the butanoate compound, the CO/H₂ selectivity shows uncommonly high values at low pressure (ca. 100, one of the highest reported to date for CO/H₂ mixtures), which falls again exponentially to reach the selectivity values similar to the acetate and propionate ones at high pressures.

In order to have deeper insight into the unusual behaviour of the butanoate analogue, we analyzed the preferential adsorptive sites from the interpretation of the potential energy maps obtained by GCMC simulations. The potential energy maps for N₂ reveal two types of adsorption cavities in the acetate compound (Fig. 13). The first one consists of two minima whose centroids are in two

symmetrically equivalent positions sandwiched by the pyrimidine rings of two adeninato ligands (site 1). The second cavity is somewhat wider and it presents four symmetrically equivalent energy minima oriented towards the Watson–Crick faces of four adenine molecules in a pseudo-tetrahedral disposition (site 2). Considering the crystallographic multiplicity of the positions of the centroids there are 32 preferential adsorption sites within the unit cell (site-1: 16 and site-2: 16). Site-2, due to its very polar nature is specially well-suited for the adsorption of CO₂ (having a relatively high quadrupolar moment) and CO (having a weak dipolar moment and relatively high quadrupolar moment). In the acetate and propionate derivatives both sites are accessible for any of the three adsorbates (CO₂, CO and H₂) according to the potential energy maps. However for the butanoate analogue, the occupancy of site 1 is hindered by the aliphatic tail of the carboxylato ligand which is oriented towards this cavity. Thus, at low pressures the guest molecules go into site 2 whose high affinity towards CO₂ and CO leads to a negligible coadsorption of H₂ and explains the high selectivity values achieved at low pressures. On the contrary, the abrupt drop in the selectivity values at high pressures is explained because although at low pressures the adsorption on site 1 is negligible for the three adsorbates (CO₂, CO and H₂), at high pressures only H₂ is able to populate site 1. Therefore, as the pressure increases, CO₂ and CO molecules saturate site 2, while H₂ molecules easily occupy site 1, leading to a more significant coadsorption of H₂ that promotes

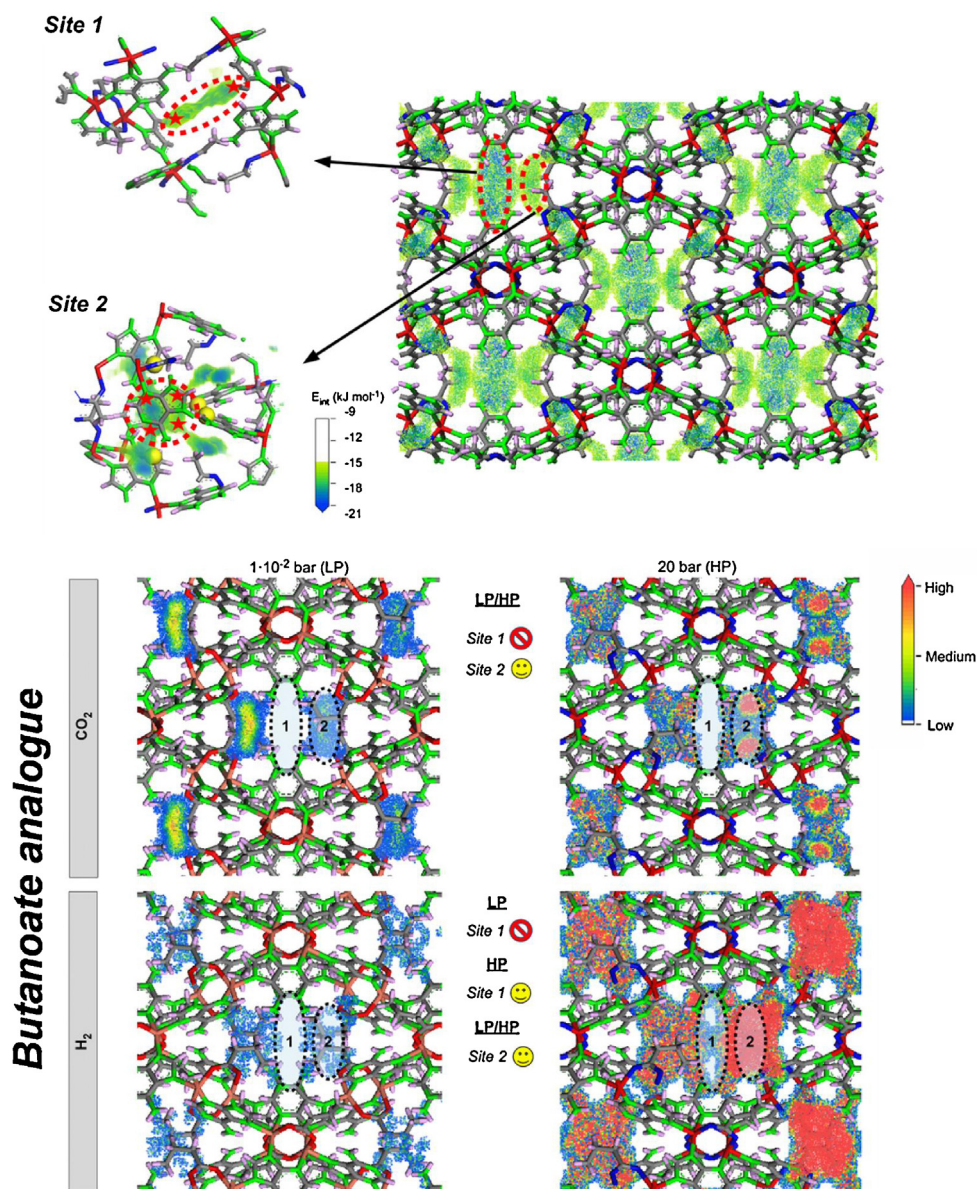


Fig. 13. Preferred adsorption sites and accessibility at low pressure (LP: 1×10^{-2} bar) and high pressure (HP: 20 bar). Reproduced from Ref. [38]. Copyright (2012) WILEY-VCH Verlag GmbH & Co. KGaA, Weinheim.

the marked exponential decrease in the selectivity observed for the butanoate compound.

4.3. Overtaking gas uptake capacity limited by the crystal structure

During our work with this family of porous MBioFs we noticed that to ensure the complete miscibility of monocarboxylic acids longer than propionate it is mandatory to use a mixture of water and methanol as solvent. This fact is something not surprising as far as we all know that short chain carboxylic acid such as acetic and propionic acids are completely miscible in water but long chain ones are immiscible. However at intermediate situations there is an opportunity to obtain stable microemulsions and the micelles present in it can be used as templating agents. Therefore we take some time to search for information about the miscibility of these acids in different solvents and we found an old paper, published in 1929, that clearly indicates the formation of a stable microemulsion in mixtures of butyric acid and water [46]. After that, there was

some research based on this paper in subsequent years but after 1952 the interest for this system apparently ceased and references to butanoic acid as surfactant almost disappeared [47].

We reproduced this work to ensure the presence of the micelles and to determine, by means of conductivity measurements, the critical micelle concentration (CMC) above which a stable microemulsion is obtained. The value obtained at 4 °C is around 1 M for a butyric acid/water mixture in agreement with the data previously published. However, in the presence of copper(II) ions the CMC drops to a 0.05 M value, that ensures the presence of micelles under the common reagent concentrations used for the synthesis of the butanoate MBioF.

As previously mentioned the micelles are usually employed as templating agents to incorporate pores within a material by means of the removal of the surfactant molecules from the embedded micelles. Obviously, depending on the size of the template the resulting pore will fall into the micropore (<2 nm), mesopore (2–50 nm) or macropore (>50 nm) regime. It becomes clear that due to the length of the commonly employed surfactants (SDS,

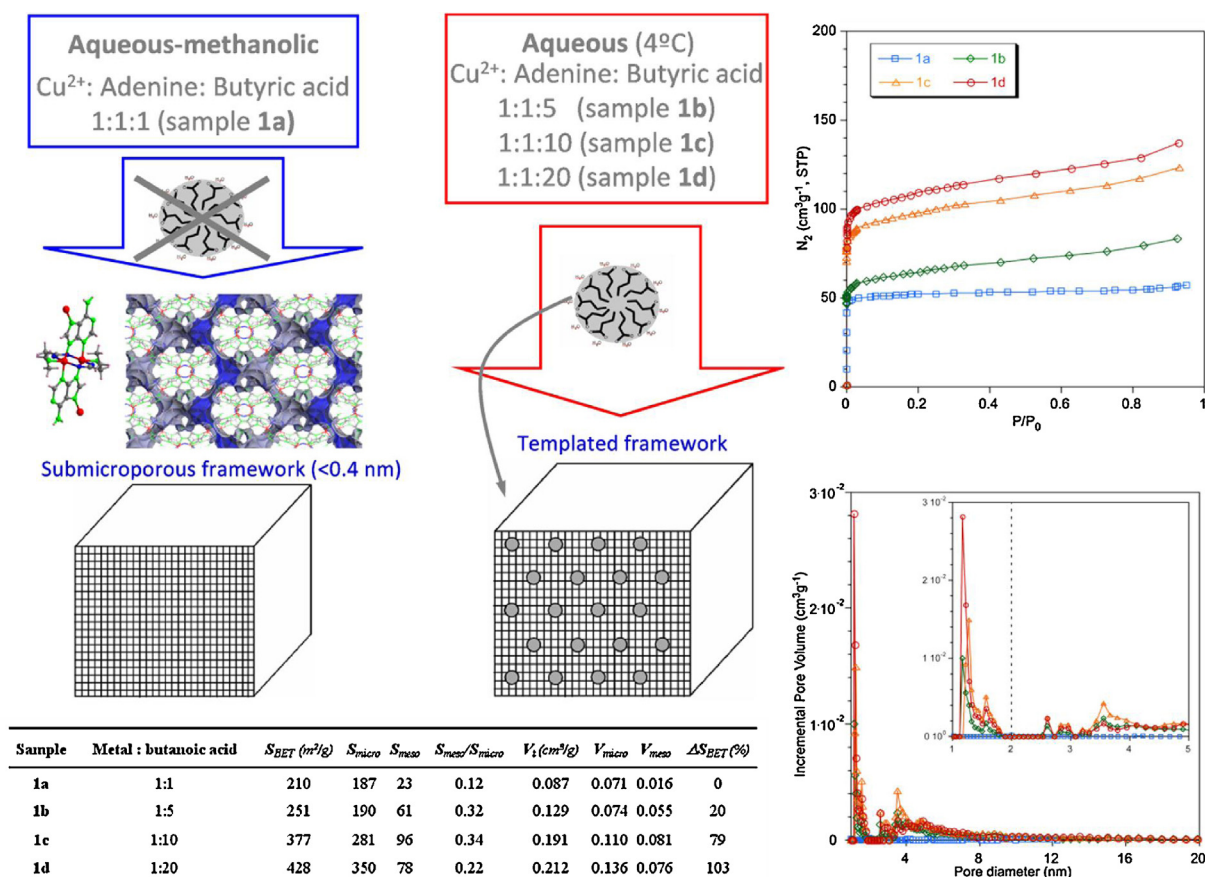


Fig. 14. Schematic representation of the butanoic acid templating effect, N_2 adsorption isotherms at 77 K and pore size analysis [48].

AOT, Tween, etc.), the generated pores fall well into the mesopore regime. Before the publication of the work described below there was no reported method able to incorporate extra microporosity to a material. This work took advantage of the relatively short tail of the butyric acid, around 6.4 Å, to generate small micelles that will fall into the micropore regime [48].

The use of micelles to incorporate porosity is a well-known strategy in many areas such as the synthesis of mesoporous silicates, carbons and other ceramics [49]. More recently, it has been applied to the synthesis of hierarchically ordered micro- and mesoporous MOFs in which the microporosity is limited by the crystal structure and the mesoporosity arises from the inclusion of long chain micelles [50,51]. Unfortunately, the methods developed that provide the mesoporous characteristics to the starting material usually also affect the material by lowering the contribution of the microporosity to the total porosity and by decreasing the available total surface area [50,52]. In many cases, the addition of mesoporous features is a desired objective for example to provide technologically relevant ordered mesoporous materials with high specific surface areas. However, in other cases, for instance to improve the performance in gas separation and purification processes [53], it is a superior option to increase the porosity just in the micropore range.

In order to ensure the viability of this route to enhance the microporosity (Fig. 14), we prepared several samples of $[Cu_2(\mu_3\text{-adeninato})_2(\mu\text{-butanoato})_2]_n$ with the following metal:butanoic acid ratios: **1a** (1:1), **1b** (1:5), **1c** (1:10) and **1d** (1:20). The first sample **1a**, to be used as reference material, was synthesized in a water: methanol mixture to avoid strictly any micelle formation. In contrast, samples **1b–1c** were prepared at 4 °C using solely water as solvent to favour the micellar aggregation. The crystallinity of the

material was retained after the inclusion of the micelles and even after the release of the butyric acid molecules from the incorporated micelles. The N_2 adsorption isotherms at 77 K for the four samples shows that a significant increase in the total gas uptake takes place as the amount of butanoic acid is raised. The sample prepared with the highest butanoic acid concentration (**1d**) doubles the surface area of the reference material (**1a**), reaching a maximum value of 428 m² g⁻¹.

The pore size distribution, modelled by density functional theory (DFT), shows the appearance of a maximum around 1.3 nm, followed by some contribution of pores between 2.6 and 4 nm. The maximum, located in the microporous range, shows a continuous raise as the micelle concentration increases and its diameter agrees fairly well with the expected one. No clear trend was observed for the less contributing pores of greater size, which source is probably related to the presence of some bigger aggregates of butanoic acid coming from the coalescence of some original micelles during the crystallization process. None of these maxima were observed in the untemplated sample (**1a**).

5. $[Cu_2(\mu\text{-carboxylato})_4]$ secondary building unit

The correct selection of the polycarboxylato ligand can direct the resulting crystal structure from the assembly of the well-known $[Cu_2(\mu\text{-carboxylato})_4]$ entities towards a great variety of architectures ranging from polynuclear discrete entities to 3D crystal structures. As example: flexible dicarboxylic connectors provide 1D infinite chains, rigid linear dicarboxylates generate 2D infinite sheets, rigid angular carboxylates afford octahedral clusters, and linear but not coplanar carboxylates give rise to 3D porous nets (Fig. 15) [13a,54]. There are many other combinations using

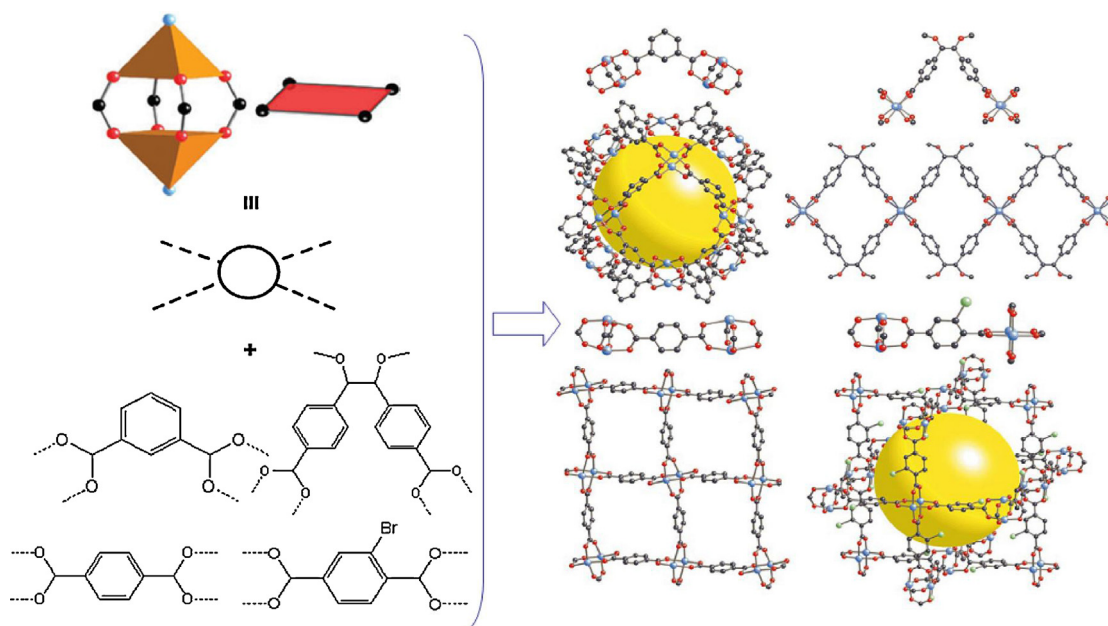


Fig. 15. Dimmensionality control of the $[\text{Cu}_2(\mu\text{-carboxylato})_4]$ paddle-wheel units assembly by means of precise dicarboxylate linker geometry [13a,54].

connectors containing additional carboxylate groups that provided different topologies [55]. The axial positions of these entities, usually occupied by solvent molecules, can be replaced by nucleobase ligands increasing the ability of the systems to establish molecular recognition processes [4].

Adenine molecules methylated at N3/N9 positions were employed to preclude the adenine $\mu\text{-}\kappa\text{N3}:\kappa\text{N9}$ bridging mode that is the key factor to obtain the mixed dimeric $[\text{Cu}_2(\mu\text{-adenine})_2(\mu\text{-carboxylato})_2]$ entities that were used as building blocks in Section 4. In this way, we promoted the formation of the $[\text{Cu}_2(\mu\text{-carboxylato})_4]$ entities and their polymerization through the careful selection of the dicarboxylato bridge. In the first stage of this research line we prepared a series of infinite 1D metal-organic structures using long chain dicarboxylato ligands: $^-\text{OOC}(\text{CH}_2)_n\text{COO}^-$ [n being 3 (glutarate) and 5 (pimelate)] altogether with 3-methyl- and 9-methyladenine. The obtained compounds $\{[\text{Cu}_2(\mu_4\text{-glutarato})_2(3\text{-methyladenine-}\kappa\text{N7})_2]\cdot 4\text{H}_2\text{O}\}_n$, $\{[\text{Cu}_2(\mu_4\text{-glutarato})_2(9\text{-methyladenine-}\kappa\text{N7})_2]\}_n$, and $\{[\text{Cu}_2(\mu_4\text{-pimelato})_2(9\text{-methyladenine-}\kappa\text{N7})_2]\cdot 2(\text{pimelic acid})\}_n$ contain chains of interconnected paddle-wheel entities in which the dicarboxylato ligands show the expected $\mu_4\text{-}\kappa\text{O1}:\kappa\text{O2}:\kappa\text{O3}:\kappa\text{O4}$ binding mode. The methylated nucleobases exhibit their usual monodentate N7-coordination pattern to anchorage to the apical positions of the dimeric entity [37]. This assembling strategy provides neutral chains where the paddle-wheel motifs are doubly bridged by the tetratopic dicarboxylate anions (Fig. 16). The supramolecular architecture of glutarato based ones is essentially knitted by pairing interactions between the Watson–Crick faces of adjacent adenines, whereas that of pimelato shows the inclusion of guest pimelic molecules which are anchored to the polymeric chains through fork-like hydrogen bonding interactions between one of the carboxylic groups and the peripheral adenine moieties, affording a supramolecular layered structure.

6. Other metal–carboxylato–adenine systems

As previously mentioned short chain dicarboxylate ligands have a great tendency to coordinate metal centres establishing five or six member chelating rings. This precludes the presence of the paddle-wheel shaped dimeric entities that we were using

to generate the previously described systems. In any case they provide many interesting systems ranging from discrete monomers and dimers to infinite polymeric chains that can, in some cases, be rationalized on the basis of their coordination properties.

6.1. Metal-malonato-adenine discrete systems. Magnetic properties

Malonato ligand exhibits a remarkable versatility in adopting different modes of bonding, including monodentate, chelating and bridging, with more than one of these modes sometimes occurring in the same compound. Fig. 17 shows the most usual coordination modes of this short chain dicarboxylato ligand [56]. There is

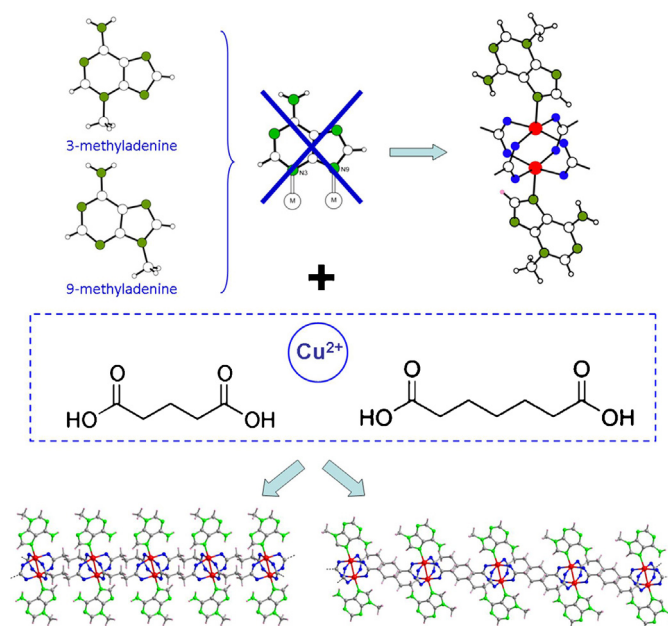


Fig. 16. Schematic representation of the design of infinite 1D chains based on $[\text{Cu}_2(\mu\text{-carboxylato})_4]$ with long chain dicarboxylato ligands and decorated with methylated adenine moieties [37].

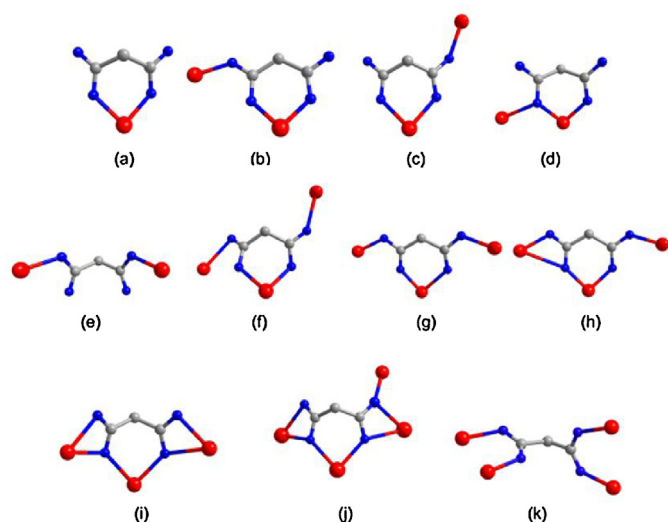


Fig. 17. Most common coordination modes of malonato ligand.

only one crystal structure registered in the CSD with the malonate ligand coordinated to a first row transition metal centre showing the $\mu_4\text{-}\kappa\text{O1}:\kappa\text{O1}':\kappa\text{O2}:\kappa\text{O2}'$ bridging mode, which is the key factor to obtain the extended systems described in Section 5. The trend of malonate ligand to establish five membered chelate rings hinders the individual carboxylate groups to afford the $\mu\text{-}\kappa\text{O}:\kappa\text{O}'$ bridging mode which is necessary to obtain the $[\text{M}_2(\mu\text{-carboxylato-}\kappa\text{O}:\kappa\text{O}')_4]$ or $[\text{M}_2(\mu\text{-adenine-}\kappa\text{N3}:\kappa\text{N9})_2(\mu\text{-carboxylato-}\kappa\text{O}:\kappa\text{O}')_2]$ secondary building units. In spite of all the above drawbacks, we obtained pseudo “paddlewheel” dinuclear $[\text{M}_2(\mu\text{-adenine-}\kappa\text{N3}:\kappa\text{N9})_2(\mu\text{-malonato-}\kappa^2\text{O1},\text{O2}:\kappa\text{O1})_2(\text{H}_2\text{O})_2]$ ($\text{M}^{\text{II}} = \text{Ni}, \text{Co}$) units (Fig. 18) [57]. Each metal is coordinated to three oxygen atoms from the malonato ligands and two nitrogen atoms of adenine nucleobases. The octahedral distorted polyhedron is completed with a water molecule to give a $\text{N}_2\text{O}_3\text{Ow}$ donor set. The malonate anion shows an unusual tridentate $\mu\text{-}\kappa^2\text{O1},\text{O2}:\kappa\text{O1}$ coordination mode where O1 links both metal atoms and O2 is only bonded to one

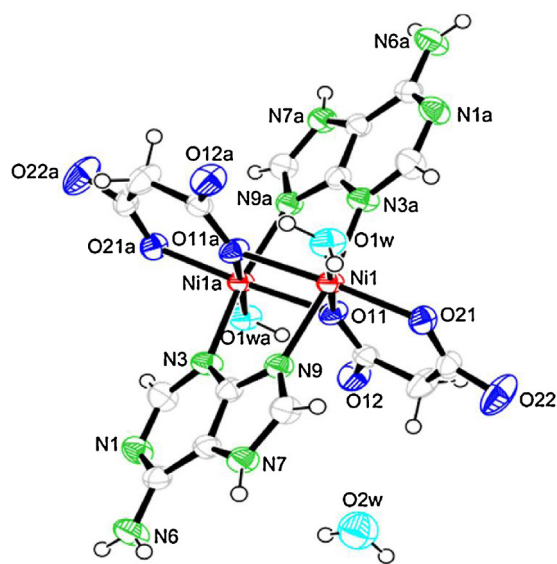
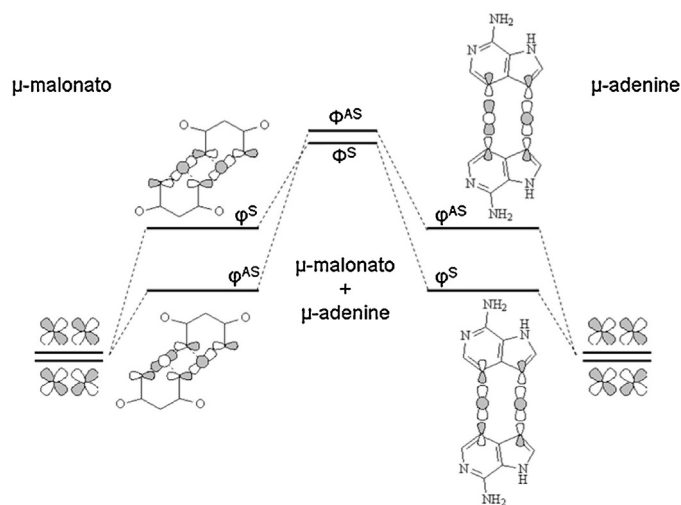


Fig. 18. Pseudo paddle-wheel shaped entities in compounds $[\text{M}_2(\mu\text{-adenine})_2(\mu\text{-malonato})_2(\text{H}_2\text{O})_2]$ ($\text{M}^{\text{II}} = \text{Ni}, \text{Co}$). Reproduced from Ref. [57]. Copyright (2012) WILEY-VCH Verlag GmbH & Co. KGaA, Weinheim.



Scheme 6. Orbital countercomplementarity of the $\mu\text{-malonato-}\kappa^2\text{O1},\text{O2}:\kappa\text{O1}$ and $\mu\text{-adenine-}\kappa\text{N3}:\kappa\text{N9}$ bridging ligands. Reproduced from Ref. [57]. Copyright (2009) WILEY-VCH Verlag GmbH & Co. KGaA, Weinheim.

of these metal centres, thus forming a six-membered chelate ring (coordination mode d in Fig. 17).

The hexacoordination of the metal centres in these pseudo paddle-wheel units contrast with the pentacoordination found in normal paddle-wheel units. Additionally the coordinated water molecules and the angles between the M-Ow bond and the metal \cdots metal axis are around $34\text{--}45^\circ$. This differs significantly with the collinear disposition between the M-X axial bonds ($\text{X} = \text{Cl}, \text{H}_2\text{O}$) and the $\text{M}\cdots\text{M}$ axis in common carboxylate/adenine PW motifs. This structural feature precludes the controlled polymerization through the malonate ligand but it leaves open the opportunity to achieve it by means of the deprotonation and further coordination of the adenine ligands to the apical position of adjacent dimeric entities.

The study of the magnetic properties of these compounds provided a striking difference with respect to the behaviour of the common paddle-wheel dimeric entities. At low temperatures the ferromagnetic nature of the interaction mediated simultaneously by the bridging adenine and malonato becomes evident. This behaviour is in great contrast with the strong antiferromagnetic interaction observed for the $[\text{Cu}_2(\mu\text{-adenine-}\kappa\text{N3}:\kappa\text{N9})_2(\mu\text{-carboxylato-}\kappa\text{O}:\kappa\text{O}')_2]$ units. The differences come from the coordination mode of the malonate which resembles a $\mu\text{-oxo}$ bridge. As a consequence, the splitting of the molecular magnetic orbitals is reversed for each type of bridging ligand (adenine and malonato), thus leading to an almost negligible energy difference between them (Scheme 6). This phenomenon, called orbital countercomplementary, favours a parallel alignment of the unpaired electron spins and it is responsible for the observed ferromagnetic behaviour.

6.2. Metal-oxalato-adenine extended systems

The oxalato ligand (dianion of oxalic acid; ox) has appeared as a fruitful tecton for the design of a great diversity of homonuclear and heteronuclear transition metal compounds, which have played a key role in areas such as inorganic crystal engineering and molecule-based magnetism [58]. The main reasons for the extensive use of this old but evergreen ligand are (a) its remarkable ability to mediate electronic effects between metal centres, affording compounds with a wide range of magnetic properties; and (b) the prevalence of its rigid bischelating bridging mode, that provides

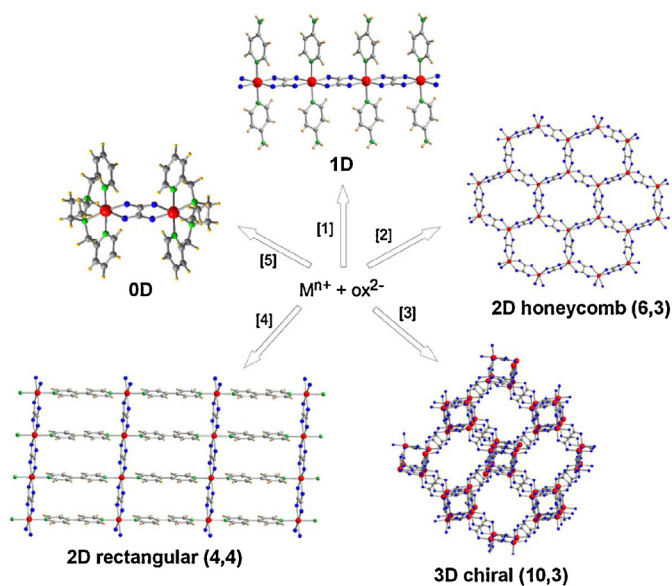


Fig. 19. Tailoring of metal-oxalato frameworks by using different organic ligands and/or templating counterions: [1] monodentate N-containing rings; [2] achiral cations; [3] chiral tris-chelated diimine cationic complexes; [4] bidentate ligands such as 4,4-bipy, piperidine, bpe, and bpa; and [5] multidentate blocking N- or O-donor ligands.

Reproduced from Ref. [59]. Copyright (2006) American Chemical Society.

some degree of predictability with regard to the structural characteristics of the resulting metal-oxalato networks. The topology and dimensionality of polymeric networks based on the oxalato bridging ligand essentially depend on the shape of the templating counterions, on the features of the auxiliary organic ligands used to complete the metal coordination sphere, or on both (Fig. 19) [59].

In the framework of our previous research on the chemistry of polymeric complexes based on the oxalato-bridging ligand, a strategy for the design of one-dimensional complexes with general formula $[M(\mu\text{-ox})(L)_2]_n$ containing substituted pyridine derivatives as terminal ligands has been derived [60]. By using similar synthetic routes, a family of one-dimensional (1D) complexes has been prepared, in which the pyridine bases are replaced by nucleobases, such as purine (pur) and/or adenine (Hade), whose structural characterization allows one to perform a fruitful data harvesting on the effects of the supramolecular interactions on the adenine preferred coordination mode and tautomeric form [61,62].

The main structural feature common to all compounds is the presence of 1D zigzag chains (Fig. 20) in which *cis*- $[M(H_2O)(\text{adenine/purine})]^{2+}$ ($M^{2+} = \text{Cu, Co, Mn, Zn}$ and Cd) units are sequentially bridged by bis-bidentate centrosymmetric oxalato ligands. The metal atoms exhibit a distorted octahedral MO_4OwN chromophore formed by four oxygen atoms from two bridging oxalato ligands, one water molecule and one endocyclic nitrogen atom of the nucleobase in the *cis* position. The main differences comprise the coordination mode of the nucleobase and the tautomeric form it exhibits.

With regard to the coordination mode of purine, in all cases, it binds to the metal centres through N9 whereas adenine molecule always uses N3 position. If we consider the basicity of the adenine donor positions (basicity order: $N9 > N1 > N7 > N3 > N6$ -exocyclic) an N9-binding mode would be expected, like in purine. As it is not the case, it becomes clear that this behaviour cannot be attributed to inherent electronic effects of the adenine molecule [63]. Therefore the source must be found somewhere else. Several authors have explained the modifications observed in the coordination sites by the presence of additional intramolecular hydrogen

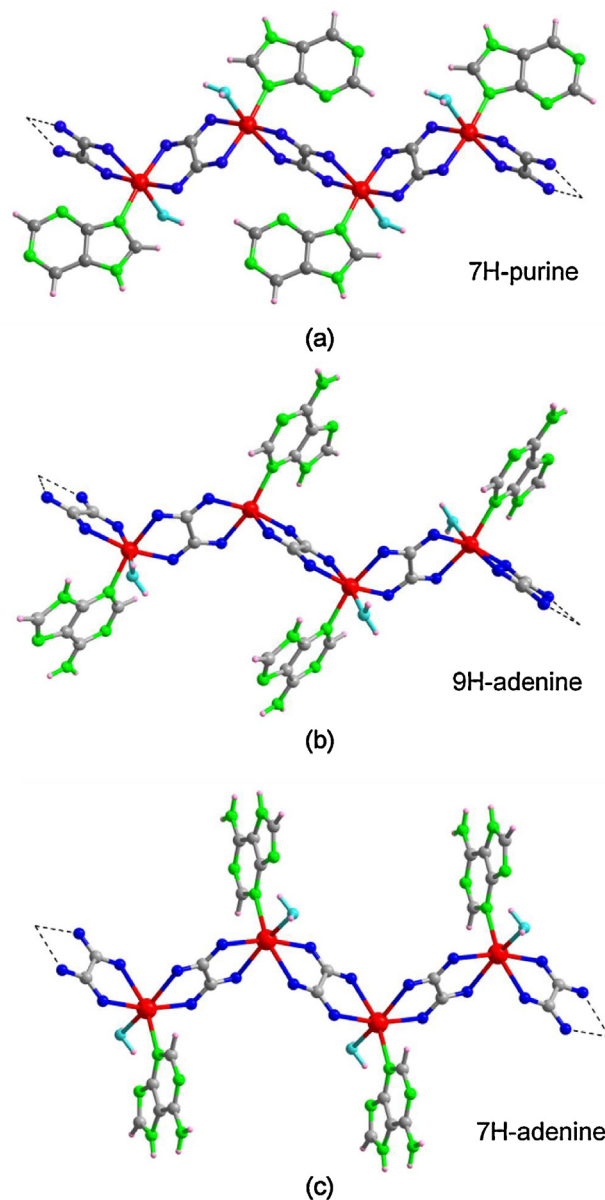


Fig. 20. Polymeric chains of compounds (a) $[M(\mu\text{-ox})(H_2O)(7H\text{-purine-}\kappa N9)]_n$ ($M^II = \text{Cu, Co, Mn, Zn}$) [61], (b) $\{[M(\mu\text{-ox})(H_2O)(9H\text{-adenine-}\kappa N3)] \cdot 2(9H\text{-adenine}) \cdot (H_2O)\}_n$ ($M^II = \text{Co, Zn}$) [61] and (c) $\{[Cd(\mu\text{-ox})(H_2O)(7H\text{-adenine-}\kappa N3)] \cdot H_2O\}_n$ [62].

bonding interactions that deviate the coordination site from the most basic and usually preferred N9 nitrogen atom [64,65]. However in our case, less basic N3-binding mode is not responsible for the intramolecular interactions, as usually pointed, because both purine and adenine ligands are pointing the same hydrogen bonding donor/acceptor groups towards the metal-oxalato backbone. Therefore the reasons must be found in the different intermolecular interactions that they present. As evidence of this fact, it is possible to perform a random partial substitution of purine ligands in compound $[Co(\mu\text{-ox})(H_2O)(7H\text{-purine-}\kappa N9)]_n$ by adenine molecules rendering compound $[Co(\mu\text{-ox})(H_2O)(7H\text{-purine-}\kappa N9)_{0.76}(7H\text{-adenine-}\kappa N9)_{0.24}]_n$ in which the adenine binds metal centre by N9 site [61].

The second difference that must be mentioned is the presence of two tautomeric forms of the adenine molecule although retaining the same N3-coordination mode: 9H tautomer for the adenine bonded to Co(II) and Zn(II) and 7H-adenine when coordinated to

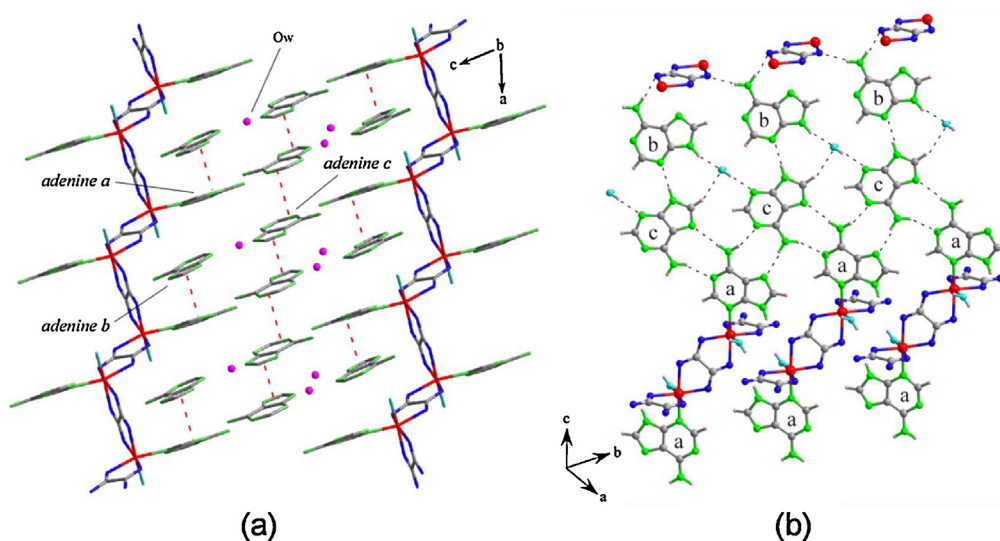


Fig. 21. Supramolecular interactions among the 9*H*-adenine molecules in compounds $\{[M(\mu\text{-ox})(\text{H}_2\text{O})(9\text{H}\text{-adenine-}\kappa\text{N3})]\cdot 2(9\text{H}\text{-adenine})\cdot (\text{H}_2\text{O})\}_n$ (M^{II} : Co, Zn): (a) π - π contacts and (b) hydrogen bonds [61].

Cd(II). This apparently insignificant hydrogen dissimilar placement and the absence/presence of the exocyclic amino group lead to a very different supramolecular arrangement.

In the case of purine containing compounds, the parallel orientation of the nucleobase with respect to the metal-oxalato framework locates the nonprotonated minor groove N3 atom over the carbon-carbon bond of one oxalate ligand with a mean intrachain N3...C distance of 3.0 Å and a dihedral angle between the pyrimidinic ring and the oxalato plane of $\sim 90^\circ$. This fact precludes the involvement of the potential hydrogen-bonding N3 atom in any other interaction. In fact, the supramolecular cohesion among the chains is ensured by means of π - π aromatic stacking and hydrogen bonding interactions between the coordinated water molecules, the oxalate and the purine ligand that do not imply this position.

On the other hand, the adenine molecules in compound $\{[M(\mu\text{-ox})(\text{H}_2\text{O})(9\text{H}\text{-adenine-}\kappa\text{N3})]\cdot 2(9\text{H}\text{-adenine})\cdot (\text{H}_2\text{O})\}_n$ (M^{II} : Co, Zn) are arranged perpendicularly to the chain propagation direction providing bulkier chains, which pack less effectively allowing the inclusion of crystallization water molecules and noncoordinated adenine molecules. All these coordinated and noncoordinated adenines establish an intricate network of π - π aromatic stacking interactions and of hydrogen bonding interactions involving both the Watson-Crick and Hoogsteen sides of the adenines (Fig. 21). In compound $\{[Cd(\mu\text{-ox})(\text{H}_2\text{O})(7\text{H}\text{-adenine-}\kappa\text{N3})]\cdot \text{H}_2\text{O}\}_n$, the proton placement at N7 permits the formation of an intramolecular hydrogen bond involving the coordinated water molecule (donor) and the N9 atom (acceptor) which reinforces the observed metal-binding pattern of the nucleobase. Moreover, the intermolecular interactions do not require the presence of additional adenine molecules and it is sustained by hydrogen bonding pairing interactions between the Watson-Crick faces of adenines belonging to adjacent faces and with those established with the crystallization water molecules (Fig. 22).

On the other hand, there are reported examples of Mn(II) binding to N donor sites of nucleobases in biopolymeric systems, but coordinative Mn-N linkages involving non-substituted nucleobases, as seen in $[Mn(\mu\text{-ox})(\text{H}_2\text{O})(\text{purine-}\kappa\text{N9})]_n$, are extremely rare in structurally characterized coordination compounds [66]. Probably because of this, all attempts to obtain 1D chains with the adenine nucleobase being anchored to a manganese(II)-oxalato framework were unsuccessful, obtaining compound $\{[Mn(\mu\text{-ox})(\text{H}_2\text{O})_2]\cdot (7\text{H}\text{-adenine})\cdot (\text{H}_2\text{O})\}_n$ [67]. Its crystal structure is made

up of zigzag chains with the Mn(II) centres bridged by bisbidentate oxalato ligands, but the adenine nucleobase remains free within the crystal and the metal coordination polyhedron is filled by two water molecules.

Interestingly, the adenine nucleobase exists in the lattice in its 7*H*-amino form due to the efficient stabilization of this non-canonical tautomer by means of a molecular recognition process among the nucleobase, the water molecules, and the manganese-oxalato framework (Fig. 23). In 2006, this compound represented the first X-ray crystallography characterization of the 7*H*-amino tautomer of the adenine nucleobase as free molecule (without metal coordination). Thereafter, Mastropietro et al. isolated the 7*H*-adenine tautomeric form in compounds $[Mg(\text{H}_2\text{O})_6]X_2\cdot 2(7\text{H}\text{-adenine})$ ($X = \text{Cl}^-$ and Br^-) [66a]. It is well known that DNA bases can undergo proton shifts while keeping their neutrality and form different tautomers. Each tautomer has a specific H-bonding donor and acceptor pattern, which increases the possibility of mispairing of purine and pyrimidine bases in DNA, leading to spontaneous point mutations in the genome [68]. Due to its biological impact, the tautomerism of nucleobases has been largely studied using a variety of experimental and theoretical methods which support the relevance of the isolation of unusual tautomeric forms in the solid state [69].

A similar synthetic procedure to that employed for the family of metal/oxalate/nucleobase compounds described above but using $\text{K}_2[\text{Cu}(\text{ox})_2]\cdot 2\text{H}_2\text{O}$ as metal source gives a different compound $\{[\text{Cu}(\mu\text{-ox})(\text{H}_2\text{O})(7\text{H}\text{-adenine-}\kappa\text{N9})][\text{Cu}(\mu\text{-ox})(\mu\text{-OH}_2)(7\text{H}\text{-adenine-}\kappa\text{N9})]\cdot \sim 10/3\text{H}_2\text{O}\}_n$ [67]. Its structure consists of crystallization water molecules and two crystallographically independent and roughly planar $[\text{Cu}(\text{ox})(\text{H}_2\text{O})(7\text{H}\text{-adenine-}\kappa\text{N9})]$ units, molecule A and molecule B, as shown in Fig. 24. In both complex fragments, the Cu(II) atoms are coordinated to two oxygen atoms from a bidentate oxalato ligand, one water molecule, and the imidazole N9 atom from the adenine ligand. The planar complex units are connected through weaker axial Cu-O interactions to create neutral ribbons. The adenine ligands are located in the same side of the polymeric framework and they are ring-to-ring stacked, suggesting that π - π stacking interactions contribute to the formation of the one-dimensional chains. Polymeric one-dimensional chains are further interlinked through an intricate hydrogen bonding network that implies again the Watson-Crick and Hoogsteen edges, but in this case there is not direct interaction between the adenines.

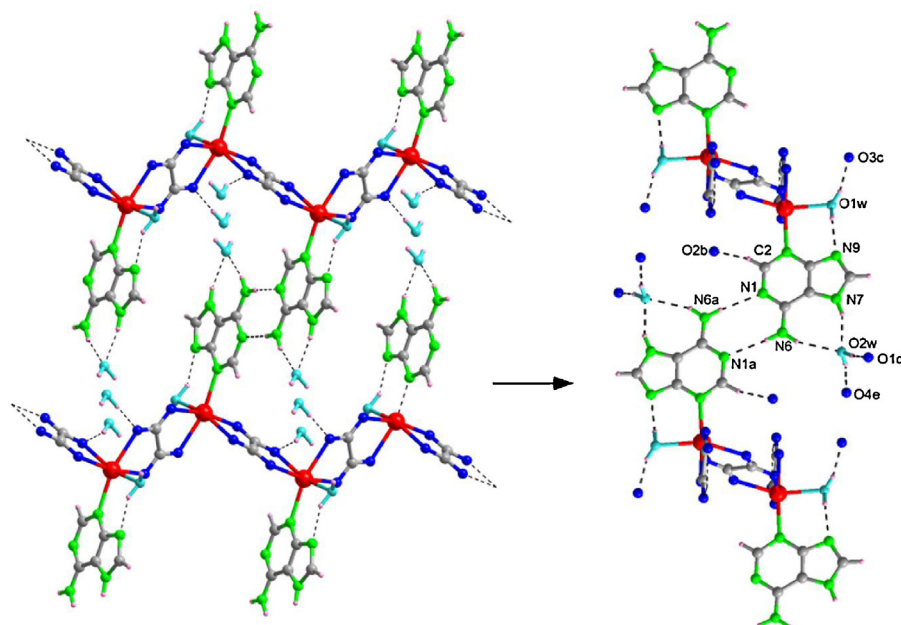


Fig. 22. Supramolecular interactions in compound $\{[\text{Cd}(\mu\text{-ox})(\text{H}_2\text{O})(7\text{H-adenine-}\kappa\text{N3})]\cdot\text{H}_2\text{O}\}_n$.

Reproduced from Ref. [62]. Copyright (2011) Elsevier B.V.

After the success in the coordinative anchorage of non-substituted nucleobases to metal-oxalato frameworks, the next step was to explore new coordination modes apart from N3 and N9, which was achieved by methylating the adenine at N3 and guanine at N9. The alkylation by itself and otherwise the steric hindrance exerted by the methyl group will force the coordination of the nucleobase through any of the remaining positions except N3 and N9. For that purpose copper-oxalato skeletons were employed obtaining compounds $\{[\text{Cu}(\text{ox})(\text{H}_2\text{O})(3\text{-methyladenine-}\kappa\text{N7})]\cdot\text{H}_2\text{O}\}_n$ and $[\text{Cu}(\text{ox})(\text{H}_2\text{O})_2(9\text{-methylguanine-}\kappa\text{N7})]\cdot 2.5\text{H}_2\text{O}$ in which both nucleobases act as monodentate ligands through N7 that is the most frequent coordination metal binding pattern for both 3-methyladenine and 9-methylguanine ligands (Fig. 25) [62,70,71].

Compound $\{[\text{Cu}(\text{ox})(\text{H}_2\text{O})(3\text{-methyladenine-}\kappa\text{N7})]\cdot\text{H}_2\text{O}\}_n$ shows again the presence of zigzag chains comprised of

$\text{cis-}[\text{Cu}(\text{H}_2\text{O})(3\text{-methyladenine-}\kappa\text{N7})]^{2+}$ fragments joined by bisbidentate oxalato ligands (Fig. 23). In contrast, compound $[\text{Cu}(\text{ox})(\text{H}_2\text{O})_2(9\text{-methylguanine-}\kappa\text{N7})]\cdot 2.5\text{H}_2\text{O}$ is comprised of discrete distorted square pyramidal complexes (A and B) in which the basal plane is occupied by a bidentate oxalato ligand, one water molecule, and the N7 site of the nucleobase. The apical position is occupied by the remaining water molecule. These monomeric complexes are held together establishing a complicated recognition process that involves, among others, the formation of a triple hydrogen bonding interaction between the adenine Watson–Crick face and the oxygen atoms of an adjacent unit that resembles the complementary guanine–cytosine molecular recognition pattern. This interaction is extended by additional hydrogen bonds to give rise to centrosymmetric metal-organic quartets which resembles the homonucleobase tetrameric aggregates (G4) presented in the guanine-rich zones of the multistranded nucleic acid structures. These tetrameric aggregates are further interconnected to give rise to infinite tapes.

Apart from the relevance of this work in a merely crystal design sense, 3-methyladenine is highly cytotoxic and mutagenic as a result of its ability to block DNA replication since the N3-methyl group protrudes into the minor groove of the DNA double helix and thereby stops replication [72]. So that, the design and structural analyses of coordination compounds containing this methylated adenine can supply useful information to understand the conformational damages induced by the N-alkylation of nucleobases in biological systems and the molecular recognition processes to repair them.

6.3. Hybrid systems based on metal-oxalato entities and protonated nucleobases

The metal-oxalato matrix has demonstrated a high efficiency not only to permit the covalent anchorage of nucleobases but also to embed supramolecular nucleobase architectures by means of molecular recognition processes involving non-covalent interactions such as those in the organic–inorganic hybrid compounds $(1\text{H},9\text{H-adeninium})_2[\text{Cu}(\text{ox})_2(\text{H}_2\text{O})]$, $(3\text{H},7\text{H-adeninium})_2[\text{M}(\text{ox})_2(\text{H}_2\text{O})_2]\cdot 2\text{H}_2\text{O}$ ($\text{M}^{\text{II}} = \text{Co}, \text{Zn}$) and

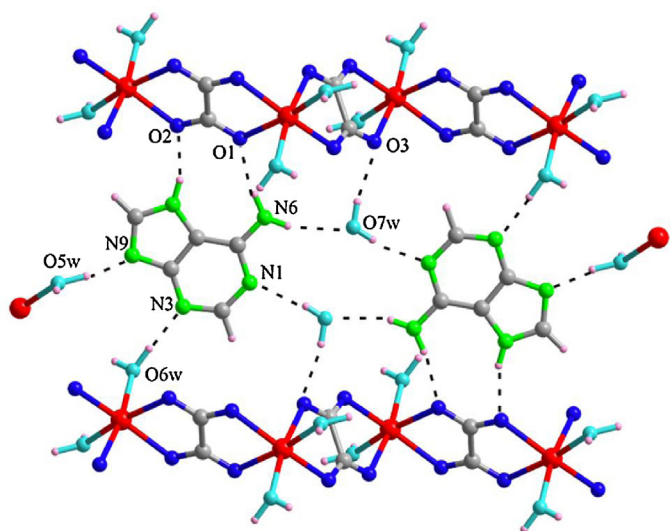


Fig. 23. Hydrogen-bonded network (dashed lines) around the 7H-adenine tautomer in compound $\{[\text{Mn}(\mu\text{-ox})(\text{H}_2\text{O})_2]\cdot(7\text{H-adenine})\cdot(\text{H}_2\text{O})\}_n$ [67].

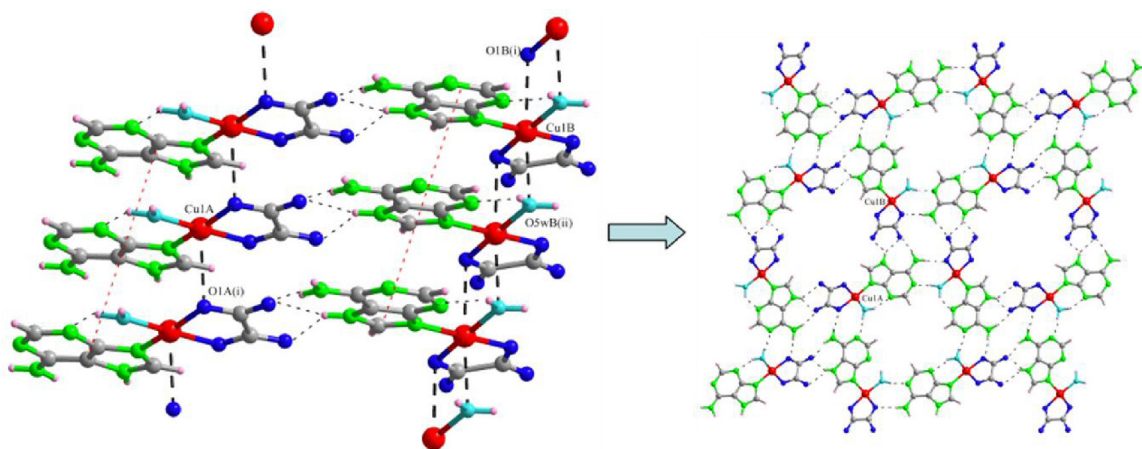
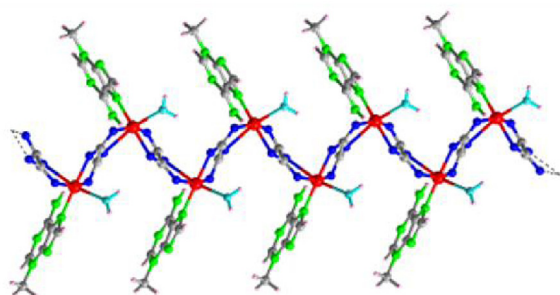
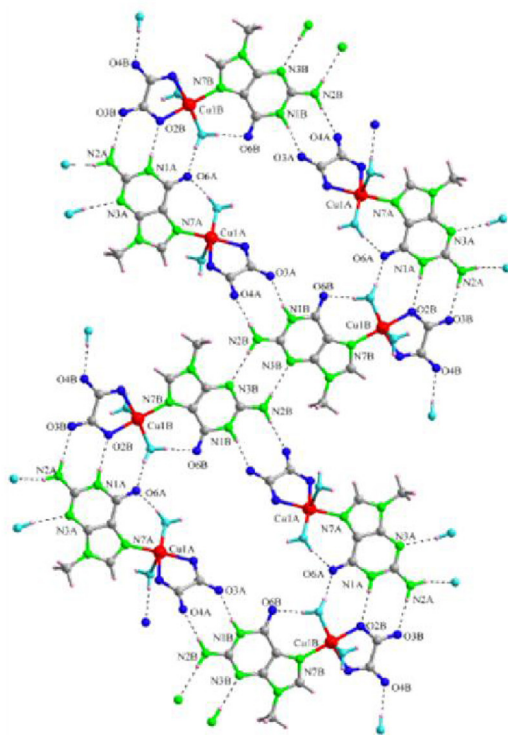


Fig. 24. One-dimensional chains and hydrogen bonding scheme in compound $\{[\text{Cu}(\mu\text{-ox})(\text{H}_2\text{O})(7\text{H-adenine-}\kappa\text{N9})][\text{Cu}(\mu\text{-ox})(\mu\text{-OH}_2)(7\text{H-adenine-}\kappa\text{N9})] \sim 10/3\text{H}_2\text{O}\}_n$ [67].



(a)

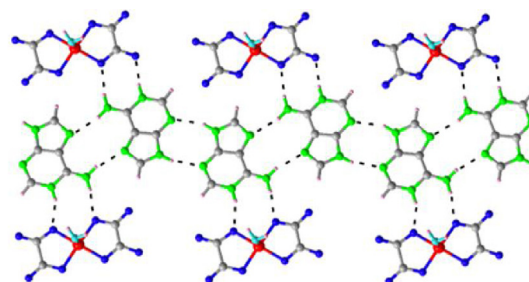


(b)

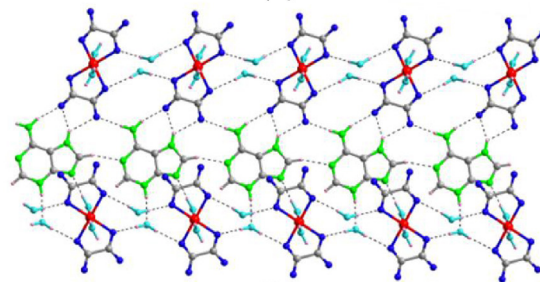
Fig. 25. (a) Polymeric chain of compound $\{[\text{Cu}(\text{ox})(\text{H}_2\text{O})(3\text{-methyladenine-}\kappa\text{N7})\cdot\text{H}_2\text{O}\}_n$ and (b) infinite tapes of metal-organic quartets in compound $[\text{Cu}(\text{ox})(\text{H}_2\text{O})_2(9\text{-methylguanine-}\kappa\text{N7})]\cdot 2.5\text{H}_2\text{O}$.

Reproduced from Ref. [62]. Copyright (2011) Elsevier B.V.

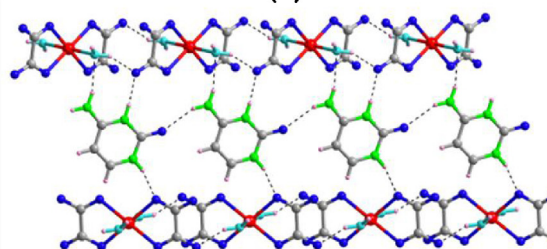
(*1H,3H*-cytosinium) $_2[\text{M}(\text{ox})_2(\text{H}_2\text{O})_2]$ ($\text{M}^{\text{II}} = \text{Mn, Co, Cu, Zn}$) [73,74]. In all the cases, the supramolecular architecture is quite similar and its overall crystal packing can be regarded as a lamellar network built up of anionic sheets of metal-oxalato-water complexes and cationic nucleobase layers sandwiched among them. Each wide organic layer serves as “double-sided adhesive tape” to tightly join adjacent inorganic layers by means of electrostatic forces and a strong hydrogen bonding network.



(a)



(b)



(c)

Fig. 26. Supramolecular surrounding of the protonated nucleobases in compounds (a) (*1H,9H*-adeninium) $_2[\text{Cu}(\text{ox})_2(\text{H}_2\text{O})]$ [73], (b) (*3H,7H*-adeninium) $_2[\text{M}(\text{ox})_2(\text{H}_2\text{O})_2]\cdot 2\text{H}_2\text{O}$ ($\text{M}^{\text{II}} = \text{Co, Zn}$) [73] and (c) (*1H,3H*-cytosinium) $_2[\text{M}(\text{ox})_2(\text{H}_2\text{O})_2]$ ($\text{M}^{\text{II}} = \text{Mn, Co, Cu, Zn}$) [74].

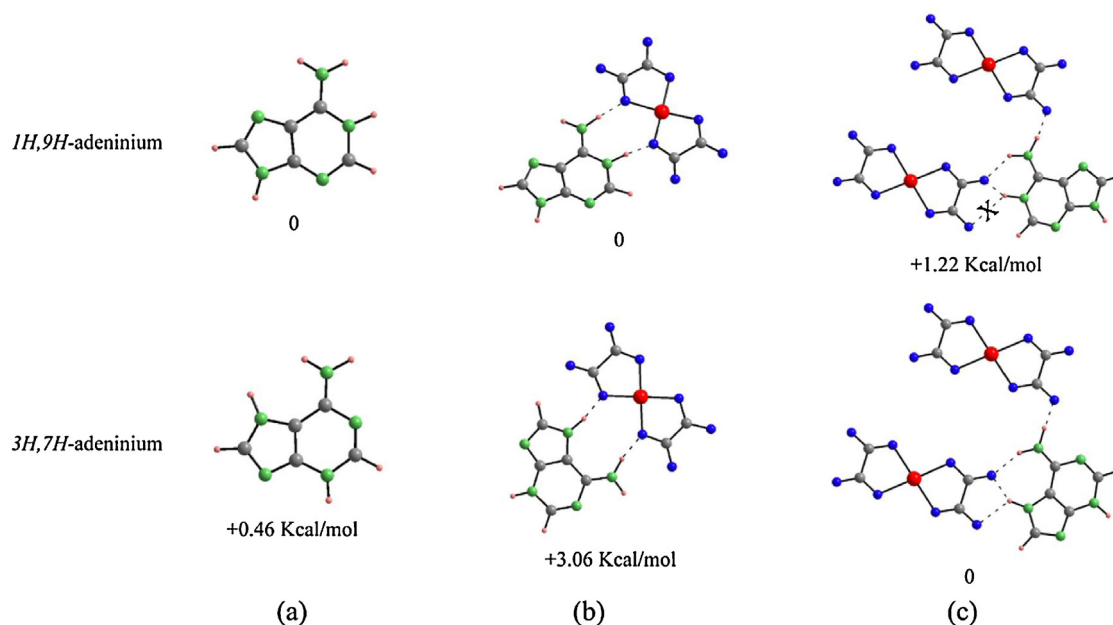


Fig. 27. Relative energies between the 1H,9H- and 3H,7H-adeninium forms for different environments: (a) gas phase, (b) interacting with a $[M(ox)_2]^{2-}$ fragment and (c) interacting simultaneously with two $[M(ox)_2]^{2-}$ fragments [73].

The supramolecular structure of these inorganic–organic hybrids is created by three types of molecular recognition: between complex anions, between cationic nucleobases, and between ribbons of nucleobases and layers consisting of oxalato-complexes (Fig. 26). Molecules of complexes located within the anionic layers are joined among them by hydrogen bonds. The interaction between the organic base molecules results in the hydrogen bonding recognition unit and leads to ribbon formation. Finally, the third group of hydrogen bonds completes the closely packed structure. The most interesting aspect of this family of compounds is that the metal-oxalato matrix exerts a decisive effect on the tautomerism of the nucleobase cations. In fact, compounds $(3H,7H\text{-adeninium})_2[M(ox)_2(H_2O)_2] \cdot 2H_2O$ ($M^{II} = Co, Zn$) represent the first solid-state characterized 3H,7H-adeninium tautomer (CSD mining statistics and gas phase calculations indicate that the canonical form is 1H,9H-adeninium).

DFT calculations for this compound including the presence of one $[M(ox)_2]^{2-}$ fragment in all of its possible dispositions around the adeninium cation show that the energy order of 1H,9H- and 3H,7H-tautomers is not altered. However, when two $[M(ox)_2]^{2-}$ fragments with the experimental disposition of compounds are included, the 3H,7H-adeninium cation becomes the most stable (Fig. 27). This fact is due to the demanding conditions for an efficient hydrogen bonding interaction that are better fulfilled by the 3H,7H-adeninium cation than by the 1H,9H-form. The optimized 1H,9H-adeninium entity establishes only three hydrogen bonds with the $[Cu(ox)_2]^{2-}$ fragments, indicating a less efficient hydrogen bonding stabilization.

7. Summary and perspective

Herein we have presented a complete overview of the preparation and properties of a series of metal–carboxylato–nucleobase architectures that range from supramolecular assemblies to 3D porous materials. In particular, we have taken advantage of the synthetic control over the three dicopper paddle-wheel entities built up from the adenine nucleobase and carboxylato ligands. These entities can further polymerize to obtain extended systems, connecting the dimeric entities either through the equatorial positions or/and by means of the axial positions.

The polymerization of the $[Cu_2(\mu\text{-adenine})_4]$ entity was first achieved in the $\{[Cu_2(\mu\text{-adeninato})_4(H_2O)_2][Cu(ox)(H_2O)]_2\}_n$ compound, by means of the deprotonation of the adenine and its coordination to less sterically hindered $[Cu(ox)(H_2O)]$ units. This building unit also allowed us to obtain a porous material, $[Cu_2(\mu\text{-adenine})_4Cl_2]Cl_2 \cdot 2CH_3OH$, based only on supramolecular interactions, with a high thermal stability and a computed accessible surface area of $790\text{ m}^2\text{ g}^{-1}$.

The replacement of two adenine molecules by two dicarboxylato ligands led to a family of 3D metal–organic compounds based on $[Cu_2(\mu\text{-adenine})_2(\mu\text{-dicarboxylato})_2]$ entities. This fact suggested us to use monocarboxylic acids, with which we obtained the corresponding isostructural series of compounds but with an accessible free volume. The adsorption measurements of these porous compounds demonstrated that the length of the aliphatic chain of the carboxylato ligands modifies the porosity of the open-framework structures. Additionally, the study of the adsorption selectivity of binary mixtures of CO_2/H_2 and CO/H_2 at 298 K carried out for these compounds shows that the selectivity towards CO_2 and CO can be tuned by changing the carboxylato ligand, increasing its value with increasing the length of the aliphatic chain.

In the light of these results, the next step of this research consists on preparing core–shell particles employing this family of MBioFs, starting from a core of a porous MBioF which will be covered with a thin layer of a compatible metal–organic compound. Moreover, there is work in progress to extrapolate the systems described in this work to other metal centres (Ni^{II} , Co^{II} , Zn^{II} , etc.), which may have higher thermal stability for a subsequent use in adsorption applications, as well as, expand this study to other purine bases (guanine, purine, hypoxanthine, xanthine, etc.) with ability to form analogous SBUs capable to generate novel MBioFs.

Another remarkable fact is the pronounced increase of microporosity achieved through the template effect of butanoic acid micelles in the reaction media of compound $[Cu_2(\mu_3\text{-ade})_2(\mu_2\text{-OOC}(CH_2)_2(CH_3)_2)]_n$, doubling the intrinsic adsorption capacity of the pristine crystal network. Thus, one of our research areas attempts to extrapolate this methodology to other systems.

In case of using $[Cu_2(\mu\text{-carboxylate})_4]$ entity, long chain flexible dicarboxylate connectors promote the formation of one-dimensional metal–organic architectures, where methylated

adenine nucleobases decorate the axial positions of the paddle-wheel units. When these flexible linear ligands are replaced by rigid dicarboxylate connectors the structural variability can be directed towards extended systems of higher dimensionality.

On the other hand, the chelating nature of short chain dicarboxylic ligands, such as the oxalate and malonate anions, leads to substantially different structures. When the malonic acid is used, the pseudo paddle-wheel entities are obtained with Ni(II) and Co(II) salts. In the case of the oxalate ligand, two different families of compounds are achieved. When the adenine is in its neutral form, polymeric chains are obtained, whereas lamellar inorganic–organic compounds are achieved by using it as a cation.

Magnetic properties have also been analyzed for all the compounds reported. The magnitude of the antiferromagnetic coupling in the $[\text{Cu}_2(\mu\text{-adenine})_4]$ entities has been evaluated on the basis of different structural parameters. In the case of $[\text{M}_2(\mu\text{-adenine})_2(\mu\text{-carboxylato})_2]$ entities, the splitting order of the molecular magnetic orbitals is the same for each type of bridging ligand leading as a consequence to J values intermediate between the ones found for the non-mixed paddle-wheels. Surprisingly, in the case of $[\text{M}_2(\mu\text{-adenine})_2(\mu\text{-malonato})_2]$, (where $\text{M} = \text{Ni(II)}$, Co(II)), the orbital countercomplementarity leads to ferromagnetic interactions.

Acknowledgements

Financial support from the Gobierno Vasco (IT477-10, SAIOTEK S-PE12UN004) and the Universidad del País Vasco/Euskal Herriko Unibertsitatea (UFI 11/53, postdoctoral and predoctoral fellowships) is gratefully acknowledged.

References

- [1] Chem. Rev. 112 (2012) and references therein.
- [2] I. Imaz, M. Rubio-Martínez, J. An, I. Solé-Font, N.L. Rosi, D. Maspoch, Chem. Commun. 47 (2011) 7287.
- [3] (a) P. Amo-Ochoa, P.J. Sanz Miguel, O. Castillo, A. Houlton, F. Zamora, in: N. Hadjiladis, E. Sletten (Eds.), Metal Complex–DNA Interactions, Wiley, Chichester, 2009, p. 95 (Chapter 4); (b) O. Castillo, A. Luque, J.P. García-Terán, P. Amo-Ochoa, in: A.S. Abd-el-Aziz, C.E. Carraher, C.U. Pittman, M.M. Zeldin (Eds.), Macromolecules Containing Metal and Metal-Like Elements, vol. 9, Wiley & Sons, Hoboken, 2009, p. 407 (Chapter 9); (c) K.C. Stylianou, J.E. Warren, S.Y. Chong, J. Rabone, J. Bacsa, D. Bradshaw, M.J. Rosseinsky, Chem. Commun. 47 (2011) 3389; (d) J. An, S.J. Geib, N.L. Rosi, J. Am. Chem. Soc. 132 (2010) 38; (e) S. Verma, A.K. Mishra, A. Kumar, Acc. Chem. Res. 43 (2010) 79.
- [4] (a) L. MacGillivray, Metal–Organic Frameworks: Design and Application, John Wiley and Sons, New Jersey, 2010; (b) S.T. Meek, J.A. Greathouse, M.D. Allendorf, Adv. Mater. 23 (2011) 249; (c) M. Köberl, M. Cokoja, W.A. Hermann, F.E. Kühn, Dalton Trans. 40 (2011) 6834; (d) A. Carné, C. Carbonell, I. Imaz, D. Maspoch, Chem. Soc. Rev. 40 (2011) 291; (e) R. Mas-Ballesté, J. Gómez-Herrero, F. Zamora, Chem. Soc. Rev. 39 (2010) 4220; (f) G. Givaja, P. Amo-Ochoa, C.J. Gómez-García, F. Zamora, Chem. Soc. Rev. 41 (2012) 115.
- [5] (a) B. Bleany, K.D. Bowers, Proc. R. Soc. Lond. Ser. A 214 (1952) 451; (b) J.B. Van Niekerk, F.R.L. Schoening, Acta Crystallogr. 6 (1953) 227.
- [6] H. Abourahma, G.J. Badwell, J. Lu, B. Moulton, I.R. Pottie, R.B. Walsh, M.J. Zaworotko, Cryst. Growth Des. 3 (2003) 513.
- [7] (a) S.I. Vagin, A.K. Ott, B. Rieger, Chem. Ing. Tech. 79 (2007) 767; (b) B. Chen, S. Xiang, G. Quian, Acc. Chem. Res. 43 (2010) 1115; (c) D. Zhao, D.J. Timmons, D. Yuan, H.C. Zhou, Acc. Chem. Res. 44 (2011) 123.
- [8] W.L. Leong, J. Vittal, Chem. Rev. 111 (2011) 688.
- [9] (a) A. Rodríguez-Fortea, P. Alemany, S. Alvarez, E. Ruiz, Chem. Eur. J. 7 (2001) 627; (b) S. Youngme, A. Cheansirisomboon, C. Danvirutai, C. Pakawatchai, N. Chai-chit, C. Engkagul, G.A. van Albada, J.S. Costa, J. Reedijk, Polyhedron 27 (2008) 1875; (c) M. Fontanet, A.–R. Popescu, X. Fontrodona, M. Rodríguez, I. Romero, F. Teixidor, C. Viñas, N. Aliaga-Alcalde, E. Ruiz, Chem. Eur. J. 17 (2011) 13217; (f) R. Cejudo, G. Alzuet, J. Borraís, M. Liu-González, F. Sanz-Ruiz, Polyhedron 21 (2002) 1057; (g) L. Gutiérrez, G. Alzuet, J. Borraís, A. Castiñeiras, A. Rodríguez-Fortea, E. Ruiz, Inorg. Chem. 40 (2001) 3089.
- [10] (a) D. Sonnenfroh, R.W. Kreilick, Inorg. Chem. 19 (1980) 1259; (b) J. Cepeda, O. Castillo, J.P. García-Terán, A. Luque, S. Pérez-Yañez, P. Román, Eur. J. Inorg. Chem. (2009) 2344.
- [11] Y. Nishida, S. Kida, J. Chem. Soc. Dalton Trans. (1986) 2633.
- [12] V. McKee, M. Zvagulis, C.A. Reed, Inorg. Chem. 24 (1985) 2914.
- [13] (a) O.M. Yaghi, M. O’Keeffe, N.W. Ockwig, H.K. Chae, M. Eddaoudi, J. Kim, Nature 423 (2003) 705; (b) K. Biradha, Y. Hongo, M. Fujita, Angew. Chem. Int. Edn Engl. 39 (2000) 3843; (c) M. Eddaoudi, J. Kim, J.B. Wachter, H.K. Chae, M. O’Keeffe, O.M. Yaghi, J. Am. Chem. Soc. 123 (2001) 4368; (d) B. Moulton, J. Lu, A. Mondal, M.Z. Zaworotko, Chem. Commun. (2001) 863; (e) M. Eddaoudi, J. Kim, M. O’Keeffe, O.M. Yaghi, J. Am. Chem. Soc. 124 (2002) 376.
- [14] P. de Meester, A.C. Skapski, J. Chem. Soc. A (1971) 2167.
- [15] A. Terzis, A.L. Beauchamp, R. Rivest, Inorg. Chem. 12 (1973) 1166.
- [16] E. Sletten, Acta Crystallogr. B58 (1992) 1480.
- [17] F.H. Allen, Acta Crystallogr. B58 (2002) 380.
- [18] J.P. García-Terán, O. Castillo, A. Luque, U. García-Couceiro, P. Román, L. Lezama, Inorg. Chem. 43 (2004) 4549.
- [19] J.M. González-Pérez, C. Alarcón-Payer, A. Castiñeiras, T. Pivetta, L. Lezama, D. Choquesillo-Lazarte, G. Crisponi, J. Niclós-Gutiérrez, Inorg. Chem. 45 (2006) 877.
- [20] (a) T. Chifotides, K.R. Dunbar, Acc. Chem. Res. 38 (2005) 146; (b) P.X. Rojas-González, A. Castiñeiras, J.M. González-Pérez, D. Choquesillo-Lazarte, J. Niclós-Gutiérrez, Inorg. Chem. 41 (2002) 6190.
- [21] M.A. Salam, K. Aoki, Inorg. Chim. Acta 314 (2001) 71.
- [22] (a) C.B. Aakeroy, N.R. Champness, C. Janiak, CrystEngComm 12 (2010) 22; (b) R. Zou, A.I. Abdel-Fattah, H. Xu, Y. Zhao, D.D. Hickmott, CrystEngComm 12 (2010) 1337; (c) A.D. Naik, M.M. Dirtu, A. Leonard, B. Tinaut, J. Marchand-Brynaert, B.L. Su, Y. García, Cryst. Growth Des. 10 (2010) 1798.
- [23] (a) Y.-Q. Tian, C.-X. Cai, Y. Ji, X.-Z. You, S.-M. Peng, G.-H. Lee, Angew. Chem. Int. Ed. 41 (2002) 1384; (b) A. Gadet, O. Lefebvre-Soubeyran, Acta Crystallogr. Sect. B 30 (1974) 716.
- [24] J. Thomas-Gipson, G. Beobide, O. Castillo, J. Cepeda, A. Luque, S. Pérez-Yañez, P. Román, CrystEngComm 13 (2011) 3301.
- [25] G.V. Oshovsky, D.N. Reinhoudt, W. Verboom, Angew. Chem. Int. Ed. 46 (2007) 2366.
- [26] (a) For examples see: M. Byres, P.J. Cox, G. Kay, E. Nixon, CrystEngComm 11 (2009) 135; (b) M.A. Galindo, D. Amantia, W. Clegg, R.W. Harrington, R.J. Eyre, J.P. Goss, P.R. Bridson, W. McFarlane, A. Houlton, Chem. Commun. (2009) 2833; (c) A.F.A. Peacock, S. Parsons, P.J. Sadler, J. Am. Chem. Soc. 129 (2007) 3348; (d) A.C. Morel, D. Choquesillo-Lazarte, C. Alarcón-Payer, J.M. González-Pérez, A. Castiñeiras, J. Niclós-Gutiérrez, Inorg. Chem. Commun. 6 (2003) 1354; (e) S. Verma, A. Kumar-Mishra, J. Kumar, Acc. Chem. Res. 43 (2010) 79.
- [27] (a) J.J. Jiang, M. Pan, J.M. Liu, W. Wang, C.Y. Su, Inorg. Chem. 49 (2010) 10166; (b) J.J. Jiang, L. Li, M.-H. Lan, M. Pan, A. Eichhöfer, D. Fenske, C.-Y. Su, Chem. Eur. J. 16 (2010) 1841.
- [28] (a) K.M. Ok, J. Sung, G. Hu, R.M.J. Jacobs, D. O’Hare, J. Am. Chem. Soc. 130 (2008) 3762; (b) T.K. Maji, R. Matsuda, S. Kitagawa, Nat. Mater. 6 (2007) 142; (c) W. Steele, Chem. Rev. 93 (1993) 2355.
- [29] J.I. Feldblyum, M. Liu, D.W. Gidley, A. Matzger 133 (2011) 18257.
- [30] (a) D.L. Reger, A. Debreczeni, M.D. Smith, Inorg. Chim. Acta 386 (2012) 102; (b) D.L. Reger, A. Debreczeni, M.D. Smith, J. Jezierska, A. Ozarowski, Inorg. Chem. 51 (2012) 1068.
- [31] E.-C. Yang, H.-K. Zhao, B. Ding, X.-G. Wang, X.-J. Zhao, New J. Chem. 31 (2007) 1887.
- [32] J. An, S.J. Geib, N.L. Rosi, J. Am. Chem. Soc. 131 (2009) 8376.
- [33] J. An, O.K. Farha, J.T. Hupp, E. Pohl, J.I. Yeh, N. Rosi, Nat. Commun. 3 (2012) 604.
- [34] E.-C. Yang, Y.-N. Chan, H. Liu, Z.-C. Wang, X.-J. Zhao, Cryst. Growth Des. 9 (2009) 4933.
- [35] J. Kumar, S. Verma, Inorg. Chem. 48 (2009) 6350.
- [36] S. Pérez-Yañez, G. Beobide, O. Castillo, J. Cepeda, A. Luque, A.T. Aguayo, P. Román, Inorg. Chem. 50 (2011) 5330.
- [37] S. Pérez-Yañez, G. Beobide, O. Castillo, J. Cepeda, A. Luque, P. Román, Cryst. Growth Des. 12 (2012) 3324.
- [38] S. Pérez-Yañez, G. Beobide, O. Castillo, M. Fischer, F. Hoffmann, M. Fröba, J. Cepeda, A. Luque, Eur. J. Inorg. Chem. (2012) 5921.
- [39] S. Sircar, T. Golden, Sep. Sci. Technol. 35 (2000) 667.
- [40] K. Sumida, D.L. Rogow, J.A. Mason, T.M. McDonald, E.D. Bloch, Z.R. Herm, T.H. Bae, J.R. Long, Chem. Rev. 112 (2012) 724.
- [41] B.S. Hoffmann, A. Szkló, Appl. Energy 88 (2011) 3917.
- [42] N. Armaroli, V. Balzani, ChemSusChem 4 (2011) 21.
- [43] V. Colombo, C. Montoro, A. Maspero, G. Palmisano, N. Masciocchi, S. Galli, E. Barea, J.A.R. Navarro, J. Am. Chem. Soc. 134 (2012) 12830.
- [44] (a) M. Gallo, T.M. Nenoff, M.C. Mitchell, Fluid Phase Equilib. 247 (2006) 135; (b) E.D. Akten, R. Siriwardane, D.S. Sholl, Energy Fuels 17 (2003) 977; (c) Q. Yang, Q. Xu, B. Liu, C. Zhong, S. Berend, Chin. J. Chem. Eng. 17 (2009) 781; (d) Q. Yang, C. Zhong, J. Phys. Chem. B 110 (2006) 17776; (e) J. Jiang, AlChE J. 55 (2009) 2422; (f) R. Babarao, J. Jiang, J. Am. Chem. Soc. 131 (2009) 11417.
- [45] M. Fischer, F. Hoffmann, M. Fröba, RSC Adv. 2 (2012) 4382.
- [46] J. Grindley, C.R. Bury, J. Chem. Soc. (1929) 679.
- [47] D. Moulet, G.C. Benson, Can. J. Chem. 37 (1959) 2083.

- [48] S. Pérez-Yáñez, G. Beobide, O. Castillo, J. Cepeda, M. Fröba, F. Hoffmann, A. Luque, P. Román, *Chem. Commun.* 48 (2012) 907.
- [49] (a) C.T. Kresge, M.E. Leonowicz, W.J. Roth, J.C. Vartuli, J.S. Beck, *Nature* 359 (1992) 710;
(b) W. Wang, J.E. Lofgreen, G.A. Ozin, *Small* 6 (2010) 2634;
(c) P. Yang, D. Zhao, D.I. Margolese, B.F. Chmelka, G.D. Stucky, *Nature* 396 (1998) 152;
(d) Y. Wan, D. Zao, *Chem. Rev.* 107 (2007) 2821.
- [50] (a) K.M. Choi, H.J. Jeon, J.K. Kang, O.M. Yaghi, *J. Am. Chem. Soc.* 133 (2011) 11920;
(b) L.-G. Qiu, T. Xu, Z.-Q. Li, W. Wang, Y. Wu, X. Jiang, X.-Y. Tian, L.-D. Zhang, *Angew. Chem. Int. Ed.* 47 (2008) 9487;
(c) J. Górká, P.F. Fulvio, S. Pikus, M. Jaroniec, *Chem. Commun.* 46 (2010) 6798.
- [51] (a) X.-D. Do, V.-T. Hoang, S. Kaliaguine, *Microporous Mesoporous Mater.* 141 (2011) 135;
(b) X. Roy, M.J. MacLachlan, *Chem. Eur. J.* 15 (2009) 6552.
- [52] D. Yuan, D. Zhao, D.J. Timmons, H.-C. Zhou, *Chem. Sci.* 2 (2011) 103.
- [53] (a) M. Fischer, F. Hoffmann, M. Fröba, *ChemPhysChem* 11 (2010) 2220;
(b) Y.-S. Bae, O.K. Farha, A.M. Spokoyniy, C.A. Mirkin, J.T. Hupp, R.Q. Snurr, *Chem. Commun.* (2008) 4135.
- [54] M. Eddaoudi, J. Kim, D. Vodak, A. Sudik, J. Wachter, M. O'Keefe, O.M. Yaghi, *Proc. Natl. Acad. Sci. U. S. A* 99 (2002) 4900.
- [55] H. Furukawa, Y.B. Go, N. Ko, F.J. Uribe-Romo, J. Kim, M. O'Keefe, O.M. Yaghi, *Inorg. Chem.* 50 (2011) 9147.
- [56] Y. Rodríguez-Martín, M. Hernández-Molina, F.S. Delgado, J. Pasán, C. Ruiz-Pérez, J. Sanchiz, F. Lloret, M. Julve, *CrystEngComm* 4 (2002) 522.
- [57] S. Pérez-Yáñez, O. Castillo, J. Cepeda, J.P. García-Terán, A. Luque, P. Román, *Eur. J. Inorg. Chem.* (2009) 3889.
- [58] (a) M. Pilkinton, S. Decurtins, in: J.A. McCleverty, T.J. Meyer (Eds.), *Comprehensive Coordination Chemistry II*, vol. 7, Elsevier, University of Berne, Switzerland, 2004, p. 214;
(b) C.N.R. Rao, S. Natarajan, R. Vaidyanathan, *Angew. Chem. Int. Ed.* 43 (2004) 1466.
- [59] U. García-Couceiro, O. Castillo, A. Luque, J.P. García-Terán, G. Beobide, P. Román, *Cryst. Growth Des.* 6 (2006) 1839.
- [60] (a) O. Castillo, A. Luque, P. Román, F. Lloret, M. Julve, *Inorg. Chem.* 40 (2001) 5526;
(b) O. Castillo, A. Luque, F. Lloret, P. Román, *Inorg. Chim. Acta* 324 (2001) 141;
(c) O. Castillo, A. Luque, M. Julve, F. Lloret, P. Román, *Inorg. Chim. Acta* 315 (2001) 9.
- [61] J.P. García-Terán, O. Castillo, A. Luque, U. García-Couceiro, P. Román, F. Lloret, *Inorg. Chem.* 43 (2004) 5761.
- [62] S. Pérez-Yáñez, O. Castillo, J. Cepeda, J.P. García-Terán, A. Luque, P. Román, *Inorg. Chim. Acta* 365 (2011) 211.
- [63] B. Lippert, *Coord. Chem. Rev.* 200–202 (2000) 487.
- [64] M.M. Taqui-Khan, C.K. Krishnamoorthy, *J. Inorg. Nucl. Chem.* 42 (1971) 1417.
- [65] (a) S. Verma, M. Ashutosh, J. Kumar, *Acc. Chem. Res.* 43 (2010) 79;
(b) A. Marzotto, A. Ciccicarese, D.A. Clemente, G. Valle, *J. Chem. Soc. Dalton Trans.* (1995) 1461;
(c) E.R.T. Tiekink, T. Kurucsev, B.F. Hoskins, *J. Crystallogr. Spectrosc. Res.* 19 (1989) 823;
(d) Y. Rosopolos, U. Nagel, W. Beck, *Chem. Ber.* 118 (1985) 931;
(e) J.-P. Charland, A.L. Beauchamp, *Croat. Chem. Acta* 57 (1984) 679;
(f) L. Prizant, M.J. Olivier, R. Rivest, A.L. Beauchamp, *Can. J. Chem.* 59 (1981) 1311;
(g) W.M. Beck, J.C. Calabrese, N.D. Kottmair, *Inorg. Chem.* 18 (1979) 176;
(h) H. Sakaguchi, H. Anzai, K. Furuhata, H. Ogura, Y. Titaka, T. Fujita, T. Sakaguchi, *Chem. Pharm. Bull.* 26 (1978) 2465;
(i) D.B. Brown, J.W. Hall, H.M. Helis, E.G. Walton, D.J. Hodgson, W.E. Hatfield, *Inorg. Chem.* 16 (1977) 2675;
(j) P. de Meester, A.C. Skapski, *J. Chem. Soc. Dalton Trans.* 4 (1973) 424;
(k) T.J. Kistenmacher, *Acta Crystallogr.* B30 (1974) 1610;
(l) D. Badura, H. Vahrenkamp, *Inorg. Chem.* 41 (2002) 6013.
- [66] (a) T.F. Mastropietro, D. Armentano, N. Marino, G. de Mundo, *Polyhedron* 26 (2007) 4945;
(b) O.S. Sukhanov, O.V. Shishkin, L. Gorb, Y. Podolyan, J. Leszczynski, *J. Phys. Chem. B* 107 (2003) 2846;
(c) A.F. Jalbout, L. Adamowicz, *J. Phys. Chem. A* 105 (2001) 1033.
- [67] J.P. García-Terán, O. Castillo, A. Luque, U. García-Couceiro, G. Beobide, P. Román, *Dalton Trans.* (2006) 902.
- [68] M.F. Goodman, *Nature* 378 (1995) 237.
- [69] J. Sponer, J. Leszczynski, P. Hobza, *Biopolymers* 61 (2002) 3.
- [70] (a) W.S. Sheldrick, P. Gross, *Inorg. Chim. Acta* 156 (1989) 139;
(b) J.D. Orbell, C. Solorzano, L.G. Marzilli, T.J. Kistenmacher, *Inorg. Chem.* 21 (1982) 2630.
- [71] P. Brandi-Blanco, P.J. Sanz-Miguel, B. Müller, E. Gil-Bardaji, M. Willermann, B. Lippert, *Inorg. Chem.* 48 (2009) 5208.
- [72] M.D. Wyatt, J.M. Allan, A.Y. Lau, T.E. Ellenberger, L.D. Samson, *Bioessays* 21 (1999) 668.
- [73] J.P. García-Terán, O. Castillo, A. Luque, U. García-Couceiro, G. Beobide, P. Román, *Inorg. Chem.* 46 (2007) 3593.
- [74] J.P. García-Terán, O. Castillo, A. Luque, U. García-Couceiro, G. Beobide, P. Román, *Cryst. Growth Des.* 7 (2007) 2594.

Paddle-Wheel Shaped Copper(II)-Adenine Discrete Entities As Supramolecular Building Blocks To Afford Porous Supramolecular Metal–Organic Frameworks (SMOFs)

Jintha Thomas-Gipson,[†] Garikoitz Beobide,^{*,†} Oscar Castillo,^{*,†} Michael Fröba,[‡] Frank Hoffmann,[‡] Antonio Luque,[†] Sonia Pérez-Yáñez,[†] and Pascual Román[†]

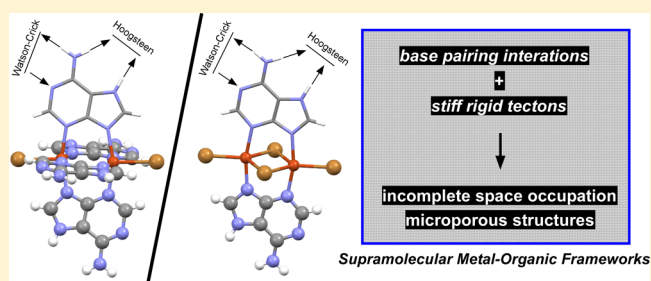
[†]Departamento de Química Inorgánica, Facultad de Ciencia y Tecnología, Universidad del País Vasco (UPV/EHU), Apartado 644, E-48080 Bilbao, Spain

[‡]Institute of Inorganic and Applied Chemistry, Department of Chemistry, University of Hamburg, Martin-Luther-King-Platz 6, D-20146 Hamburg, Germany

Supporting Information

ABSTRACT: The present work assesses the ability of $[\text{Cu}_2(\mu\text{-adenine})_4(\text{X})_2]^{2+}$ and $[\text{Cu}_2(\mu\text{-adenine})_2(\mu\text{-X})_2(\text{X})_2]$ (X: Cl^- or Br^-) metal-nucleobase dinuclear entities to build up supramolecular metal–organic frameworks (SupraMOFs) based on the complementary hydrogen bonding interactions established by the Watson–Crick and Hoogsteen faces of adjacent adenine moieties. The noncoplanar disposition of these synthons in the $[\text{Cu}_2(\mu\text{-adenine})_4(\text{X})_2]^{2+}$ building unit leads to an open framework with one-dimensional (1D) channels of ca. 6 Å in compounds $[\text{Cu}_2(\mu\text{-adenine})_4(\text{Cl})_2] \cdot 2\text{MeOH}$ (**1**, SMOF-1) and $[\text{Cu}_2(\mu\text{-adenine})_4(\text{Br})_2] \cdot 2\text{MeOH}$ (**2**, SMOF-2) sustained through the hydrogen bonding base pairing interactions among the Watson–Crick faces.

In the case of the second building unit, $[\text{Cu}_2(\mu\text{-adenine})_2(\mu\text{-X})_2(\text{X})_2]$, the coplanar arrangement of the two adenines in the dimeric unit does not allow a three-dimensional (3D) supramolecular architecture based only on the complementary hydrogen bonding interactions between the nucleobases. Therefore, other supramolecular interactions involving the halide ions and solvent molecules are crucial for determining the features of the crystal packing. In compound $[\text{Cu}_2(\mu\text{-adenine})_2(\mu\text{-Cl})_2(\text{Cl})_2] \cdot 2\text{MeOH}$ (**3**, SMOF-3), base pairing interactions between adjacent adenines produce 1D supramolecular ribbons of dinuclear entities. These ribbons establish additional hydrogen bonds between the Hoogsteen face and the chloride anions of adjacent ribbons that are also reinforced by the presence of $\pi\text{-}\pi$ stacking interactions among the adenines leading to a rigid synthon that gives rise to a robust 3D skeleton with the presence of micropores occupied by solvent molecules. In the case of the bromide analogue, the weaker hydrogen acceptor capacity of the bromide allows the solvent molecules to disrupt the self-assembly process of the dinuclear entities and prevents the formation of an open-framework supramolecular structure leading to the nonporous $[\text{Cu}_2(\mu\text{-adenine})_2(\mu\text{-Br})_2(\text{Br})_2] \cdot 2\text{PrOH}$ (**4**) compound. According to gas adsorption studies, SMOF-1, SMOF-2, and SMOF-3 present a surface instability that creates a diffusion barrier that can be permeated only by strong interacting adsorbate molecules with high kinetic energy such as CO_2 but not N_2 , H_2 , and CH_4 . This feature makes them attractive for selective gas adsorption and separation technologies.



INTRODUCTION

The coordination chemistry of metal ion interactions with purine nucleobases has attracted enormous attention because of its biological relevance, structural diversity, molecular recognition behaviors, and potential applications as advanced functional materials.¹ Adenine (6-aminopurine) has a wide range of binding possibilities through the endocyclic N9, N7, N3, N1, and exocyclic N6 nitrogen atoms as donor sites² resulting in a vast number of products. Moreover, when a metal–adenine complex is formed, the noncoordinated nitrogen donor sites confer the ability to establish a wide variety of hydrogen bonding based supramolecular interactions.³ On the other hand, the purine ligands are well-known for their ability

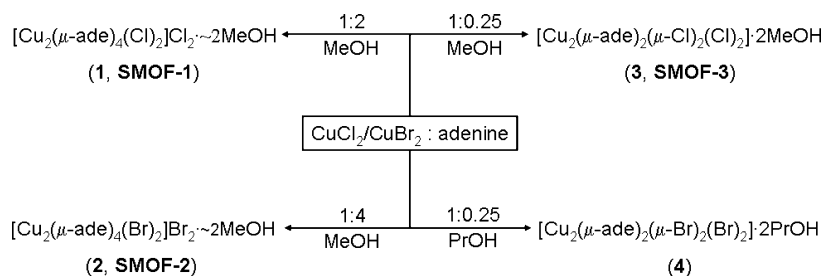
to build dinuclear complexes by means of the N3 and N9 bridging mode,⁴ and previous works have demonstrated that either adenine or adeninate ligands tend to form paddle-wheel shaped dinuclear complexes, such as $[\text{Cu}_2(\mu\text{-adenine})_4]^{4+}$, $[\text{Cu}_2(\mu\text{-adeninato})_4]$, or $[\text{Cu}_2(\mu\text{-adeninato})_2(\text{X})_2]$ (where X: RCOO^- , halide \cdots).⁵ These entities can self-assemble by means of the well-known base pairing of the Watson–Crick (N6–H, N1) and Hoogsteen faces (N6–H, N7) and by $\pi\text{-}\pi$ stacking interactions. Nonetheless, additional factors present in the

Received: May 2, 2014

Revised: June 11, 2014

Published: June 13, 2014

Scheme 1



reaction media, such as interactions with solvent molecules or counterions, can disrupt the direct hydrogen bonding interactions between the nucleobases.⁶

On the basis of these facts, we have designed a synthetic strategy to develop rigid supramolecular open-networks showing permanent microporosity as an alternative to more conventional metal–organic frameworks (MOFs).⁷ It deserves mentioning that examples of microporous compounds whose crystal structure is sustained by noncovalent interactions are scarce, mainly due to the difficulties inherent to the design of such systems and the usually assumed weakness of the supramolecular connectivity.⁸ Our approach is based on employing as supramolecular building blocks discrete metal–adenine complexes in which two or more nucleobases are tightly anchored to the metal centers by at least two donor positions (N3, N9 sites of the adenine in the present case). This coordination motif imposes a rigid structure to the building unit that is a key factor of our crystal design. In addition, the geometrical arrangement of the nucleobases around the metal centers is otherwise difficult to achieve for other systems such as organic molecules functionalized with adenine residues. In these discrete complexes, as many hydrogen donor/acceptor positions of the nucleobase remain free, the entities are able to self-assemble among them by means of rigid double or triple complementary hydrogen bonds. Due to the geometric restraints of the H-bonding synthons and of the metal–nucleobase complex itself, an efficient packing of the supramolecular building units is hindered allowing the presence of a large empty volume: an open-framework supramolecular crystal building. The voids will be usually occupied by solvent molecules, and as consequence, in order to achieve a compound with permanent porosity, the scheme of supramolecular interactions established among the metal–nucleobase entities must be strong enough to avoid the collapse of the crystal structure when the solvent is evacuated. This fact is the reason to select metal–nucleobase systems. The nucleobases self-recognize by double or triple hydrogen bonding ensuring a superior strength of the resulting supramolecular crystal building. The pioneering example that makes use of this strategy to provide a molecular porous material with formula $[\text{Cu}_2(\mu\text{-adenine})_4\text{Cl}_2]\text{Cl}_2$ was published by us in 2011.⁹ Later, Zaworotko et al. reported an analogous compound replacing the chlorides by bulkier TiF_6^{2-} anions improving the chemical stability of the supramolecular network toward humidity.¹⁰

In this work we assess the ability of two types of metal–nucleobase dinuclear entities $[\text{Cu}_2(\mu\text{-adenine})_4(\text{X})_2]^{2+}$ and $[\text{Cu}_2(\mu\text{-adenine})_2(\mu\text{-X})_2(\text{X})_2]$ (where X: Cl^- or Br^-) to build up supramolecular metal–organic frameworks (SMOFs) based on base pairing interactions between either Watson–Crick faces or Hoogsteen faces. The control over the molecular

structure of the dinuclear entities is easily achieved by means of the copper(II) halide/adenine ratio. As a result of the non-coplanarity of the adenines in $[\text{Cu}_2(\mu\text{-adenine})_4(\text{X})_2]^{2+}$ entities, the base pairing sustained self-assembling process yields an open framework with one-dimensional (1D) channels occupied by methanol solvent molecules: $[\text{Cu}_2(\mu\text{-adenine})_4(\text{Cl})_2]\text{Cl}_2 \cdot 2\text{MeOH}$ (**1**, SMOF-1) and $[\text{Cu}_2(\mu\text{-adenine})_4(\text{Br})_2]\text{Br}_2 \cdot 2\text{MeOH}$ (**2**, SMOF-2). Regarding $[\text{Cu}_2(\mu\text{-adenine})_2(\mu\text{-X})_2(\text{X})_2]$ dinuclear entity, compounds $[\text{Cu}_2(\mu\text{-adenine})_2(\mu\text{-Cl})_2(\text{Cl})_2] \cdot 2\text{MeOH}$ (**3**, SMOF-3) and $[\text{Cu}_2(\mu\text{-adenine})_2(\mu\text{-Br})_2(\text{Br})_2] \cdot 2\text{PrOH}$ (**4**) were yielded. In the latter cases, the coplanar arrangement of the adenines reduces the dimensionality of the supramolecular polymer obtained from the base pairing interactions. As a consequence, the coordinated halides and solvent molecules play a crucial role stabilizing the overall three-dimensional (3D) crystal structure. In the case of the chloride-based compound **3** (SMOF-3), the combination of base pairing, π – π stacking, and additional hydrogen bonding interactions involving the chloride anions provides a rigid scheme of supramolecular interactions that precludes an efficient occupation of the space leading to a robust open-framework supramolecular structure. The weaker nature of the hydrogen bonds involving bromide anions allows the solvent molecules to disrupt the previously described supramolecular interaction scheme leading to nonporous compound **4**. Even though previously reported N_2 adsorption experiments performed on samples of $[\text{Cu}_2(\mu\text{-adenine})_4(\text{Cl})_2]\text{Cl}_2$ (SMOF-1)¹¹ did not show significant adsorption, the present work will prove the permanent porosity of SMOF-1, SMOF-2, and SMOF-3 compounds by means of CO_2 adsorption isotherms at 273 K. The different adsorption behavior is attributed to a surface instability, because of the air humidity, that creates a diffusion barrier that only can be permeated by well-suited adsorbates under specific adsorption conditions. Therefore, these compounds can be envisaged as potential materials for selective gas adsorption or separation purposes.

EXPERIMENTAL SECTION

Synthesis. All the chemicals were of reagent grade and were used as commercially obtained. The purity of the synthesized samples was checked by means of powder X-ray diffraction, along with the elemental and thermogravimetric analyses. Scheme 1 describes the most notorious synthesis conditions to afford compounds 1–4.

$[\text{Cu}_2(\mu\text{-adenine})_4\text{Br}_2]\text{Br}_2 \cdot 2\text{MeOH}$ (2**, SMOF-2).** A total of 0.0112 g of cupric bromide (0.05 mmol) dissolved in 5 mL of methanol was added dropwise to the hot stirring solution of 0.0273 g of adenine (0.2 mmol) dissolved in 30 mL of methanol at 50 °C. Immediately after the reagents were mixed, compound **2** precipitated as a blue polycrystalline product. Yield: 90%. Anal. Calcd (found) for $\text{C}_{22}\text{H}_{28}\text{Br}_4\text{Cu}_2\text{N}_{20}\text{O}_2$: C, 25.13 (25.24); H, 2.68 (2.81); N, 26.65 (26.53); Cu, 12.09 (11.97). IR (KBr, cm^{-1}): 3330s, 3170s, 1650vs, 1515w, 1460m, 1348w, 1320m, 1260w, 1215m, 1182w, 1148w,

Table 1. Single-Crystal Data and Structural Refinement Details of Compounds 2, 3, and 4

compound	2	3	4
formula	C ₂₂ H ₂₈ Br ₄ Cu ₂ N ₂₀ O ₂	C ₁₂ H ₁₈ Cl ₄ Cu ₂ N ₁₀ O ₂	C ₁₆ H ₂₆ Br ₄ Cu ₂ N ₁₀ O ₂
MW [g mol ⁻¹]	1051.36	603.24	837.19
crystal system	trigonal	monoclinic	monoclinic
space group	R $\bar{3}m$	C2/c	P2 ₁ /c
a [Å]	27.1979(9)	22.2245(18)	9.1344(7)
b [Å]	27.1979(9)	13.8069(10)	11.0778(10)
c [Å]	15.4999(4)	7.0204(6)	13.0778(11)
α [°]	90	90	90
β [°]	90	108.280(6)	103.873(7)
γ [°]	120	90	90
V [Å ³]	9929.6(5)	2045.5(3)	1284.7(2)
Z	9	4	2
ρ_{calcd} (g·cm ⁻³)	1.582	1.959	2.164
μ (mm ⁻¹)	4.630	2.636	7.912
reflections collected	31767	9439	18741
unique data/parameters	2837/109	9439/127	3059/161
R _{int}	0.0465	0.0695	0.0942
goodness of fit (S) ^a	1.234	1.089	1.119
R ₁ ^b /wR ₂ ^c [I > 2 σ (I)]	0.0927/0.2997	0.0778/0.2048	0.0504/0.0927
R ₁ ^b /wR ₂ ^c [all data]	0.1112/0.3107	0.1119/0.2342	0.0688/0.1005

^aS = $[\sum w(F_o^2 - F_c^2)^2 / (N_{\text{obs}} - N_{\text{param}})]^{1/2}$. ^bR₁ = $\sum ||F_o| - |F_c|| / \sum |F_o|$. ^cwR₂ = $[\sum w(F_o^2 - F_c^2)^2 / \sum w|F_o|^2]^{1/2}$; w = $1/[\sigma^2(F_o^2) + (aP)^2 + bP]$ where P = (max(F_o², 0) + 2Fc²)/3 with a = 0.2000 (2), 0.1437 (3), 0.0235 (4), and b = 9.0683 (4).

1117m, 1022w, 970w, 934w(sh), 922w(sh), 790m, 738m, 683w, 610w, 563w, 545m. Crystals suitable for single crystal X-ray diffraction studies were grown by using the slow diffusion of a methanolic solution (12 mL) of adenine (0.0111 g, 0.08 mmol) into a propanolic solution (12 mL) of cupric bromide (0.0088 g, 0.04 mmol). After 1 week, compound 2 crystallized as deep blue colored single crystals along with some poor quality red crystals of compound 4.

[Cu₂(μ -adenine)₄Cl₂Cl₂·2MeOH (1, SMOF-1). Compound 1 was prepared following the synthetic method mentioned in one of our previous works.¹¹ A total of 0.0171 g of cupric chloride dihydrate (0.1 mmol) dissolved in 5 mL of methanol were added dropwise to a hot stirring solution (50 °C) of 0.0273 g of adenine (0.2 mmol) dissolved in 30 mL of methanol. A blue precipitate corresponding to compound 1 was formed immediately on the addition of the cupric chloride solution. Yield: 90%. Anal. Calcd (found) for C₂₂H₂₈Cl₄Cu₂N₂₀O₂: C, 30.25 (30.19); H, 3.23 (3.19); N, 32.07 (32.26); Cu, 14.55 (14.62). IR (KBr, cm⁻¹): 3360s; 3170s; 1650vs; 1515w; 1460m; 1400m; 1350w; 1320m; 1210m; 1110w; 785w; 740w; 550m.

[Cu₂(μ -adenine)₂(μ -Cl)₂(Cl)₂·2MeOH (3, SMOF-3). A total of 0.0682 g of cupric chloride dihydrate (0.4 mmol) dissolved in 10 mL of methanol were added dropwise to a hot stirring solution (50 °C) of 0.0136 g of adenine (0.1 mmol) dissolved in 20 mL of methanol and stirred for half an hour. After the reagents were mixed, compound 3 appeared as a green precipitate. Yield: 95%. Anal. Calcd (found) for C₁₂H₁₈Cl₄Cu₂N₁₀O₂: C, 23.89 (23.92); H, 3.01 (3.14); N, 23.22 (23.18); Cu, 21.07 (21.03). IR (KBr, cm⁻¹): 3387s, 3142s(sh), 3103s(sh), 1666vs, 1611m, 1580m, 1520m, 1478m, 1450s, 1404vs, 1383w, 1356w(sh), 1347w(sh), 1318vs, 1262w, 1244w, 1215m, 1291w, 1170m, 1111vs, 1016w, 976w(sh), 970w(sh), 931m, 788m, 737m(sh), 722m(sh), 680m, 633w, 597m, 573w, 548s. Single crystals were obtained by slow diffusion of a methanolic solution (10 mL) 0.0171 g of cupric chloride (0.1 mmol) into another methanolic solution (30 mL) containing 0.0277 g of adenine (0.2 mmol) and 16.9 μ L of concentrated hydrochloric acid (37%). Green-colored single crystals of compound 3 were formed along with blue colored crystals of compound 1.

[Cu₂(μ -adenine)₂(μ -Br)₂(Br)₂·2PrOH (4). A hot propanolic solution (40 mL, 50 °C) of 0.0136 g of adenine (0.1 mmol) was added dropwise to a second propanolic solution (10 mL) of 0.0893 g of cupric bromide (0.4 mmol). Immediately, an unidentified brown precipitate appears. The reaction mixture was left stirring for half an

hour. Afterward the precipitate is collected by filtration, and the mother-liquid solution is left evaporating at room conditions. One month later, red crystals of compound 4 are obtained. Yield: 20%. Anal. Calcd (found) for C₁₆H₂₆Br₄Cu₂N₁₀O₂: C, 22.96 (22.91); H, 3.13 (3.09); N, 16.73 (16.78); Cu, 15.18 (15.15). IR (KBr, cm⁻¹): 3380s, 3226s, 3293s, 3240s, 3193s, 3130s, 2953s, 1666vs, 1612m, 1476w, 1460w, 1405m, 1384w, 1357w, 1344w, 1320s, 1262w, 1220m, 1175w, 1112m, 1050w, 1002s, 972w, 930w, 875m, 802w, 876m, 736m, 711w, 677w, 663w, 613m, 569m, 538w, 472w, 463w.

Physical Measurements. Elemental analyses (C, H, N) were performed on a Euro EA elemental analyzer, whereas the metal content was determined by inductively coupled plasma atomic emission spectrometer (ICP-AES) from Horiba Yobin Yvon Activa. The IR spectra (KBr pellets) were recorded on a FTIR 8400S Shimadzu spectrometer in the 4000–400 cm⁻¹ spectral region. Thermal analyses (TG/DTA) were performed on a TA Instruments SDT 2960 thermal analyzer in a synthetic air atmosphere (79% N₂/21% O₂) with a heating rate of 5 °C·min⁻¹. Prior to gas adsorption measurements all samples were activated in vacuum at 100–180 °C for 6–24 h. Lower and greater activation temperatures did not result in samples with higher gas uptake capacity. The powder X-ray diffraction patterns on the outgassed samples showed that the structure remains stable without loss of crystallinity. Nitrogen physisorption data were recorded with a Quantachrome QUADRASORB-SI-MP at 77 K. The specific surface area was calculated from the adsorption branch in the relative pressure interval from 0.01 to 0.10 using the Brunauer–Emmett–Teller (BET) method. Volumetric carbon dioxide and hydrogen physisorption data were recorded at 273 K on a Quantachrome Autosorb-iQ-MP and at 77 K on a Quantachrome Autosorb-1C (purity of hydrogen: 99.999%).

X-ray Diffraction Data Collection and Structure Determination. The single crystal X-ray diffraction data collections were done at 293(2) K for compound 2 and at 100(2) K for compounds 3 and 4 on an Oxford Diffraction Xcalibur diffractometer with graphite-monochromated Mo-K α radiation (λ = 0.71073 Å). The data reduction was done with the CrysAlisPro program.¹² All the structures were solved by direct methods using the SIR92 program¹³ and refined by full-matrix least-squares on F² including all reflections (SHELXL97).¹⁴ All calculations for these structures were performed using the WINGX crystallographic software package.¹⁵ After the initial structure solution was completed, the difference Fourier map for

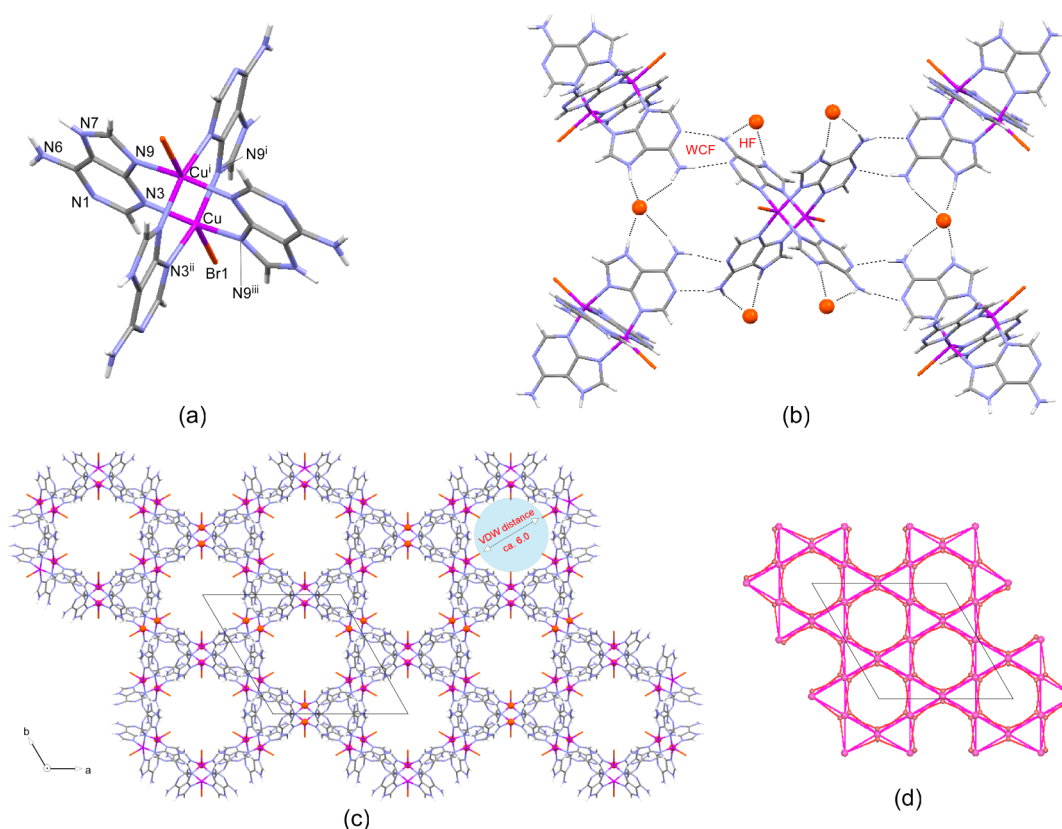


Figure 1. Crystal structure features of **SMOF-2**: (a) Structural units with the atomic numbering scheme. (b) Details of the adenine base pairing interaction through the Watson–Crick face (WCF) and of the Hoogsteen Face (HF) mediated adenine...bromide interaction (free bromide anions are represented as orange spheres). (c) Perspective view of the 3D framework along the *c*-axis showing the pores. Solvated methanol molecules are omitted for clarity. (d) Network topology.

Table 2. Selected Bond Lengths (Å) and Angles (deg) of Compounds **2**, **3**, and **4**^a

compound 2		compound 3 (X = Cl)		compound 4 (X = Br)
Cu–N3	1.994(5)	Cu–N3 ⁱ	2.006(4)	1.963(5)
Cu–N9 ⁱ	2.016(6)	Cu–N9	1.983(4)	1.962(5)
Cu–Br1	3.080(2)	Cu–X1	2.241(1)	2.378(1)
		Cu–X2	2.342(1)	2.540(1)
		Cu–X2 ⁱ	2.757(1)	2.656(1)
Cu...Cu ⁱ	3.082(1)	Cu...Cu ⁱ	2.942(1)	2.902(1)
N3–Cu–N3 ⁱⁱ	88.1(3)	N3 ⁱ –Cu–N9	164.83(17)	165.8(2)
N3–Cu–N9 ⁱ	86.5(2)	N3 ⁱ –Cu–X1	96.71(13)	98.02(14)
N3–Cu–N9 ⁱⁱⁱ	161.6(3)	N3 ⁱ –Cu–X2	87.19(14)	87.23(14)
N3–Cu–Br1	100.2(2)	N3 ⁱ –Cu–X2 ⁱ	83.77(13)	86.58(13)
N9 ⁱ –Cu–N9 ⁱⁱⁱ	93.1(3)	N9–Cu–X1	94.32(13)	95.56(14)
N9 ⁱ –Cu–Br1	98.0(2)	N9–Cu–X2	87.19(14)	86.78(14)
		N9–Cu–X2 ⁱ	83.21(13)	83.73(14)
		X1–Cu–X2	144.00(6)	132.35(3)
		X1–Cu–X2 ⁱ	105.81(6)	115.45(3)
		X2–Cu–X2 ⁱ	110.07(4)	112.12(3)

^aSymmetry codes. Compound 2: (i) $x-y, -y, -z+2$; (ii) $-x+y+1, y, z$; (iii) $-x+1, -y, -z+2$. Compound 3: (i) $-x+1/2, -y+1/2, -z+1$. Compound 4: (i) $-x+1, -y, -z+2$.

compound **SMOF-2** showed the presence of substantial electron density at the voids of the crystal structure that was impossible to model. Therefore, its contribution was subtracted from the reflection data by the SQUEEZE method¹⁶ as implemented in PLATON.¹⁷ Crystal parameters and details of the final refinements of compounds **2**, **3**, and **4** are summarized in Table 1. The X-ray powder diffraction (PXRD) patterns for polycrystalline samples were collected on a Phillips X'PERT powder diffractometer with Cu–K α radiation ($\lambda =$

1.54060 Å) over the range $5 < 2\theta < 70^\circ$ with a step size of 0.02° and an acquisition time of 2 s per step at 20 °C.

RESULTS AND DISCUSSION

Structural Description of [Cu₂(μ -adenine)₄Br₂]Br₂· \sim 2MeOH (2**, **SMOF-2**).** This compound is isostructural to compound **1** (**SMOF-1**) whose crystal structure has been previously reported by us.¹¹ The crystal structure consists of

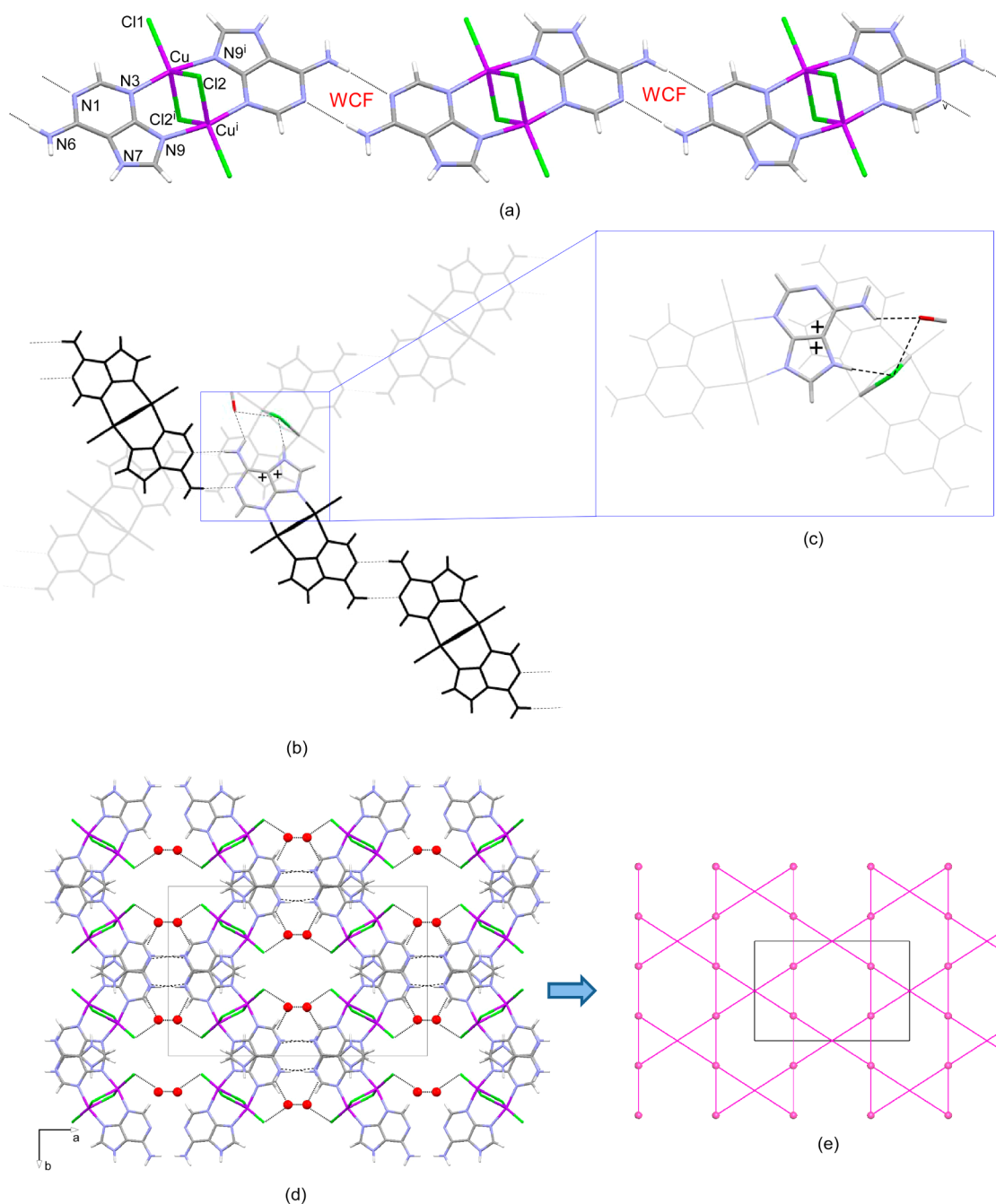


Figure 2. Crystal packing features in SMOF-3: (a) Strips of $[\text{Cu}_2(\mu\text{-adenine})_2(\mu\text{-Cl})_2\text{Cl}_2]$ dinuclear complexes grown by Watson–Crick base pairing interactions. (b, c) Dinuclear entities interacting through $\text{Cl}\cdots\text{Hoogsteen face}$ and $\pi\text{-}\pi$ interactions and the methanol hydrogen bonding mediating role. (d, e) View of the crystal packing along $[1\ 0\ 0]$ direction and overall supramolecular connectivity. Dashed lines indicate hydrogen bonds, while double plus signals represent $\pi\text{-}\pi$ interactions.

paddle-wheel like $[\text{Cu}_2(\mu\text{-adenine})_4\text{Br}_2]^{2+}$ complexes, bromide counterions, and disordered methanol molecules. Figure 1 shows a perspective view of the dimeric entity together with the labeling scheme which is conventionally accepted for the adenine nucleobase for chemical and biological purposes, while coordination bonds and angles are gathered in Table 2. Four bridging adenine molecules are linked to the copper(II) atoms through their N3 and N9 nitrogen atoms to provide the core of the paddle-wheel shaped dinuclear entity. Two bromide anions occupy the apical positions resulting in an elongated square pyramidal coordination environment of the metal centers. The dimeric complex is sited on a $2/m$ crystallographic position and

shows a UDD conformation, referring the terms U(up) or D(down) to the coordination of each pyrimidinic N3 atoms to the upper or lower metal center.

The $[\text{Cu}_2(\mu\text{-adenine})_4\text{Br}_2]^{2+}$ dinuclear entities are cross-linked together by pairs of symmetry-related $\text{N6}\text{-H}\cdots\text{N1}$ hydrogen bonding interactions between the Watson–Crick faces of two adjacent nucleobases to give a $R_2^2(8)$ ring. It deserves mentioning that this hydrogen bonding interaction scheme is a well-known structural synthon between self-assembling adenines.^{5f,18} In the present compound the geometry and rigidity of the $[\text{Cu}_2(\mu\text{-adenine})_4\text{Br}_2]^{2+}$ entity (Figure 1) and the rigidity of the previously described hydrogen

bonding synthon make it suitable to assemble in such a way that it generates an open-supramolecular-framework because of the inefficient occupation of the space. This synthon involving the Watson–Crick faces yields by itself a four-connected uninodal 3D net with *nbo* topology and $(6^4.8^2)$ point symbol (Figure 1d).¹⁹ However, the cohesion of the structure is further strengthened by $R_2^1(7)$ type hydrogen bonding interaction established among the free bromide counterions and the Hoogsteen faces of two adenine of neighboring complexes. Considering both types of interactions (Watson–Crick base pairing and Hoogsteen...bromide) the supramolecular network can be alternatively described as an eight-connected uninodal with *reo* topology and $(3^8.4^8.5^8.6^4)$ point symbol.

The resulting porous structure consists of 1D tubular channels that run along the crystallographic *c* axis with a diameter of 6.0 Å (distance among van der Waals surfaces of opposite chloride anions). These channels represent the 30% of crystal total volume,²⁰ and they are occupied by solvent methanol molecules in a highly disordered manner. Due to the greater size of bromide anion, these values are somewhat lower than those found in the chloride derivative (SMOF-1; pore diameter: 6.3 Å; accessible volume: 36%).

Structural Description of $[\text{Cu}_2(\mu\text{-adenine})_2(\mu\text{-Cl})_2(\text{Cl})_2] \cdot 2\text{MeOH}$ (3, SMOF-3) and $[\text{Cu}_2(\mu\text{-adenine})_2(\mu\text{-Br})_2(\text{Br})_2] \cdot 2\text{PrOH}$ (4). Both compounds are comprised of neutral centrosymmetric dimeric $[\text{Cu}_2(\mu\text{-adenine})_2(\mu\text{-X})_2(\text{X})_2]$ entities (X: Cl^- , Br^-) (Figure 2). It shows some resemblances to the previously described $[\text{Cu}_2(\mu\text{-adenine})_4\text{X}_2]^{2+}$ dimeric entity of SMOF-1 and SMOF-2. The overall paddle-wheel shape is retained, but two opposite adenine ligands have been replaced by two bridging halide anions giving rise to a neutral dimeric entity showing an UD conformation with regard to the adenine bridges and two capping halide anions. The intradimeric Cu...Cu distances (2.942(1) and 2.902(1) Å, for chloride and bromide analogues) are slightly shorter than that of SMOF-1 and -2 (3.064(1) and 3.082(1) Å). Each copper atom is pentacoordinated by a N_2X_3 donor set which resembles a compressed trigonal bipyramid. The equatorial plane consists of three halide atoms implying longer bond distances than the apical ones (Table 2) and X–Cu–X angles within the range of 106–144° and a deviation of ca. 0.05 Å for the Cu(II) atom. The apical positions are occupied by the N3 and N9 donor sites of two symmetry related adenine molecules with a N–Cu–N angle of ca. 165° and an angle between equatorial plane and Cu–N bond of 83–86°. The coordination bond distances of the bridging halide anions are slightly longer than those of the terminal one as usually happens.

Obviously, the coplanar arrangement of adenines in the dimeric $[\text{Cu}_2(\mu\text{-adenine})_2(\mu\text{-X})_2(\text{X})_2]$ entity although does not preclude the polymerization through direct complementary hydrogen bonding interactions between the nucleobases reduces the dimensionality of the resulting supramolecular network. In the case of SMOF-3, the base pairing interaction between the Watson–Crick faces of $[\text{Cu}_2(\mu\text{-adenine})_2(\mu\text{-Cl})_2(\text{Cl})_2]$ units gives rise to linear 1D supramolecular ribbons (Figure 2a) that spread along two different crystallographic directions $[1\ 1\ 0]$ and $[1\ \bar{1}\ 0]$. These supramolecular ribbons are further cross-linked by means of both the hydrogen-bonding interactions between the Hoogsteen face and the bridging chloride and π – π stacking interactions between adjacent adenines. The combination of the latter two types of interactions leads also to a relatively rigid synthon that extends the connectivity toward a robust supramolecular 3D one and, at

the same time, precludes an efficient occupation of the space (Figure 2d). Considering both types of synthons (Watson–Crick base pairing and Hoogsteen...chloride/ π – π stacking) the supramolecular network can be described as a six-connected uninodal net with *rob* topology and $(4^8.6^6.8)$ point symbol (Figure 2e). This packing generates 1D channels along the crystallographic *c* axis with an elliptical cross-section of ca. 5.5×7.5 Å, that are filled by solvation water molecules that represent a 21% of the total volume. Again, the combination of rigid metal-nucleobase building unit and geometrically restricted supramolecular synthons leads to an ineffective space occupation providing accessible space within the crystal structure of this material. It is worthy to mention that the hydrogen bonding interaction between the Hoogsteen side of the adenine and the chloride anion is reinforced by an indirect hydrogen bonded interaction mediated by a solvation methanol molecule that will involve, as it is discussed later, a relatively significant unit cell change upon the removal of the solvent molecules.

The weaker hydrogen bond acceptor nature of the bromide anion in comparison to chloride makes the crystal packing features of compound 4, $[\text{Cu}_2(\mu\text{-adenine})_2(\mu\text{-Br})_2(\text{Br})_2] \cdot 2\text{PrOH}$ (Figure 3), to be essentially different from that of its

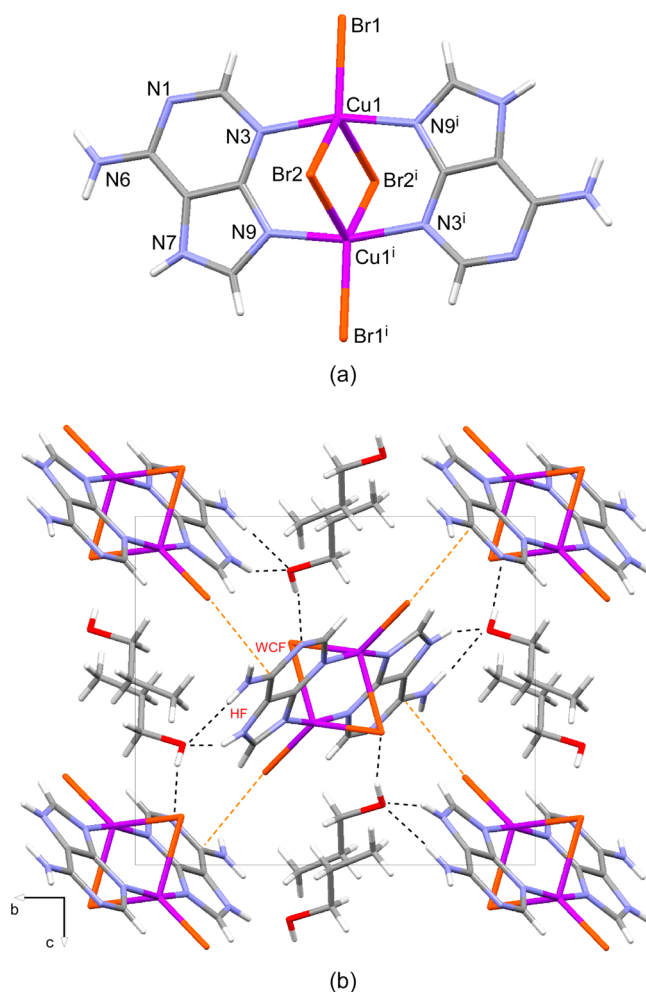


Figure 3. Dimeric unit (a) and view of the crystal packing along $[1\ 0\ 0]$ direction (b) in compound 4. Black dotted lines indicate hydrogen bonding interactions, while orange dashed lines indicate halide... π contacts.

chloride analogue (SMOF-3). It does not present base pairing interaction nor any other direct hydrogen bonding interaction between the adenine moieties and coordinated halides. In fact, the dinuclear entities are held together by the hydrogen bonding interactions mediated through the entrapped propan-1-ol molecules with the Hoogsteen and Watson–Crick faces of adjacent paddle-wheel entities. The Hoogsteen face of the nucleobase forms hydrogen bonding with the oxygen atom of the propan-1-ol molecule ($R_2^1(7)$ hydrogen bonded ring), while the Watson–Crick face of the adenine establishes a single hydrogen bond by means of the interaction of N1 with H atom of the alcohol group. The supramolecular interaction network of compound 4 is further reinforced by halide $\cdots\pi$ type interactions established between the terminal Br1 atoms and C6 carbon of the adenine (Br1 \cdots C6:3.489 Å). The lack of direct hydrogen bonding interactions among the rigid adenine moieties and the solvent mediated disruption of the hydrogen bonding network result in a nonporous crystal structure which collapses at temperatures close to 50 °C rendering an amorphous product, according to the thermogravimetric and variable temperature PXRD measurements.

Gas Adsorption Experiments on $[\text{Cu}_2(\mu\text{-adenine})_2(\text{Cl})_2]\text{Cl}_2\cdot\sim 2\text{MeOH}$ (SMOF-1) and $[\text{Cu}_2(\mu\text{-adenine})_2(\text{Br})_2]\text{Br}_2\cdot\sim 2\text{MeOH}$ (SMOF-2). Prior to gas adsorption experiments, thermal stability of both SMOFs was assessed by means of thermogravimetric and variable temperature PXRD experiments (see Supporting Information). According to the thermogravimetric data of both compounds, release of the solvent molecules hosted in the channels takes place between room temperature and 100 °C. In both cases the resulting compound remains stable up to 220 °C and the PXRD patterns at different temperatures (Figure 4a,b) do not differ substantially from that of the starting material, suggesting that the 3D open framework is retained after the removal of the methanol molecules. Above this temperature, it undergoes successive exothermic processes leading to CuO as final residue above 500 °C.

Freshly synthesized single crystals of SMOF-1 and -2 were used for gas adsorption experiments, and they were activated under a vacuum at temperatures ranging from 100 to 180 °C during 6–24 h to eliminate solvent guest molecules prior to measurements. Different outgassing conditions did not exert significant changes in N_2 uptake capacity. For clarity only the results of samples outgassed at 150 °C during 12 h are shown in subsequent figures. The adsorption curve collected at 77 K exhibits features resulting from multilayer adsorption. The fitting of the adsorption area to BET equation leads to surface area values of 26 and 14 m^2/g , respectively. These values are substantially smaller than the surface area calculated from the BET fittings on GCMC simulated N_2 adsorption isotherms (767 and 654 m^2/g , respectively), see details at the Supporting Information. Thereafter, H_2 adsorption experiments were also carried out by collecting isotherms at 77 K. Similarly to N_2 , a negligible adsorption is observed for both compounds. A common explanation to such a difference between the experimental and expected porosity includes incomplete solvent removal, crystal collapse, or a massive presence of impurities. However, the weight loss of the outgassed sample fits the one expected from the compound formula, which suggests a quantitative removal of the solvent. The PXRD data confirms that the outgassed sample retains its crystallinity and, therefore, its bulk porous framework. Finally, the comparison of PXRD patterns, chemical analysis, and scanning electron

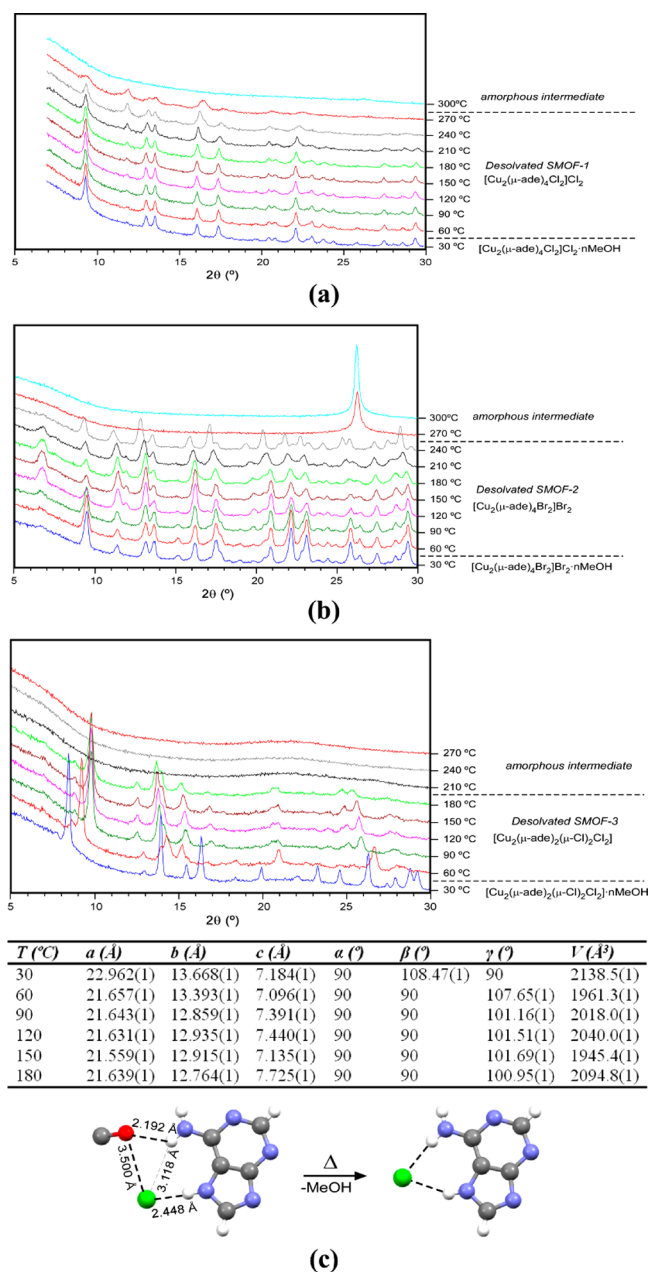


Figure 4. Thermogravimetric data of (a) SMOF-1, (b) SMOF-2, and (c) SMOF-3.

microscopy data on the fresh and outgassed samples allowed to rule out the presence of a substantial amount of impurities.

In a recent work Matzger and co-workers explained the discrepancies between crystallographic porosity and experimental gas uptake for Zn-HKUST-1 based on positron annihilation lifetime spectroscopy.²¹ The authors state that the lack of gas uptake is due to the inherent surface instability after solvent removal which renders the material impermeable to molecular guests irrespective of the handling and activation methods used in the gas adsorption experiments. However, according to the latter work, the surface collapse is overcome when the sample is immersed in a solvent, and thus the porous network is well accessible.

Nonetheless, the present SMOFs have been shown to behave as an adsorbent when they were exposed to the vapors of methanol, acetone, dichloromethane, tetrachloromethane, and

water.¹¹ Thus, it seems that the above-described diffusion barrier resulting from the surface instability is not only overcome in solution but also when adsorbate molecules in the gas phase have enough interaction energy to pass through. In order to get further evidence on the latter statement herein we have carried gas adsorption measurements at higher temperatures by collecting the isotherms for CO₂ at 273 K and CH₄ at 298 K (Figure 5). Similarly to the previous

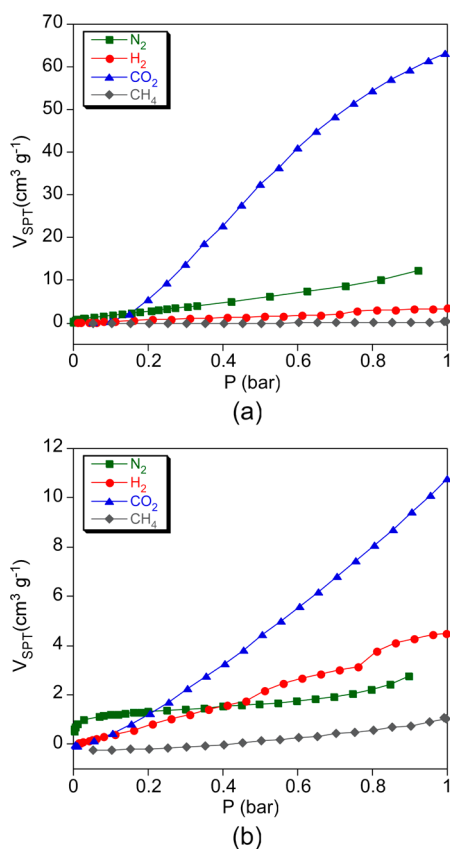


Figure 5. Adsorption isotherms for N₂ (77K), H₂ (77K), CO₂ (273 K), and CH₄ (298 K) for fresh samples of SMOF-1 (a) and -2 (b).

adsorbates methane adsorption is not observed. However, the CO₂ uptake shows a notable increase in both compounds. In fact while at pressures close to saturation, the N₂ uptake is 0.54 and 0.12 mmol/g for compounds SMOF-1 and -2, and the CO₂ uptake increases about four times to reach values of 2.81 and 0.48 mmol/g, respectively. Considering the latter results this behavior can be rationalized on the basis of the thermal energy and of the polar nature of the adsorbate. The apolar CH₄ lacks of quadrupole moment, while CO₂ presents a relatively strong quadrupole moment ($-0.8908 \text{ e} \cdot \text{\AA}^2$), substantially greater than that for N₂ or H₂ (-0.2946 and $+0.1288 \text{ e} \cdot \text{\AA}^2$, respectively).²² Methane has not been able to permeate the surface although the increase of the adsorption temperature. Nonetheless, the higher measurement temperature and the stronger quadrupole moment of CO₂ confer the ability to diffuse through the surface barrier and permeate the porous network.

An additional proof that supports the hypothesis of the surface instability of these compounds is obtained from the gas adsorption study of the sample aging. In this regard, CO₂ measurements were carried out periodically during a month on samples of SMOF-1 stored at room conditions (Figure 6a). It

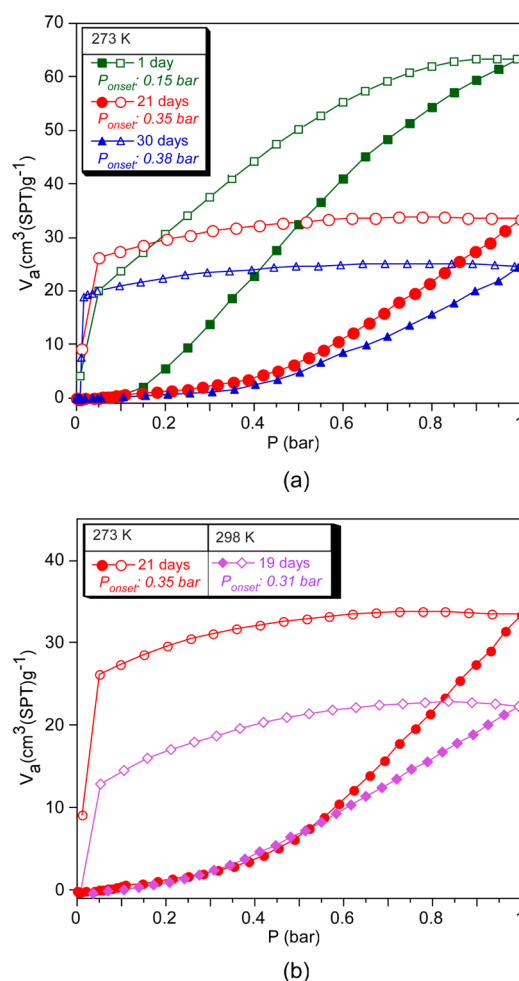


Figure 6. (a) CO₂ adsorption/desorption isotherms measured at 273 K showing the aging of SMOF-1. (b) CO₂ isotherms at 273 and 298 K. The onset pressure value is indicated for each case.

becomes clear that the CO₂ uptake capacity decreases progressively as the sample becomes older, and after a month the uptake at P = 1 bar is depleted in a ca. 60% when compared to its initial value ($V_{\text{STP}} = 63.3$ and $24.4 \text{ cm}^3 \text{ g}^{-1}$ for the initial and one month aged sample). A second phenomenon related with the sample aging is the adsorption onset pressure calculated from the intersection between the tangents at the low pressure region and at the region of maximum slope of the adsorption branch (see Supporting Information). The adsorption of the initial sample shows a plateau with a negligible CO₂ uptake at pressures below 0.1 bar, and it requires a minimum breakthrough pressure ($P_{\text{onset}} = 0.15$ bar) to permeate the surface and reach the porous network. Moreover, the breakthrough pressure is shift to higher values as the sample gets older, to reach an onset value of $P_{\text{onset}} = 0.38$ bar for the sample aged during 1 month. This progressive increase of the breakthrough pressure is related with increase of the thickness of the collapsed surface which acts as a surface permeation barrier. Another feature that supports the presence of a surface barrier that hinders the diffusion of the molecules is related to the hysteresis cycle enclosed by desorption branch and its trend with the aging of the sample (Figure 6a). It is noteworthy that even though different equilibration times were used the hysteresis cycle was not affected, and as consequence, this hysteresis seems to be induced by structural features of the

sample. In fact, the hysteresis becomes more acute as the sample is aged, and its end-pressure is delayed also progressively (P_{end} : 0.05 and 0.02 bar for fresh and one month aged samples, respectively). This behavior is also congruent with an increasing thickness of the collapsed surface (or diffusion barrier) as the storage time goes on, which would also obstruct the release of the adsorbed molecules during the desorption process.

On the other hand, comparison between adsorption experiments carried out at 273 and 298 K samples similarly aged (Figure 6b) shows that the onset pressure (0.35 and 0.31 bar, respectively) is reduced with the increase of the experiment temperature, as the potential energy of the molecules to permeate the surface is increased.

In order to analyze the bulk crystal stability during CO₂ adsorption PXRD patterns were collected in a sample subjected to a CO₂ atmosphere with pressure ranging between 0.5 and 6 bar. Prior to the experiment the sample was outgassed at 150 °C during several hours. As it can be observed (Figure 7)

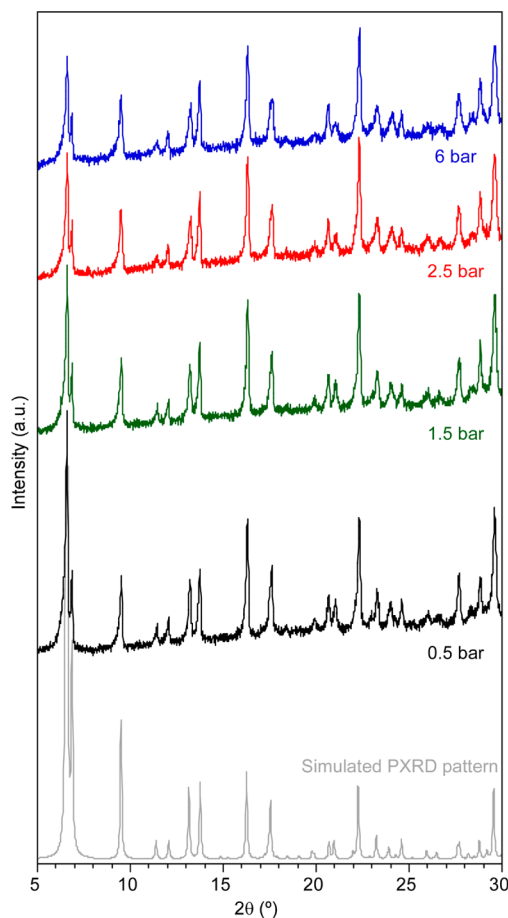


Figure 7. Comparison between experimental PXRD patterns collected at different CO₂ pressures and simulated PXRD pattern for the pristine crystal structure of SMOF-1.

all the experimental reflections match the ones corresponding to the simulated patterns of SMOF-2, and in any case no shift in 2θ positions is observed which stands for stability of the bulk crystallinity and for the bulk framework rigidity during the CO₂ adsorption process (i.e., reversible structural changes caused by CO₂ uptake can be disregarded, as for example, the so-called breathing effect).²³

Regarding to the peak intensity, even though most of the peaks show no changes, the intensity of certain reflections is significantly affected. Figure 8a shows the trend of three

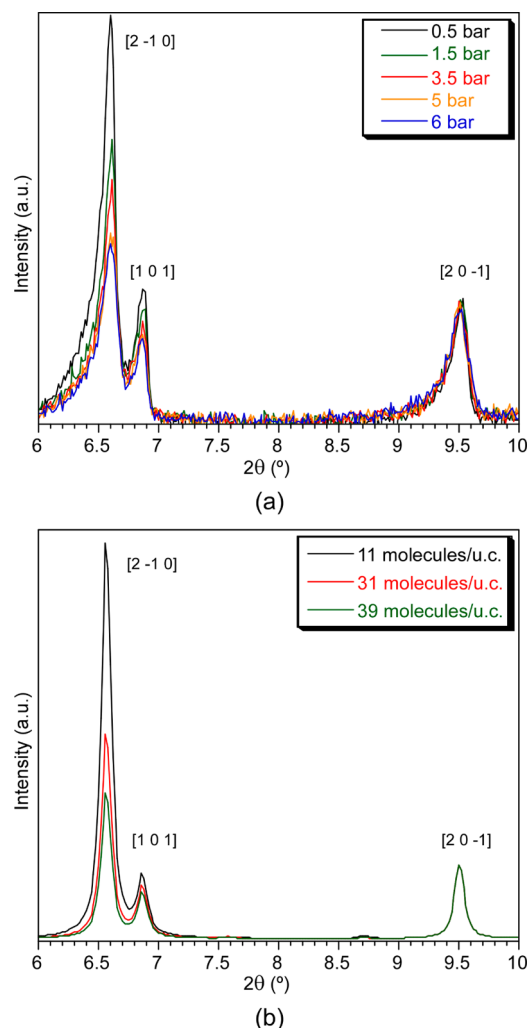


Figure 8. PXRD data for SMOF-1 within 6–10°: (a) experimental patterns with increasing CO₂ pressure. (b) Simulated PXRD patterns from GCMC low energy configurations with increasing CO₂ uptake per unit cell.

reflections within the 6–10° 2θ range. As it can be observed $[2\ 0\ \bar{1}]$ reflection remains unvarying, while the intensity of $[2\ \bar{1}\ 0]$ and $[1\ 0\ 1]$ decays continuously with the increasing CO₂ pressure, which seems to be related to the CO₂ uptake within the structural pores. In order to confirm the latter proposal Grand Canonical Monte Carlo (GCMC) calculations were carried out in which the porous framework of SMOF-1 was loaded with different amounts of CO₂ (see Supporting Information). Low energy configurations of the adsorbed molecules were used to model how the PXRD patterns are affected by the CO₂ (Figure 8b). The trend derived from the GCMC simulations matches the observed for experimental PXRD patterns, which allows us to state that intensity decay of the cited reflections ($[2\ \bar{1}\ 0]$ and $[1\ 0\ 1]$) is due the CO₂ presence within the 1D pores. When coordinates of CO₂ molecules are considered, no symmetry relation is found in any of the GCMC calculations. However, there is a periodicity of the preferential sites of adsorption (most sites derived from

probability density distribution for the center of mass of CO₂ molecule) in which electron density coming from adsorbed gas is accumulated (see Figure S5 in the Supporting Information). As a consequence, the decay of the mentioned reflections can be attributed to this periodically distributed averaged electron density of the adsorbed molecules.

Gas Adsorption Experiments of [Cu₂(μ-adenine)₂(μ-Cl)₂(Cl)₂·2MeOH (3, SMOF-3). In order to assess the stability of the unsolvated SMOF-3 thermogravimetric and variable temperature PXRD experiments were carried out (see Supporting Information). Thermogravimetric analysis (TGA) shows that the solvent molecules are released easily at temperatures below 100 °C. Afterward the TGA curve shows a stability plateau that extends up to 245 °C. At higher temperatures the compound decomposes in successive steps to yield CuO as the final residue at temperatures above 475 °C. The thermodiffractometric measurements show a significant difference between the diffractogram performed at 30 °C and those performed between 90 and 180 °C (Figure 4c). The cell parameters indexed for the PXRD pattern collected at 30 °C match the ones corresponding to the single crystal structure. However, the PXRD pattern change observed at temperatures above 60 °C lead to new unit cell parameters closely related to the previous ones but with a significant change in the unit cell transforming it to a nonstandard monoclinic setting with $\gamma \neq 90^\circ$, but maintaining the cell volume nearly constant. This transformation is related to a rearrangement of the synthon established between the Hoogsteen face and the chloride anion once the methanol molecule is released. All this indicates that although the supramolecular structure presents a moderate change its overall supramolecular crystal structure remains essentially stable up to 180 °C.

In order to assess the permanent porosity inferred from thermodiffractometric measurement we proceeded to measure gas adsorption isotherms on freshly synthesized sample of SMOF-3 which was activated under a vacuum at 140 °C during 12 h to eliminate solvent guest molecules. The results and conclusions derived from the study of the gas adsorption behavior of SMOF-1 and SMOF-2 suggest that the surface weakness of this kind of supramolecular compounds can make routine nitrogen adsorption isotherms not suitable for the study their porous features. In fact, SMOF-3 presents a computed surface area of 361 m² g⁻¹, but the experimental N₂ adsorption isotherm corresponds to a nonporous material. SMOF-3 adsorbs a significant amount of CO₂ as depicted by Figure 9, but comparatively smaller than SMOF-1 and SMOF-2, due to the greater free volume and surface area of the latter ones. Similarly to the precedent supramolecular microporous compounds, SMOF-3 presents a breakthrough pressure close to $P = 0.31$ bar.

CONCLUSIONS

It becomes clear how a combination of rigid tectons with rigid synthons spreading at least in three noncoplanar directions is a well-suited route to obtain porous supramolecular networks. In this context, the metal-nucleobase complexes can be good candidates to fulfill both requirements when the nucleobase is anchored to the discrete entity by at least two positions. This anchorage and the aromatic nature of the nucleobase provide rigid supramolecular building units. On the other hand, the well-known complementary hydrogen bonding established between the nucleobases ensures the necessary rigidity of these synthons. Therefore, as it has been probed here the

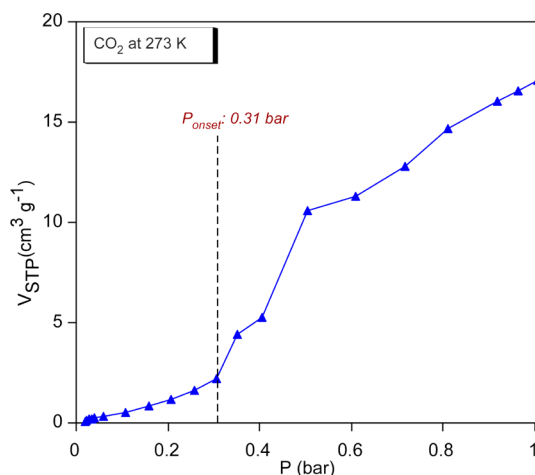


Figure 9. CO₂ adsorption isotherm SMOF-3 at 273 K.

chances to obtain 3D supramolecular metal–organic frameworks based on metal-nucleobase systems are high. However, it is necessary to take care of the synthetic conditions in order to ensure the presence of the required direct hydrogen bonding interactions between the nucleobases. Related to this latter issue, the presence of water molecules can disrupt these direct adenine...adenine hydrogen bonding interactions, leading to nonporous materials as evidenced by the crystal structure of [Cu₂(μ-adenine)₄Cl₂]Cl₂·8H₂O.²⁴ The direct hydrogen bonding disrupting capacity of the water molecule seems also to be responsible of the surface instability observed in SMOF-1, -2 and -3.

ASSOCIATED CONTENT

Supporting Information

Hydrogen bonding interaction tables, thermogravimetric measurements, thermodiffractometric analysis, onset pressure calculation on SMOFs, details on GCMC calculations, and cif files. This material is available free of charge via the Internet at <http://pubs.acs.org>.

AUTHOR INFORMATION

Corresponding Authors

*(G.B.) E-mail: garikoitz.beobide@ehu.es. Fax: (internat) +34-94601-3500.

*(O.C.) E-mail: oscar.castillo@ehu.es.

Author Contributions

[#]These authors (J.T.-G. and G.B.) contributed equally.

Notes

The authors declare no competing financial interest.

ACKNOWLEDGMENTS

Financial support from the Gobierno Vasco (IT477-10, SAIOTEK S-PE12UN004, SAIOTEK S-PE13UN016) and the Universidad del País Vasco/Euskal Herriko Unibertsitatea (UFI 11/53, postdoctoral fellowship) is gratefully acknowledged. Technical and human support provided by SGIker (UPV/EHU, MINECO, GV/EJ, ERDF and ESF) and by Mrs. Sandra Maracke from the University of Hamburg is also acknowledged.

REFERENCES

- (1) (a) Lippert, B. *Coord. Chem. Rev.* **2000**, 200–202, 487. (b) Lippert, B. In *Progress in Inorganic Chemistry*; Karlin, K. D., Ed.;

- Wiley: New York, 2005; Vol. 54, Chapter 6. (c) Sanz Miguel, P. J.; Amo-Ochoa, P.; Castillo, O.; Houlton, A.; Zamora, F. In *Metal Complex-DNA Interactions*; Hadjiliadis, N., Sletten, E., Eds.; Blackwell-Wiley: New York, 2009, Chapter 4. (d) Castillo, O.; Luque, A.; García-Terán, J. P.; Amo-Ochoa, P. In *Macromolecules Containing Metal and Metal-Like Elements*; Abd-El-Aziz, A. S., Carraher, Ch.E., Pittman, Ch.U., Zeldin, M., Eds.; Wiley, New York, 2009; Vol. 9, Chapter 9. (e) Lippert, B. In *Nucleic Acid-Metal Ion Interactions*; Hud, N. V., Ed.; RSC Publishing, Cambridge, 2009; Chapter 2. (f) Verma, S.; Mishra, A. K.; Kumar, J. *Acc. Chem. Res.* **2010**, *43*, 79. (g) Beobide, G.; Castillo, O.; Cepeda, J.; Luque, A.; Pérez-Yáñez, S.; Román, P.; Thomas-Gipson, J. *Coord. Chem. Rev.* **2013**, *257*, 2716.
- (2) (a) En-Cui, Y.; Hong-Kun, Z.; Yan, F.; Xio-Jun, Z. *Inorg. Chem.* **2009**, *48*, 3511. (b) García-Terán, J. P.; Castillo, O.; Luque, A.; García-Couceiro, U.; Román, P.; Lloret, F. *Inorg. Chem.* **2004**, *43*, 5761.
- (3) (a) Choquesillo-Lazarte, D.; Brandi-Blanco, M. P.; García-Santos, I.; González-Pérez, J. M.; Castiñeiras, A.; Niclos-Gutiérrez, J. *Coord. Chem. Rev.* **2008**, *252*, 1241. (b) García-Terán, J. P.; Castillo, O.; Luque, A.; García-Couceiro, U.; Beobide, G.; Román, P. *Dalton Trans.* **2006**, 902.
- (4) (a) Cepeda, J.; Castillo, O.; García-Terán, J. P.; Luque, A.; Pérez-Yáñez, S.; Roman, P. *Eur. J. Inorg. Chem.* **2009**, 2344. (b) Suggs, J. W.; Dube, M. J.; Nichols, M. J. *Chem. Soc., Chem. Commun.* **1993**, 307. (c) Wei, C. H.; Jacobson, K. B. *Inorg. Chem.* **1981**, *20*, 356. (d) Gagnon, C.; Hubert, J.; Rivest, R.; Beauchamp, A. L. *Inorg. Chem.* **1977**, *16*, 2469.
- (5) (a) Terzis, A.; Beauchamp, A. L.; Rivest, R. *Inorg. Chem.* **1973**, *12*, 1166. (b) de Meester, P.; Skapski, A. C. *J. Chem. Soc. A* **1971**, 2167. (c) Mastropietro, T. F.; Armentano, D.; Marino, N.; De Munno, G. *Polyhedron* **2007**, *26*, 4945. (d) González-Pérez, J. M.; Alarcón-Payer, C.; Castiñeiras, A.; Pivetta, T.; Lezama, L.; Choquesillo-Lazarte, D.; Crisponi, G.; Niclós-Gutiérrez, J. *Inorg. Chem.* **2006**, *45*, 877. (e) Sletten, E. *Acta Crystallogr., Sect. B* **1969**, *25*, 1480. (f) Pérez-Yáñez, S.; Beobide, G.; Castillo, O.; Cepeda, J.; Luque, A.; Román, P. *Cryst. Growth Des.* **2012**, *12*, 3324.
- (6) Amo-Ochoa, P.; Sanz-Miguel, P. J.; Castillo, O.; Sabat, M.; Lippert, B.; Zamora, F. *J. Biol. Inorg. Chem.* **2007**, *12*, 543.
- (7) (a) Eddaoudi, M.; Moler, D. B.; Li, H. L.; Chen, B. L.; Reineke, T. M.; ÓKeeffe, M.; Yaghi, O. M. *Acc. Chem. Res.* **2001**, *34*, 319. (b) Yaghi, O. M.; ÓKeeffe, M.; Ockwig, N. W.; Chae, H. K.; Eddaoudi, M.; Kim, J. *Nature* **2003**, *423*, 705. (c) Kitagawa, S.; Kitaura, R.; Noro, S. *Angew. Chem., Int. Ed.* **2004**, *43*, 2334. (d) Perry, J. J.; Perman, J. A.; Zaworotko, M. J. *Chem. Soc. Rev.* **2009**, *38*, 1400.
- (8) (a) Desiraju, G. R. In *Crystal Engineering: The Design of Organic Solids*; Elsevier: New York, 1989. (b) Etter, M. C. *Acc. Chem. Res.* **1990**, *23*, 120. (c) Etter, M. C. *J. Phys. Chem.* **1991**, *95*, 4601.
- (9) Reger, D. L.; Debreczeni, A.; Smith, M. D.; Jezierska, J.; Ozarowski, A. *Inorg. Chem.* **2012**, *51*, 1068.
- (10) Nugent, P. S.; Rhodus, V. L.; Pham, T.; Forrest, K.; Wojtas, L.; Space, B.; Zaworotko, M. J. *J. Am. Chem. Soc.* **2013**, *135*, 10950.
- (11) Thomas-Gipson, J.; Beobide, G.; Castillo, O.; Cepeda, J.; Luque, A.; Pérez-Yáñez, S.; Aguayo, A. T.; Román, P. *CrystEngComm* **2011**, *13*, 3301.
- (12) *CrysAlisPro*, version 1.171.35.15; Agilent Technologies, Yarnton, UK, 2011.
- (13) Altomare, A.; Cascarano, M.; Giacovazzo, C.; Guagliardi, A. J. *Appl. Crystallogr.* **1993**, *26*, 343.
- (14) Sheldrick, G. M. *SHELXL-97, Program for X-ray Crystal Structure Refinement*; University of Göttingen: Göttingen, Germany, 1997.
- (15) Farrugia, L. J. *J. Appl. Crystallogr.* **1999**, *32*, 837.
- (16) Van der Sluis, P.; Spek, A. L. *Acta Crystallogr.* **1990**, *A46*, 194.
- (17) Spek, A. L. *Acta Crystallogr.* **1990**, *A46*, C34.
- (18) (a) Pandey, M. D.; Mishra, A. K.; Chandrasekhar, V.; Verma, S. *Inorg. Chem.* **2010**, *49*, 2020. (b) Mishra, A. K.; Purohit, C. S.; Kumar, J.; Verma, S. *Inorg. Chim. Acta* **2009**, *362*, 855. (c) Beck, W. M.; Calabrese, J. C.; Kottmair, N. D. *Inorg. Chem.* **1979**, *18*, 176. (d) Sánchez-Moreno, M. J.; Choquesillo-Lazarte, D.; González-Pérez, J. M.; Carballo, R.; Castiñeiras, A.; Niclós-Gutiérrez, J. *Inorg. Chem. Commun.* **2002**, *5*, 800. (e) Pérez-Yáñez, S.; Castillo, O.; Cepeda, J.; García-Terán, J. P.; Luque, A.; Román, P. *Inorg. Chim. Acta* **2011**, *365*, 211. (f) An, J.; Fiorella, R. P.; Geib, S. J.; Rosi, N. L. *J. Am. Chem. Soc.* **2009**, *131*, 8401.
- (19) Blatov, V. A.; TOPOS Main Page; **2006**, 7, 4.
- (20) Spek, A. L. *J. Appl. Crystallogr.* **2003**, *36*, 7.
- (21) Feldblyum, J. L.; Liu, M.; Gidley, D. W.; Matzger, A. J. *J. Am. Chem. Soc.* **2011**, *133*, 18257.
- (22) NIST Computational Chemistry Comparison and Benchmark Database NIST Standard Reference Database Number 101, Release 16a, , Johnson, R. D., III, Ed.; National Institute of Standards and Technology: Gaithersburg, MD , August 2013; <http://cccbdb.nist.gov/>.
- (23) (a) Ramsahye, N. A.; Maurin, G.; Bourrelly, S.; Llewellyn, P. L.; Loiseau, T.; Serre, C.; Férey, G. *Chem. Commun.* **2007**, 3261. (b) Serre, C.; Bourrelly, S.; Vimont, A.; Ramsahye, N. A.; Maurin, G.; Llewellyn, P. L.; Daturi, M.; Filinchuk, Y.; Leynaud, O.; Barnes, P.; Férey, G. *Adv. Mater.* **2007**, *19*, 2246.
- (24) de Meester, P.; Skapski, A. C. *J. Chem. Soc. A* **1971**, 2162.

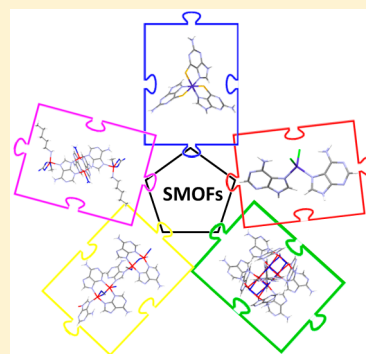
Unravelling the Growth of Supramolecular Metal–Organic Frameworks Based on Metal–Nucleobase Entities

Jintha Thomas-Gipson,[‡] Rubén Pérez-Aguirre,[‡] Garikoitz Beobide, Oscar Castillo,* Antonio Luque, Sonia Pérez-Yáñez,* and Pascual Román

Departamento de Química Inorgánica, Facultad de Ciencia y Tecnología, Universidad del País Vasco (UPV/EHU), Apartado 644, E-48080 Bilbao, Spain

Supporting Information

ABSTRACT: The present work provides the basis to obtain three-dimensional (3D) extended porous supramolecular assemblies named supramolecular metal–organic frameworks (SMOFs). This goal can be achieved by considering three key factors: (i) the use of rigid building units, (ii) the establishment of predictable and rigid synthons between the building units, and (iii) the non-coplanarity of functional groups involved in the predictable synthons. Throughout this report we demonstrate the suitability of this synthetic strategy supported by six new SMOFs based on metal–nucleobase entities which fulfill the stated requirements: [Co(ThioG)₃] (SMOF-4; ThioG = thioguaninato), [Co(Hade)₂X₂] (SMOF-5, SMOF-6; Hade = adenine and X = Cl[−], Br[−]), [Cu₈(μ₃-OH)₄(μ₄-OH)₄(ade)₄(μ-ade)₄(μ-Hade)₂] (SMOF-7; ade = adeninato), [Cu₄(μ₃-ade)₄(μ-ade)₂(pentylNH₂)₂(CH₃OH)₂(CO₃)₂(H₂O)₂] (SMOF-8; pentylNH₂ = 1-pentylamine), and [Cu₂(μ-ade)₂(ade)(μ-OH)(H₂O)(CH₃OH)]_n (SMOF-9). SMOF-4 is built up from monomeric entities in which bidentate thioguaninato ligands establish complementary hydrogen bonding interactions in non-coplanar directions leading to supramolecular layers that are further connected resulting in a porous structure with one-dimensional (1D) channels. The hydrogen bonding interactions among Watson–Crick and sugar edges of monomeric entities in SMOF-5 give rise to a triply interpenetrated supramolecular framework. Octameric clusters in SMOF-7 are self-assembled by hydrogen bonding to yield a porous 3D network. SMOF-8 is built up from tetranuclear units that are linked via base pairing interactions involving Watson–Crick faces to afford layers whose assembly generates a two-dimensional pore system. SMOF-9 is in between pure MOFs and SMOFs since it consists of 1D infinite coordination polymers held together by complementary hydrogen bonding interactions into a 3D supramolecular porous structure.



INTRODUCTION

Metal–organic frameworks (MOFs) encompass an area of chemistry that has experienced impressive growth during the last decades because of their various potential applications in catalysis, gas storage, chemical separations, sensing, ion exchange, drug delivery, and optics.¹ Regarding the adsorption field, it is worth mentioning that their large surface areas, adjustable pore sizes, and controllable functionalities are key factors that make MOFs promising candidates for adsorptive separations and purification purposes.^{2,3} Taking into account the great potential of MOFs, we decided to explore a related type of material, in which the coordination bonds are replaced with hydrogen bonds as connectors, which are also directional and predictable interactions, to sustain the three-dimensional (3D) crystal building containing potentially accessible voids (Figure 1).^{4,5} Although such kinds of alternative materials can arise a similar fascination to that of MOFs, the crystal engineering principles and the synthetic approach are not yet settled, and examples of this kind of material are rather scarce. In this sense a first clue to reach this goal can be inferred using the naive analogy of soft and rigid balls. Soft balls can adjust their shape to provide an efficient packing leaving almost no space in between. However, rigid balls do not have the option

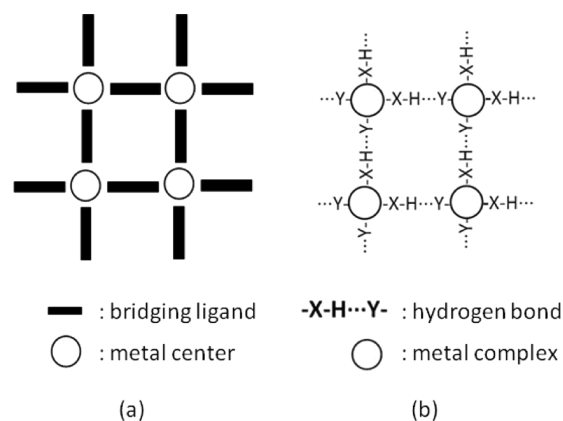


Figure 1. Similarity between (a) coordination bonds and (b) hydrogen bonding interactions as structure directing agents.

Received: December 10, 2014

Revised: January 7, 2015

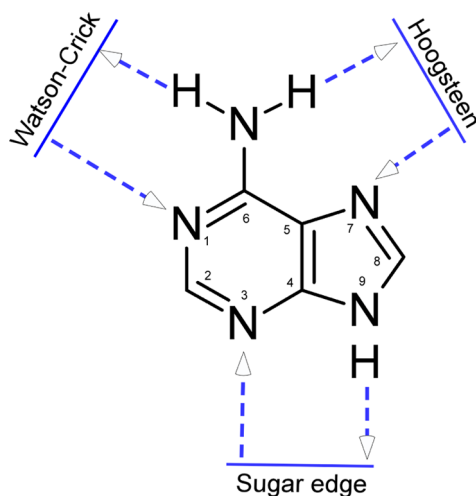
Published: January 12, 2015

of changing their shape, and, as a consequence, their packing is less effective giving rise to the presence of voids. In other words, flexible objects pack effectively, while rigid objects do not unless they present very specific and appropriate shape, such as cubes, triangular, rectangular and hexagonal prisms, etc.⁶ This simple idea has helped us develop a synthetic strategy to obtain supramolecular metal–organic frameworks (SMOFs)^{7,8} with potentially accessible voids as an alternative to more conventional metal–organic frameworks (MOFs).

The synthetic strategy is based on the following key factors: (i) the use of rigid building units, (ii) the establishment of predictable and rigid synthons between the building units, and (iii) the noncoplanarity of functional groups involved in the predictable synthons. The rigidity of the building units (discrete complexes) can be achieved using rigid ligands bonded through multiple positions. It means, in most common cases, a double anchoring of the ligand by means of two simultaneous coordination bonds or the combination of a coordination bond and an intramolecular hydrogen bond. The predictability and rigidity of the synthons require the presence of adjacent functional groups, incorporated into the rigid ligands, able to establish complementary hydrogen bonding interactions. Finally, the requisite of noncoplanar arrangement of the synthons comes from our objective of obtaining 3D extended systems that is achieved by the presence of at least three noncoplanar synthons. The use of nonplanar coordination geometries for the complexes makes this last condition easy to accomplish.

From previous studies we realized that a suitable system that would fulfill all of the above-described requirements for obtaining SMOFs are the discrete metal–nucleobase systems, especially those based on purine nucleobases.^{9–11} These ligands provide, on the one hand, the advantage of increased rigidity of the supramolecular building block due to the coordination through multiple positions, and, on the other hand, they present many edges capable of establishing complementary hydrogen bonding interactions that provide rigid and predictable synthons (Scheme 1). Therefore, the adequate selection of the metal–nucleobase discrete entity that would afford a non-coplanar arrangement of the nucleobases could provide the desired supramolecular porous materials.

Scheme 1. Adenine Edges Capable of Establishing Rigid Complementary Double Hydrogen Bonding Synthons



The preliminary results were achieved employing $[\text{Cu}_2(\mu\text{-adenine})_4(\text{X})_2]^{2+}$ (SMOF-1 and SMOF-2; $\text{X} = \text{Cl}^-$, Br^-) as supramolecular building blocks in which two or more nucleobases are tightly anchored to the metal centers by two donor positions (N3 and N9 sites), imposing a rigid building unit.^{7,12} Moreover, this coordination motif imposes a rigid geometrical restraint among the nucleobases providing a set of noncoplanar synthons that otherwise would be very difficult to achieve. As many hydrogen donor/acceptor positions of the nucleobase remain free, these discrete entities are able to self-assemble among them by means of double hydrogen bonds to provide extended supramolecular solids in which great channels are present. These compounds present a surface instability that creates a diffusion barrier permeated only by strong interacting adsorbate molecules such as CO_2 but not N_2 , H_2 , and CH_4 , which makes them attractive for selective gas adsorption and separation technologies. Zaworotko et al. reported an analogous compound, based on the $[\text{Cu}_2(\mu\text{-adenine})_4(\text{X})_2]^{2+}$ dinuclear entity, replacing the halides by bulkier TiF_6^{2-} anions improving the chemical stability of the supramolecular network toward humidity, thus avoiding the surface instability, and therefore, being able to adsorb CO_2 , CH_4 , and N_2 .¹³ These studies also pointed out the relevance of the solvent selection because strong hydrogen bond donor and acceptor solvents such as water molecules could disrupt the direct hydrogen bonding interactions between the nucleobases that are the key factors to achieve this type of compound.

In this report we demonstrate the suitability of this synthetic strategy to afford the self-assembly of rigid mono- or polynuclear entities by means of a set of non-coplanar synthons into supramolecular porous materials.

■ EXPERIMENTAL SECTION

Synthesis of SMOF-4, $[\text{Co}(\text{ThioG})_3]$. 0.59 mL (0.4 mmol) of pentylamine was added dropwise to 0.0685 g (0.4 mmol) of 6-thioguanine dissolved in 20 mL of water, and the mixture was stirred in an ice bath for 1 h. To this mixture was added a 10 mL solution of 0.0291 g (0.1 mmol) of $\text{Co}(\text{NO}_3)_2 \cdot 6\text{H}_2\text{O}$ dissolved in water. The brown-colored solution was then stirred for 2 h in an ice bath and then left for evaporation. Brown-colored single-crystals were separated after 2 weeks. The compound was also obtained on replacing $\text{Co}(\text{NO}_3)_2 \cdot 6\text{H}_2\text{O}$ with $\text{CoSO}_4 \cdot 7\text{H}_2\text{O}$. Yield: 60%. Anal. Calcd (found) for $\text{C}_{15}\text{H}_{12}\text{CoN}_5\text{S}_3 \cdot 6.7\text{H}_2\text{O}$: C, 26.56 (26.68); H, 3.78 (3.70); N, 30.98 (31.29); S, 14.18 (14.21); Co, 8.69 (8.75). Main IR features (cm^{-1} ; KBr pellets): 3422s, 1611m, 1498w, 1459w, 1385m, 1306sh, 1243vs, 1190m, 1146s, 983s, 933w, 893w, 836w, 803w, 743w, 716w, 680w, 630w, 523w.

Synthesis of SMOF-5, $[\text{Co}(\text{Hade})_2\text{Cl}_2]$. This compound was obtained as deep blue polycrystalline form by the dropwise addition of a propanolic solution of adenine (0.0270 g, 0.2 mmol) into a stirring solution of 0.0238 g of $\text{CoCl}_2 \cdot 6\text{H}_2\text{O}$ (0.1 mmol). When the synthesis was performed in methanol bad quality crystals were obtained. Then, single crystals of good quality were obtained by using diffusion techniques. Yield: precipitate 70%, crystals 50%. Anal. Calcd (found) for $\text{C}_{10}\text{H}_{10}\text{Cl}_2\text{CoN}_{10}$: C, 30.02 (30.09); H, 2.52 (2.47); N, 35.01 (34.93); Co, 14.73 (14.82)%. Main IR features (cm^{-1} ; KBr pellets): 3391vs, 3258vs, 3133vs, 3058vs, 2346w, 2280w, 2186w, 2016w, 1943w, 1790w, 1696vs, 1611s, 1498m, 1459w, 1397s, 1327m, 1237m, 1171m, 1105w, 1066w, 1016w, 942m, 895m, 856w, 778m, 712m, 631w, 610m, 530m.

Synthesis of SMOF-6, $[\text{Co}(\text{Hade})_2\text{Br}_2]$. The synthesis is the same as for SMOF-5 but replacing $\text{CoCl}_2 \cdot 6\text{H}_2\text{O}$ by CoBr_2 . Yield: precipitate 60%. All the attempts to grow single-crystals were unsuccessful. Anal. Calcd (found) for $\text{C}_{10}\text{H}_{10}\text{Br}_2\text{CoN}_{10}$: C, 24.56 (24.49); H, 2.06 (2.15); N, 28.64 (28.57); Co, 12.05 (12.01)%. Main IR features (cm^{-1} ; KBr pellets): 3450s, 3341vs, 3066s, 2817w, 2671w, 2284w, 1951w, 1663vs,

Table 1. Crystallographic Data and Structure Refinement Details^a

	SMOF-4	SMOF-5	SMOF-7	SMOF-8	SMOF-9
formula	C ₁₅ H ₁₂ CoN ₁₅ S ₃	C ₁₀ H ₁₀ Cl ₂ CoN ₁₀	C ₅₀ H ₅₀ Cu ₈ N ₅₀ O ₈	C _{30.85} H _{46.80} Cu _{3.55} N _{21.55} O _{8.20}	C ₁₆ H ₁₉ Cu ₂ N ₁₅ O ₃
MW (g mol ⁻¹)	557.51	400.11	1987.72	1076.37	596.54
crystal system	trigonal	monoclinic	monoclinic	triclinic	monoclinic
space group	P $\bar{3}$	C2/c	Ccca	P $\bar{1}$	C2/c
a (Å)	16.7297(14)	11.2442(18)	20.1899(5)	12.646(5)	23.472(7)
b (Å)	16.7297(14)	6.9401(7)	28.964(2)	13.136(5)	16.398(3)
c (Å)	6.5245(4)	18.760(2)	16.5403(5)	13.158(5)	18.803(5)
α (deg)	90	90	90	73.784(5)	90
β (deg)	90	95.000(13)	90	81.840(5)	112.30(3)
γ (deg)	120	90	90	62.368(5)	90
V (Å ³)	1581.4(2)	1458.4(3)	9672.6(8)	1859.2(12)	6696(3)
Z	2	4	4	1	8
ρ_{calcd} (g cm ⁻³)	1.171	1.822	1.365	0.961	1.184
μ (mm ⁻¹)	0.769	12.758	1.790	1.047	1.899
reflections collected	4690	5201	33482	6909	5529
unique data/parameters	2300/103	1462/109	5277/272	6909/269	5529/325
R _{int}	0.1278	0.0656	0.0630	0.1840	0.0972
goodness of fit (S) ^b	1.033	1.045	1.092	0.773	0.741
R ₁ ^c /wR ₂ ^d [all data]	0.0924/0.1673	0.0664/0.1606	0.0872/0.2221	0.2330/0.2882	0.1519/0.2091
R ₁ ^c /wR ₂ ^d [I > 2 σ (I)]	0.0646/0.1585	0.0606/0.1560	0.0721/0.2115	0.1044/0.2691	0.0800/0.1840

^aReported data do not include the variable amount of solvent molecules present in the channels. ^bS = $[\sum w(F_0^2 - F_c^2)^2 / (N_{\text{obs}} - N_{\text{param}})]^{1/2}$. ^cR₁ = $\sum \|F_0 - |F_c|\| / \sum |F_0|$. ^dwR₂ = $[\sum w(F_0^2 - F_c^2)^2 / \sum wF_0^2]^{1/2}$; w = 1/[$\sigma^2(F_0^2) + (aP)^2 + bP$] where P = (max(F₀², 0) + 2F_c²)/3 with a = 0.0691 (1), 0.0897 (2), 0.1440 (3), 0.1283 (4), 0.0584 (5) and b = 4.8645 (2), 1.6779 (3).

1596vs, 1513w, 1480s, 1416s, 1360w, 1343s, 1306s, 1246s, 1170w, 1120w, 1020w, 1063w, 1030w, 973m, 910m, 870w, 791m, 763m, 722s, 680w, 638m, 627m, 557s, 545m, 532s.

Synthesis of **SMOF-7**, [Cu₈(μ_3 -OH)₄(μ_4 -OH)₄(ade)₄(μ -ade)₄(μ -Hade)₂]. Twenty milliliters of an aqueous methanolic solution (1:1) containing adenine (0.8 mmol, 0.108 g) were added to 20 mL of an aqueous solution of CuSO₄·5H₂O (0.4 mmol, 0.0998 g) leading to a solution of pH = 3. Immediately a dark blue precipitate appeared. Then, sulfuric acid was added until complete dissolution of the precipitate (pH = 1.5). A glass vial with the resulting solution was placed in an Erlenmeyer flask containing triethylamine favoring the diffusion of the base into the solution. A few days later a small amount of purple crystals appeared mixed with a major unknown phase.

Synthesis of **SMOF-8**, [Cu₄(μ_3 -ade)₄(μ -ade)₂(pentylNH₂)₂-(CH₃OH)₂(CO₃)₂(H₂O)₂]. Single crystals of this compound were obtained by adding a 10 mL methanolic solution of 0.0198 g of Cu(OOCCH₃)₂·H₂O (0.1 mmol) to a methanolic solution (20 mL) of 0.0206 g of adenine (0.15 mmol) mixed with 0.59 mL of pentylamine. The green-colored solution was stirred for 1 h and left evaporating at room temperature. On evaporating the color of the solution started changing to blue-violet. After 2 weeks, violet-colored prismatic shaped crystals appeared. The crystals are unstable out from the mother liquid.

Synthesis of **SMOF-9**, [Cu₂(μ -ade)₂(ade)(μ -OH)(H₂O)-(CH₃OH)]_n. Single crystals of this compound were obtained by the slow addition of a 10 mL methanolic solution of 0.0199 g of Cu(OOCCH₃)₂·H₂O (0.1 mmol) into a methanolic solution (50 mL) of 0.0546 g of adenine (0.4 mmol) mixed with 0.59 mL of pentylamine. The green-colored solution was stirred for 1 h and left evaporating at room temperature. Few blue needle like crystals that correspond to **SMOF-9** appeared in a time period of 1 week, mixed with violet crystals of **SMOF-8**. Yield: 5%. Anal. Calcd (found) for C₁₆H₁₉Cu₂N₁₅O₃·8.5(CH₃OH): C, 33.87 (33.77); H, 6.15 (6.08); N, 24.18 (24.09); Cu, 14.63 (14.74) %. Main IR features (cm⁻¹; KBr pellets): 3446s, 3356vs, 3123s, 1671s, 1418m, 1398m, 1385m, 1333m, 1308s, 1268m, 1251w, 1191m, 1149m, 1123w, 1022w, 979w, 939m, 910w, 875w, 845w, 797m, 738w, 723s, 641m, 620w, 570w, 541m.

Physical Measurements. Elemental analyses (C, H, N, S) were performed on an Euro EA elemental analyzer, whereas the metal content was determined by inductively coupled plasma atomic emission spectrometer (ICP-AES) from Horiba Yobin Yvon Activa.

The IR spectra (KBr pellets) were recorded on a FTIR 8400S Shimadzu spectrometer in the 4000–400 cm⁻¹ spectral region. Dinitrogen (77 K) and carbon dioxide (273 K) physisorption data were recorded on activated samples (vacuum at 100 °C for 4 h) with a Quantachrome QUADRASORB-SI-MP and a Quantachrome Autosorb-iQ-MP, respectively. The specific surface area was calculated from the adsorption branch in the relative pressure interval from 0.01 to 0.10 using the Brunauer–Emmett–Teller (BET) method.

X-ray Diffraction Data Collection and Structure Determination. Single-crystal X-ray diffraction data were collected on an Oxford Diffraction Xcalibur diffractometer with graphite monochromated Mo K α radiation (λ = 0.71073 Å) at 100(2) K for **SMOF-4** and **SMOF-7**, and at 293 K for **SMOF-8**, and on an Agilent Technologies SuperNova diffractometer with Cu K α radiation (1.54185 Å) for **SMOF-5** and **SMOF-9**. Data reduction was done with the CrysAlisPro program.¹⁴ All the structures were solved by direct methods using the SIR92 program¹⁵ and refined by full-matrix least-squares on F² including all reflections (SHELXL97).¹⁶ All calculations for these structures were performed using the WINGX crystallographic software package.¹⁷ After the initial structure solution was completed, the difference Fourier map for **SMOF-4**, **-7**, **-8**, and **-9** showed the presence of substantial electron density at the voids of the crystal structure that was impossible to model. Therefore, its contribution was subtracted from the reflection data by the SQUEEZE method¹⁸ as implemented in PLATON.¹⁹ During the data reduction process it became clear that the crystal specimen of **SMOF-8** was a non-merohedric twin with a twin law: (1.026 -0.077 0.038/0.070 0.963 0.012/-0.023 -0.000 1.003). The final result showed a percentage of twinned component of 24.3%. Additionally, one of the metal centers (Cu2) and its coordinated ligands present a partial occupation of 0.78. Relevant data acquisition and refinement parameters are gathered in Table 1. CCDC 1038651–1038655 contain the supplementary crystallographic data for this paper.

RESULTS AND DISCUSSION

Structural Description of [Co(ThioG)₃] (SMOF-4). The basic media of the reaction favored the oxidation to Co(III), as ensured by its diamagnetic nature, giving rise to neutral monomeric [Co(ThioG)₃] entities. Three thioguaninato

ligands, in its 9*H*-tautomeric form, are coordinated in a bidentate chelating mode to the Co(III) atoms by their N7 and S6 atoms affording an octahedral coordination environment. Coordination bonds lengths and angles are gathered in the Supporting Information. The coordination mode of the nucleobase analogue renders a rigid metal-complex and, at the same time, exposes its Watson–Crick (N1, N2) and sugar edges (N3, N9) providing a set of non-coplanar synthons with dihedral angles of 87° (Figure 2a). Therefore, this discrete

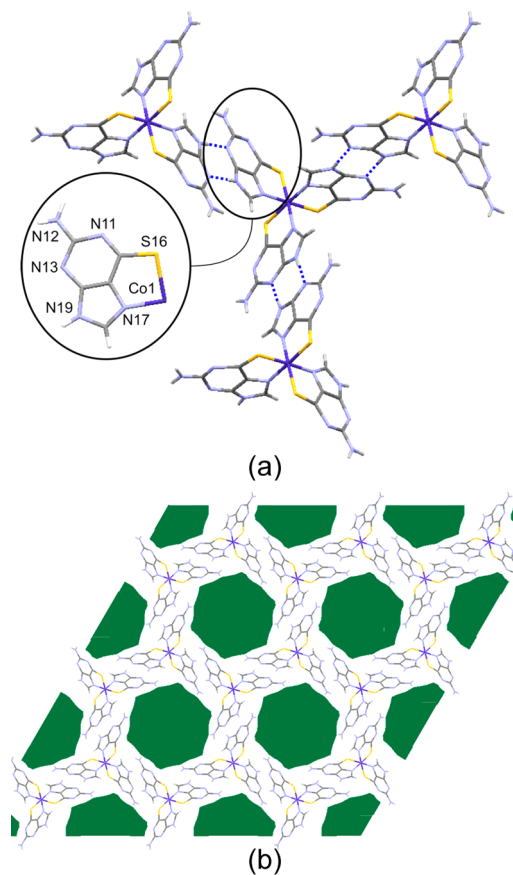


Figure 2. (a) Interactions among the monomeric entities and numbering scheme. (b) Projection of the crystal packing of SMOF-4 along the crystallographic *c* axis. Green-colored regions represent the solvent accessible void.

complex entity fulfils the previously stated requirements for the success in obtaining a supramolecular porous material. In fact, there is a previous work based on similar discrete entities but using 6-thioguanosine that provides a complementary hydrogen bonding interaction involving only the Watson–Crick face (N1, N2) as the sugar edge is blocked by the sugar residue. It affords a supramolecular assembly containing great voids that are occupied by the sugar residue of the thioguanosine.²⁰ In SMOF-4 both sides of the 6-thioguaninato are available to contribute to the supramolecular assembly. The sugar edge (N3, N9) of the nucleobases establishes a double hydrogen bonding interaction with the nucleobases of three neighboring entities to give a $R_2^2(8)$ ring (Table 2). This rigid synthon, based on direct thioguaninato⋯thioguaninato pairing interactions, leads to layers in the *ab* plane in which Δ and Λ isomers of the trischelate complex are sequentially arranged similarly to what happens in layered $[M(\text{ox})_3]^{n-}$ based compounds.^{21,22} The resulting arrangement corresponds to

Table 2. Structural Parameters (\AA , $^\circ$) of Noncovalent Interactions in SMOF-4^a

Hydrogen Bonding Interactions					
D–H⋯A ^b	H⋯A	D⋯A	D–H⋯A		
N19–H19⋯N13 ⁱ	2.03	2.875(5)	167		
N12–H12⋯S16 ⁱⁱ	2.69	3.467(4)	151		
C18–H18⋯S16 ⁱⁱⁱ	2.67	3.415(4)	138		
π – π Interactions ^c					
ring⋯ring ^d	angle	DC	α	DZ	DXY
h⋯h ^{iv}	0.0	3.46	18.5	3.28	1.10

^aSymmetry codes: (i) $-x, -y + 1, -z + 2$; (ii) $x - y, x, -z + 1$; (iii) $-x + y, -x + 1, z + 1$; (iv) $-x, -y + 1, -z + 1$. ^bD: donor; A: acceptor. ^cAngle: dihedral angle between the planes (deg), DC: distance between the centroids of the rings (\AA), α : angle between the normal to the first ring and the DC vector (deg), DZ: interplanar distance (\AA), DXY: lateral displacement (\AA). ^dh: hexagonal ring of the thioguanine.

the Shubnikov hexagonal **hcb** topology with a (6^3) point symbol.^{23–25} The interactions among the three-connected uninodal two-dimensional (2D) nets are linked via weaker hydrogen bonds (N2–H⋯S6 and C8–H⋯S6) and reinforced with π – π interactions, (Table 2) leading to an **acs** topology and $(4^9.6^6)$ point symbol that corresponds to a porous crystal structure with an estimated surface area of 887 m^2/g and 43% of void space based on theoretical calculations.^{26,19} The resulting porous structure consists of one-dimensional (1D) channels that run along the crystallographic *c* axis with a diameter of 8.2–9.4 \AA (Figure 2b). It is worth mentioning the template effect exerted by the pentylamine. This molecule provides the basic media that this reaction requires, and, at the same time, the tendency of the aliphatic tails to form aggregates in water promotes the growth of the supramolecular structure around them. In fact, the same synthesis but using different amines with shorter aliphatic tails does not provide this compound.

According to N_2 (77 K) and CO_2 (273 K) adsorption studies, this compound is highly selective toward CO_2 adsorption (Figure 3). The N_2 adsorption curve exhibits features of a nonporous material, and, accordingly, the fitting of the adsorption area to BET equation leads to a negligible value. However, it shows a significant CO_2 uptake with a non-saturating curve reaching a value of 1.4 mmol/g at 1 bar. This behavior has been described in the introduction section for

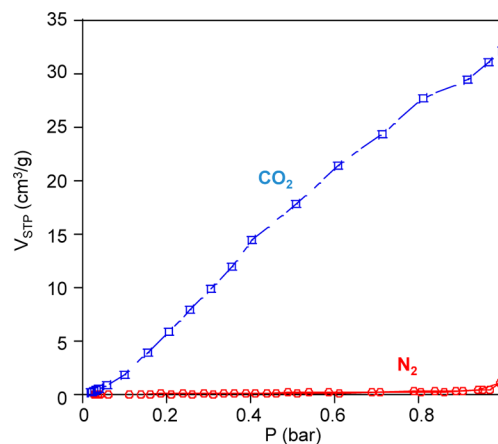


Figure 3. Adsorption isotherms for N_2 (77 K) and CO_2 (273 K), of a fresh sample of SMOF-4.

SMOF-1 and SMOF-2, and its explanation for SMOF-4 probably would also be related to a crystal surface instability.

Structural Description of [Co(Hade)₂Cl₂] (SMOF-5). SMOF-5 contains neutral monomeric [Co(Hade)₂Cl₂] units. 9H-Adenine acts as a monodentate ligand, and it is coordinated to the Co(II) metal center through the N7 position that it is very usual for unsubstituted adenine moieties, but it requires a second anchoring position of the nucleobase to be stiff enough to meet our requirements. Such stiffness is achieved by the presence of intramolecular hydrogen bonding interactions between the amino hydrogen atom and the chloride one. The adenine also exposes its Watson–Crick and sugar-edges to establish intermolecular complementary hydrogen bonding interactions with adjacent adenine molecules (Figure 4a).

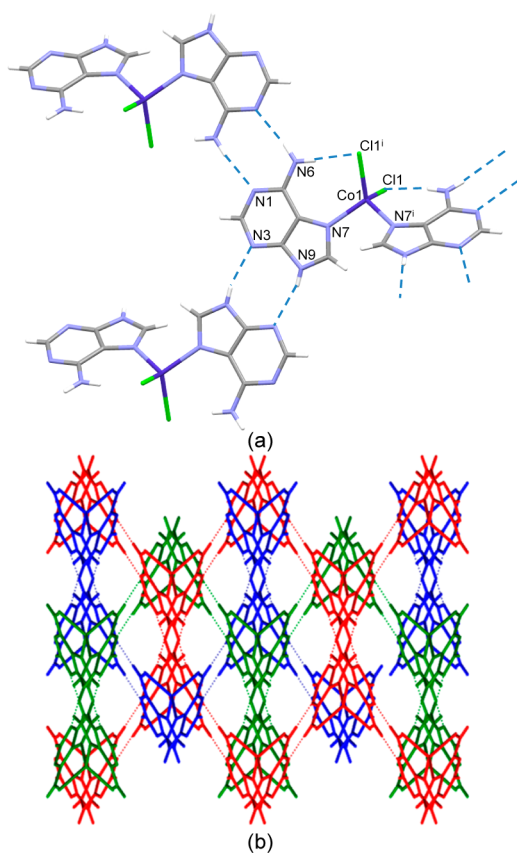


Figure 4. (a) Rigid synthon formed by direct supramolecular interactions in SMOF-5. (b) Triple interpenetrated crystal structure of SMOF-5. Each subnet is represented using a different color.

The rigid synthons involving WC...WC and sugar...sugar edges interactions give rise in both cases to $R_2^2(8)$ hydrogen bonding rings, that are well-known structural synthons between self-assembling adenine fragments.^{27–33} These interactions build up a four-connected uninodal 3D supramolecular net with dia topology and (6^6) point symbol that would represent a new porous material with an estimated internal surface area of 3600 m²/g and 67% of void space.

Nevertheless, it would contain such huge channels that the real crystal structure involves three interpenetrated networks that occupy all the available space providing a nonporous material. This entanglement problem is also common in MOFs.³⁴ Porous materials try to minimize the system energy through optimal filling of void space, but structural inter-

penetration may occur only if the pore space of an individual net is sufficiently large to accommodate an additional net. In addition to this, various weak supramolecular forces such as H-bonding, π - π aromatic stacking interactions, and van der Waals forces are believed to play vital roles in the formation of interpenetrated structures. SMOF-5 follows the same pattern, provided that it contains such a huge percentage of void. Thus, the resulting structure can be described as a 3-fold interpenetrated network as shown in Figure 4b. The attempt to avoid this interpenetration using the more voluminous bromide anion instead of chloride did not succeed, providing the same triple interpenetrated supramolecular structure (SMOF-6, see Supporting Information).

Table 3. Hydrogen Bonding Interactions (Å, °) in SMOF-5^a

D–H...A ^b	H...A	D...A	D–H...A
N6–H6A...N1 ⁱⁱ	2.06	2.912(6)	173
N6–H6B...Cl1 ⁱ	2.39	3.237(4)	167
N9–H9...N3 ⁱⁱⁱ	2.11	2.833(6)	165

^aSymmetry codes: (i) $-x, y, -z + 1/2$; (ii) $-x + 1/2, -y + 1/2, -z + 1$; (iii) $-x, -y - 1, -z + 1$. ^bD: donor; A: acceptor.

Structural Description of [Cu₈(μ_4 -OH)₄(μ_3 -OH)₄(ade)₄(μ -ade)₄(μ -Hade)₂] (SMOF-7). This compound consists of [Cu₈(μ_4 -OH)₄(μ_3 -OH)₄(adeninato- κ N9)₄(μ -adeninato- κ N3: κ N9)₄(μ -adenine- κ N3: κ N9)₂] octameric clusters formed by the stacking of four Cu₂(μ -OH)₂ dimers that are 90° rotated and linked by a semicoordination to the neighboring Cu(II) atoms through the hydroxide bridges (Figure 5a). The resulting aggregate can be described as the stacking of three cubanes (cubes with the vertices alternatively occupied by the metal and the bridging ligand). The surface of each octamer is occupied by eight adeninate and two neutral adenine ligands. Four adeninate and the neutral adenine entities act as bidentate N3,N9-bridging ligands. These bridging ligands are disordered into two coplanar arrangements with inverted orientation regarding the coordination mode (μ - κ N3: κ N9/ μ - κ N9: κ N3).^{35,36} The remaining adeninato ligands are anchored to the corners of the cluster as terminal ligands through N9, and their stiffness is reinforced by intramolecular hydrogen bonds involving the hydroxide bridges and the N3 positions of the nucleobases. All the adenines, adeninates, and hydroxides are rigidly anchored to the octameric entity because of their multiple coordination bond (OH/adenine/adeninato) or the combination of a coordination bond and an intramolecular hydrogen bond (adeninato).

The interaction of each octamer with the adjacent ones is by means of a hydrogen bonding scheme involving the hydroxide anions and the N7 imidazolic atom of terminal adeninato ligands giving rise to a bidimensional network. Moreover, the bridging adeninato ligands direct their Watson–Crick and Hoogsteen faces outward in those supramolecular layers in such a way that they establish complementary hydrogen bonding interactions with neighboring tectons. As in previous compounds the Watson–Crick faces establish a $R_2^2(8)$ hydrogen bonding ring. The combination of the above-described interactions leads to a 3D 8c uninodal supramolecular net with a sqc3 topology, point symbol being $(4^4.6^2)$, where the geometrical requirements imposed by the rigidity of the octameric unit and the hydrogen bonding interactions avoid the full occupancy of the space. This is reflected by the presence of large monodimensional channels of ca. 4.9 Å

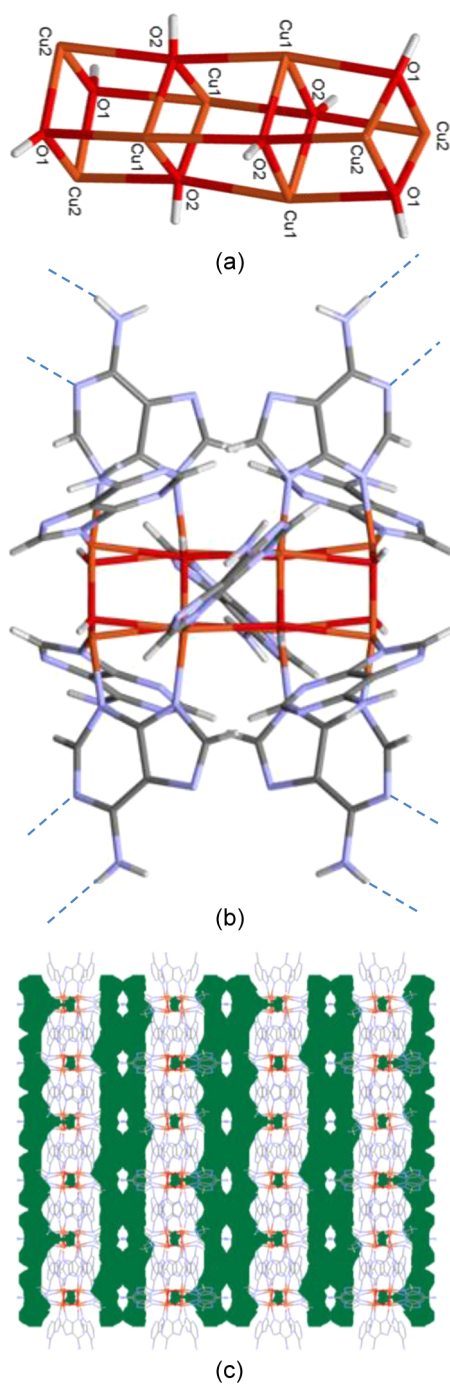


Figure 5. (a) [Cu₈(μ₄-OH)₄(μ₃-OH)₄] unit, (b) whole octameric entity, and (c) three-dimensional packing of SMOF-7.

spreading along the [100] direction, which corresponds to a calculated surface area of 366 m²/g and a 30% of void space.

Structural Description of [Cu₄(μ₃-ade)₄(μ-ade)₂-(pentylNH₂)₂(CH₃OH)₂(CO₃)₂(H₂O)₂]_n(solvent) (SMOF-8). SMOF-8 is built up by tetranuclear [Cu₄(μ₃-ade)₂(μ-ade)₂-(pentylNH₂)₂(CH₃OH)₂(CO₃)₂(H₂O)₂] units in which two types of neutral building units coexist: a dimeric [Cu₂(μ-ade)₄(H₂O)₂] entity and two monomeric [Cu(pentylNH₂)-(CH₃OH)(CO₃)] moieties (Figure 6).

The dimeric fragment is centrosymmetric and is made of two Cu(II) atoms bridged by four μ-N₃,N₉-adeninate anions in a paddle-wheel shaped arrangement. The apical position of the

Table 4. Hydrogen Bonding Interactions (Å, °) in SMOF-7^a

D–H...A ^b	H...A	D...A	D–H...A
N16–H16A...N11A ⁱⁱⁱ	2.51	3.34(3)	161
N36–H36B...N13 ⁱ	2.56	3.317(7)	148
O1–H1...N37 ^{iv}	2.09	2.947(5)	177
O2–H2...N33 ^v	2.18	3.015(6)	167

^aSymmetry codes: (i) $x, -y + 1/2, -z + 1/2$; (iii) $-x + 3/2, y, z - 1/2$; (iv) $-x + 3/2, -y + 1, z$; (v) $-x + 3/2, y, z + 1/2$. ^bD: donor; A: acceptor.

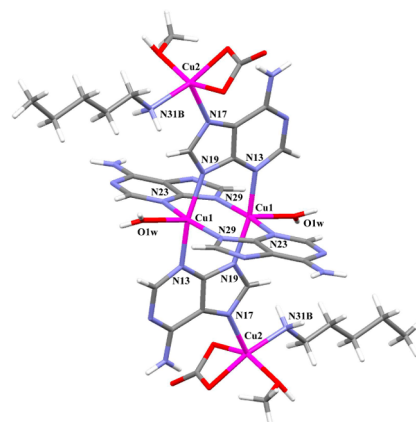


Figure 6. Structural unit of SMOF-8 with the atomic numbering scheme.

distorted square pyramidal coordination around Cu1 atom is completed with a water molecule. Each dimeric entity is linked to two neighboring monomeric units via the N7 imidazolic atoms of two adeninate ligands. Therefore, two adeninate anions behave as tridentate μ₃-N₃,N₇,N₉ bridging ligands, whereas the other two act as bidentate μ-N₃,N₉. The basal plane of the square pyramidal chromophore around Cu2 atom is completed with two oxygen atoms from a carbonato ligand, an oxygen atom of a methanol molecule, and the nitrogen atom of a pentylamine molecule.

Each tetranuclear entity is linked to four adjacent ones via double N6–H...N1 hydrogen bonding interactions between the Watson–Crick faces of neighboring entities to give a R₂²(8) ring. This assembling of tetrameric entities gives rise to layers that can be described as a four-connected uninodal net with Shubnikov tetragonal *sql* topology and (4⁴.6²) point symbol. It is worth noting that the dinuclear paddle-wheel entity of SMOF-1 and SMOF-2 presents analogous four-connected nodes (using Watson–Crick base pairing interactions), but the absence of the bulky capping monomeric entities allows the growth of a 3D supramolecular network (*nbo*, 6⁴.8²). However, in SMOF-8 the 3D cohesion requires additional hydrogen bonding interactions involving the coordination water molecule, the carbonato ligand, and the pentylamine molecule (Figure 7, Table S4) leading to an α-Po *pcu* topology. The overall packing generates a 2D pore network with channels running along the *b* and *c* axes of 3–5 Å of diameter, that represents 43% of void space and a calculated surface area of 402 m²/g. However, the crystals decompose upon removal from the mother liquor and even when immersed in pure methanol. This fact is probably due to the loss of pentylamine that seems to play a key role stabilizing the crystal structure.

Structural Description of [Cu₂(μ-ade)₂(ade)(μ-OH)-(H₂O)(CH₃OH)]_n(solvent) (SMOF-9). The basic structural

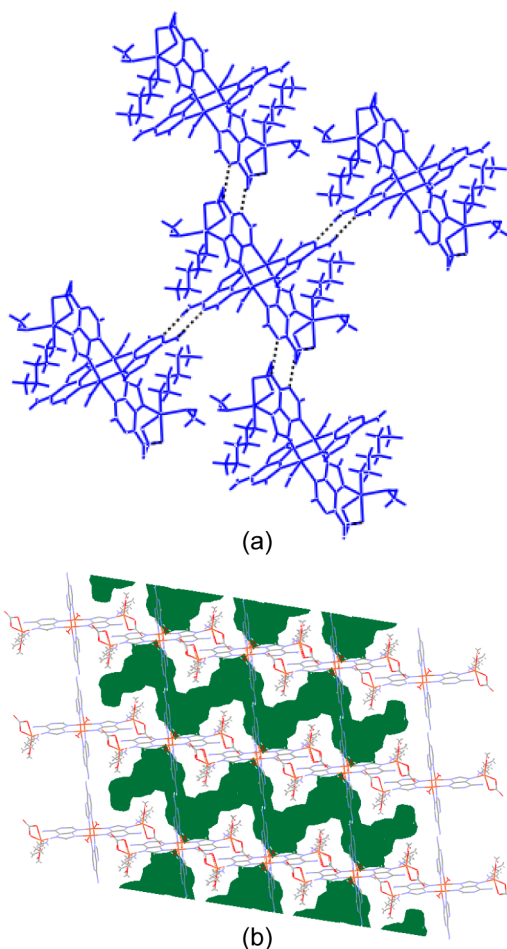


Figure 7. (a) Linkage of the tetranuclear entities by the Watson–Crick faces and (b) crystal packing along the *b* axis of SMOF-8, showing the generated voids.

Table 5. Hydrogen Bonding Interactions (Å, °) in SMOF-8^a

D–H...A ^b	H...A	D...A	D–H...A
N6–H6A...N11 ⁱⁱ	2.13	2.978(11)	167
N6–H6B...O1	2.11	2.965(13)	175
N6–H26B...N21 ⁱⁱⁱ	2.08	2.935(17)	172
O1w–H12w...O3 ^{iv}	1.94	2.790(13)	169
N31–H31A...O2 ^v	1.94	2.843(18)	176

^aSymmetry codes: (ii) $-x + 2, -y + 1, -z + 1$; (iii) $-x + 2, -y, -z$; (iv) $x - 1, y, z$; (v) $-x + 3, -y, -z + 1$. ^bD: donor; A: acceptor.

unit of this compound consists of 1D infinite coordination polymers held together by complementary hydrogen bonding interactions in a 3D supramolecular porous structure. The coordination polymer can be described as noncentrosymmetric dinuclear units (Figure 8) in which two Cu(II) atoms are bridged with two adeninate moieties by the N3 and N9 atoms and also by one hydroxyl group (Figure 9a). One of the metal centers is also coordinated to a water molecule while the other to the oxygen atom of a methanol molecule. These dinuclear units are connected by additional bridging adenines that are coordinated to the Cu(II) centers by the N7 and N9 atoms to provide a 1D coordination chain. An interesting structural feature is that the bridging adenines inside the dinuclear units are tilted by 22°, but they present wider tilt angle with respect to those connecting the dimeric units (56 and 78°, respectively)

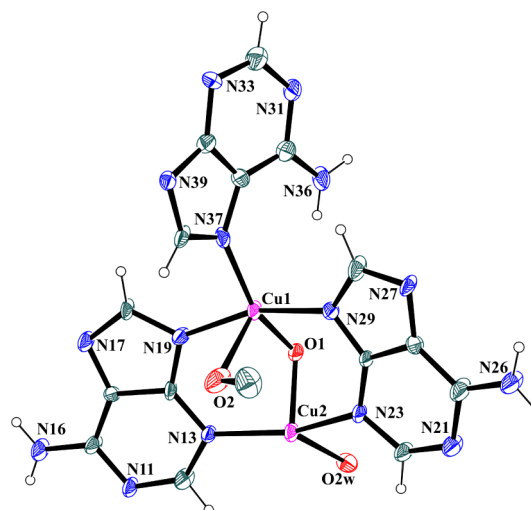


Figure 8. Ortep representation of the dimeric unit $[\text{Cu}_2(\mu\text{-ade})_2(\text{ade})(\text{H}_2\text{O})(\mu\text{-OH})(\text{CH}_3\text{OH})]$ together with the numbering scheme in SMOF-9.

in the polymeric chain. This fact together with the complementary double hydrogen bonding interactions of the nucleobases promotes a three-dimensional propagation of the supramolecular structure. The $\mu\text{-}\kappa\text{N}3:\kappa\text{N}9$ -adenines are able to establish double WC...WC and H...H synthons leading to $R_2^2(8)$ and $R_2^2(10)$ hydrogen bonding rings, respectively. On the other hand, the $\mu\text{-}\kappa\text{N}7:\kappa\text{N}9$ -adenines are hydrogen bonded to the bridging hydroxide and the coordinated water molecule of an adjacent polymeric chain through N1 and N6 positions of the Watson–Crick face. The resulting supramolecular crystal structure shows the presence of large channels along the *b* axis with a calculated surface area of 295 m²/g and 44% of void space.

This compound is an interesting case because it is in between pure MOFs and SMOFs as it polymerizes into 1D through coordination bonds and further extends to supramolecular array through complementary hydrogen bonding interactions resulting in a 3D porous network (Figure 9c).

CONCLUSIONS

In this report we have paid special attention to the design prerequisites of SMOFs: (i) rigid building unit/complex, (ii) rigid and predictable synthons, and (iii) at least three non-coplanar synthons. This approach is supported by six new SMOFs based on different metal centers, nucleobases, and synthetic conditions. It also highlights the suitability of metal-nucleobase systems, specially purine based ones, to obtain SMOFs since many of them accomplish the above stated requirements: (i) the rigidity of the building unit is achieved using nucleobases because they can be coordinated through multiple positions, normally by a double anchoring (double coordination bonds or the combination of a coordination bond and an intramolecular hydrogen bond), (ii) the well-known complementary hydrogen bonding interactions between the nucleobases ensures the necessary rigidity of the predictable synthons, and (iii) the metal coordination geometries impose, in many cases, a non-coplanar arrangement of the nucleobases affording a non-coplanar disposition of the synthons that allows three-dimensional propagation of the nucleobase...nucleobase complementary hydrogen bonding assembly.

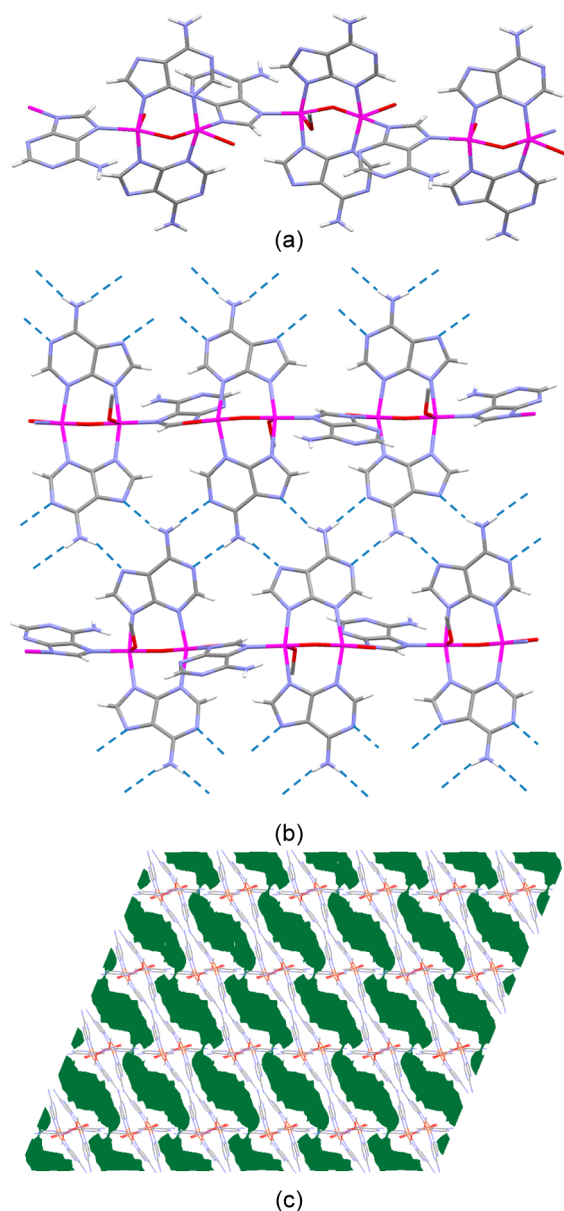


Figure 9. (a) Coordination polymeric chain. (b) Supramolecular complementary base pairing interactions among the adeninate entities. (c) Porous supramolecular architecture of SMOF-9 along the *b* axis.

Table 6. Hydrogen Bonding Interactions (Å, °) in SMOF-9^a

D–H...A ^b	H...A	D...A	D–H...A
N16–H16A...N11 ⁱⁱ	2.23	3.075(10)	170
N26–H26A...N21 ⁱⁱⁱ	2.06	2.920(11)	179
N26–H26B...N17 ^{iv}	2.08	2.904(11)	161
N36–H36B...O1 ^v	2.12	2.884(9)	148

^aSymmetry codes: (ii) $-x + 1, -y + 2, -z + 1$; (iii) $-x, -y + 2, -z$; (iv) $x - 1/2, -y + 3/2, z - 1/2$; (v) $-x + 1/2, -y + 3/2, -z$. ^bD: donor; A: acceptor.

■ ASSOCIATED CONTENT

Supporting Information

Tables of coordination bond lengths, figures of network topologies, XRPD patterns, and cif files. This material is available free of charge via the Internet at <http://pubs.acs.org>.

■ AUTHOR INFORMATION

Corresponding Authors

* (O.C.) E-mail: oscar.castillo@ehu.es. Fax: (internat): +34 946013500.

* (S.P.-Y.) E-mail: sonia.perez@ehu.es.

Author Contributions

[‡]These authors (J.T.-G and R.P.-A) contributed equally.

Notes

The authors declare no competing financial interest.

■ ACKNOWLEDGMENTS

This work has been funded by Ministerio de Economía y Competitividad (MAT2013-46502-C2-1-P), Eusko Jaurlaritza/Gobierno Vasco (Grant IT477-10, S-PE13UN016), and Universidad del País Vasco/Euskal Herriko Unibertsitatea (EHUA14/09, UFI 11/53, postdoctoral fellowship for S.P.Y.). Technical and human support provided by SGIKER (UPV/EHU, MINECO, GV/EJ, ERDF, and ESF) is gratefully acknowledged.

■ REFERENCES

- (1) Zhou, H.-C.; Long, J. R.; Yaghi, O. M. *Chem. Rev.* **2012**, *112*, 673.
- (2) Seo, J.; Jin, N.; Chun, H. *Inorg. Chem.* **2010**, *49*, 10833.
- (3) Bae, Y. S.; Farha, O. K.; Hupp, J. T.; Snurr, R. Q. *J. Mater. Chem.* **2009**, *19*, 2131.
- (4) Simard, M.; Su, D.; Wuest, J. D. *J. Am. Chem. Soc.* **1991**, *113*, 4696.
- (5) Kim, H.; Kim, Y.; Yoon, M.; Lim, S.; Park, S. M.; Seo, G.; Kim, K. *J. Am. Chem. Soc.* **2010**, *132*, 12200.
- (6) Holden, A. *Shapes, Space, and Symmetry*; Dover: New York, 1991; pp 154–163.
- (7) Thomas-Gipson, J.; Beobide, G.; Castillo, O.; Fröba, M.; Hoffmann, F.; Luque, A.; Pérez-Yáñez, S.; Román, P. *Cryst. Growth Des.* **2014**, *14*, 4019.
- (8) Reger, D. L.; Debreczeni, A.; Smith, M. D.; Jezierska, J.; Ozarowski, A. *Inorg. Chem.* **2012**, *51*, 1068.
- (9) Beobide, G.; Castillo, O.; Cepeda, J.; Luque, A.; Pérez-Yáñez, S.; Román, P.; Thomas-Gipson, J. *Coord. Chem. Rev.* **2013**, *257*, 2716.
- (10) Stylianou, K. C.; Warren, J. E.; Chong, S. Y.; Rabone, J.; Bacsá, J.; Bradshaw, D.; Rosseinsky, M. J. *Chem. Commun.* **2011**, *47*, 3389.
- (11) Kundu, S.; Mohapatra, B.; Mohapatra, C.; Verma, S.; Chandrasekhar, V. *Cryst. Growth Des.* **2015**, *15*, 247.
- (12) Thomas-Gipson, J.; Beobide, G.; Castillo, O.; Cepeda, J.; Luque, A.; Pérez-Yáñez, S.; Aguayo, A. T.; Román, P. *CrystEngComm* **2011**, *13*, 3301.
- (13) Nugent, P. S.; Rhodus, V. L.; Pham, T.; Forrest, K.; Wotjas, L.; Space, B.; Zaworotko, M. J. *J. Am. Chem. Soc.* **2013**, *135*, 10950.
- (14) *CrysAlis RED*, version 1.171.33.55; Oxford Diffraction: Wrocław, Poland, 2010.
- (15) Altomare, A.; Cascarano, M.; Giacovazzo, C.; Guagliardi, A. J. *Appl. Crystallogr.* **1993**, *26*, 343.
- (16) Sheldrick, G. M. *SHELXL-97, Program for X-ray Crystal Structure Refinement*; University of Göttingen: Göttingen, Germany, 1997.
- (17) Farrugia, L. J. *J. Appl. Crystallogr.* **1999**, *32*, 837.
- (18) Van der Sluis, P.; Spek, A. L. *Acta Crystallogr.* **1990**, *A46*, 194.
- (19) Spek, A. L. *J. Appl. Crystallogr.* **2003**, *36*, 7.
- (20) Amo-Ochoa, P.; Alexandre, S. S.; Hribesh, S.; Galindo, M. A.; Castillo, O.; Gómez-García, C. J.; Pike, A. R.; Soler, J. M.; Houlton, A.; Zamora, F. *Inorg. Chem.* **2013**, *52*, S290.
- (21) García-Couceiro, U.; Castillo, O.; Cepeda, J.; Lanchas, M.; Luque, A.; Pérez-Yáñez, S.; Román, P.; Vallejo-Sánchez, D. *Inorg. Chem.* **2010**, *49*, 11346.
- (22) Coronado, E.; Galán-Mascarós, J. R.; Gómez-García, C. J.; Laukhin, V. *Nature* **2000**, *408*, 447.
- (23) TOPOS Main Page. <http://www.topos.ssu.samara.ru> (accessed Apr. 2014).

- (24) Blatov, V. A. *IUCR CompComm Newsletter* **2006**, *7*, 4.
- (25) O'Keeffe, M.; Yaghi, O. M. *Chem. Rev.* **2012**, *112*, 675.
- (26) Sarkisov, L.; Harrison, A. *Molecular Simulation* **2011**, *37*, 1248.
- (27) Pérez-Yáñez, S.; Beobide, G.; Castillo, O.; Cepeda, J.; Luque, A.; Román, P. *Cryst. Growth Des.* **2012**, *12*, 3324.
- (28) Pandey, M. D.; Mishra, A. K.; Chandrasekhar, V.; Verma, S. *Inorg. Chem.* **2010**, *49*, 2020.
- (29) Mishra, A. K.; Purohit, C. S.; Kumar, J.; Verma, S. *Inorg. Chim. Acta* **2009**, *362*, 855.
- (30) Beck, W. M.; Calabrese, J. C.; Kottmair, N. D. *Inorg. Chem.* **1979**, *18*, 176.
- (31) Sánchez-Moreno, M. J.; Choquesillo-Lazarte, D.; González-Pérez, J. M.; Carballo, R.; Castiñeiras, A.; Niclós-Gutiérrez, J. *Inorg. Chem. Commun.* **2002**, *5*, 800.
- (32) Pérez-Yáñez, S.; Castillo, O.; Cepeda, J.; García-Terán, J. P.; Luque, A.; Román, P. *Inorg. Chim. Acta* **2011**, *365*, 211.
- (33) An, J.; Fiorella, R. P.; Geib, S. J.; Rosi, N. L. *J. Am. Chem. Soc.* **2009**, *131*, 8401.
- (34) Shekhah, O.; Wang, H.; Paradinas, M.; Ocal, M.; Schüpbach, B.; Terfort, A.; Zacher, D.; Fischer, R. A.; Wöll, C. *Nat. Mater.* **2009**, *8*, 481.
- (35) Cepeda, J.; Castillo, O.; García-Terán, J. P.; Luque, A.; Pérez-Yáñez, S.; Román, P. *Eur. J. Inorg. Chem.* **2009**, 2344.
- (36) Pérez-Yáñez, S.; Beobide, G.; Castillo, O.; Cepeda, J.; Luque, A.; Román, P. *Cryst. Growth Des.* **2013**, *13*, 3057.

This work reports a synthetic strategy to obtain supramolecular metal–organic frameworks (SupraMOFs) based on base pairing interactions with potentially accessible voids as an alternative to more conventional metal–organic frameworks (SupraMOFs) that are based on coordination bonds. This goal can be achieved by considering three key factors: (i) the use of rigid building units, (ii) the establishment of predictable and rigid synthons between the building units and (iii) the non-coplanarity of functional groups involved in the predictable synthons. Throughout this report we demonstrate the suitability of this synthetic strategy supported by several SupraMOFs based on metal–nucleobase entities which fulfill the above stated requirements. The crystal structures of these compounds are sustained through base pairing interactions taking place between nucleobases anchored to adjacent discrete metal complexes.

According to gas adsorption studies, most of these compounds present a surface instability that creates a diffusion barrier that can be permeated only by strong interacting adsorbate molecules with high kinetic energy such as CO_2 but not N_2 , H_2 , and CH_4 . This feature makes them attractive for selective gas adsorption and separation technologies.

